The development of water-based consolidants for Sydney sandstone in heritage buildings

A thesis submitted to the University of Technology, Sydney as a requirement for

Doctor of Philosophy

By

Tamae Fukumoto

2017

CERTIFICATE OF ORIGINAL AUTHORSHIP

I certify that the work in this thesis has not previously been submitted for a degree nor has it been submitted as part of requirements for a degree except as part of the collaborative doctoral degree and/or fully acknowledged within the text.

I also certify that the thesis has been written by me. Any help that I have received in my research work and the preparation of the thesis itself has been acknowledged. In addition, I certify that all information sources and literature used are indicated in the thesis.

Signature of Student:

Date:

23/06/2017

ACKNOWLEDGEMENT

I would like to gratefully acknowledge the valuable assistance and information provided for this dissertation; I owe my gratitude to all the people who have helped me and contributed to the completion of this dissertation. I would like to thank University of Technology Sydney for giving me the opportunity to participate in the significant sandstone conservation research. It has been an incredible experience to be a part of this research at University of Technology Sydney. The postgraduate research scholarship and financial support provided by University of Technology Sydney are also gratefully acknowledged.

First, I would like to express my deepest gratitude to my supervisors, Dr Paul Thomas and Associate Professor Barbra Stuart, for their advice, guidance, encouragements, patience and useful critiques of this research. I thank them for being available to help me. Their support, direction and understanding helped me overcome many challenging situations and finish this dissertation. I am also sincerely grateful to Professor Abhi Ray and Mrs Helen Ray. I appreciate that they generously gave their time to offer me valuable information, help, advice, encouragements and comments toward improving my work. I am grateful to Professor Abhi Ray for his advice and discussions that helped me sort out characterisation of montmorillonite and the composite samples. I am also much obliged to Mrs Helen Ray for her discussions and the useful information she has provided about structure, geology and conservation of sandstone.

I would like to express my appreciation to all of the faculty and technical staff members who assisted me in my laboratory work and helped me in handling the instruments. My sincere gratitude must go to Dr Barry Liu for his help in performing characterisation and analysis of consolidated Sydney sandstones. Without his support, advice and patience, the consolidation work in this thesis would not have been successful. Appreciation is extended to Mr Jean-Pierre Guerbois for his experienced and valuable technical assistance and advice with thermal analysis of my samples and for his help in the laboratory. I am also very thankful to Dr Ronald Shimmon and Dr Linda Xiao for their help with the humidity cabinets as well as the other equipment and instruments. I would

like to thank all the technical staff members for offering their support and lending me apparatuses/equipment crucial for this project, especially Ms Anthea Harris and Mr Nishath Geekiyanage. I am thankful to Mr Name Rami Haddad and Mr David Dicker for their help in cutting sandstone blocks. I would like to thank NSW public work, Arumpo Bentonite Pty Ltd. and IMCD Australia Ltd. for the supply of sandstones, montmorillonite and Silres product as well as the information provided for their products, which was valuable for the collection of my data. My special thanks must go to all the architects and stonemasons of NSW public work as well as Ms Joy Singh for their discussions and information regarding Sydney sandstone and the conservation practice of Sydney buildings.

I also owe many thanks to the postgraduate students who helped me by exchanging any ideas and information and who shared their experience and knowledge with me. I met some nice people who made my life at University of Technology Sydney a memorable experience. Without all of their support and consideration, this thesis would not have reached its completion; I am thankful to the staff and students for their help throughout my stay at University of Technology Sydney. Finally, I would like to thank my family for their encouragements, patience and understanding. This thesis is dedicated to my family members who believed in my potential to overcome all obstacles and pushed me try my best. Without their assistance and sacrifice, I could not have completed my PhD, and I am deeply indebted to them.

TABLAE OF CONTENTS

LIST OF ABBREVIATIONS

AA	Acrylic acid
Am	Acrylamide
B67	Paraloid B67
B72	Paraloid B72
BMA	Butyl methacrylate
BSE	Backscattered electrons
CR	Capillary rise absorption
DSC	Differential Scanning Calorimetry
DW	Distilled water
EA	Ethylacrylate
EMA	Ethyl methacrylate
FTIR spectroscopy	Fourier transform infrared spectroscopy
KPS	Potassium persulfate
Lascaux	Lascaux 498 HV
PAA	Polyacrylic acid
PAA100	Polyacrylic acid (100,000 g/mol)
PAA250	Polyacrylic acid (250,000 g/mol)
PAm	Polyacrylamide
PEG	Polyethylene glycol
PEG25	Polyethylene glycol (25,000 g/mol)
PEG35	Polyethylene glycol (35,000 g/mol)

PEO	Polyethylene oxide
MA	Methylacrylate
MMA	Methyl methacrylate
MMT	Montmorillonite
MMTa	Acidified MMT
RT	Room temperature
SE	Secondary electrons
SEM	Scanning Electron Microscopy
Silres	SILRES® BS OH 100
TEM	Transmission electron microscopy
TGA	Thermogravimetric Analysis
TG-MS Analysis	Evolved gas analysis using Thermogravimetric
TI	Total immersion
WVT	Water vapour transmission
XRD	X-ray Diffraction

LIST OF TABLES

LIST OF FIGURES

ABSTRACT

The work presented in this Thesis assesses the suitability and capacity of the aqueous consolidants designated for more compatible consolidation treatment of Sydney's yellow block sandstone. The aqueous consolidant systems investigated included polymer consolidants, polymer-montmorillonite composite consolidants and in situ polymerisation consolidation. Polymer consolidants incorporating montmorillonite (MMT) were prepared by aqueous solution intercalation method and demonstrated the fast and efficient preparation of composites at the wide range of MMT concentrations from 2.5 to 90%, dispersed in the water soluble polyacrylic acid (PAA), polyacrylamide (PAm), or polyethylene glycol (PEG), or in situ polymerised PAm. While the intercalation behaviour, MMT dispersion, structural variations, intermolecular interactions between polymer and MMT and thermal stability were affected by the polymer-MMT ratios and the nature of polymers; the polymer-MMT ratios determined the trend in these changes, but the extent to which these occurred depended on the nature of polymers. PAA, PAm, PEG and in situ polymerised PAm produced the interlayer separation of MMT in the range of 13.1-19.6, 15.2-26.9, 14.2-19.7 and 20.3-28.1Å with the 50 to 60% MMT threshold incorporated into the polymer matrixes. The interlayer separation of MMT were similar for PAA and PEG, while PAm and the in situ polymerised PAm increased the interlayer expansion of MMT.

The consolidant performance of PAA, PAm, PEG, the polymer-MMT composites and in situ polymerised PAA or PAm was compared with the commercial consolidants, hydrophobic Paraloid B67 (B67) and B72 (B72), water soluble Lascaux and the ethyl silicate Silres by their penetration ability, uptake, water vapour permeability, colour change and bending strength. The polymer-MMT ratio of the composite and the concentrations of polymer or monomer were critical. Practically, the composites containing less than 20% MMT were suitable and the polymerisation at greater than 10% Am or AA was unusable. Increasing the polymer concentrations reduced penetration, induced colour changes and reduced water vapour permeability. PAm and polymerised PAm showed the best performance, whereas PEG reduced mechanical strength and AA and PAA caused colour changes. In comparison, the hydrophobic commercial consolidants caused increased darkening and significantly reduced permeability although

the water soluble Lascuax did provide some beneficial effect. The consolidants developed in this research represented mild consolidation action with minor changes in the characteristics of the treated sandstone. Encouraging results were observed for the performance of these water based polymer consolidants, in particular, PAm demonstrating the best consolidant of water based consolidation systems in the conservation of heritage sandstone.

CHAPTER 1: INTRODUCTION

1.1. Heritage stone conservation

Natural stone has been an essential part of human history and has played a significant role in the development of human society (Fitzner & Heinrichs 2001, Turkington & Paradise 2005, Török & Přikryl 2010, McAfee 2011). The modification of natural stone has created various cultural stones of historical, archaeological, social, artistic and scientific importance (Rao, Brinker & Ross 1996, Pope, Meierding & Paradise 2002, Liu et al. 2006, McAfee 2011). Such stones have been tailored for the production of cultural heritage objects, such as buildings, monuments, sculptures and art (Wheeler et al. 1992, Işik-Yürüksoy, Kiş & Güven 1998, Warscheid & Braams 2000, Fitzner & Heinrichs 2001, Mola 2011).

From a mineralogical and structural point of view, stone is a highly intricate geomaterial (Warke, McKinley & Smith 2006). The general features of natural stone fabric are their heterogeneous and anisotropic nature (Siegesmund, Weiss & Vollbrecht 2002, Török 2010). The extent and type of their fabric anisotropy depend on the grain shape, micro-crack systems and preferred orientations of the rock-forming minerals (Siegesmund, Weiss & Vollbrecht 2002). The stone fabric largely determines the mechanical properties of the stone, including compressive, tensile and abrasive strengths, which are important parameters for the use of stone as a building material (Siegesmund, Weiss & Vollbrecht 2002). Each stone type differs in its chemical and physical properties from others and exhibits variations in characteristics, such as mineral composition, porosity, pore size distribution and the interconnectivity of channels (Wheeler 1992, Bugani et al. 2008, Török 2010).

For thousands of years, buildings have been constructed using natural stones as major construction materials due to their petrophysical and aesthetic characteristics as well as their availability (Weber 1985, Carta et al. 2005, Siegesmund & Snethlage 2010, Török & Přikryl 2010). In addition to limestone, tuffstone, granite and basalt, which are the types of natural stone generally employed in the construction of historical architecture, many

historic buildings were constructed from sandstone (Baglin & Austin 1980, Weber 1985, Turkington & Paradise 2005, Hugues, Steiger & Weber 2005, Giavarini et al. 2007, Ward-Harvey 2009, Siegesmund & Snethlage 2010). Sandstones vary in texture, hardness and colour and the use of sandstone in many historical structures and objects has offered a practical and attractive building material alternative (Baglin & Austin 1980, McNally and Franklin 2000, Turkington & Paradise 2005, Siegesmund & Snethlage 2010).

In contrast to the general perception that natural stone is an everlasting material, essentially unaffected during the lifetime of a building, natural stones are not exempt from natural weathering processes (Boyer 1987, Matero & Tagle 1995, Siegesmund, Weiss & Vollbrecht 2002, Warke, McKinley, Smith 2006, Siegesmund & Snethlage 2010, Doehne & Price 2011). All geomaterials slowly decay and ultimately become disintegrate (Warscheid & Braams 2000, Siegesmund, Weiss & Vollbrecht 2002, Bossert, Ožbolt & Grassegger 2004, Cnudde et al. 2004). Moving rocks from the quarry especially increases weathering action on building stone. Once removed from the natural environment, geomaterials become exposed to anthropogenic influences such as air pollution and environmental weathering (Rao, Brinker & Ross 1996, Warscheid & Braams 2000, Pope, Meierding & Paradise 2002, Siegesmund, Weiss & Vollbrecht 2002, Webster & May 2006). In fact, most natural stones are sensitive to exposed environments and stone decay in historical structures has long been observed (Weber 1985, Winkler 1987, Siegesmund, Weiss & Vollbrecht 2002, Rozenbaum et al. 2008, Schaffer 2016).

Internationally, there is no doubt that cultural heritage has the significant impact on society from political, historical, sociological and anthropological standpoints (Giorgi et al. 1986, Giovanni, Sgamellotti & Clark 1986, McAfee 2001, Pope, Meierding & Paradise 2002, Siegesmund, Weiss & Vollbrecht 2002, Smith et al. 2004, Turkington & Paradise 2005, Liu et al. 2006, Sadat-Shojai & Ershad-Langroudi 2009, Török & Přikryl 2010). The preservation of this cultural heritage from irreversible loss is of social, philosophical, cultural and historical worth (Tomaselli et al. 2000, Siegesmund, Weiss & Vollbrecht 2002, Smith et al. 2004). The conservation of cultural heritage has an important role in improving human progress and transferring culture, tradition and national identity to future generations (Giorgi et al. 1986, Tomaselli et al. 2000, Hunt 2014). The contribution of the field of cultural heritage conservation can also provide important returns from

economic and environmental prospectives (Giovanni, Sgamellotti & Clark 1986, Piacenti 1994, Pope, Meierding & Paradise 2002, Siegesmund, Weiss & Vollbrecht 2002, Department of the Environment and Heritage 2004, Smith et al. 2004, Turkington & Paradise 2005, Török & Přikryl 2010).

Due to the growing concerns about the accelerated rate of stone damage to buildings and monuments and an increasing awareness of and respect for the value of cultural heritage, the protection of historical buildings and monuments has become widespread public and political priority (Weber 1985, Giovanni, Sgamellotti & Clark 1986, Cooke 1989, Piacenti 1994, Alessandrini et al. 2000, Fitzner & Heinrichs 2001, Siegesmund, Weiss & Vollbrecht 2002, Smith et al. 2004, Australian Government Productivity Commission 2006, Turkington & Paradise 2005, Jimenez-Lopez et al. 2008, Schaffer 2016). This newfound interest has stimulated more effort and research in many fields, both nationally and internationally (Mosquera et al. 2002, Siegesmund, Weiss & Vollbrecht 2002, Wright 2002, Zárraga, Alvarez-Gasca & Cervantes 2002, De Buergo, Fort & Gomez-Heras 2004, Rodrigues & Grossi 2007, Sadat-Shojai & Ershad-Langroudi 2009). Although it should also be kept in mind that the weathering and breakdown of natural stones inescapably occurs as a part of the evolutionary cycle of life on earth, slowing down the disappearance and destruction of cultural heritage is necessary if their service life is to be extended for as long as possible (Charola, Tucci & Koestler 1986, Bell 1993, Warscheid & Braams 2000, Warke et al. 2003, Sadat-Shojai & Ershad-Langroudi 2009).

Safeguarding and maintaining built heritage involves both conservation and restoration work. While the replacement of heavily damaged stones is a widely adopted practice, replacing the original stone represents the loss of not only authenticity, but also natural stone inventory (Griswold & Uricheck 1998, Jokilehto 1999, Rodrigues 2001, Dreesen & Dusar 2004, Jimenez-Lopez et al. 2008, Rozenbaum et al. 2008, Litomyšl 2010). Additionally, the rate of decay can be accelerated because of differences in the physical properties between the original stone and the replaced stone, generating a further deterioration (Ip 2007, Schaffer 2016). Moreover, the availability of natural stone resources has been decreasing in industrialized countries and there has been more difficulty in finding suitable substitution stones that are compatible with the original stones in terms of their properties and appearance (O'Connor et al. 2001, Rozenbaum et

al. 2008, Török & Přikryl 2010, Doehne & Price 2011, Gunn 2012). Unfortunately, history has shown that most archaeological sites have experienced incorrect conservation methods through inappropriate selection of materials and through unsuitable policy decisions (Rodrigues & Grossi 2007, Török 2010). Due to this, many sites of cultural and historical significance have been definitively lost (Rodrigues & Grossi 2007). Whatever the causes of stone deterioration, the adequate treatment of the stones in historic buildings is necessary and there is an ever-increasing demand for more advancement that can lead to more effective conservation treatments (Rodrigues & Grossi 2007).

In the process of establishing an appropriate conservation strategy, it is important to recognize that conservation is a delicate and complicated multiple-step procedure as well as a multidisciplinary practice in which old and new systems are combined (Werner 1981, Griswold & Uricheck 1998, McAfee 2001, Pope, Meierding & Paradise 2002, Smith et al. 2004, Sadat-Shojai & Ershad-Langroudi 2009). To design a successful conservation treatment, it is necessary to link complex systems and integrate a wide range of information and expertise from engineers, scientists, architects and art historians (Pope, Meierding & Paradise 2002, Siegesmund, Weiss & Vollbrecht 2002, Smith et al. 2004, Turkington & Paradise 2005). A wide variety of factors must also be considered, including the intrinsic characteristics of the stones, surrounding conditions, causes of stone decay, present status of building stones, performance evaluation of consolidants applied and maintenance (Boyer 1987, McAfee 2001, Siegesmund, Weiss & Vollbrecht 2002, Török & Přikryl 2010, Litomyšl 2010). The conservation practice may involve preservation, stabilization, maintenance, restoration, renovation, adaptation, maintenance and safety and minimum intervention is desirable (Boyer 1987, McAfee 2001). Every case differs in its preservation conditions and stone types and each conservation case requires its own conservation plan (Boyer 1987, Bugani et al. 2007, Bugani et al. 2008).

1.2. Conservation of historic sites in Australia

While there has been more action taken to protect worldwide cultural heritage recently, rules and policies differ from country to country (Pope, Meierding & Paradise 2002, Smith et al. 2004, Doehne & Price 2011). In Australia, government responsibilities were recognized when heritage place conservation legislation was enacted in most states and

territories in the 1970s (Hall, McArthur & Foundation 1993, Bumbaru 2002). Under the influence of international heritage agreements and concerns, the establishment of a national estate was achieved and 19 properties in Australia were acknowledged as cultural and natural heritage sites and listed on World Heritage list sites including Hyde Park Barracks and Sydney Opera House (Australian Government Department of the Environment n.d., Hall, McArthur & Foundation 1993, The Australian National University 2009). Although the generalization of decision-making, broad-scale awareness and concern was achieved in the 1990s, heritage management in Australia has risen to a very high standard (Hall, McArthur & Foundation 1993, Australian Government Productivity Commission 2006). Both governmental and non-governmental organizations are involved in heritage conservation, with the Australian Heritage Commission emerging as a national leader of heritage management (Bumbaru 2002, Australian Government Productivity Commission 2006).

The first comprehensive heritage legislation was enacted in New South Wales in 1977, when the government began contributing to the conservation of heritage buildings (Young & New South Wales 1988). In the same year, a small unit of stonemasons was established by New South Wales Department of Public Works which is responsible for the conservation of the heritage buildings (Cramer 2002, NSW Government: NSW Public Works 2009). In New South Wales, 600 significant state-owned stone buildings and monuments were listed (Ip 2007). They are under the management of the state and over 60% of these sites have been recognized as having national heritage significance (Ip 2007). In order to meet the conservation challenges posed by Sydney's heritage, a New South Wales Government initiative has been operating since 1991 through the Minister's Centenary Stonework Program of the New South Wales Public Works, which assists in the maintenance duties of the state significant façades of Sydney's historic stone buildings (Australian Government Productivity Commission 2006, NSW Government: Public Works Advisory n.d.). The significant public buildings conserved by this program include the State Library of New South Wales and the Sydney Observatory (NSW Government: NSW Public Works 2009).

Sydney's first architectural buildings appeared during the time of Governor Macquarie of

New South Wales (1810-1821), who established the current character of heritage sites in Sydney (Stuart 1993, MacMahon 2001). Sydney is particularly recognized as having many architectural sites of heritage value that were built during the period from the late 18th century through the 19th century into the early 20th century (Baglin & Austin 1980, McNally and Franklin 2000, Cox 2002, Deirmendjian 2002, Dragovich & Egan 2011). This produced the unique heritage of Sydney and the associated architectural, social, economical, technological and cultural values (Baglin & Austin 1980, Cox 2002, Ip et al. 2004, Ip et al. 2005a). The prominent early sites have various features of historical importance, including many convict-built buildings and structures (Baglin & Austin 1980, Stuart 1993, Broadbent 2002, Deirmendjian 2002). Built heritage plays an important role in maintaining the past and helping to identify places and communities in Australia, and the built environment represents a link between history and present (Department of the Environment and Heritage 2004, NSW Government: Office of Environment and Heritage 2012).

In response to the need to adapt architectural, environmental, technological and economical changes in Sydney, the demand for stone structures was reduced after the 20th century and hundreds of historic buildings in Sydney were lost or damaged (Baglin & Austin 1980, Stuart 1993, Broadbent 2002, Cox 2002, Cramer 2002, NSW Government: Office of Environment and Heritage 2012). Although the financial aspect of historic preservation is often the main decision-making factor, the reason for decay and loss may also include neglect, lack of knowledge of the heritage importance, concern regarding safety issues of deteriorated old buildings and availability of skilled and qualified people to perform preservation tasks (Baglin & Austin 1980, Stuart 1993, Broadbent 2002).

1.3. Sandstone

Sandstone is a sedimentary rock belonging to the clastic group (Baglin & Austin 1980, McAfee 2001, Deirmendjian 2002, Mola 2011, Gunn 2012). The main composition of sandstone is sand grains, which are formed from weathered rocks and mostly rounded particles of mineral quartz (Baglin & Austin 1980, Hugues, Steiger & Weber 2005, Mola 2011). Their stiffness and resistance to weathering and mechanical abrasions made these particles outlast other common minerals (Baglin & Austin 1980, Flannery 2002, Mola

2011). The accumulated sand is cemented within the pore spaces between sand grains giving sandstone its characteristic granular appearance (Franklin 2000, Flannery 2002). Siliceous, calcareous, dolomitic and marlaceous cements are the general natural materials that bind sand grains (Baglin & Austin 1980, McAfee 2001, Hugues, Steiger & Weber 2005, Pettijohn, Potter & Siever 2005). In addition to mineral quartz as a main constituent, sandstone is composed of a range of different phases including iron oxide, calcium carbonate, which are transported by the solutions (Baglin & Austin 1980, Hugues, Steiger & Weber 2005). The colour of the sandstone results from, not only the sand grains and the cementing materials, but also the combined effect of the other phases included in the sandstone (Baglin & Austin 1980, Flannery 2002, Hugues, Steiger & Weber 2005, Pettijohn, Potter & Siever 2005, Mola 2011).

In contrast to the igneous and other metamorphic rock types including granite and crystalline marble, the sandstone structures are known for their changeable nature in response to the external conditions (Cox 2002, Deirmendjian 2002, Schaffer 2016). The unique and natural warm appearance of sandstone structures are inspired by the rich variety of colour, textures and unpolished surfaces of the sandstone (Stuart 1993, Deirmendjian 2002). Being relatively soft and readily carved, the use of Sydney sandstones were much favourred by stonemasons and architects, and Sydney sandstone was distributed and shipped all over Australia (McAfee 2001, Broadbent 2002). Sydney is characterised by the warm and gold straw-coloured Sydney sandstone, which appears quite different from Melbourne, a city of dark and cold grey stone (Broadbent 2002). Sydney sandstone contributes to distinctive characteristics of Sydney and has been a great source of irreplaceable Sydney heritage (Broadbent 2002, Cox 2002, Ip et al. 2003, Ip et al. 2004).

Sydney was fortunate to have abundant sandstone resources and Sydney sandstone was the first stone building material used in New South Wales (Carver 1940, Stuart 1993, Connell 2000, O'Connor et al. 2001, Cox 2002, Deirmendjian 2002). Many remarkable early buildings in Sydney were built using sandstone, which reflects the uniqueness of the stone-built heritage of Sydney (Connell 2000, MacMahon 2001, Broadbent 2002, Cox 2002, Deirmendjian 2002, Ip et al. 2004, Australian Government Productivity Commission 2006). The use of sandstone in Sydney was particularly intense during the

first European settlement and Sydney sandstone was the common choice as building stone for most old public buildings (Baglin & Austin 1980, Cox 2002, Deirmendjian 2002). Sydney sandstone has been used to construct educational, public, commercial and ecclesiastical buildings such as schools, hospitals, libraries, railway stations, art galleries, post offices, churches and governmental offices. It has also been used to fabricate stone structures including bridges, monuments, houses, warehouse, hotels, shops and lighthouse (Baglin & Austin 1980, Stuart 1993, Franklin 2000, Cox 2002, Deirmendjian 2002).

Sydney sandstones are argillaceous quartz sandstone and made up mostly of uniformly-sized, small sand grains (Franklin 2000, Flannery 2002). Sydney sandstones are derived from a number of quarries across the Sydney basin. The sandstones are mineralogically similar but have different colour, texture, pattern, porosity hardness, grainsize and durability (Stuart 1993, Franklin 2000, McNally and Franklin 2000, Fitzgerald 2002, Flannery 2002). Natural Sydney sandstones ranges from white to grey, including orange, yellow, pink, maroon and brown, but the discolouration of the natural looks can occur easily without care (Stuart 1993, Franklin 2000, Flannery 2002). The weathering extent of sandstones is uniform and the aged colours are stable (Stuart 1993). According to composition, colour, colour change and dimension, six groups of Sydney sandstones were identified and the principle Sydney sandstones used as the major construction material in many of Sydney heritage buildings are "yellow block" sandstone (Figure 1) and quartz-rich sandstone (Franklin 2000, McNally and Franklin 2000).

Among the Sydney sandstones used for Sydney's stone construction, yellow block sandstone produced the characteristic straw-yellow to deep honey-brown sandstone architecture (Deirmendjian 2002, Ip et al. 2003, Orwell & Peter Phillips 2008). Natural yellow block Sydney sandstone is the stone material of interest in this research. Due to its petro-physical and visual features, availability and workability, yellow block sandstone quarried from one of the major units, Triassic Hawkesbury sandstone in the Sydney basin, was a favourite material (Ray 1982, Franklin 2000, McNally and Franklin 2000, Deirmendjian 2002). It was used for the creation of cultural objects such as statues and monuments, as well as, many famous buildings including the Sydney Town Hall, the Australian Museum and St. Mary's Cathedral (Franklin 2000, McNally and Franklin

2000, Orwell & Peter Phillips 2008).

Figure 1.1. Location of Sydney Basin and Triassic rock units (Rn = Narrabeen Group, Rh = Hawkesbury Sandstone, Rw = Wianamatta Group (Swanson, Ward & Franklin 2002)

Sydney sandstone, geologically known as Hawkesbury Sandstone and upper Narrabeen Group of the Sydney Basin (Figure 1.1), was used to construct the historic buildings in Sydney and many building sandstones were quarried around the central city of Sydney (Franklin 2000, Swanson, Ward & Franklin 2002, McNally & Whitehouse 2004, Al Gahtani F 2017). The landscape within a 100 km radius of Sydney is dominated by Hawkesbury sandstone underlying the City of Sydney and occupying an area of 12500 km^2 in the Sydney basin (Pells 1977, Franklin 2000, McSkimming 2012). The Hawksbury sandstone is sedimentary quartzose sandstone from Middle Triassic period about 230 million years ago, lies flat and extends to about 20,000 km^2 (Franklin 2000). As the quarries in Pyrmont and the Eastern suburbs of Sydney were used to provide the heritage building sandstone in Sydney until 1960s (Swanson, Ward & Franklin 2002), the yellow block sandstone quarried in Pyrmont and studied in this work is of considerable importance in conservation work of Sydney's heritage buildings.

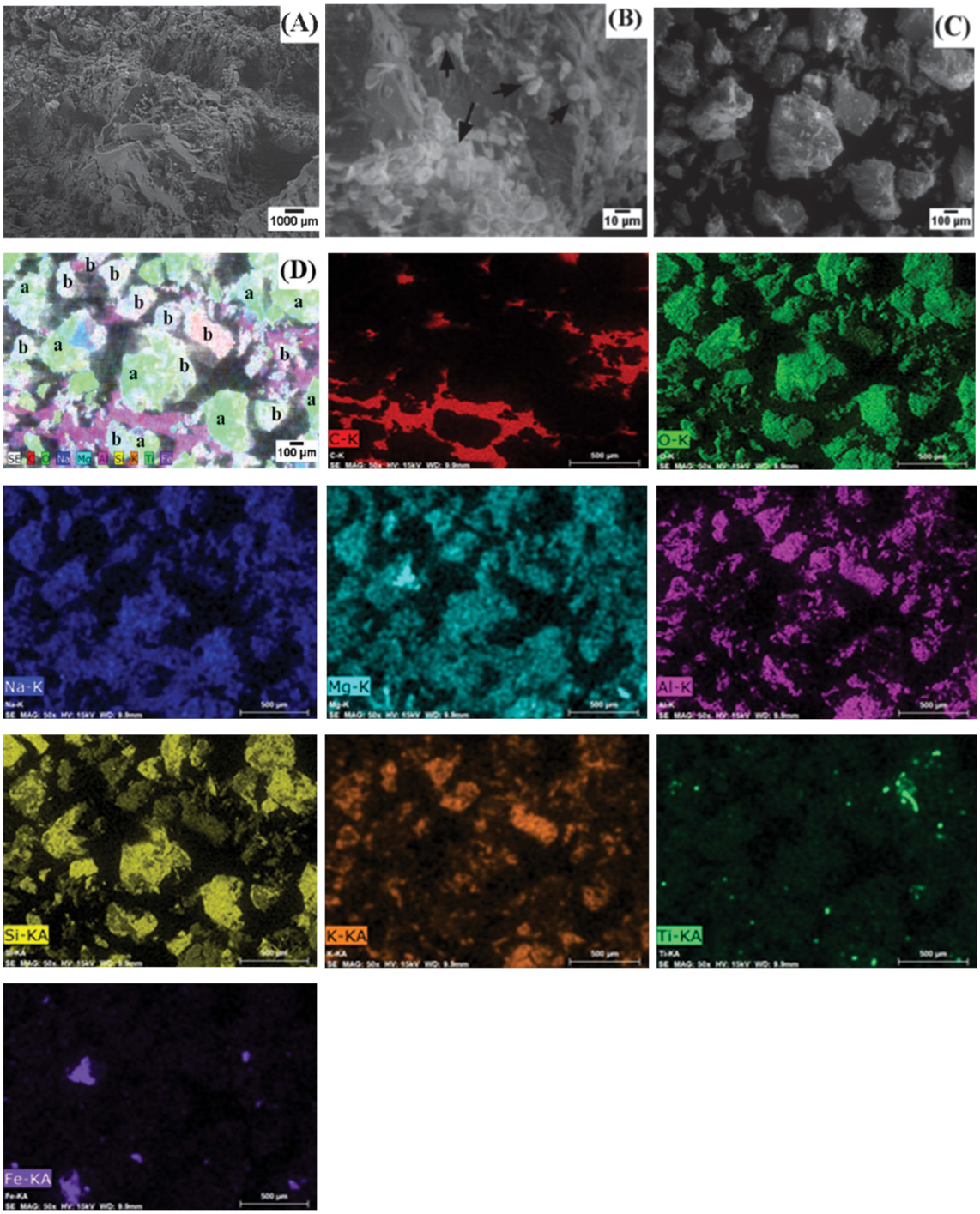

Figure 1.2. SEM images of Pyrmont sandstone taken from (A) sandstone surface, (B) hexagonal shaped kaolinite cementing clay present in the sandstone and (C) powdered sandstone. X-ray mapping images of the powdered sandstone show the presence of C, O, Na, Mg, Al, Si, K, Ti and Fe and Figure (D) shows sand grain (a) and kaolinite clay (b) in the powdered sandstone

While Sydney's quarries in Pyrmont, Ultimo and the city of Sydney first provided yellow block sandstone, it was later quarried in Paddington, Bondi and Maroubra (Flannery

2002). Yellow block sandstone in Pyrmont is of particular interest to the current research (Figure 1.2). It is one of the widely acknowledged sandstone and is plentifully available (Stuart 1993, Fitzgerald 2002). Pyrmont yellow block sandstone became recognized for its quality and toughness and sandstone quarry in Pyrmont supplied yellow block sandstone for many of Sydney's public buildings constructed during the late 19th and early 20th centuries (National Rock Garden n.d., Powerhouse museum n.d., Stuart 1993, Fitzgerald 2002, Franklin 2000, 'From heaven to hell in one easy walk' 2005, Orwell & Peter Phillips 2008, Swann 2008).

Figure 1.3. Unweathered (left) and discoloured (right) Sydney yellow block sandstone

Yellow block sandstone is a fine- to medium-grained sandstone and is generally porous (McNally and Franklin 2000, Ip 2007). The main composition of this type of stone is 60-68% sand grains, which is known as a highly stable mineral and the presence of high quartz content and secondary quartz overgrowths gives the stone its hardness, occasional sparkling appearances, durability and resistance to mechanical abrasion (Baglin & Austin 1980, Franklin 2000, McNally and Franklin 2000, O'Connor et al. 2001, Ip et al. 2005b, Ip 2007, Dragovich & Egan 2011). The sand grains are cemented with a clay binder, which is principally kaolinite (Ip et al. 2003, Ip et al. 2005a). 16-25% of yellow block sandstone content is this cementing clay binder, which is the main material responsible for the weathering process (McNally and Franklin 2000, O'Connor et al. 2001, Ip et al. 2003). Also, small amounts of iron oxide, silica and gypsum and 2-7% iron carbonate

mineral siderite are present in the stone (Franklin 2000, McNally and Franklin 2000, O'Connor et al. 2001). The stone is known to experience self-colouring and colour changes due to the oxidation of iron-bearing components of the stone, such as the iron carbonate mineral siderite, once exposed to the atmosphere (Franklin 2000, McNally and Franklin 2000). In general, the stone is light grey in colour when freshly quarried, but changes to its characteristic warm yellow-brown colour due to the action of weathering and oxidation (Ray 1982, Franklin 2000, McNally and Franklin 2000, Flannery 2002, Ip et al. 2011a) (Figure 1.3).

1.4. Sandstone weathering and deterioration mechanisms

The heritage buildings in Sydney, even if made with good-quality yellow block sandstone, have been weathered by various physicochemical processes caused by internal and external factors (Ip et al. 2004, Orwell & Peter Phillips 2008). Due to the fast changes in the environmental conditions, the visible deterioration and aesthetic damage from the surfaces of the sandstone heritage buildings in Sydney have already developed (Heiman 1981a, Heiman 1981b, Ip et al. 2003, Ip et al. 2004, Ip et al. 2005a, Ip et al. 2005b, Ip et al. 2008, Orwell & Peter Phillips 2008, Dragovich & Egan 2011). The external influences in Sydney are produced by the combined actions of natural and human-made causes. The built heritage exposed to the weather and climatic conditions is affected critically from the degradative action of temperature changes, humidity patterns, movement of water and soluble salts and attack by the atmospheric and pollution agents, and the operation of salt weathering is one of the most damaging factors (Heiman 1981a, Ip et al. 2004, Ip et al. 2005, Orwell & Peter Phillips 2008, Dragovich & Egan 2011).

Salts migrating in the form of solution through the capillary system of the sandstones can be deposited on or under the surface, depending on the environmental factors, such as type of salts and drying conditions. The flow of water influences the mobilization of salts in the porous system of sandstone and the severity of damage to the stone and maintenance of the natural flow of water is essential in order to avoid the build-up of water and salts on the surface and in the sandstone. The response of the exposed yellow block sandstones to the external weathering factors caused alterations in the mineralogical composition of cementing kaolinite and porous structure of the sandstone. The reported

studies documented the structural destabilization of kaolinite, resulting from the weathering action of iron-bearing materials as the main deterioration mechanism of yellow block Sydney sandstone and the significance to introduce suitable consolidating material and to help retain the deteriorating kaolinite sound and stable for delay in the weathering rate of the sandstone (Ip et al. 2003, Ip et al. 2004, Ip et al. 2005a, Ip et al. 2005b, Ip 2007, Ip et al. 2008).

1.5. Conservation of Sydney sandstone heritage buildings

Of the many historical buildings that remain in Sydney, there exist both well- and poorly-maintained sites and the states of deterioration and preservation vary. Heritage importance and the distinctive characteristics of historic sites in Sydney have become more recognized and interest and consciousness of the preservation of heritage sites has been developed at all levels (Baglin & Austin 1980, Broadbent 2002, Hunt 2014). An interdisciplinary field of professionals including engineers, stone masons, architects and scientists have made substantial contributions to the conservation, restoration and maintenance of Sydney heritage buildings (Ip et al. 2004, Ip et al. 2005a, Ip et al. 2005b). The future demolition of main public buildings is doubtful, but the small historic buildings in the city are still at risk of being in disrepair or destroyed and heritage buildings are reconstructed to transform them into other commercial buildings such as hotels, restaurants or shopping centres (Baglin & Austin 1980).

In the search of the appropriate decision for heritage sites, it is necessary to evaluate the many aspects of heritage sites including their historical significance and benefits of preservation (Baglin & Austin 1980). In addition to the heritage values inherent in the built environment in Sydney, the benefits of historic preservation have been realized from the environmental and economic perspectives (Department of the Environment and Heritage 2004). The preservation of historic buildings corresponds to the conservation practice of resources used for the historic buildings and the reduced consumption of energy and resources required for their destruction and new construction (Department of the Environment and Heritage 2004). Besides the positive environmental benefits, some studies reported positive economic benefits associated with the conservation of heritage buildings. Results revealed that conservation is influential in generating employment and

stabilizing local economy (Wills & Eves 2005). The reported data indicated that conservation provided long term benefits and conservation costs were minimized by the economic and social benefits (Department of the Environment and Heritage 2004, Wills & Eves 2005). Toward the aim of establishing sustainable development in order to deliver the environmental and social benefits associated with integrated heritage sites, the adaptive reuse of historic buildings was recognized as a way to conserve the built heritage. Successful examples of heritage sites across states demonstrated that adaptively reused heritage buildings accommodated both new use and heritage significance (Department of the Environment and Heritage 2004). Preservation of heritage building can contribute to the development of an environmentally sustainable economy and the preparation of a sustainable built future (Department of the Environment and Heritage 2004).

1.6. Consolidation treatment of Sydney sandstone

To protect Sydney's sandstone heritage buildings and prevent further weathering actions, treatment of remaining sandstone structures using commercially developed cleaning and consolidating materials and the replacement of decayed stones can be immediate solutions to decaying construction. These conservation practices should consider their effects on the rate of sandstone decay. In combination with the characteristics of consolidants and replaced sandstones, both intrinsic and extrinsic weathering factors may accelerate deterioration, the details of which are not exactly known (Ip 2007).

It has also been argued that, while replacing decayed sandstones with new ones can immediately restore Sydney's heritage buildings, the differential composition and extent of weathering between new and aged sandstones can further accelerate the degradation process (Ip et al. 2003, Ip et al. 2004, Ip et al. 2005a, Ip et al. 2005b, Ip et al. 2007, Ip et al. 2008a, Ip et al. 2008b). Examples of degradation include cracks formed by internal stresses due to different rates of thermal expansion and vapour absorption capacities of the used and replaced sandstones and differing aesthetic aspects of old sandstones and replaced and treated sandstones (Ip 2007). Therefore, the key issue to consider is the need to minimise the incompatible conservation interventions from aesthetic, chemical and physical points of view. It may be more appropriate to develop new and compatible

binding materials and consolidate Sydney's original heritage sandstones for future restoration work in sandstone heritage buildings.

In the search for more compatible conservation actions, the identification of suitable materials to consolidate Sydney's sandstones and the evaluation of different consolidation treatments are crucial steps. Consolidation materials must adapt well to the material parameters of the sandstone building in order to prevent further damage; consolidation materials must be tested, selected and specifically developed. To preserve cultural heritage, a wide range of consolidation products have been developed (Skoulikidis, Vassiliou & Tsakona 2005, Cnudde et al. 2006, Jimenez-Lopez et al. 2008, Stück et al. 2008). However, sandstone's characteristics, damaging factors and the climatic conditions in Sydney are considerably different from built stone in other countries. Consequently, the consolidation treatment of Sydney sandstone requires scientific study to develop new consolidating materials. This thesis explores the effectiveness of current consolidating materials used on Sydney sandstone and investigates processes for filling the void via a series of tests and analyses.

1.7. Objectives and scope of thesis

The research work comprised a synthesis of consolidants, a characterisation of prepared consolidants and an evaluation of the consolidants' performance on treated stones. This research aim was to develop a new water-based consolidation treatment that is effective, stable, compatible, eco-friendly and cost-effective for the Sydney sandstone in heritage buildings. The aqueous clay-based polymeric composite system studied in this work was investigated for chemically, physically and structurally stable and compatible binders in an aqueous environment to reduce potential adverse effects of consolidation treatment. The established research approach explored the environmentally sound consolidation treatment to meet increased demand for safe conservation practices and cost-effective alternatives in order to maximize the benefits of clay-based consolidation. The scope of this research was to investigate the consolidation performance of clay based consolidants on Sydney sandstone through the use of natural clay mineral binder and water, which can contribute to safe, eco-friendly and cost-effective consolidation practice.

This project focused on the development of water-based consolidants, which were prepared in water as the sole solvent and applied to the sandstone samples and only water-soluble or water-dispersible materials were used in this research. The preparation of consolidants was limited to the use of water-soluble polymers, in situ polymerisation of monomers and MMT as a water-dispersible clay mineral. Water soluble polymers were included to improve binding strength between sandstone and consolidant. MMT incorporation served to enhance inorganic character to the polymers and MMT was used as a physical cross linking agent to improve stability of the polymer consolidant system. The research efforts were made based on two synthetic pathways:

- one used water soluble polymer for diffusion of water soluble polymer consolidant systems
- other used monomers and produces polymers through in situ polymerisation
- in situ polymerisation uses water soluble monomer/polymer system
- both routes resulted in the formation of polymers as an end product
- in situ polymerisation was used to primarily overcome the inadequate diffusion of polymeric-consolidating materials in the pores of stones and an emphasis was placed on this technique
- inorganic clay was used to aid the binding properties of both of these systems

The different combinations of polymer/MMT intercalation composite materials were prepared using the solution intercalation technique from water through both intercalation of polymer and in situ intercalative polymerisation of monomers. Work on the direct intercalation of PAA, PAm and PEG and the in situ polymerisation of Am or AA in to MMT were conducted using different experimental conditions—including concentration of MMT, monomer or initiator, temperature, reaction time and molecular weight—in an effort to prepare suitably modified MMT/hydrophilic polymer composites. In order to study the effects of clay content and to improve the compatibility of polymer/MMT composites with sandstone, the research was devoted to the development of polymer/MMT composites with higher MMT content than those normally reported in the literature. The synthesis of intercalated hydrophilic polymer-MMT composites aimed to identify highest MMT loading levels for designing water-based consolidants wherein the structure and properties of MMT are retained to some extent and the polymers present in

the galleries remain to prevent the swelling of MMT.

The main objective for the characterisation of consolidants, based on polymer and MMT, was to perform structural, chemical, thermal and morphological characterisation of prepared consolidants. The main goal of the characterisation of clay–polymer composite was to determine its usability as stone consolidation work, based on the swelling inhibitory effects of polymers, chemical interaction of MMT with polymers, chemical structure and thermal behaviour of consolidants. Measurements were conducted to analyse changes in the interactions between MMT and polymer, the extent of intercalation and dispersion of clay platelets within the polymer matrix and the thermal characteristics of consolidating materials for samples prepared with different MMT contents.

In order to evaluate the consolidating performance of stone consolidants, both polymerised and in situ formed consolidants were introduced to the sandstones by means of capillary rise absorption or total immersion techniques. A series of consolidating solutions was prepared by the polymerised polymers and composites, using PAA, PAm, PEG, MMT and in situ polymerisation of AA and Am in the presence of potassium persulfate (KPS) as a water soluble initiator. The feasibility of the prepared consolidants has been explored by comparing their consolidation performance with the commercially available products and hydrophobic polymers (B72 and B67), water soluble acrylate (Lascaux) and ethyl silicate (Silres) were employed to consolidate the Sydney sandstone samples. The experiments for the consolidation treatment were designed to assess the differences in performance of applied consolidants under identical experimental conditions for each performance measure.

The consolidation performance was evaluated through the determination of absorbed quantity, capillary rise rate and penetration depth of consolidants, permeability of the treated sandstone to water vapor, changes in colour of consolidated sandstones caused by applied consolidants and alteration in the mechanical strength of the consolidated stones. The objectives of the performance evaluation were to investigate the effects of various experimental factors and to identify the optimal preparation condition of the aqueous consolidants developed in this thesis. This includes the changes in chemical nature of the polymers and monomers, solvents, molecular size of the polymers, acidification of MMT,

concentrations of MMT in the composites, polymer, monomer and initiator. Particularly, the compatibility and stability of consolidants, which are key concepts and the major challenges in consolidation treatment, were enhanced through this research.

The direction of performance evaluation is toward the development of a preventive treatment that can restore the mechanical and chemical properties of the treated sandstone and that could inhibit the deterioration process. The consolidation treatments were, therefore, performed only on unweathered yellow block sandstone in this research. The scope of consolidation work was to evaluate the initial changes in efficiency of consolidants under laboratory conditions and to investigate behaviors through laboratory scale testing. As expected, the performed work involved in a part of the steps towards development of consolidation treatment for Sydney sandstone and the assessment of treatment effectiveness only reflected short-term actions of the consolidants, without long-term forecasts on the ageing effects on the consolidated sandstones, which were beyond the scope of this investigation.

CHAPTER 2. WEATHERING OF SANDSTONES

2.1. Introduction

This chapter introduces weathering processes of stones due to multiple factors originated from both natural causes and human impact. It initially introduces the weathering processes generally responsible for stone deterioration and then focuses on the causes that contribute to deterioration of Sydney sandstone. Understanding the influences responsible for Sydney sandstone decay is essential to design such materials optimized for the consolidation of Sydney sandstone. This chapter is committed to identifying the main deterioration causes of sandstone in Sydney heritage sites needed as a basis for establishing strategies for possible deceleration of sandstone.

The quarrying of sandstone begins the process of change in dimension block as soon as they are removed from the ground. The transport of water changes and the migration of ions to the surface results in colour change. Initially, the stone turns black as manganese is transported to the surface and oxidised to manganese dioxide. This occurs fairly quickly over a few days or weeks and is overcome by an acid wash of the stones. With time, the iron migrates to the surface and is oxidised to Fe(III) to give the golden hue. Consequently, the deterioration of building sandstone initiates from the time it is quarried.

2.2. Stone weathering

Over long periods of time, deterioration of the stone causes changes in the appearance, aesthetic qualities, structure and composition of the historic buildings and is associated with the weakening of the stone's fabric (Karpovich-Tate & Rebrikova 1991, Fitzner & Heinrichs 2001, Tiano 2002, Rodrigues, Pinto & da Costa 2002, Warke, McKinley, Smith 2006, Bugani et al. 2007). Stone buildings and monuments encounter a variety of weathering actions that involve many different mechanisms and proceed sequentially and cumulatively (Berry 1994, Salimbeni et al. 2000, Wright 2002, Turkington & Paradise 2005, Warke, McKinley, Smith 2006, Doehne & Price 2011). The rate, type and extent of stone decay are influenced by the interaction of the stone materials and weathering factors

(Fitzner & Heinrichs 2001, Striegel et al. 2003, Warke, McKinley, Smith 2006). They vary from building to building and even across different façades on the same building (Warke, McKinley, Smith 2006). The responses to deterioration processes and weathering patterns vary by rock fabric and depend on the intrinsic parameters of the stone materials, such as mineralogical composition, porosity, pore structure as well as chemical and morphological properties (Figure 2.1) (National Research Council 1982, Bell 1993, Siegesmund Weiss & Vollbrecht 2002, De Buergo, Fort & Gomez-Heras 2004, Doehne & Price 2011).

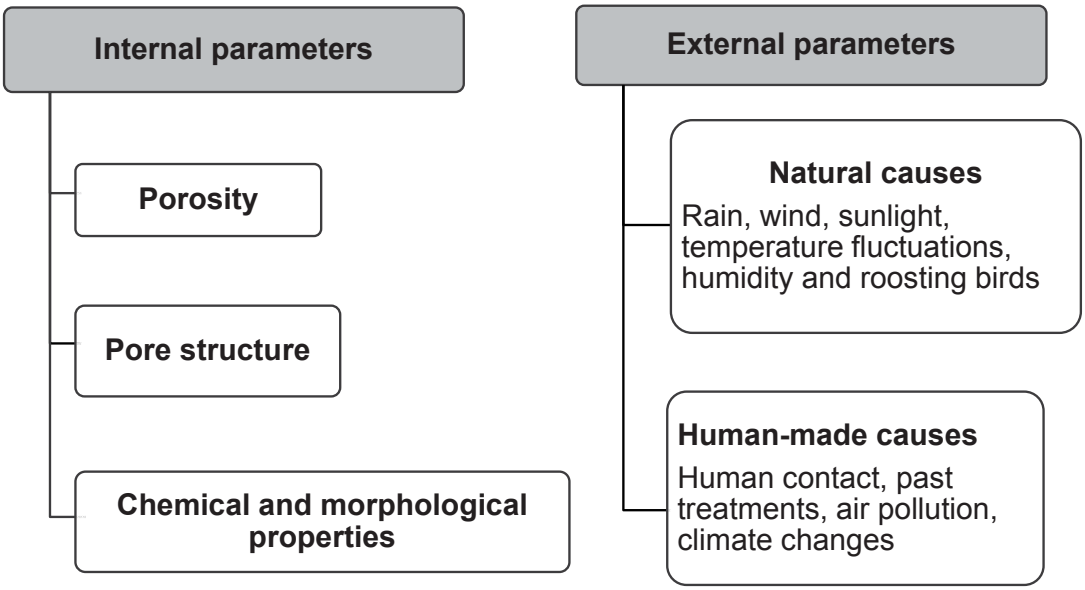

Figure 2.1. Influences of stone weathering

Together with the influence of intrinsic parameters, the weathering of stone takes place under extrinsic natural and anthropogenic influences (Warscheid & Braams 2000, Rodrigues 2001, Iñigo, Vicente-Tavera & Rives 2004). The stone decays through interaction with the surrounding environment (Rodrigues, Pinto & da Costa 2002) and these interactions are dependent on the thermodynamically and kinetically complex and persistently combined effects of chemical, physical and biological weathering actions, resulting in a wide range of decay forms (Domaslowski 1969, Giovanni, Sgamellotti & Clark 1986, Warscheid & Braams 2000, Rodrigues 2001, Siegesmund, Weiss & Vollbrecht 2002, Tiano 2002, Wright 2002, Kanellopoulou & Koutsoukos 2003, Turkington & Paradise 2005, Tiano et al. 2006, Doehne & Price 2011). The form and rate

of decay largely depends on weather conditions and the effects of climatic and environmental action, such as rain, wind, sunlight, temperature fluctuations, humidity patterns, pollution agents and roosting birds (Winkler 1987, Bell 1993, Işik-Yürüksoy, Kiş & Güven 1998, Tiano 2002, Sadat-Shojai & Ershad-Langroudi 2009, Doehne & Price 2011).

As a part of steps towards development of preservation strategy for stone conservation, it is essential to understand the stone weathering involved in the physical, chemical and biological weathering processes (Domaslowski, W. 1969, Turkington & Paradise 2005, Török & Přikryl 2010). Despite a century of scientific investigation on stone decay and stone conservation practice, some knowledge gaps exist in research and in the difficulty in predicting the rate of stone weathering as a function of the changes in environmental conditions (Viles 2005). Stone weathering is complex process and takes place nonlinearly in response to natural and urban surroundings (Turkington & Paradise 2005, Schaffer 2016). The research work on the stone weathering highlighted the need for the identification and management of nonlinear behaviour of stone decay (Wolff 2004).

2.3. Physical weathering

The physical weathering leads to an increase in stress within the fabric of the rock and results in the reduction of the stone's strength, without chemical reactions or the alteration of the stone's chemical composition (Bell 1993, Siegesmund, Weiss & Vollbrecht 2002). These processes include freeze-thaw processes and salt weathering as well as hygric, thermal and wet-dry cycling stress (Siegesmund, Weiss & Vollbrecht 2002, Doehne & Price 2011). They can induce progressive disintegration along favoured anisotropic surfaces from sites such as intra- and intercrystalline micro-cracks, cleavage planes, twin lamellae and joints (Siegesmund, Weiss & Vollbrecht 2002).

2.3.1. Salt initiated deterioration

Among these physical decay processes, the deteriorating action of soluble salts represents one of the most common and destructive deterioration problems found in cultural heritage

sites (Pope, Meierding & Paradise 2002, Cardell et al. 2003, Moreno et al. 2006, Lopez-Arce et al. 2009a, Lopez-Arce et al. 2009b, Doehne & Price 2011). Salts have long been recognized as a cause of damage to porous materials and as the central deteriorating factor of many of the greatest architectural heritage sites and monuments in the world (Heiman 1981a, Goudie and Viles 1997, Rodriguez-Navarro & Doehne 1999, Siegesmund, Weiss & Vollbrecht 2002, Cardell et al. 2003, Lopez-Arce et al. 2009a, Lopez-Arce et al. 2009b, Sadat-Shojai & Ershad-Langroudi 2009, Doehne & Price 2011). Stone deterioration due to salt attack is attributed to a variety of salt decay mechanisms that lead to decay patterns such as crumbling and disintegration (Figure 2.2) (Ruiz-Agudo et al. 2006, Warke, McKinley, Smith 2006, Lopez-Arce et al. 2009a, Lopez-Arce et al. 2009b, Doehne & Price 2011).

Figure 2.2. Image showing salt attack as found from disaggregated sandstones buildings on Sydney Harbour's Spectacle Island (Swann 2011)

Although crystallization pressure is the most important process of all mechanisms proposed, salt decay takes place due to other mechanisms as well, including the growth of salt crystals, hydration pressure, thermal expansion, osmotic pressure, hydraulic pressure and chemical weathering (Winkler 1987, Bell 1993, Goudie and Viles 1997, Rodriguez-Navarro & Doehne 1999, Siegesmund, Weiss & Vollbrecht 2002, Cardell et al. 2003, Lopez-Arce et al. 2008, Kramar et al 2010, Doehne & Price 2011, EL-GOHARY 2011, Lopez-Arce et al. 2011, Toniolo et al. 2011). Under the action of salt weathering,

historic buildings and structures mostly decay due to the different destructive forces that are capable of generating greater stress than the fracture modulus of most porous materials and of destroying the physical integrity of stones (Cardell et al. 2003, Warke, McKinley, Smith 2006, Lopez-Arce et al. 2008, Lopez-Arce et al. 2011).

Figure 2.3. Photo illustrating subfflorescence as a result of accumulated salts below the sandstone surface (Swann 2011)

The salts that are typically involved in salt damage include chlorides, sulphates, carbonates and nitrates of alkali and alkaline earth metals (Heiman 1981a, Goudie and Viles 1997, Ruiz-Agudo et al. 2006). They can originate from many different internal or external sources. Salts can be derived from the original stone matrix, unsuitable treatments and incompatible building materials (Heiman 1981a, Berry 1994, Cardell et al. 2003, Lopez-Arce et al. 2009a, Sadat-Shojai & Ershad-Langroudi 2009, Doehne & Price 2011). Salt contaminants can enter into the stone from sea spray, wind, rainwater and ground water rising through the building from the soil (Berry 1994, Cardell et al. 2003, Sadat-Shojai & Ershad-Langroudi 2009, Lopez-Arce et al. 2011, Toniolo et al. 2011). Acidic salts can also be formed from external sources, such as sulphur dioxide and carbon dioxide in the atmosphere and from biological agencies, such as bacteria, fungi, guano and lichens (Berry 1994). In particular, increased sulphur dioxide emitted from the fuel combustion in the large cites can form calcium sulphate which is the reaction product of sulphur dioxide with calcareous sandstone or mortar (Heiman 1981a).

Although the presence of salts can contribute to the destruction and acceleration of stone

decay, the extent of salt damage varies depending on the location of salt deposition. The accumulation of salts can be recognized as efflorescence or crusts on the surface of the stone, but these are less important to the deterioration of the stones, because they can be removed from the surface (Bell 1993, Berry 1994, Moropoulou et al. 2003). In cases in which the salt deposition occurs as subfflorescence or cryptoefflorescences inside the stone, these processes show much less visual impact but are more harmful than efflorescence (Figure 2.3) (Bell 1993, Berry 1994, Rodriguez-Navarro & Doehne 1999, Cardell et al. 2003, Moropoulou et al. 2003). The occurrence of efflorescences or subfflorescences is largely determined by the relationship between the rate of drying and the migration of salt solution through the capillary system, which are affected by environmental conditions such as wind, temperature, type of salt solution and the nature of the salts (Rodriguez-Navarro & Doehne 1999, Moropoulou et al. 2003, Kramar et al 2010, Doehne & Price 2011).

2.4. Chemical weathering

Unlike physical weathering, chemical bond breakage in the minerals that constitute the stones takes place in chemical weathering processes (Warke, McKinley, Smith 2006). This results in structural and compositional changes in the stones. It is involved in chemical reactions, such as the dissolution of calcite and minerals, hydrolysis, hydration and mobilization of metal ions that are produced by water, carbon dioxide and oxygen from the air (Rao, Brinker & Ross 1996, Tarasov 2001, Siegesmund, Weiss & Vollbrecht 2002). Chemically-induced fabric deterioration and structural weaknesses are also often caused by the enlargement of pores (Bell 1993).

2.5. Biological weathering

Along with physical and chemical weathering, stone buildings and monuments can deteriorate due to biological agents, which usually act on stones synergistically with other environmental factors and are involved in a secondary degradation process (Griffin, Indictor & Koestler 1991, Warscheid & Braams 2000, Doehne & Price 2011). The deterioration of stoneworks depends on the bioreceptivity of building materials and their

microbial contamination (Sadat-Shojai & Ershad-Langroudi 2009). It is associated with the establishment of a complex ecosystem from different kinds of plants and micro-organisms contingent on surrounding conditions and the physico-chemical properties of the material (Tomaselli et al. 2000, Warscheid & Braams 2000, Lisci, Monte, & Pacini 2003). As a result of the action of biotic agents ranging from bacteria, algae, fungi, mosses and lichens to higher plants, stones deteriorate and both autotrophic and heterotrophic microorganisms can colonise the stone substrates (Zanardini et al. 2000, Tiano 2002, Hugues, Steiger & Weber 2005). The biodeterioration of stones leads to not only unwanted effects on the visual appearance of historically and culturally important stone buildings and structures, such as noticeable microbial growth, related pigments and discolorations but also to both physical and chemical deteriorations (Griffin, Indictor & Koestler 1991, Karpovich-Tate & Rebrikova 1991, Tomaselli et al. 2000, Warscheid & Braams 2000, Wright 2002, Hugues, Steiger & Weber 2005, Jroundi et al. 2010).

2.6. Role of moisture and water

For most weathering processes, water on and in the stone is considered the most important factor contributing to the susceptibility of stone decay (Winkler 1973, Weber 1985, Proietti et al. 1986, Bell 1993, Rao, Brinker & Ross 1996, Cnudde et al. 2004, Siegesmund, Weiss & Vollbrecht 2002, Hugues, Steiger & Weber 2005, Warke, McKinley, Smith 2006, Beck et al. 2003, D'Arienzo, Scarfato & Incarnato 2008, Török 2010). Due to the hydrophilic nature of stones, the presence of water naturally occurs under thermodynamic equilibrium conditions with environmental humidity (Alessandrini et al. 2000, Tarasov 2001, Webster & May 2006). Water derived from different sources can enter into the porous system in the stones through gravity, osmotic pressure, capillary forces and siphoning (Rao, Brinker & Ross 1996, Bernabeu et al. 2001). Moisture present in the porous stones mostly results from the condensation of rainwater, groundwater and the atmosphere. While the movement of moisture into and within stone can play an important role in weathering, water can also act as a means of transporting contaminants, gases, pollutants and soluble salts into the porous system (Bell 1993, Alessandrini et al. 2000, Tarasov 2001, Striegel et al. 2003, Hugues, Steiger & Weber 2005, Warke, McKinley, Smith 2006). It is associated with moisture-related damage, including frost action, chemical reaction, biological degradation and salt weathering (Cnudde et al. 2004,

Hugues, Steiger & Weber 2005, Benavente et al. 2007).

Figure 2.4. Salt and water damage resulted from a sandstone building (Department of Environment and Climate Change NSW 2008a)

2.7. Anthropogenic influences on weathering

In addition to natural weathering, additional weathering results from man-made causes (Warscheid & Braams 2000). This contributes to the further deterioration of stones as a part of the natural environment. Like biodiversity and the environment, the human role in altering historic, architectural and monument places is important and the changes in surrounding conditions considerably alter the nature and rate of stone decay (Berry 1994, Rao, Brinker & Ross 1996, Salimbeni et al. 2000, Warscheid & Braams 2000, Turkington & Paradise 2005). Such effects are particularly significant in urban areas and many heritage buildings in urban areas are subjected to higher occurrences of anthropogenic pollution (Boyer 1987, Winkler 1987, Alessandrini et al. 2000, Ghedini et al. 2000, Wright 2002). As a result of various human activities, such as human contact and the previous attempts at conservation treatment of historic sites, mechanical damage to the stone of buildings and structures may occur (Sofianopoulos 1951, Pope, Meierding & Paradise 2002, Sadat-Shojai & Ershad-Langroudi 2009, Doehne & Price 2011).

Of the anthropogenic environmental factors, atmospheric pollution in urban areas is one of the most influential on the overall deterioration of exposed cultural heritage (Thomson & White 1974, Bell 1993, Işik-Yürüksoy, Kiş & Güven 1998, Ghedini et al. 2000, Striegel et al. 2003) and has a direct influence on stone-degradation mechanisms (Ghedini et al.

2000). Human influences—including population growth and industrial, agricultural and domestic activities—have led to changes in the atmospheric composition of urban areas and to higher concentrations of inorganic and organic pollutants in the form of gases, aerosols, or particles and their deposition on the exposed stone materials (Winkler 1987, Warscheid & Braams 2000, Salimbeni et al. 2000, Striegel et al. 2003, Webster & May 2006). The released airborne pollutants can involve complex interactions, depending on the physical, chemical and photochemical processes that occur during their residence (Ghedini et al. 2000, Striegel et al. 2003). Atmospheric gases (e.g., carbon dioxide, nitrogen oxides and sulfur oxides) are combined with moisture or oxygen in the environment to form acidic solutions, including sulfuric and nitric acids, which can act as a deteriorating factor in a porous surface of calcium carbonate, or the clay-binding medium of many sedimentary stones (Weber 1985, Saleh et al. 1992, Piacenti 1994, Alessandrini et al. 2000, Tarasov 2001, Sabbioni 2003, Wolff 2004, Webster & May 2006, Sadat-Shojai & Ershad-Langroudi 2009, Doehne & Price 2011). Combined with other pollution agents, the stone damage takes place due to acid deposition on the surface of stone materials that occurs through rain, other forms of precipitation, moisture through wet or dry deposition, or direct absorption of the atmospheric gases into capillary pore waters (Bell 1993, Işik-Yürüksoy et al. 1998, Sabbioni 2003, Striegel et al. 2003). The impact of air pollution on stone destruction is very complex, and its synergic effects cause a higher level of susceptibility to other weathering processes, including biodegradation and salt weathering (Zanardini et al 2000, Wright 2002, Kanellopoulou & Koutsoukos 2003, Striegel et al. 2003, Sadat-Shojai & Ershad-Langroudi 2009, Doehne & Price 2011).

Although sandstone is resistant to acid attack due to the high stability of silica to chemical weathering, acidic solutions such as acid rain may gradually dissolve the clay-based cementing medium of many sedimentary stones through hydrolysis (Blake 1967, Weaver & Pollard 1973). Even though chemical dissolution due to acid pollution affects sandstone less, acids produced from different sources can cause the salt weathering of sandstone owing to considerable amounts of salts (e.g., nitrates and sulfates) generated by the reaction of acids with building materials and the atmosphere (Wright 2002, Sabbioni 2003). Moreover, siderite present in Sydney sandstone is susceptible to acid attack. What is more, the deteriorating effect of acidic pollutants on calcareous stones and carbonate-cemented sandstones is more severe, because the chemical dissolution of $CaCO_3$ is

accelerated in the presence of acid pollutants (Kanellopoulou & Koutsoukos 2003, Rodriguez-Navarro et al. 2003, Sabbioni 2003, Bugani et al. 2007). Sulfur dioxide is particularly prone to accelerating weathering as one of the major pollution agents, especially for calcium carbonate or the carbonate-cemented sandstones (Bell 1993, Tarasov 2001, Sabbioni 2003, Striegel et al. 2003). On stone surfaces that are exposed to the action of sulfur dioxide, the deposited pollutant agents interact with the stone to form gypsum, which makes the stonework more susceptible to further deterioration (Fassina 1995, Salimbeni et al. 2000, Striegel et al. 2003). The process produces the more water soluble gypsum than the stone and results in permanent and unrecoverable loss of the soiled zone is washed away as a consequent of rains (Striegel et al. 2003).

Despite the reduction in pollution in many urban areas in recent times and, in particular, the reduced sulfur dioxide level in many urban areas, there is not sufficient evidence to support a direct relationship between sulfur dioxide levels and the rate of stone decay (Cooke 1989, Doehne & Price 2011). However, the effects of air pollution certainly represent a deterioration factor to stones of historic buildings and monuments in many industrialized areas (Giavarini et al. 2007, Doehne & Price 2011). Additionally, focus has shifted recently to carbon dioxide level, which had been treated as a minor factor in the process of stone decay, but has a significant impact on climate change (Doehne & Price 2011). In consequence of climate change and global warming, a variety of environmental conditions can be considerably modified and the impacts of the alterations in temperature, rainfall, air composition and climate fluctuations, such as floods, droughts and humidity cycles, can be significant on deterioration processes (Doehne & Price 2011).

2.8. Weathering of historic building Sydney sandstones

The sandstones used in Sydney heritage sites are deteriorated due to weathering actions in combination with intrinsic characteristics of Sydney sandstones and environmental factors in Sydney (Ip et al. 2004, Ip et al. 2011a). Located in the most populous city in Australia, the built environment in Sydney and its monuments are associated with the unfavourable consequences of anthropogenic factors that have led to the intensified deterioration of these sites (Ip et al. 2005a). As they are major international tourist destinations, it is no surprise that human contact has had an impact on these heritage sites.

The major pollutants in Sydney include particles and gases such as nitrogen dioxide, carbon monoxide and sulfur dioxide; and the human-related elements that produce such pollutants include car exhaust emissions, industries and power plants (Ip et al. 2005a, NSW Government: Office of Environment and Heritage 2016).

Figure 2.5. Deterioration of heritage sandstones taken from St Mary Cathedral in Sydney showing cracking, discoloration, detachment, biological colonization and granular disintegration (Ip 2007)

In response to rapid changes in the surrounding conditions, particularly of urban areas in Sydney, the sandstone buildings have undergone rapid deterioration and major restoration work is often required to preserve many old buildings in Sydney due to their deteriorations (Heiman 1981a, Heiman 1981b, Ip et al. 2003, Ip et al. 2004, Ip et al. 2005a, Ip et al. 2005b, Ip et al. 2008). The heritage sandstone buildings showed a great variety of deterioration forms at the microscopic levels (Figure 2.5). The sandstones, under different weathering actions, are reduced in strength, cohesion and mechanical removal of the stone surface and the sandstones becomes more brittle and crumbles as a result of

weathering processes (Ip et al. 2003, Ip et al. 2008a, Dragovich & Egan 2011, Ip et al. 2011a). The weathering actions produced a variety of weathering forms and results in discoloration, disintegration, flaking, oxidation, exfoliation, erosion, biodeterioration, structural deterioration of natural clay binders and porosity changes (Ip et al, 2003, Ip et al. 2005a). Along with the effects of pollutants, heritage buildings and monuments also face aggressive climatic conditions (Ip et al. 2005a). Generally, Sydney is known for its dry climate and high levels of solar ultraviolet radiation (Ip et al. 2005a). High summer temperatures (up to 45.8°C as recorded in 2013) and high-extreme UV index levels during summer can also have a substantial impact on the heritage buildings and monuments (Ip et al. 2005a, Australian Government Bureau of Meteorology 2016a, Australian Radiation Protection and Nuclear Safety Agency 2016). In addition, Sydney recorded a significant amount of rainfall with a mean annual rainfall of 1215 mm (Australian Government: Bureau of Meteorology 2010b).

Moreover, many heritage buildings are situated in coastal areas and sea salt spray is a source of aerosol particles (Heiman 1981a, Ip et al. 2005a, Dragovich and Egan 2011). Saltwater derived from seawater is undoubtedly one of the major causes of stone deterioration in Sydney (Flannery 2002). The penetration of saltwater in the stone's pores occurs at high tide, and the surface grains are destroyed by expansive pressure due to evaporated salt content at low tide (Flannery 2002). Compositional analysis of the rainwater in Sydney revealed aerosols across the shore can be carried via east and south-east winds that can, consequently, deposit a large quantity of sea salt on buildings (Heiman 1981a). As a result of the fast evaporation of water from the stones under hot and dry climates, salt penetrated into the sandstones are recrystallized and destruction of the structure and integrity of the sandstones results in the formation of micro-cracks between sand grains and clay binder (Ip et al. 2005a).

The estimated continuous population growth in Sydney suggests an increase in human activities that can negatively impact many heritage buildings (Australian Bureau of Statistics 2016). With continuous climate changes caused by global warming, the surrounding conditions and their effects on weathering are likely to intensify the current human-induced effects. Though it is predicted that there will be warmer and dryer days (Department of Environment and Climate Change NSW 2008b), changes in rainfall

patterns are probable with increased summer rainfall and decreased winter rainfall likely in the Sydney region. The predicted warmer and dryer conditions as well as the input of salt from sea salt spray and other contaminants are likely to result in the faster evaporation of moisture that will contribute to the formation of micro-cracks due to the crystallization of salt (Ip 2007). Additionally, ocean acidification is likely with a rise in sea level (Australian Government Department of the Environment and Energy n.d). Increased intense weather conditions, such as severe rainfall and strong winds, will likely have an impact on Sydney's heritage stone objects.

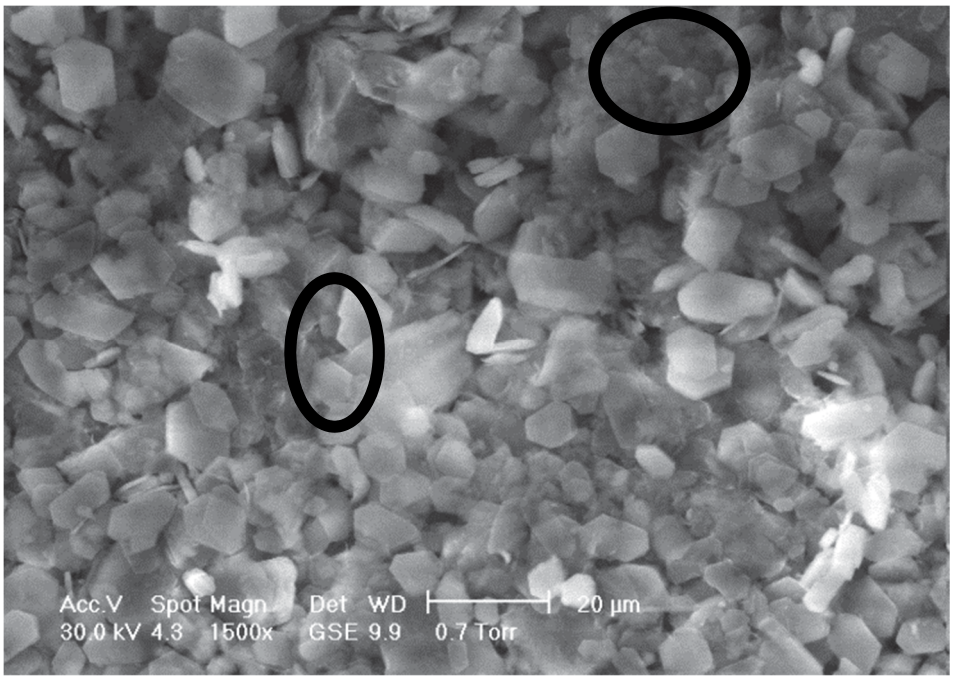

Figure 2.6. Electron micrograph presenting structural changes in weathered natural cementing clay from St Mary's Cathedral such as smaller and more irregular shapes of platelets and fused parties in circled areas (Ip 2007)

In the process of establishing a suitable conservation strategy for Sydney sandstone heritage buildings, it is essential to identify the causes and processes of sandstone deterioration. Ip et al. investigated the clay binder present in the unweathered and weathered Sydney yellow block sandstones using various analytical techniques (Figure 2.6) (Ip et al. 2003, Ip et al. 2004, Ip et al. 2005a, Ip et al. 2005b, Ip et al. 2007, Ip et al. 2008a, Ip et al. 2008b, Ip et al. 2011a). Their investigations showed the progressive structural alteration of weathered cementing materials associated with increased concentrations of iron and other impurities. In particular, the significant results of their

investigations of the cementing materials from different Sydney sandstone samples revealed that the iron concentrations of the weathered samples relative to unweathered samples were higher in both structural and non-structural iron components. Results suggested that the weathering process of the sandstones was related to the structural changes associated with the increased iron concentrations (Ip, Stuart & Ray 2003, Ip et al. 2005a, Ip et al. 2005b, Ip 2007, Ip et al. 2008a, Ip et al. 2008b). The explanation given by Ip et al. for increased iron concentration of weathered cementing clay was that iron supplied from the weathered sandstone was substituted into the aluminosilicate crystal structure of clay binder (Ip et al. 2003, Ip et al. 2004, Ip et al. 2005a, Ip et al. 2005b, Ip et al. 2007, Ip et al. 2008a, Ip et al. 2008b, Ip et al. 2011a).

Their studies indicated the presence of iron impurities such as iron oxyhydroxide, iron oxide, and high concentrations of other amorphous iron materials like goethite and ferrihydrite in the cementing materials (Ip et al. 2003, Ip et al. 2004, Ip et al. 2005a, Ip et al. 2008b). The non-structural iron impurities originated from iron-rich minerals such as iron carbonate, iron sulfate and pyrite in the sandstone as well as amorphous goethite and a trace iron impurity in groundwater (Ip et al. 2004, Ip et al. 2005b, Ip et al. 2008a, Ip et al. 2011a). The oxidization and weathering of these iron materials from the sandstone and surrounding conditions produce non-structural iron impurities such as iron oxyhydroxide and oxides that are redeposited into the porous sandstone surfaces (Ip et al. 2004). The ferrous irons in the sandstone, due to the low concentration of dissolved oxygen, are oxidized in the ferric ions upon exposure of quarried sandstone to air and cause darkening of the stone and colouring of the clay binder at the surface (Franklin 2000, McNally and Franklin 2000, Ip et al. 2004). The non-structural iron impurities from the sandstone cause discolouration of weathered sandstone and accelerate the stone deterioration by applying additional stress onto the weathered clay structure and producing a sufficient amount of iron that can be used for iron substitution into the kaolinite crystal structure (Ip et al. 2004).

In addition to iron impurities, the work of Ip et al. showed the presence of other minerals and impurities in minor concentrations arising from sandstones and the surrounding environment such as metal oxides, quartz, titanium oxide, lencoxene, anatase, by-products of burning oil in cars and other clay minerals (Ip et al. 2003, Ip et al. 2004, Ip et

al. 2008a, Ip et al. 2008b). Although structural alteration of kaolinite present in the weathered cementing clay was reported for different sandstone quarries, their studies also revealed origin-dependent stone deterioration due to different concentrations of clay mineral and impurities. Of the studied sandstones quarried from Pyrmont, Bondi and Maroubra regions, significant deviations showed higher concentrations of iron impurities and carbonate minerals, larger porosity, less ordered structure and lower concentration of kaolinite in the Bondi sandstone compared to the other sandstones. The Bondi sandstones are vulnerable to weathering impacts of the acidic environment in Sydney; therefore, they are more susceptible to stone deterioration (Franklin 2000, Ip et al. 2003).

While visible sandstone deterioration observed in Sydney heritage buildings has been reported, the external sandstone heritage buildings appear in relatively strong and sound condition to the naked eye and overall hardness and integrity of examined weathered sandstones has been sustained (Ip et al. 2004, Ip et al. 2005a, Ip et al. 2008). Although the overall crystal structure and integrity of the binding clay was unaffected, the altered porosity of the weathered sandstones induced enlargement and reduction of the pore sizes, indicating the disintegration of cementing clay (Ip et al. 2005a). The large pore population was considered to be partly formed by the destruction of the cementing clay structure, small and medium pores due to lost inter-boundaries between adjacent pores and small pores could be produced by the redistributed small mineral particles or degradation products (Ip et al. 2005b). The sandstone porosity could also be increased by the dissolution and leaching of minerals including carbonates and titanium dioxide due to acidic groundwater and rainwater in Sydney. Porosity changes illustrate the susceptibility of the weathered stones to the process of deterioration (Ip et al. 2003, Ip et al. 2005a).

Provided that sand grains are the main constituent of sandstone and are a chemically stable and durable material, the results presented by Ip at el. demonstrated that the structurally destabilized natural clay binder was identified as a key weathering mechanism of Sydney sandstone deterioration (Ip et al. 2003). It was argued that while partial and total replacement of decayed stones has been effective in some restoration work, the use of a suitable consolidant can be a means of preserving the original sandstones and slowing the degradation of Sydney heritage sandstones (Ip et al. 2003, Ip et al. 2004, Ip et al. 2005a, Ip et al. 2005b, Ip et al. 2007, Ip et al. 2008a, Ip et al. 2008b).

With a view to designing a suitable consolidant for Sydney sandstone, their work presented the need for the development of clay-based polymeric materials and suggested modification of clay with polymers as an appropriate approach to producing such consolidating materials that should be able to bind the loose particles resulting from the deteriorated clay binder, to hold similar characteristics to natural cementing clay in Sydney sandstones and to remain stable in the Sydney environment (Ip et al. 2003, Ip et al. 2004, Ip et al.2005a, Ip et al. 2005b, Ip et al. 2007). The research approach taken by this work was the development of suitable consolidation treatment underpinned with a goal to support the preservation of the original sandstones.

CHAPTER 3. STONE CONSOLIDATING MATERIALS

3.1. Introduction

A huge range of conservation products, ranging from natural substances, inorganic and organic materials, to combined materials, have long been applied to weathered stone objects in order to prevent their further deterioration and to retard their decay (Wilson 1985, Boyer 1987, Moropoulou et al. 2003b, Skoulikidis, Vassiliou & Tsakona 2005, Cnudde et al. 2006, Jimenez-Lopez et al. 2008, Stück et al. 2008, Doehne and Price 2011). This chapter attempts to give a critical literature review of the published work on stone consolidation practices and to show formulation, performance and challenges encountered by researchers developing materials for stone consolidation work. Related published literature was reviewed to establish stone consolidation techniques as the appropriate conservation strategy for this thesis. The first section focuses on the review of stone consolidants formed from a variety of materials. This review is used to identify the main groups of stone consolidants based on the chemical systems to which they can be associated. Citations were reviewed to study the chemical aspects of the stone consolidants, evaluate their consolidation efficiencies, identify their advantages and drawbacks and estimate their consolidation performance on Sydney sandstone. Consolidating materials are viewed in such a way as to address the issues according to the performance criteria established for stone consolidation in the literature. Ideal materials associated with the stone consolidation application are considered from theoretical and practical viewpoints in the following sections.

3.2. Stone consolidation

3.2.1. Traditional consolidation treatments

Dating as far back as Roman times, the importance of the protection and consolidation of stonework for long-term preservation has been recognized and conservation activities have been carried out to preserve historic stones (Weber 1985, Wheeler et al. 1992, Siegesmund, Weiss & Vollbrecht 2002, Webster and May 2006). Preservation treatments

in the early times were limited to natural substances, such as oils, waxes, glue from vegetable or animal sources and natural resins (Werner 1981, Weber 1985, Boyer 1987, Liu et al. 2006). These substances were mainly used to protect stones from direct contact with water and the sun and as adhesive surface particles for the deteriorated matrix (Wheeler et al. 1992, Siegesmund, Weiss & Vollbrecht 2002, Litomyšl 2010). The evolution of the chemical industry during 19th century resulted in the development of synthetic resins and inorganic consolidating materials (Weber 1985, Litomyšl 2010). However, very often such early treatments resulted in problems, including discoloration and dust absorption and were found to accelerate the weathering processes, due to a lack of proper understanding of the stones' characteristics and the causes and mechanisms of weathering processes (Weber 1985, Liu et al. 2006).

3.2.2. Inorganic consolidants

By the early 20th century, a range of inorganic-based consolidants had been produced and tested from inorganic materials such as alkaline earth hydroxides, alkali silicates, fluorosilicate and aluminates (Domaslowski 1969, Boyer 1987, Rodrigues 2001, Doehne and Price 2011). In these inorganic consolidating systems, efforts were made to improve stone cohesion and to provide a binding agent that was chemically compatible with the decayed stones (National Research Council (U.S.) 1982, Rodrigues 2001). Inorganic molecules that were precipitated in the pores of decayed stones bound the loose stone particles together (Rodrigues 2001). Accordingly, calcareous stones were treated with calcium hydroxide or barium hydroxide, which is converted to calcium or barium carbonates through carbonation (Eq. 1-2) (Fidler 1995, Hansen et al. 2003, Webster and May 2006, Karatasios et al. 2009, López-Arce et al. 2010).

$$Ca(OH)_2 + CO_2 \rightarrow CaCO_3 + H_2O \quad (1)$$

$$Ba(OH)_2 + CO_2 \rightarrow BaCO_3 + H_2O \quad (2)$$

$$Ba(OH)_2 + CaCO_3 \rightarrow BaCO_3 + Ca(OH)_2 \quad (3)$$

$$Ba(OH)_2 + CaSO_4 \rightarrow BaSO_4 + Ca(OH)_2 \quad (4)$$

Calcium hydroxide reacts with carbon dioxide to form calcium carbonate, which can bind the loose particles of the deteriorated carbonate stone (Eq. 1) (National Research Council

(U.S.). 1982, Webster and May 2006, Karatasios et al. 2009). Although barium hydroxide and calcium hydroxide have several similar chemical properties, barium carbonate offers certain advantages (Doehne and Price 2011). Barium carbonate converted from barium hydroxide with carbon dioxide is more resistant than calcium carbonate to acid rain and barium hydroxide can convert calcium carbonate to calcium hydroxide (Eq. 2-3) (Hansen et al. 2003, Doehne and Price 2011). In addition, barium hydroxide can react with calcium sulfate to convert calcium sulfate to barium sulfate (Eq. 4), which is less soluble in water and can lessen harm done due to the deleterious effects such as salt and osmotic pressure (Lewin & Baer 1974, Hansen et al. 2003, Doehne and Price 2011). On the other hand, sandstones were treated with siliceous consolidants (e.g., alkali silicates and fluorosilicates), which can be converted to silica gel to serve as consolidants in the stone (Eq. 5-6) (National Research Council (U.S.). 1982, Zendri et al. 2007, Siegesmund & Snethlage 2010).

$$M_2SiO_3 + CO_2 + nH_2O \rightarrow SiO_2 \cdot nH_2O + M_2CO_3 \quad (5)$$

$$2CaCO_3 + NSiF_6 \rightarrow 2CaF_2 + NF_2 + SiO_2 + 2CO_2 \quad (6)$$

$$M1 = Na^+, K^+, Li^+ \quad N = Mg^{2+}, Zn^{2+}$$

Alkali silicates, known as waterglass, react with carbon dioxide to form amorphous silica gel, after which silanols are condensed to Si-O-Si bonds and xerogel can be formed due to the evaporation of solvent (Weber 1985, Zendri et al. 2007, Siegesmund & Snethlage 2010). The waterglass products used for stone consolidation are sodium, potassium or lithium waterglass. Lithium waterglass has received recent attention due to the lower solubility of lithium carbonate compared with sodium or potassium carbonates (Siegesmund & Snethlage 2010). Likewise, the formation of silica gel can be obtained when fluorosilicate, commonly magnesium- or zinc-based fluorosilicates, reacts with the calcite for the consolidation of limestone or calcareous sandstone (Siegesmund & Snethlage 2010). The literature also contains the formation of calcium oxalate through the hydroxyl radical induced oxidation of organic compounds (Cariati et al. 2000). Research in inorganic consolidants has been conducted with calcium hydroxide nanoparticles and colloidal silica dispersions (Moropoulou et al. 2003a, Moropoulou et al. 2003b, Dei & Salvadori 2007, López-Arce et al. 2010, Zornoza-Indart et al. 2016b). However, the treatment with small silica dispersions has been reported to result in

precipitation and coagulation and the final product also depends on the relative humidity of consolidation environment (Moropoulou et al. 2003b, Zornoza-Indart et al. 2016a, Zornoza-Indart et al. 2016b). Initially, the inorganic consolidants were considered effective and have been used extensively in stone conservation (Liu et al. 2006). Despite their apparently high potential, due to a chemical compatibility between the bonding agent and the decayed stone and the interaction between the bonding agent and the stone, inorganic consolidants have been found to be less effective than expected and their use has been reduced (Lewin & Baer 1974, National Research Council (U.S.) 1982, Fidler 1995, Rodrigues 2001, Moropoulou et al. 2003b, Skoulikidis, Vassiliou & Tsakona 2005, Dei & Salvadori 2007, Zendri et al. 2007, Karatasios et al. 2009). They are often known to remain on the surface layer due to their low capacity for penetration (National Research Council (U.S.) 1982, Price, Ross & White 1988). Moreover, they lack adequate cohesive properties and instead form an unfavorable crust, salts and by-products (National Research Council (U.S.) 1982, Wheeler et al. 1992, Moropoulou et al. 2003b, Cnudde et al. 2006, Liu et al. 2006, Zendri et al. 2007, Siegesmund & Snethlage 2010).

3.2.3. Organic-based treatments

A wide range of organic-based materials—mostly synthetic organic polymers—have been increasingly found to be useful in conservation due to major advances in polymer chemistry since the 19th century (Werner 1981). Traditional natural resins were replaced by synthetic polymers in the 20th century; a change which is attributable to their physical and chemical properties (e.g., flexibility, transparency and good adhesion) that were not found in the natural materials (Werner 1981, Wheeler et al. 1992, Cocca et al. 2004, Cnudde et al. 2006, Osete-Cortina & Doménech-Carbó 2006, Litomyšl 2010). Stonework has commonly been consolidated with these synthetic polymers (Vicini et al. 2004, Cocca et al. 2004, Carretti & Dei 2004, Favaro et al. 2006, Liu et al. 2006, Liu & Zhang 2007, D'Arienzo et al. 2008, Domingo et al. 2008, Sadat-Shojai & Ershad-Langroudi 2009). The major synthetic polymers employed for stone consolidation are acrylics, vinylics, polyesters, epoxies, silicone-based polymers, polyurethanes and polyureas (Kotlík, Justa & Zelinger 1983, Giorgi et al. 1986, Tabasso 1995, Rodrigues 2001, Striegel et al. 2003, Carretti & Dei 2004, Cocca et al. 2005, Cnudde et al. 2006, Liu & Zhang 2007, Pinto & Rodrigues 2008, Vacchiano et al. 2008, Licchelli et al. 2011).

3.2.3.1. Epoxies

Epoxies have been applied as stone consolidants for limestone, marble and sandstone (National Research Council (U.S.) 1982, Ginell & Coffman 1998). Most of the commercial epoxy resins are produced with a copolymer of epichlorohydrin and bisphenol-A (Figure 3.1) and the epoxy resins used for stone conservation are dominated by these (National Research Council (U.S.) 1982, Kotlík, Justa & Zelinger 1983, Harper & Petrie 2003, Petrie 2006, Siegesmund & Snethlage 2010). The cross-linking reaction of the epoxy resins with a curing agent at ambient temperature form cross-linked polymers (National Research Council (U.S.) 1982, Kotlík, Justa & Zelinger 1983, Saleh et al. 1992, Siegesmund & Snethlage 2010). The common curing agents are primary, secondary and tertiary amines (National Research Council (U.S.) 1982, Siegesmund & Snethlage 2010). Depending on the curing agents used, the properties of the cross-linked polymers vary because of the different types of cross-linking bonds produced (Siegesmund & Snethlage 2010). The formed epoxies are strong, clear and colourless and they are chemically resistant materials (National Research Council (U.S.) 1982). They also possess an excellent adhesive strength for most materials and can be used to bond broken pieces together (National Research Council (U.S.) 1982, Kotlík, Justa & Zelinger 1983, Ginell & Coffman 1998, Siegesmund & Snethlage 2010). However, the viscosity of the epoxy resins is known to be high and organic solvents are required to produce a low viscosity consolidant for penetration as high viscosity reduces their penetration into stone pores (National Research Council (U.S.) 1982, Kotlík, Justa & Zelinger 1983, Bell 1993, Doehne & Price 2011,). Furthermore, they have a tendency to degrade and to chalk with exposure to sunlight, which can lead to further damage to the stone (National Research Council (U.S.) 1982, Kotlík, Justa & Zelinger 1983, Wheeler et al. 1992). Although the application of epoxies as stone consolidants results in considerable unsuccessful outcomes, there have been cases in which the stone consolidation was successfully implemented and further research efforts have been undertaken, such as with

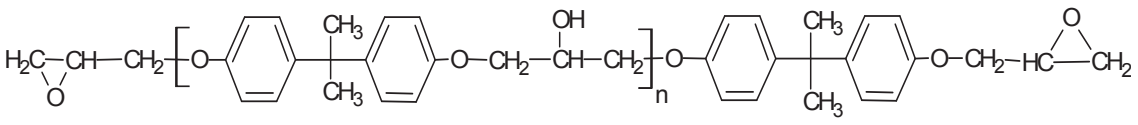

Figure 3.1. Diglycidyl ethers of bisphenol A (Harper & Petrie 2003)

the development of waterborne epoxy emulsions and epoxy-silica materials (Moncrieff & Hempel 1977, Cardiano et al. 2005, Doehne and Price 2011).

3.2.3.2. Acrylic polymers

Within the realm of organic-based synthetic polymers, acrylic polymers formed from two classes of monomers, the acrylates and the methacrylates, have been used extensively in protective and consolidating applications (Tabasso 1995, Melo et al. 1999, Mazzola et al. 2003, Cocca et al. 2004). Acrylate and methacrylate polymers have fairly hydrophobic, good adhesive and transparent coloured features that are functional for their applications as consolidating and protective products (Tabasso 1995, Mazzola et al. 2003).

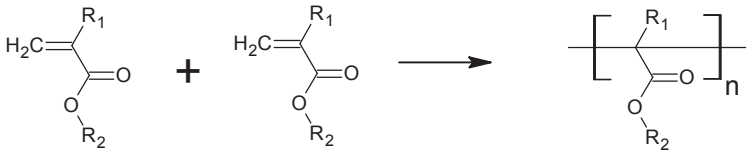

EA R_1= H $R_2 = C_2H_5$

MA R_1= H $R_2 = CH_3$

MMA R_1= CH_3 $R_2 = CH_3$

BMA R_1= CH_3 $R_2 = C_4H_9$

EMA R_1= CH_3 $R_2 = C_2H_5$

Figure 3.2. Addition polymerisation of acrylate monomers

Similar to epoxide consolidation, acrylic-based consolidants may form a polymeric network and can provide binding properties to the stone (Wheeler et al. 1992). Homopolymers and copolymers have been produced through addition polymerisation from various acrylic monomers, including ethylacrylate (EA), methylacrylate (MA), methyl methacrylate (MMA), butyl methacrylate (BMA) and ethyl methacrylate (EMA) (Munnikendam 1967, Munnikendam 1973, National Research Council (U.S.) 1982, Tabasso 1995, Carretti, Dei & Baglioni 2003, Mazzola et al. 2003, Sadat-Shojai & Ershad-Langroudi 2009) (Figure 3.2). Paraloid B72, which is a copolymer of EMA and

MA (Giorgi et al. 1986), has been widely applied in the field of conservation (Witte, Huget & Broeck 1977, Tabasso 1995, Rodrigues 2001, Casadio & Toniolo 2004, Vicini et al. 2005, Doehne and Price 2011).

Acrylic resins have been applied as preformed polymers or monomers that are introduced into the stone pores and subsequently polymerise through free-radical or frontal polymerisation inside (Bell 1993, Işik-Yürüksoy et al. 1998, Vicini et al. 2001, Vicini et al. 2002). The in situ polymerisation of monomers has been considered an alternative method to the use of preformed polymers to improve diffusion in the stones (Munnikendam 1967, Munnikendam 1973, Proietti et al. 1986, Bell 1993, Tabasso 1995, Işik-Yürüksoy et al. 1998, Bossert, Ožbolt & Grassegger 2004, Vicini et al. 2005, Vicini et al. 2006). In addition to their low penetration of polymers and the colour changes in aged polymers, synthetic polymers used in stone consolidation present various unwanted effects, largely due to incompatibility and instability in the surrounding conditions (Giorgi et al. 1986, Saleh et al. 1992, Bell 1993, Rodrigues 2001, Rodrigues, Pinto & da Costa 2002, Moropoulou et al. 2003b, Vicini et al. 2005, Liu et al. 2006, Cnudde et al. 2006, Proietti et al. 2006, Stuart 2007, Liu & Zhang 2007, Domingo et al. 2008, Vacchiano et al. 2008, Baglioni, Giorgi & Dei 2009, Sadat-Shojai & Ershad-Langroudi 2009, Doehne and Price 2011). Upon exposure to sunlight, the bond breakage of the side groups of the polymers can result in the generation of small fragments and a cross-linked structure (Glikman et al. 1986, Wheeler et al. 1992, Tabasso 1995, Mazzola et al. 2003). Although polymeric products have played an important role in stone consolidation, their use has declined and their properties apparently need improvement (Vicini et al. 2004, Vicini et al. 2005, Liu et al. 2006, Favaro et al. 2006, Liu & Zhang 2007, Sadat-Shojai & Ershad-Langroudi 2009).

3.2.4. Organosilicon compounds

Another group of consolidating agents commonly used is organosilicon compounds (Domaslowski 1969, Salazar-Hernández et al. 2009). These compounds can offer the Si-O groups and alkyl groups, which provide a chemical bond to the surface of stones and water protection, respectively (Berry 1994, Brus & Kotlík 1996a). The consolidants produced from siloxanes and silanes (e.g., alkoxysilanes, alkyltrialkoxysilanes and

dialkyldialkoxysilanes) are used in stone consolidation and are applied in various forms (e.g., monomers, oligomers and polymers) (Brus & Kotlík 1996b, Iñigo et al. 1997, Miliani, Velo-Simpson & Scherer 2007, Salazar-Hernández et al. 2010).

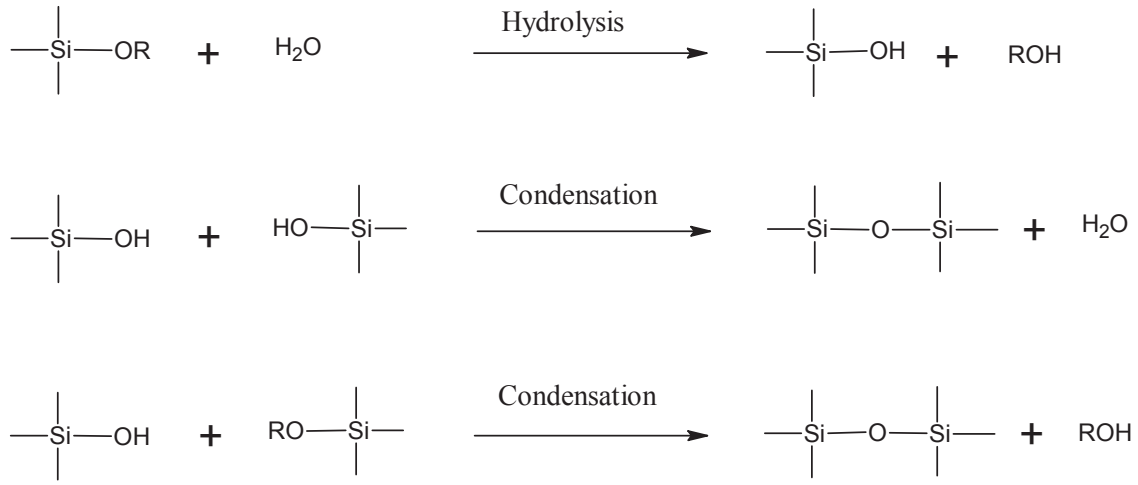

Figure 3.3. Hydrolysis and condensation of alkoxysilanes (Sadat-Shojai & Ershad-Langroudi 2009)

In recent decades, silanes have been the most commonly used and tri- or tetra-functional derivatives have been employed in conservation (Moncrieff 1976, Horie 2010, Doehne & Price 2011). Tetraethoxysilane and methyltrimethoxysilane, particularly tetraethoxysilane, which is also known as ethyl silicate, tetraethyl silicate, tetraethoxysilane and silicic acid esters are the major silane-based consolidants among those used as stone consolidants (Weber 1985, Rodrigues 2001, Oliver 2002, Mosquera, Pozo & Esquivias 2003, Mosquera et al. 2005, Park & Shin 2009, Horie 2010, Doehne & Price 2011, Zornoza-Indart et al. 2016b). The alkoxysilanes can undergo the hydrolysis reaction in the presence of water to form alkoxysilanols and alcohol and the condensation polymerisation of formed alkoxysilanols with either alkoxysilanols or alkoxysilanes produces polysiloxane/silicone polymer as a result of the elimination of water or alcohol (Figure 3.3) (Wheeler et al. 1992, Witucki 1993, Wheeler 2005, Doehne & Price 2011, Sadat-Shojai & Ershad-Langroudi 2009, Horie 2010, Zornoza-Indart et al. 2016b).

In the presence of water entering from the atmosphere, the applied monomeric silanes are polymerised in situ in the porous stone and generate a silicon polymer that is chemically

similar to silicate minerals (Bell 1993, Rodrigues 2001, Mosquera et al. 2002, Zárraga et al. 2010, Gupta 2011). With their silicate-based composition, they are very compatible with stone; sandstones are commonly consolidated with silane-based products (Bell 1993, Brus & Kotlík 1996b, Rodrigues 2001, Mosquera et al. 2002, Zárraga, Alvarez-Gasca & Cervantes 2002, Mosquera, Pozo & Esquivias 2003, Moropoulou et al. 2003b, Stück et al. 2008, Litomyšl 2010, Gupta 2011). The formed silicon polymers can covalently bond to the Si-O groups of the sandstones and form silicate linkages to quartz (Wheeler 2005, Doehne and Price 2011).

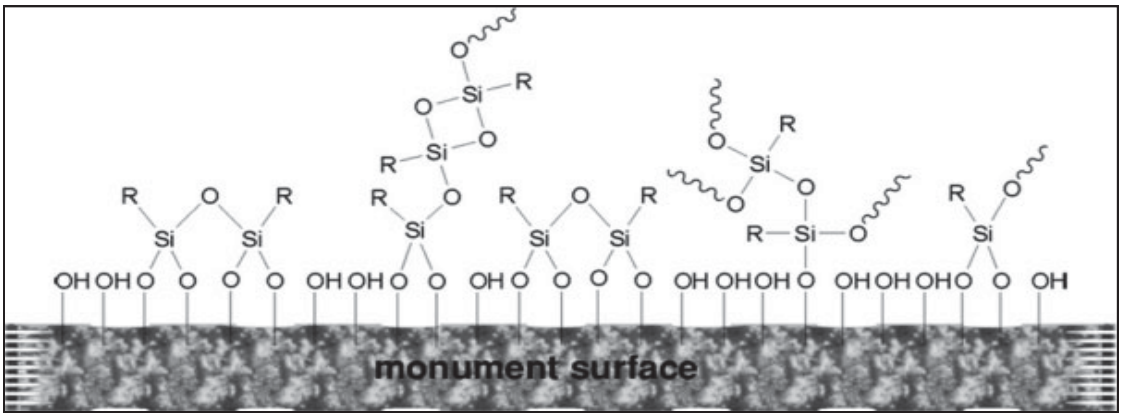

Figure 3.4. Schematic diagram of silicon polymer on the monument surface (Sadat-Shojai & Ershad-Langroudi 2009)

As a result of further hydrolysis and condensation reactions, they can be transformed into a silicon network during an in situ sol-gel process that depends on many factors including temperature, pH, reactant concentration and solvent (Figure 3.4) (Ni, Skaja & Soucek 2000, Sadat-Shojai & Ershad-Langroudi 2009, Doehne and Price 2011). They are also known as low-viscous solutions, which facilitate deep penetration into the stones and are able to produce Si-O-Si linkages of alkoxysilane polymers that are stable under UV light unlike the C-C and C-O bonding of organic polymers (Munnikendam 1973, Moncrieff 1976, Heiman 1981a, Mosquera et al. 1986, Wheeler et al. 1992, Bell 1993, Brus & Kotlík 1996b, Mosquera et al. 2002, Oliver 2002, Mosquera et al. 2005, Son et al. 2009, Salazar-Hernández et al. 2010, Zárraga et al. 2010). After the consolidation treatment with these compounds, the stones can remain permeable allowing flow of water vapor (Heiman 1981a). Despite these advantages and their widespread use in stone conservation, they still have some shortcomings, such as crack formation and colour changes and their use

has been confined due to these limitations (Mosquera et al. 1986, Brus & Kotlík 1996a, Mosquera et al. 2005, Cnudde et al. 2006, Miliani, Velo-Simpson & Scherer 2007, Kim et al. 2009, Park & Shin 2009, Salazar-Hernández et al. 2010, Zárraga et al. 2010, Zornoza-Indart et al. 2016b).

3.2.5. Combined products

With the known limitations of each type of consolidating product, efforts have been made to produce consolidants by combining different materials in order to improve their consolidating performance (Munnikendam 1973, Weber 1985, Boyer 1987, Doehne & Price 2011). To improve problems in consolidating performance (e.g., the weak binding capacity of organosilicon compounds), silicon-organic mixtures have been made by blending various organosilicon compounds with acrylic or epoxy resins to combine their beneficial characteristics (e.g., the good adhesive properties of acrylics or epoxies, the good penetration ability of organosilicon compounds) (Tabasso 1995, Brus & Kotlík 1996b, García-Talegon et al. 1998, Moropoulou et al. 2003a, Moropoulou et al. 2003b, Tsakalof et al. 2007, Favaro et al. 2007, Doehne and Price 2011, Pinna, Salvadori & Porcinai 2011). A particular acrylic-silicon mixture, commonly known as Bologna Cocktail (BC), consists of Paraloid B72 blended with DriFilm 104 (partially pre-polymerised methylsiloxane) and it has been widely used in some European countries, especially Italy (Charola, Tucci & Koestler 1986, Selwitz 1995, Favaro et al. 2007, Grassi et al. 2009). There have been some reports on its good performance in terms of penetration depth and stability under photo-oxidative/acidic conditions (Favaro et al. 2007). However, an unsuccessful treatment of BC demonstrated the need to carefully evaluate the conservation problem before applying this product (Tabasso 1995, Doehne and Price 2011). Additionally, fluorine has been introduced into the polymers in the conservation of heritage stone materials in light of its chemical properties, thermal and photochemical stability due to its more stable C-F bonds and hydrophobicity (Chiavarini et al. 1993, Chiantore et al. 2000, Alessandrini et al. 2000, Tuminello, Bracci & Piacenti 2002, Mazzola et al. 2003, Vicini et al. 2005, Sadat-Shojai & Ershad-Langroudi 2009, Licchelli et al. 2011). The fluorinated materials studied in stone conservation included fluorinated acrylics, organosiloxane and polyether (Domaslowski 1969, Chiavarini et al. 1993, Tuminello, Bracci & Piacenti 2002, Tsakalof et al. 2007). Research conducted on

fluorinated polyacrylates for use as stone consolidants involved polymerising 2,2,2-trifluoroethyl methacrylate with 1,6-hexanedioldiacrylate, MA, or a mixture of BMA and EA through in situ free-radical and frontal polymerisation in the stone (Casadio & Toniolo 2004, Vicini et al. 2004, Vicini et al. 2005, Vicini et al. 2006). The researchers demonstrated that fluorinated monomers or polymers added to the copolymerising acrylate monomer or monomer mixture improved protective efficiency compared to non-fluorinated acrylate polymers (Vicini et al. 2004, Vicini et al. 2005, Vicini et al. 2006). One recent development in stone consolidants includes the use of hybrid materials such as alkyl-modified alkoxysilanes, which have the properties of both ceramics and organic polymers. Moreover, hybrid consolidants based on tetraethoxysilane, such as colloidal silica and hydroxy-terminated polydimethylsiloxane, have shown improved porosity and elasticity in the formation of non-fractured and permeable gels (Sadat-Shojai & Ershad-Langroudi 2009, Salazar-Hernández et al. 2010). Another development is the use of a nanocomposite system derived from a blend of fluoroelastomers and acrylic polymers in which the nano-scale organically modified sodium MMT is dispersed (D'Arienzo et al. 2008). Results have demonstrated that the inclusion of organoclay MMT provides superior consolidating and protective properties such as hydrophobicity, water-vapor permeability and mechanical and abrasion resistance without significantly alternating the appearance of the treated stone.

3.2.6. Bio-consolidation

To compensate for the unsatisfactory performance of the past consolidation treatments, new and less harsh biological and bio-inspired methods have been of great interest and the contribution of applied microbiology and biotechnology to the conservation of stonework has been recognized (Webster and May 2006, Fernandes 2006, Jroundi et al. 2010). Unlike other consolidation methods, the bio-consolidation treatment of decayed historic stones provides a more compatible and more environmentally and health-friendly approach (Rodriguez-Navarro et al. 2003, Tiano et al. 2006, Webster and May 2006, Jimenez-Lopez et al. 2007a, Jroundi et al. 2010, Piñar et al. 2010). Moreover, some progress has been made through bio-mineralization, a natural method of producing minerals by utilizing living organisms (Rodriguez-Navarro et al. 2003, Liu et al. 2006, Webster and May 2006). Recent developments in the consolidation of calcareous stone

include biomimetic synthesis of the protective biofilm of calcium oxalate converted from calcium ion (Ca^{2+}) and oxalic acid and the production of bio-consolidating cements by bacterially induced calcium carbonate precipitation, called carbonatogenesis carbonate (Rodriguez-Navarro et al. 2003, Liu et al. 2006, Liu & Zhang 2007, Jroundi et al. 2010, Litomyšl 2010, Mifsud 2010). The application of bacterially induced carbonate mineralization has proven particularly effective in consolidation procedures and it offers the potential for the bio-mineralization treatment of silicate rocks (Rodriguez-Navarro et al. 2003, Jimenez-Lopez et al. 2008, Jroundi et al. 2010). Although bio-mineralization is a common process that has been known for a long time, knowledge about the potential of these techniques is still in its infancy and their risks and long-term effects on historic stones are still being discussed (Tiano, Biagiotti & Mastromei 1999, Rodriguez-Navarro et al. 2003, Webster and May 2006).

3.3. Performance criteria: Ideal stone-consolidating materials

Based on the experimental data collected through successes and failure in the development of a number of consolidants reported in the literature, the desired properties required for successful consolidation have been identified and consolidation treatment should be ideally effective, compatible, reversible, safe and cost-effective, without any destructive side effects for stones or any acceleration of the stones' deterioration (Boyer 1987, Bell 1993, Rodrigues 2001, Striegel et al. 2003, Skoulikidis, Vassiliou & Tsakona 2005, Rodrigues and Grossi 2007, Tsakalof et al. 2007). However, there is no single product that works universally in stone conservation, given the diversity and variability found from stone to stone; thus, the performance requirements should be considered on a case-by-case basis (National Research Council (U.S.) 1982, Boyer 1987, Piacenti 1994, Cnudde et al. 2004, Domingo et al. 2008, Karatasios et al. 2009).

Besides the ability of consolidants to increase mechanical durability, ideal consolidants will be effective in providing stones with an adequate depth of penetration, breathability and stability (Rodrigues, Pinto & da Costa 2002, Kim et al. 2009, Salazar-Hernández et al. 2010, Doehne and Price 2011). Penetration and distribution inside the stones are major factors in consolidating performance and the consolidant should penetrate deeply to reach the undamaged core of the stones through the deteriorated area, so as to consolidate the

entire decayed area, thus increasing the resistance to mechanical stress applied to both the exterior and interior of the porous structure (Weber 1985, Boyer 1987, Tabasso 1995, Weiss 1995, Cnudde et al. 2004, De Buergo, Fort & Gomez-Heras 2004, Favaro et al. 2006, Bugani et al. 2007, Son et al. 2009, Hameed et al. 2009, Doehne and Price 2011). Although change in porosity is inevitable as a result of the application of consolidation treatment, the treated stones should remain permeable to water vapor and air as much as possible after the application of consolidants, so that damage from conditions such as water condensation, build-up of soluble salts and biological growth is prevented (Weber 1985, Boyer 1987, Weiss 1995, García-Talegon 1998, Tuminello, Bracci & Piacenti 2002, Striegel et al. 2003, Bugani et al. 2007, Tsakalof et al. 2007, D'Arienzo et al. 2008, Hameed et al. 2009, Doehne and Price 2011, Zornoza-Indart et al. 2016a). Furthermore, good consolidants must guarantee chemical, photochemical and colour stability in face of any alteration of the surrounding conditions, including air pollution and salt attack (Weber 1985, Boyer 1987, Berry 1994, Griswold and Uricheck 1998, Tuminello, Bracci & Piacenti 2002, Iñigo, Vicente-Tavera & Rives 2004, Cnudde et al. 2006, Zornoza-Indart et al. 2016a, Favaro et al. 2007, D'Arienzo et al. 2008, Sadat-Shojai & Ershad-Langroudi 2009).

In view of long-term consolidating effects, the key feature of successful consolidation is the compatibility of consolidants, which is related to possible future treatments and consolidating performance and incompatible action must be minimized (Giorgi et al. 1986, Boyer 1987, Rodrigues and Grossi 2007, Jimenez-Lopez et al. 2007b, D'Arienzo et al. 2008, Stück et al. 2008, Piñar et al. 2010). The consolidants should be mechanically, physically and chemically compatible with the untreated stone and the properties of the treated stone, like moisture expansion, thermal expansion and mechanical resistance, should be similar to the ones of untreated stones (Boyer 1987, Tiano 1995, Griswold and Uricheck 1998, Mosquera et al. 2002, Striegel et al. 2003, Skoulikidis, Vassiliou & Tsakona 2005, Rodrigues and Grossi 2007, Doehne and Price 2011). Furthermore, significant alteration of the properties of treated stones should be avoided; treatment must not introduce new factors, like pH or mechanical stresses (Werner 1981, Griswold and Uricheck 1998). Importantly, the treatment should not modify the colour or the aesthetic appearance of the untreated stones at the initial stage or after long-term contact with the environment (Boyer 1987).

Ideally, any treatment applied to the stone should be a reversible process, in the case of any unwanted results, so that the treated stone can be recovered unharmed in its original condition (Werner 1981, Charola, Tucci & Koestler 1986, Giovanni Brunetti, Sgamellotti & Clark 1986, Striegel et al. 2003, Doehne & Price 2011). Although the reversibility of treatment is unquestionably one of the most desirable features in conservation practice, the theoretical concept of total reversibility does not exist in nature and the removal of even a soluble treatment has been found to be extremely hard in practice (Witte, Huget & Broeck 1977, Charola, Tucci & Koestler 1986, Pieper 1995, Rodrigues 2001, Doehne and Price 2011). Those developing consolidating material face a real challenge with respect to reversibility.

3.4. Consolidation treatment of Sydney's historic sandstones

Literature survey reveals that, so far, a wide range of stone consolidants has been developed for use in the conservation of heritage buildings to consolidate the deteriorated stone buildings. Despite the fact that it is the most researched technique, consolidation treatment presents many challenges and the positive aspects of such treatments have not been extensive in conservation interventions due to compositional and textural complexities (Munnikendam 1967, Rodrigues 2001, Rodrigues, Pinto & da Costa 2002, Moropoulou et al. 2003b, Jimenez-Lopez et al. 2008). It has been reported that some consolidants were effective in other countries but the same consolidants were unsuccessful to consolidate Sydney sandstone (O'Connor et al. 2001). In addition, it has become more difficult to find replacing sandstones from the common sources of yellowblock stone and surrounding quarries (Orwell & Peter Phillips 2008). All of these results obviously suggest a need for exploring suitable consolidation treatments, specifically designed for the historic Sydney sandstones.

In conservation and restoration practices, the application of protective and consolidating treatments is widely employed and is one of the most important steps (De Buergo, Fort & Gomez-Heras 2004, Domingo et al. 2008, Karatasios et al. 2009). The use of protective products is intended to prevent contact with external deteriorating factors in order to reduce the degradation rate and improve resistance to weathering agents like water,

pollutants and salts (Tabasso 1995, Rodriguez-Navarro et al. 2003, Striegel et al. 2003, Cnudde et al. 2004, Cardiano et al. 2005, Favaro et al. 2006, Cnudde et al. 2006, Domingo et al. 2008, Baglioni, Giorgi & Dei 2009). On the other hand, the major role of consolidation treatment is to restore the physical integrity of the fragile stones and thus prevent further surface loss (Rodrigues, Pinto & da Costa 2002). This involves processes to increase cohesion, adhesion and indentation strength and to bind dislodged mineral grains (Boyer 1987, Wheeler et al. 1992, Saleh et al. 1992, Bell 1993, Piacenti 1994, Durán-Suárez, García-Beltrán & Rodríguez-Gordillo 1995, Tabasso 1995, Brus & Kotlík 1996b, Rodriguez-Navarro et al. 2003, Striegel et al. 2003, Moropoulou et al. 2003b, Cnudde et al. 2004, Favaro et al. 2006, Domingo et al. 2008, Stück et al. 2008, Pinto & Rodrigues 2008, Son et al. 2009, Karatasios et al. 2009, Toniolo et al. 2011). Although a number of consolidants are intended to serve a dual function, as both consolidation and protection, the recent trend is to apply the consolidants and protective treatments separately (D'Arienzo et al. 2008, Doehne and Price 2011). This research work focused the development of materials in regard to consolidation application with aim to preserve the physical integrity of the consolidated sandstone and therefore to slow down the sandstone deterioration.

Figure 3.5. Photo image demonstrating the colour changes in the sandstone block as a result of weathering action on the uncovered surface to external environment

Given the presence of moisture derived from various sources in stone and its significant role in transporting soluble materials, such as water-soluble salts, designing a water-based system can improve the transport of water soluble salts through the porous sandstone system. This can also contribute to safety, economic and environmental demands and the reversibility of consolidation treatments—unlike conventional solvent-based consolidation treatments, which are linked to hazards and toxicity—and could be used for a number of consolidating products found on the market and in the literature. However, the research of the preparation of aqueous consolidation systems is quite limited in the

literature. The development of aqueous consolidation systems, based on water permeable materials to allow the penetration of water and the soluble salts, makes an essential component of sustainable treatment of heritage sandstones.

Provided that Sydney heritage buildings were constructed from yellowblock sandstone, which is mainly bound together by kaolinite clay, the material of choice for consolidating deteriorated stones should deposit the consolidating product, which will be similar to the original cementing clay in order to ensure its compatibility with the sandstone substrates in Sydney' heritage buildings (Ip 2007). Taking into consideration both the chemical composition of Sydney sandstones in heritage buildings and the incompatibility of organic-based synthetic polymers, the introduction of clay mineral as the consolidating system can improve both stability and compatibility of consolidating material. The significance of this research lies in the development of water-based clay, containing polymeric binders that should ideally be as similar as possible to the original cementing clay in the sandstone of Sydney's buildings, so the effect of organic polymers and inorganic clay can be combined to manipulate the adhesive properties of polymers and to improve the stability and compatibility of consolidants.

In an effort to identify the consolidation need specific to Sydney sandstone under study with the aim of focusing on the penetration depth, a single example of representative weathered sandstone specimen obtained from St Mary Cathedral was taken and the assessment of a weathered sandstone block revealed the weathered region was clearly detected as colour alternation from greyish to yellow-brown colour from the surface of sandstone exposed to external environment as illustrated in Figure 3.5. The obvious changes suggest the weathering process and the oxidation reaction of iron-bearing materials in the sandstone were extended up to 10 mm from the exposed surface.

Considered from the viewpoint that the applied consolidant should be ideally penetrated from the stone surface through the weathered area to undeteriorated area, the observations allowed presuming that the weathered Sydney sandstone should be consolidated at least 10 mm below the surface. However, the focus of the research is the development of the consolidation treatment for the unweathered sandstone. This work intended to use the unweathered Sydney sandstone for the improvement of the consolidation treatments that

may allow treated sandstones to preserve the original states of Sydney sandstone and to slow down the weathering process of treated sandstones. With knowledge of the condition of weathered and unweathered sandstone, the roles of penetration depth of consolidants for such method can be regarded to be of secondary importance and the effective penetration depth of applied consolidants can be less than 10 mm for the treatment of the unweathered sandstones.

CHAPTER 4. CONSOLIDATING MATERIALS FOR SYDNEY SANDSTONES

4.1. Introduction

This chapter focused on reviewing the materials related to consolidation treatments designed for Sydney yellow block sandstone. In order to improve the compatibility and stability, the approach to consolidant development was to develop water-based polymeric binders containing clay mineral and this review has attempted to summarize available information concerning clay mineralogy and polymer-MMT composite from published work. It is not the intent of this chapter to describe all clay minerals or composites, but rather to focus on the clay mineral groups linked with kaolinite. The purpose of this chapter was to use this information for the selection of materials, structures and preparation method that are most applicable to the need for consolidation work of Sydney sandstone from a mineralogical, physicochemical structural and practical viewpoint.

The chapter initially introduces clay mineralogy and the structural and physicochemical characteristics of clay minerals were then described, followed by the properties of the clay mineral groups belonging to kaolinite and MMT. It included a background to the structure, classification based on structures and chemical properties of natural clay materials and an understanding of the crystal structure of phyllosilicates from the fundamental level to the general clay mineral groups, presenting major layer types and subgroups. It intends to provide a basic description of natural clay minerals reported for Sydney sandstone and to examine problems associated with kaolinite and general clay mineral groups for determining suitable clay mineral as binder for consolidation work. The emphasis is placed on the reasoning applied for the consideration of MMT used in consolidation conditions for Sydney sandstone.

A brief introduction of the general characteristics, structure and preparation methods of polymer-MMT composites is then described. The essence of a polymer-MMT composite system is the capability of combining the adhesive properties of organic polymers and the stability and compatibility of MMT. To develop an aqueous consolidation system made from hydrophilic polymer and MMT for use in sandstone consolidation, knowledge of

the composite system is used as a basis for the identification of the properties, structure and preparation route that are appropriate as binding material for Sydney sandstone. While a number of polymer-MMT composites have been published, the studies on the composite materials composed of unmodified MMT with hydrophilic polymers are limited. In the last section, the intercalation process of MMT by the hydrophilic polymers and the composites containing PAA, PAm and PEG are reviewed.

4.2. Clay science

4.2.1. Clay mineralogy

In the most basic terms generalized by the joint nomenclature committees of the Association International Pour l'Etude des Argiles and the Clay Minerals Society, clay is fine-grained material that becomes plastic under wet conditions and solidifies on drying and firing (Guggenheim & Martin 1995, Douillard & Salles 2004, Guggenheim et al. 2006, Reeves, Sims & Cripps 2006, Bergaya & Legaly 2013, Mukherjee 2013). Clay is naturally derived material and mostly contains clay minerals and some other materials (Mukherjee 2013). Clay mineral generally refers to hydrated phyllosilicates mineral and mineral with plasticity characteristics (Sudo et al. 1981, Moore & Reynolds 1997, Douillard & Salles 2004, Reeves, Sims & Cripps 2006, Bergaya & Legaly 2013). Unlike clay stated according to its particle size and origin, clay mineral includes both natural and synthetic phyllosilicates and non-phyllosilicates of any size (Bergaya & Legaly 2013). Although the use of the term clay mineral is universal, clay mineral considered in this work is specified to naturally occurring hydrated phyllosilicates in the following chapters.

Chemically, clay mineral can be described as hydrous aluminosilicate, containing alkali, alkaline earth and transition metals or organic matter (Weaver & Pollard 1973, Sudo et al. 1981, Hall 1987, Moore & Reynolds 1997, Hamilton 2003, López-Galindo & Viseras 2004, Volzone 2004, Wypych 2004, Reeves, Sims & Cripps 2006, Bergaya & Legaly 2013). Clay minerals exhibit variable, diverse and complex natures of structural, chemical and physical properties (Sudo et al. 1981, Moore & Reynolds 1997, Berry, Bergaya & Lagaly 2006). Based on the chemical composition, clay minerals are inorganic materials mainly composed of oxygen, silicon, aluminum or magnesium, although chemical

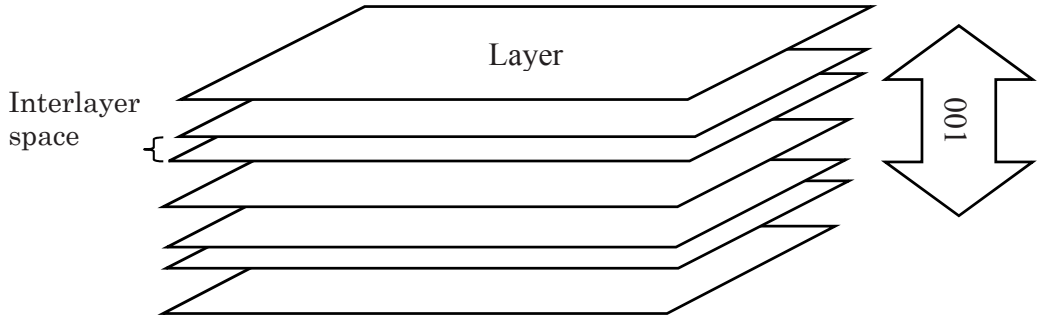

Figure 4.1. Schematic illustration of layered structure of clay minerals

structures vary, they are related by similar crystalline structure characteristics (Hall 1987, Sudo et al. 1981, Velde 1995, Worden & Morad 2003). Clay minerals can be structurally defined as layered materials in which clay sheets are cross-linked by chemical bonding of the atoms in the repeating building blocks of sheets, while neighbouring layers interact by physical forces (Weaver & Pollard 1973, Giese & Van Oss 2001, Worden & Morad 2003, Chen et al. 2008). The sheets are aligned parallel to the (001) direction and connected to form basically flat and plate-like layers (Figure 4.1) (Velde 1977, Moore & Reynolds 1997, Giese & Van Oss 2001, Velde & Meunier 2008, Bergaya & Legaly 2013). The layers stacked in the c-axis direction are interconnected to form assemblages of microcrystalline clay minerals (Velde 1995, Worden & Morad 2003). The ways of cation and anion occupations, the oxygen linkage and modes of layer stacking arrangements are important determinative factors of the shape and extent of the phyllosilicates (Velde 1977, Velde & Meunier 2008).

As with yellow block Sydney sandstone in which kaolinite has been identified as natural cementing clay (Ip et al. 2003), naturally occurring clay minerals are found in weathering crusts, soils, rocks, sediments, volcanic deposits and geothermal fields (Weaver & Pollard 1973, Velde 1977, Moore & Reynolds 1997, Giese & Van Oss 2001, Essington 2003, Celik 2004, Moronta 2004, Volzone 2004, Galán 2013). Apart from quartz and carbonate minerals, the most abundant minerals in sedimentary rocks are clay minerals and as much as 40% of the minerals comprise these rocks (Weaver & Pollard 1973). As opposed to rock where clay minerals are more common, clay minerals are found less commonly in sandstone and the five main clay minerals in sandstone generally belong to kaolin, illite, chlorite, smectite and mixed layer varieties (Worden & Morad 2003). They are generally

fine-grained components, falling within the clay-sized fraction and found in the weathering environment, the sedimentary environment, diagenetic/hydrothermal environment and metamorphic environment (Weaver & Pollard 1973, Hall 1987, Moore & Reynolds 1997, Giese & Van Oss 2001, Essington 2003, Reeves, Sims & Cripps 2006). The environments where water is abundant at low temperature and pressure are typical for the formations of clay minerals possessing structural deficiencies, such as stacking faults (Giese & Van Oss 2001). Clay minerals are frequently weathering products of rock, sediment, soils and sandstone and derived by simple or complex weathering reactions of silicates and rock though mechanisms, including diagenetic and hydrothermal alteration, neoformation, transformation and inheritance (Velde 1977, Moore & Reynolds 1997, Giese & Van Oss 2001, Essington 2003, Galán 2013). The formation of clay minerals occurs in various conditions and the genesis and formation are important for special characteristics of clay minerals (Galán 2013).

Clay minerals derived from geological formations are a widely used raw material in manufacturing processes as they are widely distributed, cost-effective, chemically inert and have a low-toxicity (Giese & Van Oss 2001, Choy & Park 2004, Reeves, Sims & Cripps 2006, El-Zahhar, Abdel-Aziz & Siyam 2007, Bergaya & Legaly 2013, Churchman et al. 2006). Clay minerals have become essential materials to modern life, considering the scope of their industrial uses across a broad range of applications, including personal consumer products, construction materials and catalytic, agricultural, geotechnical, environmental, biological, pharmaceutical and medical uses (Moore & Reynolds 1997, Giese & Van Oss 2001, Choy & Park 2004, Douillard & Salles 2004, López-Galindo & Viseras 2004, Reeves, Sims & Cripps 2006, Adams & McCabe 2013, Bishop et al. 2014, Lopes, Martins & Lanceros-Mendez 2014). Their structural, physical and chemical properties, formation and weathering processes have been extensively researched by a wide range of disciplines (Choy & Park 2004). The ability of some clay to attain nano-sized particles dispersed in a matrix phase has been of particular interest in both industrial application and scientific investigation and a challenge facing the future of clay science is to make applicable adjustments to the multi-scale method to connect studies on the nano-, micro- and macro-scale (Bergaya & Legaly 2013).

4.2.2. Structural characteristics of phyllosilicates

Phyllosilicates are commonly known as the layer or sheet silicates and related by common physical, chemical and structural features attributable to tetrahedral and octahedral units that build the framework for interrelated crystalline structures (Hall 1987, Velde 1995, Reeves, Sims & Cripps 2006, Bergaya & Legaly 2013). Each tetrahedron and octahedron, which are the fundamental building blocks of the layered silicate, consists of a cation tetrahedrally coordinated by four oxygen atoms and a metal ion octahedrally coordinated by six oxygen atoms (Moore & Reynolds 1997, Wypych 2004, Pavlidou & Papaspyrides 2008, Velde & Meunier 2008, Lopes, Martins & Lanceros-Mendez 2014). Alternatively, phyllosilicates can be viewed as inorganic polyanionic salts (Bergaya & Legaly 2013). Salts of cations counterbalance the negatively charged surface of crosslinked inorganic polymers made up of octahedron monomers and tetrahedron monomers, which in turn, are polymerised to form octahedral sheets and tetrahedral sheets (Giese & Van Oss 2001, Bergaya & Legaly 2013).

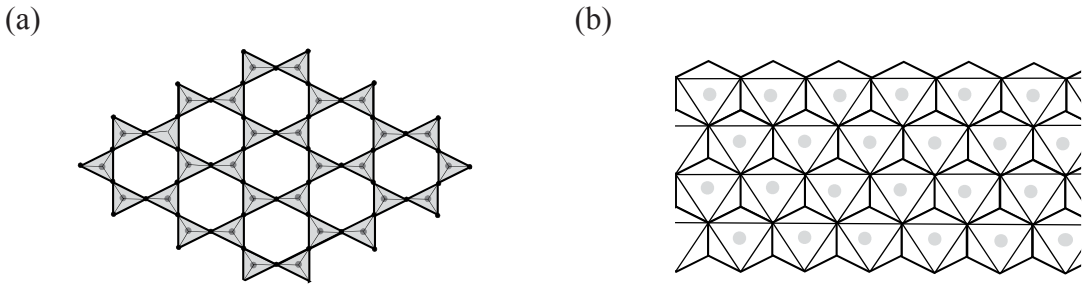

Figure 4.2. Structures of (a) tetrahedral sheet and (b) octahedral sheet

In the continuous tetrahedral sheets of phyllosilicates, the common central cations, Si^{4+}, Al^{3+} or Fe^{3+} are in tetrahedral coordination with four oxygens, three of which are basal oxygen atoms shared with a neighbouring tetrahedron (Weaver & Pollard 1973, Nemecz 1981, Velde 1995, Moore & Reynolds 1997, Choy & Park 2004, Velde & Meunier 2008, Brigatti, Galan & Theng 2013). The linked tetrahedra form a continuous two-dimensional tetrahedral sheet, which is arranged in hexagonal array structure along a and b crystallographic directions as illustrated in Figure 4.2a (Weaver & Pollard 1973, Nemecz

1981, Gúven 1992, Moore & Reynolds 1997, Giese & Van Oss 2001, Douillard & Salles 2004, Frost & Kristof 2004, Velde & Meunier 2008, Brigatti, Galan & Theng 2013).

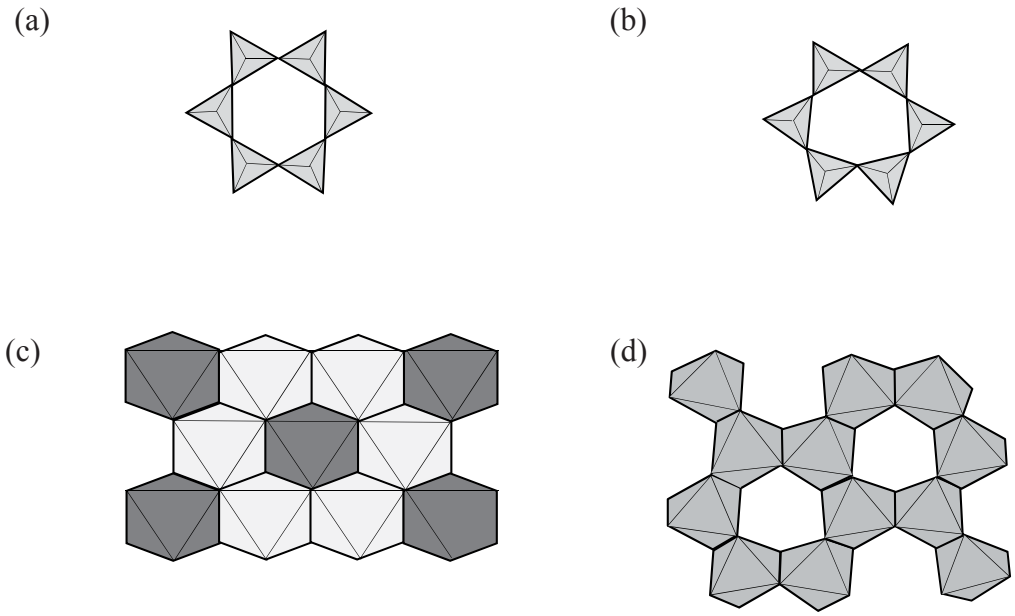

Figure 4.3. Schematic diagrams of (a) ideal hexagonal array structure, (b) deformed ditrigonal structure, (c) trioctahedral sheet and (d) dioctahedral sheet

The adjacent octahedrons, conversely, are connected by sharing all six apices, which in turn, are arranged to form regular, symmetric, hexagonal or pseudo-hexagonal pattern around the octahedral cationic sites in a two-dimensional form (Figure 4.2b) (Nemecz 1981, Velde & Meunier 2008, Brigatti, Galan & Theng 2013). The vertex of octahedral unit is hydroxyl or oxygen ions and two topological structures with trans- and cis-orientation of the OH groups can be formed in the octahedral sheet (Nemecz 1981, Brigatti, Galan & Theng 2013). The octahedral cationic position can be occupied by the divalent or trivalent cations, like Al^{3+}, Fe^{3+}, Mg^{2+} or Fe^{2+} and the octahedra in trioctahedral and dioctahedral sheets are occupied by divalent and trivalent central cations, respectively (Loughnan 1969, Weaver & Pollard 1973, Nemecz 1981, Moore & Reynolds 1997, Choy & Park 2004, Velde & Meunier 2008). In the dioctahedral sheet, each vertex anion is bonded to two trivalent cations in the octahedral site and two-thirds of octahedral sites are occupied, leaving the third vacant octahedron (Loughnan 1969, Nemecz 1981, Worden & Morad 2003, Velde & Meunier 2008, Brigatti, Galan & Theng 2013). In contrast, all octahedral sites in trioctahedral sheet are occupied and anion is connected to

three divalent cations (Loughnan 1969, Nemecz 1981, Worden & Morad 2003, Velde & Meunier 2008).

The assembled tetrahedral and octahedral sheets form a silicate layer in which one or both sides of the tetrahedral sheets are covalently bonded with octahedral sheets (Velde 1977, Reeves, Sims & Cripps 2006, Brigatti, Galan & Theng 2013). The tetrahedral sheet is connected to an octahedral sheet through apical oxygens that are unshared in tetrahedral unit and directed to the same side and the crosslinks between tetrahedral and octahedral sheets produce a shared plane with the octahedral anions located around the centre of tetrahedral sixfold ring (Velde 1995, Brigatti, Galan & Theng 2013). Because of differences in the a and b crystallographic axes of the tetrahedral and octahedral sheets, assembly of these sheets caused by sharing of apical oxygens in tetrahedral and octahedral units is accompanied by alternation of faultless geometrical structure of tetrahedral and octahedral sheets in order to organize such misfitted sheets into an assembled layer system (Nemecz 1981, Sudo et al. 1981, Velde & Meunier 2008, Brigatti, Galan & Theng 2013). The hexagonal symmetry array of tetrahedral sheet is deformed into ditrigonal structure so as to align the rotated apical oxygens in octahedral coordination (Figure 4.3a and 4.3b) (Sudo et al. 1981, Giese & Van Oss 2001, Douillard & Salles 2004, Velde & Meunier 2008). Although octahedral sheets are distorted due to a parallel axial revolution in relation to the plane, dioctahedral sheets are deformed to greater degree due to a reduction of attractive forces on anions caused by unoccupied sites, thereby leading to extended edges of the empty octahedron (Figure 4.3c and 4.3d) (Giese & Van Oss 2001, Velde & Meunier 2008).

Table 4.1. The classification of the phyllosilicate clay minerals

Layer type	Interlayer occupancy	Layer charge	Octahedral character	
			Dioctahedral	Trioctahedral
1:1	None	None	Kaolin	Serpentine
2:1	None	None	Pyrophyllite	Talc
	Hydrated cations	0.2-0.6	Smectites	
	Hydrated cations	0.6-0.9	vermiculites	
	cations	1 ~ 2	mica	
	Hydroxide sheet	variable	chlorites	

Structural classification is helpful information to provide the interrelated physicochemical and structural properties of phyllosilicate clay minerals (Essington 2003). In order to identify suitable consolidating material for Sydney sandstone, their properties and structures were reviewed. Although the criteria of the phyllosilicate clay mineral vary for different classification systems, the phyllosilicate clay minerals can be distinguished by a number of structural and chemical features and are largely organized into categories according to the type of tetrahedral-octahedral sheet combination involved in the stacking of these sheets, the distribution of electric charges of cations positioned in the sheet, net negative layer charge and the kind of the interlayer material as shown in Table 4.1 (Weaver & Pollard 1973, Sudo et al. 1981, Giese & Van Oss 2001, Essington 2003, Choy & Park 2004). They are broadly divided into two and three layer forms, depending on the number of tetrahedral sheet to octahedral sheets in the layer (Sudo et al. 1981, Essington 2003, Velde & Meunier 2008, Lopes, Martins & Lanceros-Mendez 2014). The octahedral sheet can be differentiated by either dioctahedral or trioctahedral character, which splits each layer type into two subgroups (Sudo et al. 1981, Velde 1995, Essington 2003).

4.2.3. Physicochemical characteristics

Clay minerals are porous and consist of a wide variety of sizes and shapes of particles and aggregate (Bergaya & Legaly 2013). Layers are assembled into particles, which can turn into aggregates from an assembly of particles and these particles and aggregates are arranged into different morphologies, including plates, tubules, laths and fibres (Gúven 1992, Wypych 2004, Bergaya & Legaly 2013). The pores of different size, shape and distribution are formed from the interlayer/intraparticle, interparticle and interaggregate spaces resulting from assembly of particles and aggregates (Gúven 1992, Bergaya & Legaly 2013). In addition to physicochemical properties of clay minerals and interacting materials, it is pertinent to understand their interactions with different matters in the surrounding environment, which are influenced by various factors, including thermodynamic properties, pH, ionic strength, pressure and temperature as in Figure 4.4 (Bergaya & Legaly 2013). Clay minerals can react with surrounding materials through

their interaction that takes place in different states of matter, including solid, melted solid, liquid, gas and plasma (Bergaya & Legaly 2013).

Isomorphous substitution reactions can produce permanent charge on the siloxane surface of clay minerals and polarize the basal oxygens in contact with interlayer cations (Gúven 1992, Giese & Van Oss 2001, Choy & Park 2004, Lagaly & Dékány 2013, Schoonheydt & Johnston 2013). Excess negative charge of basal oxygens due to isomorphous substitution reaction of layers causes it to increase the electron donating capacity of basal oxygens, compared to electrically neutral layers behaving as weak Lewis base to form the weak hydrogen bonds with protons (Gúven 1992, Douillard & Salles 2004, Brigatti, Galan & Theng 2013). The planar and edge surface interact with water due to the hydrogen bonds of a water proton and water oxygen interacted with a siloxane oxygen of tetrahedral sheets and a surface hydroxyl proton (Hall 1987, Brigatti, Galan & Theng 2013). Alongside the ionic bond, due to the various chemical interactions in the internal surface, the layers are linked through various chemical interactions between oxygen and oxygen, oxygen and hydroxyl, water-oxygen-hydroxyl interaction and exchangeable cation-water molecule-oxygen interactions (Sudo et al. 1981, Wypych 2004).

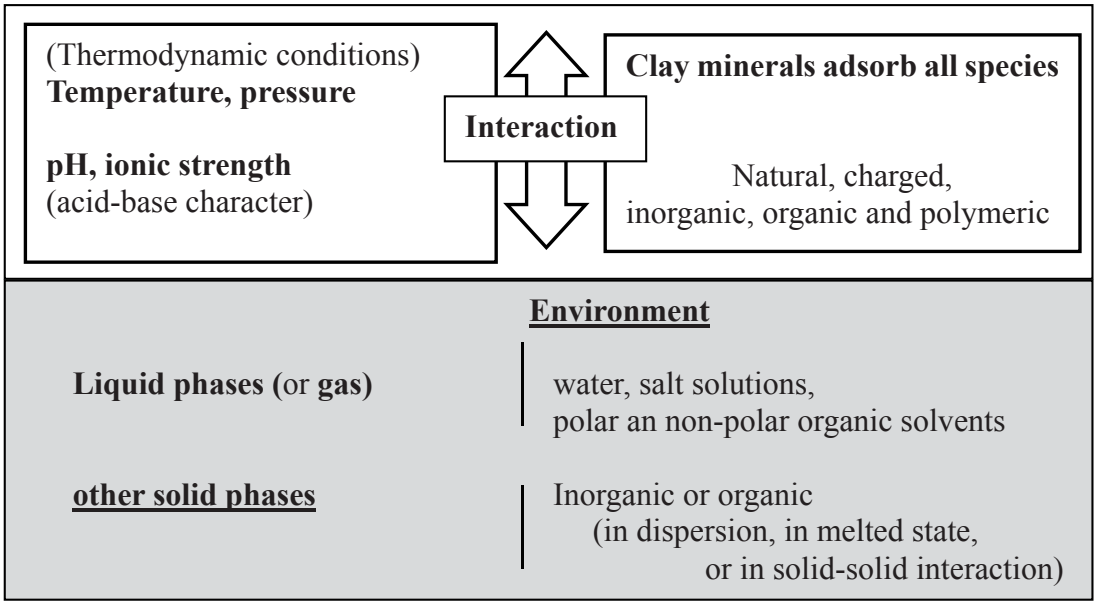

Figure 4.4. Schematic diagram illustrating clay mineral and its interaction with surroundings (Bergaya & Legaly 2013)

The alteration of chemicophysical properties of clay minerals through the structural

modification of clay mineral without the breakdown of the unit structure takes place in the external crystal surface, the crystal/particle edges, or in internal crystallographic site through the bond formation between host lattice and guest species (Sudo et al. 1981, Wypych 2004). Charged or uncharged molecular species can be adsorbed at external clay surface or absorbed within internal clay surface (Velde 1995). The ion exchange reaction and grafting reactions at layer surface and crystal edge can contribute to the surface structural modification of clay mineral (Hall 1987, Moronta 2004, Wypych 2004, Reeves, Sims & Cripps 2006, Liu 2007, Lagaly, Ogawa & Dékány 2013). The pH dependent charges of crystal edge and surface can amount to less than 5 % of total surface charge and as much as 20% of the face surface charge (Kim & Palomino 2011). Because of the pH dependence for adsorption and dissociation reaction of silonol, aluminol and hydroxyl groups exposed on the crystal edge surface, the acidic or basic condition results in positively charged or negatively charged edge sites, respectively (Celik 2004, Choy & Park 2004, Reeves, Sims & Cripps 2006, Kim & Palomino 2011, Brigatti, Galan & Theng 2013). The cationic species are adsorbed onto the negatively charged edge sites, except for the alkaline condition of the former case, while the organic molecules can be covalently bonded to the crystal edge surface (Hall 1987, Lagaly & Dékány 2013).

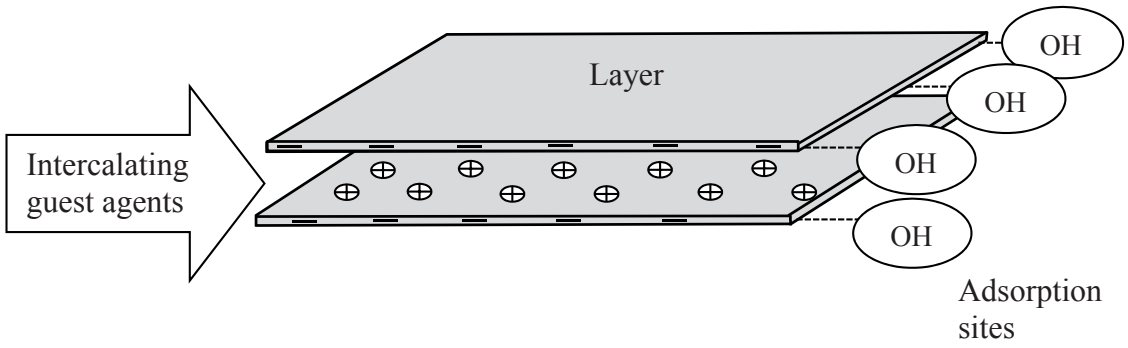

Figure 4.5. Schematic illustration showing interaction sites of clay mineral

The intercalation reaction involves in changes in the distance of gap junctions and/or alteration of the quantity or kind of interlayer materials (Sudo et al. 1981, Wypych 2004). In order to modify the interlayer volume or chemical nature of clay mineral accompanied by the arrangement and alteration of interlayer materials as illustrated in Figure 4.5, the various physical and chemical treatments, such as the dehydration of interlayer water, the dehydroxylation reaction of interlayer material, the leaching of the interlayer cations, acid activation and adsorption and replacement of interlayer materials have been used (Sudo

et al. 1981, Moronta 2004, Wypych 2004). The layer separation processes can be promoted by hydration of interlayer cations or organic materials (Reeves, Sims & Cripps 2006, Anderson et al. 2010). Besides the hydrogen bonding interaction of water with interlayer surface of clay mineral, water can be absorbed due to the interlayer cations hydrated in the interlamellar region where layer lacks electrical neutrality (Hall 1987, Reeves, Sims & Cripps 2006). The interlayer cations can also participate in cation exchange reaction, which is reversible, diffusion controlled, stoichiometric and selective and a dynamic process governed by the law of mass action (Reeves, Sims & Cripps 2006, Brigatti, Galan & Theng 2013). In addition to the cation concentration directly proportional to the exchange reaction rate, it is affected by nature, type, size, hydration states and charges of cations and pH (Hall 1987, Reeves, Sims & Cripps 2006, Anderson et al. 2010). Organic molecules can also attach to other potential interaction sites of clay mineral surface, including coordinated or uncoordinated water molecules, charged or uncharged basal oxygens (Giese & Van Oss 2001). Intercalation complexes can be formed by the penetration of a range of inorganic cations or polar, ionic or non-ionic organic matters through the replacement of interlayer cation or water or the interaction with interlayer surface of clay minerals due to hydrogen bonding, ion-dipole forces, π bonding and Van der Waals forces (Hall 1987, Giese & Van Oss 2001, Moronta 2004, Brigatti, Galan & Theng 2013). Interparticle and intraparticle interactions of various polymers have been also known in a similar manner to organic material and, particularly, the intraparticle sorption of polymers to have been extensively studied (Hall 1987).

4.2.4. 1:1 silicate layers

The naturally occurring binding material of Sydney yellow sandstone, which was identified by Ip et al., mostly belongs to 1:1 layer type (Ip et al. 2003, Ip et al. 2004, Ip et al. 2005a, Ip et al. 2005b, Ip 2007, Ip et al. 2008a, Ip et al. 2008b). It is made up of a tetrahedral sheet and an octahedral sheet, which are linked by sharing a plane of oxygen atoms, and the oxygen plane and hydroxyls are positioned on the outer side of tetrahedral sheet and the octahedral sheet (Giese & Van Oss 2001, Miranda-Trevino & Coles 2003, Pomogailo 2005, Pavlidou & Papaspyrides 2008, Lopes, Martins & Lanceros-Mendez 2014). The length of each layer made up of a tetrahedral sheet and an octahedral sheet and their intersheet distance is about 7.0 Å. The surface of this layer type consists of the

oxygen atoms of a tetrahedral sheet and oxygen atoms and hydroxyl groups of an octahedral sheet (Loughnan 1969, Weaver & Pollard 1973, Giese & Van Oss 2001, Brigatti, Galan & Theng 2013). In the stacking arrangement of the layers, the hydroxyls of an octahedral sheet interact with the oxygens of the tetrahedral sheet of the neighbouring layer and repeating layers of the mineral are strongly stuck together due to the presence of strong hydrogen bonding between the two neighbouring layers (Loughnan 1969, Giese & Van Oss 2001, Miranda-Trevino & Coles 2003, Worden & Morad 2003, Moronta 2004, Velde & Meunier 2008, Schoonheydt & Johnston 2013, Lopes, Martins & Lanceros-Mendez 2014).

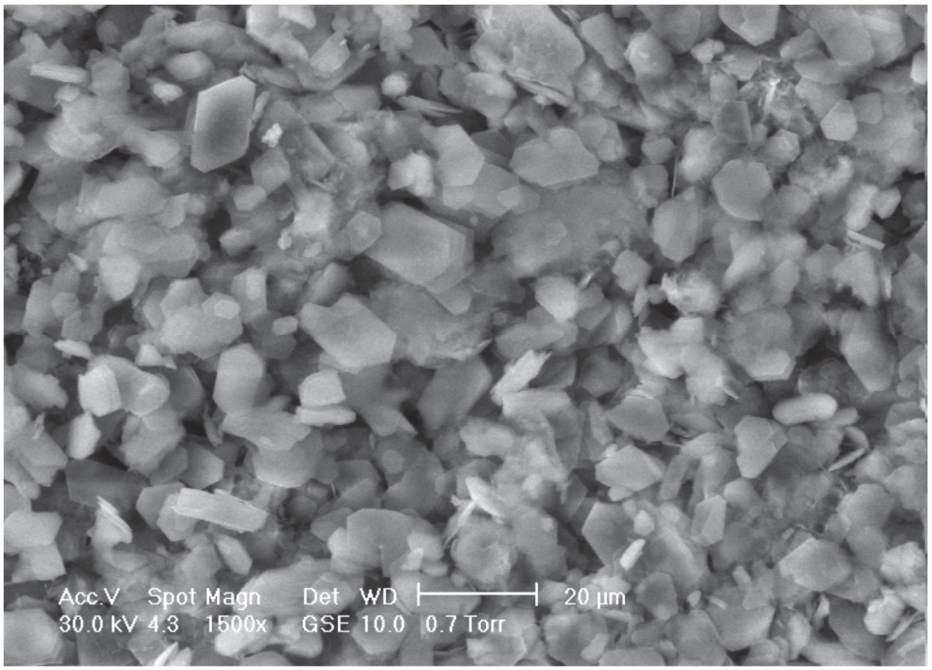

Figure 4.6. Electron microscopic image of cementing clay in Sydney sandstone (Ip 2007)

The 1:1 two sheet type is naturally quite pure and the characteristic physical and chemical features of this group are caused by the limited or absence of isomorphous substitutions in tetrahedral or octahedral sheets (Loughnan 1969, Giese & Van Oss 2001, Essington 2003, Celik 2004). The 1:1 phyllosilicates are considered to be neutral, as charges are counterbalanced by the tetrahedral and octahedral charges in the structure, or a low net negative charge is offset by a small number of interlayer cations (Giese & Van Oss 2001, Essington 2003, Worden & Morad 2003, Reeves, Sims & Cripps 2006, Velde & Meunier

2008). The subdivision of the 1:1 clay mineral type is made into either kaolin or serpentine, according to the occupation of octahedral sites and they morphologically differ due to the different lateral dimensions of the dioctahedral and trioctahedral sheet compared with one of the tetrahedral sheet (Weaver & Pollard 1973, Hall 1987, Essington 2003).

The dioctahedral kaolin group is one of the common clay minerals found in sandstone (Worden & Morad 2003). The results produced by Ip et al. demonstrated that the major components of natural clay mineral in Sydney yellow block sandstone are also the polytypes of Kaolin group and the majority of which were found to be the disordered state of kaolinite along with more ordered dickite and nacrite and other clay minerals (Figure 4.6) (Ip et al. 2003, Ip et al. 2004, Ip et al. 2005b, Ip 2007, Ip et al. 2008a, Ip et al. 2008b). The polytypes of kaolin are distinguished by their layer stacking mode and are morphologically different as seen from hexagonal plates of kaolinite and rhomb shaped dickite and nacrite (Weaver & Pollard 1973, Hall 1987, Giese & Van Oss 2001, Essington 2003, Velde & Meunier 2008). Kaolinite is one layer polytype and dickite and nacrite are monoclinic two layer polytypes where their layers are stacked in regular alternating orders (Millot 1970, Weaver & Pollard 1973, Sudo et al. 1981, Hall 1987, Essington 2003, Brigatti, Galan & Theng 2013). The degree of crystallinity in kaolinite varies while dickite and nacrite are more crystallised (Loughnan 1969, Hall 1987). Dickite, having a 2 layered monoclinic cell, is commonly found as a secondary clay in sandstones while nacrite, with 6 layered monoclinic cell, is the scarcest clay mineral in the kaolin group (Loughnan 1969, Weaver & Pollard 1973, Brigatti, Galan & Theng 2013). In contrast to dehydrated forms of kaolin group having the platy feature, halloysite in tabular form is structurally similar to disordered kaolinite but is hydrated due to the presence of interlayer water in interlayer gap (Loughnan 1969, Millot 1970, Hall 1987, Velde 1995, Giese & Van Oss 2001, Essington 2003, Reeves, Sims & Cripps 2006, Velde & Meunier 2008). Although the addition of certain polar and organic solutions can extend the interlayer enlargement, halloysite rarely occurs and is unstable under ambient environments, leading to the rapid loss of interlayer water (Loughnan 1969, Hall 1987, Giese & Van Oss 2001, Essington 2003). Unlike dioctahedral kaolin type, the octahedral sites are coordinated by divalent ferrous iron or magnesium cations and become unoccupied in trioctahedral serpentine group (Loughnan 1969). The movable octahedral cations, due to the replacement of the octahedral trivalent aluminium ion by the divalent cations, change

the stable structure to a destabilized state (Loughnan 1969). The larger trioctahedral sheet connected to the tetrahedral sheet forms tubular structures (Essington 2003). Their structures are rapidly damaged in weathering environment and the trioctahedral serpentine group is relatively rare (Weaver & Pollard 1973, Essington 2003).

4.2.5. Kaolinite

Amongst 1:1 layer forms of clay minerals, the most abundant material is certainly kaolinite (Weaver & Pollard 1973, Essington 2003). Kaolinite is the simplest 1:1 layer silicate and relatively anhydrous dioctahedral aluminosilicate having the ideal composition of $Al_2Si_2O_5(OH)_4nH_2O$ (Figure 4.7) (Weaver & Pollard 1973, Essington 2003, Miranda-Trevino & Coles 2003, Chen et al. 2008, Velde & Meunier 2008). Kaolinite, holding no structural weakness, is fairly pure even though the isomorphic substitution can produce a small layer charge, which can be compensated by base cations (Essington 2003). The neighbouring layers are strongly associated through the interlammelar hydrogen bonding between aluminol of octahedral sheet and oxygen of tetrahedral sheet and the basal d001 spacing of 0.71-0.73 nm is comparatively unchangeable against external effects (Essington 2003, Celik 2004, Wypych 2004, Brigatti, Galan & Theng 2013). The result of this arrangement is the well-packed and stable structure of kaolinite and neither the destruction of kaolinite particles nor the separation of the layers is easily achieved (Millot 1970, Miranda-Trevino & Coles 2003). The kaolinite particles are made up of stacked layers with specific surface area ranging from 10 to 20 m^2g^{-1} and forms large crystal in the coarse clay and slit size fraction of soil (Essington 2003).

Kaolinite is known to be inert and isomorphous substitutions are limited or absent (Giese & Van Oss 2001, Miranda-Trevino & Coles 2003, Wypych 2004). However, structural studies of kaolinite in the weathered Sydney sandstones done by Ip et al. confirmed that aluminium and silicon ions from the octahedral or tetrahedral sheets of kaolinite were lost in the weathered cementing clay where the comparatively large amount of irons became available and isomorphous substitutions of ferric ions (Fe^{3+}) or K^+ to aluminum ions (Al^{3+}) of the octahedral sheets or silicon ions (Si^{4+}) of the tetrahedral sheets (Ip et al. 2003, Ip et al. 2004, Ip et al. 2005a, Ip 2007, Ip et al. 2008a, Ip et al. 2008b, Ip et al. 2011a).

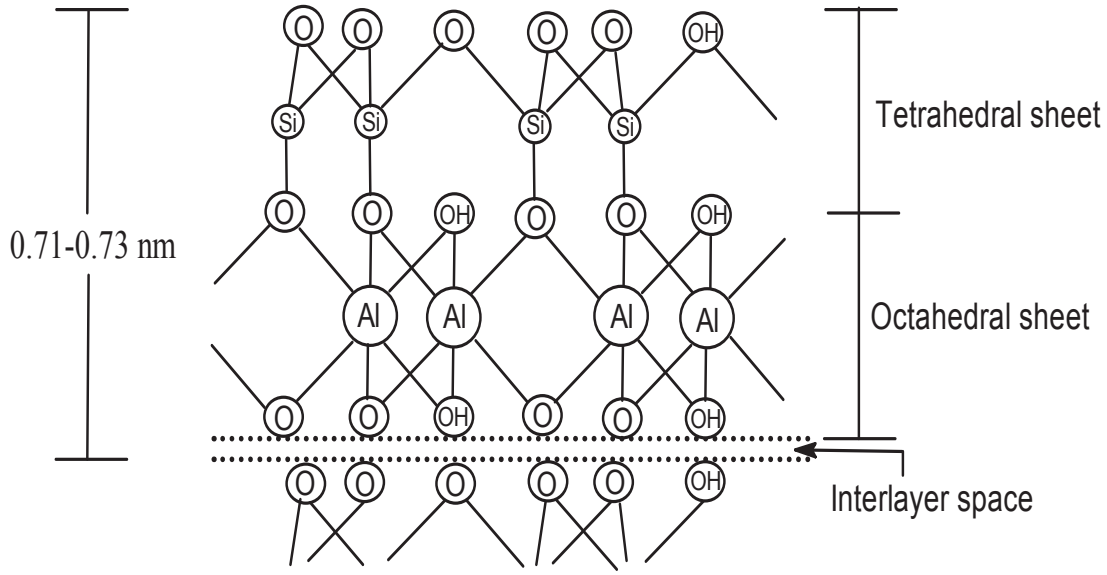

Figure 4.7. Schematic diagram of the structure of kaolinite

The weathering process on the sandstone buildings did not modify the cementing clay structure, but increased structural transition from kaolinite to dickite, indicating that kaolinite is susceptible to the stone degradation (Ip et al. 2003, Ip et al. 2008a, Ip et al. 2008b). The structural transformation of kaolinite resulted in a more ordered and thermally stable weathering product, which maintains the original kaolinite structural framework and is similar to characteristics of dickite of kaolin group (Ip, Stuart & Ray 2003, Ip et al. 2008a, Ip et al. 2008b). Although the weathering level of Sydney sandstone through the iron substitution of kaolinite is not extensive, the isomorphous substitution of Fe^{3+} ions are believed to lead to kaolinite deterioration through the structural disorder and distortion, induced by the crystal stress and strain of kaolinite (Ip et al. 2003, Ip et al. 2004, Ip et al. 2005a, Ip 2007, Ip et al. 2008a, Ip et al. 2008b, Ip et al. 2011a). Their results showed the altered and weakened crystalline structure, reduced crystallinity and binding interactions of kaolinite layers and the destabilization of its structure caused such structural weaknesses as seen from brittleness of the weathered sandstones. Ip et al. proposed that the further weathering process eventually collapses the kaolinite binder, leading to the breakdown of Sydney sandstone (Ip et al. 2003, Ip et al. 2004, Ip et al. 2005a, Ip 2007, Ip et al. 2008a, Ip et al. 2008b, Ip et al. 2011a). The weakening of the cementing kaolinite found in the weathered Sydney heritage buildings suggests that there is a need to apply new cementing materials to the sandstone in order to strengthen the destabilized and weathered cementing kaolinite (Ip et al. 2005b, Ip et al. 2008a).

Due to the strong attractions between the octahedral sheet and the tetrahedral sheet of the neighbouring layer, the silicate layers of kaolinite are closely packed in ordered hydrogen bonded structure and form pseudohexagonal book-like shapes similar to the kaolinite in Sydney sandstone reported by Ip (2007) (Frost & Kristof 2004, López-Galindo & Viseras 2004, Ip 2007). The negative charge on the surface of kaolinite is weak and a small number of counterbalancing interlayer cations are available for ion exchange reaction as reflected by the low cation exchange capacity of kaolin (Giese & Van Oss 2001, Choy & Park 2004, López-Galindo & Viseras 2004, Wypych 2004, Reeves, Sims & Cripps 2006). Therefore, kaolinite is known as non-swelling clay and the intercalation of water and organic molecules into kaolinite layers is not readily attained (Cornejo et al. 2004, Reeves, Sims & Cripps 2006, Inyang et al. 2007, Chen et al. 2008). For this reason, the intercalation of organic molecules to kaolinite has been less studied compared to swelling clays (Zhao, Wang & Li 2008). Although the formation of covalent bonds and bond modification can be made through the salvation process of aluminol and grafting reactions, the intercalation reaction of polymers requires the pre-treatment of kaolinite with small polar organic species, which can be replaced by polymers or monomers followed by in situ polymerisation in the latter case (Sudo et al. 1981, Gardolinski et al. 2000, Giese & Van Oss 2001, Wypych 2004, Chen et al. 2008). The deprotonation and/or protonation of aluminol, silanol and basal plane hydroxyl groups can contribute to the pH-dependent surface charges or surface acidity of kaolinite but basal plane surface sites mostly are not involved in the protonation and deprotonation reactions (Celik 2004, Wypych 2004).

Provided that Sydney heritage buildings were constructed from yellow block sandstone, which is mainly bound together by kaolinite, the material of choice for the consolidation of Sydney sandstone should deposit the consolidating product, which will be similar to the original cementing material in order to ensure its compatibility with the sandstone substrates in Sydney's heritage buildings (Ip 2007). Considerations of the issues in regards to application of large kaolinite aggregate and its low reactivity to separate and modify the interlayer area of kaolinite suggests the use of alternative clay based materials to kaolinite as enforcing material for the Sydney sandstone and a need for exploring new consolidation treatments that are specifically designed for the historic Sydney sandstones in heritage buildings.

4.2.6. 2:1 silicate layers

Analysis of natural binding materials of Sydney sandstones also showed the inclusion of minor clay minerals belonging to 2:1 silicate layer group (Ip, Stuart & Ray 2003, Ip et al. 2008b). Most clay minerals belong to triple layered sandwich structure, based on their availabilities and the number of species (Nemecz 1981). Each layer of this group is composed of an octahedral sheet centred between two external tetrahedral sheets and connected through the oxygen ions of the octahedral sheet shared with the tetrahedral sheets (Weaver & Pollard 1973, Giannelis 1996, Alexandre & Dubois 2000, Sinha Ray & Okamoto 2003, Chen et al. 2008, Pavlidou & Papaspyrides 2008, Kiliaris & Papaspyrides 2010, Brigatti, Galan & Theng 2013, Lopes, Martins & Lanceros-Mendez 2014). This structural arrangement substitutes two-thirds of the octahedrally coordinated hydroxyl groups by the apical tetrahedral oxygens pointing towards the centre of octahedral sheets and the oxygen atoms of the tetrahedral sheet are exposed basal surface atoms of a 2:1 clay mineral (Weaver & Pollard 1973, Gúven 1992, Giese & Van Oss 2001, Wypych 2004, Brigatti, Galan & Theng 2013, Schoonheydt & Johnston 2013).

In describing their structure from physicochemical points of view, the 2:1 type where the degree of isomorphous substitution in 2:1 phyllosilicates and the layer charges vary, can be differentiated by the levels of net surface layer charge reflecting the similar properties within the range (Hall 1987, Giese & Van Oss 2001, Ross & Guggenheim 2002, Essington 2003, Brigatti, Galan & Theng 2013). Their structural distinction is also ascribed to the deviating nature of interlayer cations, octahedral occupancy or the extent of tetrahedral or octahedral charges (Loughnan 1969, Weaver & Pollard 1973, Giese & Van Oss 2001, Essington 2003, Bergaya & Legaly 2013). Six different subgroup classifications have been identified and are listed in Table 4.1. Each subgroup is further subdivided into dioctahedral or trioctahedral species (Bergaya & Legaly 2013). In pure form of 2:1 phyllosilicates with limited isomorphous substitution, the electroneutrality is satisfied within the layers of dioctahedral pyrophyllite and trioctahedral talc and the electrically neutral layers are joined by van der Waals interactions in the absence of interlayer cations (Weaver & Pollard 1973, Nemecz 1981, Sudo et al. 1981, Giese & Van Oss 2001, Ross & Guggenheim 2002, Essington 2003, Brigatti, Galan & Theng 2013). The charges of basic 2:1 units of smectite, vermiculite, mica and chlorite are balanced and the excessive

negative layer charge produced by isomorphous substitution of cations of lesser charge is neutralized by cationic material present in the interlamellar area (Weaver & Pollard 1973, Nemecz 1981, Bergaya & Legaly 2013, Brigatti, Galan & Theng 2013).

In the case of a negatively charged layer of chlorite aligned along the c axis, a positively charged brucite-like octahedral hydroxide sheet is bonded to talc-like layers through hydrogen bonding interaction (Worrall 1968, Weaver & Pollard 1973, Nemecz 1981, Giese & Van Oss 2001, Essington 2003, Bergaya & Legaly 2013). A variety of ionic substitution reactions occur in both 2:1 layer and interlayer sheet and chlorites show a wide range of compositional variations with different proportions of magnesium, aluminium and iron on octahedral sites (Weaver & Pollard 1973, Nemecz 1981, Velde 1995, Giese & Van Oss 2001, Brigatti, Galan & Theng 2013). Although chlorites are abundantly found in clay size fraction minerals, the most chlorites are macroscopic in size and the more common trioctahedral chlorite can weather easily under moderate acid leaching conditions (Weaver & Pollard 1973, Giese & Van Oss 2001, Reeves, Sims & Cripps 2006). Similarly, naturally occurring macroscopic and trioctahedral vermiculite is common and its structural unit is similar to the talc-like layer (Loughnan 1969, Weaver & Pollard 1973, Sudo et al. 1981, Hall 1987, Giese & Van Oss 2001, Brigatti, Galan, Theng 2013, Brigatti, Galan & Theng 2013). The negative charge on layers of vermiculite is neutralized by the presence of exchangeable cations in a hydrated form, most commonly magnesium ions, which separate the vermiculite layers in a manner similar to the interlayer ions in smectite (Loughnan 1969, Sudo et al. 1981, Hall 1987, Essington 2003, Reeves, Sims & Cripps 2006). However, the better ordered three dimensional crystal arrangement and greater charge density of vermiculite layer can limit the degree of layer expansion of vermiculite in comparison to smectite (Weaver & Pollard 1973, Nemecz 1981, Sudo et al. 1981, Velde 1995, Moronta 2004, Brigatti, Galan & Theng 2013). Smectite, on the other hand, forms pyrophyllite-like dioctahedral and talc-like trioctahedral structures in which the isomorphous substitution in both tetrahedral and octahedral sheets of smectite is extensive (Loughnan 1969, Hall 1987, Essington 2003).

As with vermiculite, the negative charge on the lattice is offset by a wide range of the absorbed interlayer cations at exposed surfaces, which are loosely bound, hydrated and exchangeable (Loughnan 1969, Hall 1987, Essington 2003, Reeves, Sims & Cripps 2006).

Aside from smectite, most mica, which is one of the most abundant clay minerals and commonly large crystals, is tetrahedrally charged and the negative layer charges are counteracted by non-exchangeable ions, like sodium, calcium but almost exclusively potassium ion, which can be accommodated into the hexagonal ring of tetrahedral sheets to strongly connect them together (Worrall 1968, Weaver & Pollard 1973, Velde 1977, Sudo et al. 1981, Hall 1987, Velde 1995, Giese & Van Oss 2001, Essington 2003, Lopes, Martins & Lanceros-Mendez 2014). There are also dioctahedral and trioctahedral types of mica, which can be subdivided according to the combination of octahedral cations (Weaver & Pollard 1973, Brigatti, Galan & Theng 2013). The dioctahedral muscovite is coarse grained and was also detected as a minor component from the mixed layer in the cementing material of Sydney sandstone along with vermiculite and illite (Hall 1987, Essington 2003, Ip et al. 2003, Ip et al. 2008b). Illite is the fined grained and frequently dioctahedral mica mineral with a larger degree of octahedral substitution than muscovite and is most abundant in soils and sediments (Weaver & Pollard 1973, Hall 1987, Giese & Van Oss 2001, Brigatti, Galan & Theng 2013).

4.2.7. Expandability of 2:1 phyllosilicates

In consideration of aggregation behaviour of clay minerals leading to the formation of large particles under aqueous environment, the deaggregation process to produce a small particle in size is essential to develop a consolidation system with adequate penetration into porous Sydney sandstone. Therefore the expandability of 2:1 phyllosilicates is a decisive factor for their potential use in the consolidation treatment of Sydney sandstone and the 2:1 phyllosilicates in the layer charge range for expanding forms is the material of choice as a basis of stone consolidant, because the aggregative behaviour of 2:1 phyllosilicates is dependent on their layer charges (Thomas et al. 1999). The hydrophobic siloxane surface of the unaltered 2:1 layer type is the least reactive and the neutral layer, as in talc and pyrophyllite, is electrically satisfied without the interlammer cations unavailable for ion-exchange reaction (Giese & Van Oss 2001, Ross & Guggenheim 2002, Choy & Park 2004, Moronta 2004, Schoonheydt & Johnston 2013). Likewise, highly charged layers stacked due to the strong electrostatistic interactions with interlayer species is unbreakable and chlorites and mica are considered as uncharged non-swelling clay minerals (Giese & Van Oss 2001, Ross & Guggenheim 2002, Essington 2003, Choy

& Park 2004, Moronta 2004, Reeves, Sims & Cripps 2006). Therefore, uncharged and high charged layers are considered to be non-expanding and nondispersible in aqueous solution, which restricts the separation of stacked layers (Thomas et al. 1999).

In the 2:1 phyllosilicates falling in the low to medium levels with a layer charge less than about 1.8, the loosely bound interlayer cations are exchangeable and available for ion exchange reactions and the interlayer regions can be expanded in vermiculite and smectite (Velde 1977, Thomas et al. 1999, Ross & Guggenheim 2002, Choy & Park 2004, Moronta 2004, Lopes, Martins & Lanceros-Mendez 2014). Particularly, smectites with low layer charges, also commonly known as swelling clays, are characterised by cation exchange and extensive swelling capacity caused by expanded interllammelar gaps due to the presence of loosely bound cations and layers of water or polar organic molecules between the layers (Weaver & Pollard 1973, Velde 1995, Giese & Van Oss 2001, Mckinley, Worden & Ruffell 2003, Moronta 2004). The smectite is almost found in the fined ground particles and the significance of smectite in sandstones has not been recognized unlike other clays (Loughnan 1969, Hall 1987, Mckinley, Worden & Ruffell 2003). The additional differentiation of smectites to the octahedral occupation can be made, based on octahedral chemical composition and density and location of layer charges and various cations are occupied in the octahedral, tetrahedral and interlayer area (Loughnan 1969, Giese & Van Oss 2001, Essington 2003, Brigatti, Galan & Theng 2013). The most general naturally occurring interlayer cations are sodium, calcium, hydrogen, magnesium, potassium, iron and aluminium while the octahedral aluminium, ferrous, ferric, magnesium, nickel, zinc and lithium ions are common (Weaver & Pollard 1973, Moronta 2004, Brigatti, Galan & Theng 2013). The trioctahedral smectite include octahedrally charged hectorite and magnesium-rich and tetrahedrally charged saponite (Weaver & Pollard 1973, Hall 1987, Velde 1995). As with the other groups, the chemical composition of trioctahedral smectite is more variable than the dioctahedral smectite (Nemecz 1981, Weaver & Pollard 1973).

In contrast to trioctahedral smectite, which are rarely found in the sediment, the dioctahedral smectite is more abundant (Weaver & Pollard 1973, Essington 2003, Reeves, Sims & Cripps 2006). The main dioctahedral subgroups include montmorillonite, beidellite and nontronite and the charge deficit in their layers are mainly based on the

isomorphous substitution of Si(IV) by AI(II1) in the tetrahedral sheet and Al(II1) by Mg(I1) in the octahedral sheet (Loughnan 1969, Hall 1987, Essington 2003). In the octahedral sheet of beidellite, more aluminium and less magnesium ions are found and the tetrahedral substitution exceeding the octahedral substitution contributes to the total negative charges (Weaver & Pollard 1973, Hall 1987, Giese & Van Oss 2001, Ross & Guggenheim 2002, Mckinley, Worden & Ruffell 2003, Worden & Morad 2003). Although the iron-rich nontronite consists of both tetrahedrally and octahedrally substituted layers, the degree of tetrahedral substitution is greater than the octahedral substitution (Hall 1987, Velde 1995, Giese & Van Oss 2001, Essington 2003). In contrast to beidellite and nontronite, which are largely charged in the tetrahedral sheets, the negative layer charge of aluminium-rich montmorillonite is mainly arisen from the octahedral substitution along with some tetrahedral substitution (Hall 1987, Velde 1995, Giese & Van Oss 2001, Ross & Guggenheim 2002, Essington 2003, Mckinley, Worden & Ruffell 2003). The diotahedral layers are more stable than the trioctahedral layers and the exchangeable cations located closer to tetrahedraly charged layers are bound more firmly (Essington 2003). While the extensive swelling capability of smectite through the exchangeable reactions and hydration of interlayer cations provide their ability to separate the interlamellar space, the swelling capacity and stacking disorderness of octahedrally charged smectite are particularly known (Giese & Van Oss 2001, Essington 2003, Moronta 2004). Therefore, the octahedrally charged MMT is more favourable to produce the better layer separation and MMT can be an effective source of clay mineral for use in consolidation material from the standpoint of its availability, expandability, structure, stability and physicochemical property.

4.2.8. Montmorillonite

As in the other 2:1 phylosilicates, the layer lattice structure of MMT consists of two external tetrahedral sheets and a centred octahedral sheet as in Figure 4.8 and displays the replacement of some octahedral aluminium site by the divalent magnesium or trivalent iron and some tetrahedral substitution (Hall 1987, Giannelis 1996, Alexandre & Dubois 2000, Sinha Ray & Okamoto 2003, Reeves, Sims & Cripps 2006, Pavlidou & Papaspyrides 2008). MMT possesses both pH-dependent charges on OH groups at the edge surface and pH-independent cation exchangeable sites at permanent negative charge

at the internal surface (Bleam 1990, Avena & Pauli 1998). The negative charges caused by the isomorphous substitution of some Al^{3+} cations in MMT by Mg^{2+} are cancelled by exchangeable alkali-metal or alkaline-earth interlayer cations (Celik 2004). This results in charge imbalance about 0.66 per unit cell and the structure of MMT with ideal chemical composition $M^{n+}_{x/n} \cdot yH_2O[(Al_{4-x}Mg_x)(Si_8)O_{20}(OH)_4]$ where M, x and n denote exchangeable cation, degree of isomorphous substitution and exchangeable cation charge (Pinnavaia 1983, Celik 2004). The thickness of the layers is about 1 nm and the lateral dimensions of the layers range from 30 nm to greater than several microns with an aspect ratio of greater than 1000 (Alexandre & Dubois 2000, Sinha Ray & Okamoto 2003, Okada & Usuki 2006, Pavlidou & Papaspyrides 2008, Kiliaris & Papaspyrides 2010).

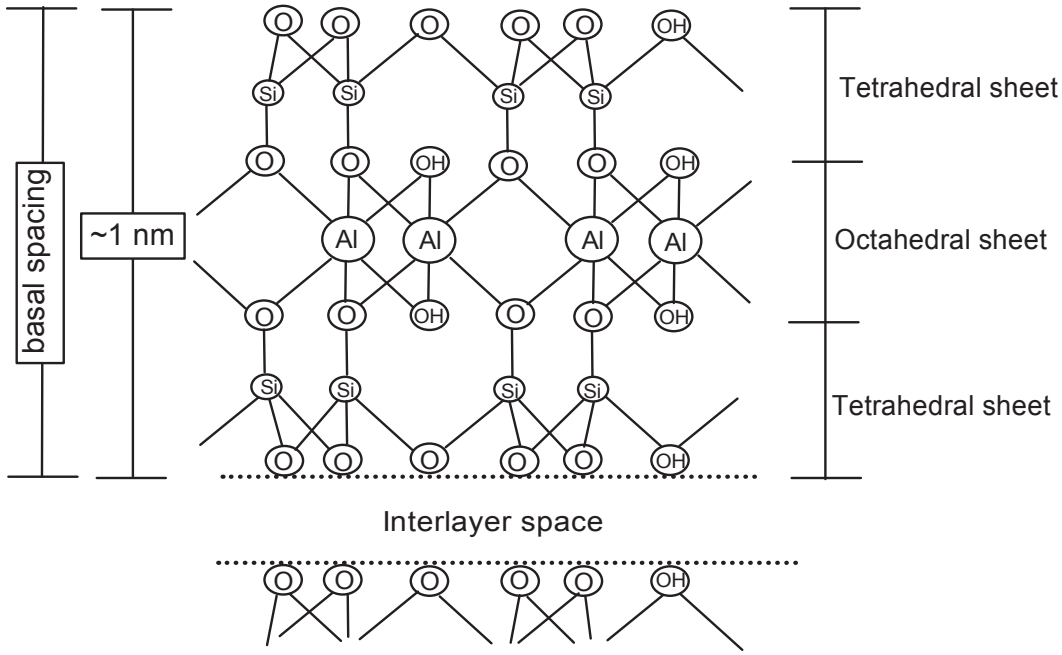

Figure 4.8. Schematic representation of MMT structure

In the interlayer regions, the various mono- and divalent cations occupying the interlayer area of MMT include Na^+, Li^+, K^+, Ca^{2+}, Mg^{2+} and these exchangeable interlayer cations provide MMT with catioinic exchange capacity of 80-124 meq/100g (Worrall 1968, Moore & Reynolds 1997, Thomas et al. 1999, Celik 2004, Reeves, Sims & Cripps 2006, Zadaka, Radian & Mishael 2010). Although the cationic exchange capacity of MMT is affected by the varied composition depending on its own genesis, its cationic ability is higher than kaolinite (Wypych 2004). Exchangeable cations are hydrophilic and lead to

the polarization of the surface oxygen atoms (Moronta 2004, Schoonheydt & Johnston 2013). In marked contrast to kaolinite, the MMT layers tend to produce the stacking arrangement by the formation of the weak dipolar or van der Waals gap between them (Worrall 1968, Alexandre & Dubois 2000, Sinha Ray & Okamoto 2003, Chen et al. 2008, Pavlidou & Papaspyrides 2008, Kiliaris & Papaspyrides 2010). The stacks of MMT are bound together by relatively weak forces and the silicate layers are loosely packed together to form interlayer spaces (Giannelis 1996, Alexandre & Dubois 2000, Chin et al. 2001, Sinha Ray & Okamoto 2003, Gao 2004, Chen et al. 2008, Pavlidou & Papaspyrides 2008).

When brought into contact with water, due to the sorption of water molecules into the pores or the interlayer space, the interlayer water is attached to exchangeable cations to form hydration shells or fill up the gap between the hydration shells in the latter case (Petit 2006, Lagaly & Dékány 2013). Based on the studies of MMT molecular dynamics simulations of hydrated MMT, the strong hydration of divalent magnesium cations are presented and are placed in the midplane of interlayer space of MMT in contrast to the sodium, lithium or potassium interlayer cations, which coordinate to the surface oxygen (Lagaly & Dékány 2013). The interlayer Na^+ and K^+ ions are associated with both surface oxygen and water to form coordination and inner- and outer-sphere surface complexes and the solvation behaviour of Na^+ cations lie between the strong solvated Li^+ and the weakly solvated potassium cations (Chang, Skipper & Sposito 1995, Skipper, Sposito & Chang 1995, Chang, Skipper & Sposito 1998, Lagaly & Dékány 2013). The simulation studies done by Hensen et al. showed that sodium and lithium cations are arranged closer to MMT surface compared to potassium cation mainly located in the midplane (Hensen et al. 2001). The extensive delamination ability of sodium and lithium MMT has been recognized and the hydrated sodium and lithium MMT under the same conditions can absorb three or more water layers in comparison to intercalated water bi-layers for the water uptake profile of potassium MMT (Chang, Skipper & Sposito 1995, Skipper, Sposito & Chang 1995, Chang, Skipper & Sposito 1998).

The published experimental work have demonstrated the different properties of the interlayer water from those of bulk water and the hydration states are altered dependent on water vapour pressure, water content, type and concentration of salts in salt solution,

interlayer charge and interlayer cation (Skipper & Sposito 1995, Lagaly & Dékány 2013). Swelling of clay minerals is known to be caused by crystalline swelling or osmotic swelling and the former proceeds through a stepwise and discrete manner for all clay minerals (Anderson et al. 2010). It can form a quasi-crystalline structure in the interlayer region due to the hydration of one, two, three and four pseudo-layers of water molecules and sodium MMT can absorb up to three layers at 90% humidity (Reeves, Sims & Cripps 2006, Anderson et al. 2010, Lagaly & Dékány 2013). In addition to crystalline swelling, the swelling studies of MMT showed osmotic swelling due to the presence of higher concentration of interlayer exchangeable ions relative to surrounding water, giving rise to extensive swelling capacity of MMT in the presence of monovalent interlayer cations (McFarlane, Bremmell & Addai-Mensah 2005, Anderson et al. 2010). The microscopic swelling of sodium saturated MMT is resulted from repulsive forces between the platelets formed by an electric double layer on the surface (Pham & Nguyen 2014).

The volumetric changes of MMT caused by the extensive uptake of water are source of concern to some practical uses (Anderson et al. 2010). As with buildings and other stoneworks, which were reported to be deteriorated by resultant deformation caused by the swelling action of clay, the consolidated sandstone can be expanded due to such drastic lamellar ability and cracking of consolidated sandstone can occur as a consequence of volume change caused by swelling-shrinkage behaviour of MMT in response to moisture (Dunn & Hudec 1966, Delgado Rodrigues 2001). In order to realise the full advantages of the properties of MMT employed as a stone consolidant, the interlayer space of MMT must be occupied by hydrophilic polymers, which can promote aggregate separation, as well as inhibit the high drying shrinkage of MMT in response to changes in moisture content and wetting state of sandstone.

Without primary chemical bonds and strong interlayer forces, its ability to participate in interactions with polar molecules promotes water and polar molecules to enter into the interlayer space, which can lead to the enlargement of the lattice and the separation of the stacked layers of MMT (Worrall 1968, Pinnavaia 1983, Komarneni 1992, Chin et al. 2001, Chen et al. 2008, Gupta, Kennel & Kim 2010, Olad 2011). Owing to its low cost, effectiveness to improve physical and mechanical properties and ability to intercalate polymers, the use of MMT to introduce organic molecules has been extensively

investigated and MMT has become one of the most frequently used clays in the preparation of polymer-clay nanocomposites (Pinnavaia 1983, Okada & Usuki 2006, Chin et al. 2001, Sinha Ray & Okamoto 2003, Pomogailo 2005, Ruiz-Hitzky & Van Meerbeek 2006, Chen et al. 2008, Pavlidou & Papaspyrides 2008, Olad 2011). With the ability to absorb organic molecules in the galleries, high cation-exchange capacities, a high aspect ratio and a large surface area and the use of MMT can also be an effective way of inserting hydrophilic polymers into the galleries of MMT in aqueous environment (Luo & Daniel 2003, Sinha Ray & Okamoto 2003, Okada & Usuki 2006, Chen et al. 2008, Pavlidou & Papaspyrides 2008, Zadaka, Radian & Mishael 2010, Huang & Ye 2014b). MMT as a source of aluminosilicate clay minerals is an alternative approach to the preparation of clay-containing polymeric material for use as sandstone consolidants. The intercalation and stabilization of hydrophilic polymers in the interlayer region of MMT can modify the properties of MMT required for its possible use as stone consolidant.

4.3. Polymer MMT composite systems

4.3.1. General characteristics of polymer MMT composite systems

Composites based on polymers and clays are formed by combining polymer and natural or synthetic clays, which have quite different structural, physical or chemical characteristics (Akelah 1995, Vasiliev & Morozov 2001, Ruiz-Hitzky & Van Meerbeek 2006, Twardowski 2007, Chen et al. 2008, Olad 2011). Like other composite materials, polymer-clay composites contain mixtures, wherein a continuous phase and a dispersed phase are formed by a polymer and a clay and the incorporation of polymer into host clay yields a composite of polymers and clays with structure and properties that are absent from and better than in each component (Akelah 1995, Giannelis 1996, Vasiliev & Morozov 2001, Jordan et al. 2005, Ruiz-Hitzky & Van Meerbeek 2006, Kickelbick 2007, Olad 2011, Natkański et al. 2012). Together with the reduction of production cost, composites formed from polymer and clay not only offer ease of manufacturing, light weight, low energy consumption and the ductile nature of polymers but also improve their properties, including stiffness, strength, chemical resistance and thermal property (Akelah 1995, Jordan et al. 2005, El-Zahhar, Abdel-Aziz & Siyam 2007, Kickelbick 2007, Olad 2011, Lopes, Martins & Lanceros-Mendez 2014).

Although many polymeric materials have long found their applications in the stone conservation, the improved consolidation properties of organic polymer-MMT nanocomposites have been realized quiet recently (D'Arienzo, Scarfato & Incarnato 2008). Taking into consideration both the chemical composition of Sydney sandstones in heritage buildings and the incompatibility of organic-based synthetic polymers, the introduction of clay mineral as the consolidating system can improve both stability and compatibility of polymers. The inclusion of polymer can increase the limited binding ability of MMT only if organic polymers with effective adhesive properties are utilized in consolidation work (Tabasso 1995). In the polymer-MMT composite system, the effect of organic polymers and inorganic clay can be combined to manipulate the adhesive properties of polymers and to improve the stability and compatibility of consolidants and the benefits of such combined influence can be extended beyond the inadequate consolidating ability of MMT or polymer alone. The stone deterioration has arisen mainly from the structural modifications of the clay binder, according to the previous studies of Ip et al. on the weathering of sandstones in heritage buildings and their results led to the development of polymer-MMT composites with high MMT contents to meet the demand for producing more compatible and stable materials to consolidate heritage buildings. Therefore, the principle behind the approach to the development of a consolidation treatment for Sydney sandstone is the synthesis of clay containing polymeric binders that should ideally be as similar as possible to the original cementing material in the sandstone of Sydney's buildings. As expected, the method of fulfilling such requirements can be aided by the synthesis of polymer-MMT composites at high MMT loading levels, unlike polymer-clay composites, which are typically prepared at low MMT loading levels (Boulet et al. 2003, Chen et al. 2008).

Given that the presence of moisture derived from various sources in stone and its significant role in transporting soluble materials, such as water-soluble salts, designing a water-based system can improve safety, economic and environmental demands. Hydrophilic MMT is capable of forming stable suspension in aqueous medium and the use of hydrophilic polymers as intercalating agents can be formulated into an aqueous based system, which can improve dispersibility, solubility, stability and ease of preparation process. This may also contribute to the reversibility of consolidation treatments—unlike conventional solvent-based consolidation treatments, which are

linked to hazards and toxicity—and could be used for a number of consolidating products found on the market and in the literature. Therefore, the direction of the present research is toward the development of a water-based consolidants that can be water-soluble or dispersible and could be re-dissolved and removed with water where necessary. The development of consolidants, therefore, is limited to the use of water-soluble or dispersible materials in this research.

4.3.2. Structure of polymer-clay nanocomposites

Based on the degree of separation of the silicate layers, polymer-layered silicate composites can be classified into three types, as depicted in Figure 4.9 (Sinha Ray & Okamoto 2003, Pomogailo 2005, Chen et al. 2008, Kiliaris & Papaspyrides 2010, Albdiry et al. 2013). In the conventional composite, phase-separated composites are formed as the layers are aggregated without diffusion of the polymer into the interlayer space of the clay, which leads to the minor improvement of properties similar to conventional micro-composites (Giannelis 1996, Pomogailo 2005, Ruiz-Hitzky & Van Meerbeek 2006, Chen et al. 2008, Pavlidou & Papaspyrides 2008, Kiliaris & Papaspyrides 2010, Albdiry et al.

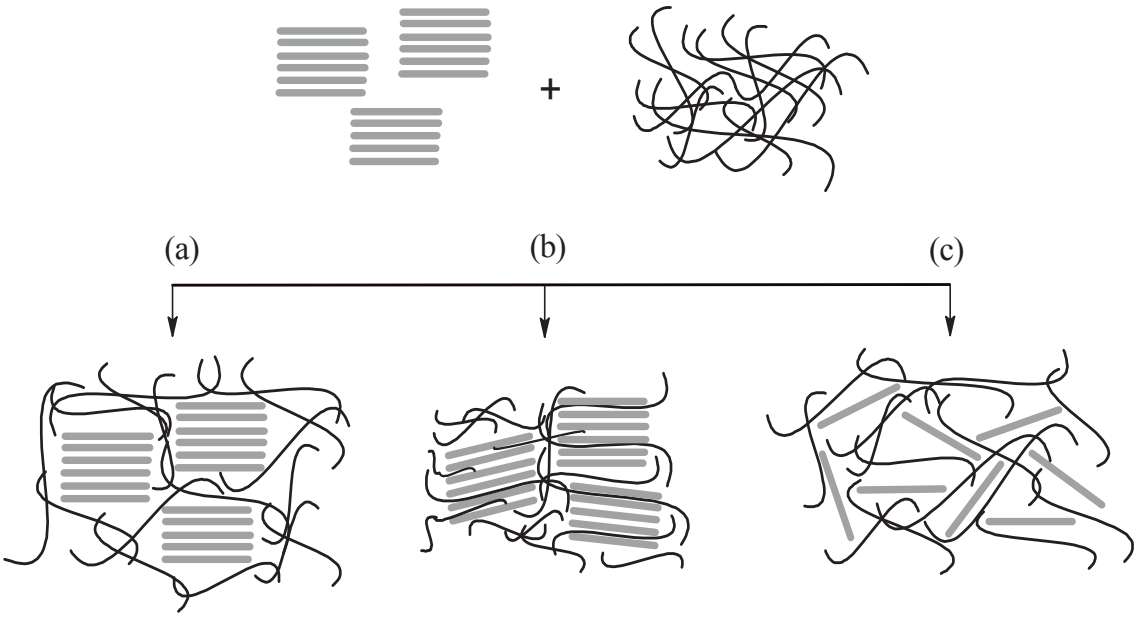

Figure 4.9. Different types of composite: (a) conventional composite, (b) intercalated nanocomposite and (c) exfoliated nanocomposite

2013). An efficient way to overcome traditional limitations is through incorporating the polymer matrix into the gallery of the clay. An intercalated composite is produced if the penetration of one or more extended polymer chain(s) to the interlayer spacing of clay leads to the enlargement of the basal plane spacing up to 2-3 nm with the layers remaining stacked, while the interlayer spacing of the exfoliated structure can be 5-15 nm, which is comparable to the radius of gyration of the polymer (Giannelis 1996, Sinha Ray & Okamoto 2003, Pomogailo 2005, Chen et al. 2008, Pavlidou & Papaspyrides 2008, Kiliaris & Papaspyrides 2010). The extent of clay dispersion depends on the polymer, clay, organic surfactant, clay loading, polymer-clay interaction and processing conditions (Luo & Daniel 2003, Chen et al. 2008, Kiliaris & Papaspyrides 2010). The mixture of different structures is frequently found (Morgan & Gilman 2003, Ruiz-Hitzky & Van Meerbeek 2006, Kiliaris & Papaspyrides 2010).

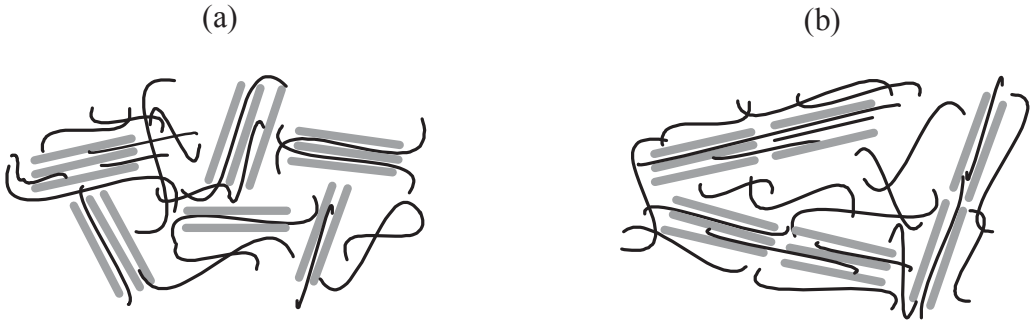

Figure 4.10. Schematic of (a) intercalated and (b) flocculated composite structure (Sinha Ray & Okamoto 2003)

The resulting intercalation structure is a regular multilayered arrangement of alternating polymeric and inorganic layers with a repeat distance between them (Giannelis 1996, Carrado 2000, Zanetti, Lomakin & Camino 2000, Biswas & Ray 2001, Sinha Ray & Okamoto 2003, Lagashetty & Venkataraman 2005, Pavlidou & Papaspyrides 2008, Kim & Palomino 2011, Albdiry et al. 2013). The intercalated nanocomposites can be sorted into intercalated and flocculated structures (Sinha Ray & Okamoto 2003, Chen et al. 2008). In the flocculated structure, the stacked silicate layers are connected though hydroxylated edge-by-edge interaction of the silicate layers and the intercalation of the long molecular chains into two or more clay galleries (Figure 4.10) (Sinha Ray & Okamoto 2003). The presence of single and several linked layer stacks in the intercalated

structures, as well as intercalated and exfoliated layers in the nanocomposites, is common and can be caused by the processing conditions, such as the incomplete adsorption and intercalation and insufficient dispersion (Morgan & Gilman 2003, Chen et al. 2008). Although the miscibility and properties of the intercalated structure is inferior to the exfoliated nanocomposites, the physical, mechanical and thermal properties can be improved and the electrostatic interaction between platelets is reserved in the intercalation structure (Giannelis 1996, Zanetti, Lomakin & Camino 2000, Albdiry et al. 2013).

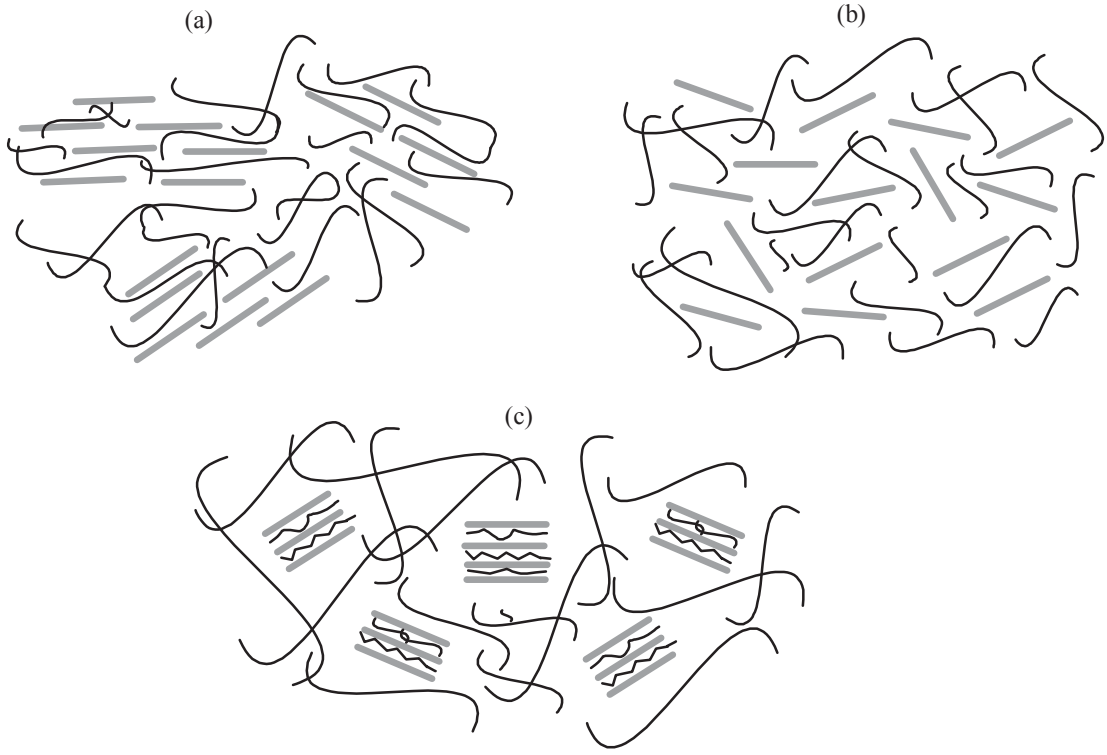

Figure 4.11. Schematic representation of (a) ordered, (b) disordered and (c) semi-exfoliated nanocomposites (LeBaron, Wang & Pinnavaia 1999, Carrado 2000)

The complete separation of 1 nm-thick clay layers can be achieved when the individual silicate layers are well dispersed as a single clay platelet in a continuous polymer matrix and there is no interaction between the adjacent layers (LeBaron, Wang & Pinnavaia 1999, Tolle & Anderson 2002, Biswas & Ray 2001, Sinha Ray & Okamoto 2003, Lagashetty & Venkataraman 2005, Ruiz-Hitzky & Van Meerbeek 2006, Pavlidou & Papaspyrides 2008, Natkański et al. 2012, Albdiry et al. 2013). The silicate layers that are dispersed in either an ordered or disordered manner or semi-exfoliated structure in which the small layer

stacks are intercalated by polymers and dispersed (Figure 4.11) (LeBaron, Wang & Pinnavaia 1999, Carrado 2000, Chen et al. 2008). It can take full advantage of the polymer-clay interactions and the entire surface of the layers is made available to the polymer (Pavlidou & Papaspyrides 2008). Significant improvements in the physical, barrier and mechanical properties of the composite can be attained by using an exfoliated structure that is considered more favourable (Carrado 2000, Biswas & Ray 2001, Pavlidou & Papaspyrides 2008, Natkański et al. 2012). Such exfoliated structure produces light, transparent and non-fragile materials (Natkański et al. 2012). Exfoliated nanocomposite is formed by the much lower clay content than that of intercalated structure (LeBaron, Wang & Pinnavaia 1999, Boulet et al. 2003, Sinha Ray & Okamoto 2003, Morgan & Gilman 2003, Pomogailo 2005). It is difficult to produce fully exfoliated silicate layers, owing to electrostatic attraction between silicate layers and interlayer cations and the formation of consistently oriented particles presents a real challenge

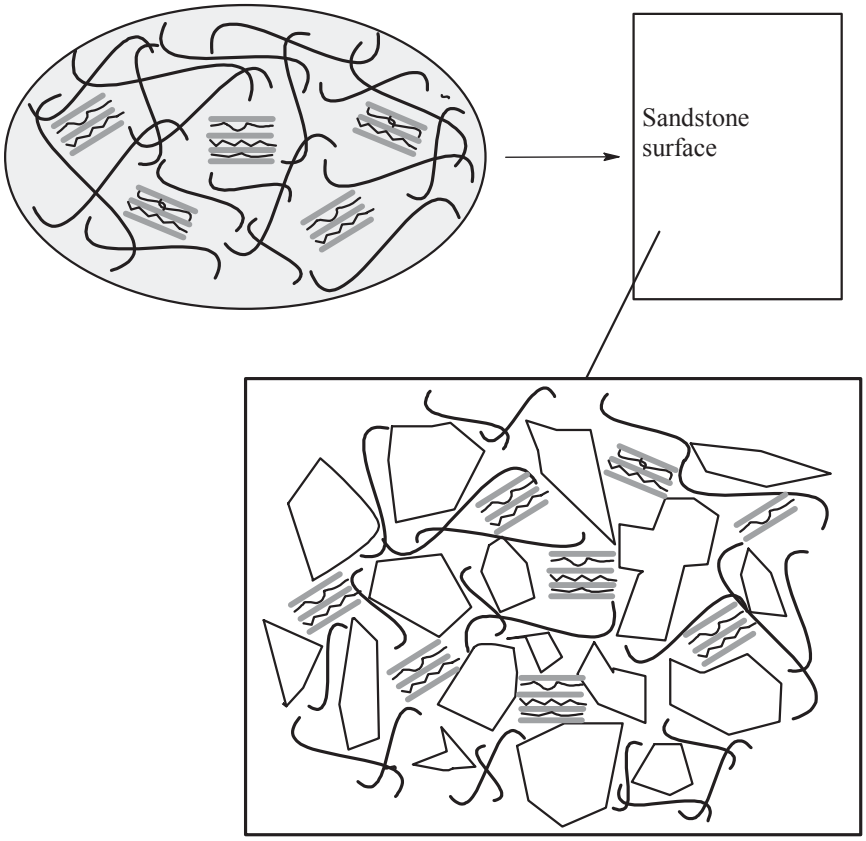

Figure 4.12. Schematic drawing of structural model designed for consolidation work of Sydney sandstone

(Ruiz-Hitzky & Van Meerbeek 2006, Pavlidou & Papaspyrides 2008). Depending on external factors, such as temperature and pressure, the equilibrium condition is influenced and the exfoliated state can be converted back to intercalated arrangement or microstructure under the thermodynamically unfavourable or unstable condition (Ruiz-Hitzky & Van Meerbeek 2006, Manias et al. 2007).

Much work in the literature on the development of polymer-MMT composites that are prepared using low clay content in order to enhance the polymer properties can be found (Lagashetty & Venkataraman 2005). In contrast, the primary interest in this study is in the development of hydrophilic polymer-MMT composites with high MMT content employed to retard the deterioration rate of sandstone heritage buildings and to meet the need for producing more compatible and stable materials to consolidate deteriorating heritage buildings. Therefore, the synthesis of intercalated hydrophilic polymer-MMT composites at higher MMT loading levels is an effective approach for designing water-based consolidants, wherein the structure and properties of MMT are retained to some extent and the polymers present in the galleries remain to prevent the swelling of MMT. The polymer must intercalate into the MMT layered structure in order to inhibit any potential drying-wetting shrinkage-expansion cycles. The objective of this study is to prepare intercalated structure using a relatively high loading of MMT (20 to 50%) in the composites to act as both a physical cross-linking agent for the water soluble polymer and as an inorganic filler in the sandstone pore structure as illustrated in Figure 4.12.

4.3.3. Preparation methods of polymer-clay composites

Polymer-clay nanocomposites have been prepared from nearly all polymers belonging to different polymer systems, such as thermoplastic and thermoset polymers and water-soluble and organic solvent-soluble polymers (Akelah 1995, Alexandre & Dubois 2000, Sinha Ray & Okamoto 2003, Chen et al. 2008). The different kinds of polymer matrices include vinyl polymers, condensation polymers, Polyolefins and biodegradable polymers (Sinha Ray & Okamoto 2003). Based on the starting materials and processing methods, the preparation routes of polymer-clay nanocomposites can be broadly divided into the following: solution intercalation (Figure 4.13a), in situ intercalative polymerisation (Figure 4.13b) and melt intercalation (Figure 4.13c) (Sinha Ray & Okamoto 2003,

Ahmadi, Huang & Li 2004, Chen et al. 2008, Anandhan & Bandyopadhyay 2011). The intercalation of a variety of hydrophobic materials requires the pre-treatment of MMT to convert hydrophilic MMT to organophilic MMT (Ruiz-Hitzky & Van Meerbeek 2006). The chemical modification of untreated MMT generally involves the cationic exchange reaction between interlayer cations with organic cationic surfactants, such as the alkylammonium ion or through a grafting reaction (Sinha Ray & Okamoto 2003, Ruiz-Hitzky & Van Meerbeek 2006). The hydrophilic polymers or monomers, on the other hand, can be directly intercalated into pristine MMT, as unmodified MMT is hydrophilic and miscible with hydrophilic polymers (Sinha Ray & Okamoto 2003, Ruiz-Hitzky & Van Meerbeek 2006, Chen et al. 2008, Pavlidou & Papaspyrides 2008). The preparation technique is critical to the nanostructure formation and important characteristics, such as mechanical properties (Albdiry et al. 2013).

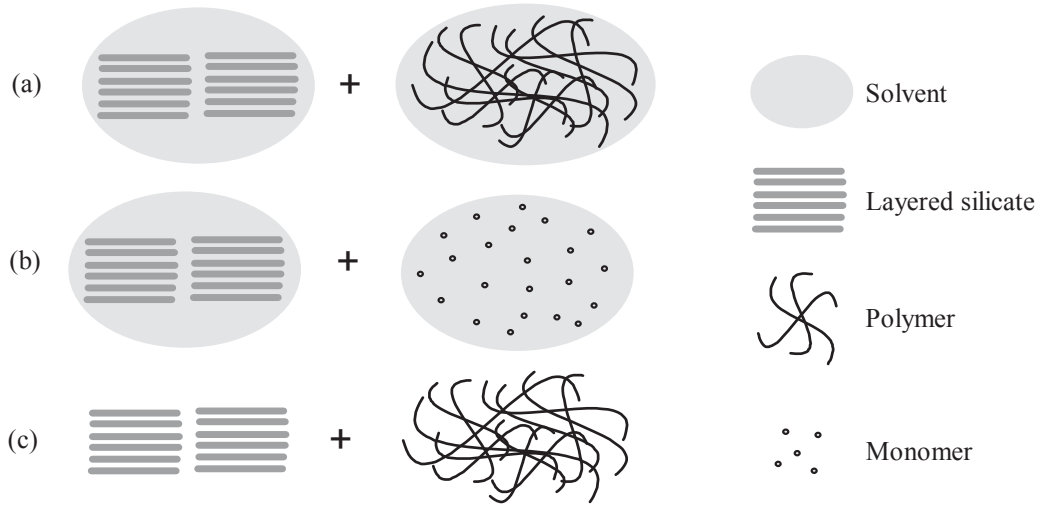

Figure 4.13. Schematic drawing of preparative techniques for polymer-MMT composite systems used in consolidation work of Sydney sandstone

Polymer-clay nanocomposites may be prepared through the melt intercalation method, in which the layered silicate mixed with the thermoplastic polymer matrix is annealed under shear above the glass transition temperature of the polymer and the penetration of the polymer can occur from the molten polymer to the interlayer of the layered silicate (Giannelis 1996, Alexandre & Dubois 2000, Zanetti, Lomakin & Camino 2000, Ahmadi, Huang & Li 2004, Pavlidou & Papaspyrides 2008, Kiliaris & Papaspyrides 2010). Melt intercalation methods are generally applied to improve the performance of polymer rather than clay mineral (Kim & Palomino 2011). Melt intercalation also offers advantages over

the in situ intercalative polymerisation and intercalation of polymer from solution methods (Shen, Simon & Cheng 2003, Sinha Ray & Okamoto 2003, Pavlidou & Papaspyrides 2008, Kiliaris & Papaspyrides 2010, Albdiry et al. 2013) as melt compounding is a solvent-free method, it is more cost-effective, environmentally friendly and simpler than the in situ polymerisation and solution intercalation methods (Shen, Simon & Cheng 2002, Sinha Ray & Okamoto 2003, Pavlidou & Papaspyrides 2008, Kiliaris & Papaspyrides 2010, Albdiry et al. 2013). Melt intercalation is a promising method for the industrialization of nanocomposite technology (Pavlidou & Papaspyrides 2008). Moreover, this technique can be utilized to prepare nanocomposites from polymers and clays that are not appropriate for the other methods (Sinha Ray & Okamoto 2003).

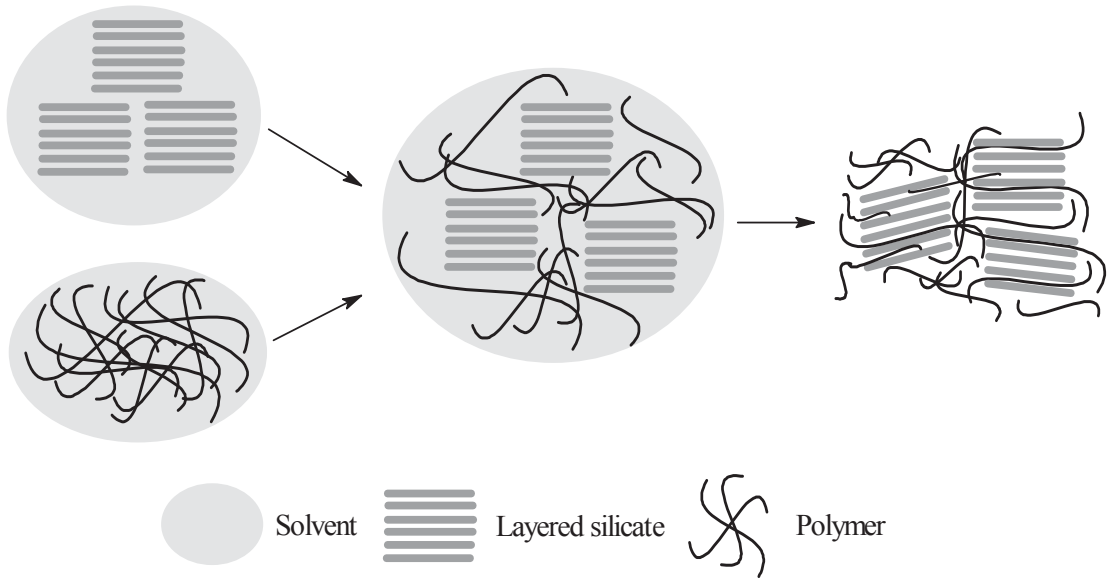

Figure 4.14. Solution intercalation of polymer

For intercalation of polymer from solution, a solvent (in which the polymer is soluble and the layered silicate is swellable) is used to mix the clay and polymer together (Figure 4.14) (Alexandre & Dubois 2000, Sinha Ray & Okamoto 2003, Kiliaris & Papaspyrides 2010, Anandhan & Bandyopadhyay 2011, Albdiry et al. 2013). In this method, the clay is expanded in a solvent before being mixed with the polymer and the polymer-clay composite is obtained when the solvent is removed from the mixture via solvent evaporation or polymer precipitation (Alexandre & Dubois 2000, Sinha Ray & Okamoto 2003, Kiliaris & Papaspyrides 2010, Anandhan & Bandyopadhyay 2011, Albdiry et al. 2013).

The solvent used for the solution intercalation method facilitates the mobility and thus intercalation of dissolved polymers (Anandhan & Bandyopadhyay 2011). It has been suggested that the intercalation of the polymer can occur by spontaneous displacement of the solvent present in the gallery of the layered silicates for which negative variation in the Gibbs free energy is required (Akelah 1995, Zanetti, Lomakin & Camino 2000, Sinha Ray & Okamoto 2003). The entropy gained by desorption of interlayer water compensates for the reduced total entropy of the intercalated polymers and is the major driving force for solution intercalation of polymer (Vaia & Giannelis 1997, Biswas & Ray 2001).

The solution intercalation has been used for a variety of polymers in both aqueous and non-aqueous solvents (Zanetti, Lomakin & Camino 2000, Sinha Ray & Okamoto 2003, Pomogailo 2005). This method has been applied to intercalate polar polymers directly to smectites in polar solvents, including water and methanol, through the formation of hydrogen bonding between the polymers and clay mineral surface (Sinha Ray & Okamoto 2003, Ruiz-Hitzky & Van Meerbeek 2006, Chen et al. 2008). Direct solution intercalation showed successful intercalation of water soluble polymers including polyvinyl alcohol and PEG, PAm and chitosan (Alexandre & Dubois 2000, Strawhecker & Manias 2000). Physical and mechanical properties of composite system can be improved by such direct intercalation of polymer, thus offering significant understanding of the polymer adsorption process (Pomogailo 2005). The nanofillers in the solution are frequently dispersed by the ultrasonication technique, which has been considered to be effective to deagglomerate and disperse clay assemblies (Manias et al. 2007).

From a practical and industrial viewpoint, the need of the plentiful amount of solvent and disposal is a concern and the use of solution intercalation has been limited (Zanetti, Lomakin & Camino 2000, Biswas & Ray 2001, Shen, Simon & Cheng 2002, Sinha Ray & Okamoto 2003, Ahmadi, Huang & Li 2004). Especially, the use of organic solvent is unfavourable from the economic and environmental standpoint (Zanetti, Lomakin & Camino 2000, Pomogailo 2005). Additionally, desorption of the solvent is necessary in order to acclimatise the entered polymer chains in the MMT galleries (Biswas & Ray 2001). The solution intercalation process depends considerably on the various preparation conditions, such as polymer solution concentration, clay mineral, pH, polymer molecular

weight, solvent, temperature and processing time (Sinha Ray & Okamoto 2003). Due to the interaction between polymer and solvent, the dispersion of clay is restricted for many solvent-polymer pairs (Kiliaris & Papaspyrides 2010, Albdiry et al. 2013). It is important to consider the effects of experimental conditions on the solution intercalation process and the interaction with solvent (Kim & Palomino 2011). The advantage of the solution intercalation technique is its simplicity and generally does not require extra heat treatment (Alexandre & Dubois 2000, Sinha Ray & Okamoto 2003, Kiliaris & Papaspyrides 2010, Anandhan & Bandyopadhyay 2011, Kim & Palomino 2011). The solvent removal results in a thin film and this technique has been applied to produce coating, adhesives and films (Sinha Ray & Okamoto 2003, Anandhan & Bandyopadhyay 2011).

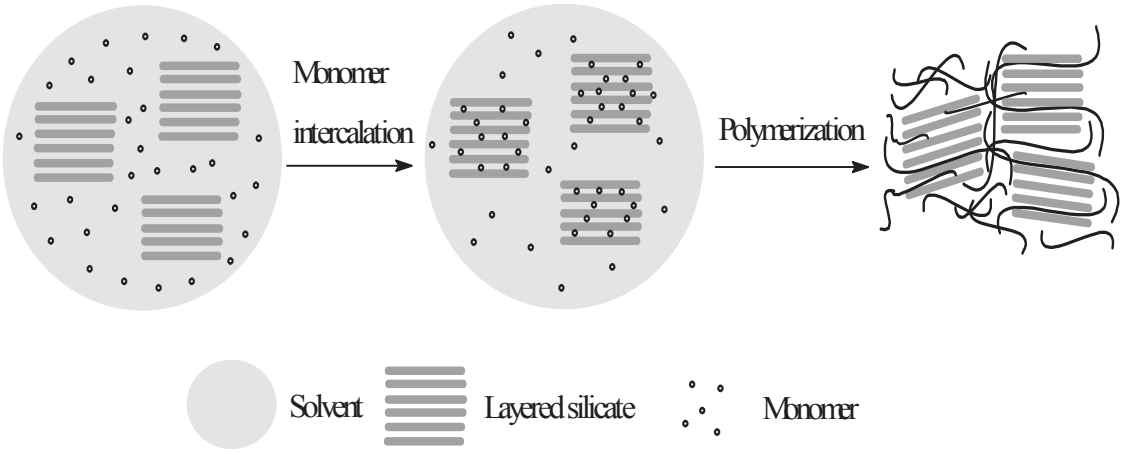

Figure 4.15. Composite preparation of in situ polymerisation

Intercalation can also be achieved through in-situ polymerisation. A monomer solution is intercalated into the interlayer space and polymerisation occurs within the interlayer space of the layered silicates (Figure 4.15) (Akelah 1995, Alexandre & Dubois 2000, Zanetti, Lomakin & Camino 2000, Biswas & Ray 2001, Sinha Ray & Okamoto 2003, Ruiz-Hitzky & Van Meerbeek 2006, Pavlidou & Papaspyrides 2008, Kiliaris & Papaspyrides 2010, Anandhan & Bandyopadhyay 2011). Marked interlayer expansion occurs when the strong interaction between intercalated monomer and solvent and the intercalated solvent serves to increase wetting and diffusion of monomers (Biswas & Ray 2001). A variety of polymers have been successfully formed through the various polymerisation reactions, such as bulk, emulsion and suspension polymerisation (Giannelis 1996, Manias et al. 2007). The initiation of the polymerisation reaction of a monomer can be achieved by

heat treatment, radiation or the penetration of a suitable initiator or catalyst in the interlayer space (Alexandre & Dubois 2000, Biswas & Ray 2001, Pomogailo 2005, Pavlidou & Papaspyrides 2008). Due to the better penetrating ability of smaller monomer into interplatelet space than the larger polymer chains, the in situ intercalative polymerisation method is more effective and more thermodynamically favourable to attain better nano-dispersion and delamination of silicate layers in comparison to melt and solution polymer intercalation methods (Manias et al. 2007). The disadvantage of using the in situ polymerisation technique is the additional preparation steps required for the application of heat or radiation that are economically and practically favourable in a large-scale environment (Kim & Palomino 2011).

Although the melt intercalation technique possesses some attractive features not present in the solution method, the consolidating material applied must be in liquid form and thus, the intercalation of polymers from solution method is more appropriate. For this reason, the synthetic routes to the polymer-MMT composites were constrained to the intercalation of water-soluble polymers or monomers from water. In addition to the consolidants produced from preformed water-soluble polymers, in situ polymerised consolidating systems are an alternative approach, with the aim of improving the penetration depth and overcoming the limited penetration of polymers in the stone. Accordingly, two synthetic strategies for developing water-based consolidants are based on the use of preformed and in situ polymerised polymers, which can lead to the development of more effective, compatible, reversible, innocuous and economical stone consolidants for treating the sandstone of Sydney's heritage buildings.

4.4. Intercalation of MMT

4.4.1. Intercalation of MMT by hydrophilic polymers

In contrast to the hydrophobic polymers, the hydrophilic polymers or monomers are miscible with pristine MMT and superior dispersion of MMT is achievable in hydrophilic polymers (Sinha Ray & Okamoto 2003, Pavlidou & Papaspyrides 2008, Ruiz-Hitzky & Van Meerbeek 2006, Chen et al. 2008). The polarity of the polymer is essential in governing the structure at nanoscale and the hydrophilic polymers are compatible with

surface polarities of MMT due to the presence of polar side groups of hydrophilic polymers (Sinha Ray & Okamoto 2003). The silicate layer separation is very different for polar and nonpolar polymers and the better separation of filler generally can be obtained for the former due to the similar polarity and the better interfacial interaction of polar polymers to the polar surface of the MMT (Mittal 2010). The absorption of hydrophilic molecules is facilitated in the presence of the dipolar or van der Waals forces between silicate layers (Gao 2004). The polar molecules interact with inorganic solids though electrostatic and noncoulombic forces, such as Van der Waals, hydrogen bonding, ion-dipole, coordination and electron transfer (Ruiz-Hitzky 2003).

The extensive studies to understand the mechanism responsible for polymer-clay mineral interaction and intercalation/exfoliation and adsorption of polymer has been performed and reviewed by Theng (1982) (Theng 1982, Akimkhan 2013). The bonding interaction between polymer and clay minerals is very complex and the intercalation and exfoliation processes are not fully understood at the molecular level (Boulet et al. 2003, Bae & Inyang 2006, Akimkhan 2013). Due to the long, flexible, polyfunctional and multisegment nature of polymers, the different conformations can be adapted and various interactions between the multiple polymer segments, solvent and mineral surface are formed (Stuart, Scheutjens & Fleer 1980, Theng 1982, Nadler, Malik & Letey 1992). The intercalation and adsorption process of polymer chains are also affected by accessibility, solubility, steric hindrance and the order and way to combine the different components are accompanied by the conformational changes from the random coil chains in the solution to variable extended shapes at polymer-solid interface (Theng 1982). The polymer adsorption is practically irreversible due to low likelihood of the simultaneous detachment of all adsorbed segments and slow desorption rate of polymer (Stuart, Scheutjens & Fleer 1980, Theng 1982).

The processes and interaction associated with the intercalation and adsorption are affected by the polymer charges and the behaviour of uncharged polymers differ from the polyelectrolyte chains (Theng 1982). In the case of uncharged chains that are intercalated and adsorbed from aqueous solution, the interlayer water plays an important role in adsorption of large uncharged molecules and the driving force for the solution intercalation of uncharged polymers is often believed to be the entropic gain resulting

from desorption of interlayer water, although Chen and Evans (2005b) demonstrated that PEG was intercalated to dehydrated smectite (Parfitt & Greenland 1970a, Parfitt & Greenland 1970b, Chen & Evans 2005b). In addition to entropy gain due to the desorption of water from the clay surface, unfavourable entropy loss resulting from the polymer intercalation can be compensated by increased number of intercalated polymer (Biswas & Ray 2001). The uncharged polymer molecules is sorbed, depending on surface accessibility, entropy effects, the interaction between the functional group and the exchangeable cation and nearest-neighbour interactions and tends to be randomly coiled in aqueous solution (Theng 1982, Inyang & Bae 2005). To offset the reduced conformational energy opposing polymer intercalation, multiple segment-clay contacts must be formed and the rotational and translational motion of the polymer should be inhibited by these interactions (Biswas & Ray 2001). The adsorption energy may possibly arise from hydrogen bond between the hydrated exchangeable cations and the organic molecules with water bridge formation (Parfitt & Greenland 1970a, Parfitt & Greenland 1970b).

The charged polymers are mainly attached through the long-range electrostatic interactions and the interaction of charged polymers are complicated by the other effects, such as pH and ionic strength of the solution, in addition to the aforementioned effects subjected to uncharged chains (Theng 1982, Akimkhan 2013). The polycations and negatively charged clay surface interact through electrostatic force and the absorption of positively charged organic matters occurs due to an exchange reaction with the interlayer exchangeable cation (Theng 1982, Inyang & Bae 2005). On the other hand, the negatively charged polymers and clay surface are likely to repel each other and the little adsorption of polyanions on the clay surface occurs, unless the negative charges of polyanions are neutralized under such settings, like acid conditions and high ionic strength (Theng 1982, Inyang & Bae 2005). In contrast to neutral or positively charged polymers, the polyanions are not intercalated into the interlayer space and attached onto the clay crystal edges that are positively charged under acid pH condition and interact through the electrostatic interactions with the negative charges of the polyanions (Theng 1982, Inyang & Bae 2005).

Understanding the binding mechanisms operated on polymer-clay interaction associated

with the formation of clay containing polymers is an important topic for many water-based systems and their practical application in agricultural, industrial and chemical technology (Theng 1982, Nadler, Malik & Letey 1992). The particular interest to this research is the inhibitory properties of water soluble polymers and stability of swellable MMT. The expansion of clay mineral can be inhibited by the use of suitable materials that can be intercalated to the interlayer space of clay minerals and bind particles of clay minerals together (Inyang & Bae 2005, Deng et al. 2006, Inyang et al. 2007, Anderson et al. 2010). Water soluble polymers may function as inhibitors and the intercalated polymers can prevent the entry of water due to hydrophobic portion and the interaction between hydrated interlayer cations and hydrophilic portion of polymers (Anderson et al. 2010). Because of the intricate and heterogeneous nature of clay minerals, the improvement of practical and environmental performance of swelling inhibitors has been a challenge (Anderson et al. 2010). Although both uncharged and charged water soluble polymers have been studied as swelling inhibitor to design the water based system, the polyelectrolytes are extended in solutions due to intra-molecular charge repulsion and known to be a more effective flocculating agent to stabilize and to form clay aggregates (Inyang & Bae 2005, Anderson et al. 2010). The concern of this work is the inhibition process by which the intercalated polymers can reduce interlayer hydration and the presence of uncharged and hydrophilic water-soluble polymers, PAA, PAm and PEG can act as intercalating agent, swelling inhibitor and stone consolidant.

4.4.2. Intercalation of MMT by PAA

PAA is one of the most important hydrophilic water-soluble polymers and PAA-containing products have been explored for use in a broad range of application fields, including personal care, adhesives, coatings, synthetic fibres and pharmaceuticals (Kabanov, Dubnitskaya & Khar'kov 1975, Dong, Ozaki & Nakashima 1997a, Dong, Ozaki & Nakashima 1997b, Çatalgil-Giz et al. 2004). PAA-clay composites have been previously investigated for their absorbance properties and the preparation of PAA-intercalated MMT was performed by few research works, which showed the direct intercalation of PAA into MMT via the solution mixing method using water as a polar solvent (Billingham, Breen & Yarwood 1997, Tran et al. 2005, Trans et al. 2006, Ip 2007). The work done by Trans et al. demonstrated temperature dependent adsorption of PAA

onto MMT interlayer distance and improved extent of MMT layer separation with increasing temperature from 20 to 85°C (Tran et al. 2005, Trans et al. 2006). Their results, gained using conventional stirring method, showed the reaction temperatures up to 60°C produced the intercalated structure with the interlayer distance up to 20Å, while the temperature 80°C formed a mixed structure having both exfoliated and intercalated layers. Ip prepared the PAA-intercalated MMT composites at a wide range of clay content from 10 to 90% using water bath sonication method for dispersion of MMT and PAA in water (Ip 2007). The interlamellar spacings (d001) data indicated the interlayer separation to form intercalated PAA-MMT composites and the interlayer distance progressively increased up to 30-40% PAA. The interlayer distance of MMT was not increased much beyond 30-40% PAA and this concentration range was identified as the saturation point corresponding to the maximum absorption of PAA was attained (Ip 2007). Morphological analyses of PAA-MMT composite containing 20% MMT using AFM showed the clay particles of different sizes, orientation and degree of embedment were well distributed with similar separation distance between particles in the polymer matrix. Additionally, Billingham et al. investigated polymer charge influence on the nature and extent of adsorption, the interaction of PAA to a clay mineral surface and absorption and desorption behaviors of water soluble polymers on the MMT surface and the penetration of single PAA was reflected by the MMT layer distance of 14.6Å in the PAA-MMT films with 2 and 5 % MMT contents formed after the dispersions were shaken at room temperature for 2 hours (Billingham, Breen & Yarwood 1997). Their study showed the protonated form of PAA in the dried films was exchanged by cationic polymer that apparently interacted more strongly with MMT.

4.4.3. Intercalation of MMT by PAm

PAm is also one of non-ionic and a significant technical and applicable polymers because of its water solubility, hydrophilicity, colourless, availability, non-toxicity and low cost (Kulicke, Kniewske & Klein 1982, Gao & Heimann 1993, Lu & Wu 2002, Anderson et al. 2010, Lu, Shan & Shang 2010, Bhat et al. 2014, Koç et al. 2014). It has been extensively used as an effective flocculant, swelling inhibitor and stabilizer in wastewater treatment, sludge dewatering, drilling fluids, enhanced oil recovery and soil stability (Bottero et al. 1988, Lu & Wu 2002, Bolto & Gregory 2007, Bhat et al. 2014, Huang &

Ye 2014b). The sorption of PAm onto clay mineral surfaces is a significant process for the systems in which clay mineral interact with PAm and a number of works have studied the properties, mechanisms, interaction and forces involved in PAm sorption to search optimal condition of each use (Yan & Zhang 2014).

Although the understanding of the bonding mechanisms between PAm and clay mineral is important for the reactions and interaction involved in the sorption process of PAm and improvement of the efficiency of PAm on the properties of clay mineral for intended application, the mechanisms responsible for the intercalation of PAm and polymerisation of Am into MMT is not well known (Gao & Heimann 1993, Deng et al. 2006, El-Zahhar, Abdel-Aziz & Siyam 2007). The literature dealing with interactions of MMT and PAm can be bonded to clay minerals through the interaction originated from (1) van der Waals and hydrogen bonding of acrylamide group with surface oxygen and hydroxyl groups of crystal edges, (2) ion-dipole interaction with interlayer cations, (3) protonation of PAm that can involve ion exchange reaction with interlayer cations or ionic bonding with negative MMT surface, (4) hydrophobic effect of carbon backbones or hydrophobic parts of PAm and (5) water bridging formation with hydrated interlayer cations of MMT (Greenland 1963, Pefferkorn 1999, Bottero et al. 1988, Ogawa, Kuroda & Kato 1989, Volpert et al. 1998, Güngör & Karaoğlan 2001, Ulusoy, Şimşek & Ceyhan 2003, Mpofu, Addai-Mensah & Ralston 2004, Mpofu, Addai-Mensah & Ralston 2005, Deng et al. 2006, El-Zahhar, Abdel-Aziz & Siyam 2007, Li & Gao 2011, Kurochkina & Pinskii 2012, Akimkhan 2013, Natkański et al. 2013, Huang & Ye 2014a, Huang & Ye 2014b). It is unlikely for hydroxyl group of PAm to form hydrogen bond with the basal tetrahedral oxygens of siloxane surface, which are weak electron donors (Deng et al. 2006).

The literature included the intercalation of PAm through either the solution intercalation of PAm or in situ intercalative polymerisation of Am. In the former method, the intercalation of non-ionic, cationic or anionic homopolymer or cationic copolymer has been investigated (Durand-Piana, Lafuma & Audebert 1987, Bottero et al. 1988, Güngör & Karaoğlan 2001, Churchman 2002, Inyang & Bae 2005, Deng et al. 2006, Inyang et al. 2007, Wang et al. 2010, Kim & Palomino 2011, Huang & Ye 2014b). The latter method was used to prepare homopolymer or copolymers of PAm and the polymerisation of Am initiated by UV irradiation, gamma radiation, electron-beam irradiation, heat treatment

and redox initiators (Ogawa, Kuroda & Kato 1989, Gao & Heimann 1993, Biasci et al. 1995, Yeh et al. 2004, El-Zahhar, Abdel-Aziz & Siyam 2007, Long et al. 2007, Dangge et al. 2009, Helvacıoğlu et al. 2011, Li & Gao 2011, Koç et al. 2014, Huang & Ye 2014a). Their studies as to the effects of various physicochemical factors on the extent of PAm intercalation indicated the influential parameters including molecular weight of PAm, cationicity, clay mineral content and pH but insignificant impact of exchangeable cations and temperature. The work of Durand-Piana et al. (1987), Ogawa et al. (1989), Yeh et al. (2004) and Kim & Palomino (2011) demonstrated the strong dependence of intercalation degree of PAm or Am on MMT concentration. Churchman (2002), Ogawa et al. (1989) and Koç et al. (2014) showed the extent of PAm/Am intercalation increased with increasing PAm/Am concentration until a distinct plateau corresponding to the maximum interlayer expansion.

Similar effects of MMT concentration was reported for the adsorption studies of PAm-MMT systems, which are investigated by their adsorption isotherms and kinetics of non-ionic, cationic or anionic homopolymers or copolymers or hydrolyzed or hydrophobic PAm (Yan & Zhang 2014). Whereas the considerable effects of charges and molecular weight of PAm and interlayer exchangeable cations on the degrees of PAm adsorption and flocculation were reported by the studies of Yan and Zhang (2014), irreversible adsorption of PAm was observed, regardless of the nature of PAm (Yan & Zhang 2014). The increase of adsorption extent and flocculation power of PAm onto sodium saturated MMT was reported in the order non-ionic > cationic > anionic and cationic > non-ionic > anionic correspondingly (Yan & Zhang 2014).

4.4.4. Intercalation of MMT by PEG

Many studies have reported on the solution intercalation of the homopolymer or copolymer of PEG by using water onto homoionic MMT (Burchill et al. 1983, Billingham, Breen & Yarwood 1997, Vaia et al. 1997, Shen, Simon & Cheng 2002, Rossi, Luckham & Tadros 2003, Chaiko 2003, Strawhecker & Manias 2003, Boulet et al. 2003, Chen & Evans 2005a, Reinholdt, Kirkpatrick & Pinnavaia 2005, Su & Shen 2008, Zampori et al. 2010, Krzaczkowska et al. 2010, Cui & van Duijneveldt 2010, Lombardo et al. 2013, Sengwa & Choudhary 2014, Shami et al. 2014, Choudhary & Sengwa 2014, Zhao et al.

2014, Clegg, Breen & Khairuddin 2014, Sengwa, Choudhary & Dhatarwal 2015). The literature shows the intercalation of PEG via melt intercalation, microwave irradiation, solvent-free sonication-assisted intercalation and in situ polymerisation technique (Parfitt & Greenland 1970b, Pusino et al. 1990, Vaia et al. 1997, Liao et al. 2001, Shen 2002, Rossi, Luckham & Tadros 2003, Shen, Simon & Cheng 2003, Aranda et al. 2003, Ratanarat et al. 2003, Chen & Evans 2005a, Chen & Evans 2005b, Reinholdt, Kirkpatrick & Pinnavaia 2005, Hikosaka et al. 2006, Kim & Park 2007, Carretero-Gonzalez et al. 2008, Zhu, Chen & Li 2009, Thuc et al. 2010, Cui & van Duijneveldt 2010, Choudhary & Sengwa 2011, Thanh et al. 2012, Lombardo et al. 2013, Onder et al. 2013, Chrissopoulou et al. 2013, Derho, Soulestin & Krawczak 2014, Choudhary & Sengwa 2014, Erceg et al. 2014, Malathi & Tamilarasan 2014, Clegg, Breen & Khairuddin 2014). The solution method is advantageous because PEG intercalated via melt intercalation is prone to thermal PEG degradation (Ratna & Abraham 2011).

A water-soluble, linear, crystalline and non-ionic polymer, PEG is used as an intercalating agent. It is known for its unique characteristics, such as conductivity, environment friendliness, low melting point, film forming ability, non-toxicity, biodegradability and hydrophilicity–hydrophobicity character (Choi et al. 2001, Shen 2002, Rossi, Luckham & Tadros 2003, Chaiko 2003, Kim & Park 2007, Su & Shen 2008, Yahiaoui, Hachemaoui & Belbachir 2009, Belova et al. 2009, Sengwa, Choudhary & Sankhla 2009, Abraham et al. 2009, Sarier & Onder 2010, Chrissopoulou et al. 2011, Lombardo et al. 2013, Onder et al. 2013, Krishnan, Saharay & Kirkpatrick 2013, Choudhary & Sengwa 2014, Erceg et al. 2014, Sengwa, Choudhary & Dhatarwal 2015). The composites of PEG with MMT have been studied and developed for many applications, such as drilling fluids, thermal storage, organoclay, electrolytes and medical applications (Billingham, Breen & Yarwood 1997, Liao et al. 2001, Rossi, Luckham & Tadros 2003, Fan, Nan & Li 2003, Kim & Park 2007, Sengwa, Choudhary & Sankhla 2009, Sarier & Onder 2010, Zampori et al. 2010, Choudhary & Sengwa 2011, Thanh et al. 2012, Onder et al. 2013, Zhao et al. 2014, Sengwa, Choudhary & Dhatarwal 2015).

The reported works conducted on the intercalation or adsorption behaviours of PEG investigated the effects of various factors, such as preparation method, polymer molecular weight, synthesising temperature, MMT content, interlayer alkali metal and solvents

(Parfitt & Greenland 1970a, Billingham, Breen & Yarwood 1997, Shen, Simon & Cheng 2002, Chaiko 2003, Aranda et al. 2003, Rossi, Luckham & Tadros 2003, Boulet et al. 2003, Shen, Simon & Cheng 2003, Chen & Evans 2005a, Reinholdt, Kirkpatrick & Pinnavaia 2005, Hikosaka et al. 2006, Kim & Park 2007, Jeong et al. 2007, Krzaczkowska et al. 2010, Sarier & Onder 2010, Zampori et al. 2010, Lombardo et al. 2013, Zhu et al. 2013a, Onder et al. 2013, Chrissopoulou et al. 2013, Choudhary & Sengwa 2014, Erceg et al. 2014, Clegg, Breen & Khairuddin 2014). The interlayer absorption of PEG was reported to be enhanced with an increase in polymer molecular weight or by solution intercalation method (Parfitt & Greenland 1970b, Billingham, Breen & Yarwood 1997, Jeong et al. 2007, Choudhary & Sengwa 2014). Conversely, some studies indicated the insignificant effects of the preparation method and molecular weight on the intercalation of PEG/PEO (Billingham, Breen & Yarwood 1997, Chen & Evans 2005a). The solution or melt intercalation increased the MMT interlayer d001 with increasing PEG concentrations up to 15%–30% PEG (Aranda & Ruiz-Hitzky 1992, Wu & Lerner 1993, Boulet et al. 2003, Kim & Park 2007, Jeong et al. 2007, Carretero-Gonzalez et al. 2008, Zhu et al. 2013a, Erceg et al. 2014, Clegg, Breen & Khairuddin 2014).

While studies also reported the MMT proportion dependence of crystallisation behaviour and the conformation of polymer chains, these effects remain debatable (Hikosaka et al. 2006, Chrissopoulou et al. 2011, Zhu et al. 2013b). Theoretical, thermal, morphological and structural investigations identified the amorphous and/or crystallised PEG polymer of PEG-MMT composites as a result of the reduced crystallinity of intercalated and adsorbed PEG in the former state, the crystallised PEG outside of MMT galleries and the proposed helical, zigzag, crown-ether-like or random conformation of adsorbed or intercalated PEG (Aranda & Ruiz-Hitzky 1992, Wu & Lerner 1993, Aranda & Ruiz-Hitzky 1994, Lemmon & Lerner 1994, Hackett, Manias & Giannelis 1995, Giannelis 1996, Vaia et al. 1997, Aranda & Ruiz-Hitzky 1999, Bujdák, Hackett & Giannelis 2000, Kwiatkowski & Whittaker 2001, Strawhecker & Manias 2003, Sun et al. 2005, Elmahdy et al. 2006, Hikosaka et al. 2006, Suter & Coveney 2009, Lebovka et al. 2011, Chrissopoulou et al. 2011). Some studies showed the disordered structure of the intercalated PEO/PEG (Hackett, Manias & Giannelis 1995, Shen, Simon & Cheng 2002, Strawhecker & Manias 2003, Krishnan, Saharay & Kirkpatrick 2013, Zhu et al. 2013a). Based on the estimated size of the polymer, the interlayer distance of ~4.5Å can be

interpreted as a single zigzag chain conformation or flattened arrangements of the bilayer or helical structure at a low PEG content and a gallery size of ~ 8Å; where, the saturated PEG content corresponds to a two-layer zigzag conformation or a monolayer in helical conformation (Aranda & Ruiz-Hitzky 1992, Ruiz-Hitzky 1993, Shen, Simon & Cheng 2002, Strawhecker & Manias 2003, Reinholdt, Kirkpatrick & Pinnavaia 2005, Hikosaka et al. 2006, Zhu et al. 2013a). A published work showed the excellent compatibility and intercalation of PEG and suggested the formation of hydrogen bonding, the hydrophobic interaction between CH_2-CH_2 groups and siloxane surface and ion–dipole coordination acting as a driving force for the intercalation reaction (Parfitt & Greenland 1970b, Aranda & Ruiz-Hitzky 1992, Hackett, Manias & Giannelis 1995, Aranda & Ruiz-Hitzky 1999, Bujdák, Hackett & Giannelis 2000, Chaiko 2003, Hikosaka et al. 2006, Su & Shen 2008, Sengwa, Choudhary & Sankhla 2009, Lebovka et al. 2011, Choudhary & Sengwa 2014, Clegg, Breen & Khairuddin 2014).

CHAPTER 5. MATERIALS AND METHODS

5.1. Introduction

The present chapter describes experimental work carried out in the preparation and characterisation of stone consolidants and the development of the experimental setup for performance evaluation of consolidants applied to sandstone. For the preparation of stone consolidants, this work performed on polymer based consolidants and on consolidants which where the polymerisation occurred in situ. Four series of experiments were undertaken to determine the potential use of preformed and in situ formed polymers with and without MMT. The experiments were organized to investigate the effects of various parameters on the structural, morphological, thermal and interactional properties of prepared polymers and composites and to examine their actual contribution to consolidation performance on Sydney sandstone.

5.2. Materials

5.2.1. Materials for synthesis of sandstone consolidants

5.2.1.1. Hydrophilic polymer/monomer-MMT systems

PAA100 (100,000 g/mol, 250,000 g/mol, 35wt. % aqueous solution), PAA250 (250,000 g/mol, 35wt. % aqueous solution) and PAm (10,000 g/mol, 50wt. % aqueous solution) were supplied by Sigma Aldrich (Germany) and used as received without further purification. PEGs with an average molecular weight of 25,000 g/mol (PEG25) and 35,000 g/mol (PEG35) were used as received from Fluka. Am (Sigma Aldrich, India) and AA (Sigma Aldrich, USA, 99.9%) were selected as the two water soluble monomers and KPS (Sigma Aldrich, Germany, 99.99%) as initiator in this work. AA, Am and KPS were used as received, prior to a series of in situ polymerisation in MMT. All chemicals used as intercalating agents in this study were reagent grade.

The MMT used in this work was a purified sodium MMT provided by Arumpo Bentonite Pty Ltd, Australia. The fine MMT powder contained 3% w/w quartz and 1% w/w anatase.

The MMT was dried in an oven at 60°C to remove any trace of moisture and kept in a desiccator prior to its use. The well-dispersed MMT contained large silicate nanolayer stacks to form tactoids or microparticles in a size range between 500 nm and 75 μm according to SEM and particle size analysis. The MMT powder had a specific surface area of 166.3 m^2/g measured by nitrogen Brunauer Emmett Teller method. The elemental analysis for powder MMT was determined by X-ray fluorescence analysis and data analysed by the Mark Wainwright Analytical Centre of the University of New South Wales based on sample dried at 105°C are presented in Table 5.1. Distilled water (DW) was used as a solvent to prepare all dispersions of polymer and MMT and to conduct in situ polymerisation reactions.

Table 5.1. Physicochemical characteristics of MMT

Chemical analysis Oxides (wt. %)	SiO_2	50.85	Na_2O	1.30	P_2O_5	0.01	SrO	BLD
	Al_2O_3	16.34	K_2O	0.95	ZrO_2	0.01	ZnO	BLD
	MgO	3.98	TiO_2	0.46	CaO	0.03	BaO	BLD
	Fe_2O_3	3.71	SO_3	0.10	Cr_2O_3	0.02	PbO	BLD
	Mn_3O_4	0.01	NiO	0.01	L.O.I.	22.40		
	L.0.I. = loss on ignition at 1,050°C. BLD = below level of detection (<0.01%)							
Surface area (BET, Nz)	166.3 m^2/g							
Specific gravity	~ 2.3 g/cm^3							
Bulk density	1.12 $tonne/m^3$							
pH (2.5 wv aq %)	7.4 (nonacidifed MMT), 6.7 (acidified MMT (MMTa)							

5.2.1.2. Commercial stone consolidants

The commercial consolidants were selected from acrylic polymer and organosilicon compound in order to compare and evaluate their consolidating effects (Table 5.2). The acrylic polymeric materials used in this work were Lascaux 498 HV (Lascaux), Paraloid B72 (B72) and Paraloid B67 (B67) and were purchased from Preservation Australia (Newtown, Australia). Lascaux is a water soluble acrylic adhesive having a pH between 8 and 9. After drying, the colour turns from white to colourless and dried Lascaux is water

insoluble but remains soluble in acetone, toluene and xylene. Hydrophobic acrylic polymers tested in this work were B72 and B67. B72 in the form of colourless beads and was dispersed in acetone to use as a 20 ww% solution of B72 for application of B72 to sandstone samples. B67 was supplied as a 20% B67 in white spirits. SILRES® BS OH 100 (Silres) based on ethyl silicate (100 wt%) was kindly provided by IMCD Australia Limited and used as received. Silres is a colourless and solventless consolidant with 100 wt% ethyl silicate. All consolidants were used as received without any further purification.

Table 5.2. Commercial stone consolidants used in this work

Consolidant	Concentration (w/w %)	Colour of dried form
Lascaux 498 HV	20	Colourless
Paraloid B72	20	Colourless
Paraloid B67	20	Colourless
SILRES® BS OH 100	approx. 100 wt. %	Colourless

5.2.2. Sandstones for consolidation treatment

The consolidation treatment in this project was conducted on the unweathered Sydney sandstone and this work forms the consolidation treatment on an initial weathering stage of Sydney sandstone. Sydney yellow block sandstone under study was Pyrmont sandstone and was supplied by the NSW Department of Public Works and Services. The sandstone block used in this work was freshly quarried from the segment below sandstone surfaces exposed to atmosphere corresponding to the zone of surface weathering. The sandstone piece was light grey in colour with minerals spread in sandstone and stored in a dark place in the absence of sunlight. The sandstone specimens in small size with a very thin thickness were selected for increased number of testing specimens in order to produce the average of triplicate samples for enhancement of the reproducibility and the homogeneity of the consolidation treatment. Unweathered sandstone block was cut into rectangle specimens with 5 cm x 1.5 cm x 0.5 cm (l×w×t), which were treated with a series of stone consolidants and their consolidating performance were subsequently evaluated. All stone samples were washed with DW and left air-dried until equilibrium was obtained. In order

to remove traces of moisture, all sandstone samples were placed in an oven at 60°C to a constant weight prior to sandstone consolidation treatments.

5.3. Preparation of stone consolidants

5.3.1. Overview of experimental work for preparation of sandstone consolidants

This study adopted two preparation approaches: solution intercalation of preformed polymers and in situ intercalative polymerisation of water soluble monomers. A set of five composite systems were prepared to evaluate their characteristics and Figure 5.1 illustrates the procedure for the preparation and characterisation of stone consolidants for Sydney sandstone.

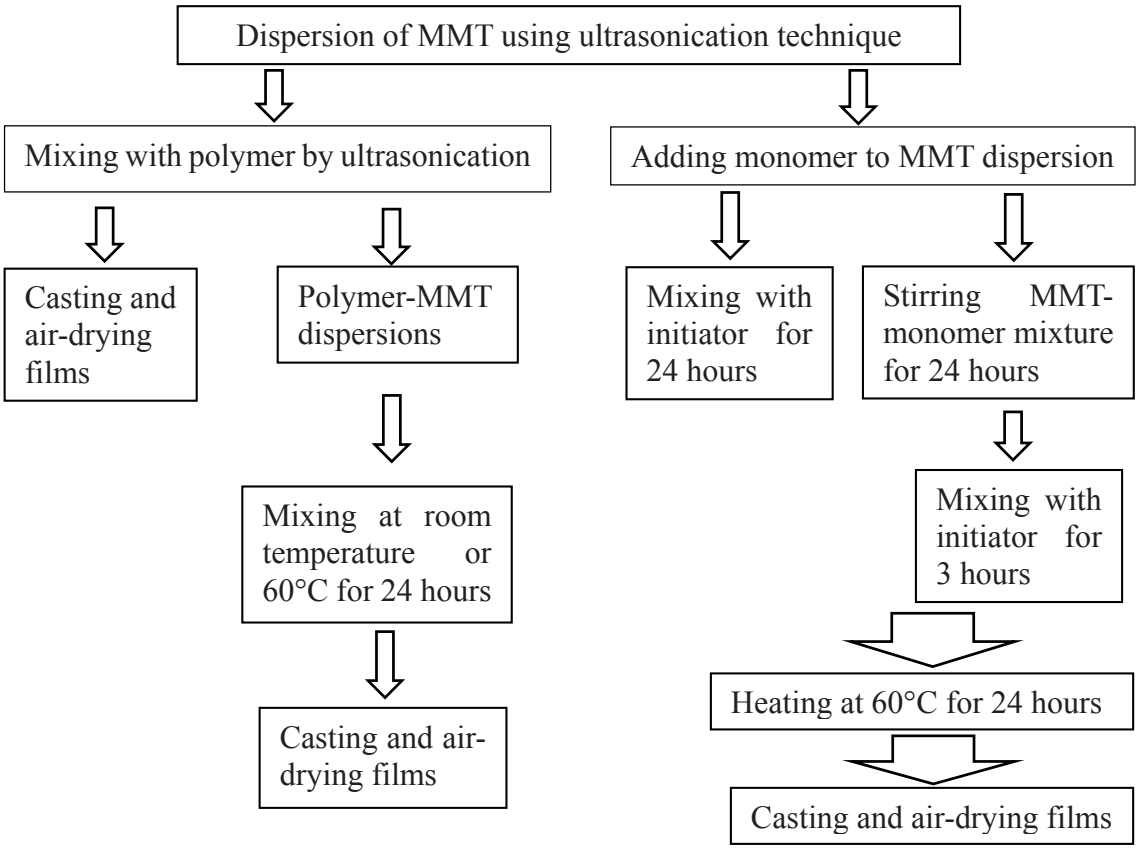

Figure 5.1. Flowdiagram shows the experimentalprocedure for stone consolidants produced from hydrophilic polymer or monomer and MMT prepared for Sydney sandstone

The preparation was initiated by dispersion and deagglomeration of MMT and this was followed by the addition of intercalating agents. The first preparation method used PAA, PAm and PEG as water soluble intercalating agents and produced PAA-MMT, PAm-MMT and PEG-MMT systems using aqueous solution intercalation technique. In the latter method, the water soluble AA or Am were first intercalated and polymerised in the presence of water soluble KPS initiator. This method sought to study the potential consolidation treatment of sandstone using AA-MMT and Am-MMT systems which can be penetrated to and polymerised within untreated sandstone. The present work has also included determinations of the effects of temperature, processing time, polymer molecular weights and acidity of MMT upon the sorption of polymers by MMT.

5.3.2. Acid-treatment of MMT

5.3.2.1. Acid-modification of MMT

Acid-treatment of clay minerals has been extensively studied for commercial and scientific uses, such as commercial catalysts and as oil decolourizers (Moronta 2004, Komadel & Madejová 2013). A great number of experimental studies have demonstrated chemical and structural modification of clay minerals after the acid treatment and such changes were found from surface area, decolouring capacity, acidity and porosity (Moronta 2004, Komadel & Madejová 2013). The reported results on acid activation treatments, which included data obtained for a variety of clay mineral and bentonite, documented that acidification processes caused disaggregation of clay particles, removal of mineral impurities, elimination of metal-exchange cations, proton exchange, colour removal capacity and enhanced surface accessibility. The surface properties of clay mineral can be affected by the nature of exchangeable ions and the acid modification was employed as an effective means to improve sorption capacity of polymers and enhance surface accessibility of MMT (Akimkhan 2013).

The acidification processes involved reacting clay minerals with a solution of mineral acid. The acid treatment proceeds with the initial replacement of exchangeable interlayer cations of clay minerals by protons of the activating acids, which can occupy the interlayer area and also enter into the layer structure (Komadel & Madejová 2013). The

penetrated protons undergo interlayer and edge attack on the structural hydroxyl groups and bonding between oxygen and cations and the cations from such broken bonds can be leached into the exchangeable positions, due to the dissolution of octahedral and tetrahedral sheets with the subsequent release of the octahedral cations and tetrahedral aluminium ion (Komadel 2003, Steudel et al. 2009, Komadel & Madejová 2013). The acid-treatment can partially destruct the crystal lattice with the gradual conversion of the tetrahedral sheets into three-dimensional SiO_4 structure and the acid-treatment products can include unaltered layers and amorphous, porous, protonated and hydrated silica, depending on condition and extent of acid treatment and type and chemical compositions of clay mineral (Tkac, Kodamel & Müller 1994, Komadel & Madejová 2013).

As for many applications for which the complete destruction of MMT is unwanted, the acidification of MMT under mild condition is more desirable for the preparation of acidified MMT modified without significant structural changes. The composition of the untreated clay minerals is significant for the determination of the extent of acidification treatment required for the optimised acid-modification and resistance of silicate layers against acid attack (Komadel & Madejová 2013). In comparison to the trioctahedral layers that showed faster dissolution, the dioctahedral layers of smectites are more stable (Steudel et al. 2009, Komadel & Madejová 2013). In general, the reported changes caused by acid treatment is strongly dependent on acid strength, time and temperature of the acidification process and the dissolution rate increases with increasing concentration of acid, temperature, time and octahedral Mg and Fe content (Komadel et al. 1990, Madejová et al. 1998, Komadel 2003, Steudel et al. 2009). The preparation of acidified MMT necessitates a control of variables to obtain improved sorption capacity and enhanced surface accessibility of MMT and the acid treatment of MMT under mild acidification condition.

5.3.2.2. Acidification of MMT

The procedures employed for the acidification process of MMT were based on the technique described by Ip (Ip 2007). 1g of MMT powder was added portion wise to 1L of DW over a period of 30 min with magnetic stirring at room temperature. Once MMT powder was uniformly suspended in DW, the pH of 1 % w/v suspension of MMT in DW

was adjusted with 0.1M sulfuric acid to about pH = 5 and the acidified suspension was agitated for 1 h. The acidified MMT was separated by repeated sedimentation and decantation and collected on a Buchner funnel. The separated acidified MMT was repeatedly washed with DW to remove water soluble sulfate related salts. The acidified MMT dried over a Buchner funnel was afterwards placed in an oven overnight at 50°C to remove traces of water.

5.3.3. Solution intercalation method

The procedures employed for the direct intercalation of hydrophilic polymers to MMT were based on the technique described by Ip (Ip 2007). The composite samples of a total solid content of 2.5 wv% were prepared with different weight ratios of polymer to MMT (Table 5.3). The specified amount of non-acidified or acidified MMT was dispersed in DW in polycarbonate tube and the dispersion was sonicated with a high-intensity ultrasonic liquid processor (Misonix, XL2020) for 1 min. The MMT suspensions were left at room temperature for 24 hours and MMT was allowed to swell in water. The predetermined amounts of polymers were mixed with the clay suspensions and the mixture of clay and polymer was then sonicated for 1 min. To study the effect of reaction time and temperature, the mixture of clay and polymer was then stirred with a magnetic stirrer at room temperature or kept in a shaker at 60°C for 24 hours further. The polymer/MMT aqueous suspensions were cast on to glass slides for XRD analysis and then into a Petri dish to evaporate water at room temperature overnight. The films that formed were then dried further in a vacuum oven at 50°C until the weights were constant and kept in desiccators prior to thermal, SEM and FTIR analysis.

Table 5.3. Summary of the stone consolidants prepared using direct intercalation method

Sample	Molecular weight of polymer (g/mol)	MMT	Temperature after ultrasonication
PAA100Mx	100,000	Non-acidified	-
PAA100Mx-RT	100,000	Non-acidified	RT

PAA100Mx-60ºC	100,000	Non-acidified	60°C
PAA250Mx	250,000	Non-acidified	-
PAA250Mx-RT	250,000	Non-acidified	RT
PAA250Mx-60ºC	250,000	Non-acidified	60°C
PAmMx	10,000	Non-acidified	-
PAmMx-RT	10,000	Non-acidified	RT
PAmMx-60ºC	10,000	Non-acidified	60°C
PAmMxa	10,000	Acidified	-
PAmMx-RTa	10,000	Acidified	RT
PAmMx-60ºCa	10,000	Acidified	60°C
PEG35Mx	35,000	Non-acidified	-
PEG35Mx-RT	35,000	Non-acidified	RT
PEG35Mx-60ºC	35,000	Non-acidified	60°C
PEG35Mxa	35,000	Acidified	-
PEG35Mx-RTa	35,000	Acidified	RT
PEG35Mx-60ºCa	35,000	Acidified	60°C
PEG25Mx	25,000	Non-acidified	-
PEG25Mxa	25,000	Acidified	-

x = ww% MMT (weight ratios of PAA/PEG to MMT) = 1(9:1), 2(8:2), 3(7:3), 4(6:4), 5(5:5), 6(4:6), 7(3:7), 8(2:8) and 9(1:9)

x = ww% MMT (weight ratios of PAm to MMT) = 2.5(39:1), 5(19:1), 10(9:1), 20(8:2), 30(7:3), 40(6:4), 50(5:5), 60(4:6), 70(3:7), 80(2:8) and 90(1:9)

5.3.4. In situ intercalative polymerisation

The specified quantity of non-acidified or acidified MMT powder was dispersed in DW contained in a polycarbonate tube using a sonication probe with a high-intensity ultrasonic liquid processor for 1 min. For the comparison of mixing conditions on the in situ polymerisation of Am or AA used as water soluble monomers, two mixing methods were studied for the preparation of monomer-MMT dispersions in the presence of KPS in DW (Table 5.4). In the first mixing method, the required amounts of monomer and KPS were added to the clay suspension and the mixtures were agitated with a magnetic stirrer at room temperature for 24 h. The second mixing method involved in the two mixing steps in which mixing of monomer and clay suspension for 24h was followed by the addition of KPS and further 3h agitation of the clay suspension in the presence of monomer and KPS. The prepared mixtures of MMT, monomer and KPS in DW were deoxygenated using nitrogen and heated at 60°C for 24 h.

Table 5.4. Summary of the stone consolidants prepared using intercalative polymerisation method

Sample	MMT	Method	Mixing time before heating (h)
AAMx	Non-acidified	I	24
AAMx-3H	Non-acidified	II	3
AmMx	Non-acidified	I	24
AmMx-3H	Non-acidified	II	3
AmMxa	Acidified	I	24
AmMx-3Ha	Acidified	II	3

x = ww% MMT = 2, 3, 4, 9, 10, 20, 30, 40, 50, 60

To study reaction conditions for the concentrations of KPS and monomer, the ratio of monomer to MMT was kept at 9:1 while the concentration ranges of KPS and monomer were 0.1-1 wt % and 1-10 % w/v respectively. The effect of clay content was examined using 4 % w/v of monomer and 0.8 wt % of KPS with respect to monomer at all MMT to

monomer ratios. The composite samples were prepared with compositions comprising ten different ratios of MMT to monomer (1:50, 1:30, 1:25, 1:10, 1:9, 2:8, 3:7, 4:6, 5:5, 6:4). All composite samples were cast on to glass slides for XRD analysis or into a Petri dish to remove water at room temperature. The resulting films dried further in a vacuum oven at 35°C to constant weight were stored in a desiccator until required for FTIR and thermal analysis.

5.4. Characterisation of polymer-MMT composites

5.4.1. FTIR spectroscopy

5.4.1.1. Background

FTIR has been an important tool employed in various applications for qualitative and quantitative analysis of infrared active molecules in a wide variety of organic, inorganic, biological, pure or mixed materials in any form, including bulk/powdered solid, liquid or gas samples (Stuart & Ando 1997, Stuart 2004, Jaggi & Vij 2006, Griffiths & de Haseth 2007, Smith 2011). This technique, when used in combination with other analytical measurements, may provide further structural details unattainable by other methods and FTIR studies have been extensively used to measure the structural changes, determination and identification of clay minerals, polymers and their composites (Grim 1968, Siesler & Holland-Moritz 1980, Hall 1987, Russell 1987, Besson & Drits 1997, Madejova & Komadel 2001, Petit 2006, Griffiths & de Haseth 2007, Crompton 2008, Anderson et al. 2010).

The FTIR studies on the clay mineralogy has been extensively undertaken as a supplemental tool not only for mineral identification in conjunction with XRD analysis, but also for the structural identifications (Farmer & Russell 1964, Grim 1968, Hall 1987, Russell 1987, Besson & Drits 1997, Madejova & Komadel 2001, Madejova 2003, Petit 2006, Diaz-Perez, Cortés-Monroy & Roegiers 2007, Anderson et al. 2010). In common with all clay minerals, the FTIR spectra of MMT are mainly characterised by hydroxyl group, silicate anion, octahedral and interlayer cations and the other main peaks in the fingerprint region, reflecting the bending vibrations of O-H and Si-O groups coordinated to octahedral or tetrahedral cations (Stuart & Ando 1997, Madejová 2003, Petit 2006).

FTIR analysis of triple layered dioctahedral structure is based on pyrophyllite used as parent structure and the FTIR spectral features of MMT are modified, depending on the nature and extent of isomorphous substitution (Farmer & Russell 1964, Petit 2006). In the 3400 and 3800 cm^{-1} region, O-H stretching vibrations due to the structural hydroxyl groups are influenced by cationic environment and have been studied to provide qualitative and quantitative information on octahedral cation occupation of dioctahedral clay minerals, such as the cationic distribution, nature and content (Velde 1983, Slonimskaya et al. 1986, Robert & Kodama 1988, Besson & Drits 1997, Petit 2006).

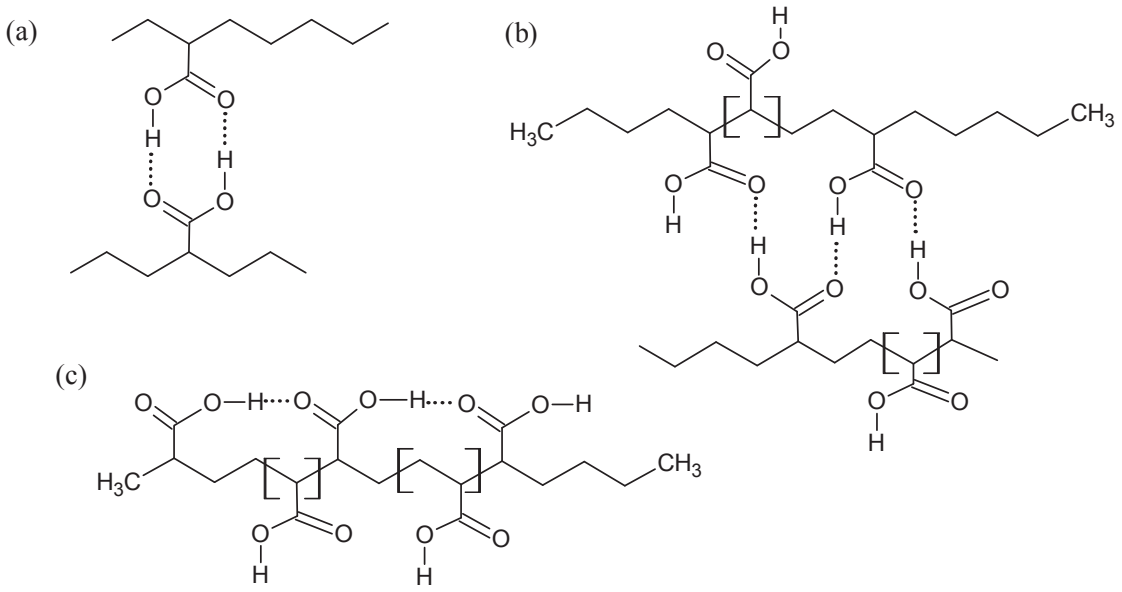

Figure 5.2. Schematic diagrams of hydrogen bonds formed by intra and intermolecular hydrogen bonding interactions of carboxyl group of PAA due to (a) cyclic dimer, (b) face to face hydrogen bonds and (c) lateral hydrogen bonds (Sun, Kepley & Crooks 1992, Dong et al. 1997b, Setoguchi et al. 2004)

Generally, the position and intensity of OH stretch bands of clay minerals have been used as diagnostic bands for the determination of octahedral cation occupation and dioctahedral smectite is characterised by a single O-H stretch band (Madejova 2003). The presence of water is detected by the structural hydroxyl groups and the OH stretch vibration of water molecules at 1500-1900 cm^{-1} (Frost et al. 1998, Madejova et al. 2002, Anderson et al. 2010). The O-H bending vibration of water is mostly used to study water-smectite interaction and is affected by the polarization of the interlayer cations, hydration level and strength of hydrogen bonding (Farmer & Russell 1964, Johnston, Sposito &

Erickson 1992, Frost et al. 1998, Madejova et al. 2002, Petit 2006, Anderson et al. 2010).

Table 5.5. Collected information for infrared absorptions of OH and CO stretch of PAA and their peak assignments

cm^{-1}	Assignments	References
3453	v(OH) of PAA	Liufu, Xiao & Li 2005
3392–3172	v(OH) of PAA	Moharram & Khafagi 2007
3140	v(OH) of PAA	Dong et al. 1997a
3126	v(OH) of PAA	Daniliuc et al. 1992
3101	v(OH) of PAA	Dong et al. 1997b
3000	v(OH) of PAA	Wang et al. 1997, Sun et al. 2000
1745	v(C=O) of unassociated PAA	Jo, Cruz & Paul 1989
1743	v(C=O) of PAA	Liufu, Xiao & Li 2005
1742	v(C=O) of unassociated PAA	Nyquist, Platt & Priddy 1982, Dong et al. 1997b
1736	v(C=O) of unassociated PAA	Daniliuc et al. 1992
1718	v(C=O) of PAA	Moharram & El-Gendy 2002, Moharram, Rabie & El-Gendy 2002
1714	v(C=O) of PAA	Morent 2009, Ma et al. 2009
1711	v(C=O) of PAA	Moharram & Khafagi 2007
1710	v(C=O) of associated PAA	Daniliuc et al. 1992, Song, Goh & Lee 2002, Zhou et al. 1998
1709	v(C=O) of PAA	Wang et al. 1997
1707	v(C=O) of PAA	Sun et al. 2000, Dong et al. 1997a
1705	v(C=O) of associated PAA	Dong et al. 1997b
1704	v(C=O) of associated PAA	Jo, Cruz & Paul 1989
1700	v(C=O) of associated PAA	Nyquist, Platt & Priddy 1982

Clay minerals show Si-O stretching and bending modes and O-H bending modes in the 1300-400 cm^{-1} and the peak shapes and positions are influenced by layer arrangement and the occupancy of the octahedral sheet (Farmer & Russell 1964, Stuart 1997, Madejova 2003).

FTIR spectroscopy is one of the powerful and important instrumental techniques for its application in structural characterisation of macromolecular systems (D'Esposito & Koenig 1978, Siesler & Holland-Moritz 1980, Jaggi & Vij 2006, Griffiths & de Haseth 2007). Given that all water soluble polymers and monomers used in this work contain proton donor and acceptor groups, changes in hydrogen bonding certainly need to be considered. The self-associated structures of PAA, PAm and PEG are formed by various forms of either intermolecular or intramolecular hydrogen-bonding interactions among hydroxyl groups in PEG, carboxyl groups in PAA and amide groups in PAm and the possible hydrogen bonded structures of PAA are illustrated in Figure 5.2. Significant to studying the contribution of the hydrogen bonding interactions for PAA and PAm is the absorption bands arising from stretching vibrations of OH, NH and CO and their peak assignments groups (Witkowski 1967, Daniliuc et al. 1992, Max & Chapados 2004, Duarte et al. 2005, Reddy et al. 2012). Their frequencies reported in the literature are included in Table 5.5 and 5.6.

The stretching vibrations of OH and NH groups in PAA are typically broad and strong and their spectra can exhibit the presence of both unassociated and associated forms (Excoffon & Marechal 1972, Daniliuc et al. 1992, Lu, Shan & Shang 2010). The hydrogen bonded forms of carboxylic acid groups of PAA exist even in extreme diluted solutions (Excoffon & Marechal 1972, Bellamy 1980). The markedly broad and moderately strong absorption of hydrogen bonded OH groups is characteristic of associated carboxylic acids units of PAA (Jo, Cruz & Paul 1989, Moharram & El-Gendy 2002, Morent 2009). While maximum absorption of the broad peak is situated at around 3000 cm^{-1} due to hydrogen bonded hydroxyl group, OH stretching of unassociated carboxylic acid groups of PAA can be assigned for a weak shoulder at about 3520 cm^{-1} by Nyquist, Platt & Priddy 1982 (Bellamy 1980, Nyquist, Platt & Priddy 1982, Daniliuc et al. 1992). The NH stretching vibrational band of amide groups for PAm and Am appear as a sharper doublet assigned to asymmetric and symmetric stretching bands of NH at 3430-3330 and 3224-3175 cm^{-1}

respectively (Table 5.6).

Table 5.6. Reported data for infrared absorptions of N-H and C=O stretching bands of PAm and their peak assignments

cm^{-1}	Assignments	References
3430	v_a(NH) of PAm	Lu, Shan & Shang 2010
3350	v_a(NH) of PAm	Yeh, Liou & Chang 2004
3343	v_a(NH) of PAm	Pan & Chen 2011
3342	v_a(NH) of PAm	Deng et al. 2006
3331	v_a(NH) of Am	Jonathan 1961
3330	v_a(NH) of PAm	Kulicke & Siesler 1982, Kulicke, Kniewske & Klein 1982
3224	v_s(NH) of PAm	Lu, Shan & Shang 2010
3200	v_s(NH) of PAm	Kulicke & Siesler 1982
3199	v_s(NH) of PAm	Deng et al. 2006
3198	v_s(NH) of PAm	Pan & Chen 2011
3190	v_s(NH) of PAm	Kulicke, Kniewske & Klein 1982, Yeh, Liou & Chang 2004
3180	v_s(NH) of PAm	Wang et al. 2004
3175	v_s(NH) of Am	Jonathan 1961
1688	v(C=O) of Am	Sugahara et al. 1990
1686	v(C=O) of Am	Ogawa, Kuroda & Kato 1989
1681	v(C=O) of Am	Jonathan 1961
1679	v(C=O) of PAm	Biswal & Singh 2004
1674	v(C=O) of Am	Wang et al. 2004
1670	v(C=O) of Am	Schmuckler & Limoni 1977
1670	v(C=O) of PAm	Moharram & El-Gendy 2002, Moharram, Rabie & El-Gendy 2002, Abdelhak, Abdelkarim & Barbara 2012
1670	v(C=O) of Am	Schmuckler & Limoni 1977
1668	v(C=O) of PAm	Pan & Chen 2011, McGuire, Addai-Mensah & Bremmell 2006

1666	v(C=O) of PAm	Wang et al. 2004, Huang & Ye 2014
1661-1666	v(C=O) of PAm	Gao & Heimann 1993
1664	v(C=O) of PAm	Pan & Chen 2011
1660	v(C=O) of PAm	Kulicke, Kniewske & Klein 1982, Deng et al. 2006
1658		Sowwan et al. 2008
1655	v(C=O) of PAm	Guerrero, Boldarino & Zurimendi 1985
1653	v(C=O) of PAm	Lu, Shan & Shang 2010
1651	v(C=O) of PAm	Bhat et al. 2014

Similarly, the C=O stretching absorption bands of COOH and $CONH_2$ can be used as an indicator of spectral changes due to their intra- and intermolecular interactions. The spectra of Am or PAm are characterised by the absorption bands typical for amide group, including amide I, amide II and amide III for C=O stretching vibration, N–H bending vibration and C–N stretching vibration, respectively. The strong resonance electron donor NH_2 group gives the low carbonyl stretching frequencies and the maximum amide I bands of amides, Am and PAm were reported as ranging from 1688 to 1651 cm^{-1} (Table 5.6). The carbonyl stretching bands of PAA at 1700-1710 cm^{-1} and 1745-1742 cm^{-1} correspond to self-associated carbonyl and free carbonyl groups (Table 5.5). The carbonyl stretching bands of associated carboxyl groups of PAA and organic compounds showed hydrogen bonding to form various forms of cyclic, open and sideway dimers (Sun, Kepley & Crooks 1992, Song et al. 1992, Dong et al. 1997b, Setoguchi et al. 2004). The changes in C=O and O–H stretching absorptions show the separation of hydrogen bonded dimers at elevated temperature (Nyquist, Platt & Priddy 1982, Dong et al. 1997b).

A great deal of literature has been produced to study the interaction of clay mineral with organic compounds, inorganic species and polymers (Petit 2006, Anderson et al. 2010). Useful information on hydration behaviour of clay, the structural alternation, acidification extent and surface acidity of clay mineral caused by the acidification reaction has been provided by IR spectral studies (Petit 2006, Anderson et al. 2010). IR measurements are powerful means to understand the interactions between organic and inorganic moieties at molecular level (Finocchio et al. 2014). In combination with other methods, FTIR technique has been extended to study the structure of polymer-clay composite systems

and the nature of bonding between polymer and MMT (Akelah 1995, Wu et al. 2001, Loo & Gleason 2003, Lagashetty & Venkataraman 2005, Pavlidou & Papaspyrides 2008, Sengwa, Choudhary & Sankhla 2009). The intercalation extent of polymers into MMT has been investigated though the analysis of the intensity, shape and frequency of the Si–O stretching environment (IJdo, Kemnetz & Benderly 2006, Tzavalas & Gregoriou 2009). Although FTIR spectroscopic analysis can be conducted to reveal the changes in bonding environment of the mixture and related composites, the resultant changes relating to peak position and shape are commonly small to determine the interactions and structural modification through FTIR measurements of many polymer-clay composite systems (Pavlidou & Papaspyrides 2008). The lack of the optimal condition to provide effective, fast and convenient determination of the dispersion of clay platelets is one of main remaining problems for the characterisation of polymer nanocomposites and the development and use of IR spectroscopy is limited, despite the potential of this technique as a powerful characterisation tool to provide information on the exfoliation state of nanocomposites (IJdo, Kemnetz & Benderly 2006, Tzavalas & Gregoriou 2009).

5.4.1.2. Experimental methods and analysis conditions

Infrared spectra of the dried powder samples were recorded on a Nicolet 6700 Fourier-transform infrared spectrophotometer, equipped with a DTGS detector and XT-KBr Beamsplitter. All spectra were obtained at room temperature by accumulation of 64 scans with a resolution 4 cm^{-1} in the range of 400-4000 cm^{-1}. The air dried polymer-MMT films were placed in a vacuum oven at room temperature and then grounded in mortar. The powder samples were further dried in the vacuum oven to remove residual moisture from the powders prior to the preparation of KBr pellets. For each sample, approximately 1 mg of the dried powder sample and 170 mg of spectroscopic grade KBr powder were ground in sample-KBr ratio about 1:170, using an agate mortar and the mixture was pressed into 13 mm diameter disk in a 10 tonne hydraulic press. The KBr pellets were placed in a spectrometer sample chamber purged with nitrogen gas and the spectra were recorded under a nitrogen flow so that the absorption bands of H_2O and CO_2 from atmospheric air and absorbed moisture were minimized. The system was operated with the use of Omnic32 software that allowed experimental set-up, automated data acquisition, as well as processing of raw data. The collected spectra were baseline corrected and processed

by performing peak detection and minimum smoothing. In order to compare the peak shifts and changes in peak intensity, the corrected spectral data were normalized with regards to the intensities of carbonyl stretching peaks of PAA-MMT, PAm-MMT and Am-MMT relative to those of PAA, PAm and Am at 1712, 1668 and 1674 cm^{-1} respectively. The normalization of spectrum for MMT was conducted using the Si–O stretching band for MMT at 1038 cm^{-1} compared to that of the corresponding Si–O stretching band of PAA-MMT, PAm-MMT and Am-MMT that included 90 w/w% MMT. The normalized spectra of PEG-MMT were obtained by adjusting the relative peak intensities of CH rocking band at 40-100% PEG and Si–O stretching band at 60-100% MMT.

5.4.2. Thermal Analysis

5.4.2.1. Thermogravimetric Analysis (TGA)

5.4.2.1.1. Background

Thermogravimetric measurements are used to determine the mass changes caused by certain thermal reactions of the heated samples, such as dehydration and the removal of the degradation products and volatile components and to study chemical, physical and thermal processes, heat stability, degradation mechanism, reaction rate and composition (Cheremisinoff 1996, Ramachandran et al. 2002, Galwey & Craig 2007, Pavlidou & Papaspyrides 2008, Kamal & Ionescu-Vasii 2010, Naskar & De 2010, Crompton 2010, Crompton 2013). The changes in chemical reaction occurred at characteristic temperature and thermal stability resulted from heating a wide variety of pure, natural and mixture materials, including polymer, clay mineral and organoclays and polymer-clay nanocomposites can be studied by TG examination (Cheremisinoff 1996, Galwey & Craig 2007, Diaz-Perez, Cortés-Monroy & Roegiers 2007, Prime et al. 2009, Kamal & Ionescu-Vasii 2010, Crompton 2010, Crompton 2013).

TG studies of MMT on the degradation of MMT commonly showed three main mass loss steps. The first step up to about 150°C to 200°C is attributable to the evaporation of physisorbed and interlayer water and is followed by the water loss of both MMT and associated phases present in the sample (Worrall 1968, Gridi-Bennadji et al. 2012). The thermal dehydroxylation reaction of MMT are commonly detected as the main last step

at around 600-700°C (Worrall 1968, Gridi-Bennadji et al. 2012). The dehydration of interparticle water, adsorbed water and interlayer water occurred upon heating (Önal & Sarıkaya 2007). Russell and Farmer suggested the interlayer water may be described as labile water and more firmly held water and the former is liquid-like water in outer co-ordination spheres of the exchangeable cations (Russell & Farmer 1964). The loss of the directly coordinated water occurs at higher temperatures (Russell & Farmer 1964). Previous experimental studies demonstrated that the dehydration and dehydroxylation step was determined by the size, charge and shape of the interlayer cations arisen from the nature of the cations and various conditional changes, such as fugacity of water on the actual recorded temperature (Worrall 1968, Guggenheim & Van Groos 2001). TGA analysis of clay mineral has been useful to analyse water distribution and the swelling processes involved in hydration of clay mineral (Diaz-Perez, Cortés-Monroy & Roegiers 2007).

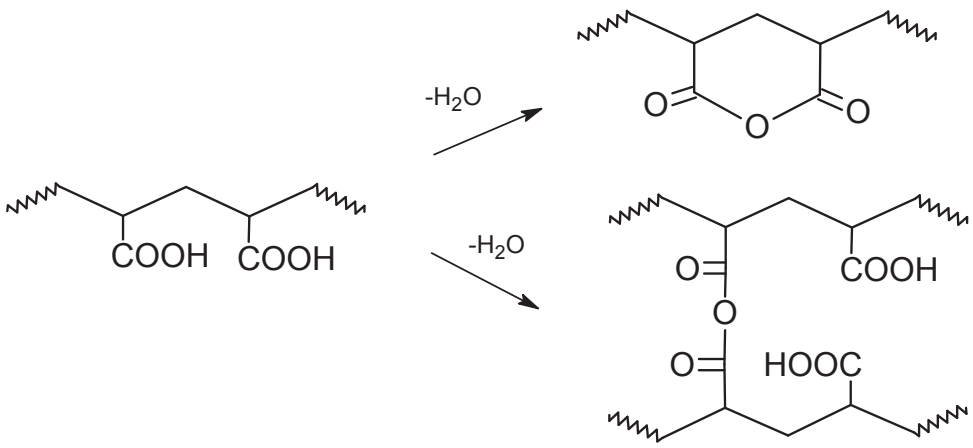

Figure 5.3. Proposed dehydration reactions of PAA (McGaugh & Kottle 1967, Maurer, Eustace & Ratcliffe 1987, McNeill & Sadeghi 1990)

The literature dealing with thermo-decomposition behaviour of PAA has shown that PAA is thermally broken down by a series of consecutive steps (Figure 5.3 and 5.4). The mass loss of dried PAA upon heating has been reported in three or four stages and the thermal decomposition proceeded two or three-step decomposition under aerobic or antibiotic conditions (Kabanov, Dubnitskaya & Khar'kov 1975, McNeill & Sadeghi 1990, Dubinsky et al. 2004). The TGA analysis of PAA in conjunction with DSC, FTIR, GC-MS and evolved volatiles analysis via mass spectroscopy revealed the elimination of the degradation products, including water, carbon dioxide, acrylic acid and unsaturated

compounds and suggested that the thermal decomposition of PAA involved a set of reactions, including dehydration, decarboxylation, depolymerisation, oxidation and chain scission (McGaugh & Kottle 1967, McGaugh & Kottle 1968, Eisenberg, Yokoyama & Sambalido 1969, Maurer, Eustace, & Ratcliffe, C.T. 1987, McNeill & Sadeghi 1990, Gurkaynak et al. 1996, Lepine & Gilbert 2002, Dubinsky et al. 2004).

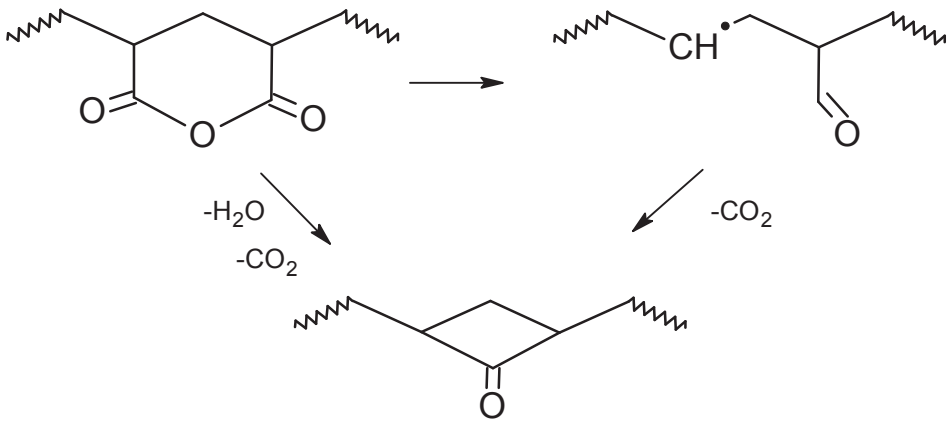

Figure 5.4. Proposed decarboxylation reactions (Kabanov, Dubnitskaya & Khar'kov 1975, Maurer, Eustace & Ratcliffe 1987, McNeill & Sadeghi 1990)

In the work of McGaugh & Kottle (1967), Maurer, Eustace & Ratcliffe (1987) (1987), McNeill & Sadeghi (1990) and Dubinsky et al. (2004), the dehydration reaction occurred as the first step in the degradation of PAA over 170°C. Although decreased with increasing temperature, the thermal conversion of carboxylic acid to anhydride was detected over a wide range of temperatures (Maurer, Eustace & Ratcliffe 1987, McNeill & Sadeghi 1990, Dubinsky et al. 2004). The anhydride structure can be potentially formed through intra- or intermolecular dehydration reaction while the latter reaction likely necessitates higher temperature above 200°C and takes place for the unreacted acrylic acid units in the chains (McGaugh & Kottle 1967, McNeill & Sadeghi 1990). Six-membered glutaric anhydride rings can be formed by the intramolecular cyclisation due to the water elimination from the adjacent carboxyl groups of PAA with a head-to-tail configuration and are thermally more stable than isobutyric anhydride structures that occur by intermolecular crosslinking (McNeill & Sadeghi 1990, Dubinsky et al. 2004). The study of Eisenberg, Yokoyama & Sambalido (1969) on the dehydration kinetics and glass transition temperature of PAA reported that anhydride formation is a first order process and intra-molecular dehydration reaction is the main reaction.

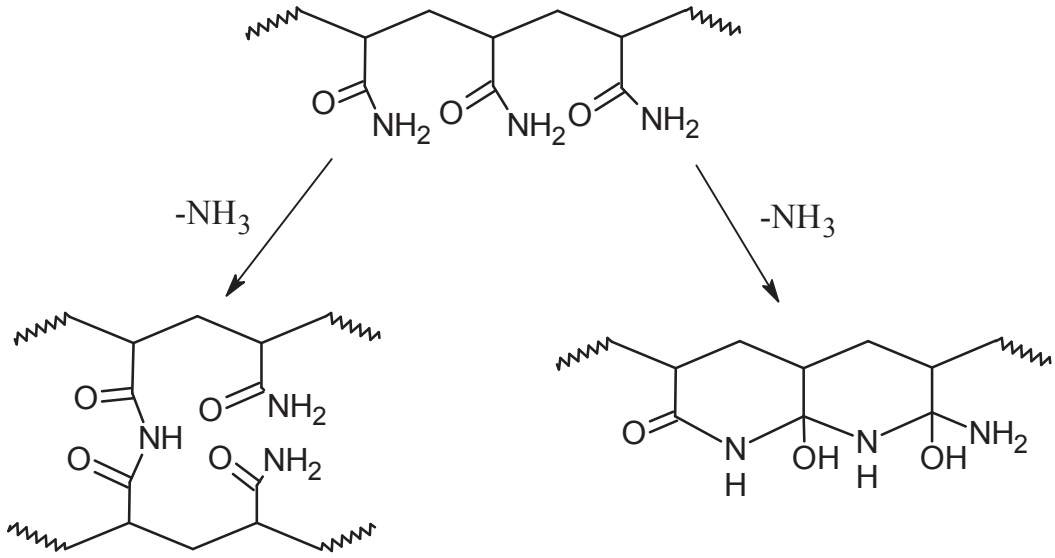

Figure 5.5. Intra and intermolecular imidization reactions of PAm

The dehydration reaction of PAA was followed by decarboxylation reaction with carbon dioxide evolution over 200°C and the anhydride structure was thermally converted to cyclic ketone in the decarboxylated PAA chains (McGaugh & Kottle 1967, McNeill & Sadeghi 1990, Dubinsky et al. 2004). The possible formation of minor products, including ketenes, ketones and unsaturated compounds from intermediate species, was also proposed by McNeill & Sadeghi (1990). Gurkaynak et al. (1996), who investigated the decarboxylation reaction of PAA, claimed the decarboxylation reaction is complex and can proceed through other possible facile decarboxylation. The studies of Eisenberg, Yokoyama & Sambalido (1969) and Gurkaynak et al. (1996) concluded that the carboxylation reaction was a first order process but slower than the dehydration reaction. Although the results of Kabanov, Dubnitskaya & Khar'kov 1975 (1975) indicated that PAA decomposed by decarboxylation reaction without dehydration reaction due to the lack of evidence of anhydride formation, Lepine & Gilbert (2002) reported that the degradation mechanism of PAA is more complex than a single decarboxylation reaction. Over the temperature 350°C, the breakdown of polymer chains occurs to form a variety of short chain fragments due to chain scission and combustive oxidation in air (McGaugh & Kottle 1967, McNeill & Sadeghi 1990, Dubinsky et al. 2004).

In comparison to other polymers, the thermal degradation of PAm is considered to be

rather complex and the multiple step decomposition of PAm was suggested by some researchers (Dollimore & Heal 1967, Burrows, Ellis & Utah 1981, Toth et al. 1990, Van Dyke & Kasperski 1993, E. Silva et al. 2000, Shi 2000). In the studies of the thermal degradation of PAm, TGA analysis combined with various methods has been employed to detect the structure of decomposed products and the combined techniques, including FTIR, DSC, mass spectrometry, gas chromatography, volatilization analysis and solid state nuclear magnetic resonance, provided information on the kind and functionality of the degradation products (Leung, Axelson & Van Dyke 1987, Toth et al. 1990, Van Dyke & Kasperski 1993, Schild 1996, Shi 2000, Abdelhak, Abdelkarim & Barbara 2012). On heating to 200~250°C, the initial mass loss of undried PAm is mostly attributed to the removal of all surface moisture, matrix-bound or hydrogen bonded water (Guerrero, Boldarino & Zurimendi 1985, Tutas et al. 1987, Leung, Axelson & Van Dyke 1987, Toth et al. 1990, Van Dyke & Kasperski 1993, E. Silva et al. 2000, Shi 2000, Pan & Chen 2011). The evolved gas analysed by Leung et al (1987) also indicated the release of degradation products due to the breakdown of monomer.

The thermally induced decomposition of PAm was initiated over 220-250ºC and thermal decomposition behaviours of PAm studied using TGA systems occurred in two or three distinct mass change regions, which were interpreted as two or three main reaction stages of PAm thermal degradation (Burrows, Ellis & Utah 1981, Vilcu et al. 1987, Tutas et al. 1987, Leung, Axelson & Van Dyke 1987, Toth et al. 1990, Van Dyke & Kasperski 1993, Gao & Heimann 1993, Biasci, Aglietto & Ruggeri 1995, Schild 1996, Yang 1998, Yang 1999, E. Silva et al. 2000, Shi 2000, Yang 2002, Han et al. 2010, Pan & Chen 2011, Abdelhak, Abdelkarim & Barbara 2012, Rakhshani et al. 2012). In the first decomposition region, intra-/intermolecular imidization, dehydration and deammonation of pendant amide groups and subsequent decarboxylation of the imide group eliminated ammonia, water and carbon dioxide and the formation of various imide groups, crosslinked and cyclic structures, nitrile groups, isocyanide groups and aliphatic compounds was documented (Burrows, Ellis & Utah 1981, Leung, Axelson & Van Dyke 1987, Toth et al. 1990, Van Dyke & Kasperski 1993, Schild 1996, E. Silva et al. 2000). Van Dyke & Kasperski (1993) suggested the remaining water can be desorbed in this temperature range. The works of Leung, Axelson & Van Dyke (1987), Vilcu et al. (1985), Toth et al. (1990) and Dyke & Kasperski (1993) showed the initial decomposition was mostly

ascribed to imidization reaction to produce NH_3 (Figure 5.5).

Following the first thermal conversion of the amide groups, Leung, Axelson & Van Dyke (1987) and Van Dyke and Kasperski (1993) included the former reactions and the chain-breaking actions, including decarboxylation of the imide groups below 440°C. During the mass loss of this region, the side chains reactions are completed and the breakdown of the polymer backbone into long chain hydrocarbons became significant and dominant. The subsequent decomposition proceeded in a complex manner (Tutas et al. 1987, Toth et al. 1990, Shi 2000). In addition to carbon dioxide, Toth et al. (1990) and Van Dyke and Kasperski (1993) identified various degradation products that can contain small portion of molecules less than 200 molecular weights, glutarimide and substituted analogs (Toth et al. 1990, Van Dyke & Kasperski 1993, Schild 1996, Han et al. 2010). The breakdown process of main PAm chain undergoes the thermooxidative degradation and the chain scission is triggered by free radical mechanisms including inter/intramolecular hydrogen transfer (Vilcu et al. 1987, Toth et al. 1990, Van Dyke & Kasperski 1993, Han et al. 2010).

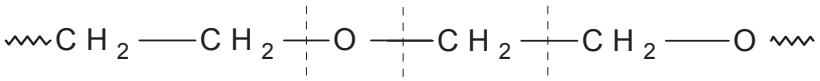

Figure 5.6. Random scission of C-O and C-C bonds of PEG chains (Fares, Hacaloglu & Suzer 1994)

In contrast to two-three mass change regions of PAA and PAm, the published TG trace showed a rapid mass loss of PEG and indicated the thermal degradation of PEG mainly in one step that begins at 230°C and is completed by 450°C (Grassie & Mendoza 1984, Fares, Hacaloglu & Suzer 1994). The thermal degradation processes of PEG were evaluated using TG analysis combined with mass spectrometry, gas chromatography and FTIR (Grassie & Mendoza 1984). The presence of oxygen can greatly affect the thermal decomposition of PEO (Costa et al. 1992). Grassie and Mendoza (1984) identified the losses of non-condensable, condensable and cold ring fraction, including different aldehydes, alkanes, carbon monoxide, hydroxyl, carbonyl and ethereal compounds and showed that the main radical chain mechanism was initiated by the random scission of C-O and C-C bonds of PEG chains and the formation of water ethylene glycol at chain terminal structures (Grassie & Mendoza 1984). Yang et al. (1996) reported the oxidative

thermal degradation of PEG in air at 150°C and showed the formation of the formate ester and hydroxy end-groups (Yang et al. 1996). The changes in molecular weight with thermal degradation time of PEO are in accordance with random scission reaction of the PEG molecular chain (Yang et al. 1996). Fares, Hacaloglu & Suzer et al. (1994) showed that PEO was degraded by both C-O and C-C scission with the former being predominant and the formation of degradation products up to six monomer units and small stable compounds, such as $C_2H_5OC_2H_5$, CH_3CHO, CO_2, CO and C_2H_4 (Fares, Hacaloglu & Suzer 1994). Due to more degradable carbon-oxygen bond cleavage, Fares, Hacaloglu & Suzer et al. (1994) suggested that thermal degradation of PEO undergoes C-O bond cleavages of the polymer chain more significantly as shown in Figure 5.6 (Fares, Hacaloglu & Suzer 1994).

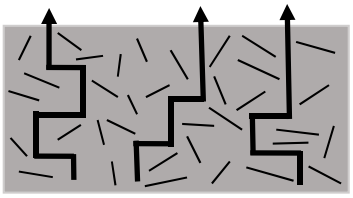

Figure 5.7. Tortuous path effect of clay minerals on thermal decomposition of polymer-clay minerals composite systems

As with MMT and polymers, the thermal characterisation of polymer-MMT composite systems is an important analysis to evaluate their thermal performance and the effect of filler modification (Pavlidou & Papaspyrides 2008, Kamal & Ionescu-Vasii 2010, Mittal 2012). The overall thermal behaviour of nanocomposites is synergistically enhanced, which is a direct consequence of thermal performance of both filler and pure polymers (Mittal 2012). These effects were determined through TGA measurements that can be used to compare the changes in thermal stabilities of organically modified fillers and to measure increase in thermal onset decomposition temperatures for higher thermal resistance of the modified fillers (Akelah 1995, Biswas & Ray 2001, Mittal 2012). It has been reported that the thermal stability of product can be improved upon by the introduction of clay minerals to polymeric matrix and the stabilizing effect of MMT on the thermal decomposition process of polymer-MMT composite systems has been described as a tortuous pathway effect that can delay the emission of volatile degradation products (Figure 5.7) (Alexandre & Dubois 2000, Kalaleh, Tally & Atassi 2013, Ferfera-

Harrar et al. 2014). Weight loss, due to decomposition into volatile products which are expelled during the heat treatment, is used to detect the amount of the sorbed polymer on clay mineral. However, the TGA data can show averaged results and distinguishing between adsorbed and intercalated matters is often difficult (Chen et al. 2008).

5.4.2.1.2. Experimental methods and analysis conditions

TGA scans of hydrophilic polymers, monomers and their composites were obtained on a TA Instruments SDT 2960 simultaneous DTA-TGA analyser. The experimental measurements of the tested samples were obtained from the apparatus, which was calibrated, based on baseline calibration, mass calibration and temperature calibration. In the baseline calibration, balance in sample stage contained empty crucibles and the apparatus was heated at 10°C/min in the heating temperature range from RT to 1200°C. For the mass calibration, alumina standard masses were used and heated at 10°C/min in the heating temperature range from RT to 1200°C. The temperature calibration was based on five-point calibration and high purity metal standards of indium, tin, aluminium, copper and gold were used.

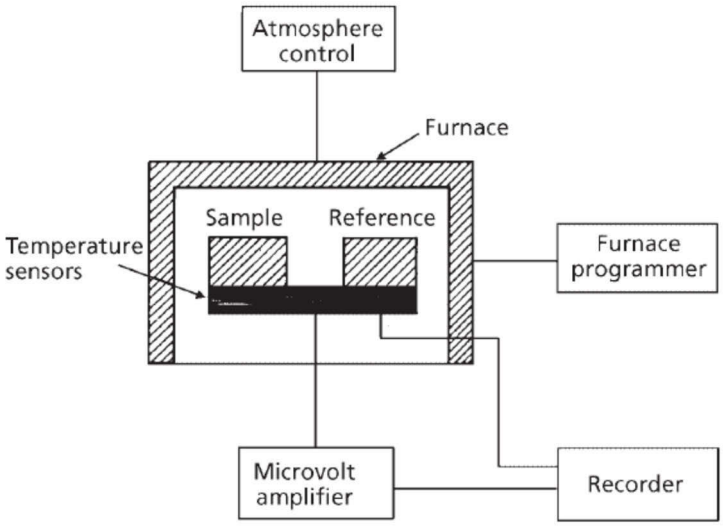

Figure 5.8. Schematic representation of TG apparatus (Wendlandt & Gallagher 1981)

Dried PAA, PAm and PEG were heated at heating rates of 0.5, 1, 2, 5 and 10°C/min and the temperature ranges used were from 35°C to 700°C. TG data of dried PAA-MMT,

PAm-MMT, PEG1-MMT and Am-MMT samples were obtained between 35°C and 1100°C at a heating rate of 10°C/min. For all runs, the atmospheric gases used in the study were air and the flow rates were 25 ml/min. An empty aluminium pan was used as a reference and the balance arms for reference and sample were located horizontally (Figure 5.8). The samples containing about 10-15 mg were measured in open sample platinum pans. TA Instruments Thermal Advantage Software, Version 1.1A was used to produce automated data acquisition and data collection. The thermal analysis was assisted by the use of TA Instruments Universal Analysis software.

5.4.2.2. Evolved gas analysis using Thermogravimetric Analysis (TG-MS)

5.4.2.2.1. Background

Although useful quantitative information can be obtained from TGA, which can measure the mass changes of heated sample, TGA is incapable of providing information on chemical reactions of the tested material in response to thermal treatment and is able to provide limited information (Crompton 2010, Crompton 2013). The additional information from complementary analytical measurements is often needed to support the interpretation of TG observations (Galwey & Craig 2007). TG observations can be studied in conjunction with the results from a variety of other techniques, such as FTIR, MS, DSC, gas chromatography and nuclear magnetic resonance spectroscopy and they are important for enthalpy measurements, evolved gas analysis and structural information (Galwey & Craig 2007, Crompton 2013). The conjoint use of multiple thermal and analytical tools to study the thermal behaviour of materials is more advantageous and the usefulness of TGA measurements is often extended by the multiple analytical technique, which incorporates one or more types of adjunct techniques to TGA.

In combination with TGA measurement, evolved gas analysis has been performed with various analytical techniques, which are used for quantitative or qualitative examination of the thermal breakdown products (Galwey & Craig 2007, Crompton 2013). In evolved gas analysis, combined or simultaneous analysis has been employed and the former utilizes multiple samples for each instrument (Xie & Pan 2001, Galwey & Craig 2007). For the simultaneous analysis, the same sample is analysed and the simultaneous

techniques coupled with TGA are real time, faster and helpful to lessen uncertainties produced by a single technique (Xie & Pan 2001, Menczel, Prime & Gallagher 2009). The simultaneous analysis involves heating the sample in TGA under controlled conditions of time, temperature, heating rate and atmosphere, while the gases released from the heated sample in TG apparatus are simultaneously introduced to and monitored by the suitable instrument(s) (Xie & Pan 2001, Galwey & Craig 2007, Crompton 2010, De 2010, Crompton 2013).

By coupling TGA with MS or FTIR, the same sample and thermal environments are shared and near simultaneous analysis with the small time delay between the mass loss and the gas detection is achievable (Xie & Pan 2001, Menczel, Prime & Gallagher 2009, Crompton 2013). TG/FTIR and TG/MS analysis allow continuous and simultaneous examination of the decomposition products and identification of complex processes from detected mass losses most frequently utilized in the field of material science (Menczel, Prime & Gallagher 2009, De 2010, Crompton 2013). The TG/MS model has been the most common and popular combination and a valuable identification tool for the evolved elements (Crompton 2013). In comparison to FTIR, MS detects mass to charge ratio of ions over a mass range of the specimens with more sensitivity and quicker response times (Xie & Pan 2001, De 2010). Disadvantageously, however, it is unable to distinguish the evolved gases of identical masses, isomers and high molecular mass species (Xie & Pan 2001).

TG/MS technique has been used for polymer analysis and produced information on thermal stability and degradation of polymers studies (Kamal & Ionescu-Vasii 2010, Crompton 2013). The thermal decomposition study of PAA, MMT and PAA-MMT composites using TG/MS technique was performed in this work. TG/MS analysis of PAA and MMT has been investigated by different researchers. Kabanov, Dubnitskaya & Khar'kov 1975 (1975) showed carbon dioxide as the main degradation product over 150°C in air but no confirmation for depolymerisation to release acrylic acid and dehydration reaction to form anhydride rings (Kabanov, Dubnitskaya & Khar'kov 1975). The TG-MS observations reported by Maurer, Eustace & Ratcliffe (1987) indicated the release of water and carbon dioxide due to anhydride formation and decomposition in helium. McNeill and Sadeghi (1990) also reported the evolved water, carbon dioxide and

short chain fragments due to the dehydration, decarboxylation and chain scission reactions, based on the thermal degradation products of PAA examined by TG, IR, MS and gas chromatography. Similarly, Dubinsky et al. (2004) indicated the release of water, carbon dioxide, acrylic acid and short fragmented chains from the TGA data combined with FTIR and MS.

5.4.2.2.2. Experimental methods and analysis conditions

The TG-MS measurements were acquired with a TGA/MS system, consisting of a Setaram Setsys 16/18 thermoanalyser and a Balzers ThermoStar quadrupole mass spectrometer. The Setaram was equipped with a vertical hand down balance system (Figure 5.9). Setaram was calibrated though baseline calibration, mass calibration, temperature calibration and heat flow calibration. To calibrate the baseline, empty pans were heated in air purge at a flow rate of 20 mL/min from 20 to 1200°C. The mass calibration was also conducted using standard masses and the high purity metals of indium, tin, aluminium, copper and gold were used for five-point temperature calibration. The heat flow calibration is based on analysing the melting endotherms of the temperature calibration standards.

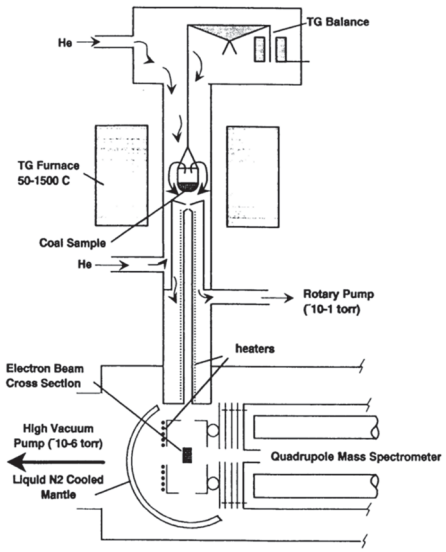

Figure 5.9. Schematic diagram of atmospheric TG-MS apparatus (Szekely, Nebuloni & Zerilli 1992)

The Setaram and the mass spectrometer were connected by a capillary that was preheated

to 160ºC to prevent condensation of gases. A small amount of dried PAA and PAA-MMT composite samples (20mg) was loaded in a 100 μL platinum sample pan and heated from room temperature at heating rates of 10ºC/min. TG-MS analyses were conducted in an air atmosphere. The MS signals up to 120 amu were measured as functions of temperature. The data acquisition and data processing were carried out using SetSys software.

5.4.3. X-ray Diffraction (XRD)

5.4.3.1. Background

The XRD profiles of every prepared sandstone consolidant based on MMT and hydrophilic polymers were obtained to investigate the interlayer structure of MMT. Clay minerals are most commonly characterised by the well-established XRD measurement method (Hall 1987, Moore & Reynolds 1997). XRD is a non-contact and destructive analytical technique that employs an intrinsic property of the x-rays and its interaction with electrons of atoms to determine crystalline nature of materials (Chung 1993, Will 2006). It gives information about the atomic arrangement of crystalline substances in

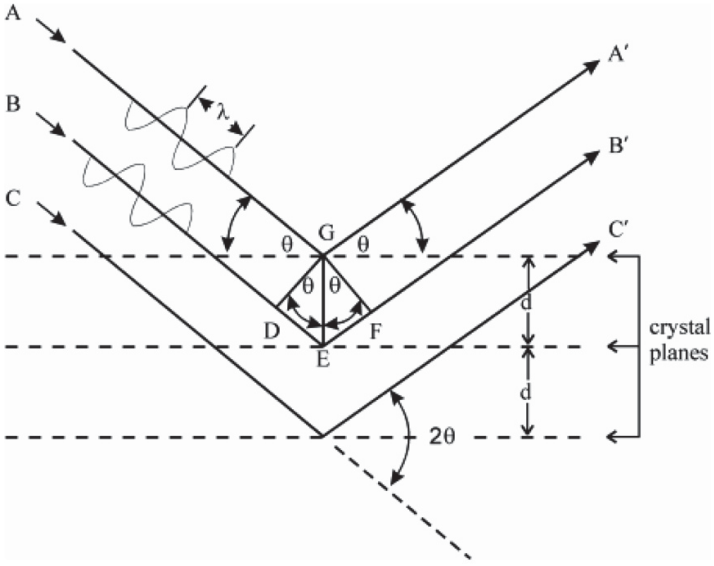

Figure 5.10. Schematic diagram for X-ray reflection from regularly spaced planes of atoms in a crystal structure (Saravanan & Rani 2012)

detail for the study of various structural properties of crystallographic structure (Baltá-Calleja & Vonk 1989, Arnold & Chung 1993, Moore & Reynolds 1997, Vaia & Liu 2002, Will 2006, Sharma et al. 2012).

The diffraction of X-ray beams are produced when the incident light is scattered from periodically assembled atoms or molecules of crystal lattice and information about the atomic order in crystal can be revealed (Figure 5.10) (Alexander 1969, Moore & Reynolds 1997, Lagashetty & Venkataraman 2005, Sharma et al. 2012, Chauhan & Chauhan 2014). When scattering of x-rays by the electron density around atoms occurs, atoms in ordered arrays cause constructive and destructive interference resulting in observable diffraction at only certain angles defined by Bragg's law ($n\lambda = 2d\sin\theta$) (Kovacs 1969, Lipson & Steeple 1970, Cullity 1978, Reynolds 1989, Arnold & Chung 1993, Moore & Reynolds 1997, Bowen & Tanner 1998, Kasai & Kakudo 2005, Will 2006, He 2009, Waseda, Matsubara & Shinoda 2011, Sharma et al. 2012, Chauhan & Chauhan 2014).

Although non-expandable phyllosilicates can be regarded as crystalline materials with long range periodicity, which can be characterised by diffraction phenomenon produced by XRD, the crystal definition is often inappropriate when applied to smectite clays devoid of the periodicity along the c axis and the structure of smectite is more related to an assemblage of silicate layers (Moore & Reynolds 1997, Giese & Van Oss 2001, Velde & Meunier 2008). The structure of clay minerals consists of the interlayer space between stacked layers in the c direction but naturally occurring clay minerals are considered as amorphous materials with lack of perfect crystal structure (Giese & Van Oss 2001). The crystal defects can disrupt three-dimensional periodicity in the a-b plane or in the c direction and can modify their diffraction characteristics (Grim 1968, Velde & Meunier 2008). Such crystal imperfection can cause the loss of certain reflections and broader and weaker bands (Grim 1968, Velde & Meunier 2008). The crystal defects in the c direction decrease the size of the coherent scattering domains and the diffraction profiles are modified by the faults in the a-b plane (Velde & Meunier 2008). Due to the imperfect lattice of clay minerals, the effects of the shape and size of the crystal particles become insignificant and result in the similar diffraction characteristics and diffused background, which lessens intensity of the Bragg reflections (Grim 1968, Arnold & Chung 1993). Crystallinity of a polymer, on the other hand, generally refers to three phase system

consisting of crystallites spread in amorphous background and their boundary regions (Alexander 1969, Baltá-Calleja & Vonk 1989, Kasai & Kakudo 2005). The structural analysis of high polymers is similarly intricate due to the imperfect crystallite orientation and the smaller number of diffraction peaks (Kasai & Kakudo 2005).

Figure 5.11. Schematic diagram illustrating orientations of clay particles (Essington 2003)

Despite extensive investigation on the identification and the structural characterisation of clay minerals by XRD technique, this technique is generally limited to qualitative data analysis of clay mineral due to issues, such as degree of structural disorder, making their XRD interpretation difficult or time-consuming (Grim 1968, Minichelli 1982, Giese & Van Oss 2001). While XRD measurements of clay mineral are mainly investigated from oriented or non-oriented samples (Figure 5.11), the former is most widely employed to analyse the d_{001} basal reflections (Gibbs 1965, Gillott 1968, Grim 1968, Viani, Gualtieri & Artioli 2002). The orientation of the sample can produce the most diagnostic d_{001} basal plane spacing and the intensified basal reflection and suppressed non-basal reflections of the oriented sample can improve detection limit (Gibbs 1965, Gillott 1968). The measurements of basal spacing can generate d_{001} values, characteristic of main clay mineral groups (Worrall 1968, Essington 2003). Analysis of randomly oriented layers produces the hk reflection pattern, which are two-dimensional reflections for one dimensionally disordered structure and gives rise to broad diffraction bands (Grim 1968).

Of practical importance to clay minerals is often the first-order basal reflection, which is used for measuring basal spacing of clay minerals (Grim 1968). The characterisation of polymer layered silicate materials has been also performed by X-ray powder diffraction techniques for the structural identification of layered silicate minerals (Akelah 1995, Zanetti, Lomakin & Camino 2000, Biswas & Ray 2001, Morgan & Gilman 2003, Sinha Ray & Okamoto 2003, Ahmadi, Huang & Li 2004, Chen & Evans 2005a, Manias et al. 2007, Utracki, Sepehr & Boccaleri 2007Zhu & Wilkie 2007, Anderson et al. 2010, Kiliaris

& Papaspyrides 2010, Mittal 2010, Olad 2011, Alateyah, Dhakal & Zhang 2013). Particularly, changes in distance between adjacent layers are important measurements as a clue to polymer incorporation into interlayer gap and the (nano)composites of polymer and clay minerals can be characterised in terms of interlayer separation (Akelah 1995, Vaia & Liu 2002, Morgan & Gilman 2003, Manias et al. 2007, Zhu & Wilkie 2007, Pavlidou & Papaspyrides 2008, Anderson et al. 2010, Olad 2011, Alateyah, Dhakal & Zhang 2013). Increase in d_{001} basal spacings is often used as an indication that guest materials have been intercalated within the interlayer space of layered silicate minerals and the position, direction, shape, full width at half-maximum and intensity of the (00l) basal reflections are analysed to identify the morphology as immiscible, intercalated or exfoliated structure (Akelah 1995, Alexandre & Dubois 2000, Zanetti, Lomakin & Camino 2000, Vaia & Liu 2002, Morgan & Gilman 2003, Sinha Ray & Okamoto 2003, Zhu & Wilkie 2007, Chen at al. 2008, Anderson et al. 2010, Kiliaris & Papaspyrides 2010, Olad 2011, Alateyah, Dhakal & Zhang 2013). In general, immiscible systems do not change the d-spacing and at the other extreme, layer exfoliation is believed to result in the absence of the basal reflection due to large interlayer distance and disordered clay layers (Akelah 1995, Vaia & Giannelis 1997, Alexandre & Dubois 2000, Vaia & Liu 2002, Morgan & Gilman 2003, Sinha Ray & Okamoto 2003, Lagashetty & Venkataraman 2005, Ruiz-Hitzky & Van Meerbeek 2006, Manias et al. 2007, Chen at al. 2008, Pavlidou & Papaspyrides 2008, Anderson et al. 2010, Kiliaris & Papaspyrides 2010, Mittal 2010, Alateyah, Dhakal & Zhang 2013). Increased d-spacing from the distinct basal reflection has been used as evidence for the formation of intercalated structure and XRD measurement of d_{001} spacings is considered an efficient and convenient tool to determine the basal plane spacing up to 4~5 nm for the periodically stacked layers of intercalated structure (Alexandre & Dubois 2000, Morgan & Gilman 2003, Sinha Ray & Okamoto 2003, Ahmadi, Huang & Li 2004, Manias et al. 2007, Zhu & Wilkie 2007Pavlidou & Papaspyrides 2008). It can only provide the averaged basal spacing between neighbouring silicate layers but is incapable of producing reliable and detailed information concerning the interlayer arrangement of intercalating agents, their interactions with the silicate layers, the conformation of the clay sheets and clay particle dispersions (Zanetti, Lomakin & Camino 2000, Vaia & Liu 2002, Filippi et al. 2007, Utracki, Sepehr & Boccaleri 2007, Chen at al. 2008, Anderson et al. 2010).

Caution is required in making the direct interpretation of exfoliation degree from the absence of obvious reflection patterns, which can indicate the disordered structure or large interlayer distance of exfoliated clay layers (Vaia & Liu 2002, Morgan & Gilman 2003, Ruiz-Hitzky & Van Meerbeek 2006, Filippi et al. 2007, Manias et al. 2007, Zhu & Wilkie 2007, Chen at al. 2008, Anderson et al. 2010). The analysis of featureless reflection deserves considerations of orderliness and orientation of silicate layers, detection limit, peak broadening and weakening and other experimental conditions that are suspected causes of errors in interpretation of such patterns (Vaia & Liu 2002, Morgan & Gilman 2003, Chen at al. 2008). Certainly, the reflections for randomly oriented layers can be misinterpreted as the lack of exfoliated layers or disoriented layers, low concentration, weakened and broadened peaks can be readily overinterpreted as the exfoliation state (Morgan & Gilman 2003, Chen at al. 2008). Consequently, the XRD investigation of the MMT-polymer composite systems is only of limited use in interpreting the diffused and weaken peaks but can provide clues to approximate the intercalation degree of polymers.

5.4.3.2. Experimental methods and analysis conditions

The XRD scans of MMT and hydrophilic polymer-MMT composites were collected to determine the degrees of MMT layer separation in samples based on the interplanar distance of the planes parallel to the sample surface and changes in their crystalline structures. The XRD analysis was performed on a Siemens D5000 diffractometer fitted with a fine focus Cu X-ray tube and a graphite post-monochromator at 40 kV and 30 mA and operated in Bragg-Brentano geometry (Figure 5.12). Different slit sizes and other diffractometer options, such as count times/step, were attempted while all experiments were conducted by a power detector. The first step was to find X-ray diffraction optimal setup to provide minimal scan time for analysis of diffraction peaks of MMT in the samples, which focus on the d_{001} plane corresponding to the variation in basal spacing of MMT silicate layers.

The XRD profiles of oriented MMT and polymer-MMT composite films were tested from samples deposited onto glass slides. The oriented MMT sample was first collected from the < 20 μm fraction separated by gravity sedimentation technique and transferred onto glass slide for XRD analysis. The middle of the glass slide mounts was placed on a small

ball of adhesive clay in the well of the sample holder and the samples were pressed into the clay, such that XRD data was scanned from the flat level surface of films and oriented MMT mounted on the glass slides. The data of selected composite samples was collected in the 2θ range between 2.7° and 25°. Each film sample was recorded with a step size of 0.02° 2θ, a count time per step of 3 secs and a scanning rate of 0.4°/min and the samples were scanned through a divergence slit set at V20. For receiving optics, a 2.0 mm antiscatter slit and 0.2 mm receiving slit were used. To analyse some samples that exhibited no clear diffraction peak of MMT, a low angle section of the diffraction pattern was measured in the 2θ range 1.2-7° with a step size of 0.02° 2θ, a count time per step of 10 seconds and a scanning rate of 0.4°/min. As weak reflections were observed using the same setup 3 secs count time per step unlike the higher-angle reflections from 2.7 to 25º, the count time per step was increased to 10 seconds to enhance weak signals for the low-angle analysis. A 0.5 div 20 deg divergence slit, a 0.6 mm antiscatter slit and a 0.2 mm receiving slit were used. The data were analysed by Diffrac Plus EVA software.

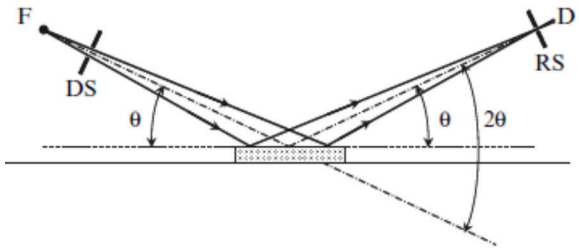

Figure 5.12. Schematic diagram of bragg-brentano geometry using a flat sample (DS-divergence slit, RS-receiving slit, D-detector, θ-Bragg angle, D-detector) (Pecharsky & Zavalij 2009)

The selected powder and film samples that exhibited clear (001) basal reflection peaks were used to validate that the results recorded from the film surfaces reasonably matched the d_{001} peaks produced by the corresponding powder samples. The powder samples were scanned over the range of 2.7-80° 2θ using the same diffraction setup used for the films. The dried composite and MMT samples were ground with a mortar and pestle to produce uniform and fine powder while care was taken in an effort to decrease risks that structural damage could occur to crystal structure resulting in broadened diffraction lines. The fine-grained powders were densely packed into a sample holder and pressed flat using a glass plate. The excessive powder was scraped off to produce a flat, stable and smooth surface

being parallel with the top of the well of the sample holder.

The randomly oriented MMT powder and selected powder PAm-MMT samples were also tested under the same XRD scan setup and the obtained X-ray diffraction patterns of PAm-MMT samples were compared with the one of random mount of MMT powder. Unlike basal 001 reflections of MMT that change according to the intercalation reaction in interlayer space of MMT, hk diffraction reflection of MMT is unique to the structure of MMT layers and independent of the basal plane spacing (Kornmann 1999). Therefore, the hk reflection patterns of random powder mount of PAm-MMT samples were assessed to identify the concentrations of MMT corresponding to the disappearance of hk diffraction bands.

5.4.4. Scanning Electron Microscopy (SEM)

5.4.4.1. Background

The particle diameters of clay mineral usually fall in the sizes smaller than 2 μm, which is less than the resolution of an optical microscope (Worrall 1968, Velde 1995, Moore & Reynolds 1997, Velde & Meunier 2008). The limited resolution in an optical microscope is approximately 1700-2000Å and MMT aggregates are often distinguishable. Limited information of clay minerals is identifiable, as most fractions of clay particles exist below or near this boundary, which are outside the resolving power of the optical system for deagglomerated MMT particles (Worrall 1968, Zhou et al. 2007, Velde & Meunier 2008). Superior spatial resolution and a much larger depth of field can be obtained, owing to the shorter wavelength of electron radiation and the use of electron microscopy undoubtedly provides more structural information of clay minerals (Worrall 1968, Sawyer, Grubb & Meyers 2008, Gupta, Kennel & Kim 2010).

SEM is an electron microscopy method, which produces information about the sample from signals derived from interactions of sample with electron in the beam (Echlin 2009, Reichelt 2007, Zhou et al. 2007). It employs an electron beam, which is emitted from an electron gun, focused to a small probe and scanned over a surface (Figure 5.13) (Reichelt 2007, Zhou et al. 2007, Sawyer, Grubb & Meyers 2008). When the electron beam hits the

sample surface, the interaction of electron with the sample yields the various types of signals and the reflected signals from the specimen surface can be collected with the electron detector and converted into digital images (Reichelt 2007, Zhou et al. 2007, Sawyer, Grubb & Meyers 2008, Khursheed 2011).

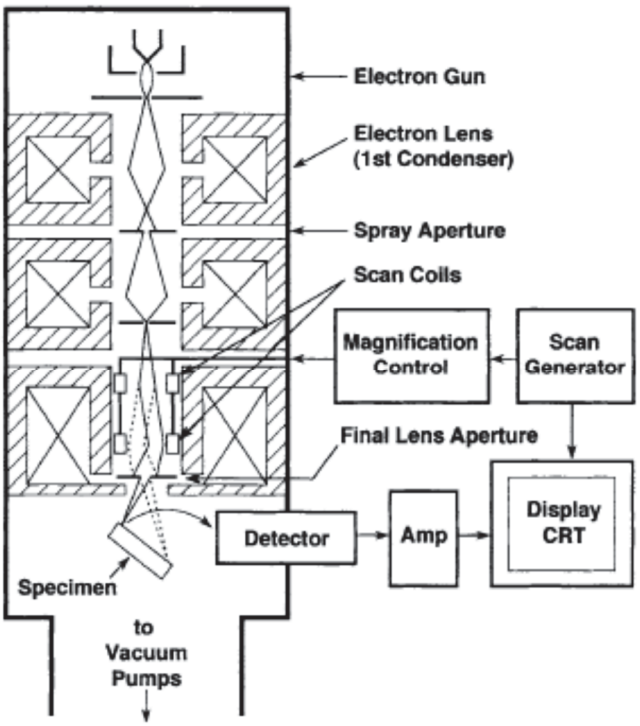

Figure 5.13. Schematic diagram of conventional SEM (Cullity & Stock 2001)

As the primary beam penetrates the sample surface to depths of up to a few μm, electrons passed through the thin surface layer are significantly scattered from a range of depths, which are directly dependent on the energies of the primary beam and inversely related to the atomic number of the atoms in the specimen (Sawyer, Grubb & Meyers 2008, Khursheed 2011). In response to the primary beam entering the specimen, various interactions can take place and broadly fall into two types of interactions: elastic and inelastic interactions (Reichelt 2007, Zhou et al. 2007, Sawyer, Grubb & Meyers 2008). The complex interaction of the primary beam with the atoms of the sample develops electron scattering and generation of photons and X-rays in an electron interaction volume where the variety of interactions occurs and a range of signals are emerged (Zhou et al. 2007, Sawyer, Grubb & Meyers 2008, Gupta, Kennel & Kim 2010, Khursheed 2011).

Of the signals produced through the interaction of primary electron with specimens, the most common imaging mode is the detection of secondary electrons (SE), which are in-elastically scattered from atoms of excited specimen by the electron beam as a result of interaction of the incident electrons with electrons and atoms in the specimen (Reichelt 2007, Zhou et al. 2007). During inelastic collision with specimen atoms, a substantial energy transfer from primary electron to the atom occurs and energy of in-elastically scattered electrons is significantly reduced (Reichelt 2007, Zhou et al. 2007). Depending on the excitation and binding energy of the electron, the energy loss of electrons takes place to different extents and SE are known to have low energy with the maximum of 50eV (Reichelt 2007, Zhou et al. 2007, Echlin 2009). The resulting image is determined by the quantity of collected SE by the detector and the relative position of incident beam on the surface (Reichelt 2007). Indirect SE that are generated by multiple scattering of electrons derived far from the position of the incidence beam carry the low-resolution images (Reichelt 2007). Direct SE of low energies are produced from a small region of the specimen and emitted from the top few nanometers of the specimen (Reichelt 2007). The collected secondary electrons provide good-resolution imaging of morphology and topographic contrast of the specimen surface and more structural information on the sample surface can be obtained (Reichelt 2007, Zhou et al. 2007, Sawyer, Grubb & Meyers 2008, Echlin 2009, Shimizu & Mitani 2010).

In comparison to SE, backscattered electrons (BSE) are scattered back from deeper and wider inside the target specimen from a larger interaction volume (Zhou et al. 2007, Sawyer, Grubb & Meyers 2008, Echlin 2009, Khursheed 2011). The elastic scattering of the primary electron beam produce BSE through its interaction with the electrostatic field of the positively charged nuclei (Reichelt 2007, Sawyer, Grubb & Meyers 2008). The electrons that elastically collide with atoms are deflected with alteration in electron trajectory and scattered through large angles (Reichelt 2007, Zhou et al. 2007). During elastic collisions, little or no energy is transferred to the specimen and the energies of BSE are greater than 50 eV (Reichelt 2007, Zhou et al. 2007, Sawyer, Grubb & Meyers 2008). In contrast to SE, backscattering increases monotonically as atomic number of the scattering atoms increases and there is a higher likelihood of generating more electrons backscattered from the higher average atomic number of the specimen region being analysed (Echlin 2009). BSE imaging can differentiate between areas of low and high

atomic number and information about the differentiations in chemical composition of the object (Echlin 2009).

As many materials are electronically poor conductors, sensitive to electron beam or hydration, the specimen preparation is a critical process (Reichelt 2007, Echlin 2009). In order to maintain the electron gun filament and avoid the scattered electrons strikes with water molecules in the SEM chamber, specimens should be degassed under a high vacuum to produce very dry samples (Chung 1993). Considering both MMT and hydrophilic polymers used in the prepared composite systems that are sensitive to moisture absorption and prepared from aqueous solutions, the specimens should be carefully dried and moisture absorption must be minimized during the specimen preparation (Echlin 2009). What is more, they are electronically poor conductive materials and polymers are prone to radiation damage under high voltage (Reichelt 2007, Sawyer, Grubb & Meyers 2008, Echlin 2009). On the surface of the nonconductive materials, the build-up of negatively charged electrons causes charging, which produces distorted secondary electron images and charging artefacts (Sawyer, Grubb & Meyers 2008, Echlin 2009). To facilitate the reduction of charging effects and increase the surface conductivity, non-conducting materials were coated with a thin conductive coating layer (Reichelt 2007, Sawyer, Grubb & Meyers 2008, Echlin 2009).

SEM has been used for imaging surfaces and investigating morphology of clay minerals and polymers (Bohor & Hughes 1971, Diaz-Perez, Cortés-Monroy & Roegiers 2007, Reichelt 2007, Crompton 2008, Sawyer, Grubb & Meyers 2008). SEM is one of the familiar instrumentation methods for mineralogical study and SEM observations using secondary and backscattered electron imaging can provide microstructural and compositional information in combination with energy-dispersive spectroscopic analysis or wavelength-dispersive spectrometry (Mata, Peacor & Gallart-Martí 2002, Zhou et al. 2007). SEM can be used to study configuration, texture and fabric of clay samples (Bohor & Hughes 1971). The SEM observation of MMT made by Zou and Pierre (1992) have presented house of cards structures with edge-to face and edge-to-edge particle associations (Zou & Pierre 1992). SEM examinations have been also carried out as a means of providing information on many morphological and microstructural aspects of composite systems comprising of MMT and various polymers (Akelah 1995, Biswas &

Ray 2001, Lagashetty & Venkataraman 2005, Utracki, Sepehr & Boccaleri 2007, Sengwa, Choudhary & Sankhla 2009).

The major shortcoming of SEM analysis lies in the limited resolution of SEM, as the individual platelets are too small to be resolved in SEM (Mata, Peacor & Gallart-Martí 2002). Although TEM has been used as a complementary technique to XRD, the sample preparation and operation required for higher resolution of TEM is more difficult and time-consuming, especially for samples that are vulnerable or unstable under the microscopic operating environment (Alexandre & Dubois 2000, Zanetti, Lomakin & Camino 2000, Biswas & Ray 2001, Sinha Ray & Okamoto 2003, Nguyen & Baird 2006, Utracki, Sepehr & Boccaleri 2007Zhu & Wilkie 2007, Chen at al. 2008, Paul & Robeson 2008, Sawyer, Grubb & Meyers 2008, Kiliaris & Papaspyrides 2010, Shimizu & Mitani 2010, Olad 2011). Moreover, there are limitations of TEM technique in the structural characterisation, including the extremely small examined sample area (Zanetti, Lomakin & Camino 2000, Sinha Ray & Okamoto 2003, Zhu & Wilkie 2007, Manias et al. 2007, Paul & Robeson 2008). On the contrary, the SEM characterisation is less effective but is advantageous, considering the sample handling procedures for SEM that are faster, easier, and more flexible than TEM (Biswas & Ray 2001, Reichelt 2007). Morphological analysis by microscopic examination commonly supports mixed states, which are hierarchically arranged systems, comprising individual layers as primary structural section and a collection of individual layers and/or of stacked layers as secondary structural segment (Akelah 1995, Vaia & Liu 2002, Morgan & Gilman 2003). The complete exfoliation or intercalation of layers is rarely seen and such idealised structures are rarely achieved (Vaia & Liu 2002, Ruiz-Hitzky & Van Meerbeek 2006, Manias et al. 2007, Chen at al. 2008). Although the SEM technique is insufficient for the complete structural characterisation of MMT, combining SEM and XRD diffraction data can be an alternative approach to detect hierarchical changes in morphological structure (Akelah 1995).

5.4.4.2. Experimental methods and analysis conditions

SEM analyses were performed on the surface of composite films for inspection of morphology and dispersion of MMT particles. The SEM images were observed from both

the coated and non-coated surface, using a Zeiss Supra 55VP scanning electron microscopy with an in-lens detector. All polymer-MMT composite films were dried under a vacuum to constant weight at room temperature prior to SEM analysis. The composite films or MMT powder were firmly attached to carbon adhesive pad and the sample surface was flushed with nitrogen gas to remove excess and dirt particles prior to SEM observation or coating. Coating of samples was conducted using a sample coating unit and the samples were coated with a conducting carbon or gold layer to reduce surface charging during SEM-imaging. The coated surfaces and cross-sections were recorded at accelerating voltage of 20kV with 3 mm working distance and viewed along the sides and at the centre of each sample using different magnifications at the same point of the samples. The SEM images of the uncoated surfaces and cross-sections were taken to compare them with the images of the coated samples and an accelerating voltage of 5 kV was utilized in the microscopic analysis to reduce image distortion or drift caused by charging. For the inspection of MMT dispersed in polymer matrix, the uncoated top and the cross-sectional surface were also viewed in a Zeiss Evo LS15, operated at an accelerating voltage of 15 kV and 103 Pa pressure with working distance between 9 and 10mm. The microscopic analysis was conducted, using Variable Pressure Secondary Electron mode equipped with a backscattering detector, to enhance the contrast between MMT and polymers in the micrographs were recorded. The enhanced colour contrast between MMT and polymers were obtained by modifying brightness, contrast and balance of obtained images using ImageJ freeware.

5.5. Consolidation treatment of Sydney sandstone

5.5.1. Application of consolidants

5.5.1.1. Background

The complexity and delicacy of stone conservation makes the decision making process difficult for the identification of a suitable consolidation strategy, which involves considering many intrinsic and extrinsic factors from the chemical and mineralogical composition of the stone to environmental factors which control the rate mechanism and extent of weathering (Piacenti 1994, Mosquera, Benítez & Perry 2002, Ferreira Pinto & Delgado Rodrigues 2008). While it is commonly considered that consolidating

performance and strength of treatment are improved by higher quantity of consolidating materials absorbed by stone substrate, there is little information concerning the amount of absorbed consolidants based on technical sheets or detailed investigations devoted to establishing criteria or standards for the accomplishment of desirable consolidation outcome (Tabasso 1995, Borgia et al. 2003, Ferreira Pinto & Delgado Rodrigues 2008).

The critical factors influencing the uptake of consolidating materials include chemical, physical and structural characterisation of consolidating material, as well as structure, surrounding conditions, pore space and surface dimension of stone under consolidation treatment (Ferreira Pinto & Delgado Rodrigues 2008). The characteristics of stone consolidants are certainly a critical factor influencing their uptake and penetration to the sandstone. The extent of penetration depth is known to be determined by the molecular size and viscosity of consolidating agents and it is important to optimize the viscosity of the treatment solution (Kim et al. 2009). The absorption of a polymer solution by a substrate is restricted by increased polymer solution viscosity resulting in poor penetration and low uptake of the polymeric materials (Munnikendam 1967, Cheraghian et al. 2014). The several applications of diluted consolidating fluid required for the satisfactory consolidant absorption is time-consuming and the accumulated polymers in the stone surface upon the solvent vaporization can lead to further stone deterioration (Munnikendam 1967).

Given the poor penetrations of polymeric materials, one alternative to improve penetration of polymer based consolidants has been absorption of monomer solutions, which were polymerised within the stone (Munnikendam 1967). Combined with the low viscosity of monomer solutions, this technique also provides fast penetration of more concentrated monomers with less steric hindrance to reduce accumulated polymers of stone surface due to solvent evaporation (Munnikendam 1967, Munnikendam 1973, Tabasso 1995). The literature contains various intitation systems, such as the use of peroxide initiators and ɤ-ray or UV irradiation, for the in situ polymerisation of various organic based polymers, including acrylic polymers (Munnikendam 1967, Witte, Huget & Broeck 1977, Tabasso 1995). Previous reports in literature showed the issues of in situ treatments, such as stress produced during the polymerisation and importance of meticulously monitoring variables, including polymerisation time (Munnikendam 1967,

Tabasso 1995).

In addition to the properties of stone and consolidants, the application technique is a critical influence on the penetration and performance of consolidants (Alessandrini et al. 2000, Borgia et al. 2003, Pinto & Rodrigues 2008). A wide range of application techniques were employed in the reported consolidation works while the common methods for the application of consolidation to stones are the uses of brush, spray, pipette, total immersion or capillary rise absorption (De Buergo, Fort & Gomez-Heras 2004, Doehne & Price 2011, Domaslowski 1969, Pinto & Rodrigues 2008). The other application techniques in the literature included the systems to supply the consolidants by means of pocket, bottles, intravenous tubes, three-way tap, vacuum impregnation and syringe injection (Munnikendam 1967, Hempel 1976, Witte, Huget & Broeck 1977). Although the full immersion and capillary rise absorption of consolidants commonly employed in the literature is impractical, the capillary absorption test is more practical than full immersion (Moropoulou 2003a).

Of practical importance to evaluate suitability of stone consolidation treatment are the measurements of quantity of consolidant absorbed by sandstone and time and rate of consolidant absorption (Boyer 1987, Borgia et al. 2003, Ferreira Pinto & Delgado Rodrigues 2008). The amount and penetration depth of consolidation treatments were directly measured by the comparison of stone sample weights before and after consolidation treatment (Tsakalof et al. 2007). The literature work reported different indirect measurement techniques to determine the distribution and penetration of consolidants in terms of visual evaluation, drilling resistance, ultrasonic tracer, water drop absorption time, capillary water absorption, polarisation microscopy and electronic microprobe (Boyer 1987). For the consolidation treatment of Sydney sandstone under study, the capillary rise absorption was used as application method to compare the consolidating performance with regard to the penetration rate, penetration depth and absorption.

This current work also investigated the consolidating behaviours of both organic and inorganic consolidants to Sydney sandstone. The consolidating performance of prepared stone consolidants can be examined by experimental comparison of the prepared

consolidant with commercial products. B72 and B67 have been used in the stone conservation of art work and frequently applied to consolidate sandstones in some European countries (Witte, Huget & Broeck 1977, Tabasso 1995, Striegel et al. 2003). Despite good solubility in some solvents, low glass transition temperature, transparency and adhesiveness of B72, its extensive use was limited due to its poor penetration and discoloration (Tabasso 1995). In addition to these water insoluble acrylic polymers, a comparative study for the consolidating capability of water soluble acrylic adhesive Lascaux can allow the comparison of the hydrophilic nature of polymers with the polymers tested in this study. Silres, selected as a representative organosilicon compound, is an inorganic ethyl silicate consolidant and is a solvent-free consolidant used for construction materials. Given that previous publications demonstrated the effective consolidation of ethyl silicate due to good penetration, water vapour permeability and stability, Silres can be a useful indicator of consolidation measures and the evaluation of the performance of Silres toward Sydney sandstone can be used as a standard of relative efficiency of the formulations under current work.

5.5.1.2. Experimental methods and analysis conditions

Stone consolidant absorption tests were carried out on samples wholly or partially immersed in the consolidating solutions. Test methods reported here were developed based on the methods reported in the literature (Domaslowski 1969, Brus & Kotlík 1996b). All absorption tests of stone consolidants were performed on previously oven-dried conditioned rectangular specimens under standard laboratory conditions (22 +/- 1°C) and the stone consolidants were absorbed by capillarity method or total immersion. All absorption experiments were conducted in an enclosed space in a sealed glass sample bottle (15 mm diameter, 50 mm tall) containing a sandstone sample and consolidant solution (Figure 5.14). For both methods, the quantity of consolidant solutions absorbed was recorded until constant weights of absorbed samples were obtained. The sandstone specimens were treated with both pre- and in situ formed consolidants and the summary of treatment solutions that were used in this work is shown in Table 5.7. The capillary rise experiment was also performed with DW to study the capillary rise of DW for comparison purposes.

Table 5.7. Consolidants tested in this work

Treatment solution	Solid content (w/v) %	(w/w) % MMT	wt % KPS	Application method
DW	-	-	-	CR
MMT	2.5	100	-	CR
Acidified MMT	2.5	100	-	CR
PAA100	2.5, 10	-	-	CR
	2.5	-	-	TI
PAA250	2.5, 10	-	-	CR
	2.5	-	-	TI
PAA100M	2.5	10, 20, 40, 60, 80	-	CR
	10	10	-	CR
	2.5	20	-	TI
PAm	2.5, 10	-	-	CR
	2.5	-	-	TI
PAmM	2.5	5, 10, 20, 40, 60, 80	-	CR
	10	10	-	CR
	2.5	5	-	TI
PAmMa	2.5	5, 10, 20, 40, 60, 80	-	CR
	10	10	-	CR
	2.5	5	-	TI
PEG20	2.5, 10	-	-	CR
	2.5	-	-	TI
PEG20M	2.5	20, 40, 60, 80	-	CR
	2.5	20	-	TI
PEG20Ma	2.5	20, 40, 60, 80	-	CR
	2.5	20	-	TI
PEG35	2.5, 10	-	-	CR
	2.5	-	-	TI

PEG35M	2.5	10, 20, 40, 60, 80	-	CR
	10	10	-	CR
	2.5	20	-	TI
PEG35Ma	2.5	10, 20, 40, 60, 80	-	CR
	10	10	-	CR
	2.5	20	-	TI
B67	20	-	-	CR
B72	20	-	-	CR
Lascaux	20	-	-	CR
Silres	99	-	-	CR
AA*x*	5, 10, 20, 30, 40, 50	-	0	CR
AA*x*-*y*	2.5, 5, 10, 20	-	0.5, 1.0	CR
Am*x*	5, 10, 20, 30, 40, 50	-	0	CR
Am*x*-*y*	2.5, 5, 10, 20	-	0.5, 1.0	CR
	10		0.1, 0.25	CR
	20		0.05, 0.1,0.25	CR
	30		0.5	CR
	40		0.1	CR
	50		0.025,0.05, 0.1	CR

CR=capillary rise absorption, TI= total immersion

x = w/v% AA or Am

y = wt% KPS

The aqueous dispersions of 2.5 % (w/v) MMT, polymer and their composite systems were prepared with DW and the weight concentrations of 10, 20, 40, 60 and 80 (w/w) % MMT were tested for composite systems with additional 5 % (w/w) MMT for PAm-MMT systems. In order to study the effect of consolidant concentrations, 10 % (w/v) aqueous solutions of polymer and composite systems with a polymer to MMT ratio of 9:1 were applied by capillary absorption and comparisons were made with 2.5 % (w/v) aqueous solutions of polymer and composite systems. The pre-formed commercially available

stone consolidants were applied to sandstones in the same manner to composite systems by capillary absorption, and their solution concentrations were 20 w/v %, except for Silres, containing 99% monomers. The total immersion of polymer and composite samples were performed on 2.5 % (w/v) aqueous solutions of polymer and polymer-MMT systems and the MMT concentrations of 20, 40, 60 and 80 (w/w) % were selected for composite systems. The in situ formed consolidants were prepared by the polymerisation of water soluble AA and Am using KPS as an initiator in the sandstone and their penetrations to sandstones were performed by means of capillarity. The penetration of the monomers was studied from 5, 10, 20, 30, 40 and 50 % (w/v) aqueous solutions of AA and Am, which were magnetically stirred in DW prior to their application. The in situ polymerisation of AA and Am was performed using 2.5, 5, 10 and 20 % (w/v) aqueous solutions of AA and Am in the presence of 0.5 and 1.0 wt % KPS. To study the changes produced by differing KPS concentrations, 0.05, 0.1 and 0.25 wt % KPS were additionally tested with 10, 20, 30, 40 and 50 % (w/v). To the well-mixed aqueous solution of AA or Am, the required amount of KPS was added and stirred with a magnetic stirrer. The prepared solutions containing monomer and KPS were immediately applied to sandstone samples and all consolidants tested in this work were applied in a similar manner.

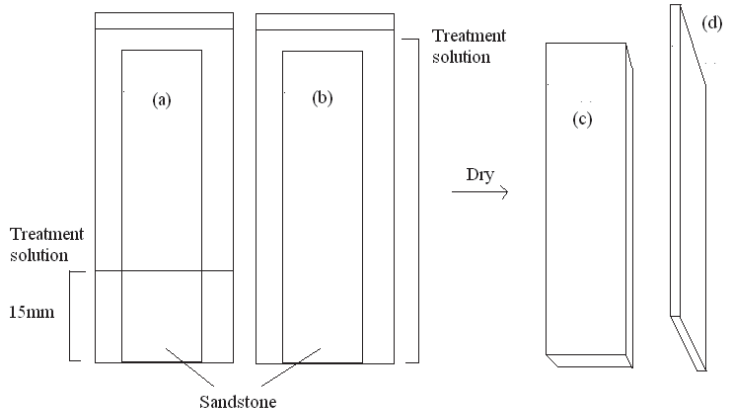

Figure 5.14. (a) capillary rise saturation and (b) total immersion of sandstone via the whole cross-section of a sample (vertical displacement)

In the case of capillary absorption of consolidants, the untreated sandstone samples were carefully placed in the centre of a glass tube without contact between the sandstone side edge and the wall of the glass tube and care was taken to minimize leanness of sandstone (Figure 5.14). The treatment solutions were added using a pipette so that the length of the

solution was 1.5 cm from the bottom of the glass tube. The sandstones were dipped in the solutions from the bottom up to 1.5 cm and this height was positioned as an initial level for the rate of capillary rise. The height of capillary rise was measured as a function of time until the sandstone was fully covered by the fluid. In order to provide better conditions for the strength measurements of being conducted on the treated sandstones, uniform absorption of consolidant by sandstone is desirable and the sandstones were completely soaked in the solutions resulting in total immersion.

For both application methods, capillary rise and total immersion, the absorption of consolidant to the sandstones was carried out in the glass tube until the constant weight of treated sandstones was attained and saturation of the sandstones with the consolidants was assumed to have occurred. Sample weights were measured by after quickly drying the treated samples with tissue in order to remove the excess treatment solution. Their weights were measured daily for one week and every 2-3 days for four weeks and then weekly measurements were conducted when weight gains became comparable until no changes occurred. The increases in weights of treated sandstone samples due to absorption of treatment solution was calculated by the difference of absorbed sample and dry sample as wet weight percentage as follows,

$$\text{Wet weight uptake (\%)} = (W_{t0} - W_o) / W_o$$

The difference of initial weights of dry sandstone samples, W_o and weights of those absorbed by treatment solutions, W_{t0}, at time (hour) t, with respect to the initial weights, W_o, was expressed as a percentage of wet weight uptake and plotted as a function of time. Capillary rise absorption curve of the treatment solution was obtained plotting the percent wet weight uptake versus time and this allowed the determination of the increased weight percentage of treatment solutions absorbed by sandstone samples. Once the absorption period was complete and the samples had reached a constant weight, the sandstone samples were removed and left to dry at room temperature. The treated sandstones were initially dried such that one (Figure 5.14 (c)) or both (Figure 5.14 (d)) of large surfaces of sandstones were exposed in air. Selected sandstone samples treated by capillary and the total immersion were dried as shown in Figure 5.14 (d) in order to study the influence of drying positions on the distribution of absorbed consolidant in the former and to provide

uniform distribution of absorbed consolidants in the latter. To remove remaining moisture with further drying, the samples treated with polymers and composite systems were dried in an oven at 35°C and other samples were placed in a vacuum oven at room temperature until no further weight changes were observed. Weight differences before and after consolidant application process were measured and the amount of the product remaining in the fully dried sample was calculated. Dry weight % uptake was calculated in a similar way as wet weight % uptake,

$$\text{Consolidant uptake } (\%) = (W_t - W_o) / W_o$$

Where , W_o is initial weights of dry sandstone samples and W_t is weights of sandstone samples treated with treatment solutions and dried to a constant weight. The procedure was adapted to produce the triplicate samples for each consolidant tested and all results are reported as average values.

5.5.2. Colour analysis

5.5.2.1. Background

Together with water vapour permeability changes and other chemical and physical characteristics of untreated sandstones, the original properties of treated stones, such as colour and texture, should be preserved and aesthetic modification of treated stone should be minimized (Durán-Suárez et al. 1995, García-Talegon 1998, D'Arienzo, Scarfato & Incarnato 2008, Licchelli et al. 2011). With regard to aesthetical and ornamental aspects of building materials, colour is one of the most important characteristics (García-Talegon 1998, Iñigo et al. 1997, Iñigo, Vicente-Tavera & Rives 2004). The treatment of stones should not produce any variations in colour and surface appearance of the treated stones at the initial stage or after long-term contact with the environment (Iñigo et al. 1997, Iñigo, Vicente-Tavera & Rives 2004). Considering the unique aesthetic appearance and colour of Sydney yellow block sandstones in heritage buildings, a great importance is placed on the preservation of their unique appearance and colour.

Critical to inspecting suitability of consolidation treatment and to evaluating the

consolidation efficiency is the ability to preserve the original colour of stone (Iñigo et al. 1997, Iñigo, Vicente-Tavera & Rives 2004). In response to the need to develop quantitative colour measurements of treated stones, instrumental colour determinations were adapted to replace the visual inspection based on the colour chart, according to Munsell notation (Durán-Suárez et al. 1995). The effect of consolidation treatment on the chromatic characteristics of the treated stones has been reported using a range of instrumental techniques for measuring colour most notably colorimetry, chromametry and spectrophotometry with colour measurements taken from the consolidated sandstone, marble, tuff stone, limestone, carbonate stone and granite (Mosquera, de los Santos & Rivas 1986, Durán-Suárez et al. 1995, Selwitz 1995, Iñigo et al. 1997, García-Talegon 1998, Ginell & Coffman 1998, Tiano, Biagiotti & Mastromei 1999, Cocca et al. 2004, Iñigo, Vicente-Tavera & Rives 2004, Cnudde et al. 2006, Favaro et al. 2006, Tiano et al. 2006, Favaro et al. 2007, Miliani, Velo-Simpson & Scherer 2007, Tsakalof et al. 2007, D'Arienzo, Scarfato & Incarnato 2008, Domingo et al. 2008, Vacchiano et al. 2008, Karatasios et al. 2009, Park & Shin 2009, Jroundi et al. 2010, López-Arce et al. 2010, Török 2010, Licchelli et al. 2011).

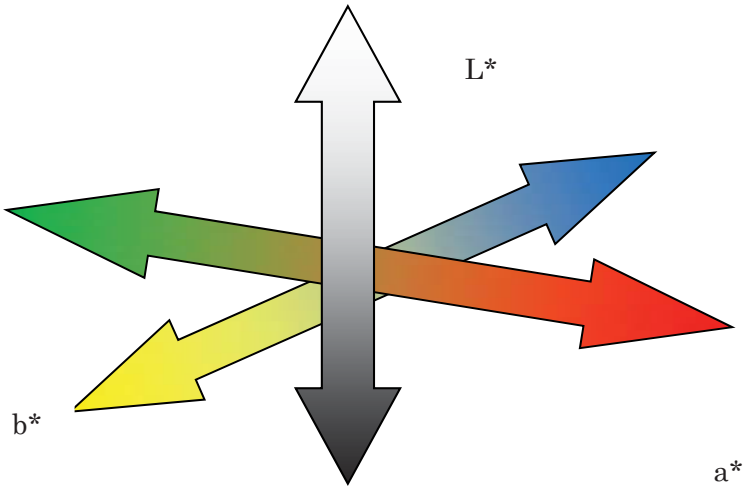

Figure 5.15. Diagram of three dimensional colourimetric coordinates according to Commission Internationale de l'Eclairage

Based on the perceptual attributes of colour, there are three main perceptual attributes, brightness, hue and colourfulness, to characterise colours (Hunt & Pointer 2011). It is generally accepted that relative colour appearance can be described based on hue, lightness and chroma and perceptually, colours are represented by a three dimensional

system. CIELab colour system, recommended by Commission Internationale de l'Eclairage, is perceptually more uniform and based on the opponent colour theory of colour vision. In the CIELab colour space, colours are represented by using the coordinates in a uniform colour space and represented by three axes for variable L* and chromaticity a* and b* (Figure 5.15). The L* values shown on central vertical axis indicate the relative brightness from white to black. The a* and b* values correspond to red-green and yellow-blue colour axis. The L* value represents the luminosity, while a* and b* refer to the chromaticity coordinates (García-Talegon 1998). The colorimetric analysis of consolidated stones were characterised by L*, a* and b* coordinates that provide information on black-white, red-green and yellow-blue colour space (Selwitz 1995, Török 2010). The L* variable represents the degree of darkness/lightness of the samples (García-Talegon 1998).

In order to obtain the numerical colour determination with the instrumentally obtained coordinates, the colorimetric characteristics of the consolidated stones have been evaluated using L*, a* and b* coordinates, according to the CIE 1976 colour space (García-Talegon 1998, Tiano, Biagiotti & Mastromei 1999, Tsakalof et al. 2007, Karatasios et al. 2009, Park & Shin 2009, Jroundi et al. 2010). The a* coordinate indicates ranges between positive and negative a* values identified with redness and greenness, respectively (García-Talegon 1998). Similarly, the b* coordinate expresses blueness and yellowness detected by the negative and positive b* values (García-Talegon 1998). The colour changes can occur with ageing or be caused by the different treatments and stone types (Iñigo et al. 1997, García-Talegon 1998, Iñigo, Vicente-Tavera & Rives 2004, Cnudde et al. 2006). Although no modifications in the appearance, particularly colour, of the original stonework should ideally be made by the consolidation treatment, colour alteration is practically acceptable if the visual changes are imperceptible (Park & Shin 2009). Rodrigues and Grossi (2007) suggested that the incompatibility risk for stone consolidation work can be considered to be low for the total colour difference values less than 3 (Rodrigues & Grossi 2007).

5.5.2.2. Experimental methods and analysis conditions

Colorimetric analyses of sandstone specimens were carried out digitally on digital images

captured using a Canon EOS 450D digital SLR camera with a Canon EF-S 17-85mm f/4-5.6 IS USM lens in a tightly controlled lighting environment. A Polaroid MP-4 Multipurpose Camera Systems lighting stage, consisting of four 150W tungsten light bulbs with each set at 45° and at equal distance, was used (Figure 5.16). The camera was mounted on the vertical column set at a height of 33 cm directly above the specimens. Images were captured in the camera's manual mode to ensure consistent exposure values. In addition, images were captured in RAW format. The exposure values were determined using spot metering on a Kodak neutral grey card at a fixed focal length of 35 mm, ISO 100 and aperture f/8.0. These values, in conjunction with having the specimen in the centre of the frame, ensured that chromatic aberration, noise and light falloff were minimised. Once the exposure was determined (i.e. shutter speed of 1/15 second) the camera was raised to a height of 100 cm to capture an image of the Datacolor's SpyderCheckr™ colour checker, a professional colour reference tool, to calibrate for the camera's sensor in order to achieve accurate colour reproduction. The camera was raised in order to fit the entire colour checker in frame without changing the focal length of the lens. The camera was then re-adjusted to 33 cm in height again to capture an image of the neutral grey card. This image was then used to set the in-camera custom white balance.

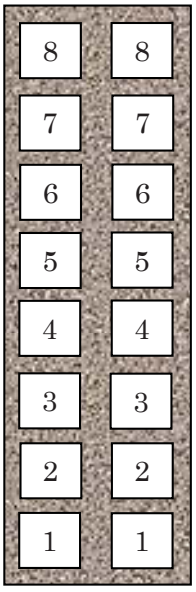

Figure 5.16. Polaroid MP-4 Multipurpose Camera Systems lighting stage with four 150W tungsten light bulbs angled at 45°(left) and order of colour sampling of sandstone specimens as processed in Photoshop CS5 (right)

All image capturing utilised Canon's camera remote control shutter release to avoid shadows being cast onto the specimens by the operator. A black cardboard was used as the background while capturing images of the sandstone specimens to avoid colour spills from coloured backgrounds.

A custom camera colour profile was created using the SpyderCheckr^{TM} software on the captured image of the SpyderCheckr^{TM} colour checker. The colour profile was generated in colorimetric mode in order to produce the most literal result. The saved colour profile was then applied to all images using batch processing in Adobe Camera Raw software. The corrected images were then opened and processed in Adobe Photoshop CS5. Colours were sampled using the Eyedropper tool with an average sample area of 101 x 101 pixels. A total of 16 regions were sampled per specimen as illustrated in Figure 5.16. A hex colour code was produced from each region and the CIE-LAB colour space data were extracted and analysed.

Colour measurements were performed on both untreated and treated sandstones and the untreated sandstone was used as a control to monitor the colour changes of treated sandstones relative to data obtained before treatment. Prior to image acquisition, the sandstone specimens were fully dried as described above to reduce the darkness of sample surfaces caused by the moisture absorption of sandstones. The photographic images were taken from the treated sandstones after the capillary absorption of MMT suspension, polymer solutions, polymer-MMT composite dispersion, commercial products and monomer solutions. For each specimen, the digital images were taken from both sides of untreated and treated sandstone and colour alternation caused by consolidation treatment was determined based on the L*, a* and b* coordinates of the CIELAB space. The colour differences for the three components of lightness, perceived chroma and hue, ΔL*, Δa* and Δb* based on colour difference formula and the total colour difference ΔE given in terms of ΔL*, Δa* and Δb* were calculated according to the standard ASTM D2244 – 09b as follows:

$$\Delta L^* = L^*_t - L^*_u$$

$$\Delta a^* = a^*_t - a^*_u$$

$$\Delta b^* = b^*_t - b^*_u$$

$$\Delta E = [(\Delta L)^2 + (\Delta a)^2 + (\Delta b)^2]^{1/2}$$

where L^*_t, a^*_t and b^*_t denote the collected data from the treated samples and L^*_u, a^*_u and b^*_u denote the untreated specimen (ASTM Standard international 2011a). Two sandstone samples were used to analyse untreated and treated samples for each consolidant treatment and the procedure was adopted to take from four spots in each section. The calculated values of ΔL^*, Δa^*, Δb^* and ΔE and their average values of quadruplicate colour determinations were plotted as functions of length from the bottom of the treated sandstone as illustrated in Figure 5.16.

5.5.3. Permeability to water vapour

5.5.3.1. Background

The behaviour of stone and the processes of absorption, condensation, evaporation and migration of water are affected by the internal structure of stones, such as porosity, pore size distribution, pore shape and interconnected pores (Cnudde et al. 2004, Bugani et al. 2007). Owing to the role of water that is absorbed and penetrated though porous structure, stones with high porosity are more susceptible to stone decay processes and the diffusion of salt solutions spreading the marred area is facilitated by the extensively interconnected pores (Bugani et al. 2007). Conversely, the severe reduction in the permeability of treated stones to the water vapour can lead to further stone deterioration due to any accumulation of trapped water and soluble salts inside the stone and the blocked pores to hinder the passage of water or water vapour (Munnikendam 1973, Tuminello, Bracci & Piacenti 2002, Bugani et al. 2007, Doehne & Price 2011). The porosity of the applied consolidants are often so different from those of the original stone (Rodriguez-Navarro et al. 2003). The consolidation effect is largely influenced by porosity (Cnudde et al. 2004).

Because of an important role of porous stone structure in the deterioration process of treated stone, characterisation of changes in porous network is particularly significant for the evaluation of consolidation effect (Mosquera, Benítez & Perry 2002). The determination of the pore-size distribution and the porosity of the surface have been made using the mercury porosimetry technique (Tiano 1995, Brus & Kotlík 1996b, Mosquera, Benítez & Perry 2002, Moropoulou et al. 2003b, Mosquera, Pozo & Esquivias 2003, Rodriguez-Navarro et al. 2003, Cardiano et al. 2005, Mosquera et al. 2005, Stück et al.

2008, Vacchiano et al. 2008, Karatasios et al. 2009, Park & Shin 2009). However, Mosquera, Benítez & Perry (2002) concluded that this technique was inappropriate to analyse the microstructure of consolidated rocks (Mosquera, Benítez & Perry 2002). Some employed micro x-ray computed tomography to study the porosity and other morphological parameters of the treated biocalcarenite (Cnudde et al. 2004, Bugani et al. 2007, Bugani et al. 2008).

Porosity and permeability are characterised by the movement of moisture into and within the stones and porosity refers to the space between solid particles in a specified volume (Warke, McKinley & Smith 2006). Permeability measurements may provide a more accurate and reliable way to predict long-term weathering reaction and moisture movement in stone (Warke, McKinley & Smith 2006). Permeability describes ease of water vapour to flow through stone under a pressure gradient and water vapour permeability is defined as the quantity of water vapour passing through a stone sample (Warke, McKinley & Smith 2006, D'Arienzo, Scarfato & Incarnato 2008). To determine the consolidation efficiency, the cup test has been employed to measure water vapour permeability of consolidated marble, sandstone, limestone and tuff-stone using the water method (Piacenti 1994, Borgia et al. 2003, Carretti & Dei 2004, Vicini et al. 2004, Vicini et al. 2005, Cnudde et al. 2006, Tsakalof et al. 2007, D'Arienzo, Scarfato & Incarnato 2008). In the cup test, water vapour permeability can be determined by either the water method or desiccant method. The water method measures loss of water vapour transmitting though tested stones out of the test cell and the desiccant method is used to detect the amount of absorbed water vapour passing through tested stones into the test cell (ASTM Standard international 2011b). The changes in the permeability of the consolidated sandstones to water vapour were evaluated by the desiccant method in this work.

As a result of a consolidation treatment, the penetration of consolidation products through the porous structure is unavoidably accompanied by the decrease in porosity of the treated stone (Tabasso 1995). The penetration of macromolecule is restricted and the superficial films of the polymer remain (Vicini et al. 2004, Vicini et al. 2005, Bugani et al. 2007). The water vapour permeability of treated stones can be rigorously decreased by the formation of superficial polymeric layers or a high number of pores filled with the

conservation materials (Bugani et al. 2007). The unsatisfactory consolidation effects resulted from surface crust that can be formed by the poor penetrating materials with high viscosity (Munnikendam 1973, Bugani et al. 2007). It is indispensable that the consolidated stones should remain permeable to water vapour and the permeability of consolidated sandstones should be maximized (Vicini et al. 2005, Bugani et al. 2007, Hameed et al. 2009). According to the incompatibility risk indicator of stone consolidants assessed by Rodrigues and Grossi (2007), the reductions of water vapour permeability of consolidated stones between 10 and 25% are considered to present medium risk (Rodrigues & Grossi 2007).

5.5.3.2. Experimental methods and analysis conditions

The determination of water vapour permeability measurements was performed based on the desiccant method, which was a modified version of standard ASTM E96/E96M–10 test method (ASTM Standard international 2011b). All measurements were carried out using a clear PVC cylindrical plastic sample bottle having length of 50 mm and diameter of 15 mm. Silica gel, as desiccant to absorb water vapour from the surrounding environment, thus providing the concentration gradient to drive permeability, was added to the sample bottle. Each sample tube was packed with 3 +/-0.01g silica gel. The sandstone specimens were placed on and firmly attached to the open side of the sample bottle by way of hot glue gun, such that the stone specimen was used to cover the open top of the bottle. Particular efforts were made in filling gaps between stone and tube using glue and a schematic diagram of the experimental set up is illustrated in Figure 5.17. The system was designed to cover all sides of the stone specimens so that water vapour flow was allowed to be diffused through the 5 +/- 0.5 mm thick stone specimen within the test area, which was within the diameter of the open top side of the plastic bottle and to be absorbed by silica gel.

A set of experiments was intended to measure the changes in permeability of the sandstone influenced by different consolidants and their penetration depth. The permeability measurements were conducted on the specimens, which were applied by capillary rise action for all consolidated sandstones and the tested consolidating agents and their compositions are given in Table 5.7. The permeability changes caused by the

consolidant penetration were evaluated and Figure 5.17 is included to show the measurements conducted from the immersed, middle and top parts of each consolidated sandstone specimen. For all three parts of each consolidated specimen, duplicate samples were measured in order to report average values obtained from two stone samples. Prior to the measurement cell preparation, the sandstone plate and plastic tube were fully dried in vacuum oven at room temperature and silica gel was left in an oven at 100°C. In order to minimize absorption of moisture from the surrounding air, the prepared measurement cells were immediately placed in a desiccator and stored in the vacuum oven at room temperature until they were tested.

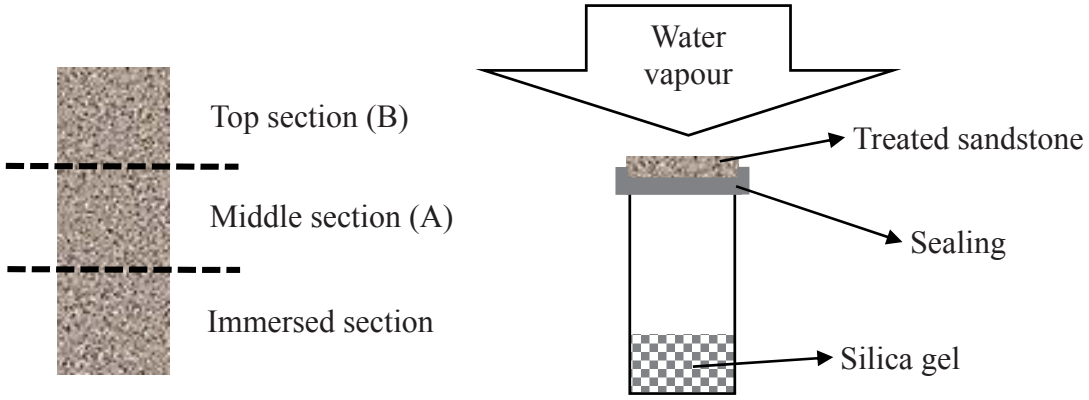

Figure 5.17. Illustration of the set-up for the water vapour permeability test

The permeability to water vapour after the consolidation treatment was determined by the weight of the measuring cells, which were increased by the moisture absorption of silica gel. The changes in the weights due to absorbed moisture were monitored under controlled environments to provide constant humidity and temperatures and the absorption of moisture was conducted in either a humidity cabinet or desiccators. Whereas the tested measurement cells were divided into three experimental groups, which were tested on separate occasions, the duplicated sandstone samples were tested in the same group for each consolidated sample. In order to compare experimental variants of each group, duplicate determinations of the untreated sandstone specimens were performed in each batch for the control observations. The samples of the two groups were measured in the temperature/humidity cabinet set at 23°C and 75% relative humidity. In the case of determinations of the third group, constant humidity was controlled using aqueous salt solutions of sodium chloride based on the standard ASTM E104–02 method

and the reported data for salt solutions (ASTM Standard international 2012). A desiccator was used as a container to provide a secured airtight seal and the sodium chloride salt produced 65% relative humidity. The measurement cells were placed in a desiccator containing a saturated aqueous solution of sodium chloride. The humidity chamber was used to keep the temperature of the system at a constant temperature and the desiccator containing the samples and saturated sodium chloride solution was left in the chamber set at 21°C for three weeks. The desiccator containing the cells and the saturated sodium chloride solution was then kept under laboratory conditions and the measurements were undertaken at ambient temperature. For each group of experimental work, monitoring and recording the data for experimental temperature and humidity was made by the temperature and humidity data logger.

Once the measurement cells were exposed to relative humidity and temperature established as above, the changes in the weight of cells were monitored until a clear plateau was reached. The daily measurements were initially performed and the frequency was reduced as conditions stabilized. The differences between the weights of the cells and the initial weights of the corresponding cells allowed evaluation of weight increase due to water absorbed by the absorbent within the cells and the percentage weight increase of the cells proportionate to the initial weight of the cells was calculated as follow:

$$(W_t - W_o) / W_o \times 100\%$$

The cells initially had weights, W_o, before the permeability tests and W_t is denoted as the weight of the cells measured after t days. Plotting the percentage weight increase against time elapsed enabled recording of the course of absorbent saturation with water. The water vapour transmission (WVT) was also calculated according to the standard test method (ASTM E96/E96M – 10) as follow:

$$\text{WVT } (g/hm^2) = (G/t)/A$$

The weight changes (G) were measured during time, t (hours) and the slope of the straight line, G/t, was calculated between 0h (t_0) and 240h (t_{240}). The test area, A, was cup mouth area of the plastic bottle in m^2.

5.5.4. Mechanical strength

5.5.4.1. Background

One of the key roles of the stone consolidation treatment is to strengthen loosed materials in order to avoid its loss of surface materials and further deterioration and to slowdown the breakdown process (Bell 1993, Piacenti 1994, Selwitz 1995, Rodrigues, Pinto & da Costa 2002, Moropoulou et al. 2003b, Cnudde et al. 2004, Domingo et al. 2008, Stück et al. 2008, Karatasios et al. 2009). When the forfeiture of the surface layer of the stone results in the subsequent damage of the historical or artistic value or endangers the stability of the overall structure of the object or its area, the decision for consolidation can be substantiated (Rodrigues 2001). The consolidation intervention is essential for decayed stones of loose cohesion in the exposed surfaces to a particular depth (Rodrigues 2001). In order to restore the physical and mechanical characteristics of the consolidated stones and to improve the resistance and coherence of damaged stone, the consolidation treatment should be able to provide sufficient penetration of consolidating agent and increased bonding between consolidating material and consolidated stone (Brus & Kotlík 1996b, Zendri et al. 2007, Hameed et al. 2009, Baglioni et al. 2009, Salazar-Hernández et al. 2010).

The durability of building stones was described as a measure of its capacity to resist weathering and to preserve its original properties, such as size, shape, strength and appearance over a prolonged period of time (Bell 1993). Factors that affect durability of a consolidated stone include many chemical and physical parameters, the durability and properties of the consolidant, compatibility of the consolidant with the stone and the environment (Moropoulou 2003a). Due to the complex interaction among these factors, the development of appropriate accelerated durability tests is problematic (Moropoulou 2003a). The deviations in stone strength often proceed and affect the stone by only a slight penetration of the outermost area (Moropoulou 2003a). The parameters related to stone strength are important in the understanding of material properties and in the analysis of decay processes and they can be used for description and characterisation of decay profiles and evaluation of efficiency of stone consolidants (Rodrigues, Pinto & da Costa 2002).

Mechanical strength tests were used to provide a method of change in the mechanical and physical properties of the consolidated stones relative to the untreated stones. The efficiencies of stone consolidation treatments applied to stones have been evaluated by mechanical characteristics, such as determinations of cohesive properties, adhesion between stone constituents, strength and density of stone surfaces and hardness of consolidated sandstones (Karatasios et al. 2009). The method used for mechanical testing can be destructive or non-destructive (Török 2010). The literature work reported various mechanical tests, including ultra-sonic velocity variations, Rockwell Indenter, peeling tape test, drilling resistance measurement, shearing meter, abrasion test, uniaxial tensile test, hardness measurement, uniaxial compression test, flexural strength and ultrasonic treatment (Mosquera, de los Santos & Rivas 1986, Saleh et al. 1992, Piacenti 1994, Selwitz 1995, Brus & Kotlík 1996b, Işik-Yürüksoy, Kiş & Güven 1998, Moropoulou 2003a, Moropoulou 2003b, Rodriguez-Navarro et al. 2003, Cocca et al. 2004, Mosquera et al. 2005, Cnudde et al. 2006, Favaro et al. 2006, Tiano et al. 2006, Favaro et al. 2007, Miliani, Velo-Simpson & Scherer 2007, D'Arienzo, Scarfato & Incarnato 2008, Domingo et al. 2008, Jimenez-Lopez et al. 2008, Pinto & Rodrigues 2008, Stück et al. 2008, Vacchiano et al. 2008, Son et al. 2009, Salazar-Hernández et al. 2010, Török 2010). The measurement of stone strength is one of the most important physical parameters and micro-drilling resistance, Schmidt hammer and Duroscope are commonly used for documenting on site (Török 2010).

In order to evaluate the consolidation performance in regard to the enhancement of mechanical strength, the measurements of bending strength have been conducted on calcareous sandstone and limestones (Rodrigues, Pinto & da Costa 2002, Moropoulou et al. 2003b). The bending test is a standard method and the bending test measurements are useful for establishing reference values to assess or compare different testing methods (Rodrigues, Pinto & da Costa 2002). In the detailed study of the mechanical characterisation of consolidated stones, Rodrigues et al. (2002) compared the mechanical characterisation of the consolidated stones using microdrilling resistance and bending strength measurements. Although Rodrigues et al. (2002) claimed that the interpretation of the mechanical strength measurements requires consideration of consolidant penetration, which can be studied by the drilling resistance, their results demonstrated good correlations between the bending strength and drilling force of the stones

consolidated by total immersion (Rodrigues, Pinto & da Costa 2002). Therefore, the mechanical strengths of the consolidated sandstones in this study were assessed by the bending tests and the tested results were intended to compare the consolidation efficiencies of the treated sandstones. Taking into account effects of consolidant penetration on the mechanical characteristics of consolidated sandstones, the consolidated sandstones for bending strength measurements were prepared by total immersion of sandstone.

5.5.4.2. Experimental methods and analysis conditions

The measurement of three point bending strength was conducted on consolidated and unconsolidated sandstone samples. The rectangular specimens were used for all measurements and the consolidated samples were prepared by full immersion, which aimed to produce the better and more uniform distribution of consolidants in the treated sandstones. A series of consolidated sandstones were prepared using polymer, polymer-MMT composites and in situ polymerisation of AA and Am as summarized in Table 5.7, which provided the selected consolidants for the three-point bending test. The triplicate samples were prepared for each consolidant and all of the results are expressed as average values obtained from the triplicate samples. The treated sandstones were dried in air for the removal of moisture and both untreated and treated sandstone specimens were stored in laboratory conditions in order to obtain equilibrium state. All procedures and tests were performed under laboratory conditions. Prior to the bend tests, the lengths were recorded from the middle position of each sandstone specimen whilst the width and thickness were recorded from the left, middle and right positions. The measured sizes of the treated sandstone specimens ranged from 4.6 to 5.0 cm in length, from 1.4 to 1.8 cm in width and from 0.4 to 0.6 cm in thickness. The width and thickness used for the calculation of bending strength correspond to average values obtained from three measurements.

The procedures employed for bending strength measurements was based on some modifications to the method that was established in the Standard ASTM D790–10 test and the measurements were performed on an the universal testing machine (Shimadzu AGS-X) with a 10 kN load capacity (ASTM Standard international 2010). The bending test was conducted using a cross-head speed of 2 mm/min in a laboratory environment at

22.2°C and 55.0 % relative humidity. Two round bars provided two supporting points.

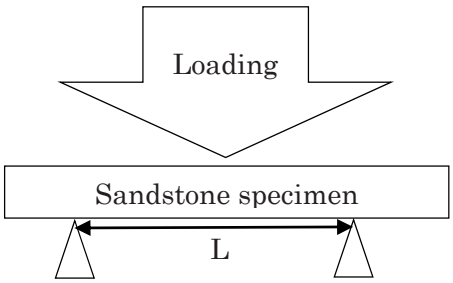

Figure 5.18. Schematic diagram of three point bend testing

The rectangular sandstone specimens were placed on two support spans and the central positions of the sandstone specimens were situated at the midpoint of support spans (Figure 5.18). The loading span above the sandstone specimen was situated at the midspan, such that the force was applied to the central positions of the sandstone specimens.

In order to evaluate the changes in the mechanical strength of the consolidated sandstone specimens relative to the unconsolidated sandstone, the flexural stress of tested sandstone specimens was calculated according to the following equation (ASTM Standard international 2010):

$$\sigma_f = 3 \cdot 38.13P/2wt^2$$

where P is maximum load applied, span length is 38.13 (mm) and w and t stand for width and thickness of specimen, respectively.

CHAPTER 6. RESULTS AND DISCUSSION: CHARACTERISATION OF SANDSTONE CONSOLIDANTS

6.1. Introduction

In this chapter, the composites composed of MMT prepared from the preformed or in situ polymerised polymers, as described in Chapter 5, were characterised. To begin, the prepared composite films were characterised by macroscopic inspection, followed by X-ray diffraction, microscopic, infrared spectral and thermal methods were applied to the study of the microstructure of MMT, bonding interaction of polymers with MMT and thermal stability of the polymer/MMT composites. The experiments were planned to study how composite formation was affected by preparation conditions, MMT content, reaction time, reaction temperature and molecular weight of the polymer. The intent of investigating the different experimental factors in this chapter was to reduce any experimental variables that are likely to be insignificant for the sandstone consolidation treatment. Of the tested variables, the emphasis was placed on whether the content of MMT, as the hydrophilic polymer-MMT composites at high clay concentrations, would be an effective way for designing water-based consolidants, wherein the structure and properties of clay are retained to some extent and the polymers present in the galleries remain to avoid the swelling of MMT. Because of the important role of MMT to improve the chemical compatibility and stability of the composite materials, efforts were made to characterise the composites containing a wide range of MMT concentrations and to identify the critical range of MMT concentration that are potential and practical in the consolidation work of Sydney sandstone.

6.2. PAA-MMT composite system

6.2.1. Microscopic evaluation of PAA-MMT composite films

The composite films containing 10–70% MMT and PAA100 prepared using ultrasound treatment are presented in Figure 6.2.1. The preservation of the natural appearance of consolidated stone is one of the most important considerations in evaluating the suitability

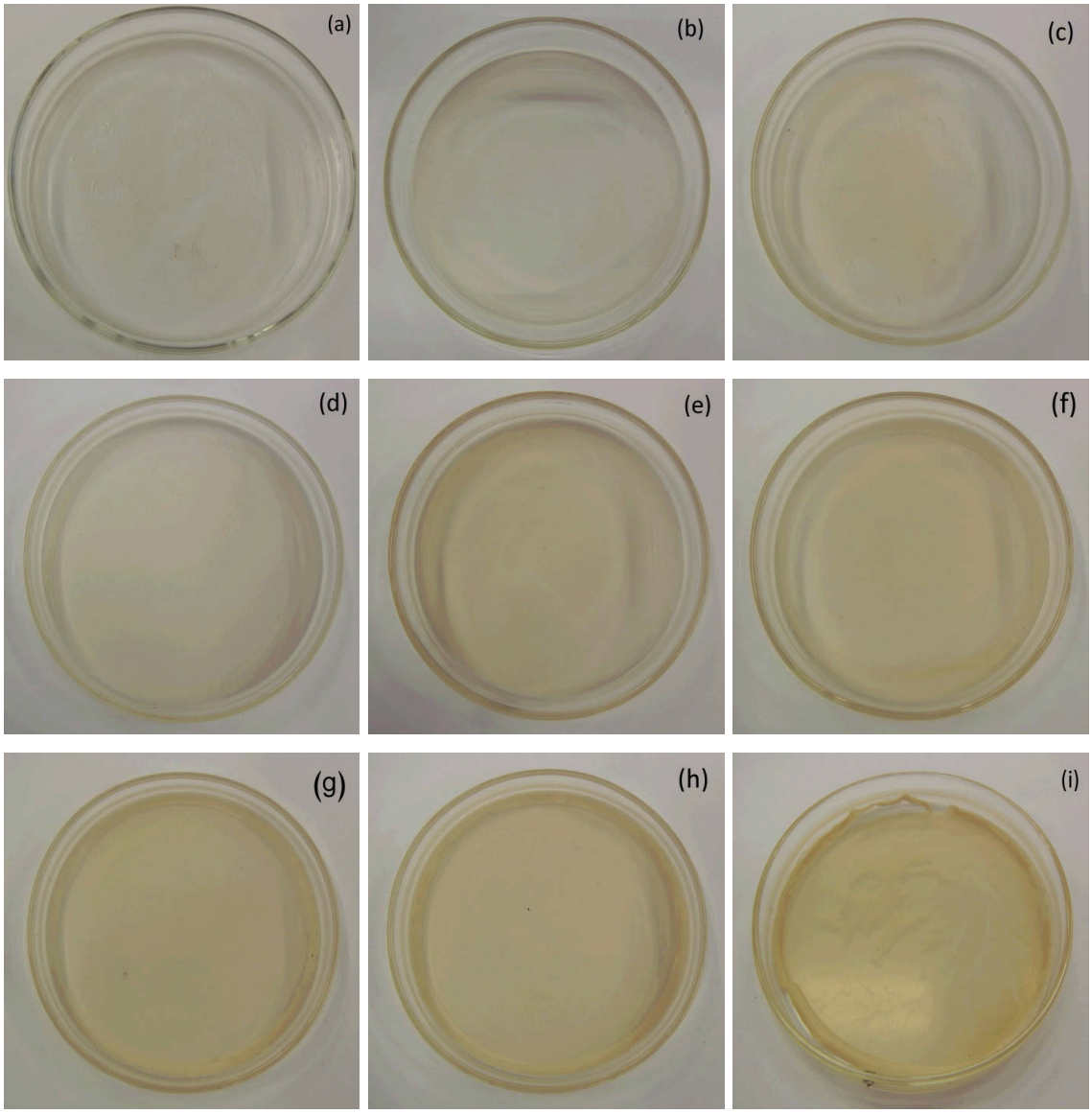

Figure 6.2.1. PAA100M composite films dried after the ultrasonication treatment at (a)10% MMT, (b) 20% MMT, (c) 30% MMT, (d) 40% MMT, (e) 50% MMT, (f) 60% MMT, (g) 70% MMT, (h) 80% MMT and (i) 90% MMT

of the composite samples as stone consolidants. Consequently, the appearance and colour of the composites are of great significance as consolidating materials. It was observed that the mixtures of PAA100 and MMT produced the composite films in which the distribution of MMT was macroscopically homogeneous. The films produced from lower clay loading appear clearer and more cohesive, whereas the use of higher MMT contents produced more fragile and opaque films. Compared to the brittle composite films containing 70–90% MMT, the opacities and brittleness of the films increase with higher

MMT contents, but the films remained fairly transparent up to 60% MMT loadings. Although a similar trend was observed for the composite films produced by PAA250, the composite samples containing PAA250 were noticeably more opaque, but showed improved cohesive properties. Based on their colours, uniformness and clarity, the composites using 10–60% MMT demonstrate appearance characteristics matching the need of the intended application.

6.2.2. XRD analysis of PAA-MMT

The XRD patterns in the range of 2θ = 2.5-25 and 2.5-10.5° for the composites are illustrated in Figure 6.2.2 and 6.2.3. The oriented clay displays a broad basal reflection of (001) plane at 2θ = 7.0 corresponding to a c-axis basal spacing of 12.6 Å. Although all samples at all PAA-MMT ratios exhibit the peaks near 2θ = 8.9, 12.5, 17.5 and 19.9°, the first basal reflection of MMT appearing as a broad peak shifts from 7.0° 2θ to lower angles after the treatment of MMT with PAA. The measured d-spacing of PAA-MMT composites indicates the separation of the silicate layers up to approximately 19.6 Å

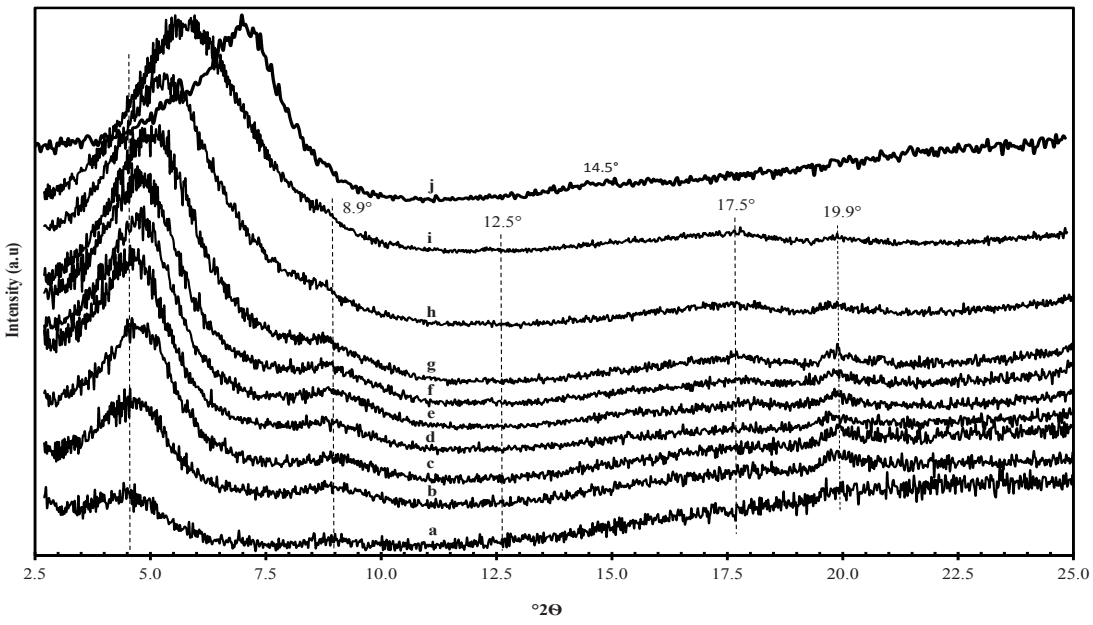

Figure 6.2.2. XRD patterns of (a) PAA100M1, (b) PAA100M2, (c) PAA100M3, (d) PAA100M4, (e) PAA100M5, (f) PAA100M6, (g) PAA100M7, (h) PAA100M8, (i) PAA100M9 and (j) MMT

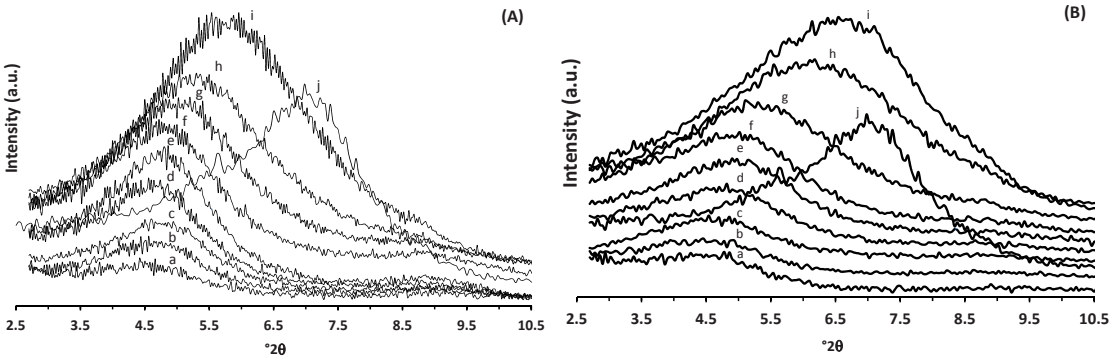

Figure 6.2.3. Basal (001) reflection of the ultrasonicated composites formed from (A) PAA100 and (B) PAA250 at (a)10% MMT, (b) 20% MMT, (c) 30% MMT, (d) 40% MMT, (e) 50% MMT, (f) 60% MMT, (g) 70% MMT, (h) 80% MMT, (i) 90% MMT and (j) 100% MMT

(Figure 6.2.4) and, therefore, the PAA-MMT composites at all MMT-PAA ratios display the penetration of PAA between the gallery evident by the increased d-spacing of PAA-MMT composites.

The XRD profiles of the further-mixed PAA-MMT ultrasonicated dispersions yielded the essentially unchanged degree of PAA100 penetration into MMT, but resulted in reduced penetration of PAA250 at MMT concentrations less than 80%. The results at both temperatures were interpreted as having a negligible effect of processing time on the MMT layer separation by the PAA intercalation and the equilibrium state of PAA-MMT intercalated structure after the ultrasonic treatment. Although the intercalation degree of PAA to MMT layers prepared by the ultrasonication treatment in this work corresponds fairly well to the results for the solution intercalation of PAA into sodium MMT using the conventional mixing method or water bath sonication, the rapid rate of intercalation during the process of ultrasonication results in what appears to approach saturation of the galleries with PAA, as no further intercalation is observed on subsequent treatment.

The XRD data obtained for the specimens prepared at 60°C in the current work showed an essentially unchanged or a small decrease in the interlamellar spacing for both PAA100 and PAA250 series. Although the longer heat treatment was used in an attempt to increase the PAA penetration into silicate layers by enhancing PAA mobility and penetration rate within the MMT galleries, it did not induce further lattice expansion of MMT layers,

indicating a negligible effect of temperature on the intercalation of PAA. The further heat treatment, in fact, had a small adverse effect on the PAA100 penetration, resulting in a small reduction in interlayer spacing. The further treatment appeared to reverse the processes of PAA250 intercalation to a higher degree. The removal of PAA250 after heat treatment demonstrates the better stability of PAA100 over PAA250 in the interlayer space. The ultrasonication resulted in a similar interlayer distance of MMT to that made by Tran et al. (Tran et al. 2006), who used the conventional mixing method and showed an increase in the interlayer spaces of MMT after heat treatment of PAA and sodium MMT at 60°C. The results are independent of processing temperature and the similar interlayer distance of MMT after the ultrasonication treatment without further heat treatment may indicate effectiveness of ultrasonic treatment which significantly enhanced the accessibility of lamellar spaces to PAA.

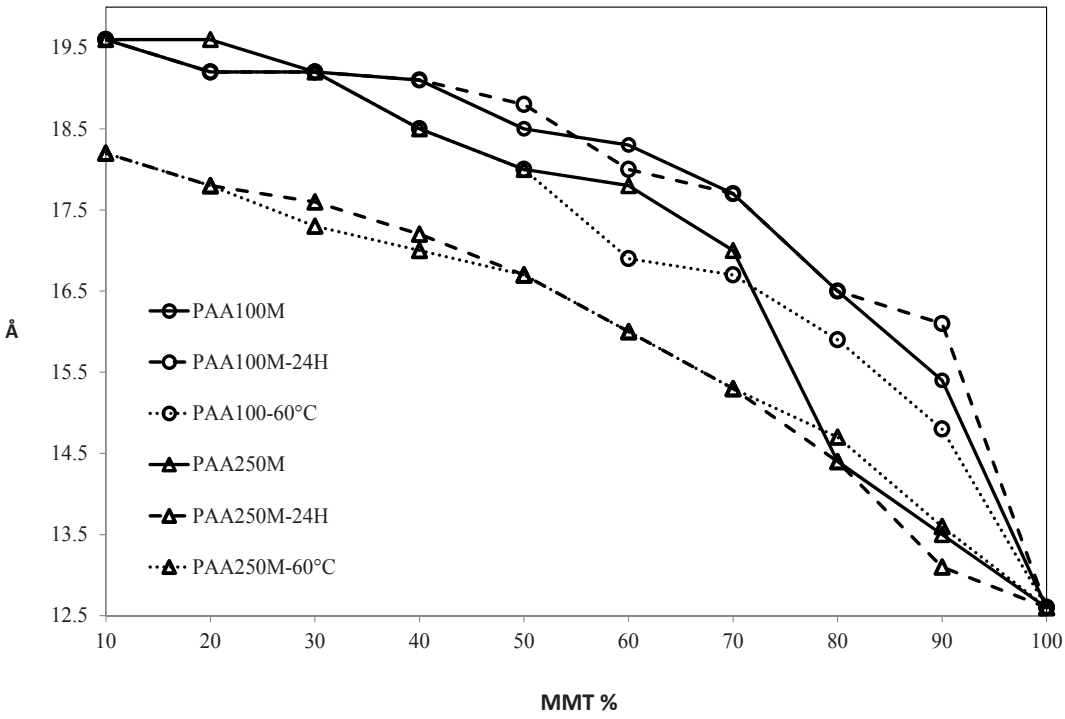

Figure 6.2.4. Changes in d_{001} spacing plotted as a function of the MMT loadings

In agreement with the study on aqueous solution intercalation of hydrophilic polymers, including PAA and PVA (Strawhecker & Manias 2000, Ip 2007, Ip et al. 2011b), the general trend is the same; that is, the interlayer expansion is inversely related to clay contents under all experimental conditions conducted in this investigation. In all cases,

the extent of interlayer enlargement falls within the values for the intercalated structure, which is indicative of the layers remaining stacked in all compositions. Although diffusion of PAA clearly occurs with increasing concentration of PAA, the (001) reflections identify the upper limit for the PAA uptake. The XRD curves show that the interlamellar expansion progressively increases up to 40% PAA, beyond which no further increase in the interlamellar spacing is observed indicating that the galleries have a maximum capacity of PAA (Ip 2007).

6.2.3. SEM study of PAA-MMT composites

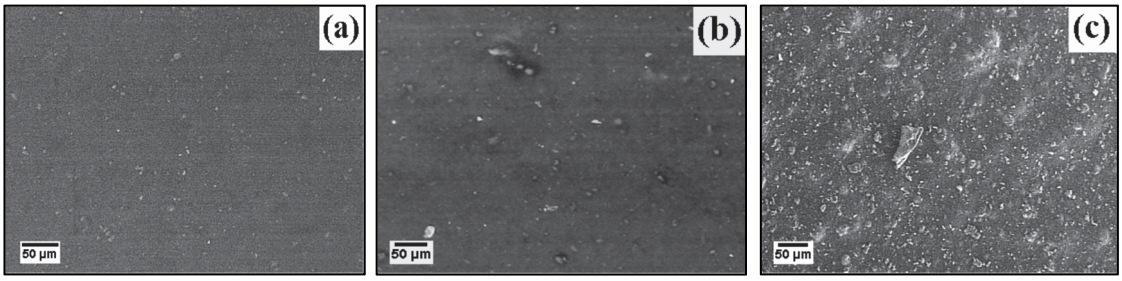

Figure 6.2.5. Backscattered images of (a) PAA100M1, (b) PAA100M4 and (c) PAA100M7 at magnification of 200

Backscattered electron imaging was performed to inspect the distribution of MMT in PAA100 and produced contrast between MMT and PAA100. As seen in Figure 6.2.5, the backscattered images of PAA100-MMT composite systems displayed the MMT particles as bright spots against dark background of the PAA100 matrix. Although these images revealed the homogeneous distributed MMT within PAA100 and the increase in the size of MMT particles and the surface roughness with increasing clay loadings, the images obtained at low magnification were found to be insufficient to observe detailed surface information of MMT particles and higher magnification was used to obtain further morphological information on unmodified MMT and PAA100-MMT composites.

The microstructures observed from the ultrasonicated MMT and oriented MMT were examined by SEM at higher magnification and are presented in 6.2.6(a) and (b). The SEM

images obtained from the sonicated MMT dispersion showed a flaky layered appearance of large MMT aggregates and silicate layers are self-assembled to form a disordered stacking arrangement (Figure 6.2.6 (a)). As seen from the SEM images taken from the surface of oriented MMT specimen in Figure 6.2.6 (b), the gravity sedimentation technique resulted in the parallel orientation of the MMT platelets and particle size of the oriented MMT revealed the lateral dimension of MMT platelets around 100-150 nm. The analysis of dried and uncoated MMT showed the presence of MMT clusters up to 10 μm and the measured particle size range indicated the formation of MMT clusters after the ultrasonication treatment of MMT (Figure 6.2.6 (c)).

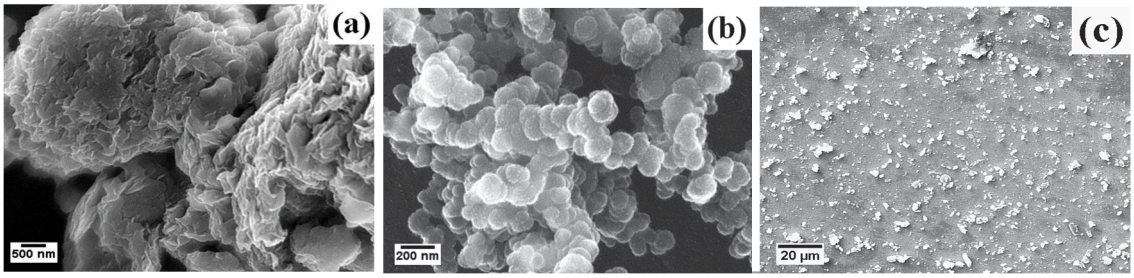

Figure 6.2.6. SEM micrographs of gold-coated MMT particles (a) dispersed by ultrasonication and (b) prepared by sedimentation technique and (c) uncoated MMT particles dispersed by ultrasonication of 2.5 wv% MMT suspension

In order to examine nano scales and morphology changes of PAA100-MMT composites at various MMT loading, surface and cross sections of the samples were viewed and compared by SEM at higher magnification, as shown in Figure 6.2.7 and 6.2.8. The similar observations to backscattered electron analysis were seen from these images, which were taken under coated conditions at higher magnifications. However, it has been noted that in the SEM images of the samples containing 10-20% MMT, the presence and position of MMT were not clear, which implies that it produced the images from the coating at low MMT concentrations as illustrated in Figure 6.2.7(a) and 6.2.8(a). Although the samples were coated to improve conductivity of the samples and to dissipate electron charge accumulation on the surface, the images were also observed from the uncoated samples at low voltage and compared with the coated samples.

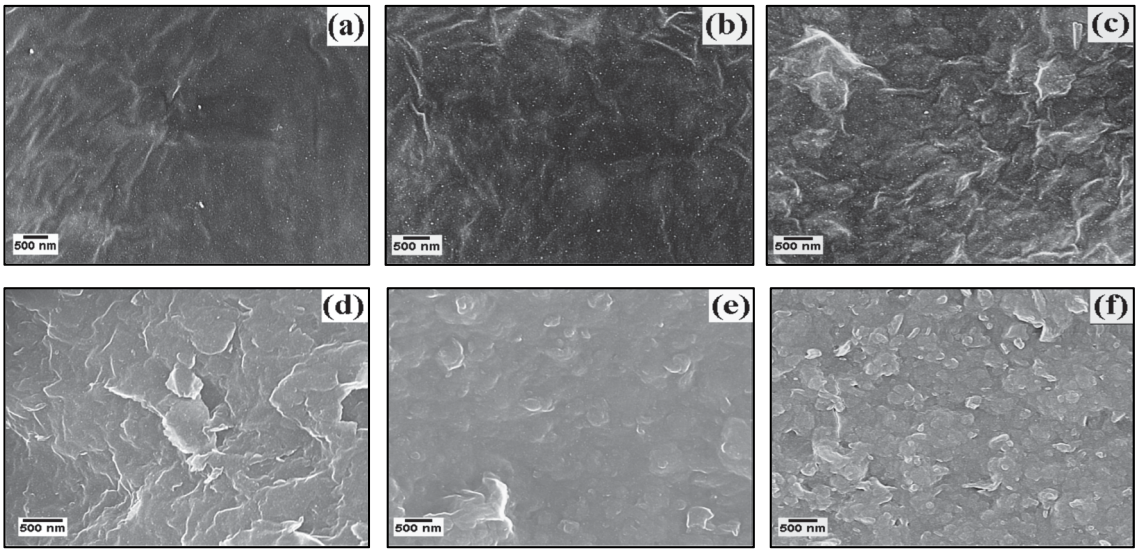

Figure 6.2.7. Carbon coated surface images of (a) PAA100M1, (b) PAA100M2, (c) PAA100M4, (d) PAA100M5, (e) PAA100M7 and (f) PAA100M9

From SEM analysis of surface morphology and the cross-sectional microstructure of the ultrasonicated PAA100-MMT samples, clay particles of irregular shapes and various sizes were observed. In contrast to silicate layers stacked together to form a flaky surface of MMT, the large aggregates present in MMT appear to be broken apart into smaller

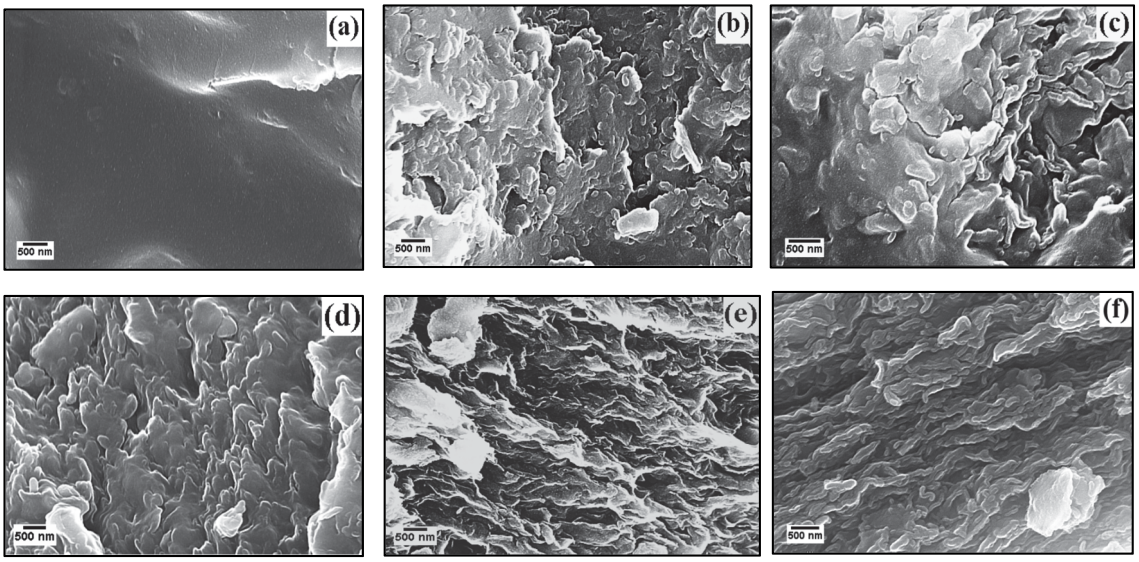

Figure 6.2.8. Carbon-coated cross-sectional images of (a) PAA100M1, (b) PAA100M2, (c) PAA100M3, (d) PAA100M5, (e) PAA100M7 and (f) PAA100M9

sizes in the composites with decreasing clay ratio and are spread more uniformly in the PAA matrix. Although there appears to be an increase in the degree of separation and disordered orientation of MMT particles with decreasing clay content, the particle size of the composite, even at 10% MMT, shows many particles having thicknesses in the range of 15-55 nm. This signifies that reduced size agglomerates of a few (10 to 50) stacked clay layers remained after the intercalation of PAA as indicated by the reflection at 4.5° 2θ in Figure 6.2.9. The SEM images at 10–40% MMT display a smoother surface, a more disordered orientation of clay particles in PAA matrix, a greater variability in particle size and shape and a generally increased particle size in comparison to higher MMT contents, which show a rougher and flakier surface characteristic of clay aggregate. With increasing MMT content, there appears to be a systematic increase in size and degree of order of the clay particle orientation and the overall effect gradually approaches more uniform systems of clay aggregates. The increase in dispersibility and a reduction in particulate size with increasing PAA content suggest that there is a significant degree of intercalation of the clay galleries as observed in the XRD.

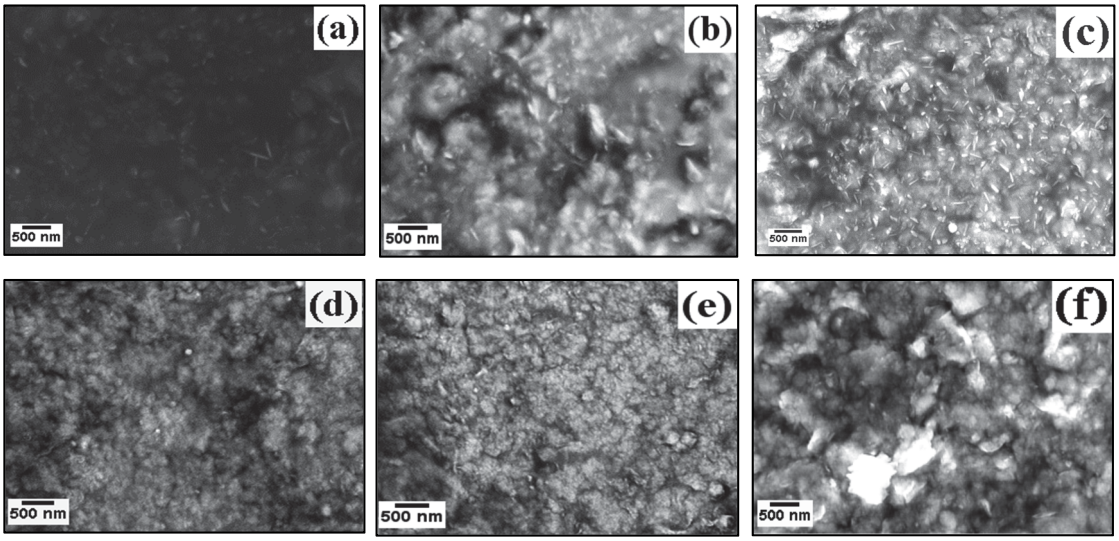

Figure 6.2.9. Non-coated surface images of (a) PAA100M1, (b) PAA100M3, (c) PAA100M4, (d) PAA100M5, (e) PAA100M6 and (f) PAA100M7

6.2.4. FTIR analysis of PAA-MMT composites

The FTIR spectra of the PAA100-MMT composites show the presence of bands typically related to both PAA and MMT (Figure 6.2.10). The assigned peaks of MMT and PAA are summarized in Table 6.2.1 based on FTIR data available in the literature for raw MMT and PAA (Nyquist et al. 1982, Hu et al. 1991, Dong et al. 1997a, Dong et al. 1997b, Alexander, Payan & Duc 1998, Moharram & El-Gendy 2002, Moharram & Khafagi 2007). The absorption bands associated with MMT include OH stretching and bending modes of lattice water, the stretching modes of structural hydroxyls and Si-O-Si and the bending vibrations of Al_2OH, Si-O-Si and Al-O-Si are observed at 3431, 1640, 3628, 1038, 925, 471 and 526 cm^{-1}, respectively (Farmer & Russell 1964, Madejová 2003). The characteristic absorption bands pertaining to PAA are OH and CH stretching, CH_2 deformation, carbonyl stretching and CO stretching coupled with the O-H in-plane bending at 3180, 2958, 1454, 1712 and 1414 cm^{-1} (Don Dong et al. 1997b). These

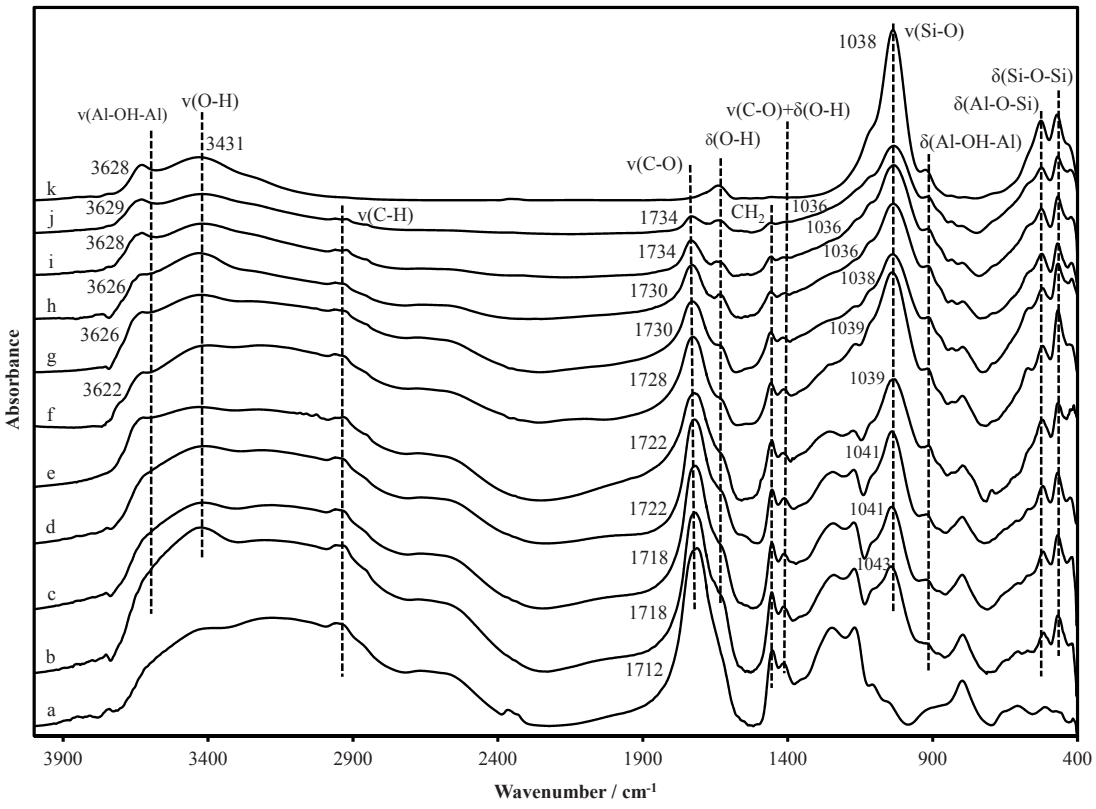

Figure 6.2.10. FTIR spectra of (a) PAA100, ultrasonicated PAA100-MMT composites at (b) 10% MMT, (c) 20% MMT, (d) 30% MMT, (e) 40% MMT, (f) 50% MMT, (g) 60% MMT, (h) 70% MMT, (i) 80% MMT and (j) 90% MMT and (k) MMT

Table 6.2.1. Infrared Bands of PAA and MMT and their peak assignments

cm^{-1}		Assignments
PAA	MMT	
-	3628	Al-OH-Al stretching
-	3431	O-H stretching vibrations of the interlayer water
3180	-	O-H stretching vibration of hydrogen-bonded OH groups
2958	-	CH_2 or CH stretching vibration
2669	-	Overtones and combinations of bands
1712	-	C=O stretching vibration
-	1640	O-H deformation vibrations of the interlayer water
1454	-	Bending vibration of CH_2
1414	-	Coupling of C–O stretching and O–H deformation vibrations
1246	-	Coupling of C–O stretching and O–H deformation vibrations
1169	-	Coupling of C–O stretching and O–H deformation vibrations
1109	-	C-CH_2 stretching vibration
-	1038	Si-O-Si stretching
-	925	AlAlOH bending
900	-	Out-of-plane bending OH
	876	AlFeOH
-	837	AlMgOH
798	-	CH_2 twisting and C-COOH stretching
-	792	Si-O vibrations of amorphous silica
-	526	Al-O-Si bending of tetrahedral layer
-	471	Si-O-Si bending

characteristic absorption bands become weaker for the composites with decreasing PAA and increasing MMT contents in the composites. There appears to be no significant changes in the positions of the majority of the characteristic bands associated with PAA and MMT for all compositions, apart from the C=O stretching bands.

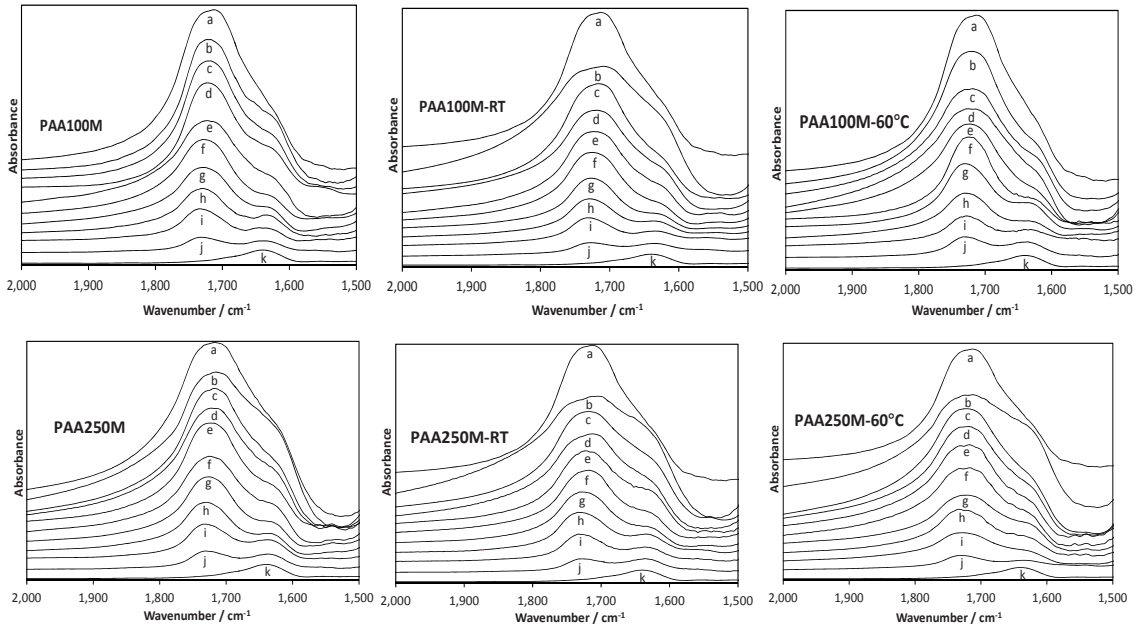

Figure 6.2.11. Carbonyl FTIR stretching vibrations of (a) PAA, ultrasonicated PAA-MMT composites at (b)10% MMT, (c) 20% MMT, (d) 30% MMT, (e) 40% MMT, (f) 50% MMT, (g) 60% MMT, (h) 70% MMT, (i) 80% MMT (j) 90% MMT and (k) 100% MMT

The absorption band at 1712 cm^{-1} assigned to the carbonyl stretching band, exhibits a gradual upward shift with increasing MMT content (Figure 6.2.11 and 6.2.12). The shift of carbonyl stretching bands suggests a reduction in the degree of hydrogen bonding of PAA, which indicates that the PAA is absorbing on or intercalating in the MMT galleries (Dong 1997b). The reduced degree of hydrogen bonding due to the increase in adsorption can be observed in the relative increases in the pH (Figure 6.2.13). Intercalation, in particular, will reduce availability of the CO_2H proton for dissociation. This increase in pH may also be attributed to ion exchange with the MMT as there also appears to be a small new peak at around 1550 cm^{-1} attributable to the anti-symmetric stretching mode of carboxylate groups (McCluskey, Snyder & Condrate Sr 1989, Jones et al. 1998).

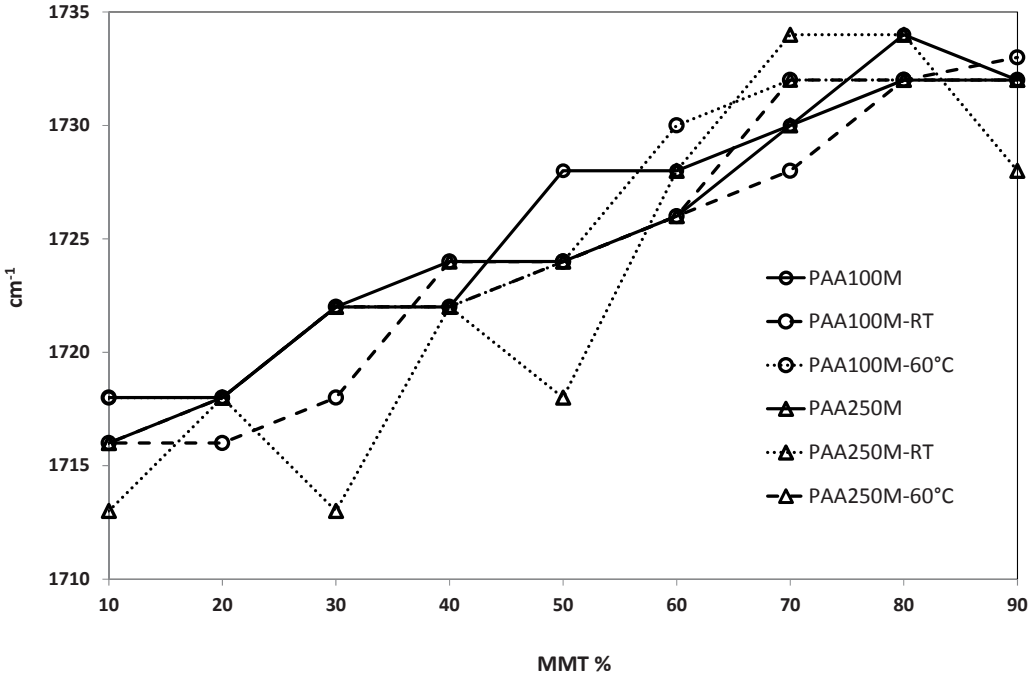

Figure 6.2.12. Plot of carbonyl stretching absorption band positions against MMT loadings

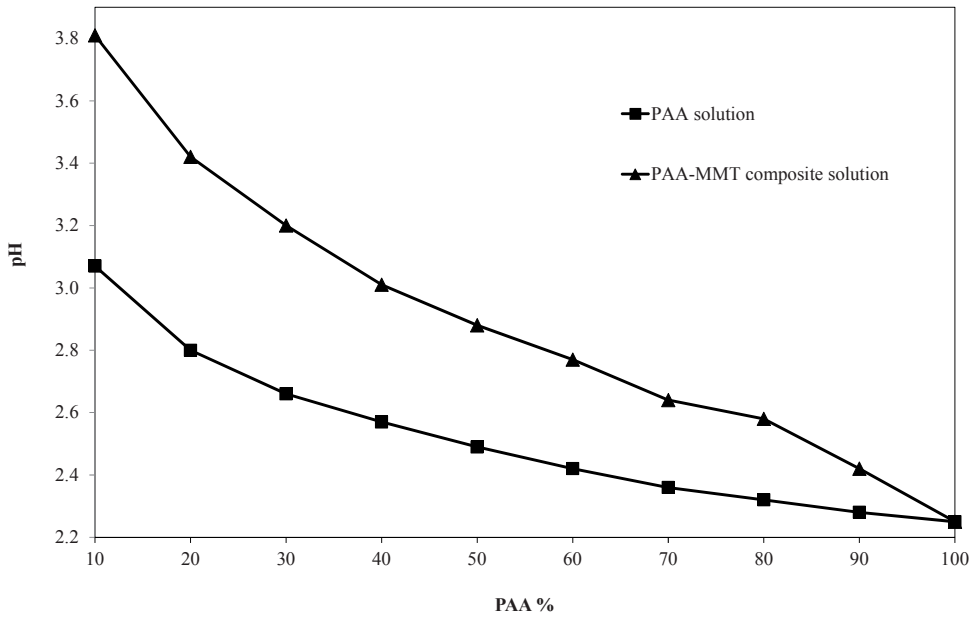

Figure 6.2.13. Changes in pH values plotted as a function of the PAA concentrations. The PAA solutions contained the same amount of PAA used for the corresponding composite solutions having a total solid concentration of 2.5 w/v%

Based on pH change, 92 and 2.8% of Na^+ or K^+ ions in MMT were exchanged with proton of PAA at 10 and 90% MMT and there was less exchange reaction with increasing MMT content as there was less PAA and more MMT. The amount of proton exchange ranged from 0.5 to 1.1% and the nondissociated form of PAA predominates at all MMT concentrations. The pH values and concentrations of the studied composites together with the weak carboxylate absorption bands suggest, however, small proton exchange of PAA with exchangeable interlayer cations, with the carboxylic acid groups of PAA mostly non-dissociated in all composite solutions. These results are consistent with the small concentration of exchangeable interlayer cations available for proton exchange reaction, since elemental analysis detected only 1.3% Na_2O and 0.95% K_2O by weight in MMT.

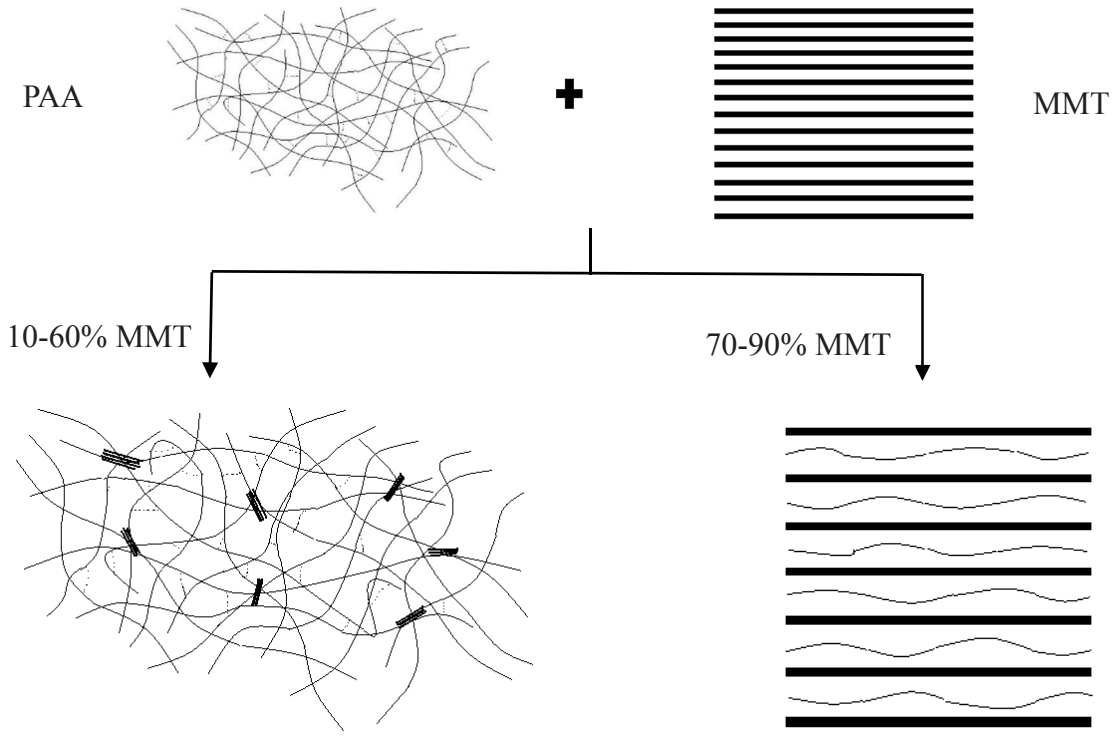

Figure 6.2.14. Schematic presentation of formation of PAA-MMT composites having intercalated structures

Consequently, the non-dissociated form exists in the interlayer space of MMT because the negatively changed species cannot be absorbed. The intercalation of protonated PAA is evidenced in particular by the shift in the carbonyl peak to higher wavenumber. The IR spectra recorded on the further treated and heat-treated samples showed the similar results to the ones observed for the ultrasonicated samples. The shift in the carbonyl peaks

correlates with the intercalation of the PAA and shows an increased proportion of PAA intercalated as the MMT content increases. Thus, the composite system can be modelled according to Figure 6.2.14. This correlation also applies to the XRD data.

6.2.5. Thermal analysis of PAA-MMT

Figure 6.2.15 and Figure 6.2.16 show the differential TG (DTG) results obtained for PAA100, MMT and each of the ultrasonicated PAA100-MMT composites and the TG and DTA curves of PAA100. The DTG and TGMS curves of the thermal decomposition of PAA reflected the occurrence of three different mass reduction steps as identified by the maximum peaks on the DTG curves, gravimetric loss and evolved gases in the TGMS data, as summarized in Table 6.2.2. In the first mass reduction step up to approximately 140°C, a small mass loss of 6.2 % occurred because of the removal of absorbed water as indicated by the peaks at m/z = 17 and 18 amu. In the second mass reduction step up to a DTG maximum of 264°C, a mass loss of 26.6 % occurred and it was accompanied by an endothermic peak (Kabanov, Dubnitskaya, & Khar'kov 1975, Maurer, Eustace & Ratcliffe 1987, Dubinsky et a. 2004). The TG-MS data showed peaks at m/z = 17, 18, 22, 29, 44, 45, 46, 58 and 72 amu and the second mass loss step was associated with the release of water, carbon monoxide, acetone, acrylic acid and carbon dioxide. PAA has been shown to form an intramolecular anhydride mostly at temperatures below 150-200°C (McGaugh & Kottle 1967, Eisenberg, Yokoyama & Sambalido 1969). The separation of water observed up to approximately 215°C in this mass loss region may be suggestive of anhydride formation caused by the intramolecular dehydration of adjacent monomer rings. The loss of water at around 260ºC might be attributable to the intermolecular dehydration of unreacted PAA during the intramolecular dehydration reaction (McGaugh & Kottle 1967, Eisenberg, Yokoyama & Sambalido 1969). The release of carbon dioxide identified at m/z = 22, 44, 45 and 46 amu is attributed to the decarboxylation reaction due to the breakdown of the anhydride structure to carbon dioxide. The decarboxylation process can be followed by the formation of other minor degradation products such as carbon monoxide, ketenes, ketones, unsaturated compounds and acetone, and the observed peaks at m/z = 29 and 58 are likely attributable to carbon monoxide and acetone that were separated as degradation products (McGaugh & Kottle 1967, McNeill & Sadeghi 1990,

Dubinsky et al. 2004). The acrylic acid evolved in this step may indicate a depolymerisation reaction (McNeill & Sadeghi 1990, Dubinsky et al. 2004). In the last mass reduction step from 370 to 440°C with a DTG maximum of 419°C, a mass loss of 42.5 % was observed during the thermal decomposition along with a broad exothermic peak with a maximum of 472ºC beginning during this step and extending up to approximately 480ºC (Dubinsky et al. 2004) and it was accompanied by peaks indicating the evolution of water, carbon dioxide, acrylic acid, carbon monoxide and acetone.

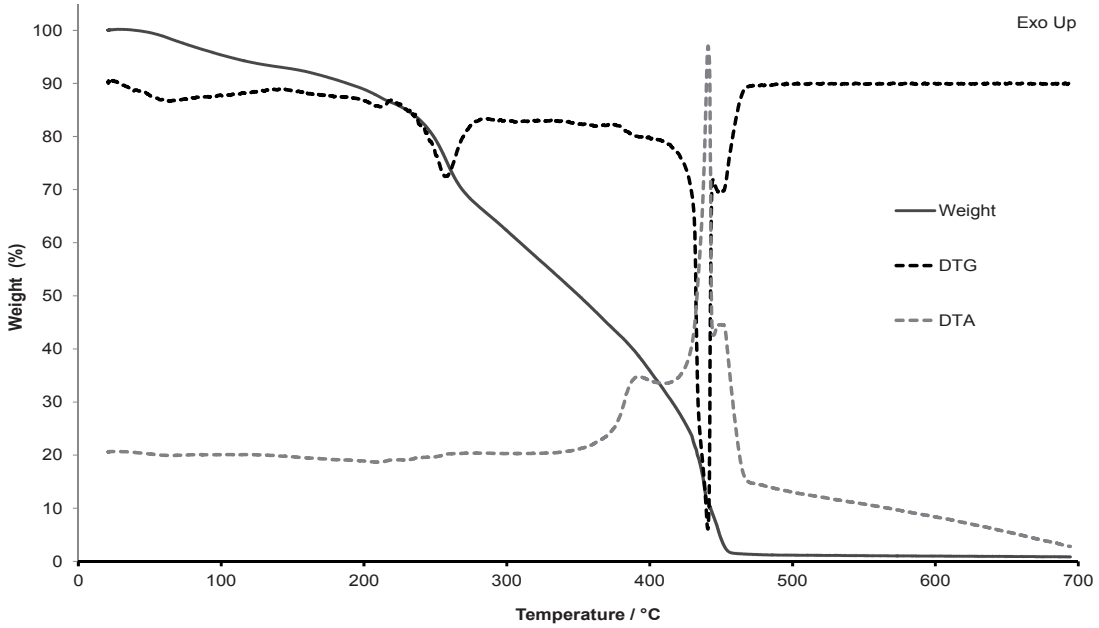

Figure 6.2.15. TG, DTG and DTA curves of PAA100 heated at 10ºC/min

Table 6.2.2. Mass losses of PAA and MMT

Sample	Interval temp (°C)	DTG Peak temp (°C)	Mass loss (%)
PAA100	25 - 140	45	6.2
	140 - 283	264	26.6
	375 - 500	419	42.5
MMT	25 - 193	76	4.6
	360 - 555	459	5.3

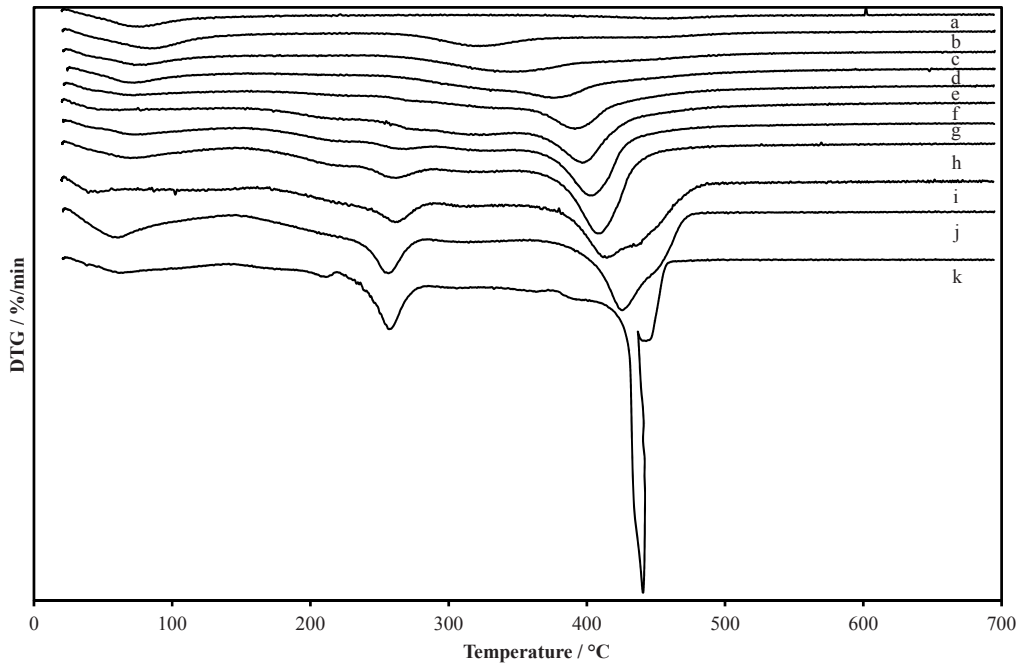

Figure 6.2.16. DTG curves of (a) MMT, the ultrasonicated PAA100M composites at (b) 90% MMT, (c) 80% MMT, (d) 70% MMT, (e) 60% MMT, (f) 50% MMT, (g) 40% MMT, (h) 30% MMT, (i) 20% MMT, (j) 10% MMT and (k) PAA100

Although the dehydration, decarboxylation, depolymerisation and production of short chain fragments appear to occur as observed in the last mass loss step, the higher-intensity ion peaks detected for carbon dioxide indicate that the decarboxylation reaction becomes more significant in this temperature region. The evolution of water and carbon dioxide as well as the 0.6% residual mass are suggestive of a complete oxidation reaction in the last step (Dubinsky et al. 2004).

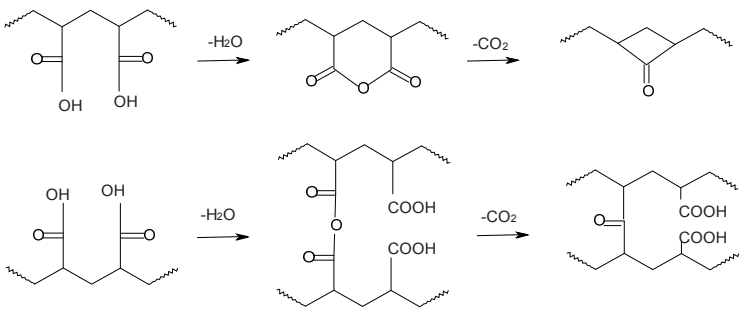

Figure 6.2.17. Intra- and intermolecular dehydration and decarboxylation of PAA

The DTG and TGMS curves of MMT exhibited two mass loss steps. Generally, the heat treatment of pristine MMT produces two mass loss steps in temperatures of up to 1000°C, and it is known to thermally decompose through dehydration and dehydroxylation (Kok 2002). The mass loss occurring at a temperature range of 100-400°C is ascribed to different water sources, due to their coordination with the exchangeable cations and surface moisture (Kok 2002). The first endothermic mass loss of 4.6%, observed in temperatures of up to 193°C, occurred with the release of water, including both free water and interlayer water. Free water evolved in this region is known to exist between MMT crystallites, while the interlayer water present between the aluminosilicate layers can include the hydration spheres of the exchangeable Na^+ ions (Hedley et al. 2007). The second mass loss step with a maximum DTG peak at about 459°C occurred between 360 and 555ºC. According to the reported thermal analysis results, structural water is understood to disappear due to the dehydroxylation of MMT layers at a higher temperature (Hedley et al. 2007, Kok 2002). Although the second mass loss may correspond to the dehydration of structural water due to the dehydroxylation of the MMT layers, in this temperature range the evolution of water based on peaks corresponding to the release of water is not clearly seen.

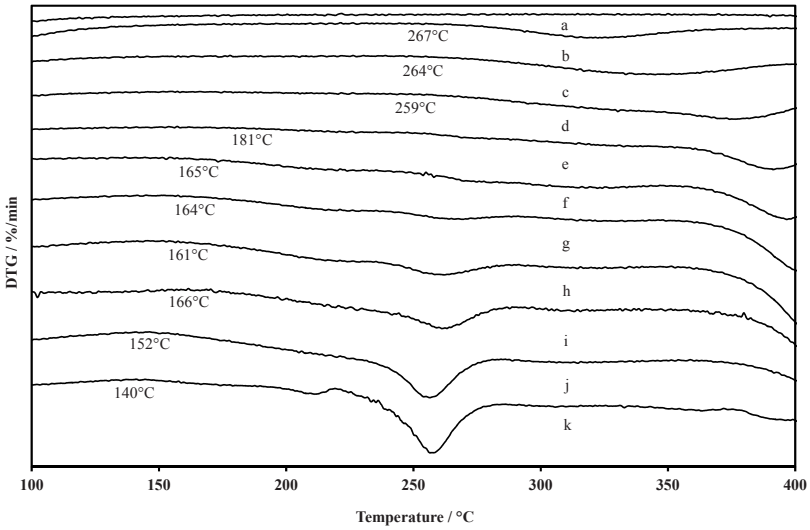

Figure 6.2.18. DTG curves of (a) MMT, the ultrasonicated PAA100-MMT composites at (b) 90% MMT, (c) 80% MMT, (d) 70% MMT, (e) 60% MMT, (f) 50% MMT, (g) 40% MMT, (h) 30% MMT, (i) 20% MMT and (j) 10% MMT and (k) PAA100, showing the initial thermal decomposition temperatures of PAA

PAA is observed to decompose through a series of decomposition steps which include dehydration and elimination of CO_2 (McGaugh & Kottle 1967, Eisenberg, Yokoyama & Sambalido 1969, Maurer, Eustace & Ratcliffe 1987, McNeill & Sadeghi 1990, Dubinsky et al. 2004). Additionally, exothermic oxidation of the PAA occurs in the 400 to 600°C range. The strongly exothermic nature of the oxidation is the cause of the unusually sharp peak of the PAA decomposition in the region. MMT, on the other hand, only undergoes dehydroxylation in the temperature range resulting in a small mass loss of ca. 5.3% (Velde 1992, Balek et al. 1999). A proposed decomposition mechanism of PAA reported in the literature is illustrated in Figure 6.2.17, which shows a two-step decomposition of PAA with the first step resulting in the elimination of water and the second step resulting in the elimination of CO_2, prior to oxidation or pyrolysation (McGaugh & Kottle 1967, Eisenberg, Yokoyama & Sambalido 1969, Maurer, Eustace & Ratcliffe 1987, McNeill & Sadeghi 1990, Dubinsky 2004).

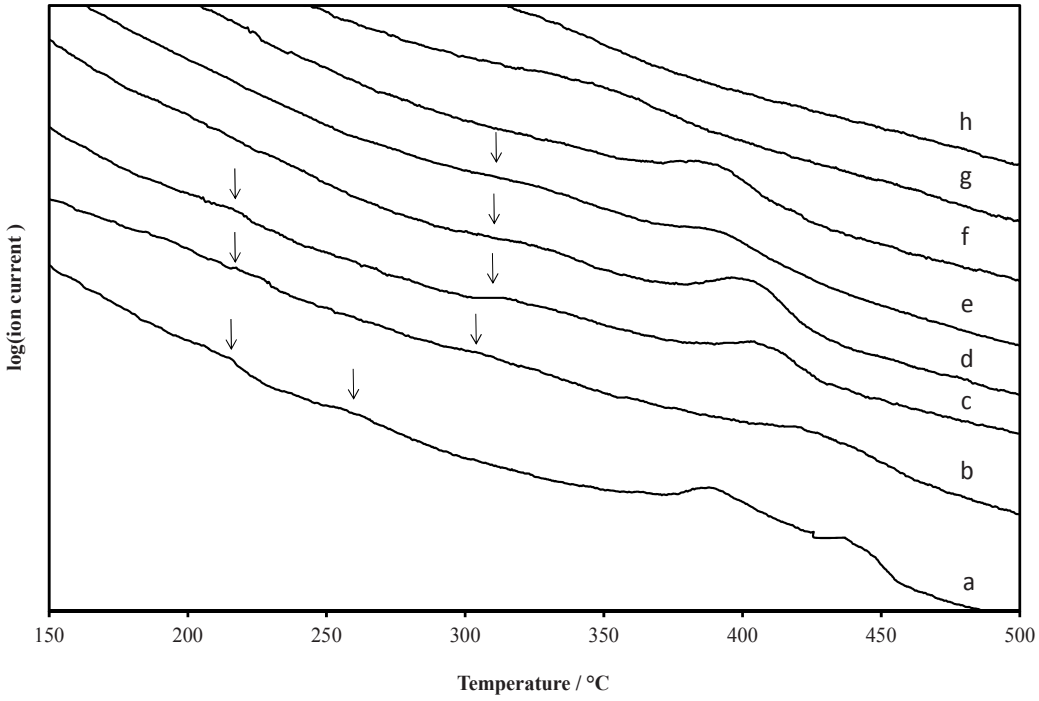

Figure 6.2.19. TGMS curves for dehydration reaction of (a) PAA100, the ultrasonicated PAA100-MMT composites at (b) 10% MMT, (c) 30% MMT, (d) 40% MMT, (e) 50% MMT, (f) 60% MMT, (g) 80% MMT and (h) 90% MMT at a heating rate of 2°C/min

Two pathways (inter- or intra-molecular elimination) are possible for the initial condensation step (McGaugh & Kottle 1967, Eisenberg, Yokoyama & Sambalido 1969,

McNeill & Sadeghi 1990). The decomposition of the PAA occurs at a relatively low temperature ca. 140°C, which correlates with the relatively labile nature of the decomposition steps identified in Figure 6.2.17 (McGaugh & Kottle 1967, Eisenberg 19 Eisenberg, Yokoyama & Sambalido 1969, Maurer, Eustace & Ratcliffe 1987, McNeill & Sadeghi 1990, Dubinsky et al. 2004). The initial decomposition for the PAA occurs at around 140°C and this peak rapidly diminishes in size with increasing MMT content. The onset temperatures of decomposition of PAA100-MMT composites increase in temperature with an increase in MMT concentration (Figure 6.2.18). The onset of decomposition for the PAA-MMT composites is delayed to a higher temperature with increasing MMT contents. The MMT is, therefore, aiding the stabilisation of the PAA through adsorption of the PAA to the MMT surface and through intercalation. The onset of thermal degradation is observed to fit into two groups. The onset temperatures of the composites with 10-60% MMT concentration are similar below 200°C. For the composites containing more than 60% MMT, the onset temperatures of decomposition are considerably higher. The noticeable changes in their DTG curves observed between 60 and 70% MMT concentrations indicate correlations. The data from in the DTG curves again correlates with the XRD, FTIR and SEM data of the composites and provides additional evidence in support of the changes in the structures and the formation of the two types of intercalated structures.

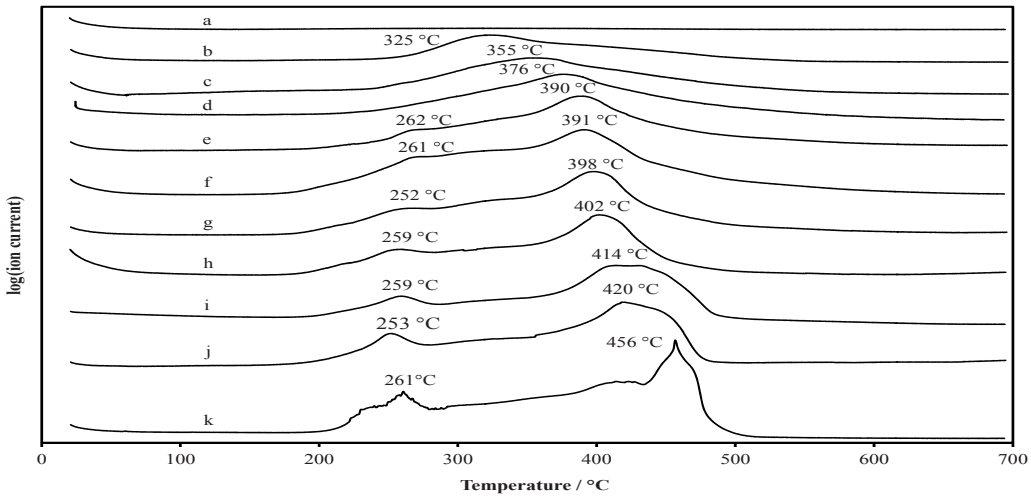

Figure 6.2.20. TGMS curves for decarboxylation of (a) MMT, the PAA100-MMT ultrasonicated composites at (b) 90% MMT, (c) 80% MMT, (d) 70% MMT, (e) 60% MMT, (f) 50% MMT, (g) 40% MMT, (h) 30% MMT, (i) 20% MMT, (j) 10% MMT and (k) PAA100

While the PAA sample produced the three peaks due to a dehydration reaction of PAA, the corresponding peaks seem to disappear from the composite samples, as illustrated in Figure 6.2.19. Most water released for the dehydration reaction of PAA display small signals which are difficult to be detected due to the presence of high background water. Comparison of the ion current curves for evolved water vapor of the composites reveals the changes associated with the dehydration processes of PAA, and, as the clay content is increased, the disappearance of water formation. The ion current curves of PAA and the composites at 10-30% MMT show the presence of water vapour which was released at about 215°C due to the dehydration reaction of PAA. For composite compositions with greater than 30% MMT, no water release below 250°C is seen. The corresponding first dehydration process appears to be lost for the composite samples at 40-90% MMT in this temperature range. The TG-MS curves related to the CO_2 species indicate that increasing the MMT content appears to result in a shift in onset temperature and a change in peak intensity, as seen in Figure 6.2.20. Comparison of these curves shows that the composites containing 10-60% MMT loadings appear to display similar characteristics in comparison to the ones for the higher clay content. The onset temperatures due to the first decarboxylation reaction increased gradually with clay content while the peaks due to the last decarboxylation reaction shifted to lower temperature with increasing clay loading.

It is clear that PAA and MMT exhibited different thermal behaviours and superior thermal stability of the composites compared to PAA. The improvement in thermal stabilities and changes in dehydration and decarboxylation processes of PAA100 in the composites can be attributed to the high thermal stability of MMT and PAA100-MMT interactions. Analysis of evolved water from the thermal decomposition of PAA, MMT and their composites indicates that the change in ratio of PAA to MMT appears to reflect a change in the dehydration reaction of PAA and also in the interaction between PAA and MMT. The water formation attributable to the dehydration process of PAA seems to disappear due to the presence of MMT between PAA polymer chains and the intra- and inter-molecular dehydration reaction of PAA could be hindered by an interaction between PAA and MMT that would involve hydrogen bonding between the carbonyl oxygen of PAA and hydroxyl groups of MMT. Therefore, the reduction in the water formation due to the dehydration reactions of PAA depends on clay content and relates to the physically cross-linked structure in which the presence of MMT generated the coordination between PAA

and MMT. MMT can perform as a barrier towards the dehydration and decarboxylation reaction of PAA and cause a delayed decomposition of PAA-MMT composites. With its ability to enhance the thermal stability of PAA-MMT composites, the presence of MMT and the use of higher MMT contents in the composite structure show positive effects on the thermal stability of PAA-MMT composites. Therefore, the PAA-MMT ratio seems to have a noticeable effect on the stability of PAA, and the presence of MMT stabilizes the PAA system - even when the ratio of MMT increased from 0 to 1.

6.2.6. Summary

The formation of an intercalated structure of PAA-MMT composites with a direct aqueous solution intercalation technique demonstrates layer separation up to 19.6 Å due to the intercalation of PAA into MMT layers. The degree of interlayer expansion was independent of processing time and temperature, but was mainly determined by the molecular size of PAA and the accessibility of PAA to the intercalating site of MMT, which were influenced by clay-PAA ratios and the dispersibility of MMT particles. In terms of the intercalation behaviour of PAA and their structures and stabilities, the best results were attained using ultrasonicated PAA100-MMT samples. The direct aqueous solution intercalation using the ultrasonic mixing technique demonstrated not only a simple and fast method, but also a green preparation approach for the production of a PAA-MMT intercalated system.

The changes in structure and stability of the PAA-MMT composites indicated the clay concentration dependent behaviour of the intercalated composites. The thermal stabilities of composites improved with an increase in MMT loading. Only a small proportion (< 10% MMT) is required to stabilize PAA to thermo-oxidative degradation. The XRD and SEM data show that the intercalation of MMT with PAA takes place up to the saturation of the interlayer cavity. Once this is achieved, no further separation of the MMT d_{001} spacing occurs. The properties and structural frameworks are similar to those found for MMT up to this MMT concentration, which suggests the coexistence of properties of polymer and clay in composite systems. The moderate contents, up to 50% MMT, reveal structurally favourable, stable and compatible composites on the molecular level for use

as a stone consolidating material. The TG, XRD, SEM and FTIR data obtained for the series of PAA-MMT composites showed that there is intimate interaction between MMT and PAA. The intimate interaction between MMT and PAA suggests that this material will have good compatibility with the sandstone as a composite.

6.3. PAm-MMT composite system

6.3.1. Macroscopic evaluation of PAm-MMT films

The appearance and color of the PAm-MMT films were first inspected to evaluate the suitability of the samples as stone consolidants and the photographs of the representative PAm-MMT films are shown in Figure 6.3.1. The films produced from both unmodified MMT and acidified MMT changed in similar fashion and transparent and adhesive films with uniform distribution of MMT particles moved in the direction of more brittle and opaque samples closer to the features of MMT with increasing MMT loadings. At 2.5-10% MMT under all experimental conditions, the observed films were nearly transparent and possessed a considerable binding effect, showing the similar appearance and characteristics to those of PAm alone. The MMT particles at 10% MMT appeared nearly imperceptible, while the macroscopic particles became clearly visible at 20% MMT loadings. Previous studies on transparent polymers showed their optical clarities for low filler loading resulted from filler dispersion to nanoscale levels or the exfoliated state (Strawhecker & Manias 2000, Yeh, Liou & Chang 2004).

While increasing MMT concentrations from 20 to 90% was accompanied with the increase in color intensity of the produced films, the MMT loadings up to 50% resulted in the macroscopically uniform distribution of particles in the fairly transparent films. Further increase in MMT contents produced fragile and opaque films unsuited for stone consolidation work. The observations pointed to the ability of acidified MMT to improve transparency and distribution of MMT particles over 50% MMT as demonstrated in Figure 6.3.1(g) and 6.3.1(j). The more transparent films with better distribution of acidified MMT particles were noticeable in comparison to denser PAm-MMT films with a mixture of uniform and non-uniform distributions of MMT1 at 60-70% MMT. The enhanced transparency of the films can be accounted to acidified MMT to develop the transparency of MMT. Considering the performance criteria of material to meet the intended application, the films consisting of up to 50% MMT are apparently compatible with the natural look of sandstone, according to their brownish color, uniform and transparent appearances and demonstrate their sufficient cohesive and adhesive forces to cling to target stone material.

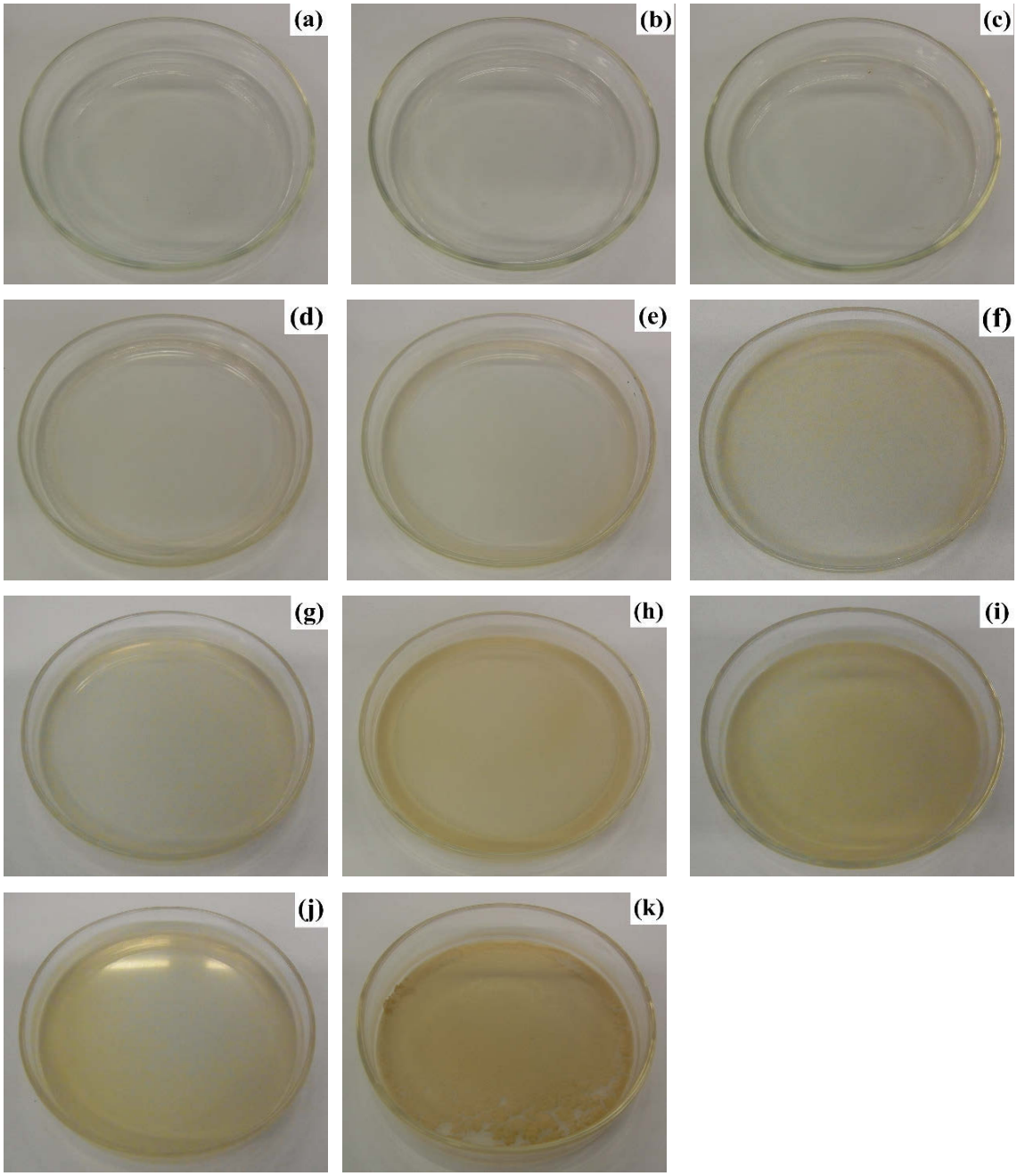

Figure 6.3.1. Photographs of the ultrasonicated PAm-MMT films at (a) 2.5% MMT, (b) 5% MMT, (c) 10% MMT, (d) 20% MMT, (e) 40% MMT, (f) 50% MMT, (g) 50% acidified MMT, (h) 60% MMT, (i) 70% MMT, (j) 70% acidified MMT and (k) 80% MMT

6.3.2. XRD analysis of PAm-MMT

Figure 6.3.2 shows the XRD patterns observed for the diffraction peaks along the (001) basal plane of MMT in the ultrasonicated samples and the oriented MMT. The peaks appeared at around 2θ = 8.5, 17.4 and 19.9° at all ratios of PAm to MMT and the variations in the XRD patterns were only found from the basal reflection along the (001) plane of layer silicates. The broad diffraction peak for the oriented MMT specimen at 2θ = 7.0 is assigned to the (001) basal plane with a lattice d-spacing of 12.6 Å and the treatment of MMT with PAm resulted in the interlayer expansion along the (001) plane of layer silicates evidenced by a shift of the (001) plane basal reflection to lower diffraction angle (Figure 6.3.3 (A) and (B)). The (001) basal plane spacing of the MMT gradually increased from 90% to 20% MMT, after which clear d_{001} basal spacing reflections were undetectable at less than 20% MMT under all experimental conditions (Figure 6.3.3 and 6.3.4).

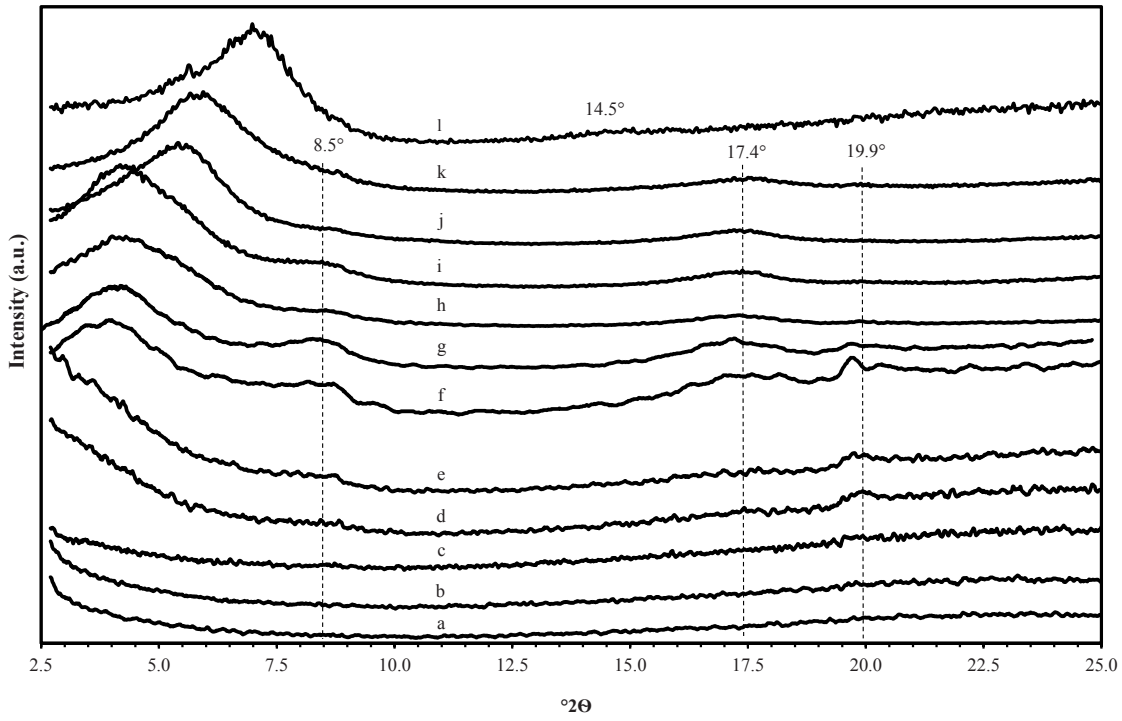

Figure 6.3.2. XRD patterns of (a) PAmM2.5, (b) PAmM5, (c) PAmM10, (d) PAmM20, (e) PAmM30, (f) PAmM40, (g) PAmM50, (h) PAmM60, (i) PAmM70, (j) PAmM80 and (k) PAmM90 and (l) unmodified MMT

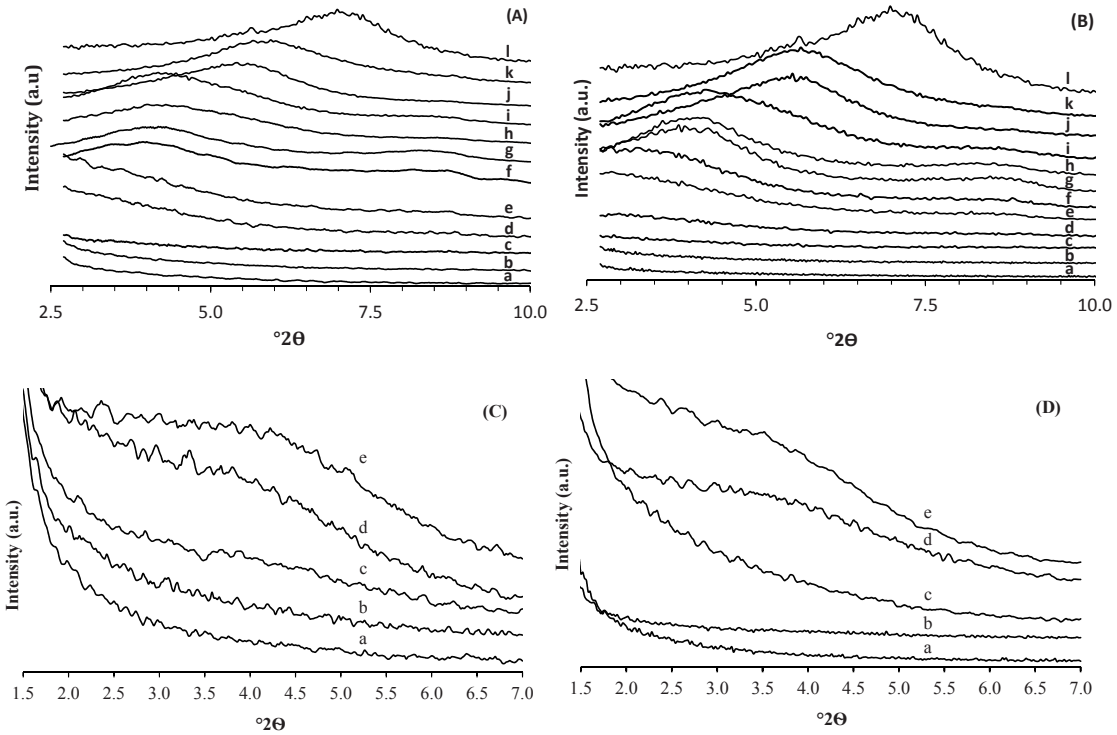

Figure 6.3.3. Basal (001) reflection of ultrasonicated samples produced from unmodified MMT ((A) and (C)) and acidified MMT ((B) and (D)) at (a) 2.5% MMT, (b) 5% MMT, (c) 10% MMT, (d) 20% MMT, (e) 30% MMT, (f) 40% MMT, (g) 50% MMT, (h) 60% MMT, (i) 70% MMT, (j) 80% MMT and (k) 90% MMT and (l) MMT

The variations in d_{001} spacings reflected the inverse relationship between the MMT loading and the interlamellar separation. This inversion was more obvious for the samples with high MMT compositions and the measured interlayer gaps up to 26.9 Å indicated the intercalated structures where the silicate layers remain stacked (Kim & Palomino 2011, Huang & Ye 2014b). At MMT contents less than 50%, the smaller extent of peak shifting and the broader peaks with higher background intensity toward lower angles were observed, making them undetectable at low MMT concentrations. The observed data suggested separation of silicate layers, in agreement with the previously reported results for the intercalation behaviour of PAm into MMT (Ogawa, Kuroda & Kato 1989, Churchman 2002, Yeh, Liou & Chang 2004, Dangge et al. 2009, Kim & Palomino 2011, Huang & Ye 2014b, Koç et al. 2014). As the MMT loading decreased, a shift in the 001 peak was observed indicating an increase in the basal spacings until at 10% loading and below, no basal plane peak was observed indicating exfoliation of the MMT.

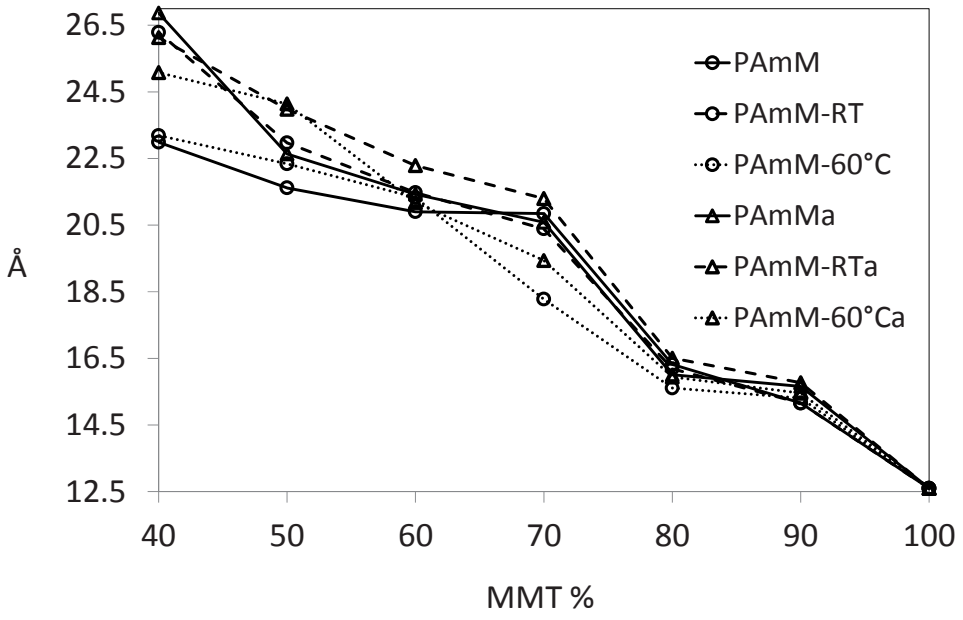

Figure 6.3.4. Comparison of d_{001} spacing plotted against the MMT loadings

While these curves could be viewed as large interlamellar separation, due to the PAm intercalation, attention was given to the fact that the featureless diffraction pattern could be related to dilution effect below 10% MMT or due to the disordered structure of these materials, due to varied interlattice magnitudes caused by the disorientation of the silicate layers. However, the (001) peaks showed a shift toward increased interlayer distance with increasing PAm concentrations across all experimental conditions and there was a systematic variation in the shifting and broadening of the (001) peaks. The reported studies have also shown the partial formation of MMT layer exfoliation at low MMT concentration based on the featureless (001) diffraction peaks (Yeh, Liou & Chang 2004, Dangge et al. 2009, Kim & Palomino 2011, Koç et al. 2014). The position and characteristics of these peaks may suggest the potential formation of exfoliated silicate layers that coexist with intercalated layer structure in considerable proportions. Therefore, these observations, whilst mixed and non-uniform structures are likely, point to interlameallar separation extended beyond the intercalated layer structure at low MMT concentrations.

The results obtained for the further treated samples produced general minor changes in the interlayer expansion up to 40-50% PAm, above which the interlayer gaps tended to

be enlarged with increasing PAm concentrations in comparison to the ultrasonicated samples. The increased interlayer spacing of the further treated samples was observed at less than 50% MMT and the layer separation was extended to a small degree in the state where the structure composed of non-intercalated and excess PAm. Some investigators reported that penetration of smaller molecules through the interlayer region was favoured due to better ability of smaller sized molecules to penetrate (Kim & Palomino 2011). As followed from the assumed increased interlayer penetration in dependence on decreasing molecular size of intercalants, the small molecular weight PAm used in this work became available as non-intercalated and excess PAm and the longer mixing time facilitated slightly the additional PAm diffusion as observed for the PAm adsorption study on MMT (Bottero et al. 1988).

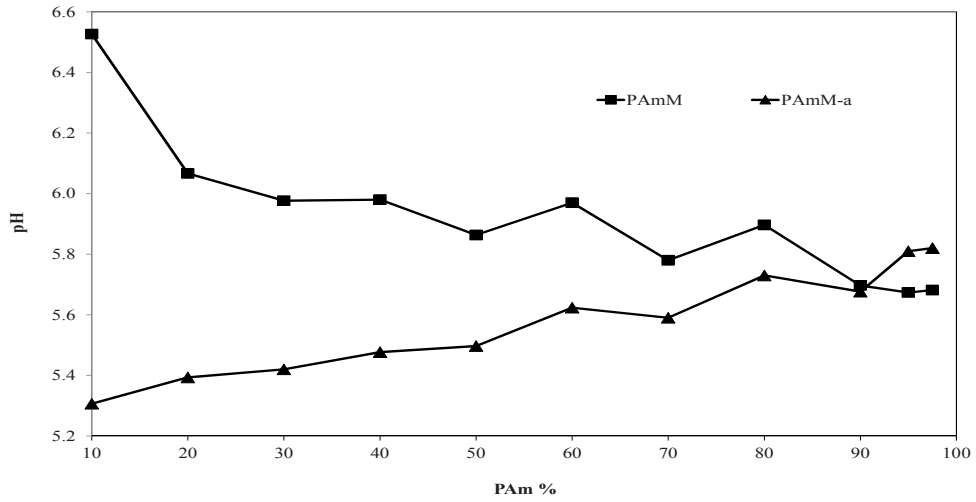

Figure 6.3.5. Measured pH values of the ultrasonicated PAm-MMT samples prepared using the unmodified MMT (PAmM) and the acidified MMT (PAmM-a) plotted against the PAm concentration

On the contrary, the heat treatment of the ultrasonicated samples slightly reduced the interlayer d-spacing of most heat treated samples. The small decrease in interlayer spaces due to the deintercalation of PAm chains indicated that the penetrated PAm chains did not orient well in the interlayer region. The interactions between MMT surface and polymer could be disrupted by the thermal motion of PAm, making them susceptible to the structural destabilization. Further PAm penetration was not detected after further heat treatment of the ultrasonicated PAm-MMT dispersions and the effect of increased

temperature was found to be insignificant, which agrees with the work of Kim & Palomino (2011).

While the variations in d_{001} interplanar spacings reflect the similar behaviours to the non-acidified samples, the acid treated samples generally enhanced the separation of the silicate layer in comparison to non-acidified samples prepared in the same manner. Similar to the results obtained for the further treatment of the ultrasonicated dispersion at room temperate, the changes in (001) reflections indicated that the acidification process of MMT resulted in slightly higher or comparable interlayer distance of MMT at 2.5-50 % MMT. The measured pH of the PAm—MMT dispersions changed with increasing MMT contents and varied from 5.7 to 6.5 for the non-acidified MMT samples and from 5.8 to 5.3 for the acidified MMT samples (Figure 6.3.5). The observed pH variations appeared to reflect the PAm conformational changes. The increased pH of non-acidified samples could be regarded as increased extent of expanded PAm structure while increasing acidified MMT concentrations reduced the pH to form more coiled conformations of PAm (Kim & Palomino 2011, Bishop et al. 2014).

Whereas the pH measurements indicated the partial coiled conformation of PAm at all PAm-MMT ratios, the extended conformation of PAm chains became more available with increasing the unmodified MMT concentration or decreasing the acidified MMT concentrations and the general tendency of more extended state of PAm with decreasing acidified MMT may facilitate the increased PAm diffusion observed for the less than 50% acidified MMT (Besra et al. 2004, Kim & Palomino 2011, Bishop et al. 2014). Although a more coiled structure of PAm for the acidified samples is expected from their lower pH values compared to the non-acidified samples, the slightly larger interlayer distance of acidified MMT indicated that more coiled PAm chains were able to be intercalated at high PAm concentrations compared to the non-acidified MMT samples and the chain conformation of PAm showed insignificant effect on their intercalation behaviours, similar to the results shown by Inyang & Bae (2005) and Kim & Palomino (2011) (Inyang & Bae 2005, Kim & Palomino 2011).

Although the longer treatments of the ultrasonicated samples at both temperatures and acidification process of MMT appeared to show some effect on the separation of the

silicate layer, the overall contribution of mixing time, temperature and pH was negligible and the intercalation extents of PAm were mostly attained after the ultrasonication treatment, which was fast and effective for MMT particle separation. The results obtained for the ultrasonication method in this work correlate with what has been reported for the absorption studies of smectite or MMT prepared by direct solution intercalation of non-ionic PAm in the works of Bottero et al. (1988), Deng et al. (2006) and Kim & Palomino (2011).

6.3.3. SEM study of PAm-MMT

Figure 6.3.6 depicts the backscattered electron images of selected ultrasonicated PAm-MMT samples to examine distribution of non-acidified and acidified MMT in PAm matrix. The MMT particles appearing bright were regularly distributed within polymer film at all PAm-MMT ratios and uniform surface morphology was observed. As MMT content increased in the samples, the particle size of dispersed MMT became larger and the smoothness of the sample surface was steadily reduced to form the rougher surface over 60% MMT. Although the MMT content dependence of the particle dispensability and separations was observed from the samples formed by both acidified and non-acidified MMT, the acid treatment of MMT caused the precipitation of impurities in the acidified MMT, indicating that the presence of sulfate-related impurities remained after the repeated washing process (Ip 2007). At 2.5-10% acid-treated MMT, leaf-like impurities appeared to be stacked up in the middle to form bow-shaped impurities that were spread in the polymer matrix. The microscopic evaluation of acidified samples suggested that the impurities were dispersed and detached, possibly due to the significantly improved separation and distribution of the MMT particles at this MMT concentration range. Conversely, the SEM observation of the high acidified MMT content showed crystal microaggregates with little or no dispersion of salt crystals as seen for the 60% acidified MMT (Figure 6.3.6 (f)).

Microstructure and morphological information of smaller MMT particles were examined from their surface and cross-sectional areas for the ultrasonicated samples at higher magnification (Figure 6.3.7). While fairly uniform distribution of MMT particles

appeared in the PAm matrix throughout all MMT concentrations, MMT particle size tended to decrease as PAm concentration increased. The stable distribution within the matrix may indicate the interactions between PAm and MMT and increase in deaggregation and separation of particles with increasing PAm concentration was observed. At high MMT concentration, MMT is clearly a major phase in the structure, the flaky and grainy surface and large MMT aggregate particles indicated similar surface morphology to that of MMT alone. The large agglomeration of MMT in the surface of the PAm-MMT composites were seen at 70-90% MMT as in Figure 6.3.7(d).

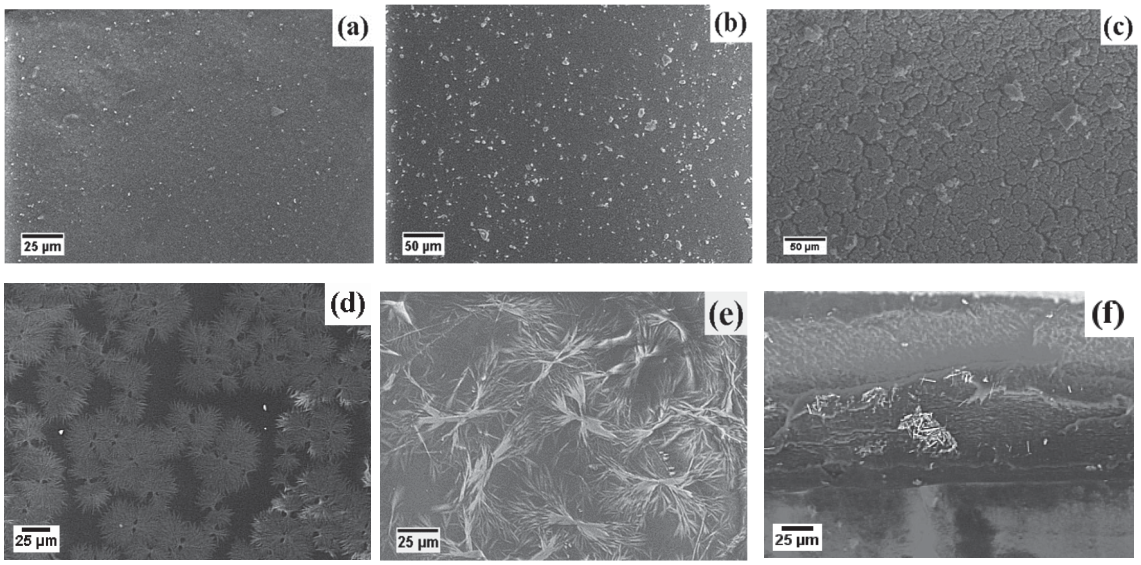

Figure 6.3.6. Backscattered images of the ultrasonicated PAm-MMT samples loaded at (a) 20% MMT, (b) 50% MMT, (c) 70% MMT, (d) 2.5% acidified MMT, (e) 5% acidified MMT and (f) 60% acidified MMT

Decreasing MMT content from 60 to 50% resulted in the transition toward PAm dominated structure in which a smoother surface and significant particle size reduction was observed. Below this MMT concentration range, the extent of the large aggregate separation to tactoids significantly increased, leading to the improved interfacial adhesion between the embedded MMT particles and the hosting PAm matrix. The SEM observations showed increased variation in particle size and shape, surface smoothness and disorderly arranged particles with increasing PAm concentration. This tendency was

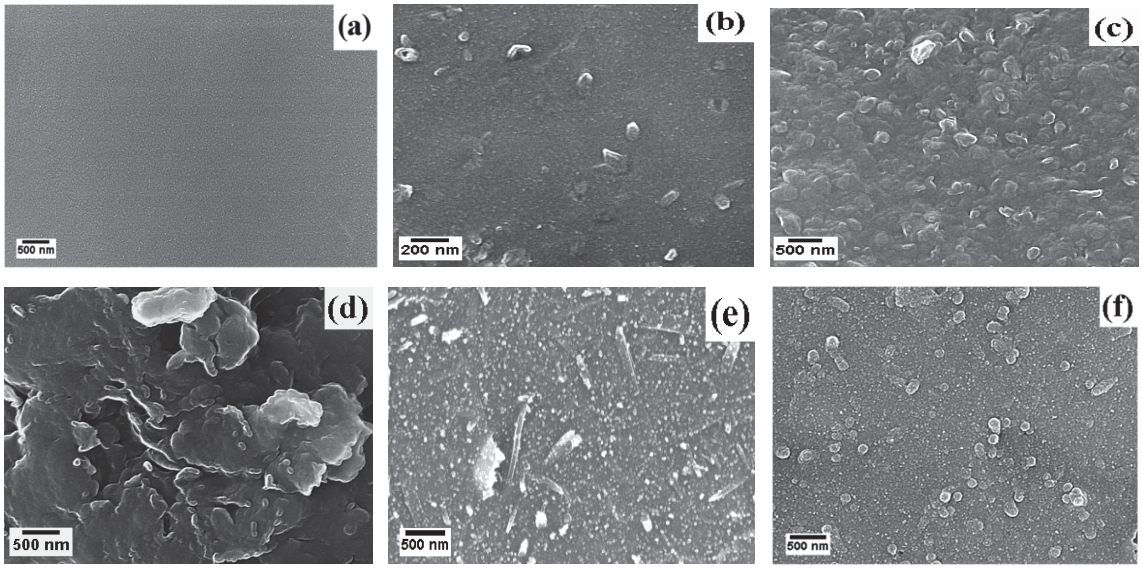

Figure 6.3.7. Carbon coated surface images of (a) PAmM2.5, (b) PAmM5, (c) PAmM60 and (d) PAmM70 and carbon coated cross-sectional images of (e) PAmM5 and (f) PAmM10

more patent for the MMT concentration of less than 20% MMT and the aggregate size reduced to smaller tactoids with decreasing MMT concentration. The surface area is also a consideration as the more intercalation of PAm can be promoted by higher surface area of MMT at lower MMT concentrations. The separation of MMT particles observed by microscopic analysis was consistent with the (001) peaks which showed increased MMT layer separation with PAm concentrations and the intercalation process was accompanied by the breakage of large MMT agglomeration into smaller tactoids and the reduced number of stacked MMT layers (Bottero et al. 1988). PAm possibly covered MMT particles at high PAm and MMT particles were invisible at 2.5 % MMT when viewed in the SEM. Although degree of silicate layer separation considerably increased at 5 and 10 % MMT, there appeared to be the mixture of dispersed MMT in different sizes and the presence of tactoids was seen by the platelet stacks, the clearly detectable thicknesses of stacked platelets greater than 1 nm under SEM examination. The presence of the tactoids in the sample having 5% MMT suggested that the complete exfoliation of MMT layers was not attained when examined under the SEM and the silicate layers persisted intact after the penetration of PAm. The microstructural surfaces and cross-sectional areas of the samples, produced from acidified MMT, demonstrated a similar pattern to the specimens prepared by non-acidified MMT, according to the observed size, shape and arrangement of distributed particles.

6.3.4. FTIR analysis of PAm-MMT

Figure 6.3.8 displays the FT-IR spectra of PAm, MMT and ultra-sonicated PAm-MMT samples and represents the typical FT-IR spectral results of the PAm-MMT samples prepared under different conditions. Table 6.3.1 lists absorption band assignment of the IR-spectra of PAm and MMT according to the infrared spectral assignments reported for PAm, MMT and their complexes (Kulicke & Siesler 1982, Lee et al. 1984, Guerrero, Boldarino & Zurimendi 1985, Deng et al. 2006, McGuire, Addai-Mensah & Bremmell 2006, Sowwan et al. 2008, Natkański et al. 2013). The spectral analysis of the PAm-MMT samples prepared by the preparation method showed the typical structural framework of both PAm and MMT and the relative intensity of most peaks were directly proportional to the concentrations of PAm and MMT in the tested samples. The characteristic absorption bands due to MMT structural framework at 3431, 1640, 3628, 1038, 925, 471 and 526 cm^{-1} were attributed to the OH stretching and bending vibrations of lattice water, the stretching vibration of structural hydroxyls and Si-O-Si and the bending modes of

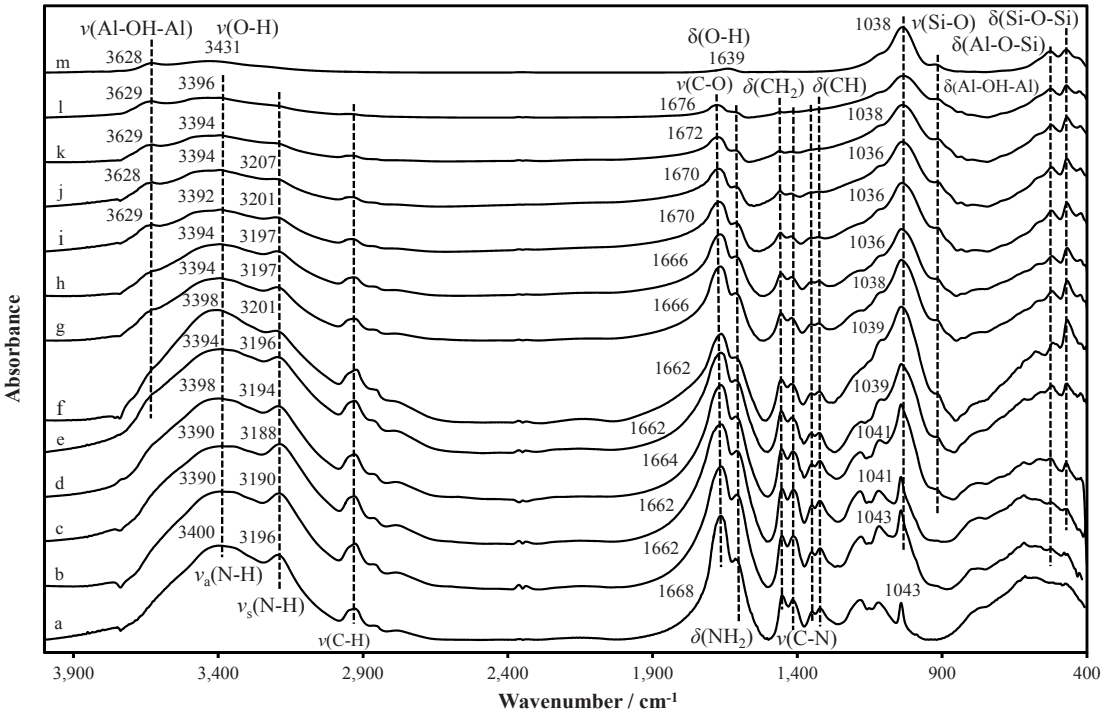

Figure 6.3.8. FTIR spectra of (a) PAm, (b) PAmM2.5, (c) PAmM5, (d) PAmM10, (e) PAmM20, (f) PAmM30, (g) PAmM40, (h) PAmM50, (i) PAmM60, (j) PAmM70, (k) PAmM80 and (l) PAmM90 and (m) unmodified MMT

Table 6.3.1. Infrared absorption bands of PAm and MMT and their peak assignments

cm^{-1}		Assignments
PAm	MMT	
-	3628	Al-OH-Al stretching
-	3431	O-H stretching vibrations of the interlayer water
3400	-	N-H asymmetric stretching vibration of NH_2 group
3196		N-H symmetric stretching vibration of NH_2 group
2929	-	C-H asymmetric stretching vibration of CH_2 group
2864		C-H symmetric stretching vibration of CH_2 group
2789	-	C-H stretching of CH group
1668	-	C=O stretching vibration of CO group (Amide I band)
-	1640	O-H deformation vibrations of the interlayer water
1616		N-H bending vibration of NH_2 group (Amide II band)
1456	-	Bending vibration of CH_2 group
1417	-	C-N Stretching vibration (Amide III band)
1350	-	CH_2 wagging vibration
1323	-	C–H bending vibration
1184	-	Wagging mode of NH_2
1122		NH rocking vibration of NH_2 group
-	1038	Si-O-Si stretching
-	925	AlAlOH bending
	876	AlFeOH
-	839	AlMgOH
-	791	Si-O vibrations of amorphous silica
760	-	C-H wagging mode
615		C-C rocking vibration
-	526	Al-O-Si bending of tetrahedral layer
-	471	Si-O-Si bending

Al_2OH, Si-O-Si and Al-O-Si, respectively. The absorption peaks characteristics of PAm included amino group, carbonyl group and C-N bond of the amide group and the bands appearing at 2929, 2864 and 2789 cm^{-1} were associated with CH asymmetric and symmetric stretching vibration of CH_2 groups and CH stretching vibrations of CH group.

The spectral examination of all samples indicated that most of the abovementioned peaks related to MMT and PAm were relatively similar. In contrast, the shifts in the absorption bands ascribed to the carbonyl stretching, asymmetric and symmetric stretching of NH_2, bending vibration of NH_2, CH_2 bending vibration and C-N stretching vibration were found at 1668, 3400, 3196, 1616, 1456 and 1417 cm^{-1}, respectively. While the changes in bonding environment of PAm were reflected by shift of the peaks, corresponding to the C=O, NH_2, CH_2 and C-N groups, variations made by these absorption bands were independent of the method by which the samples were prepared.

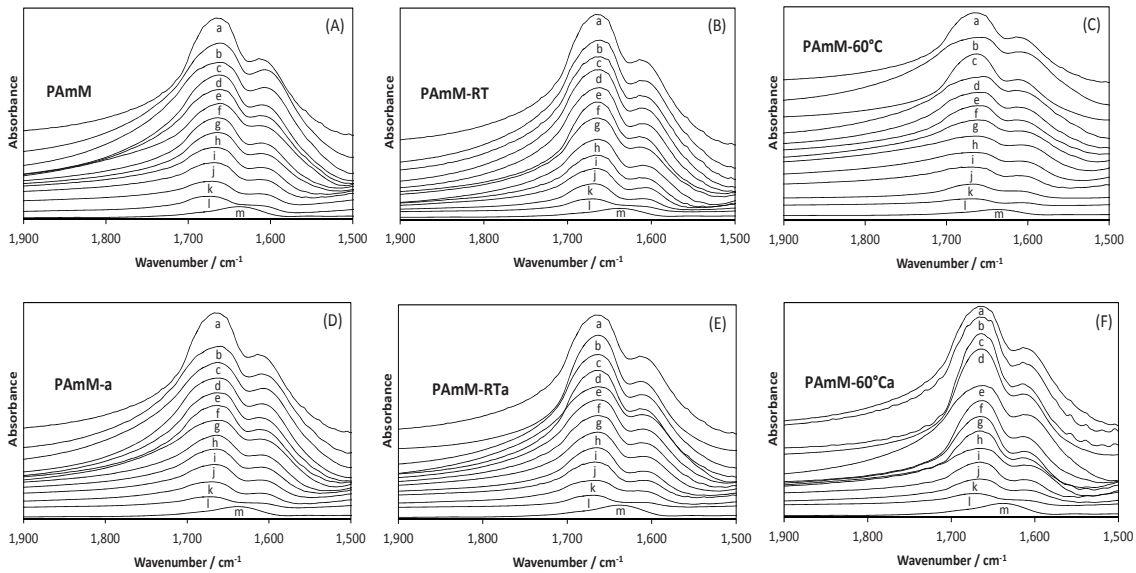

Figure 6.3.9. Carbonyl stretching region of (a) PAm, (A) PAmM, (B) PAmM-RT, (C) PAmM-60ºC, (D) PAmMa, (E) PAmM-RTa, (F) PAmM-60ºCa at (b) 2.5% MMT, (c) 5% MMT, (d) 10% MMT, (e) 20% MMT, (f) 30% MMT, (g) 40% MMT, (h) 50% MMT, (i) 60% MMT, (j) 70% MMT, (k) 80% MMT and (l) 90% MMT and (m) 100% MMT

It can be seen from Figure 6.3.9 and 6.3.10 that the carbonyl peak shifts to higher wavenumber for all experimental conditions from 1660 cm^{-1} to 1676 cm^{-1}. The band shifting of C=O band were observed up to ~1660 cm^{-1} at 2.5% MMT loading and to 1676

cm^{-1} at 90% MMT loading. The shift from 1668 to 1600 cm^{-1} on the addition of 2.5% MMT indicates that the shift to lower frequency is likely attributed to increased hydrogen bonding with MMT or ion-dipole interactions of carbonyl oxygen of PAm (Mpofu, Addai-Mensah & Ralston 2004, Mpofu, Addai-Mensah & Ralston 2005, Deng et al. 2006, Natkański et al. 2013, Huang & Ye 2014a).

At 50-60 % MMT concentrations, the C=O stretching peaks were found to shift back to original position, corresponding to carbonyl stretching absorption of PAm alone while the further shift of the C=O stretching bands beyond 50-60% MMT resulted in the higher wavenumber side of the carbonyl stretching peaks in comparison to PAm. The shifts in the carbonyl stretching bands to lower wavenumber from 2.5 up to 50-60% MMT could result from carbonyl groups of PAm participating in hydrogen bonding interaction with MMT and the carbonyl oxygen could be engaged in hydrogen bonding with the terminal hydroxyl groups of MMT and/or hydrated interlayer cations (Olodovskii & Murashko 1976, Ogawa, Kuroda & Kato 1989, Gao & Heimann 1993, Mpofu, Addai-Mensah & Ralston 2004, Mpofu, Addai-Mensah & Ralston 2005, Deng et al. 2006, El-Zahhar, Abdel-Aziz & Siyam 2007, Kurochkina & Pinskii 2012, Natkański et al. 2013). The decreased hydrogen bonding forces of PAM in the latter case suggest the disruption of self-associated hydrogen bonding interaction of intercalated PAm chains (Deng et al. 2006).

The similar MMT loading dependent shifts were found for the peaks due to symmetric stretching of NH_2, CH_2 bending vibrations, C-N stretching vibration of PAm at 3196, 1456 and 1417 cm^{-1} respectively. These peaks showed reduced bond strength of NH and CN for lower MMT concentration as seen from the peak positions towards lower frequency. The symmetric stretching of NH_2 group were shifted to lower wavenumber by up to 17 cm^{-1} from 90% to 2.5% MMT and resulted in shifts by ~3190 cm^{-1} at 2.5% MMT. The shifts of NH_2 symmetric stretch vibration with increasing PAm concentration could also be ascribed to an increase in the hydrogen bond formation of NH group, especially over 70-80% PAm, which showed the peaks at lower wavenumbers compared to that of PAm (Huang & Ye 2014a, Huang & Ye 2014b). The peaks positioned at the higher wavenumber below 70-80% PAm indicated the decrease in NH···O=C hydrogen bonds of PAm and the reduced hydrogen bonding interaction of PAm showed dissociation of

self-assembled polymer chains caused by the diffusion of PAm into interlayer region of MMT (Deng et al. 2006). CN stretch modes were also found to shift towards lower wavenumber with the increase of PAm concentrations and their frequencies changed from a higher to lower wavenumber than that of PAm at 10-20% MMT. The small shifts of CN stretching frequencies of PAm from 1417 cm^{-1} up to 1425 cm^{-1} were observed when going from 10-20% MMT to 90% MMT as was observed for non-ionic PAm intercalated sodium smectite complex (Deng et al. 2006).

The CH_2 bending vibrations of PAm at 1456 cm^{-1} also shifted to lower wavenumbers by 4~8 cm^{-1} with decreasing MMT contents and the band positions were moved to lower wavenumbers than 1456 cm^{-1} below 40% MMT. Some investigations showed the studied clay minerals could develop hydrophobic interaction with the CH_2CH backbone chains of PAm at siloxane surface of clay mineral or with hydrophobic segment of hydrophobically modified PAm (Volpert et al. 1998). Slight shifts of CH_2 bending vibrations to lower wavenumber in dependence on decreasing MMT concentrations may reveal trivial hydrophobic interactions, which is in accord with the work of Deng et al. (2006) who also suggested insignificant contribution of hydrophobic interactions for PAm.

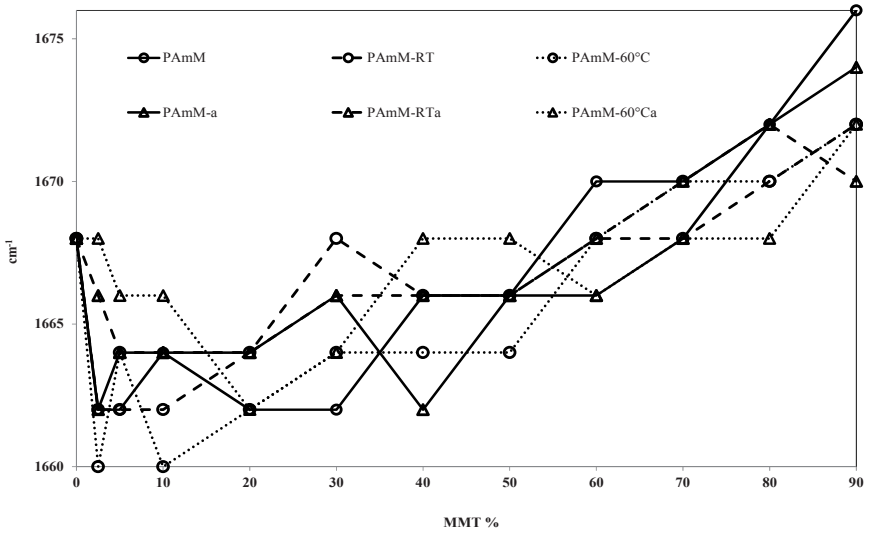

Figure 6.3.10. Variations in the carbonyl stretching bands with MMT loadings

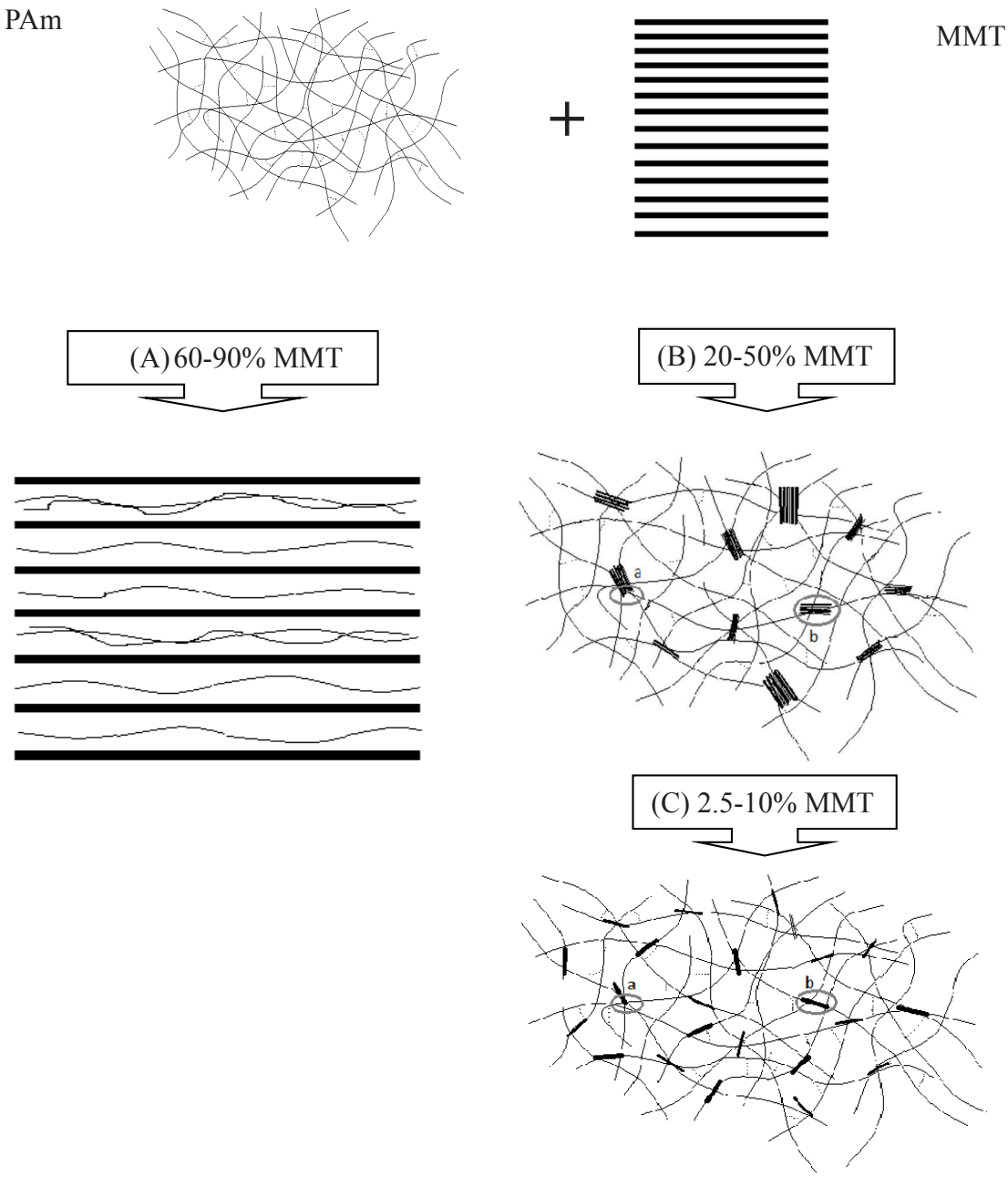

Figure 6.3.11. Schematic representation of PAm-MMT systems

In contrast to the above-mentioned peaks, the absorption bands, due to asymmetric stretching and bending vibrations of NH_2 at 3400 and 1616 cm^{-1} showed both decreased and increased bonds of NH_2 as seen from most peak positions located at lower wavenumbers than PAm. The NH_2 asymmetric stretching bands were shifted up to 3381 cm^{-1} at 2.5-5% MMT and this was followed by gradual shifts to higher wavenumber. Although the NH hydrogen bonding forces became stronger with increasing PAm concentration, as with NH_2 symmetric stretching bands, most NH_2 asymmetric stretching

bands showed shift to lower frequencies than the ones of the bulk PAm across all MMT concentrations. The shift to lower wavenumbers by up to 8 cm^{-1} were also detected for the most NH_2 bending vibrations and a small shift of NH_2 bending vibrations to lower wavenumber was similarly observed by Deng et al. (2006). The slight shifts in most NH_2 bending vibrations indicated the weakening of NH_2 bending vibrations.

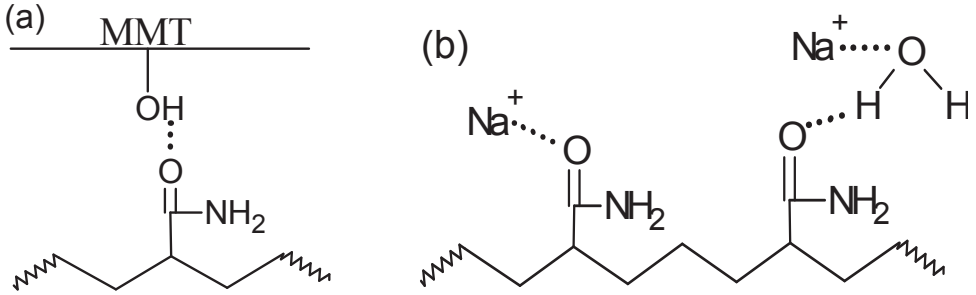

Figure 6.3.12. Schematic drawing of bonding interactions of PAm in the composite structure showing in Figure 6.3.11 (B) and (C)

Although relatively little deviations were observed for C-N stretch and CH_2 and NH_2 bending vibrations, the IR spectral analysis showed considerable changes in CO and NH_2 stretch vibrations. As suggested by the reported studies of nonionic PAm-smectite, PAm physically interacted with MMT through hydrogen bonding and van der Waals forces (Güngör & Karaoğlan 2001, El-Zahhar, Abdel-Aziz & Siyam 2007, Kurochkina & Pinskii 2012). The IR data indicated that the influence of the hydrogen bonds of PAm from the changes in hydrogen bond strength associated with carbonyl and amino groups played an important role in determining the structure of PAm-MMT systems. Under all preparation conditions, the CO stretch, NH_2 stretch and C-N stretch vibrations exhibited decreased bond strength in dependence on increasing polymer concentration, whereas, insignificant effect of sample preparation conditions on the FTIR measurements have provided additional evidence of the MMT loading dependent effect observed from the bands for C=O, N-H and C-N bonds.

Based on the examined FTIR spectral changes, together with XRD and SEM analysis, it was attempted to draw the kinds of PAm-MMT structures and to reflect changes brought about by different clay contents, illustrating the three different environments encountered

by PAm-MMT samples in Figure 6.3.11. The possible interactions of carbonyl oxygen of PAm with MMT edge surface, exchangeable Na^+ and interlayer water were schematically illustrated in Figure 6.3.12. The combined results observed for NH and C=O groups revealed the decreased hydrogen bonding links, as seen from the NH and CO stretching vibrations over 50-60% MMT, in which MMT aggregates significantly remained to form the clay dominated structure. The weakening of intra- and intermolecular hydrogen bonding strength of intercalated PAm appeared to correspond to XRD measurements exhibiting progressive penetration of PAm chains and the self-associated PAm was disconnected upon PAm intercalation into MMT (Deng et al. 2006). The concentrations over 50-60% MMT appeared to form intercalation structure where PAm chains were intercalated into more orderly arranged MMT. Figure 6.3.11 (A) and (B) illustrate schematically the probable structural changes in PAm-MMT systems.

Upon increasing the PAm concentration to 80-90% PAm, better MMT separation and the general increase in the interaction of carbonyl and amino groups of PAm with MMT was observed from XRD and SEM data and NH, CO and CN stretching vibrations. MMT aggregate were separated to smaller particles, but the proportion of PAm that remained non-intercalated and existed as excess was increased in the structure at less than 50-60% MMT. The systems were transformed to contain the varied size, orientation and interlayer separation degree of MMT as illustrated in Figure 6.3.11 (B). The changes beyond these concentration ranges coincided with PAm-MMT interaction, the diffuse basal reflections and MMT stacks as found under SEM observations. The third environment at low MMT contents could be seen as the polymer dominated structure similar to Figure 6.3.11 (C).

Several bonding possibilities could be considered to increase the overall interaction of the C-O and N-H groups in PAm. First, both clay mineral and PAm are known for their pH dependent behaviours. It is possible from the observed pH changes that the intercalation behaviour of PAm could be affected by conformational states of PAm altered according to PAm-MMT ratios and protonation of PAm or hydroxyl groups of crystal edges, resulting in the chemical attraction to the negatively charged MMT (Caulfield et al. 2003, Besra et al. 2004, Kim & Palomino 2011, Bishop et al. 2014). The FTIR spectral deviations originated from protonated amide or carboxyl groups were undetectable in all samples and showed no evidence of bands due to hydrolysed and protonated PAm under

all preparation conditions. Consistent with previous work by Deng et al. (2006), pH values showed no direct correlation between conformational and FTIR spectral changes of PAm, in spite of the altered PAm conformations derived from the MMT concentration dependent pH changes on the PAm intercalation. Second, the observed shifts in CO and NH stretching bands of PAm may indicate that PAm become bound to MMT through the hydrogen bonding interaction of amide groups of PAm with the hydrated interlayer sodium cation, hydroxyl group of crystal edge and/or the basal oxygens on the MMT surface (Greenland 1963, Ogawa, Kuroda & Kato 1989, Gao & Heimann 1993, Ulusoy, Şimşek & Ceyhan 2003, Mpofu, Addai-Mensah & Ralston 2004, Mpofu, Addai-Mensah & Ralston 2005, Deng et al. 2006, El-Zahhar, Abdel-Aziz & Siyam 2007, Natkański et al. 2013, Huang & Ye 2014a). It has been claimed that basal oxygens of MMT is a very weak electron donor (Deng et al. 2006). In this study, there was no indication to form the hydrogen bonding of PAm from the changes in the Si-O-Si stretching and bending bands of MMT. It is considered probable that the interaction sites on MMT surface or edges became more available due to considerable MMT separation that caused the intercalation and adsorption process of PAm on both external and internal MMT surfaces. The degree of interaction of the edge hydroxyl groups of clay minerals with carboxyl and amino groups of PAm could be increased with decreasing MMT concentration, although the amount of free hydroxyl group of MMT is limited (Olodovskii & Murashko 1976, Huang & Ye 2014a). The slight increase in CN stretching and decrease in NH bending vibrations over 10-20% MMT could be attributed to the partial ion-dipole interaction between the amide groups of PAm and interlayer sodium ions (Schmuckler & Limoni 1977). Even though the noticeable increase in the MMT layer separation and hydrogen bonding interactions between MMT and PAm could contribute to preserve a uniform distribution of MMT within the matrix, it is likely that neither the MMT layer separation nor the PAm-MMT interactions is insufficient to establish an exfoliation of stacked layers.

6.3.5. Thermal analysis of PAm-MMT

TGA measurement of PAm was obtained at a heating rate of 10.0 °C/min. Five different mass loss steps were identified from TG and DTG results of PAm as in Figure 6.3.13 and Table 6.3.2. Both the first and second endothermic peaks with the mass loss of 1.7

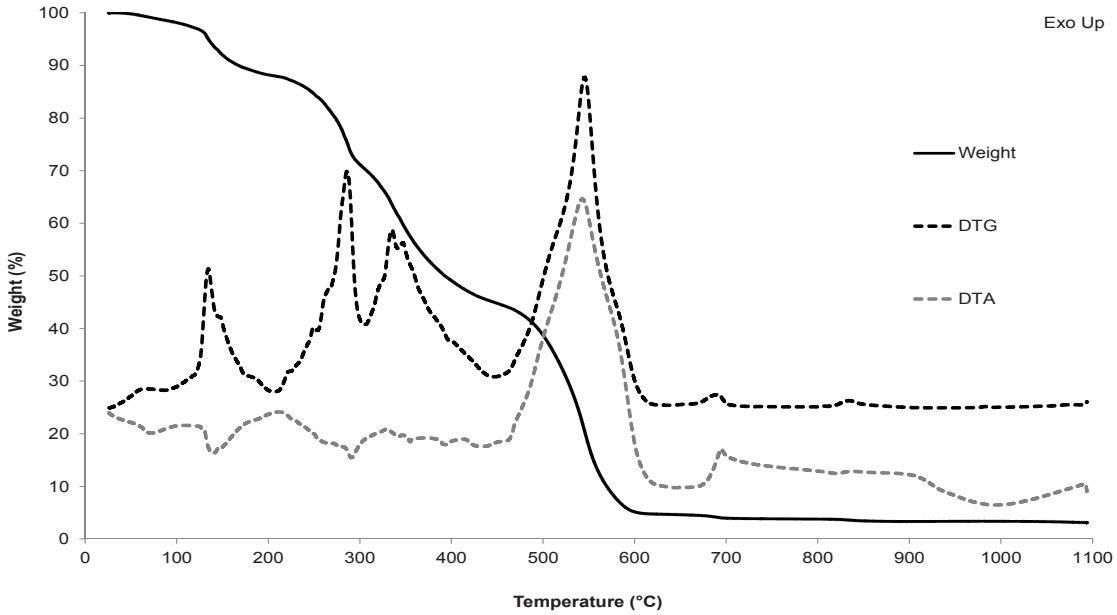

Figure 6.3.13. DTG and DTA curves of PAm measured at a heating rate of 10ºC/min

and 10.4 % could be attributable to the elimination of water molecules adsorbed to the PAm chains and other volatile impurities. The first mass loss of PAm mostly ascribed to the volatilisation of water and the loss of both weakly (low temperature) and strongly (higher temperature) bound water hydrogen bonded to the PAm could occur in the second mass loss step up to 208°C (Guerrero, Boldarino & Zurimendi 1985, Tutas et al. 1987, Leung, Axelson & Van Dyke 1987, Toth et al. 1990, Van Dyke & Kasperski 1993, E. Silva et al. 2000, Shi 2000, Pan & Chen 2011). The sharp peak due to the second endothermic step with DTG maximum at 135ºC in the 95-208ºC range may also include the release of degradation products owing to the breakdown of structure (Leung, Axelson & Van Dyke 1987).

Table 6.3.2. Mass losses of PAm heated at 10.0 °C/min

Interval temp (°C)	DTG Peak temp (°C)	Mass loss (%)
25-95	61	1.7
95-208	135	10.4
208-309	286	18.2
309-448	335	24.9
448-611	546	40.1

The third DTG peak in the temperature range between 208 and 309°C with a DTG maximum at 286°C is an endothermic process with the mass loss of 18.2% and could be related to the side chain reactions involved in the intra-/intermolecular imidization or deammonation of pendant amide groups and subsequent decarboxylation of the imide group, accompanied by the formation of various crosslinked and cyclic structure, nitrile groups, and aliphatic compounds to release ammonia and carbon dioxide (Burrows, Ellis & Utah 1981, Leung, Axelson & Van Dyke 1987, Toth et al. 1990, Van Dyke & Kasperski 1993, Schild 1996, E. Silva et al. 2000). In addition to desorption of the remaining water attached to the polymer chains, the dehydration reaction of amide groups could eliminate water and form cross-linked polymer or nitriles groups (Leung et al. 1987, Toth et al. 1990, Van Dyke & Kasperski 1993, Schild 1996). On heating from 309ºC to 611ºC, the large mass losses of about 24.9 % and 40.1 % are found in the fourth and fifth mass loss steps of PAm.

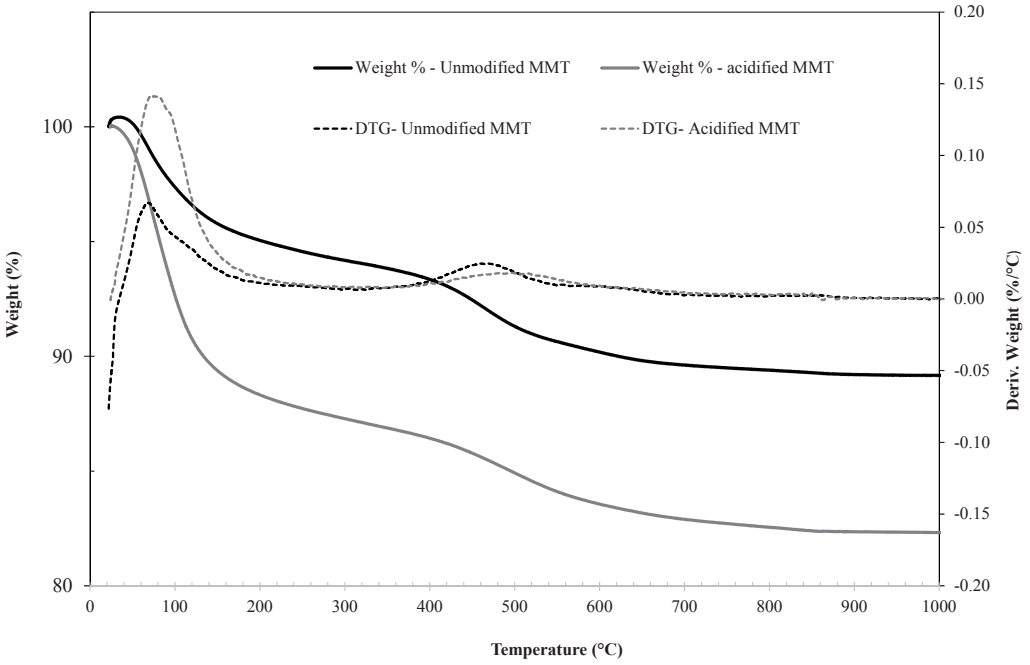

Figure 6.3.14. TG and DTG measurements made on unmodified MMT and acidified MMT

Based on the reported degradation products and structure changes, the fourth mass loss step between 309 and 448 ºC could still include the degradation products due to the side chain reactions together with more polymer chains breaking reactions such as

decarboxylation (Leung et al. 1987, Van Dyke & Kasperski 1993). A further mass loss was found with a DTG maximum of 546°C over the 448-611 temperature range and is associated with an exothermic peak, which shows a maximum at 544°C and ended at approximately 650°C. PAm decomposes almost completely by 650ºC as the last degradation step is observed with the residual mass being 3.1%. The last exothermic mass loss step was ascribed to thermooxidative degradation, combustion of remaining chains backbone and chain scission caused by free radical mechanisms (Vilcu et al. 1987, Van Dyke & Kasperski 1993, Han et al. 2010).

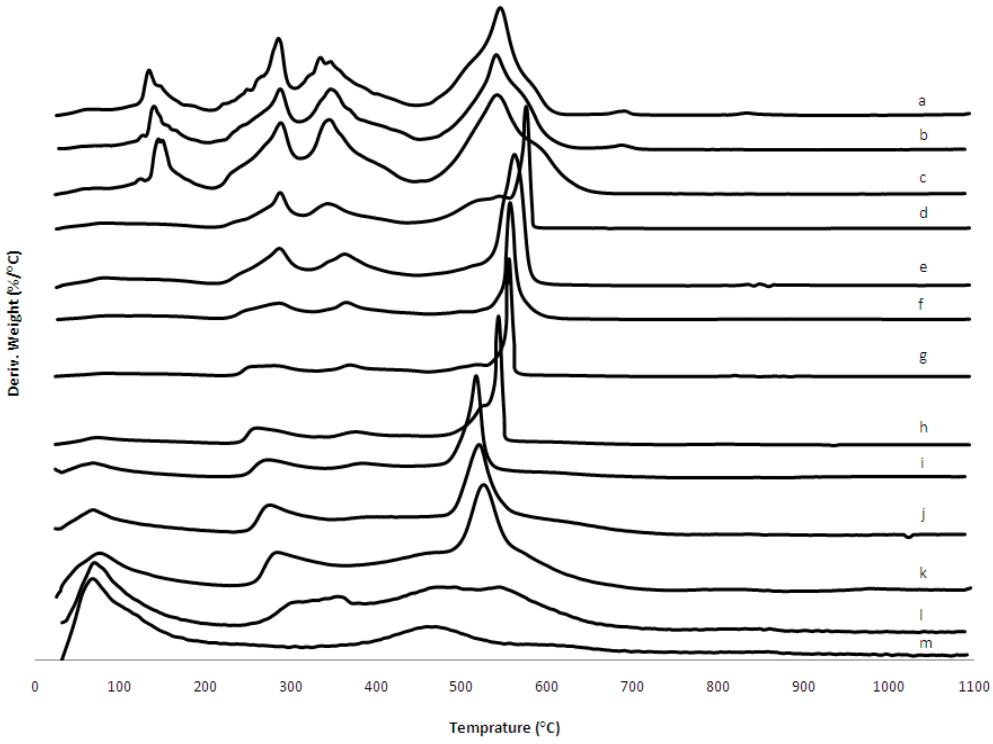

Figure 6.3.15. DTG measurements made on (a) PAm and PAm-MMT at (b) 2.5% MMT, (c) 5% MMT, (d) 10% MMT, (e) 20% MMT, (f) 30% MMT, (g) 40% MMT, (h) 50% MMT, (i) 60% MMT, (j) 70% MMT, (k) 80% MMT and (l) 90% MMT and (m) unmodified MMT

The TGA curves of MMT are shown in Figure 6.3.14 where two steps are observed. The first step of unmodified MMT was in the range of 25–193ºC due to a release of physically adsorbed and interlayer water present in unmodified MMT with a mass of 4.6%.

Following the first stage, the mass loss within the temperature of 360-555ºC was attributed to the dehydroxylation reaction of MMT layers associated by a mass loss of 5.3%. The observed total mass loss of MMT was only 9.9% when heated to 1100°C. Similarly, the dehydroxylation reaction of aluminosilicate of acidified MMT occurred in the temperature range recorded comparative to unmodified MMT and exhibited a mass loss of 4.6 %. Even though higher amounts of adsorbed and interlayer water were evaporated for the acidified MMT, The TGA profiles are fairly comparable before and after the acid-treatment of MMT.

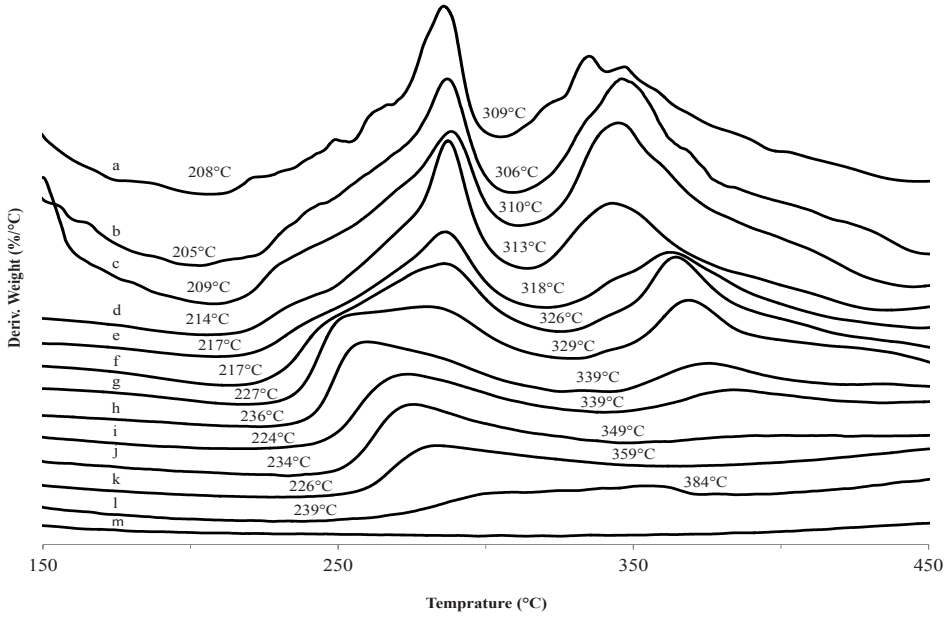

Figure 6.3.16. Onset temperatures of first and second decomposition steps of (a) PAm, (b) PAmM2.5, (c) PAmM5, (d) PAmM10, (e) PAmM20, (f) PAmM30, (g) PAmM40, (h) PAmM50, (i) PAmM60, (j) PAmM70, (k) PAmM80, (l) PAmM90 and (m) MMT

DTG curves of PAm, unmodified MMT and the ultrasonicated samples of PAm and MMT with different MMT contents are shown in Figure 6.3.15. Based on comparative TG and TGA data, referring to characteristic temperatures of PAm and MMT, the thermal breakdown of PAm was virtually completed at 700ºC, over which small mass losses were observed to leave MMT residue at 1100ºC. TGA measurements indicated that the behaviour of the PAm-MMT composites at low MMT loadings of 2.5-5% were similar to PAm and that the composites with MMT content greater than 40% MMT were closer

to the characteristics of MMT. The initial mass losses occurred due to dehydration of surface moisture present in both PAm and MMT (Natkański et al. 2013, Koç et al. 2014). The mass losses up to approximately 249ºC could have resulted from the elimination of adsorbed water of MMT and PAm (Toth et al. 1990). During this temperature range, the the DTG peak of 2.5 and 5% MMT were seen to be absent in the samples loaded with greater than 5% MMT. The absence of the second DTG peaks could be possibly attributed to the loss of strongly bound water, as a result of the intercalated and adsorbed PAm to reduce the hydrogen bonded water attached to PAm polymer chains.

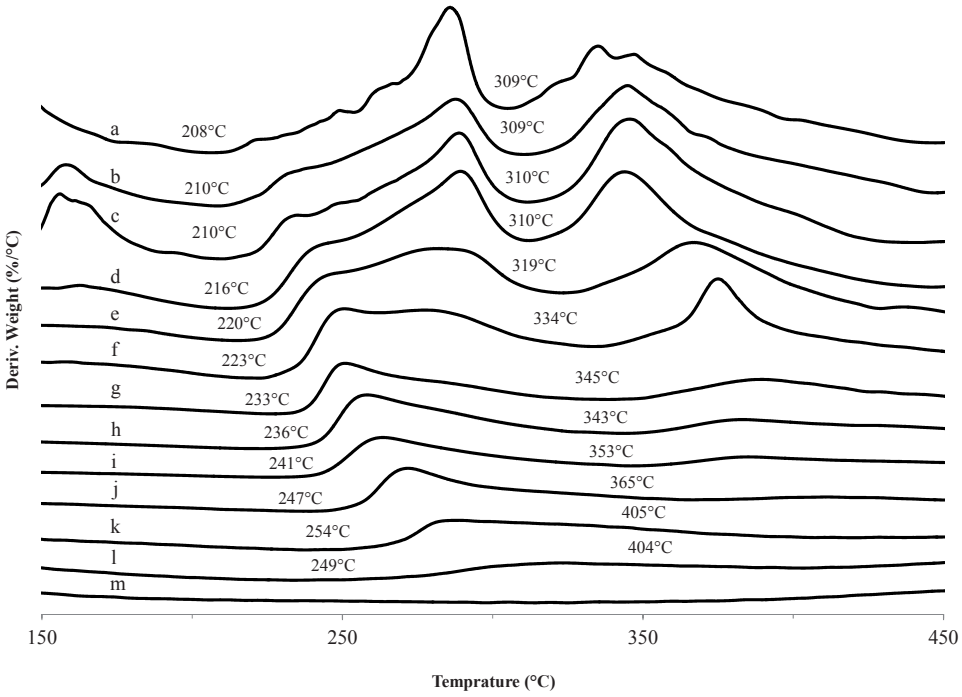

Figure 6.3.17. Onset decomposition temperatures of (a) PAm, (b) PAmM2.5a, (c) PAmM5a, (d) PAmM10a, (e) PAmM20a, (f) PAmM30a, (g) PAmM40a, (h) PAmM50a, (i) PAmM60a, (j) PAmM70a, (k) PAmM80a, (l) PAmM90a and (m) acidified MMT

Analysis of the TG and DTG curves on the degradation of PAm in the presence of MMT showed a three-stage thermal decomposition between 205 to 750ºC. The mass losses within this temperature range were mainly attributed to the decomposition processes of PAm in the PAm-MMT samples, although the second and third decomposition steps were associated with dehydroxylation reaction of MMT (Toth et al. 1990, Voorn, Ming & Van Herk 2006, Natkański et al. 2013). Figure 6.3.16 and 6.3.17 shows DTG curves used to

determine onset temperatures due to thermal degradation of the ultrasonicated PAm-nonacidified MMT and PAm-acidified MMT. Except for PAmM2.5 and PAmM5, which showed lower onset temperatures, the onset temperatures of the first and second decomposition processes of PAm incorporated with MMT were shifted to higher temperature with increasing MMT concentrations in the PAm-MMT system and the PAm-MMT samples exhibited a delayed decomposition in comparison to PAm. These observations indicated the improvement of thermal stability of both the ultrasonicated samples compared to that of PAm and previous studies reported the addition of MMT caused the thermally more stable (nano) composites of homopolymers or copolymers of Am with MMT (Toth et al. 1990, Biasci, Aglietto & Ruggeri 1995, Yeh, Liou & Chang 2004, Voorn, Ming & Van Herk 2006, Chen et al. 2008, Koç et al. 2014).

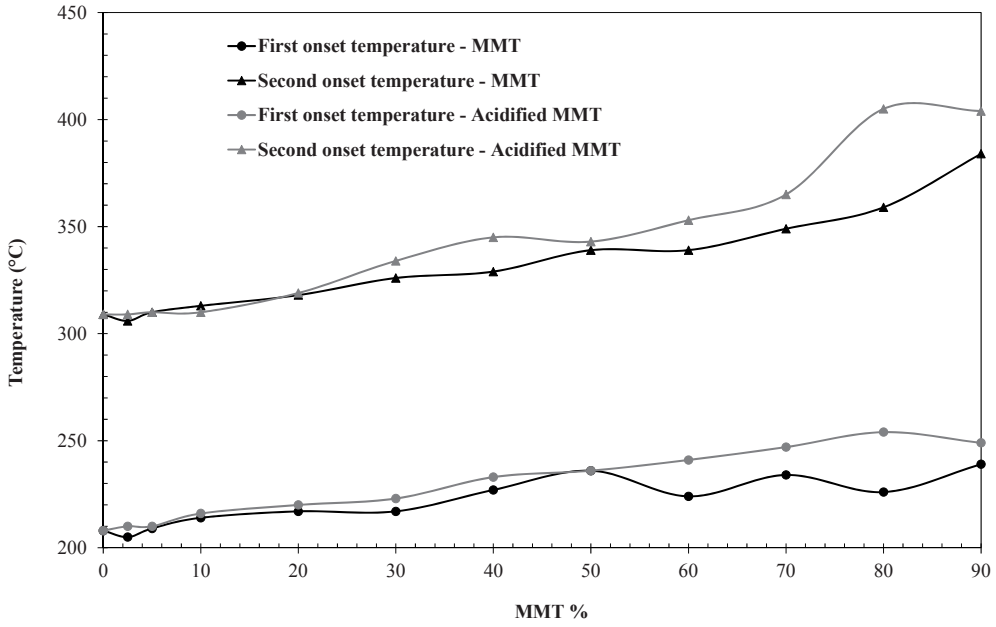

Figure 6.3.18. Plot showing first and second onset temperatures of PAm and PAm-MMT samples

In comparison, the samples prepared using modified or acidified MMT showed decompositions of PAm containing unmodified MMT began at lower temperatures. The first and second decomposition onset of the PAm-unmodified MMT samples shifted from 208ºC to 239ºC and from 309ºC to 384ºC while the shifts of the first and second onsets from 208ºC to 249ºC and from 309ºC to 404ºC were observed for the PAm-acidified MMT samples. The first and second onset temperatures were found to be higher, up to

about 10ºC and 20ºC for the PAm-acidified MMT samples and the slightly higher onset temperatures of the acidified samples indicated greater thermal stabilities than the corresponding non-acidified samples (Figure 6.3.18). The observed changes could be attributed to different PAm conformations within the structures as more coiled polymer chains in the acidified samples favour the formation of inter- and intramolecular interaction, such as hydrogen bonding forces (McNeill & Zulfiqar 1978). The increased thermal stabilities of the acidified samples could also be correlated to the slight increase in the intercalated PAm, leading to delay the onset of thermal degradation of PAm and the reduced thermal stabilities of 2.5 and 5% non-acidified MMT compared to PAm might the attachment of PAm to MMT surface (Biasci, Aglietto & Ruggeri 1995).

The stabilizing effect of MMT appeared to increase with increasing MMT content and the TGA profiles obtained in this work provided additional evidence for the changes in thermal behaviour of PAm-MMT systems based on the composition of PAm/MMT. In the presence of MMT in the structure, the molecular chains of PAm could be restricted and the thermal motion and processing of PAm are likely to be altered. This could also be caused by significantly higher thermal stability of MMT to act as thermal barrier to heat flow (Mahdavinia & Asgari 2013, Kalaleh, Tally & Atassi 2013, Koç et al. 2014, Ferfera-Harrar et al. 2014). According to previous thermal analysis studies, in conjunction with the observed results of TGA curves, the most probable first and second thermal decompositions of PAm in the PAm-MMT samples involved in imidization and dehydration reactions of the side groups and the successive decarboxylation reactions and the barrier effect of MMT could hinder these decomposition reactions to delay the thermal decomposition processes of PAm. Additionally, the uniform dispersion of MMT is known to reduce permeability of PAm-MMT samples (Voorn, Ming & Van Herk 2006). The tortuous pathway effect of MMT could also hinder the permeation of oxygen and the diffusion of volatile degradation products to result in a delay in thermal decomposition (Yano et al. 1993, Alexandre & Dubois 2000, Kalaleh, Tally & Atassi 2013, Ferfera-Harrar et al. 2014). The increased thermally stable PAm with increasing MMT concentrations could have arisen from the combined influence of increasing interaction between PAm and MMT, introducing more stable MMT and the higher proportions of intercalated PAm into MMT structure that could provide thermal protection to the intercalated PAm (Akelah 1995). The increased onset decomposition temperature for

higher MMT concentrations is related to physical attractions, such as hydrogen bonding, with the sodium ions largely linked to MMT in the structure, since the sodium ions bonded to amide groups of PAm could speed up the decomposition of side groups of PAm as suggested in the work of Toth et al. (1990).

6.3.6. Summary

The PAm-MMT systems composed of various PAm-MMT ratios were prepared from the non-ionic PAm treated with either unmodified or acidified MMT via the direct aqueous solution intercalation technique with ultrasonication-assisted dispersion of MMT and different experimental conditions were investigated through XRD, SEM, FTIR and TGA measurements. It was found that the visual appearance of the prepared films, the extent to which interlamellar intercalation of PAm, bonding interaction between PAm and MMT and their thermal stabilities were considered to be similar to the results obtained after the ultrasonication treatment of PAm-MMT dispersions. The experimental results showed the insignificant influences of processing time, mixture temperature and acidification of MMT. It can be concluded that the ultrasonication treatment presented the fast, straightforward and effective preparation method and is adequate to produce similar results for use as sandstone consolidation work.

Based on the interlayer separation of MMT, their appearance, microstructural and morphological alterations, PAm-MMT interaction and thermal behaviours, the observed changes were mainly determined by the MMT-PAm ratios. At high loadings of MMT, over 50-60% MMT, the appearance and visual, structural and thermal characteristics were similar to MMT and the self-associated hydrogen bonded PAm was separated and absorbed by MMT silicate lamellae to form the intercalated structures. The brittle and opaque composite films produced in this MMT concentration range were most likely to be unsuitable for use in stone consolidation work. On decreasing MMT concentrations, the adhesiveness and transparency of the produced films, the separation of stacked layers and interlayer space of MMT, the amount of non-intercalated PAm and the interaction between MMT and PAm increased linearly. The separation of MMT was significantly increased at 10-20% MMT as detected by XRD, SEM, FTIR and TGA analysis.

The (001) reflection of the samples appeared to show a gradual increase in the interlayer gaps up to 14.3 Å at 80% Pam, beyond which the (001) curves became broader, weaker and undetectable proportionally to PAm. The SEM evaluation revealed a reduction in the MMT aggregate size to smaller tactoids and non-intercalating PAm that adsorbed the external surface and crystal edges MMT. The various size and orientation of the dispersed MMT were converted to smaller MMT stacks without MMT layer exfoliation at less than 10-20% MMT. FTIR spectral changes in NH and CO stretching bands indicated that the interaction was developed for the amide groups of PAm with the hydrated interlayer sodium cation and hydroxyl group of crystal edge. The TGA measurements showed the delay in the first and second decomposition stage of PAm and the thermally stable systems from 10 to 90% MMT.

From a physicochemical and applied point of view, the PAm-MMT systems at MMT loading less than 50-60% MMT are more likely of practical and effective usage as stone consolidant. Although the use of the low MMT concentrations up to 10-20% MMT enhanced visual clarity, adhesiveness, MMT particle separation and interaction between PAm and MMT, significant improvements were unattained in the absence of delaminated silicate layers in comparison to the PAm-MMT composites containing greater than 10-20% MMT, which reflected the coexistence of varied size, shape and orientation of MMT tactoids. The ability of the PAm-MMT composites at higher MMT concentrations, as high as 50-60%, to provide the superior thermal and structural stability and physical and chemical compatibility of MMT could be of benefit to sandstone consolidation in application. Apart from the presence of precipitated sulphate-related impurities, the acidified MMT produced the similar changes and the more coiled states of PAm chains resulted in the slight improvement in the interlamellar separation of acidified MMT and the thermal resistance of PAm. As with the PAm-MMT systems prepared from unmodified MMT, the observed effects of acid-treated MMT presented potential use of the acid treated samples along with the non-acidified samples.

6.4. PEG-MMT composite system

6.4.1. Microscopic evaluation of PEG-MMT composite films

The preliminary assessment of the PEG-MMT films was performed to determine whether the appearance and physical characteristics of samples are potentially suitable to consolidate Sydney sandstone. The selected images of the PEG-MMT films produced using both MMT and acidified MMT in Figure 6.4.1 illustrated the decreased transparency, even distribution of MMT particles and adhesive bonding of the films to the surface with increased MMT content in the films. The similar appearance and characteristics of films to those of PEG are converted to the conditions in which visible MMT particles became more noticeable in the films with increasing the MMT-polymer ratio from 1 : 9 to 2 : 8. Further increase in MMT content gradually approached the system close to MMT film, which is brittle, dry, and opaque with inadequate adhesive bonding of the films to the surface. While the overall effect of acidified MMT is similar to that of

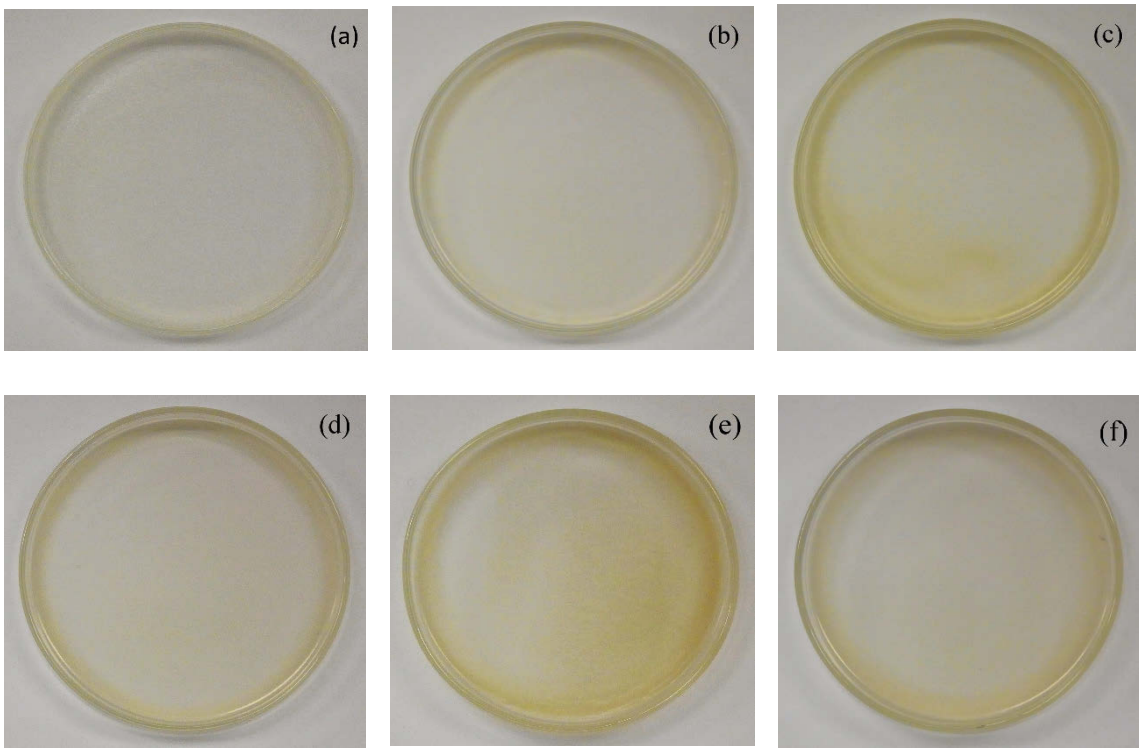

Figure 6.4.1. PEG35-MMT composite films dried after ultrasonication treatment at (a) 10% MMT, (b) 30% MMT, (c) 50% MMT, (d) 50% acidified MMT, (e) 70% MMT and (f) 70% acidified MMT

non-acidified MMT, the transparency and distribution of acidified MMT particles were enhanced over 40% acidified MMT in the corresponding systems (Figure 6.4.1c-f). The more transparent films with better distribution of acidified MMT particles are noticeable in comparison to denser PEG-MMT films with a mixture of uniform and non-uniform distributions of non-acidified MMT at 60-70% MMT. The enhanced transparency of the films can be accounted for by acidified MMT to enhance the transparency of MMT. In view of the suitability of the PEG-MMT composites films for intended use, the uniform and transparent appearances of composite samples at 10-50% MMT appear to be compatible to the natural appearance of Sydney sandstone and to possess sufficient strength, capable of binding target stone material.

6.4.2. XRD analysis of PEG

Figure 6.4.2 shows the XRD diffraction patterns of PEG35, non-acidified MMT, ultrasonicated samples formed from PEG35 and non-acidified MMT. The diffraction pattern for PEG35 contains peaks at 2θ (hkl) = 12.9°, 13.4° (100), 14.4° (021), 14.9° (110), 18.5°, 19.0° (120), 21.0° (031), 21.9° (102), 22.8° (112), 23.1° and 23.3° (032) and the observed peaks are consistent with reported diffraction patterns for helical structure of crystalline PEG (Bortel, Hodorowicz & Lamot 1979, Saujanya & Radhakrishnan 1997, Chrissopoulou et al. 2011, Deka & Kumar 2013, Choudhary & Sengwa 2014). The composites formed from PEG35 and non-acidified MMT after ultrasonication exhibited the peaks attributable to PEG35 at 2θ = 14.9°, 18.5°, 19.0°, 23.1° and 23.3° for systems that contain 10-30% MMT, but the corresponding peaks are almost undetectable at higher MMT concentration. The other peaks observed for PEG35 at 2θ = 12.9°, 13.4°, 14.4°, 21.0°, 21.9° and 22.8° almost became unidentifiable from all PEG35M composites suggesting that even at relatively low levels of MMT the PEG crystallinity is disrupted. This is consistent with reported studies of PEG (or the related PEO)-MMT composites where intercalation has been observed in conjunction with an inhibition of the crystallisation of the bulk PEG (Vaia et al. 1997b). The disappearance of crystalline PEG peaks over 30% MMT indicates that a negligible amount of free or adsorbed PEG is available for crystallisation (Shen, Simon & Cheng 2003, Kim & Park 2007, Sarier & Onder 2010, Chrissopoulou et al. 2011, Chrissopoulou et al. 2013, Choudhary & Sengwa 2014). In their studies of the PEG-MMT composites, Shen, Simon & Cheng (2003),

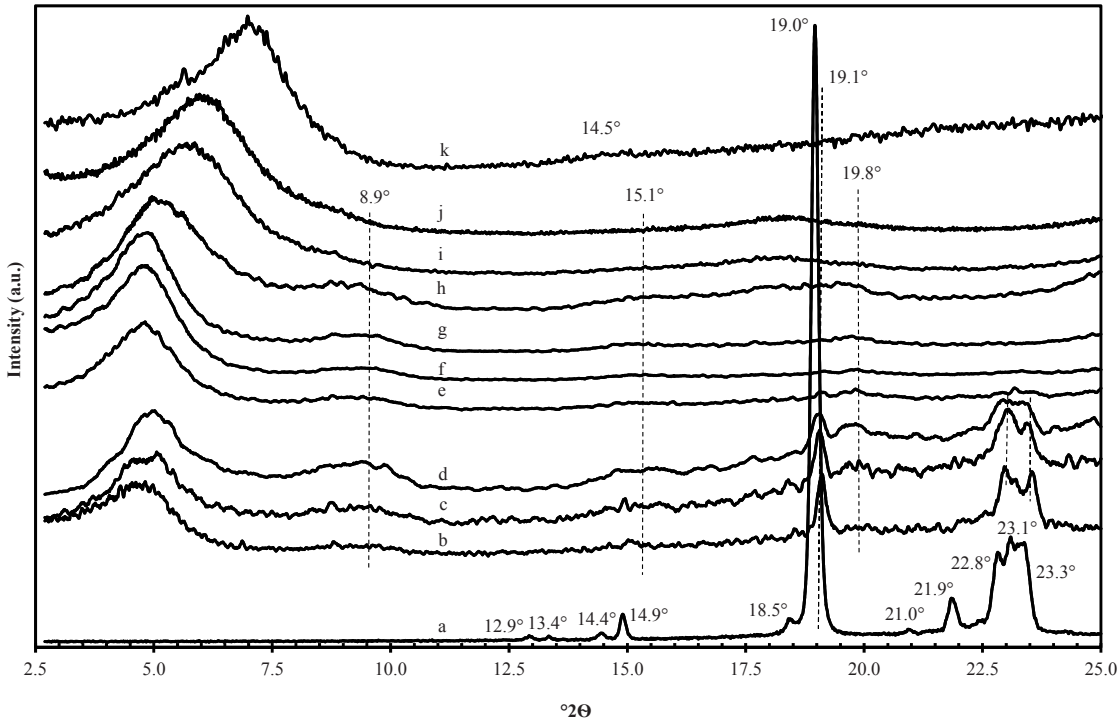

Figure 6.4.2. XRD patterns of (a) PEG35, (b) PEG35M1, (c) PEG35M2, (d) PEG35M3, (e) PEG35M4, (f) PEG35M5, (g) PEG35M6, (h) PEG35M7, (i) PEG35M8 and (j) PEG35M9 and (k) MMT

Sarier & Onder (2010), Chrissopoulou et al. (2013) and Choudhary & Sengwa (2014) reported the disappearance of crystalline peaks of PEG or PEG at MMT loadings greater than 35 % MMT while the shifts of (001) reflections showed the intercalation of polymer chains (Shen, Simon & Cheng 2003, Kim & Park 2007, Sarier & Onder 2010, Zhu et al. 2013a, Choudhary & Sengwa 2014). There appear to be new peaks at around 8.9° and 19.9° at all MMT concentrations and a new series of identifiable broad first order basal reflections corresponding to interplanar d-spacing of MMT is found in the ultrasonicated PEG35-MMT samples. The new peaks at 2θ = 8.9° and 19.9° appeared to be related to MMT in the composites. The XRD curves of PEG35Ma composites measured after ultrasonication also exhibited the new diffraction peaks at 2θ = 8.9° and 19.9° at all PEG35-MMTa ratios and the peaks at 2θ = 14.9°, 18.5°, 19.0°, 23.1° and 23.3° for 10-30% MMT. The observed peaks are located at similar positions to those observed for the PEG35M composites suggesting that some poorly ordered PEG crystallites are forming. Similar results were found for other series, PEG35M-RT, PEG35M-60°C, PEG35M-RTa, PEG35M-60°Ca, PEG20M and PEG20Ma, prepared under different experimental

conditions. The peak positions appeared to remain fairly constant and similar shapes and widths of the peaks were observed. Experimental observation of invariant XRD curves of composites under varied experimental parameters indicates that the peaks were independent of the process by which the samples were prepared and were unaltered by longer treatment, temperature, acidification process of MMT, or molecular weight of PEG.

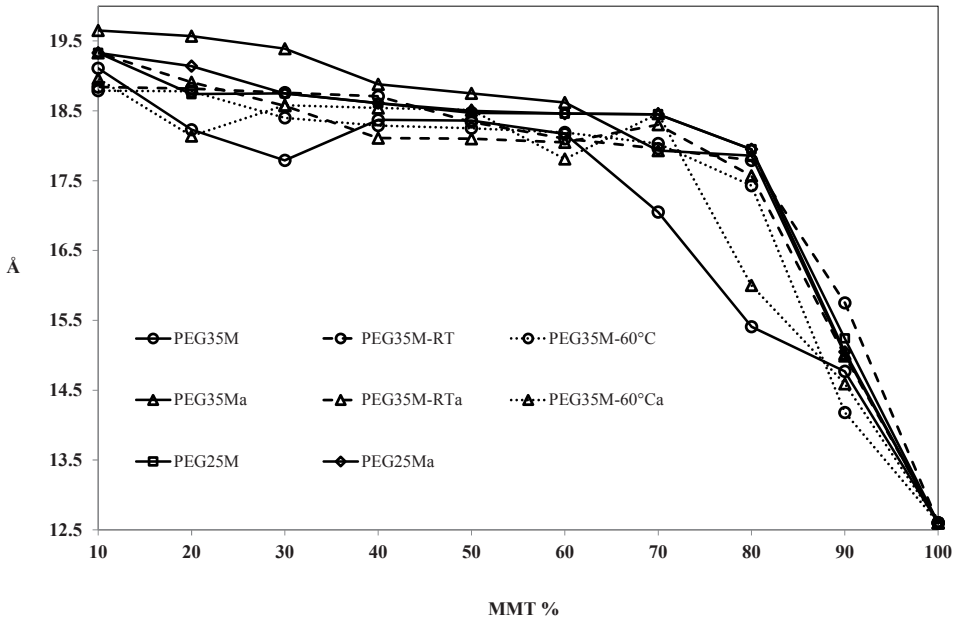

Figure 6.4.3. Plotting the changes in d-spacing against their corresponding MMT concentrations

In contrast to negligible changes associated with the abovementioned peaks, all PEG-MMT composites show major shifts of the basal (001) reflection to lower 2θ values. The variations of basal spacing for the PEG-MMT samples investigated in this study are plotted in Figure 6.4.3 and their interlayer expansions due to absorption of PEG were compared. The basal reflection of MMT at 2θ = 7.0° corresponding to 12.6 Å of the unintercalated silicate layers were substantially shifted up to 2θ=4.5° and the interlayer expansion of up to 7.1 Å was obtained at 10% MMT. It is clear from the plot that the basal plane diffraction peak shifted to higher d-spacing with increasing concentration of PEG under all experimental conditions and that the treatment of MMT with PEG obviously widened c-axis spacing of MMT due to incorporation of PEG in the MMT gallery. The basal plane spacing for PEG-MMT composites was observed to range from

14.2 Å to 19.7 Å, indicating that intercalated structure formed with silicate layers remained stacked in all compositions.

The effects of mixing time, temperature and molecular weight of PEG on the interlayer separation of MMT were first evaluated by comparing the changes in the interlayer separation of non-acidified MMT. The observed changes in the basal (001) reflection reflected the small increases in absorption of PEG35 into the interlayer gap after further treatment of the ultrasonicated dispersions at both room temperature and 60°C. The d_{001} spacing of the PEG35M-60°C composites appeared generally lower than the ones of the PEG35M-RT composites and the heat treating process did not practically improve the intercalation of PEG35. Comparisons between the interlayer distances of the ultrasonicated PEG35-MMT and PEG25-MMT composites were made to determine the influence of molecular weight on interlayer separation of non-acidified MMT. The interlayer thicknesses measured for the PEG25M composites were slightly larger than the ones of the PEG35M composites. The general increases in the diffusion of PEG25 into the interlayer galleries of MMT imply better penetration of the lower molecular weight PEG25 through the interlayer spaces of ultrasonically dispersed non-acidified MMT.

The acid treatment of MMT, on the other hand, slightly decreased interlayer space of acidified MMT layers after the longer treatment of the ultrasonicated PEG35Ma dispersions at RT and 60ºC. The acid treatment of MMT resulted in a reduced degree of intercalation of PEG35 after the longer treatment of the ultrasonicated dispersions at both temperatures. In contrast to the non-acidified composites, when the ultrasonicated dispersions of acidified MMT were treated with PEG25, the absorption of PEG25 was undertaken to smaller extents in comparison to the ultrasonicated PEG35Ma composites. The interlayer expansion of acidified MMT was not increased by smaller PEG25 in size, unlike the treatment of non-acidified MMT.

Assessing the interlayer distance of non-acidified and acidified MMT showed that the acidification process resulted in the different intercalation behaviors of PEG in response to different reaction time and temperature and the molecular weight of the PEG. For non-

acidified MMT, the intercalation of PEG35 was greater after the PEG35M dispersions were further treated at RT and the non-acidified MMT was better intercalated by the smaller PEG chains. For acidified MMT, the further treatments of the ultrasonicated PEG35-MMT dispersions decreased interlayer distance of acidified MMT possibly due to slight deintercalation of PEG35 but the intercalation degree of PEG35 into the acidified MMT was greater than that of the PEG25. The interlayer spacing appeared to be increased for the acidified samples relative to the non-acidified samples prepared under identical experimental conditions and PEG was best absorbed into the interlayer space after the ultrasonication treatment of PEG35Ma dispersions. The greater uptake of the larger PEG35 chains indicate that the acidification process of MMT may provide more accessible sites due to the better particle separation caused by the acid-treatment of MMT. However, the slight losses of intercalated PEG35 from acidified MMT could be resulted from the unstable interlayer arrangement of PEG35.

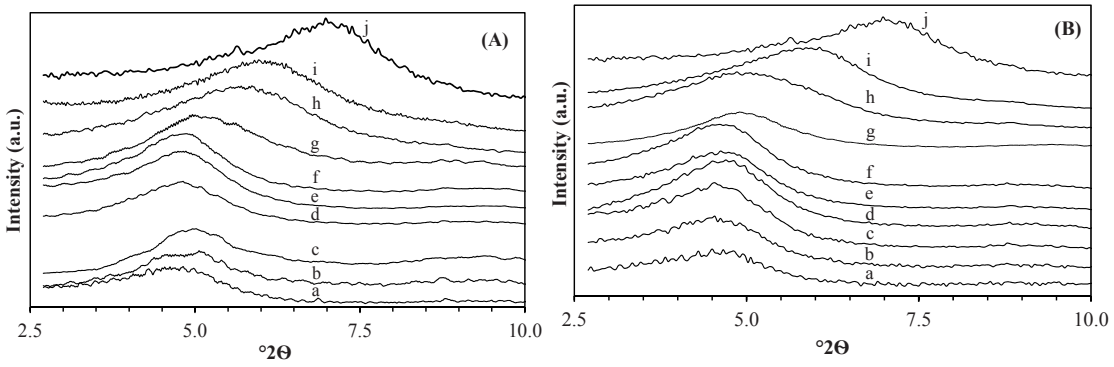

Figure 6.4.4. Basal (001) reflection of the ultrasonicated samples produced from (A) MMT and (B) acidified MMT at (a) 10% MMT, (b) 20% MMT, (c) 30% MMT, (d) 40% MMT, (e) 50% MMT, (f) 60% MMT, (g) 70% MMT, (h) 80% MMT and (i) 90% MMT and (j) MMT

Although the PEG penetration into non-acidified MMT was found to be lower, especially for the ultrasonicated PEG35M samples without the additional treatments, the increased absorption of larger PEG35 to the non-acidified MMT after the longer treatment may indicate that the composite structure formed of non-acidified MMT afforded better stability and interaction of PEG with MMT (Chen & Evans 2005a).

Even though the series of diffraction patterns in Figure 6.4.4 showed some changes produced by different experimental parameters, the overall changes occurred at comparatively small levels and the degree of d_{001} more strongly depended on the MMT-to-PEG ratio as reflected by the similar shape and position of peaks at each PEG-MMT compositions. It can be seen from Figure 6.4.4 that all PEG-MMT series showed sharp increases in interlayer spacing from 10 to 20% PEG. After progressive expansion process, slowdowns in the absorption of PEG were observed at 30-40% PEG and the extents to which increase in d-spacing of MMT of the PEG-MMT composites were considerably reduced compared to those for lower PEG concentrations. The changes in (001) basal spacing from 12.6 Å for MMT up to 18.6 Å at 60% MMT due to interlayer expansion of 6.0 Å. Further increase in PEG concentrations led to interlayer expansion of ~ 19.7 Å at 10% MMT, only 1.1 Å larger than the ones of the composites at 60% MMT. The comparable interlayer spacings indicates a limit to the PEG absorption to the interlayer space of MMT and increased proportions of unintercalated PEG with increasing PEG concentrations.

Similar observations have been reported elsewhere for PEG-MMT composites where the aqueous intercalation method reached near maximum value of 17.5-18.8 Å for the interlayer spacing of MMT at 15-30% PEG concentrations, beyond which the penetration of PEG became less dependent on their concentrations in the composites (Aranda & Ruiz-Hitzky 1992, Wu & Lerner 1993, Boulet et al. 2003, Jeong et al. 2007, Carretero-Gonzalez et al. 2008, Zampori et al. 2010, Zhu et al. 2013a, Erceg et al. 2014, Clegg, Breen & Khairuddin 2014). They also observed a loss of PEG crystallinity with increasing MMT concentration (Choi et al. 2001, Kim & Park 2007). In agreement with the work of Ip (2007) et al., the crystallinity of PEG was reduced with increasing MMT concentrations of the composite (Ip 2007). In the combination with the variation of the d-spacing, d_{001} of the basal plane in MMT, it was evident that the crystallinity of PEG was inhibited and amorphous PEG structure was formed in the interlayer region or the adsorbed surface of MMT. Conversely, the most crystalline peaks of PEG appeared at 70-90% PEG concentrations where the maximum penetration of PEG was reached as observed from the position of the (001) peak. Agreeing with the previous studies on the PEG-MMT composites, these results showed the presence of the significant portion of PEG chains in excess that were free or adsorbed onto the MMT surface as reflected by the crystallinity

peaks of PEG (Sarier & Onder 2010, Chrissopoulou et al. 2011, Choudhary & Sengwa 2014).

In combination with d_{001} basal spacing of MMT and the crystalline peaks of PEG, the observed interlayer spacing at varied clay contents broadly exhibited three different states of PEO chains: fully and partly absorbed and free states, and the results reflected the structural changes at 60 and 30% MMT. In the 60-70% PEG where no crystalline diffraction peaks of PEG and considerable interlayer expansion was found, the PEG chains were accommodated in the interlayer space of MMT and the motion and structure of the intercalated PEG chains within the interlayer space of MMT were restricted. Although the extent of PEG intercalation was reduced based on the (001) basal reflection over 40% PEG, the observed disappearance of PEG crystalline peaks at 40-60% PEG could be possibly caused by the partial intercalation of PEG and adsorption of PEG chains onto the MMT surface at high MMT portions, which may interact with PEG chains and constrain PEG chains. The concentrations greater than 60% PEG presented the formation of free PEG chains, which existed in the outer side of the MMT layer.

6.4.3. SEM study of PEG-MMT

Figure 6.4.5 shows the Backscattered electron images of the selected PEG35-MMT1 composite films. The BE images of the composites demonstrated the presence of the bright MMT particles, which were dispersed homogeneously within the dark PEG background at concentrations as high as 60% MMT, although the measured particle size became consistently larger with increasing MMT concentration. SEM comparison of the top surface of the composite films showed significant morphological and microstructural changes with MMT concentration at 60-70% MMT. Dispersion of the MMT clusters with the maximum dimension of 5, 6 and 9 μm was observed in the composites at 20, 50 and 60% MMT respectively. As the concentration of PEG increases, smaller MMT particles and larger particle size differences were seen. In the structures containing 10-60% MMT, the large MMT agglomerated MMT were broken to form the clusters and tactoids of MMT layers, which appeared to be regularly separated and distributed throughout the polymer. Although the aggregates and clusters of MMT were disaggregated with

increasing PEG35 concentration, the extent of PEG35 intercalation was apparently limited to the formation of intercalated tactoids along with the significant proportion of MMT clusters. At this MMT concentration range, the dispersion states were comparable and this result was reflected by their similar interlayer distance measured by XRD data. In contrast to the films where PEG exists predominantly, the backscattered electron image showed the much rougher and denser surfaces and cracks were developed at 70-90% MMT and the microstructures at high MMT content appeared very similar to that of MMT by the presence of larger MMT aggregates. The obvious structural differences between 60 and 70% MMT were identified due to the transformation from the MMT dominated agglomerated microstructure at 70-90% MMT to the well-dispersed states at 10-60% MMT.

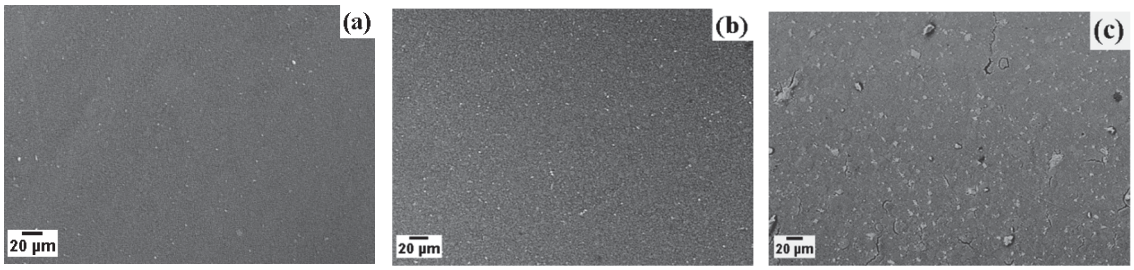

Figure 6.4.5. Backscattered electron images of the top surface of PEG35M composites at (a) 20% MMT, (b) 50% MMT and (c) 70% MMT

SEM micrographs of PEG35M composite films loaded at varied MMT content taken at higher magnification are presented in Figure 6.4.6. The SEM comparison of the top surface by SEM shows noticeable morphological changes and SEM examination of the microstructural surface condition show irregular size and shapes of MMT particles. The images of the composites with MMT loading of 10% (Figure 6.4.6a-b) and 20% (Figure 6.4.6c) depicts comparable surface morphology and their surfaces reflect fairly uniform distribution of MMT particles in the PEG matrix. The measured sizes of nano MMT particles are around 100 nm, corresponding to the lateral dimension of MMT platelets reported in the literature and indicate the dispersion of MMT platelets from the layer agglomerates due to the intercalation process of PEG35. The structure also includes the micro MMT particles having the dimension of about 500-600 nm dispersed in the polymer matrix, suggesting that the clay agglomerates still remained in the structure even at 10 % MMT loading. The nano and micron level dispersions of MMT particles were apparently

observed within the polymer matrix and the particles were well separated from the adjacent MMT particles with no apparent links. At 20% MMT, both nano and microparticles were observed, though the microparticles are more readily visualized. Disagglomeration of microparticle clusters seemingly reduced the formation of nanoparticles and more microparticles remained in the structure.

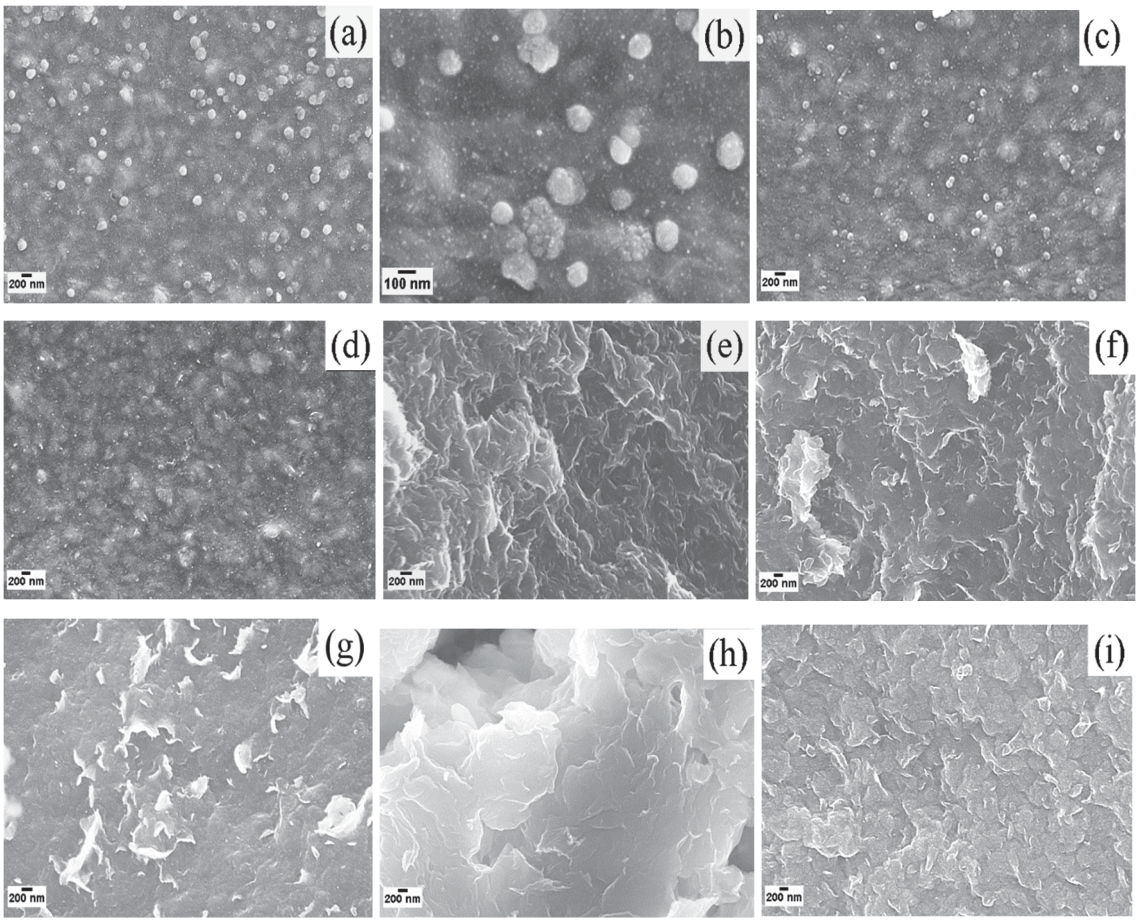

Figure 6.4.6. Representative SEM images of ultrasonicated PEG35-MMT composites at (a) and (b) 10% MMT, (c) 20% MMT, (d) 40% MMT (surface), (e) 40% MMT (cross section), (f) 60% MMT, (g) 70% MMT, (h) 80% MMT and (i) 90% MMT

The microstructure and morphology of the film surface at 30% MMT appeared to be similar to the ones at 40% MMT as shown in Figure 6.4.6(d), 4(e) and 4(f) and the SEM examination of these composites revealed the increased size and number of MMT microparticles and the absence of nanoparticles observed at the lower MMT loadings. The cross section of the films displayed flaky and layered MMT structures and the rougher surface textures compared to the lower MMT contents as seen from the cross-

sectional images for 40% MMT. The microstructures of the films containing 50 and 60% MMT could be described as composite systems similar to the SEM photographs obtained for 60% MMT in Figure 6.4.6(f). The composite films at 50 and 60% MMT also exhibited layer structures and the SEM observations of these composites indicated less flat surface topography, a more roughened surface and more opened and larger layered agglomerate at 60% MMT. Considerable increase in the surface roughness and more dense layered aggregates were observed at 70% MMT concentration while the morphological features of composites were relatively unaltered at 70-90% MMT as shown in Figure 6.4.6 (g-i). The SEM micrographs indicated that the larger MMT agglomerates appeared as dominant components and the homogeneous and dense microstructures were formed. The SEM analysis corresponds with XRD measurements, which also showed two types of composite structures. From an applied point of view, both microscopic and macroscopic observations suggested that the composite structures at high MMT content greater than 60% MMT are most likely unsuitable for use in stone consolidation.

6.4.4. FTIR analysis of PEG-MMT

Figure 6.4.7 contains the FTIR spectra of PEG35, MMT and the ultrasonicated composites incorporated with unmodified MMT concentrations ranging from 10 to 90% and represents typical spectra observed for the PEG-MMT composites. An assignment of the FTIR spectra is given in Table 6.4.1, on the basis of FTIR data available in the literature for MMT, PEG and the PEG-MMT composites (Papke et al. 1981, Ruiz-Hitzky & Aranda 1990, Shen, Simon & Cheng 2002). In the FTIR spectrum of PEG35, a broad band in the region 3600–3000 cm^{-1} contains a maximum absorption at around 3460 cm^{-1}, which can be attributed to OH stretching vibrations. The very strong and strong bands at 2888 and 2745 cm^{-1} arise from the CH stretching modes of CH_2 and CH vibrations –(CH_2CH_2O)– of PEG. The strong bands at 1468, and 1284 cm^{-1} represent the CH_2 bending vibration and CH_2 twisting vibration, respectively. The medium absorption bands at 1243 cm^{-1} appeared for CH_2 twisting mode and the strong peak derived from the CH_2 wagging vibration can be seen at 1351 cm^{-1}. The absorption bands appearing at around 1105 cm^{-1} can be assigned to the stretching and bending vibrations of C-O-C bond, respectively.

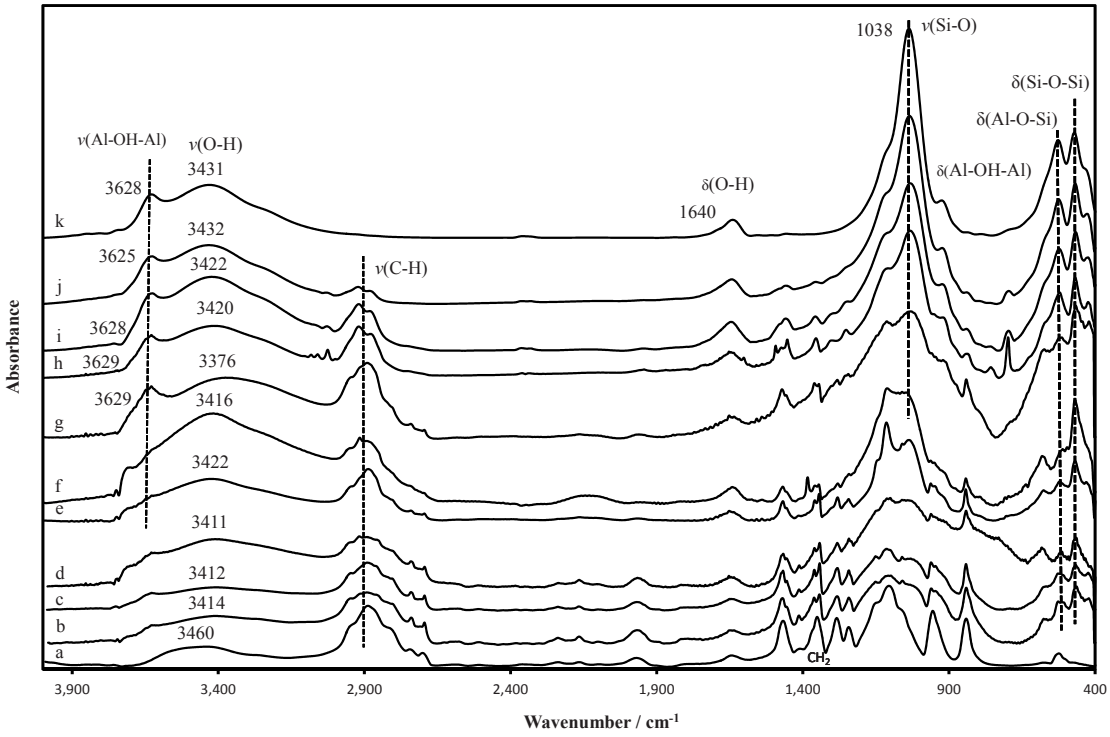

Figure 6.4.7. FTIR spectra of (a) PEG35, (b) PEG35M1, (c) PEG35M2, (d) PEG35M3, (e) PEG35M4, (f) PEG35M5, (g) PEG35M6, (h) PEG35M7, (i) PEG35M8, (j) PEG35M9 and (k) MMT

The spectroscopic analysis of PEG showed that the conformational changes of PEO were determined by be trans (CC-OC), trans (CO-CC), gauche (OC-CO), or gauche-minus(OC-CO) conformation (Papke et al. 1981). The gauche conformation of the -CH_2-CH_2- groups can be identified by the CH_2 rocking modes of methylene group at 945 and 850-880 cm^{-1} whereas trans conformation can be detected by the CH_2 rocking modes at around 773 and 992 cm^{-1} and the characteristics CH_2 stretching vibration of ethylene group in the trans form around 1320 cm^{-1} (Papke et al. 1981, Ruiz-Hitzky & Aranda 1990). In the collected FTIR spectrum of PEG, the presence of the absorption bands at 841 and 956 cm^{-1} attributed to CH_2 rocking modes of gauche configuration and the absence of band near 1320 cm^{-1} indicate the presence of gauche conformations of the -CH_2-CH_2- group in the PEG structure (Ruiz-Hitzky & Aranda 1990).

The FTIR spectra of prepared PEG-MMT composites shows the presence of bands ascribed to PEG35 and MMT (Figure 6.4.7b-j). The characteristic absorption bands of MMT corresponding to the OH stretching and bending vibrations of lattice water, the

Table 6.4.1. Observed frequencies for PEG and MMT

cm^{-1}		
PEG	MMT	Assignments
	3628	Al-OH-Al stretching
3460 (s)		OH stretching vibration
	3431	O-H stretching vibrations of the interlayer water
2888 (vs)		Symmetric and asymmetric stretching vibrations of CH_2
2745 (s)	-	
2701 (w)	-	
	1640	O-H deformation vibrations of the interlayer water
1670 (w)		C-O stretching vibration
1468 (s)		Bending vibration of CH_2
1351 (s)		CH_2 wagging vibration
1284 (s)		Twisting vibration of CH_2
1243 (m)		Twisting vibration of CH_2
1105 (vs)		C-O-C stretching vibration
	1038 (s)	Si-O-Si stretching
956 (s)		Rocking vibration of CH_2 in gauche configuration
	925	AlAlOH bending
	876	AlFeOH
841 (s)		Rocking vibration of CH_2 in gauche configuration
	839	AlMgOH
	791	Si-O vibrations of amorphous silica
	526	Al-O-Si bending of tetrahedral layer
	471	Si-O-Si bending

stretching vibration of structural hydroxyls and Si-O-Si and the bending modes of Al_2OH, Si-O-Si and Al-O-Si are found at 3628, 1640, 3628, 1038, 925, 471 and 526 cm^{-1} respectively. The PEG-MMT composites present the strong absorption bands of PEG at 2888, 1351, 1280, 1242 and 1105 cm^{-1} due to CH_2 stretching, CH_2 wagging, couple of CH_2 twisting modes, and C–O–C stretching vibrations respectively. The presence of a broad absorption band in the region 3700-3000 cm^{-1} appears due to the superimposed peaks from structural hydroxyl group of MMT at around 3431 cm^{-1} and OH stretching

vibration of PEG35 at 3460cm^{-1}. Similarly, at lower wave numbers 900-1200 cm^{-1}, the absorption bands at 1105 cm^{-1} assigned to C–O-C stretching vibrations of PEG can be seen as overlapped on the broad absorption bands at 1038 cm^{-1} due to Si-O stretching vibration of MMT in the PEG-MMT samples. Overlaid on these peaks, the peaks at high wave numbers and 900-1200 cm^{-1} were broadened and the spectral changes in structural OH and Si-O stretching bands of MMT and OH and C-O-C stretching vibration of PEG35 were not clearly defined (Aranda & Ruiz-Hitzky 1992). Previous work on the solution intercalation of PEG showed the reduced intensity of the water bending vibration and lattice hydroxyls of MMT due to the removal of the interlayer water with PEG (Pusino et al. 1990, Chen & Evans 2005b). The observed spectra of PEG-MMT composites did not show clear change in the peak intensities of OH bending vibration of the interlayer water due to a superposition of the peaks from PEG and MMT at around 1640 cm^{-1}.

As observed by the previously reported infrared analysis of intercalated PEG reported, there appeared considerable changes in the absorption bands due to CH_2 stretching vibration of PEG in the composites at 70% MMT (Aranda & Ruiz-Hitzky 1992, Shen, Simon & Cheng 2002). The CH_2 stretching vibration region of PEG of the PEG-MMT composites at 10-60% MMT appeared similar to the pure PEG, whereas the composites at 70-90% MMT converted to two well separated bands at about 2880 and 2921 cm^{-1}. The previous reports on the infrared spectral analysis of PEO-MMT intercalation compounds also showed the shifts of methylene deformation vibrations in the 1200-1500 cm^{-1} owing to the interactions between interlayer cations and the lone electron pairs of oxygens of PEG and the peaks shifts of 1-15 cm^{-1} were reported (Aranda & Ruiz-Hitzky 1992, Shen, Simon & Cheng 2002, Boulet et al. 2003).

The vibration bands at 1410 cm^{-1} were slightly shifted to higher wavenumber with increasing MMT concentration. The peaks at 1468 cm^{-1}, which are ascribed to bending vibration of CH_2 group, were shifted up to 1475 cm^{-1} over 40% MMT. Similarly, the upward shift of the bands corresponding to twisting vibrations were detected. These absorption bands were shifted from 1284 and 1243 cm^{-1} up to 1308 and 1261 cm^{-1} for the PEG-MMT composites containing greater than 50 and 40% MMT respectively. Comparing with the spectra of PEG-MMT composites below 50-60% MMT loading, the

position and shape of these peaks remained unchanged at the MMT concentrations from 10 up to 50-60% MMT for the absorption bands at 1243, 1284 and 1468 cm^{-1}. In contrast, these adsorption bands of PEG-MMT composites were shifted over 50-60% MMT, which may indicate the alteration in the bonding environment of PEG in the composites at 50-60% MMT and two PEG-MMT composite structures. Additionally, the appearance of new absorption bands at around 1361 and 1343 cm^{-1} was found. It has been reported that the absorption band of PEO/PEG at 1350 cm^{-1} was split into two bands at 1360 and 1340-1345 cm^{-1} upon the intercalation of PEO/PEG (Billingham, Breen & Yarwood 1997, Ruiz-Hitzky & Aranda 1990, Shen, Simon & Cheng 2002). Ruiz-Hitzky and Aranda suggested the observed peak splitting at 1350 cm^{-1} may be attributed to ion-dipole interactions between the oxygen of oxyethylene units and the interlayer cations (Ruiz-Hitzky & Aranda 1990).

Consistent with XRD and SEM observations, it was found from the FTIR spectra of the PEG-MMT composites that similar FTIR spectra were detected for the PEG-MMT composites prepared using different experimental conditions and no significant effects of preparation conditions on the PEG-MMT structures were found. The FTIR results corresponded with XRD and SEM measurements and considerable changes were observed when comparing the FTIR spectra of PEG-MMT composites 10-40% MMT with the ones at higher than 50-60% MMT. In the crystalline state, PEO showed helical structure with gauche conformation of PEO chains due to the absorption bands at 956 and 841 cm^{-1} ascribed to the rocking vibration of PEG and the lack of CH_2 stretching vibration of ethylene group around 1320 cm^{-1} (Ruiz-Hitzky & Aranda 1990, Shen, Simon & Cheng 2002). In confirmation of earlier studies, the FTIR measurements of PEG-MMT composites revealed the absence of stretching vibration ascribed to trans CH_2 conformation at all MMT concentrations and showed the lack of the trans conformation of PEG for the indication of the planar zigzag chain conformation of PEG in the composites (Ruiz-Hitzky & Aranda 1990, Shen, Simon & Cheng 2002). However, the peaks at 956 cm^{-1} were not clearly detected at 50-90% MMT and the bands at 841 cm^{-1} overlapped with the band of MMT at 839 cm^{-1}. Shen et al. showed similar observations and suggested the distorted helix structure of PEG in the composites (Shen, Simon & Cheng 2002). Based on the changes in the FTIR and XRD observations, the helical

structure with gauche conformation of crystalline PEO chains were distorted in the composite structures and the crystalline of the intercalated PEG were lost over 50-60% PEG.

6.4.5. Thermal analysis of PEG-MMT

Figure 6.4.8 shows the DTG and TG curves for PEG35 showing one major mass loss step in the thermal degradation of PEG35 as illustrated in TG, DTG and TG curves of PEG35. The mass loss steps of PEG was summarized in Table 6.4.2. The initial small mass loss of 0.3 % due to evaporation of adsorbed water up to 99°C was followed by the exothermic decomposition reaction of PEG35 between 164 and 500°C with a mass loss of 99.7 %. The thermal degradation that PEG35 underwent mainly in a single step was initiated by the random scission reaction of C-O and C-C bonds of PEG chains. The reported thermal degradation studies of PEO showed that the thermal decomposition of PEG mainly involved the scission reaction of C-O bond cleavage and consequent formation of various degradation products, including oligomers up to hexamer, formate ester, aldehydes, alkanes, hydroxyl, carbonyl and ethereal compounds (Grassie & Mendoza 1984, Costa et al. 1992, Fares, Hacaloglu & Suzer 1994, Yang et al. 1996).

Table 6.4.2. Mass losses of PEG35 measured at a heating rate of 10°C/min

Mass loss step	Interval temp (°C)	DTG Peak temp (°C)	Mass loss (%)
M1 endo	66 - 99		0.3
M2 exo	164 - 500	288	99.7

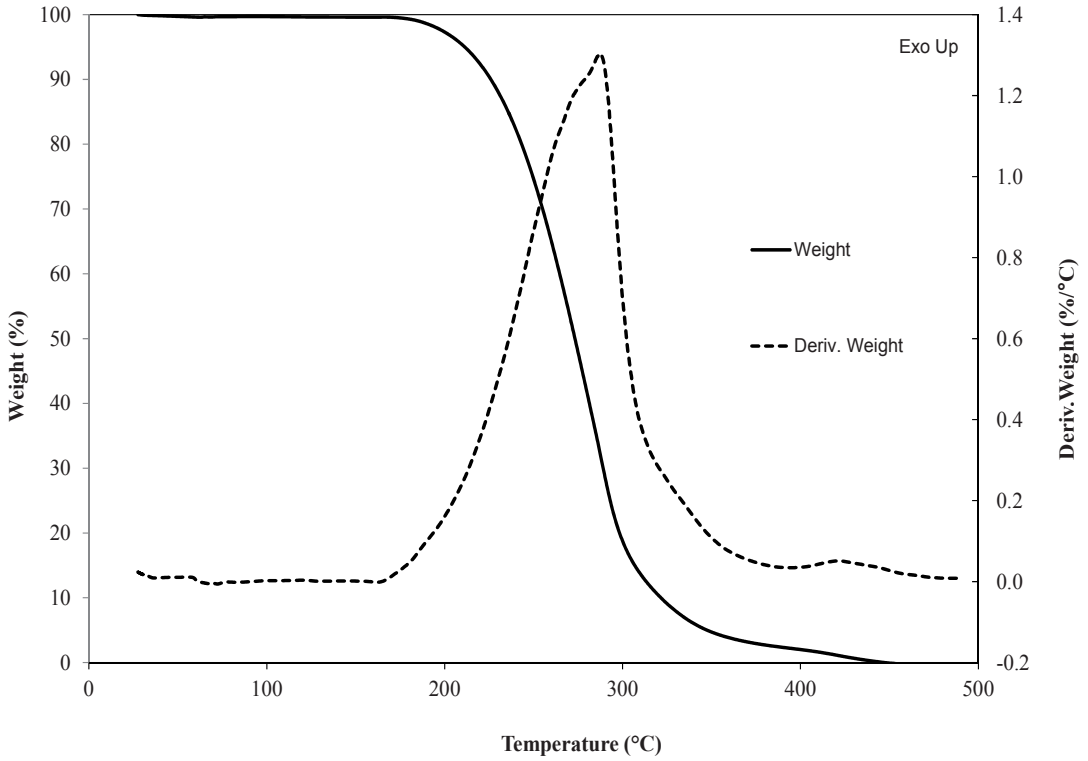

Figure 6.4.8. DTG and TG curves of PEG35 measured at a heating rate of 10ºC/min

TGA analysis of the composites prepared using non-acidified or acidified MMT intercalated by PEG35 were performed to find the amount of PEG and water present in the PEG-MMT composites. Figure 6.4.9 shows the TG and DTG profiles for PEG35, MMT, and the ultrasonicated PEG35-MMT composite systems. In contrast to PEG, a total mass of only 9.9% was detected for MMT on heating to 1100°C and the thermal decompositions of MMT occurred in two steps as seen from the TGA and DTG curves of MMT. The first step is attributed to the evaporation of physisorbed and interlayer water to ~193ºC with a mass loss of 4.6% and to dihydroxylation reaction of MMT in the temperature range 360-555ºC. Following the dehydration of PEG-MMT composites, it is clear from the Figure 6.4.9 that, compared to neat PEG35 and MMT, the DTG curves of the PEG-MMT composites exhibited the degradation of PEG occurring in a single step from 132°C and the total losses of PEO being completed by around 600°C. When heated to 1100°C, all tested PEG-MMT composites revealed the total weight losses attributed to PEG and the partial decomposition of MMT and resulted in the MMT residues.

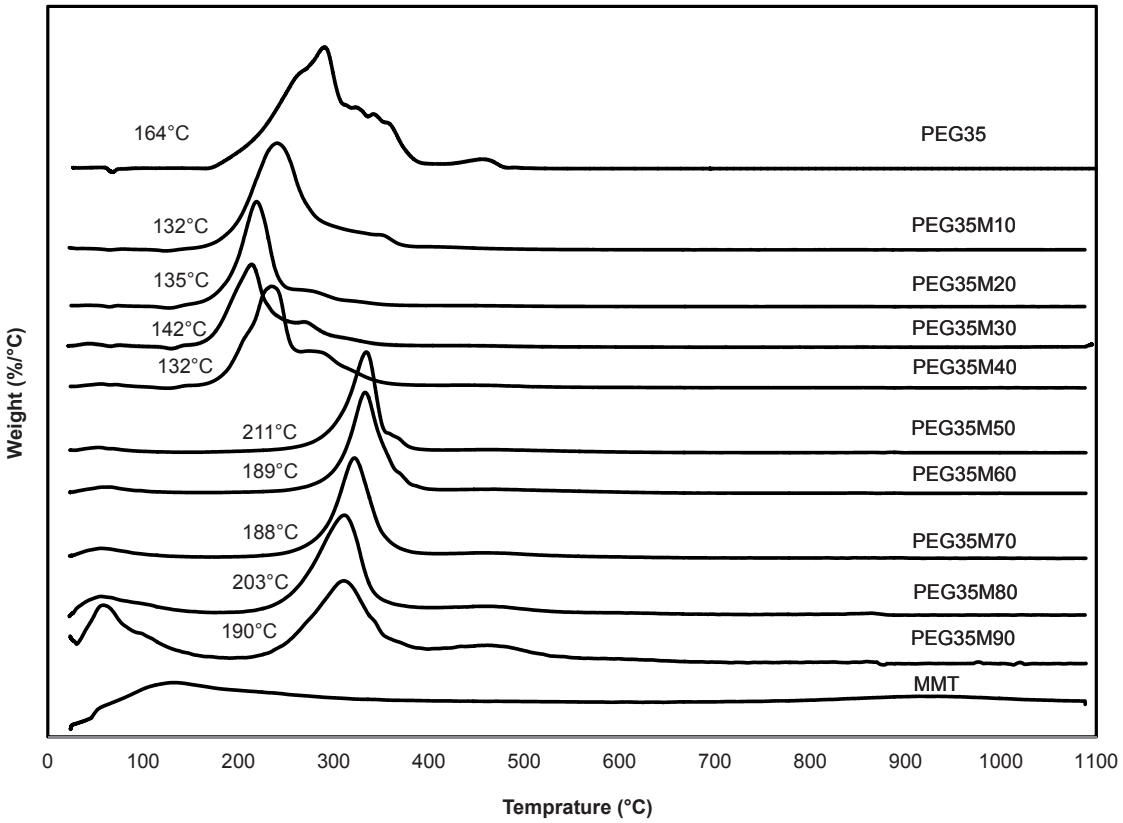

Figure 6.4.9. Thermograms of PEG35, MMT and the ultrasonicated PEG35-MMT composite systems measured at a heating rate of 10ºC/min

In the temperature range from 130°C to about 350°C, the two mass loss regions of PEG were identified from the TG and DTG curves of the PEG-MMT composites. The first onset temperatures of the PEG35M composites were found at 132-135°C at 10-40% MMT, whereas the onset decomposition temperatures for the higher MMT concentrations were found to be 188°C or higher. The reduced first onset temperatures of PEG35M composites at 10-40% MMT indicates disruption of the crystallinity of PEG35. It has been demonstrated that the intercalated PEG chains in MMT were thermally more stable and the mass loss of the intercalated PEG are detected by higher degradation temperature (Sarier & Onder 2010, Deka & Kumar). When PEG is intercalated in the galleries of MMT, the effects of torturous path are increased on the diffusion of oxygen into and the escape of degradation products from the galleries of MMT.

Table 6.4.3. Decomposition temperatures and mass losses with respect to PEG mass for the ultrasonicated PEG-MMT samples

	First onset temperature	Amount of Free PEG	Second onset temperature	Intercalated PEG (%)
PEG35	164	-	-	-
9:1	132	70.6	280	29.4
8:2	135	64.2	248	35.8
7:3	142		248	
6:4	132	56.3	264	43.7
5:5	-		211	100
4:6	-		189	100
3:7	-		188	100
2:8	-		203	100
1:9	-		190	100

In agreement with the similar TGA data reported by Shen, Simon & Cheng (2003), the higher onset temperatures of the PEG-MMT composites at 10-50% PEG, corresponding to the degradation of intercalated PEG, indicated the absence of PEG remaining outside the galleries (Shen, Simon & Cheng 2003). Conversely, the lower onset temperatures at 60-90% PEG showed the presence of PEG remaining in the outer surface of MMT where PEG is weakly adsorbed and the non-intercalated PEG moved more freely. In addition to the thermal degradation of the free PEG, the mass losses ascribed to the thermal degradation of the absorbed PEG between MMT layers were detected over 200°C from their TG and TGA curves of the PEG-MMT composites at 60-80% PEG. As summarized in Table 6.4.3, the calculated proportions of free PEG were increased with increasing PEG concentrations.

Correlating TGA and XRD data, PEG was intercalated into MMT at 10-50% PEG and the intercalation of PEG was accompanied by the lost crystallinity and increased thermal stability of PEG. The observed TGA and XRD results are in accord with the FTIR analysis of PEG-MMT composites, which also showed the peaks shifts and indicated the changes in the bonding environments of PEG at about 50-60% MMT. The SEM observations made on PEG35M were consistent with the structural transformation from the well-dispersed MMT in the PEG matrix to the states corresponding to predominantly MMT-like surface structure at 50-60% MMT. Based on the combined results from the macroscopic, XRD, SEM, FTIR, and TGA observations, the structural changes of PEG-MMT composites were taken place at 50-60% MMT where the interlayer space of MMT were occupied by the bilayer of PEG chains.

6.4.6. Summary

The solution intercalation technique was used to prepare a series of PEG-MMT composites in the concentration range from 10 to 90% MMT and the influences of processing time, temperature, acidity of MMT and molecular weight of PEG were studied. XRD, SEM, FTIR and TGA measurements have been conducted to study the changes in the intercalation degree of PEG, bonding interactions between PEG and MMT and microstructures, morphology and thermal characterisation of PEG-MMT composites and all the results revealed and the observed changes were largely determined by the MMT-PEG ratios. The overall effects of the tested parameters were found to be relatively negligible, demonstrating that the ultrasound assisted solution-casting method was an effective, fast, simple and green approach for the preparation of PEG-MMT composites.

The XRD data showed the interlayer spacing of MMT was increased up to 19.7 Å and the formation of composites structures where mono- and bilayers of PEG chains were intercalated at all tested series. The interlayer expansions were progressive, going from 10 to 20 % PEG and the MMT interlayer separation of MMT was reduced and reached the state corresponding to insignificant interlayer separation of MMT by PEG with further increase over 20% PEG concentrations. Likewise, the inhibited semicrystalline structure

of PEG from 10 to 50-60% PEG and the reserved crystallinity of PEG at 70-90% PEG were observed. The XRD data indicated fully and partly intercalated and free states of PEG and the crystalline structure of bulk PEG was transformed to amorphous after full intercalation of PEG.

SEM observations also revealed the morphological changes at 50-60% MMT. The well-dispersion of stacked MMT layers in PEG matrix were found at 10-40% MMT and the agglomeration of MMT layers were increased to form over 50-60% MMT. Similarly, the altered local environments of PEG were observed from FTIR results of the composite structure at 50-60% MMT and the PEG-MMT composites were formed by the interactions between interlayer cations and the lone electron pairs of oxygens of PEG. The FTIR spectra exhibited no evidence of the trans configuration of PEG to indicate the planar zigzag chain conformation of PEG in the composites and the helical structure with gauche conformation of PEO chains was increasingly distorted and lost in the composites. Over the 50% MMT concentrations, the TGA curves indicated the increased thermal stability of PEG that was intercalated into MMT. In the composites over 50% PEG, the presence of intercalated and free PEG was found and the amounts of excess PEG increased with increasing PEG. The thermal stability of free PEG was reduced and the excess PEG was weakly interacted with MMT.

From the visual appearance and physical characterises in conjunction with XRD, SEM, FTIR and TGA analysis of the formed PEG-MMT composite film, the structural and characteristic changes in dependence on MMT concentrations were observed. The results showed that the composite system was in a saturated state over 50% PEG, which indicated that PEG chains were available both in the locality of the clay surface and in the bulk state. It follows that the intercalated portions of PEG chains can provide the structural miscibility with MMT while the free PEG can provide the physical and adhesive characteristics of PEG. PEG chains stuck within the interlayer space of MMT that is in confined environment of MMT would not be useful as a binder for the intended application. From the practical point of view, the PEG-MMT composites over 60% PEG can meet the need to provide for the intended use as stone consolidation work.

6.5. In situ intercalative polymerisation method

6.5.1. Introduction

In addition to the investigation of polymer consolidants, in situ polymerisation was also considered. In this section, the potential for use of in situ polymerisation on a method to promote intercalation in MMT is addressed. Am and AA have been investigated as a function of the initiator KPS concentration. The in situ intercalative polymerisation was performed over the concentration range of 1-7 w/w% AA or Am and 0.1-1.0 wt% KPS. The effects of monomer and initiator concentrations on the physical characteristics of polymerised samples were evaluated by keeping MMT concentration constant at 10 wt% relative to concentration of Am or AA. The first step was to examine their appearance, cohesiveness and mechanical strength of prepared composite films. These observations were included to determine ranges of monomer and initiator concentrations that are able to procedure uniform film of good adhesion for the treatment of sandstone.

6.5.2. In situ intercalative polymerisation of Am

This section considers the potential for use as stone consolidant of in situ polymerisation of water soluble monomers in the presence of MMT. The in situ polymerisation of Am in the concentration range from 1 to 7 w/w% was initiated by 0.1-1.0 wt% KPS in the presence of 10 wt% MMT relative to Am. It was observed that increasing KPS concentration generally decreased the polymerised Am concentration. These observations are exemplified in the images of Figure 6.5.1. As seen from Figure 6.5.1a, the unreacted Am-MMT dispersions showed the agglomerated MMT separated from the dissolved solution. Figure 6.5.1b illustrates the uniform dispersion of MMT in the solution which became viscous likely due to the polymerisation reaction of Am and produced the film upon drying. At 0.1 wt% KPS, polymerisation of Am was observed over 4 w/w % Am. Although increasing KPS concentration from 0.1 to 0.8 wt% reduced Am concentrations brought about the polymerisation reaction of Am, further increase in KPS concentration above 0.8 wt% considerably reduced the effect of KPS concentrations on the polymerised Am concentration and viscosity and appearance of polymerised samples caused by the extent of MMT particle separation.

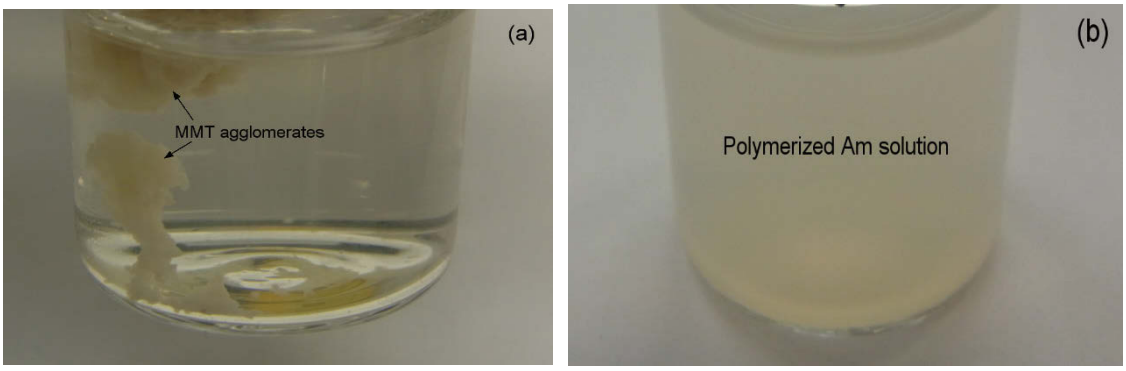

Figure 6.5.1. Photographic images taken for the in situ polymerisation of Am in the presence of 10 ww% MMT using (a) 2w/w% Am and 0.1wt% KPS and (b) 2w/w% Am and 1wt% KPS.

Although initiator concentrations influenced polymerised Am concentration, the samples polymerised at the identical Am concentrations produced similar results even at different KPS concentrations and all results demonstrated the main effect of Am concentrations on the physical characteristics of the polymerised samples. The reaction conducted using 3-5 w/w % Am generated honey-like viscosity and relatively uniform and milky appearance. The observed results indicate that the concentration of Am plays a significant role in dispersion and separation of MMT particles to improve evenness and stability of MMT particles in polymer matrix. The gel polymerised in this concentration showed no obvious phase separation, considerable adhesiveness and the formation of smaller MMT particles and more stable particle distribution within the polymer matrix, which appeared to meet the requirements for the intended use.

Higher Am concentrations resulted in the formation of neither water insoluble nor non-dispersive gels in which the separation of MMT aggregates became significant. Similar observations were seen from the Am-MMT samples containing high Am concentrations which were reacted at room temperature. Although the polymerisation of various Am concentrations was attempted at 1.0 wt % KPS, the gelation was not observed for the Am concentrations less than 7 w/w % Am. The Am concentrations higher than 5 w/w % Am was polymerised at both temperatures to form hard, inflexible and water insoluble materials where MMT portion was separated from polymer without MMT dispersion. The unfavourable gel formations were observed for high Am concentrations.

Apart from the above-mentioned criteria, considerations were applied to potential issues concerning unreacted materials that can remain in consolidated sandstone. In an effort to reduce impurity levels which can be resulted from unreacted Am and KPS, attentions were initially made to prepare in situ polymerised Am-MMT systems that are prepared using lowest concentrations of both Am and KPS as possible. MMT particle separation at Am concentrations less than 6 w/w % was improved and the Am-MMT sample prepared at up to 4 w/w % Am and 1.0 wt% KPS particularly appears to provide the uniformity, dispensability and viscosity that are more suitable for use in stone consolidant. Such results were used as a guideline to estimate the effects of concentration of Am and KPS on the intercalation separation of MMT in the Am-MMT samples in the following section.

6.5.3. In situ intercalative polymerisation of AA

Experiments also showed the similar trends that give indications about the influence of the KPS concentrations on polymerisation reaction of AA and revealed a clear decrease of AA concentrations that polymerised at the given reaction time and temperature with increasing KPS concentration. The in situ polymerisation of 1-7 w/w% AA in the presence of 0.1-1.0 wt% KPS were observed in similar way to Am-MMT samples. In contrast to Am-MMT samples, the shorter mixing time after the addition of KPS used for the second method polymerised the slightly lower AA concentrations than the longer mixing time and the polymerised AA-MMT samples revealed that the changes occurred in physical characteristics were different from Am-MMT samples. Irrespective of the preparation method and concentration of AA and KPS, the polymerised AA-MMT samples showed unfavourable visual effects from noticeable separation of MMT and non-uniform dispersion of MMT after the polymerisation of AA. The polymerisation time of AA was decreased likely due to acidic conditions of the AA-MMT dispersions and the fast polymerisation reaction of AA could similarly reduce the extent of AA diffusion to the interlayer gap of MMT. In comparison to the Am-MMT samples, the use of AA significantly reduced the extent of MMT dispersion and separation and formed inhomogeneous gels. The observed appearance of the AA-MMT samples was apparently unsatisfactory for the intended use of AA-MMT samples and therefore no further XRD, SEM, FTIR and TG analysis of the AA-MMT samples was performed.

6.5.4. XRD analysis of Am-MMT

6.5.4.1. Effect of Am concentrations on interlayer separation

The influence of Am, KPS and MMT concentrations on interlayer separation introduced by absorption of polymerised Am was investigated from position of the (001) peaks and the d_{001} interlayer spacing of the Am-MMT composite samples and comparisons were made by varying one of the Am, KPS or MMT concentrations while keeping the other two parameters constant. Figure 6.5.2 illustrates the (001) peak of Am-MMT films prepared using 1, 1.5, 2, 2.5 and 4 w/w % Am under the first mixing technique. The observed results were considered under two complementary viewpoint: the extent of MMT interlayer separation and the design of MMT based stone consolidant. At all Am concentrations, most samples resulted in gel formation polymerised at 60°C and the heat treatment of MMT in the presence of Am and KPS showed a shift of the (001) reflection to lower angles across all experimental condition. The relative increases in basal spacing of treated MMT imply the absorption and following polymerisation of Am in the interlayer gap. With increasing Am concentrations, there was a general increase in interlayer distances accompanied by increase in polymerisation degree, viscosity, clarity, adhesiveness and homogeneous dispersion of MMT particles. The Am-MMT samples containing 4 w/w % Am exhibited much improved interlayer expansion, transparency, uniform dispersion of MMT particles and adhesiveness compared to lower Am loadings which tended to produce visible MMT aggregates from polymer.

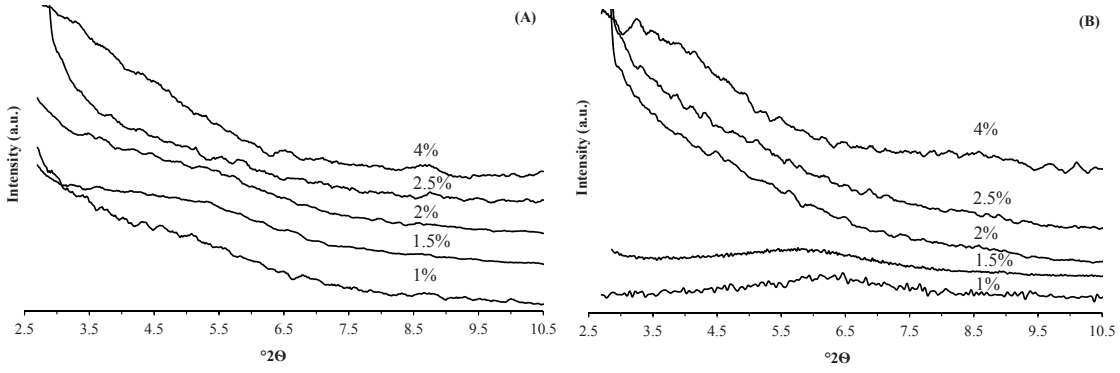

Figure 6.5.2. Basal (001) reflection of the samples prepared from 1 wt% KPS using (A) 10 w/w% non-acidified MMT or (B) 10 w/w% acidified MMT at various AM concentrations

Contrasting Method I versus Method II, the patterns from the (001) reflection of the non-acidified Am-MMT samples prepared by Method I and II were unchanged and the similar observations were found for the acidified Am-MMT samples. The interlayer distance was apparently independent of the methods by which the samples were prepared in this work and indicate that the extent of Am absorption in the interlayer space was not affected by the different mixing time. In contrast, the acidification process of MMT considerably reduced the interlayer separation at 1 and 1.5 w/w % whereas this effect was decreased to produce similar results to non-acidified samples and no substantial difference between acidified or non-acidified samples at higher Am concentrations. With increasing Am concentration, the effect of acidifications process becomes insignificant and the resultant structural and visual effects seemed to be determined mainly by the fraction of Am content. Together with comparative results of all samples at 4 w/w % Am which presented a major improvement in interlayer separation of MMT, the enhanced transparency, uniform dispersion of MMT particles and adhesiveness of this concentration were consistent with the initial experimental observations on their visible appearance and the results suggested the use of 4 w/w % Am for preparation of suitable stone consolidating system.

6.5.4.2. Effect of KPS concentrations on interlayer separation

The influences of KPS concentration on the interlayer separation of MMT layers and physical appearance of produced films were assessed by changing the KPS concentration with 4 w/w % Am and MMT concentration being constant at 10 wt % relative to Am concentration. There seems to be no obvious difference from the shape and position of (001) peaks as shown in Figure 6.5.3. The insignificant effect of KPS on the degree of interlayer distance at all initiator concentrations suggests that the diffusion speeds and penetration levels of Am were apparently similar at all initiator concentrations. Like with the results of the position of the (001) peaks observed from varied Am concentrations, no considerable differences were detected for the samples prepared using Method I and II and mixing time has practically no influence upon Am absorption into the interlayer space of MMT. The results of these series indicates that the overall effect of variation in KPS concentration, acidification treatment of MMT and mixing time of Am-MMT dispersion are likely to be low for interlayer separation of MMT.

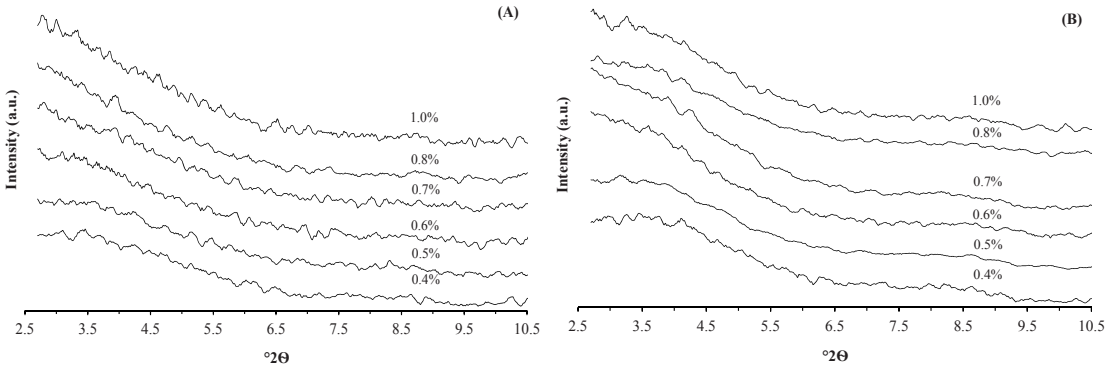

Figure 6.5.3. Basal (001) reflection of the samples prepared under Method I from 4 w/w% Am using (A) 10 w/w% non-acidified MMT or (B) 10 w/w% acidified MMT at various wt% KPS

As was to be expected from the results discussed above, the polymerisation of 4 w/w % Am using various KPS concentrations resulted in the similar appearance of produced films which provided clear colour, evenly dispersed MMT particles in polymer matrix and good adhesiveness throughout all initiator concentrations applied in these series. As indicated by apparent increase in viscosity and adhesiveness of the films, the extent to which polymerisation of Am occurred was increased with higher KPS concentration, whilst marked increases in film strengths were seen to occur at 0.9 and 1.0 wt % KPS to produce significant viscosity and glueyness. Increasing KPS concentrations gradually approaches the adhesive film suitable as stone consolidant at 0.8 wt % KPS over which the film strength became a slightly higher. Therefore the results demonstrated the concentrations of 0.8 wt % KPS and 4 w/w % Am to provide the better visual characteristics and separation of MMT layers for intended use in consolidating work.

6.5.4.3. Effect of MMT concentrations on interlayer separation

The effect of MMT concentrations on intercalation behaviours were studied by different MMT loading at the constant concentrations of 0.8 wt % KPS and 4 w/w % Am. It is apparent that clear change in positions of (001) reflection was observed from Figure 6.5.4 which shows the XRD pattern obtained from the films prepared using Method I without acidification process of MMT. Irrespective of MMT concentrations in the samples, the

examined Am-MMT samples produced the peaks located around at 2θ = 8.9, 12.5, 17.5 and 19.9° and the changes in these peak positions appear to be small in comparison to the marked effect of MMT contents on the position of the basal (001) reflection. Similarly, the Am-MMT samples prepared by Method I after acidification process of MMT produced the XRD peaks at 2θ = 8.9, 12.5, 17.5 and 19.9° at all MMT concentrations while considerable variation in the (001) basal plane of MMT was observed. The Am-MMT samples prepared using Method II with or without acidification process of MMT also resulted in similar patterns. The shape of peaks appeared similar at each composition across all experimental conditions but the positions of the basal (001) reflection are dependent on the ratio of MMT concentration to Am concentration (Figure 6.5.5). As the Am concentration is increased, the (001) peak shifts to lower 2θ angle and interlayer expansions increased as a result of the absorption of Am into interlayer gap of MMT.

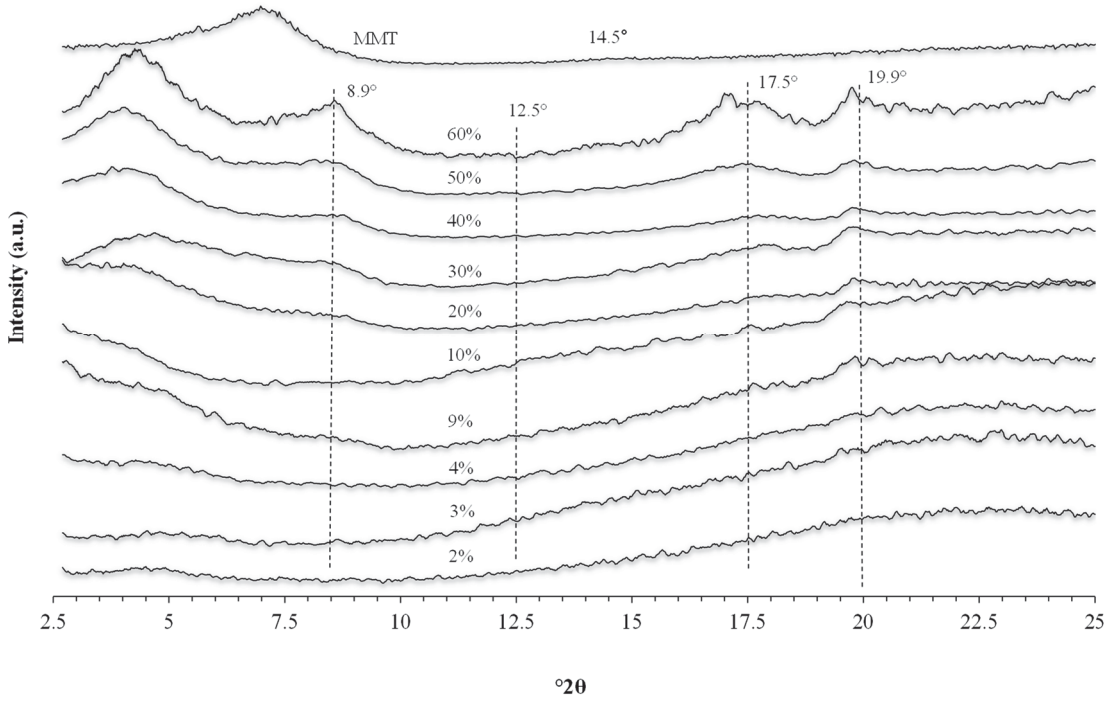

Figure 6.5.4. XRD profiles of the Am-MMT samples produced using 0.8 wt% KPS and 4 ww% Am at various MMT concentrations

Some adsorption and absorption studies of Am revealed the influence of the ratio between the amount of absorbent and expandable clay minerals including MMT on the extent of interlayer intercalation of Am (Ogawa et al. 1989, Inyang et al. 2007, Koç et al. 2014).

The results obtained in this work brought the results of XRD measurements into agreement with the previously reported investigation and the measured separation of MMT layers showed the tendency to increase with MMT loading in the samples. In general, the clay concentration-dependent changes in the position of the basal (001) reflection reveals that the intercalation process of Am occurred in two steps. With decreasing MMT concentrations going from 60 down to 20%, there appears gradual downshift of identifiable (001) peak maxima and the more distorted peak due to broadening and higher background intensity. A steady increase in interlayer gap was observed up to 28.1 Å corresponding to interlayer enlargement of 15.5 Å at 20% MMT and these measurable peaks were found to be located in a range that indicate the formation of intercalated structure (Zanetti et al. 2000, Sinha Ray & Okamoto 2003, Chen 2004, Pomogailo 2005, Chauhan et al. 2006, Zhu & Wilkie 2007, Chen at al. 2008b, Pavlidou & Papaspyrides 2008, Kiliaris & Papaspyrides 2010). This was followed by a further decreased in intensity and collapse of peak upon increasing the Am concentrations greater than 80 %. No clear basal reflection of MMT may indicate the presence of exfoliated and disordered silicate layers throughout the polymer matrix resulting from improved interplatelet expansion due to absorption of Am between the layers (Koç et al. 2014).

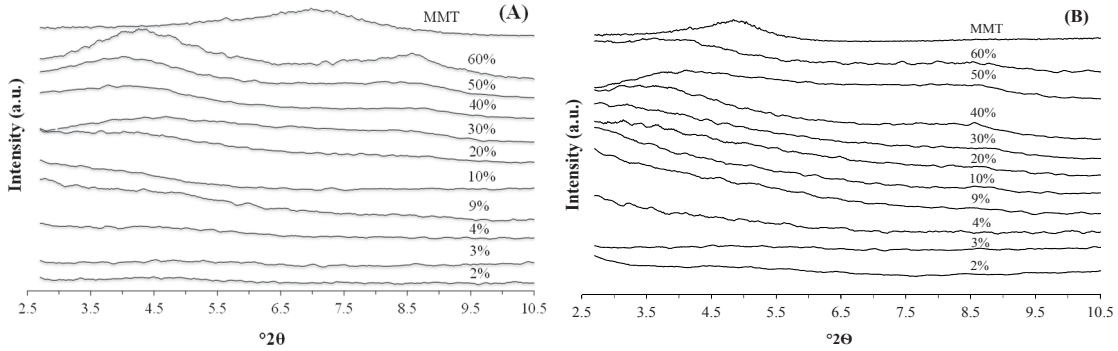

Figure 6.5.5. Basal (001) reflection of the samples prepared under Method I from 0.8 wt% KPS and 4 ww% Am using (A) non-acidified MMT or (B) acidified MMT at various concentrations of MMT

However, it is worth noting that the observed featureless flat curves can be associated with misorientation of layer silicates in the structure. As with the XRD data observed for PAm-MMT complexes, reducing the concentration of MMT down to 20% MMT showed

an increased interlayer separation accompanied by increased peak distortion. It is probable from the observed shift of (001) peak together with the increased peak distortion, the interlayer separation is accompanied by the increase of disordered MMT layers with decreasing MMT loadings. Accordingly, the observed pattern is consistent with the view that the significant interlayer separation was likely to be taken placed in the compositions below 20% MMT and MMT-Am ratio probably plays an important role in establishing the structural changes of the products. However, on the basis of the featureless curve, the misorientation of silicate layers should be considered and the complete exfoliation of MMT layers was unlikely achieved. It is likely that the decisive concentrations are found to be 20% MMT where interlayer separation significantly begins to increase, going from more homogeneous intercalated structure to an inhomogeneous system where intercalated and exfoliated layers coexist with the varied degree of layer separation, irregularity and misorientation in the mixed layer structure.

6.5.4.4. Effect of acidification and mixing condition on interlayer separation

The interlayer separation of MMT modified with or without acidification process in the polymerised PAm matrix was examined by the measurable d_{001} spacing of the samples as plotted against MMT concentrations between 20 and 60% in Figure 6.5.6. The influences of acidification of MMT and mixing modes were evaluated by the comparison of non-acidified and acidified samples for which all other preparation conditions were held constant. Comparisons made between two mixing modes demonstrated the different intercalation behaviour for the non-acidified and acidified MMT. The interlayer distance of the non-acidified samples prepared using the second mixing method were found to be generally greater than the ones for the first mixing method. Presumably, the longer mixing time reduced the interlayer absorption of Am in the presence of KPS and the smaller interlayer spacing of non-acidified MMT in the presence of KPS indicates inhibitive effect of KPS on the interlayer absorption of Am on non-acidified MMT. The addition of KPS to the well-stirred Am and MMT solution may facilitate the better intercalation of Am. After acidification of MMT, generally similar d_{001} spacing at each MMT loading was obtained and the results indicated that the swelling behaviour of acidified MMT was almost unaffected by mixing methods. The higher interlayer distance of acid-treated

MMT in comparison to non-acidified samples prepared by the long mixing time may be resulted from the better interaction of Am with the acidified surface of MMT.

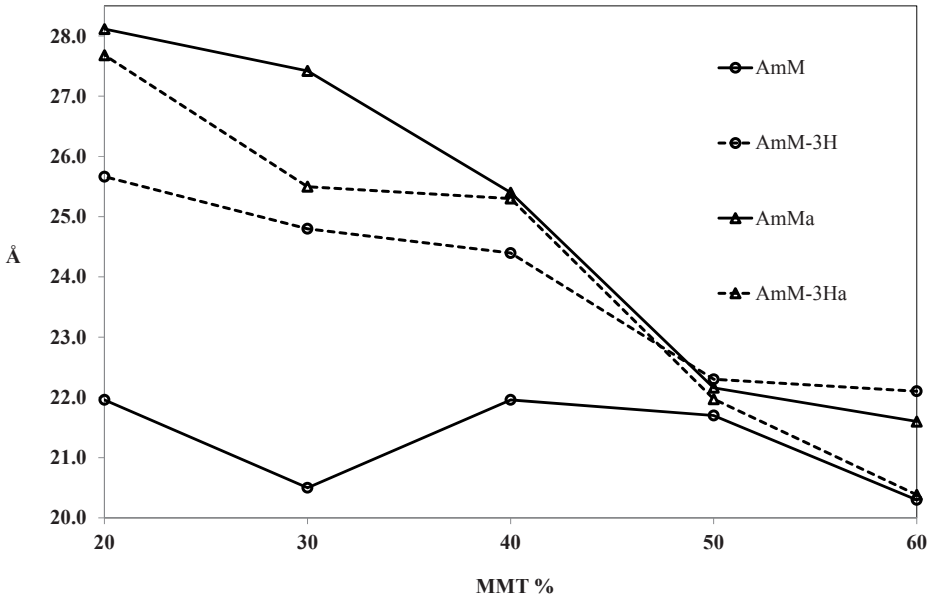

Figure 6.5.6. Interlayer distance of MMT plotted versus MMT loading

6.5.5. Microscopic evaluation of in situ polymerised Am-MMT films

The visual effect of MMT concentrations were determined through the evaluation of any changes that occurred from the produced films having different MMT loadings but the same concentrations of 0.8 wt % KPS and 4 w/w % Am (Figure 6.5.7). The first sight of produced films reflected polymerisation reaction at all MMT loading under all experimental conditions and clarity, adhesiveness and surface smoothness of produced films as well as evenness of clay dispersion were generally found to increase with Am concentration in all tested series. The low concentrations of 2-3 % MMT produced the uncoloured and transparent films in which MMT particles appeared microscopically invisible. At the concentrations as high as 20-30% MMT, the uniform distribution of MMT particles became visible in the light brown and transparent films but the evenness and transparency of films were reduced to produce darker, denser, thicker films over 30 % MMT. Macroscopically, the films at 40-60 % MMT loadings produced the heterogeneous and non-transparent films. The similar qualitative picture was deduced from the visual

examination of the produced films showing the changes in their appearances according to MMT loading. The increased interlayer gap of MMT with decreasing MMT concentrations is consistent with an apparent general trend of increasing clarity, uniformity, degree of MMT distribution of the produced films. A combination of XRD data on d_{001} spacings and their microscopic observations that the samples produced at 40-60 % MMT loadings appeared unsuitable for their use in stone consolidation work.

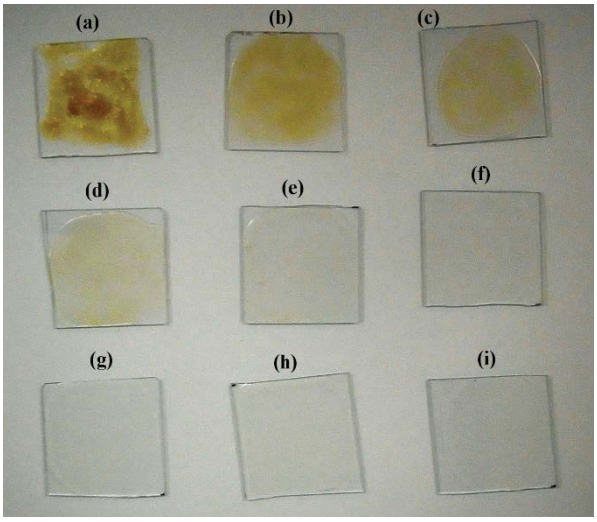

Figure 6.5.7. Am-MMT films at (a) 50% MMT, (b) 40% MMT, (c) 30% MMT, (d) 20% MMT, (e) 10% MMT, (f) 9% MMT, (g) 4% MMT, (h) 3% MMT and (i) 2% MMT

6.5.6. FTIR analysis of Am-MMT

The spectra of Am, MMT and their Am–MMT composites using the first method are presented in Figure 6.5.8. The assignments of the peaks are presented in Table 6.5.1 according to the data reported for MMT and Am (Jonathan 1961, Schmuckler & Limoni 1977, Günzler & Gremlich 2002, Duarte et al. 2005, Girma et al. 2006). In the FT-IR spectrum of Am, the characteristic bands in the NH stretching region are observed from the double bands of the primary amide at about 3352 and 3190 cm^{-1} and are assigned to the asymmetric and symmetric stretching vibration, respectively. The small absorption bands at 3105 and 3035 cm^{-1} may be attributed to unsaturated CH stretching vibrations due to the presence of C=C bonds of Am and the peaks between 3000 and 2700 cm^{-1} are assigned to saturated CH stretching vibrations. The intense absorption band at 1674 cm^{-1}

is originated from the C-O stretching vibration corresponding to carbonyl group of the amide moiety and the bending vibrations of CH_2 and NH_2 are found at 1429 and 1612 cm^{-1} respectively. The peaks at 1387 cm^{-1} could be assigned to the C-N stretching vibration.

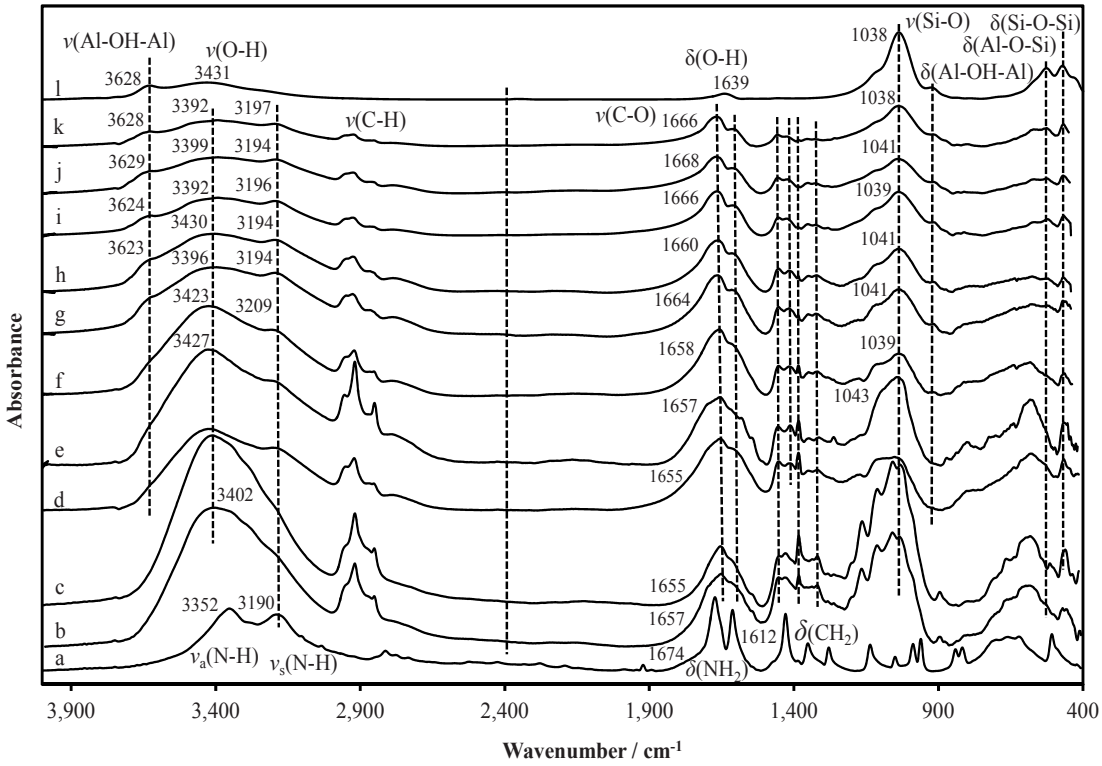

Figure 6.5.8. FTIR spectra of (a) Am and Am-MMT samples prepared using the first method at (b) 2% MMT, (c) 3% MMT, (d) 4% MMT, (e) 9% MMT, (f) 10% MMT, (g) 20% MMT, (h) 30% MMT, (i) 40% MMT, (j) 50% MMT and (k) 60% MMT and (l) MMT

For the FTIR spectra of Am-MMT samples with different MMT contents, the absorption bands due to the presence of MMT and PAm can be found. The spectra of the Am-MMT samples contain bands present in MMT at about 3628, 1038, 926, 520 and 471 cm^{-1} attributed to the stretching vibrations of structural OH group, Si-O-Si stretching and the bending vibrations of Al-OH-Al, Si-O-Al and Si-O-Si bonds (Table 6.5.1). The characteristic absorbance bands originating from PAm occurred for N-H symmetric stretching vibration, CH symmetric and asymmetrical stretching vibrations, C-O stretching vibration and N-H bending vibrations at around 3190, 2814, 2777, 2735, 1674

Table 6.5.1. Infrared absorptions of Am and MMT and their peak assignments

cm^{-1}		Assignments
Am	MMT	
-	3628	Al-OH-Al stretching
-	3431	O-H stretching vibrations of the interlayer water
3352	-	N-H asymmetric stretching vibration
3190	-	N-H Symmetric stretching vibration
3105		Asymmetric stretching vibration of CH_2 group
3035		Symmetric stretching vibration of CH_2 group
2814	-	Symmetric and asymmetric CH stretching vibrations
2777		
2735	-	
1674	-	C=O stretching band
-	1639	O-H deformation vibrations of the interlayer water
1612	-	Amide II: Bending vibration of NH_2 group
1429	-	Bending vibration of CH_2 group
1352	-	C-N stretching vibration
1279	-	C-H Bending + C–N stretching vibrations
1136		NH_2 and CH_2 rocking vibrations
1049	-	NH_2 and CH_2 rocking and CH bending vibrations
-	1038	Si-O-Si stretching
987	-	HC=CH wagging vibration
960	-	CH_2 wagging vibration
-	926	AlAlOH bending
-	876	AlFeOH
841	-	C–C stretching vibration
-	839	AlMgOH
818	-	NCC and CCC out of plane bending vibrations
-	791	Si-O vibrations of amorphous silica
660	-	NCC and CCC out of plane bending vibrations
621	-	NH_2 and CH_2 rocking vibrations
-	520	Al-O-Si bending of tetrahedral layer
507	-	NH_2 and CH_2 rocking vibrations

-	471	Si-O-Si bending

and 1612 cm^{-1}. The broad bands with the maximum absorptions between 3352 and 3431 cm^{-1} appear due to the overlapping the absorption bands of asymmetric NH stretching vibrations of Am and structural OH stretching vibrations of MMT. The additional peaks were detected at around 1320, 1417 and 1454 and cm^{-1} at all Am-MMT ratios except for the bands at 1417 cm^{-1} which were undetected at less than 9% MMT. These bands absent in Am, were observed in the spectra of Am-MMT samples and could be attributed to the presence of C-H bending vibration, C-N stretching vibration and CH_2 bending vibration coming from PAm in the samples as a result of polymerisation of Am in the samples. The disappearance of unsaturated CH stretching vibrations due to the C=C bonds of Am at 3105 and 3035 cm^{-1} may also indicate the polymerised Am monomers in the Am-MMT samples. The spectral analysis of Am-MMT samples show no clear peaks for C=C bond and the observations suggest that Am was intercalated and polymerised in the system (Ogawa, Kuroda & Kato 1989). For the samples up to 20-30% MMT, two new peaks at around 1166 and 1111 cm^{-1} were observed. The intensity of most bands representing characteristics of PAm and MMT were found to be enhanced with raising their concentrations while the most peaks exhibited little or no changes on their shapes and positions.

The bands ascribed to N-H symmetric stretching vibrations in amide groups of PAm tended to be shifted to lower wavenumber with increasing MMT content, whereas the bands occurring at 1674, 1454, 1352, 1320 and 1279 cm^{-1} exhibited gradual shift to lower frequency with rising PAm concentration. The slightly higher frequencies of the peaks at 1454, 1352, 1320 and 1279 cm^{-1} than those in Am were found but the results presented considerable change in the band positions of N-H symmetric stretching and carbonyl stretching of PAm after addition of MMT to Am with different ratios. The absorption bands of N-H symmetric stretching in the Am-MMT samples were positioned at higher wavenumber relative to the corresponding bands of Am and their increased peak positions compared to Am reflected the weakening of hydrogen bonding interaction of NH bond upon the addition of MMT. The bands were shifted from 3190 cm^{-1} up to 3222 cm^{-1} and resulted in upshifting of ~ 32 cm^{-1} with increasing Am concentration. The observed increased bond strength of NH group of amide may indicate the reduced self-associated

interactions of NH bonds of Am units with increasing Am concentrations in the samples (Deng et al. 2006). As for the aforementioned absorption bands which revealed a linear dependence of band shifts on the MMT concentration, there appear no clear and significant changes of symmetric NH stretching bands observed for different parameter including mixing time, temperature and acidification of MMT.

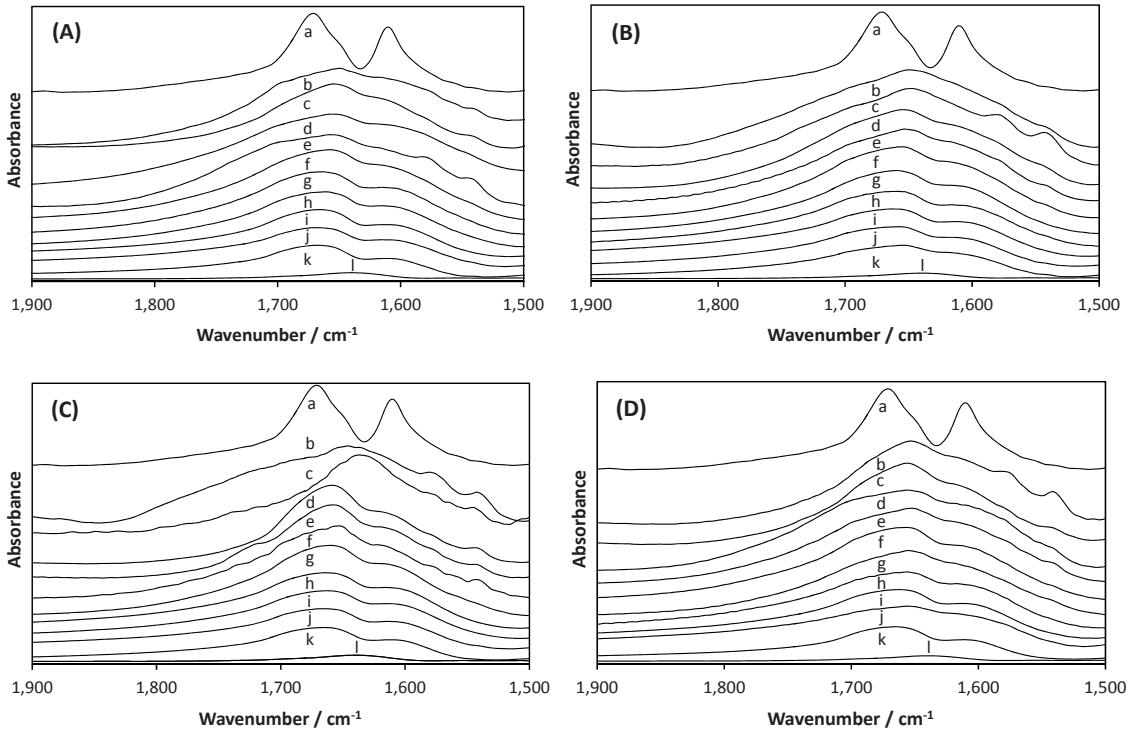

Figure 6.5.9. Carbonyl stretching bands of (A) AmM, (B) AmM-3H, (C) AmMa and (D) AmM-3Ha at (a) PAm, (b) 2% MMT, (c) 3% MMT, (d) 4% MMT, (e) 9% MMT, (f) 10% MMT, (g) 20% MMT, (h) 30% MMT, (i) 40% MMT, (j) 50% MMT and (k) 60% MMT and (l) MMT

In contrast, the bands corresponding to the CO stretching absorption of amide groups decreased carbonyl bond strength with rising Am concentration and some observable changes were caused by the preparation method as illustrated in Figure 6.5.9 which presents the FTIR spectra of the Am-MMT samples in the carbonyl stretching region. Plotting the peak position of maximum absorption bands against their corresponding MMT loading (Figure 6.5.10) showed that the carbonyl stretching band shifted from 1674 cm^{-1} for Am up to 1648 cm^{-1} for Am-MMT samples and the maximum absorptions of the C-O stretching band were found to be downshifted by up to 26 cm^{-1}. These figures

represent the lower frequency of C-O stretching bands at all Am-MMT ratios after the addition of MMT and indicated carbonyl oxygen of amide group is involved in the hydrogen bond formation with the terminal hydroxyl groups of MMT and hydrated interlayer sodium ions (Olodovskii & Murashko 1976, Mpofu, Addai-Mensah & Ralston 2004, Mpofu, Addai-Mensah & Ralston 2005, Deng et al. 2006, Kurochkina & Pinskii 2012, Natkański et al. 2013). The perceptible peak shifts to higher wavenumbers from 10 and 20% MMT were found in all series and the similar peak positions and shapes were found with the further increase in MMT contents. The observed changes correspond to the variations in the (001) reflection of MMT, which showed the significant changes in the interlayer separation accompanied by the reduced intensities and increased distortions from 10 and 20% MMT.

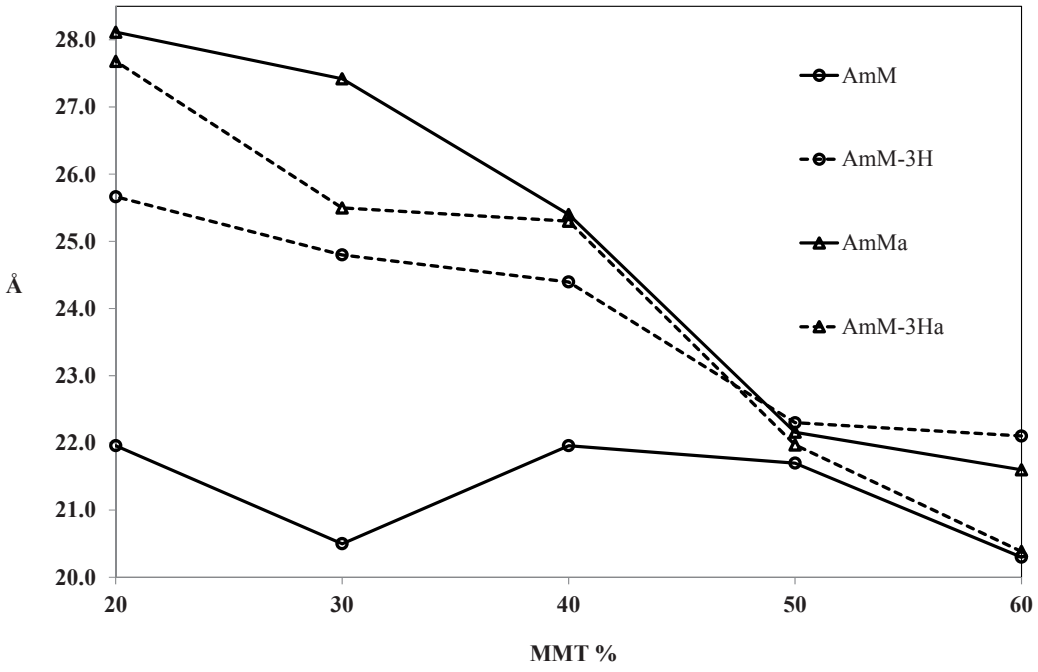

Figure 6.5.10. Maximum absorption band position plotted versus the concentration of MMT

Observation of Figure 6.5.11 also reveals that the carbonyl stretching bands of the samples prepared by the first mixing method tend to shift to slightly higher wavenumber than the samples prepared using the second method. The lower frequencies observed for the second mixing conditions indicate that the intermolecular interactions of carbonyl group were increased to a higher extent in comparison to the longer mixing conditions

which resulted in the reduced carbonyl hydrogen bonding interaction. The slightly higher wavenumber of carbonyl bands were found for the non-acidified samples using the first method, which exhibited correspondingly noticeably smaller interlayer distances as manifested by their d_{001} spacings in Figure 6.5.6. These observations seem to indicate the relation between the interaction of the carbonyl of the amide group and the intercalation degree of Am and it is probable that the intercalation of Am was partly associated with its increased interaction with MMT surface. In addition to the preparation condition, the frequencies for carbonyl bands of the acidified MMT samples appeared somewhat smaller than the non-acidified samples prepared under corresponding preparation condition. The results can be similarly viewed as the likelihood of forming more interactions of PAm with the acidified MMT and the observed changes may suggest that PAm was connected more strongly to the acid-treated MMT. However, the overall effects of both acidification treatment and mixing condition are insignificant relative to the ratio of MMT to PAm which is likely to be the main factor for the changes in interaction of carbonyl oxygen with MMT.

Summarizing analysis of IR spectral data for all Am-MMT series, there was no clear structural changes caused by the positions and intensities of most bands and the overlapped regions which likely covered the bands from the asymmetric NH stretch and interlayer water of MMT. The only noticeable variations were found from the MMT loading dependent shifts of NH symmetric stretch and carbonyl stretch bands and FTIR technique, therefore, revealed no formation of chemical bonds but physical forces which likely govern the sorption process in Am-MMT systems. Increasing concentrations of Am caused weakened N-H hydrogen bonding and increased CO hydrogen bonds and these results suggest the disconnection of self-associated intermolecular hydrogen bonds of the polymerised Am leading to the replacement of NH···OC hydrogen bonding by hydrogen interaction of carbonyl oxygen with MMT surface. The amino groups showed a negligible part in the formation of bonding interactions and MMT mainly interacted through the formation of hydrogen bonding of carbonyl oxygen unlike MMT intercalated by PAm or in situ intercalative polymerisation of Am that indicated the interaction of MMT with NH bond of amide group (Ogawa, Kuroda & Katso 1989, Huang & Ye 2014a). The slight deviations in the positions and shapes of Si-O stretching bands in Am-MMT samples

were observed for the intercalation process of Am and little or no changes were found for hydrogen bonding of the tetrahedral oxygens of siloxane surface with Am.

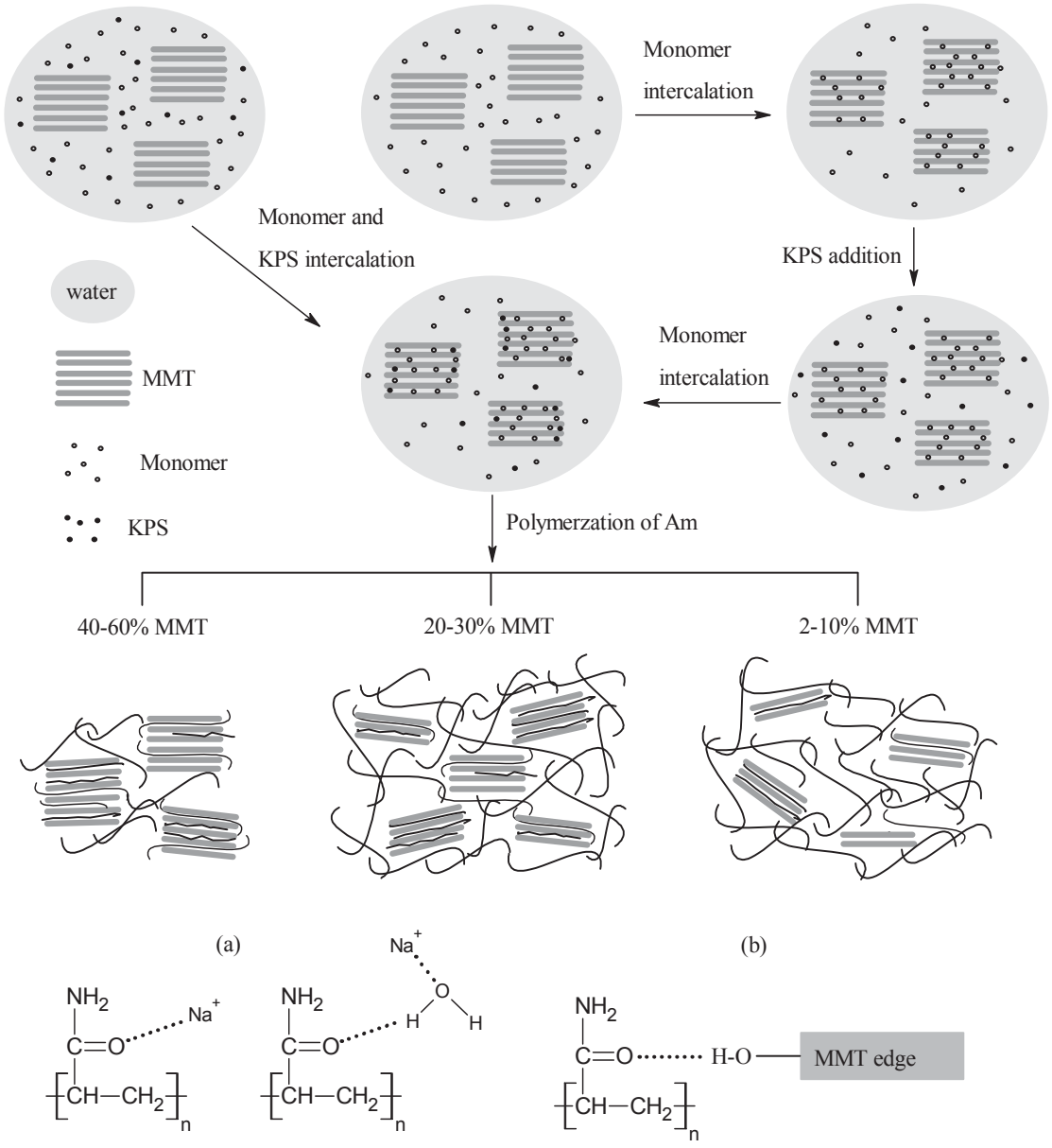

Figure 6.5.11. Schematic illustration of structural changes as a function of the amount of MMT

In addition to the interaction of the carbonyl oxygens of amide moiety with clay mineral, the previous studies have also included possible bonding mechanisms contributing from ion-dipole interaction with interlayer cations, hydrophobic associations and protonation of PAm or MMT that can involve in ion exchange reaction with interlayer cations or ionic

bonding with negative MMT surface (Deng et al. 2006). The FTIR analysis showed no indications for the protonation of the polymerised Am due to the absence of evidence to form new bands ascribed to protonated PAm (Ogawa, Kuroda & Kato 1989, Deng et al. 2006). The slight lower wavenumber in the carbonyl stretching bands of PAm observed for the acidified MMT samples may indicate the interaction of PAm with the protonated aluminol groups of the acidified MMT (Deng et al. 2006). The slight variations in the bands ascribable to methylene group of PAm were suspected to be effected by significant hydrophobic interaction with basal oxygens of MMT (Deng et al. 2006, Li & Gao 2011). Of these possible bonding interactions, the partial decrease in the carbonyl bond strength can be possibly caused by the ion-dipole interaction between sodium ions and carbonyl oxygen and the protonation of MMT in the case of acidified MMT samples (Deng et al. 2006).

The observed changes can be qualitatively pictured in Figure 6.5.11 illustrating the two probable structures in the range of concentrations used in this system. With increasing Am concentration, the interlayer expansion and destruction of MMT aggregates increased. The ion-dipole or hydrogen bonding interaction of carbonyl oxygens with sodium ions or hydrated interlayer sodium ions in interlayer region can contribute to the intercalation of Am (Figure 6.5.11a). The crystal edge surfaces consisting of aluminol or silanol groups can account for hydrogen bond formation with carbonyl oxygens of amide group (Figure 6.5.11b). Considering the restricted amounts of interlayer sodium ions and the lack of evidence for hydrogen bonding effects of amino group and other interaction forces, the interaction of Am with MMT edges can be increased by the available surface and a possible explanation of increased hydrogen bonding effects of carbonyl oxygens is that the total surface and terminal edge of MMT becomes more accessible to produce more binding sites at which Am can interact to promote the sorption of Am onto MMT (Inyang et al. 2007). The increased interactions between carbonyl moieties and terminal hydroxyl groups of MMT may also imply higher concentration of Am around the crystal edge of MMT with increasing Am concentrations (Huang & Ye 2014a). Upon the decrease in MMT concentration to 10-20% MMT, the noticeable increase in the adsorption of Am and particle separation can be explained by noticeable differences in visual assessment, interlayer expansion and carbonyl stretch bands of Am-MMT samples.

6.5.7. Thermal analysis of Am-MMT

The TG, DTG and DTA profiles of Am are presented in Figure 6.5.12. In the course of heating up to 500°C, the DTG curve showed the three distinct mass reduction steps as shown in Table 6.5.2. The first mass loss occurred below about 177ºC and the large mass loss of 56.2 % was accompanied by endothermic peak. Most of the mass loss occurring during the first stage is attributed to the decomposition of Am in the samples after the initial evaporation of small amount of moisture in the sample. The melting point of Am is 84°C and the evaporation of Am is likely during this main volatilisation step of Am. This was followed by two consecutive steps and these steps occurred with mass losses of 3.7% and 22.3%. The second mass loss is started at about 211ºC and the next mass loss step ranges from 275 to 458ºC. It is probable that polymerised Am was formed in the subsequent polymerisation reaction during heating. After the elimination of Am, the mass losses of heated Am sample beyond 177°C account for the decomposition of polymerised Am for these consecutive endothermic steps.

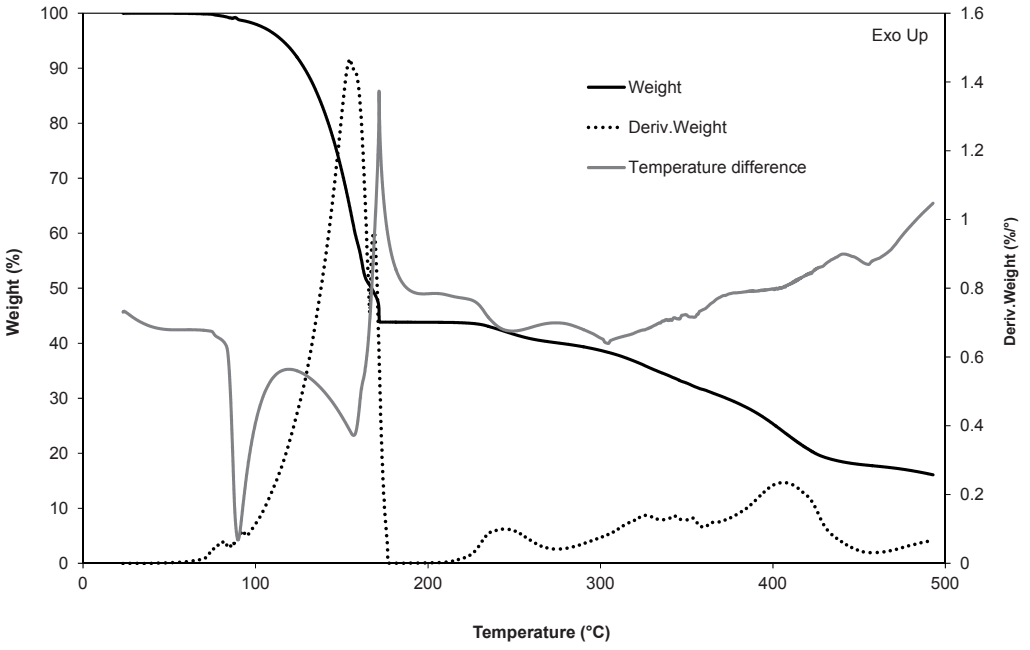

Figure 6.5.12. TGA thermogram of Am

The effect of MMT on the thermal stability of polymerised PAm-MMT systems was studied and Figure 6.5.13 shows curves for TGA measurements used to find mass losses

and to compare the thermal degradation of Am-MMT systems prepared by the first mixing condition. According to the TG and DTG curves of Am-MMT samples, four mass loss regions can be seen from the samples. Unlike the large mass of Am with DTG peak temperature at about 155°C, the first mass loss stages of the Am-MMT samples accounted for much smaller mass losses with respect to Am component of the Am-MMT samples. The reduced mass losses relative to Am below 200°C indicate the presence of PAm due to persulfate initiated polymerisation of Am during the sample preparation and the intercalated Am could be polymerised in the intercrystalline regions of MMT (Ogawa, Kuroda & Kato 1989).

The first mass reductions of the Am-MMT samples mostly resulted from the removal of moisture and absorbed water of PAm and MMT or unreacted Am (Natkański et al. 2013, Koç et al. 2014). Thereafter, the decomposition of Am-MMT samples proceeded in three steps and these consecutive steps were ended by 900°C which was followed by small mass losses to leave MMT residues persisted at 1100ºC due to the much higher thermal persistence of MMT as clearly observed from the TGA traces of MMT. Comparison of these curves shows fairly similar DTG curves with those observed for PAm and it is likely that are mainly related to the thermal decomposition of polymerised Am component in the samples.

Table 6.5.2. Mass losses of Am heated at 10.0 °C/min

Interval temp (°C)	DTG Peak temp (°C)	Mass loss (%)
25-177	155	56.2
211-275	243	3.7
275-458	407	22.3

Following the first mass loss stage, the initial decomposition step in the second mass loss stages over 203°C can be assigned to the elimination of ammonia and carbon dioxide and can be connected with the reaction of side groups of PAm including dehydration, intra-/intermolecular imidization or deammonation and subsequent decarbxylation of the imide group, crosslinked and cyclic structure, nitrile groups and aliphatic compounds (Burrows, Ellis & Utah 1981, Leung, Axelson & Van Dyke 1987, Toth et al. 1990, Van Dyke &

Kasperski 1993, Schild 1996, E. Silva et al. 2000). This was followed by the second decomposition steps over 329°C which can involve in the decomposition reactions of the side groups but more polymer chains breaking reactions such as decarboxylation (Leung, Axelson & Van Dyke 1987, Van Dyke & Kasperski 1993). The last decomposition step can be attributed to the main chain breaking process due to chain scission and PAm portion was completely combusted by the oxidative degradation (Vilcu et al. 1987, Toth et al. 1990, Van Dyke & Kasperski 1993, Han et al. 2010).

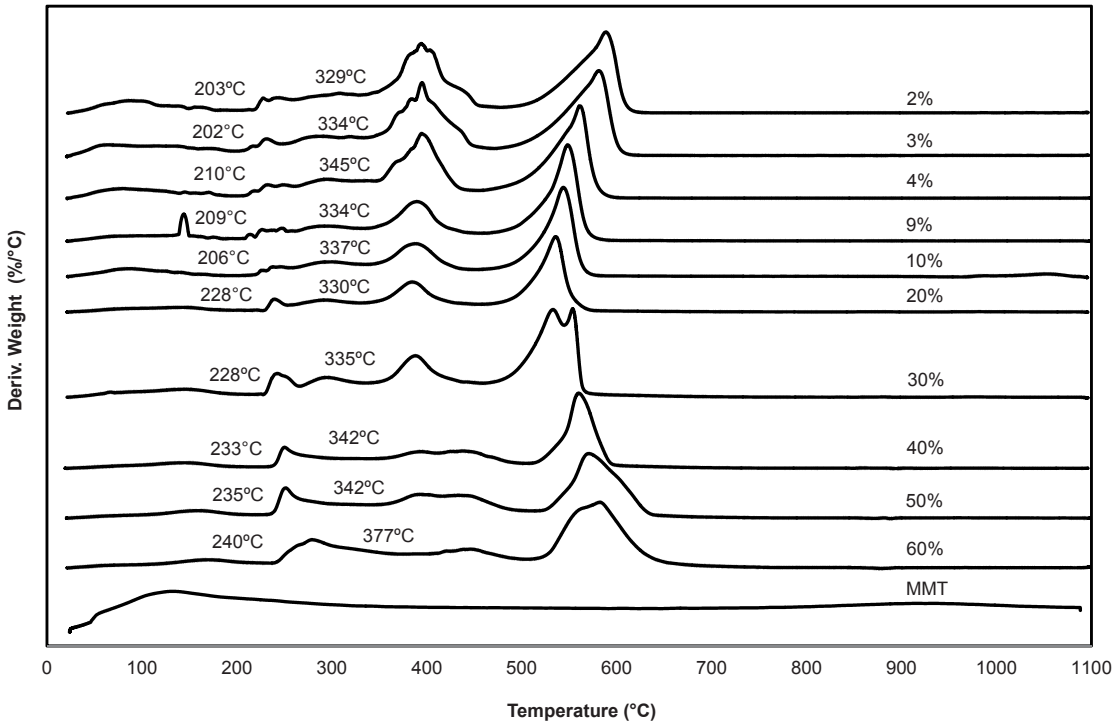

Figure 6.5.13. DTG curves of AmM samples at various MMT loadings

It is obvious from Table 6.5.3 that the enhanced thermal resistance of Am-MMT systems was revealed by the shifting of both onset and maximum decomposition temperatures toward higher values with increasing MMT concentrations. The first decomposition onset temperatures were shifted from 203°C at 2.0% MMT to 240°C at 60% MMT and the onset temperatures were found to be increase by almost 37°C at 60% MMT. The noticeable increase from 206°C at 10% MMT to 228°C at 20% may indicate the improved interaction between the PAm molecules and clay particles. Likewise, a shift of up to 48°C was observed from a shift of the second decomposition temperature from 329°C at 2.0% MMT to 377°C at 60.0% MMT. The increase in MMT concentrations caused the higher

onset temperatures of the first and second decomposition steps corresponding to the thermal decomposition of side chains of PAm contents. The addition of MMT had a retarding effect on the thermal decomposition of adsorbed or intercalated PAm in the structures.

Table 6.5.3. Decomposition onset temperatures (left) and mass losses (right) for the AmM and AmMa samples

Mass loss step	T1 (Mass loss %)	T2 (Onset, Mass loss %)	T3 (Onset, Mass loss %)
Am	56.2	211, 3.70	275, 22.3
AmM2	9.5	203,14.6	329, 37.4
AmM3	10.7	202, 15.5	334, 34.4
AmM4	9.2	210, 17.2	345, 30.3
AmM9	9.0	209, 15.5	334, 27.1
AmM10	7.8	206, 15.1	337, 24.4
AmM20	6.8	228, 12.4	330, 23.7
AmM30	6.6	228, 12.3	335, 19.8
AmM40	5.3	233, 11.3	342, 19.4
AmM50	5.4	235, 11.5	342, 19.5
AmM60	4.4	240, 11.9	377, 8.60

The thermal stability of Am-MMT systems was also considerably changed in relation to Am-MMT ratios and was resulted from the ability of MMT to enhance thermal stability of the corresponding polymer-MMT composite systems as observed in the literature. The improved stability of Am-MMT systems could be originated from the effects of MMT that can behave as interruption to slow down the decomposition of PAm. The presence of MMT in the structure can produce tortuous-path which can deter the diffusion of the volatile decomposition products. Moreover, MMT present between PAm chains could partially restrict the thermal motion of PAm and may interact with PAm to delay the thermal decomposition reactions on side group of PAm. The observed higher decomposition temperatures for higher MMT loading might also be attributed to protective effects of MMT for the degradation of PAm intercalated into the MMT layers

(Akelah 1995). Combined with XRD data which showed the increased intercalation degree of PAm with increasing the amount of MMT, the increased thermal stabilities for lower Am concentrations imply that the extent of PAm intercalation was increased with increasing MMT as a consequence of the interactions of intercalated PAm with internal surface of MMT.

6.5.8. Summary

The in situ polymerisation of AA and Am in the presence of MMT was conducted using KPS initiator. The in situ polymerisation of AA at 60°C and Am at room temperature produced the heterogeneous dispersion of MMT and their uses for in situ preparation of stone consolidant appeared to be unsuitable due to their unfavourable appearance. The effects of the concentrations of Am and KPS on film appearance and interplatelet separation of MMT were monitored. The interlayer expansion, MMT particle separation and the extent of Am polymerisation were generally increased with increasing Am and KPS concentrations but the observed changes were decreased over 0.8 wt % KPS and 4 % w/w Am corresponding to their upper limit where their effects became insignificant. The comparative results for 3-5 w/w % Am and 0.8 wt% KPS as intercalating agent and initiator appeared to meet the requirements for the in situ formation of stone consolidant. The changes in the separation of interlayer space and particles were partially explained by monomer interlayer penetration which was inversely related to the concentrations of monomer and KPS.

For the acidification treatment of Am-MMT samples, different concentrations of KPS, Am and MMT produced the insignificant effects of mixing conditions on the visual appearance as well as disaggregation, dispersion and interplatelet separation of acidified MMT but the slight improvement in the interlayer separation and CO hydrogen bonding interaction were observed. Under the longer mixing condition, the interlayer expansion of the non-acidified MMT due to Am intercalation was reduced and carbonyl hydrogen bonding force was slightly weaken. Considering the slight increase in interlayer enlargement and hydrogen bonding interaction observed for the acidified samples and the

short mixing time in the presence of KPS, the acidification treatment of MMT and shorter mixing time facilitated in situ intercalative polymerisation of Am.

The combined results of FTIR data, XRD patterns, TG measurements and visual inspections of the produced Am-MMT films showed strong dependence of changes in the structure and interaction of Am-MMT systems on MMT concentrations. Generally, the decreased MMT concentrations resulted in larger interlayer enlargement of MMT, better distribution of MMT particles, reduced NH hydrogen bonds and greater hydrogen bonding force at the carbonyl oxygen and thermal stability and uniformity, clarity and adhesiveness of the produced films. The intercalation and adsorption processes of onto MMT were accompanied by breaking of self-associated interaction of NH with C=O in amide group and the hydrogen bonding interaction of carbonyl oxygen with hydroxyl groups of MMT edges and hydrated interlayer cations in addition to possible ion-dipole interaction and the protonation of MMT.

Critical concentration of MMT were found to be about 20% MMT where the significant structural changes occurred. At the high MMT concentrations of 20-60% MMT, the basal distance of MMT was increased up to 28.1Å at 20% MMT and the intercalation and polymerisation of Am resulted in the formation of intercalated MMT structure. Even though high MMT concentrations showed thermally more stable Am-MMT systems due to the better intercalation of Am, the non-uniform, non-transparent and fragile films over 30% MMT were unsuited as stone consolidants. Below 20% MMT, the weak diffuse (001) reflection may indicate the mixed morphology that possibly includes partial intercalation, exfoliation or misorientation of MMT layers. The MMT particle separation and surface adsorption of polymerised Am were found to increase as observed from the noticeable increase in carbonyl hydrogen bonding interaction of Am and decrease in thermal stability observed in correlation with changes in appearance of the Am-MMT films. The use of less than 20% MMT produced macroscopically homogeneous films which provided uniform distribution of MMT particles, transparency and good adhesiveness and is likely to be more practical for intended use as stone consolidant. The described results are intended to serve as a preliminary study on the potential usage of in

situ preparation of sandstone consolidants in the presence of water soluble monomer, initiator and MMT under the laboratory condition.

6.6. Comparison of polymer-MMT composite systems

6.6.1. Microscopic evaluation of composite films

The preliminary assessment of the macroscopic appearance, as well as physical characteristics of the prepared polymer-MMT composite films, is a critical step in identifying their suitability for stone consolidation work. For all MMT composite systems with PAA, PAm, PEG, or in situ polymerised PAm, there was a clear, general trend of increasing the uniformity, transparency, adhesiveness and flexibility of the composite films with decreasing MMT loading, irrespective of polymers and experimental parameters. The opposite tendency was observed with increasing MMT loading and the formation of agglomerated MMT particles became visible with increasing MMT concentration for the solution intercalation of all polymers. The observed changes in the macroscopic properties was found to correspond well with the microscopic analysis of the prepared composite systems studied by the structural characterization of polymer-MMT composite systems XRD and SEM analysis.

Although it was observed that the dispersion behaviour of MMT was found to be comparative with all polymers and the dispersed MMT particles were distributed in a uniform manner at all polymer-MMT ratios, the addition of MMT had some unfavourable effects at higher concentrations. From 70% MMT of all polymer-MMT composites onward, increasing MMT concentrations caused the produced films to appear dark and opaque and to reduce significantly their cohesiveness, flexibility and strength based on visual inspections of the films. In a consistent fashion with the XRD and SEM observations, the composites comprising of low polymer concentrations corresponded to the intercalation of most polymers in the MMT structure, and these changes were reflected by the lack of sufficient adhesiveness, flexibility, strength, and transparency characteristics of polymers and by their macroscopic and physical characteristics similar to MMT. The observations indicated that the composite systems consisting of polymer loaded with high MMT content and MMT are most likely unsuitable in view of the importance of macroscopic appearance for intended use as stone consolidants.

More practical uses of the composite systems consisting of polymer loaded with lower MMT content in consolidation work were apparent from the inspected films, which were

more adhesive to the surface, flexible, transparent and uniform. At the MMT concentrations less than 70% MMT, the solution cast method used for the direct intercalation of all polymers was found to be effective to form sound films and the good dispersing ability of MMT was maintained for all polymer/MMT systems. The effects of different polymers on the visual and physical features were evaluated and the PAA-MMT and PEG-MMT composite films showed a similarity of their appearance and physical characteristics in comparison to the produced films formed with PAm. In agreement with the XRD and SEM observations of the composite systems prepared by the direct polymer intercalation method, PAm-MMT films appeared more transparent, particularly for the addition of small amounts of MMT up to 10% MMT and the better dispersion of MMT was demonstrated not only microscopically, but also macroscopically. There appeared, however, to be reduced transparency, adhesiveness, flexibility and strength of PAm-MMT films compared with the PAA-MMT and PEG-MMT composite films. The observations are in accord with the microscopic evaluations of the tested composite systems showing that the extent of PAm intercalation was greater than PAA and PEG. PEG and PAA acted as better dispersing agents favouring the dispersion of higher MMT loading and better ability of PAA or PEG to form good films can be related to the higher amounts of PAA and PEG that adsorbed on the outer MMT surface or existing free bulk chains. In addition to the adsorbed or free polymer chains that resulted in the better films needed for consolidation work, PAA and PEG were more flexible and could attach more strongly to the surface, making them more suitable at higher MMT loading for consolidating work on a macroscale level. The PAm films were harder and more brittle and the observations suggested that using low MMT loading and PAm-MMT concentration is better suited to provide optically clear and uniform appearance and to reduce the negative effect possibly caused by the hardness of PAm.

Comparison of the series of the solution intercalation of PAm with in situ polymerisation of Am showed the similar changes occurred in physical characteristics at low MMT loading, and both methods produced optically clear, uniform and solid films up to 40% MMT. The higher MMT contents in the Am-MMT films increased the extent of heterogeneous surface roughness and agglomeration of MMT compared with the PAm-MMT films showed the better dispersion of MMT in PAm. It was observed that the mixtures containing Am, MMT, and KPS were uniform prior to the heat treatment, but

the re-agglomeration process increased upon in situ polymerisation of Am in the presence of high MMT contents. It is likely that the use of low MMT loading is necessary to minimise the unfavourable appearance and to provide effective consolidation for the in situ preparation of Am-MMT in applied sandstones. The visual inspection of PAm-MMT, PEG-MMT and Am-MMT composite films showed that the appearance of films were changed toward slightly more transparent and uniform, especially at highly acidified MMT content when the acid-treated MMT was solvent-cast mixed with Am, PAm and PEO. Therefore, the acid treatment of MMT could be worth pursuing for the enhanced transparency of PAm-MMT or in situ polymerised Am-MMT films at high MMT concentrations.

6.6.2. XRD analysis

XRD was used as main technique to study the effects of different polymers, MMT concentrations, processing times, temperatures and molecular weights of polymer and acidity of MMT on the interlayer separation of MMT. The longer treatment of PAm-MMT, and PEG35-MMT dispersions at RT showed the slight increases in the penetration of PAm and PEG35, whereas the effect of longer treatment was negligible and the intercalation degree of PAA was not increased after the further treatment of the ultrasonicated samples. Conversely, the heat treatment was found to have negative impact on the intercalation of polymers as seen from the slight deintercalation of PAA and PAm and smaller interlayer separation than the treatment at RT. The changes in the d_{001} spacing of MMT showed the better stability or small increase in the intercalation of smaller PAA100 or PEG20 in comparison to larger PAA250 and PEG35. The intercalation behaviours of PAm and PEG into the acidified MMT were different in that the former showed comparable results to the non-acidified MMT and the latter produced variations in the opposite direction to the non-acidified MMT.

Despite the changes in the measured d_{001} spacing of MMT, the interlayer distances of MMT obtained by the ultrasonicated composites were similar to or higher than the ones of the samples prepared using different processing time and temperature or acidity of MMT at each MMT loading. Irrespective of the procedure and the nature of the polymer,

the ratios between MMT and polymer were found to be the most important factor influencing the interlayer swelling of MMT. The overall effects of the other experimental conditions on the interlayer expansion of MMT were found to be small and the effectiveness of ultrasonication treatment was demonstrated by the XRD results. These results showed that the deagglomeration process and homogenization of MMT, assisted by ultrasonication technique, played key roles in absorption behaviour of polymers and the pre-treatment of MMT using ultrasonication technique was found to be useful in increasing the surface of MMT accessible to the polymers.

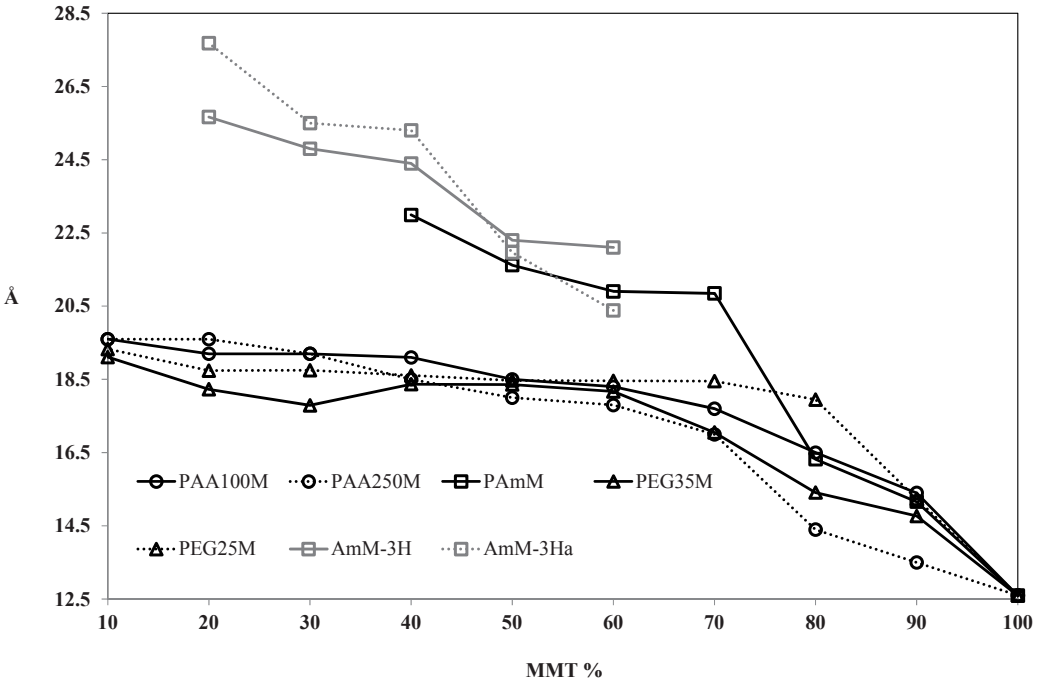

Figure 6.6.1. Comparison of d_{001} spacings of the ultrasonicated polymer-MMT composite samples and in situ intercalative polymerisation of Am

Comparison of the d_{001} spacing for the ultrasonicated samples demonstrated the changes that occurred in the interlayer expansion of MMT were dependent on the different MMT loading (Figure 6.6.1). Along with the increased concentration of polymers, the interlayer expansion of MMT was increased up to 30-40% polymers and the extents of polymer intercalation were reduced afterward. Despite the large difference in the molecular weights of PAA and PEG, the influences of PAA and PEG on intracrystalline swelling of MMT were small and similar interlayer behaviours of PAA and PEG were observed. One

major difference in the solution intercalation of polymers was observed when comparing the d_{001} spacing of MMT intercalated by PAm with those of the PAA and PEG on the MMT at 70% MMT. The intercalation of PAm was greater than the ones observed for PAA and PEG and large amounts of PAm were absorbed by the interlayer space of MMT. The intercalation degree of PAm was considerably greater below 80% MMT. The greater interlayer enlargement of MMT was induced by the in situ polymerisation of Am and the greater level of in situ polymerised PAm was obtained for the AmM-3H samples.

6.6.3. SEM study

The SEM images were compared to study the effect of different polymers on the microscopic structures and morphology of MMT, which was solvent-cast mixed with PAA, PAm and PEG. For all three combinations, there was found to be a clear, general trend as to the shape, size, orderliness and dispersion of MMT and microscopic surface texture and topography of the examined polymer-MMT composite systems. SEM evaluations of MMT mixed and dispersed in all polymers revealed the same trend and there appeared a gradual increase in the size and the degree of separation and disordered orientation of the MMT particles with decreasing MMT concentrations in the structures. Despite these observed changes, considering the hydrophilic natures of MMT, PAA, PAm and PEG, good miscibility and interactions between polymer and MMT may account for the similar dispersion pattern of MMT and the reasonably uniform distribution of MMT particles in all polymer phases. Although all polymer-MMT composite systems showed the same trend and revealed the structural changes mainly dependent on polymer-MMT ratios, the same variances were seen at low MMT concentrations.

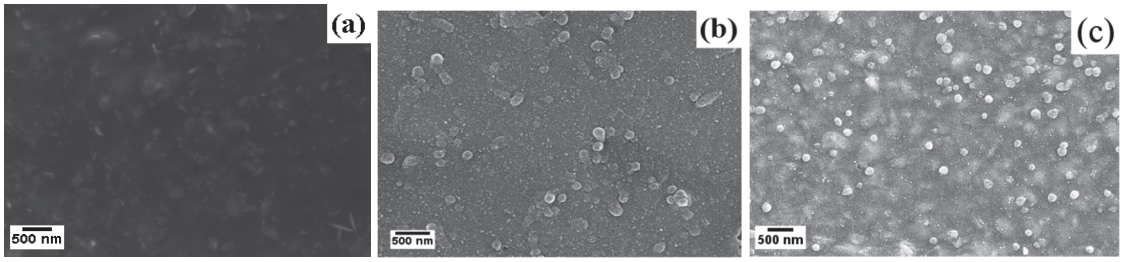

Figure 6.6.2. Comparison of SEM images of (a) PAAM10, (b) PAmM10 and (c) PEG35M10

A comparison of the SEM images for the films of PAA100M10, PAmM10 and PEG35M10 showed morphological changes of MMT between the three systems and provided some indications for the different (001) reflections of PAm-MMT system (Figure 6.6.2). Although relatively similar surface morphologies and textures were observed at 10-20% MMT loading, the SEM observations of all composites loaded at 10% MMT exhibited the good dispersions of MMT particles and the extents of MMT particle separation were noticeably greater at 10% MMT as reflected by the decreased portions of micro-sized MMT particles. The SEM images of the PAm-MMT and PEG-MMT composites revealed the stacks of parallel MMT layers present within the range of 100-200 nm in diameter, whereas the MMT particles were distributed more randomly in the PAm matrix. While stacked MMT lamellae were oriented more randomly in the PAA matrix, the proportion of micro-sized MMT particles appeared to be higher for PAA-MMT and PEG-MMT composites than PAm-MMT composites and SEM examinations showed the comparable degree of MMT layer separation as observed from the (001) reflections in comparison to the increased amounts of smaller sized stacked MMT layers in the PAm-MMT system.

In consistent manner to the XRD and macroscopic observations, SEM images of all polymer-MMT systems over 20% MMT loading depicted comparable surface morphology at each MMT concentrations. At 30-40% MMT, the dispersed MMT were stacked to form more micro-sized particles with significantly reduced numbers of smaller layer stacked MMT layers. Upon increasing the MMT concentrations to 50-60 % MMT, the agglomeration process of MMT led to the development of large layered MMT, which appeared piled up in larger sizes and different shapes. The availability of a large number of MMT layers over 60% MMT, the agglomerated and layered MMT structure resulted in rough and dense surface and their structures and characteristics are similar to MMT. In agreement with the microscopic appearances of all composites at 70-90% MMT, the SEM images reflected unsuitable micro-scale structures in the view of their uses to the consolidation of sandstones.

6.6.4. FTIR analysis

FTIR spectra of the series of prepared composite samples were analysed to characterize the local environments of polymers in the interlayer space of MMT and the composite structures and the interaction between polymers and MMT. The effects of different polymers, MMT concentrations, processing times, temperatures and molecular weights of polymer and acidity of MMT were also studied by FTIR measurements. For all polymer-MMT composite systems, the tested preparation conditions revealed slight influences on the interaction of polymers with MMT and bonding environment of polymers in the composite structures. The FTIR analysis of the prepared composite samples revealed the physical interactions of polymers with MMT. In the cases of PEG-MMT composites, FTIR results indicated the ion-dipole interactions between the oxygen of oxyethylene units and the interlayer cations. The peak shift observed for PAA, PAm and Am in the composite structures due to CO stretching bands of the COOH or $CONH_2$ groups, indicated that the changes in hydrogen bonds of PAA, PAm and Am played an important role in determining their composite structures.

Regardless of the preparation condition and the nature of the polymer, the ratios of polymers to MMT were found to be the most important factor influencing the changes in hydrogen bonding of PAA, PAm and Am. The increased hydrogen bonding between CO and NH bonds of PAm may indicate that the hydrogen bonding interaction of amide groups of PAm with the hydrated interlayer sodium cation or hydroxyl group of crystal edge up to 50-60% MMT, whereas the intra- and intermolecular hydrogen bonding strength of NH and CO bonds of PAm were reduced over 50-60% MMT, as a result of the extensive intercalation of PAm into MMT. In contrast to PAm, which indicated the hydrogen bonding formation of NH and CO bonds, the in situ polymerisation of Am developed the hydrogen bond formation between CO and MMT as the main interaction and the negligible effect of amino group on the bonding interactions may imply the development of stronger interaction between PAm and MMT for the solution intercalation of PAm into MMT. Unlike $CONH_2$ groups of PAm or Am, the intercalation of PAA was associated with the disconnection of decreased OH···O=C hydrogen bonds of PAA and the nondissociated carboxylic acid of PAA was intercalated without proton exchange of PAA with exchangeable sodium cations.

6.6.5. Thermal analysis

The TGA measurements of the polymer-MMT composite systems were performed to determine the thermal stability of polymers in the presence of MMT in their structures. For all polymer-MMT composite systems, the thermal stabilities of polymers were strongly dependent upon the polymer-MMT ratios and the onset temperatures for the degradation of all polymers were found to be increased with increasing MMT concentrations in the composite structures. The onset temperatures of PAA, PEG, PAm and in situ polymerised PAm were found to be increased by almost 127, 45, 31 and 37 °C at the 90% MMT concentrations respectively. The measured onset temperatures reflected the larger increase in the onset temperatures of PAA in comparison to PEG, PAm and in situ polymerised PAm, which may be attributed to better interaction between MMT and PAA.

In contrast to the PAm-MMT and Am-MMT samples, which showed the gradual increases in the onset temperatures with increasing MMT contents, there was found to be large onset shifts going from 60 to 70% MMT for PAA-MMT composites and from 40 to 50% MMT for the PEG-MMT composites. The observed changes in the onset temperature may indicate the presence of two composite structures and the results mostly correlate with the XRD data, which revealed the upper limits for the intercalation of PAA and PEG at 50-60% MMT. The gradual increases in the onset temperatures with increasing MMT contents for PAm-MMT and Am-MMT samples are also consistent with the XRD results that showed more steady increases in the intercalation of PAm. The considerable differences were found for PEG-MMT composites at 10-40% MMT, as the onset temperatures of free PEG were lower than the bulk PEG due to crystallinity of the PEG, possibly due to the weaker interactions of free PEG with outer surface of MMT in comparison to excess PAA and PAm present in the composite structures.

6.7. Conclusions on characterisation of sandstone consolidants

The intercalation into MMT and morphological changes of polymer MMT composites for PAA, polymerised and in situ polymerised PAm and PEG were compared. This study included determinations of the effects of various physicochemical conditions using MMT concentration, processing time, temperature, polymer molecular weight and the acidity of MMT on polymer intercalation from solutions. The tested parameters contributed negligible effects in improving the intercalation of polymers and the interaction of polymers with MMT. Monitoring of the d_{001} spacing and FTIR absorption bands resulted in the conclusion that the ultrasonication treatment was effective to produce similar results in regard to the intercalation of polymers.

Overall, the observed changes were found to be mostly determined by the polymer-MMT ratios for each polymer-MMT composite system. Critical concentrations of MMT were found in the 50-60% MMT where polymers begin to have two states, going from intercalated to free polymers. At concentrations over 50-60% MMT, polymer chains are intercalated in the interlamellar space of MMT, causing surface characteristics somewhat similar to MMT. At concentrations below 50-60% MMT, the excess polymers are attached to the MMT outer surface, which could lead to their characteristics being closer to polymers. Pertaining to MMT loading induced changes, the PAA-MMT and PEG-MMT composites showed similar variations but were surpassed by the degree of intercalation of PAm or Am into MMT.

Focusing on a specific application of the polymer-MMT composite, which will be tested to consolidate Sydney sandstones, the goal is to use the polymer-MMT composites having sufficient adhesive properties with the MMT loading as high as possible to improve the compatibility of the composites with the sandstones. To achieve consolidation needs, the incorporation of MMT up to 50-60% MMT to the polymers is most likely to be more appropriate to provide the composite structure having both characteristics of polymer and MMT and transparent system. The attempt to link the macro observations with the micro investigations was useful and supports the use of up to 50-60% MMT for changing their behaviour and effectiveness of the consolidation treatments though colour may limit loading to significantly lower level of 10 to 20% MMT. For the determination of their performance in consolidation treatments, the polymer-MMT composite dispersions prepared using the ultrasonication treatment were tested in the following chapter.

CHAPTER 7. RESULTS AND DISCUSSION: CHRACTERISATION OF CONSOLIDATED SYDNE SANDSTONE

7.1. Introduction

This chapter examines and compares the consolidation performance of water soluble PAA, PAm or PEG and the composite systems consisting of PAA, PAm, or PEG loaded with various MMT contents on Sydney sandstones. In addition to the consolidants containing the water soluble polymers or the water dispersible polymer-MMT composites, the in situ polymerisation method, using AA and Am, was applied to overcome the limited penetration of the larger macromolecules. The consolidant systems were tested on unweathered Sydney sandstone for the development of preventive treatment to enhance resistance to stone disintegration and to delay sandstone deterioration. Such protective approach aimed to focus on a more compatible method and to enable the enhancement of consolidated sandstones that can be deteriorated by weathering actions. In order to identify the optimal conditions of the consolidant preparations for the treatment of Sydney sandstone, this work investigated various conditions of the consolidant preparation, the effects of acid-modification of MMT, the concentrations of polymers, MMT, monomers and initiators on the consolidation actions of the water based materials. The goal of the consolidation work performed in this chapter was to assess their suitability as sandstone consolidants and the comparative studies of the water based consolidation systems with the commercially available consolidants were included to assess consolidation efficiency. Experiments were designed to evaluate the consolidation performance of the consolidated sandstones and the deviations in rate and depth of the consolidant penetration, absorption of the applied consolidants, permeability to air or water vapour, colour, appearance and mechanical strength were analysed. The measurements were intended to reflect the initial stage of changes in the consolidated sandstones and short-term impacts of the consolidation treatments.

7.2. PAA and PAA-MMT composite system

7.2.1. Application of PAA and PAA-MMT

In order to investigate penetration and absorption of consolidants and their performance, the initial step was to carry out a capillary rise test. The method is based on the partial immersion of a sandstone specimen in the consolidant solution and the rise in the solvent front was monitored as well as the wet weight uptake of the consolidant in the sandstone as a function of time. These data were determined as a percentage and are plotted in Figure 7.2.1 for DW, PAA, MMT and PAA100-MMT composite systems. The absorption curves in Figure 7.2.1 were found to be comparable except for 10% PAA100 and PAA250 solutions. The upward movement of DW was rapid and the wetting front almost reached the top of the sandstone specimens located 35mm above the immersed DW after 4 hours. The initial uptake of DW rapidly increased and 74.7% of total wet weight uptake was obtained upon the completion of capillary rise. Afterward, the water uptake slowly increased up to about 72 days and approached the saturated state, which showed 7.6% weight uptake with respect to the dried sample.

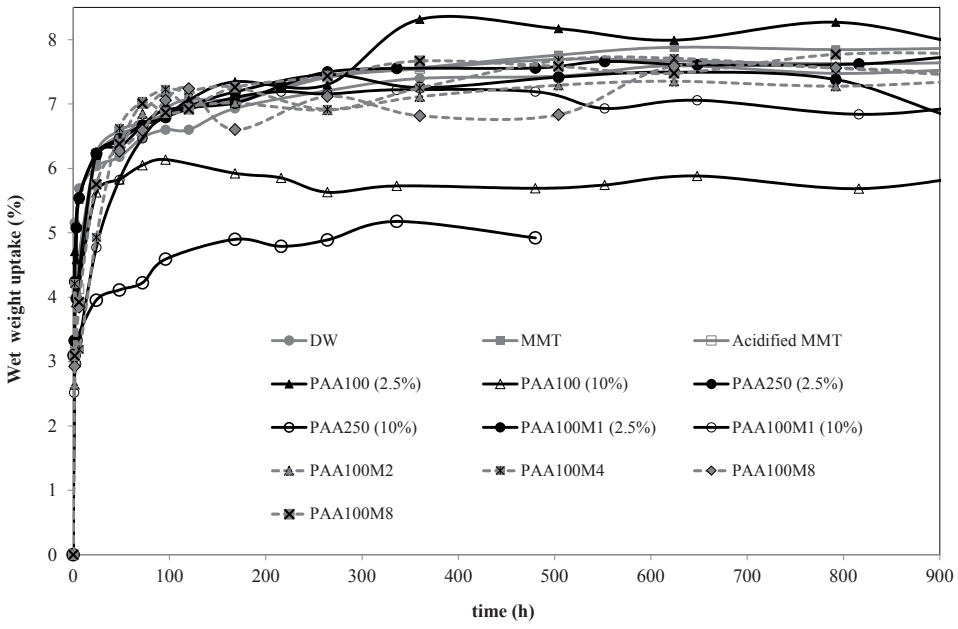

Figure 7.2.1. Absorption curves of DW, PAA, MMT and PAA100-MMT composites solutions versus time

Although the similar wet weight increases were obtained for all the treatment solutions were absorbed by the sandstones in a similar way to DW, the capillary rise actions became slower in the following order: DW > 2.5% PAA > PAA100-MMT > MMT > 10% PAA. The absorption process of DW and 2.5% PAA solution by the sandstones were comparable but the capillary rise was noticeably slower in the presence of PAA. In comparison to PAA, the capillary rise front of ultrasonically stirred suspensions of both non-acidified and acidified MMT moved more slowly and the amounts of MMT actually absorbed by the sandstones were found to be smaller (Figure 7.2.2). Likewise, the reduced uptake and slower flow of the 2.5% PAA100-MMT composites were observed with increasing MMT concentrations and these observations may be partially related to the reduction in the intercalated PAA chains into MMT available to inhibit water absorption as the MMT concentration increased. For the PAA100-MMT composites over 20% MMT, gel formation was visible in the solution that remained in the tube. Polymer/MMT aggregates could be absorbed into the surface layers only resulting in a carrier to further aggregates but water continued to diffuse through the sandstone making the solution more concentrated and leading to gel formation in the bottom of the tube. These observations demonstrated that MMT concentrations over 20% were found to be impractical due to the small uptake of PAA100-MMT composites. Conversely, the better uptake and faster penetration of the PAA100-MMT composite at 10 and 20% MMT suggest the potential use of PAA100-MMT composite at 10 and 20% MMT in the consolidation of sandstone.

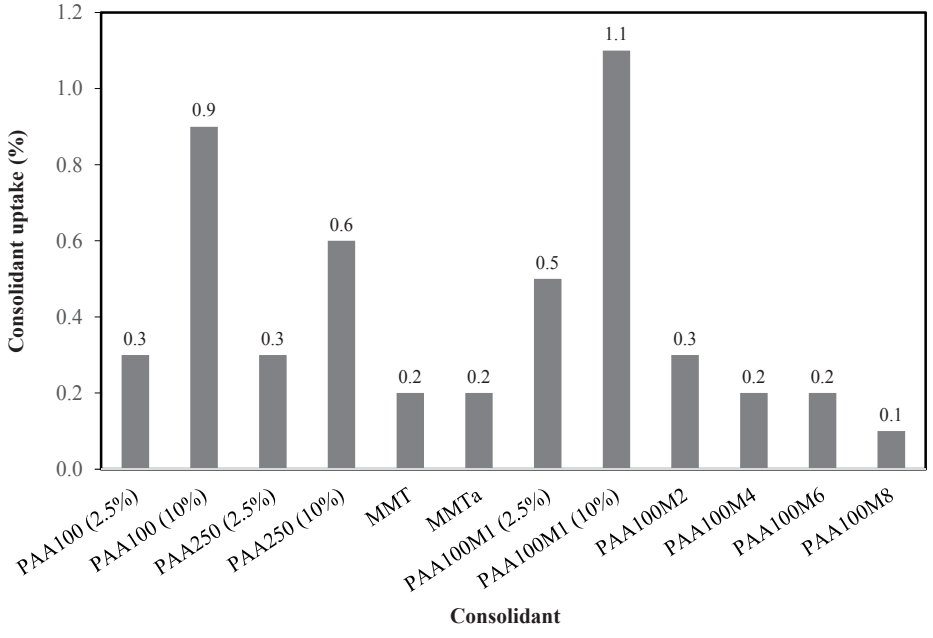

Figure 7.2.2. Comparison of uptake of PAA, MMT and PAA100-MMT composites

Upon increasing the concentrations of PAA100 and PAA250 solutions from 2.5% to 10%, the absorbed amounts of PAA100 and PAA250 were almost three and two times greater than the ones of 2.5% PAA solutions (Figure 7.2.2). As expected from the increased viscosity, the capillary penetrations of 10% PAA solutions were considerably slowed and their penetrations were reduced from 35mm for the 2.5% PAA solutions to 20 mm for the 10% PAA100 solutions and to 10 mm for the 10% PAA250 solutions. The higher PAA concentrations resulted in the increased uptake of PAA, but reduced both rate and extent of PAA penetration. The reduced uptake, penetration level and penetration rate of 10% PAA250 solution indicated a better penetrating performance of the PAA100, which is likely facilitated by the lower molecular weight of the PAA100. The absorption of the 10% PAA100M1 was also doubled and the capillary rise reached the top of the specimens (35 mm) after 48 hours, even though the penetration of 10% PAA100M1 solution was slower than that of the 2.5% PAA100M1. The capillary rise tests showed that 10% PAA100M1 resulted in the highest absorption within the tested PAA, MMT and their composite and the PAA100M1 was found to be the best absorbed consolidant based on % weight gain of the specimens.

7.2.2. Variations in appearance and colour

The treated and untreated sandstones were visually evaluated to determine whether colour change and/or appearance change were produced by application of PAA, PAA100-MMT, and MMT (Figure 7.2.3). The similar appearance of the untreated sandstones was obtained by the treatment with MMT suspensions and the application of MMT had no visual effects on the colour and appearance of sandstones. Conversely, the treatment with PAA and PAA100-MMT composites, significantly, changed the sandstone colour to orange and alterations in colour during the capillary rise absorptions of PAA and PAA100-MMT composites may be ascribed to the dissolution and oxidization of iron-bearing materials in the sandstones such as siderite. The treated sandstones became darker and more orange with increasing PAA concentrations.

In Figure 7.2.4, the influences of PAA, MMT and PAA100-MMT composites on the

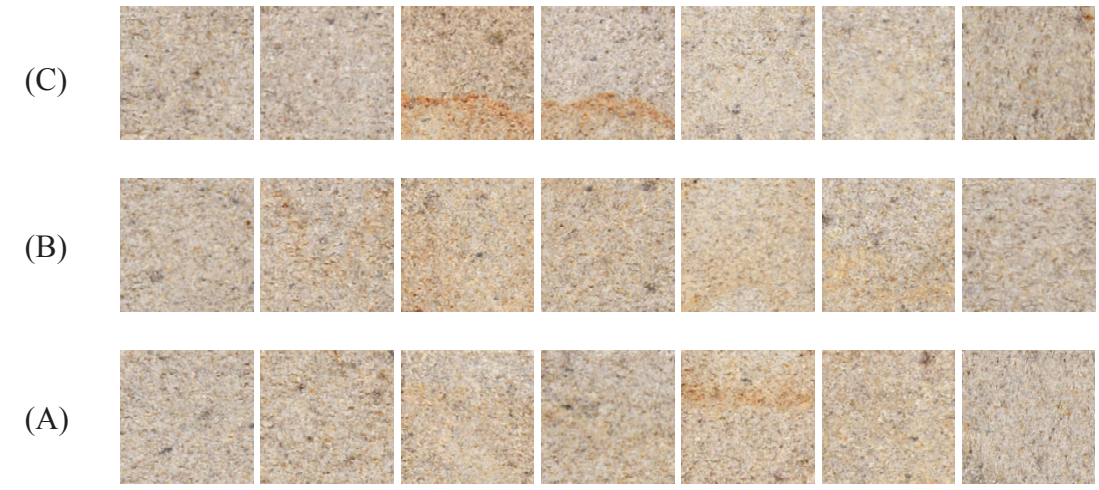

Figure 7.2.3. Photographic images taken from (A) immersed, (B) middle and (C) upper parts of sandstones treated with (a) DW, (b) PAA100, (c) PAA100M2, (d) PAA100M4, (e) PAA100M6, (f) PAA100M8 and (g) MMT

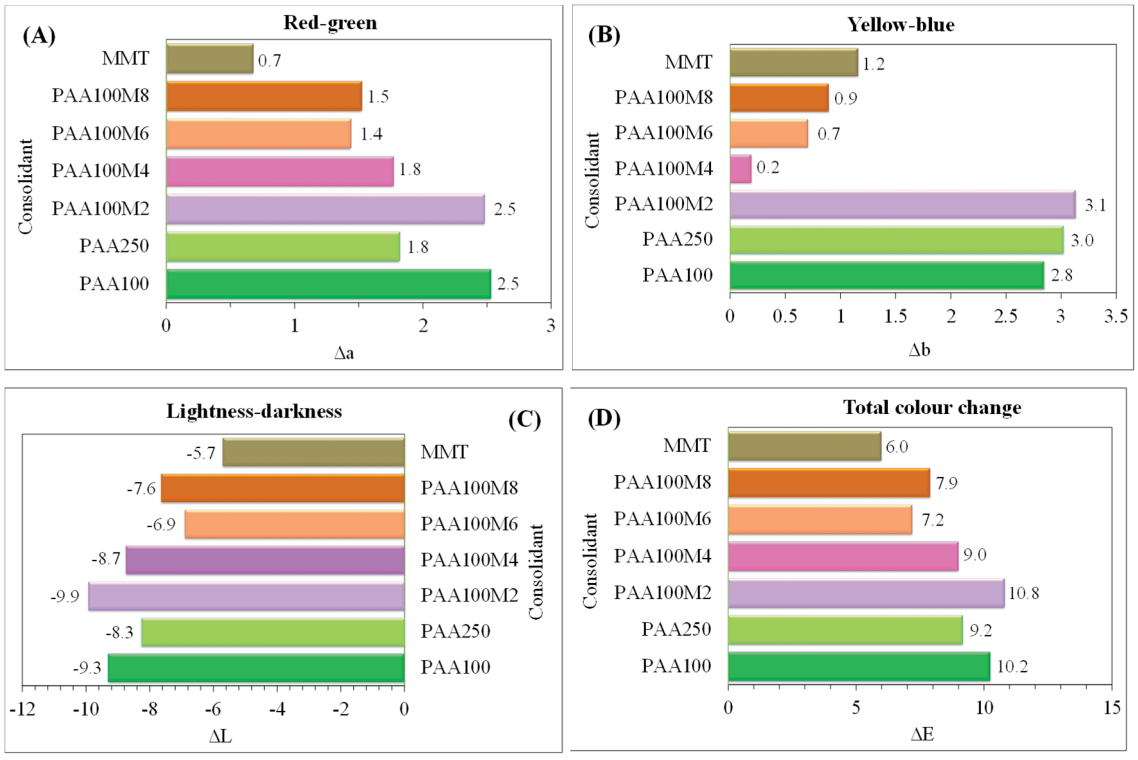

Figure 7.2.4. Variations in (A) Red-green component (a*), (B) yellow-green component (b*), (C) Luminosity (L*) and (D) total colour caused by PAA, MMT and PAA100-MMT composites from the images taken from the immersed sections of the treated sandstones

treatments with PAA100-MMT composites. The ΔE* values were found to be between 6 and 10.8 and the colour changes appeared to be greater for the higher PAA concentrations. The total colour values of the chromatic coordinate values are shown for the immersed section of the treated sandstones. The L* values displayed darkening of all treated sandstones and the coordinates a* and b* indicated the increases in the red and yellow components. The lower and upper sections of the sandstones corresponding to the treatment after the penetration of consolidant displayed the relatively similar a*, b* and L* values to the immersed sections for all the samples. This may indicate the penetration and uniform distribution of the applied consolidants through the sandstones or at least the transport of hydrogen ions. Comparison of the treatments with PAA, MMT and PAA100-MMT composites revealed the losses of luminosity tended to be greater for the higher PAA100 concentrations and the darkening effects appeared to be slightly increased with increasing PAA concentrations, possibly due to H^+ ion exchange reducing the pH of the consolidating solutions. Increasing MMT concentrations exhibited decreases in Δa* and Δb* values and implied that MMT caused decreases in red and yellow hues for the colour changes greater than 5 signified the considerable effects of PAA and PAA100-MMT composites (Rodrigues & Grossi 2007). In the case of PAA250, the chromatic coordinate values indicated less darkening and reddening effects and less total colour change than PAA100. Consistent with the visual appearance of the treated sandstones, it was found that increasing PAA concentrations produced the greater colour changes and the visual impact of MMT was lower than PAA and PAA100-MMT composites.

7.2.3. Water vapor permeability of consolidated sandstones

The effects of PAA, MMT and PAA100-MMT composites on the permeability of the treated sandstones to water vapour and the degree of their penetrations were studied by changes in mass of silica gel and the WVT values. Assuming the applied consolidants were penetrated or coated on the sandstone surfaces, then any relative reduction in water vapor permeability of the middle and upper sections of the treated sandstones can indicate the consolidant penetrations. Figure 7.2.5 shows the absorption of water vapour passing through sandstones obtained after the immersions of PAA and PAA100-MMT composites and the measured mean WVT were compared in Figure 7.2.6. The sandstones

treated with MMT showed similar WVT rates to the untreated sandstones and the effects of MMT were almost negligible. Although the absorption of water vapour was slower than MMT, the WVT rates tended to be higher with increasing MMT contents in the PAA100-MMT composites and the treated sandstones with MMT and composite with high MMT contents were more permeable, which may be attributed to the reduced product uptake due to the inhibitive effect of MMT. It was found from absorption curves in conjunction with the WVTs that the rates of water vapour absorptions were reduced with increasing PAA concentrations from 2.5 to 10% and the mean WVT values of PAA100 and PAA250 were comparable, which indicates insignificant effect of PAA molecular weights on the water vapour permeability of the treated sandstones. For the treatments with 10% PAA, the WVTs were highest for the upper sections, followed by the middle sections and the immersed sections, indicating decreased water vapour permeabilities, increasing the penetration depth of 10% PAA.

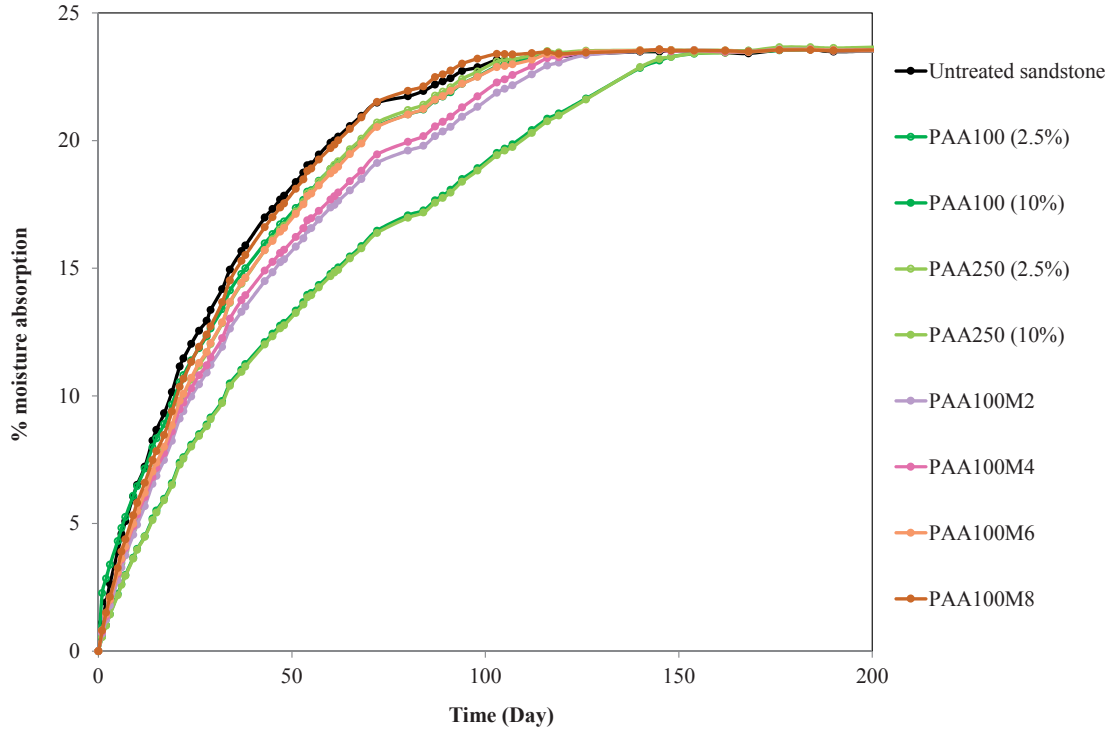

Figure 7.2.5. Plot of moisture absorption by desiccant against time observed by the untreated sandstone and the immersed sandstones consolidated with PAA and PAA100-MMT composites

Contrasting the WVT values of the immersed sections of the treated sandstones with the ones for the penetrated sections of the treated sandstones, it was observed that, although the higher WVT values were seen with increasing MMT concentrations of PAA100-MMT composites, the WVT values of the sandstones treated with PAA did not seem to produce considerably higher WVT values, as shown in Figure 7.2.6. Likewise, Figure 7.2.7 also presented the comparable WVT values for PAA100-MMT composite samples, except for the samples treated with PAA100M4 and PAA100M8 and the treated sandstones did not reveal a clear general trend of increasing permeabilities in relation to the penetration depth of PAA100-MMT composites. The similar WVT values can be considered as insignificant effects of consolidated sandstones that remained permeable for the treated samples penetrated by PAA and PAA100-MMT composites. Observation of Figure 7.2.7 and 7.2.8 showed the lower WVT values of the sandstones treated with PAA than the ones for PAA100-MMT composites at 20-60% MMT.

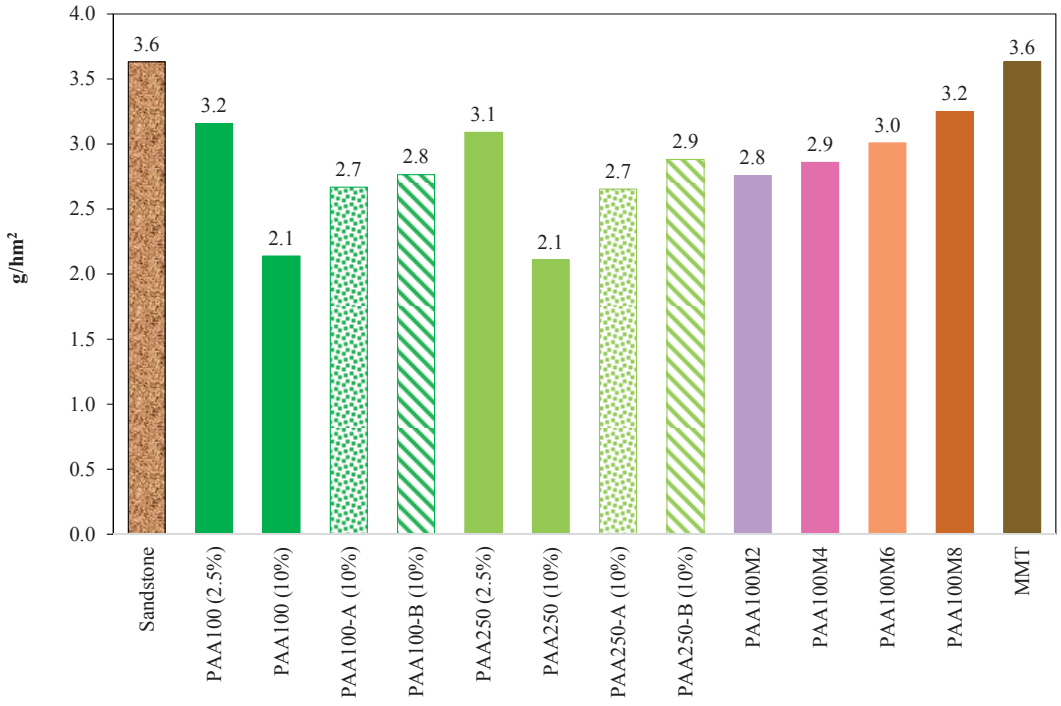

Figure 7.2.6. Averaged WVT values measured from the sandstones consolidated with PAA, MMT and PAA100-MMT composites

Comparison of the immersed sections of the treated sandstones showed the decreased WVT values in the order MMT > 2.5% PAA ≈ PAA100-MMT > 10% PAA and

demonstrated the sandstones treated with 2.5% PAA, MMT and PAA100-MMT composites were more permeable than the ones for 10% PAA. The observed WVT values correlated with the uptakes of the most tested samples. The reduced WVT values of the sandstones treated with 10% PAA indicate the higher amounts of absorbed PAA by the sandstones and the comparable WVT values for 2.5 % PAA to PAA100-MMT composites are also consistent with their uptakes by the sandstones. Although the sandstones treated with 2.5% PAA and PAA100-MMT composites were more permeable to water vapor, the uptakes of 10% PAA by the sandstones was higher and the water vapor permeabilities for 10% PAA were rather similar to the ones for 2.5% PAA and PAA100-MMT composites. The results indicated the better ability of PAA or PAA100-MMT composites with low MMT content to produce the higher uptake by the sandstone and to maintain the permeability of the treated sandstones.

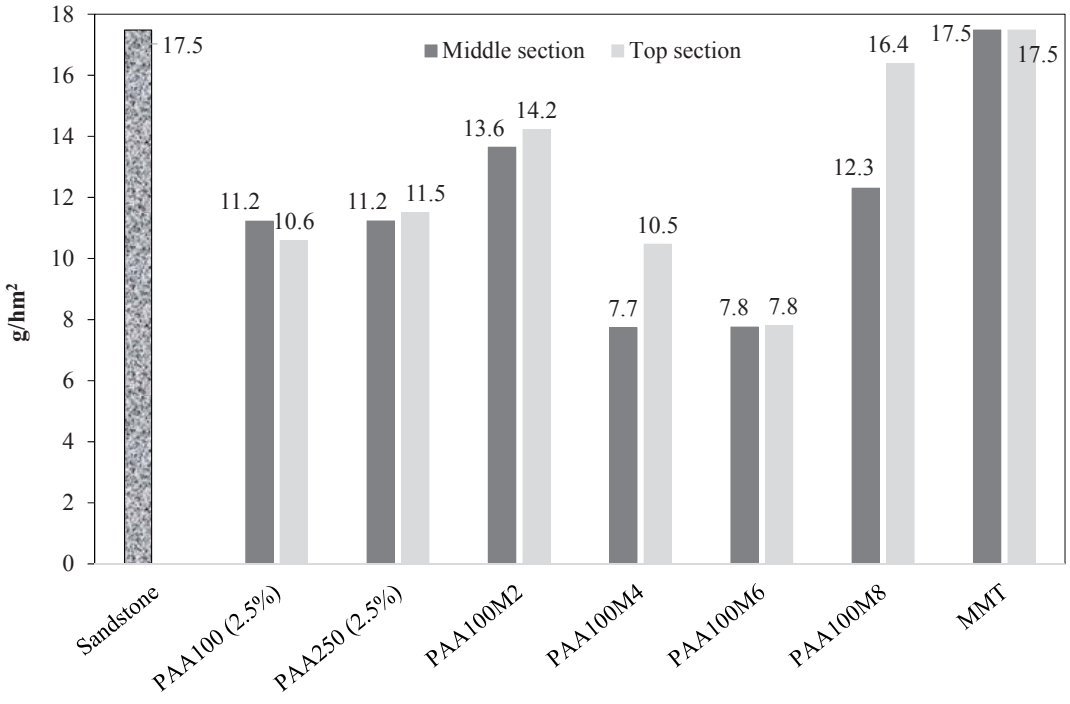

Figure 7.2.7. The WVT values averaged from the penetrated sections of the sandstones treated with PAA100, PAA250, MMT and PAA100-MMT composites

7.2.4. Bending tests

Bending tests were performed on sandstone specimens immersed in consolidant solutions for investigation of effect of consolidants on the change in mechanical properties of the consolidated sandstones. The three point bend testing was used to qualitatively determine the consolidating efficiency of the consolidant system as an applied tensile force to the outer surface indicates the potential of the consolidant for binding and consolidating the surface of sandstone. Figure 7.2.8 shows the results for bending strength tests performed for the sandstones immersed in the 2.5% PAA100, 2.5% PAA250 and 2.5% PAA100M2 solutions and dried. The average values of the bending strength of all consolidated sandstones were higher than untreated sandstones. The bending strengths were found to be higher after the treatments with PAA and the treatments with PAA100, PAA250 and PAA100M2 resulted in 27, 24 and 7% increases of strength values. The larger standard deviations for PAA100M2 may indicate more inhomogeneous treated sandstones by PAA100M2.

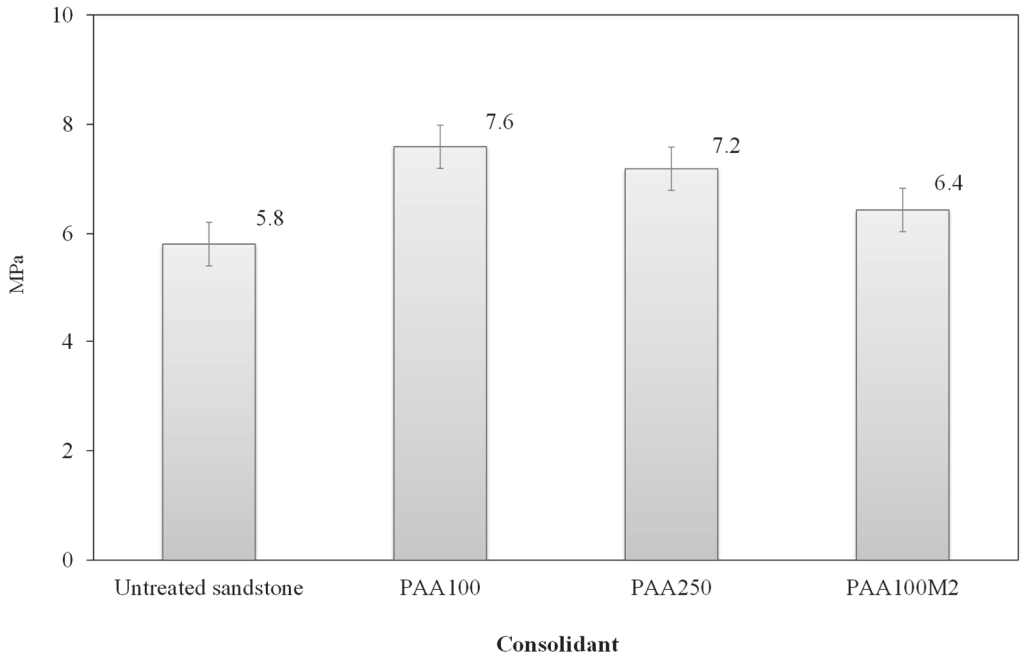

Figure 7.2.8. Average flexural stress of the sandstones after the treatments with PAA100, PAA250 and PAA100M2 prepared at 2.5 w/w%

The important role of the consolidation treatment is to increase the mechanical strength of the treated sandstone against the external forces acting on sandstone. The increased bending strengths of the treated sandstones indicated the absorbed PAA100, PAA250 and

PAA100M2 helped reduce the crack propagations caused by the applied force. It is therefore likely that the consolidation actions of PAA100 and PAA250 were greater than the one of PAA100M2.

7.2.5. Summary of consolidation treatment with PAA and PAA-MMT

The present work investigated the consolidation efficiencies of PAA and PAA-MMT composites for the consolidation of Sydney yellow block sandstones used in many Sydney heritage buildings. The consolidated sandstones were examined by measurements of colour variations, water vapour permeability, bending strength and rate and extent of penetration and uptake of the applied consolidants and the effectiveness of the applied consolidants were assessed with regard to their changes. The capillary rise experiments were performed to examine the rate and depth of capillary penetration and capillary absorption of the applied consolidants.

As the concentration of MMT and PAA or the molecular weights of PAA increased, the penetration rates of PAA and PAA100-MMT composites decreased. Increasing PAA concentration was found to increase the uptake of PAA, while the uptake was reduced with increasing MMT concentrations. The highest uptake and good penetration depth of PAA100M1 indicated the improved absorbing ability of PAA100-MMT composites at less than 20% MMT. Except for 80 and 100% MMT, the water vapour permeabilities of the sandstones were reduced after the consolidation treatments and were found to decrease in the following order: 2.5% PAA ≈ 2.5% PAA100-MMT composites > 10% PAA. In correlation with capillary uptakes and penetrations, the water vapour permeabilities were increased with decreasing PAA concentrations and increasing penetration depth of 10% PAA and MMT content of PAA100-MMT composites.

The consolidated sandstones were visually evaluated and PAA consolidated sandstones developed an orange colour through the acid dissolution and oxidation of the iron in the siderite present in the sandstone. While increases in darkness were the major contribution to the total colour changes of all tested consolidants, the colour alterations tended to

increase with increasing PAA concentrations, generally becoming darker, redder and yellower. The presence of MMT apparently increased the effectiveness in reducing the colour alternation, thus, compatibility of the consolidation treatments with PAA100-MMT composites. The bending strength of the treated sandstones increased with increasing PAA concentrations and PAA was potentially more effective to consolidate the sandstone.

In summary, PAA were able to provide higher absorption, relatively comparable water vapour permeability to PAA-MMT composites and higher mechanical strength of the treated sandstones, demonstrating improved consolidation actions over PAA-MMT composites. Even though the uptakes and capillary penetration rates were reduced with increasing MMT concentrations, the compatibility of the consolidation treatments with PAA-MMT composites was enhanced in view of the aesthetic aspects, water vapour permeability and bending strength and the results suggested the use of low MMT contents for improving composite uptake by Sydney sandstone.

7.3. PAm and PAm-MMT composite system

7.3.1. Application of PAm and PAm-MMT

The penetration rate and depth and uptake of DW, PAm, MMT and PAm-MMT were studied and compared by the capillary rise method. In Figure 7.3.1, the absorption curves of DW, PAm, MMT and PAm-MMT solutions are reported. When applied to the dried sandstones, capillary rise was observed to reach and most solutions were absorbed after 24 hours. Their absorptions slowly approached the capillary saturation after 72 days. Even though the capillary penetrations of the MMT suspensions were slightly slower than the 2.5% PAm solutions, the take-up of MMT was found to be greater than the 2.5 w/w% PAm solution and the absorption of acidified MMT was increased by twice in comparison to the one of non-acidified MMT suspensions (Figure 7.3.2). While the similar absorption curves and the complete capillary penetrations after 24 hours were also observed for the PAm-MMT dispersions prepared using non-acidified and acidified MMT, the sandstones treated with the acidified PAm-MMT samples became saturated before the treated sandstones were saturated by the non-acidified PAm-MMT samples. Despite the better uptake of the suspended particles of the acidified MMT, the effect of the acidification process of MMT was found to be insignificant on the extents and rates of penetration and uptake at each ratio of MMT to PAm.

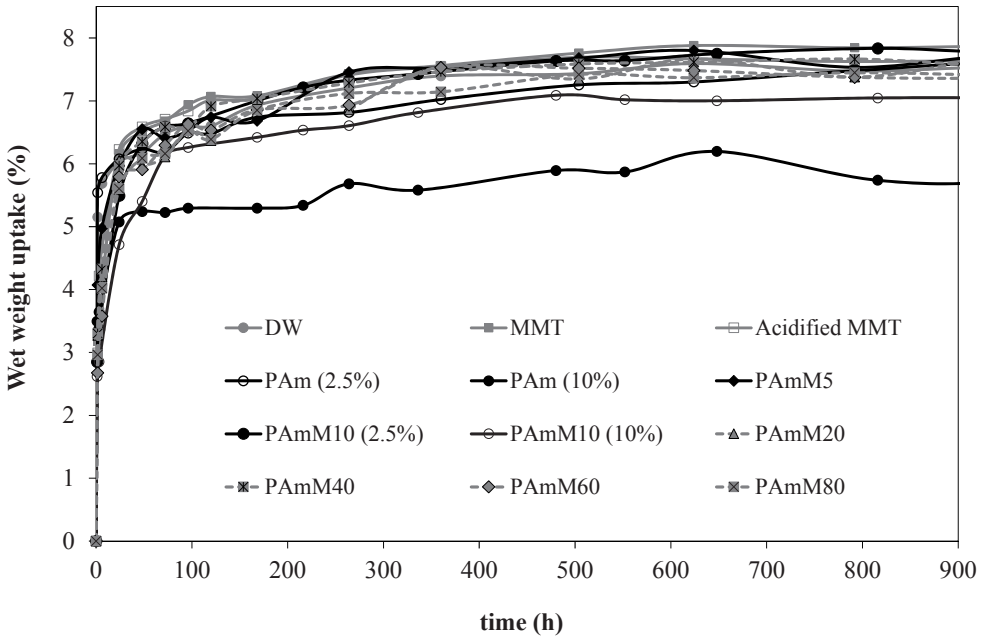

Figure 7.3.1. Capillary rise absorption curves of DW, PAm, MMT and PAm-MMT

Upon increasing the MMT concentration of the PAm-MMT samples, the absorbed amount and the penetration rate tended to be decreased slightly and the PAm-MMT uptake was found to be lower for MMT contents of over 20% MMT (Figure 7.3.2). As in the MMT particles suspended in DW, the PAm-MMT solutions in the tubes became viscous over 20% MMT and the agglomerated PAm-MMT were absorbed into the sandstone surface and gel formation was resulted from the concentrated solutions due to the diffusion of water through the sandstones. It was obvious the 40-80% MMT in the PAmM samples were most likely to be inappropriate from their low absorptions and increased viscosities.

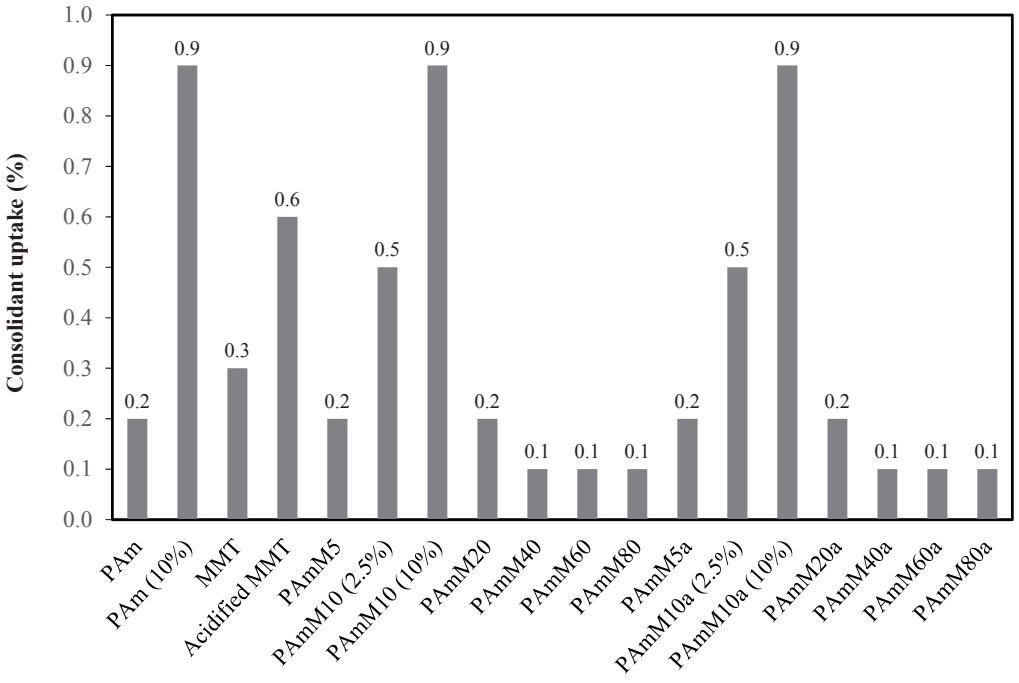

Figure 7.3.2. Uptake of PAm, MMT and PAm-MMT

The opposite effect was observed with increasing the PAm solution concentration. The absorbed amounts of 10% PAm and PAmM10 solutions increased to 0.9% and the weight increases were more than four times for the treatment with 10% PAm solutions. The 10% PAmM10 solutions slowly penetrated to 35mm while the 10% PAm solution was only observed to 15-25 mm. Compared with the 2.5% PAmM10 solutions, the absorption profiles of the PAm-MMT dispersions containing 10% non-acidified and acidified MMT appeared relatively similar and the better penetration ability of the 10% PAmM10 solutions than the 10% PAm solution demonstrated the best result among the tested PAm,

MMT and PAm-MMT composite systems.

7.3.2. Variations in appearance and colour

The visual inspection of the sandstones treated with PAm, MMT, PAm-MMT composites, and the commercial consolidants was performed to determine their effects on the appearances and colour of the stone surface (Figure 7.3.3). The treatments of sandstones with PAm and PAm-MMT composites did not seem to affect the appearance and colour markedly and resulted in visually homogeneous treatments on the stone surface. The colour of the sandstones treated with PAm was slightly lighter, whereas the sandstones treated with the PAm-MMT composites appeared darker and resulted in a slightly wet appearance. With increasing MMT contents, the surface appearance of the sandstones treated with the PAm-MMT composites became similar to the ones after treatment with MMT.

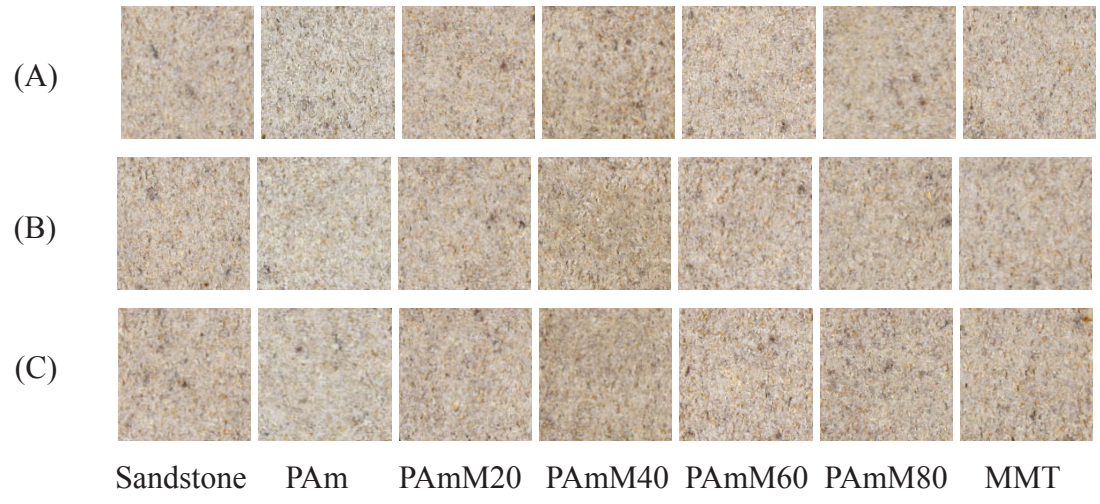

Figure 7.3.3. Digital pictures obtained from (A) immersed, (B) middle and (C) top sections of sandstones treated with PAm, MMT and PAm-MMT composites

Figure 7.3.4 presents the colour alternations of the treated sandstones evaluated, based on brightness value (L*), a* and b* coordinates and chromatic difference ΔE*. The treated sandstones with PAm, MMT and PAm-MMT composites yielded slight increases in the a* and b* mean values and decreases in the L* values. The PAm-MMT composites showed higher a* values than PAm and revealed the increased reddening effects than the

ones for the treatment with PAm. The slight decrease in redness of the sandstones treated with PAm-MMT composites was seen with increasing MMT concentrations. The composites prepared by the unmodified MMT tended to decrease the Δb* values with increasing MMT concentrations, whereas the acidified MMT produced the Δb* values with no clear trend. The increase in yellowing coloration of the PAm-MMT composites containing the acidified MMT was greater than non-acidified MMT. The L* values for the sandstones treated with PAm-MMT composites are smaller than the ones of PAm and the composites caused increased darkening of the consolidated samples. The L* values of the PAm-MMT composites were similar at all acidified MMT concentrations, whereas the *L values increased with increasing unmodified MMT concentrations.

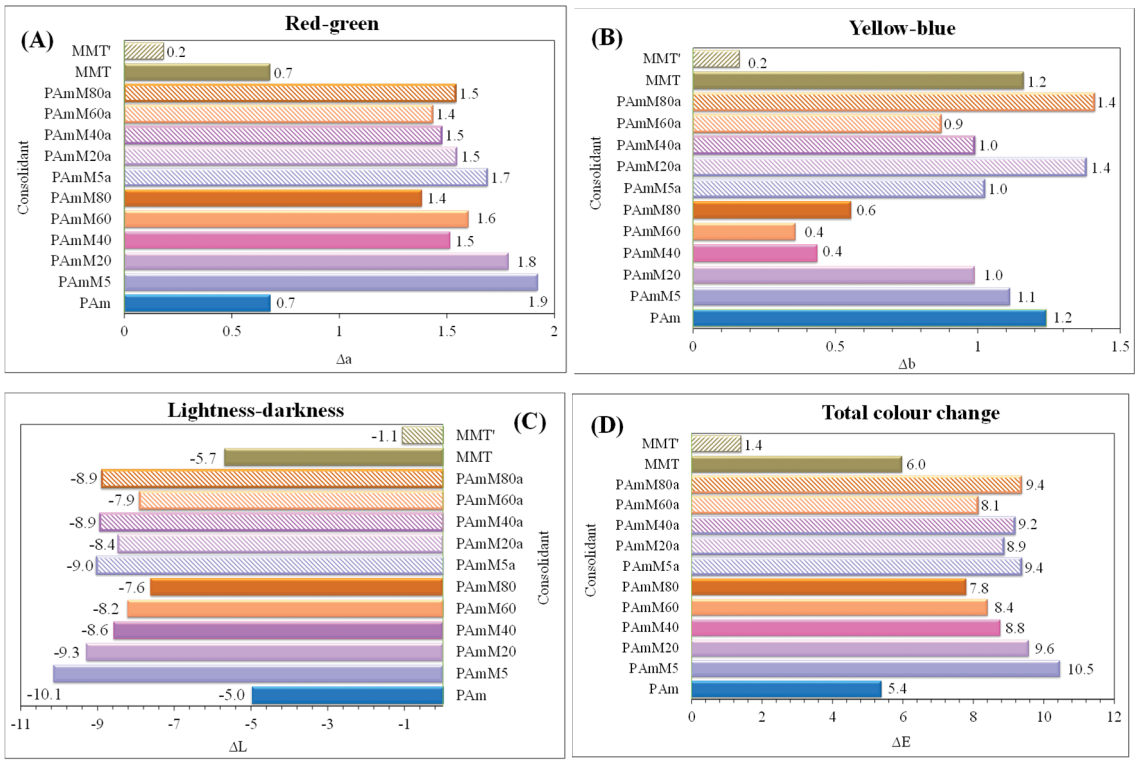

Figure 7.3.4. Comparison of (A) red-green component (a*), (B) yellow-green component (b*), (C) Luminosity (L*) and (D) total colour change (ΔE*) resulted from the sandstones consolidated with PAm, MMT and PAm-MMT composite

These indicate that unmodified MMT was more effective to reduce the darkening effect of PAm-MMT composites, but insignificant effects of acidified MMT on the darkening effect was detected. In contrast to the L* values that displayed considerable darkening of the treated sandstones with the composites, the a* and b* coordinates showed relatively smaller modifications in the redness and yellowness of the treated sandstones. The total

colour alterations of most of the sandstones treated with PAm-MMT were found to be greater than 5 and less than 10, indicating the considerable visual effect of PAm-MMT (Rodrigues & Grossi 2007). The total colour changes tended to be reduced with increasing unmodified MMT, but the acidified MMT revealed insignificant impact. Compared with PAm-MMT composites, the sandstones treated with PAm resulted in decreased redness, darkness and total colour changes and the significantly reduced colour variations were caused by the treatment with PAm. Agreeing with the visual appearance modifications, the total colour changes of the treated sandstones were found to decrease in the following order: PAm-MMT > unmodified MMT > PAm and there appeared insignificant changes across the capillary rise distances for all the samples.

7.3.3. Water vapor permeability of consolidated sandstones

The changes in weight of the silica gel and WVT values were analysed and compared to study the effects of PAm, MMT and PAm-MMT composites on water vapour permeability of the treated sandstone and their penetration depth. Figure 7.3.5 illustrated the changes in the weight increases caused by water vapour absorbed through some consolidated sandstones and Figure 7.3.6 reported the WVT values measured from the sandstones

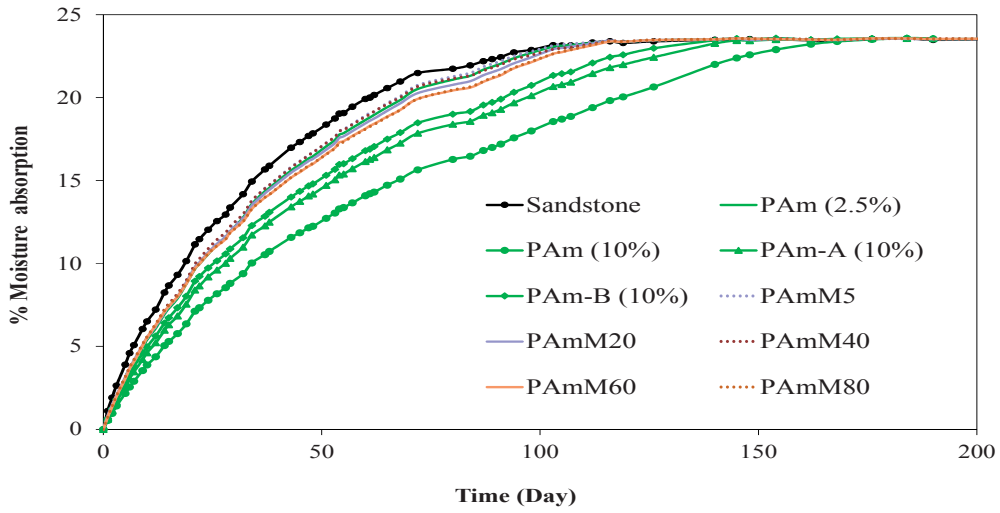

Figure 7.3.5. Moisture absorption by desiccant plotted against time after the treatments with PAm and PAm-MMT composites. The middle and top parts of the consolidated sandstones are denoted by A and B.

consolidated with PAm and PAm-MMT composites. It was apparent from the absorption curves and the WVT values measured from the immersed parts of the consolidated sandstones that 2.5% PAm and the composites comprising PAm with unmodified or acidified MMT yielded similar WVT values and the obtained diffusion rates were almost independent of the MMT contents in the composites or acidity of MMT. Conversely, the effect of PAm concentrations on the diffusion rates of water vapour was more evident as reflected by the reduced WVT values of the sandstone treated with 10% PAm and the decreases in the sandstone's permeability were associated with the increased amounts of absorbed PAm. The treatments with 10% PAm showed increased values of WVT with increasing height of capillary rise, thus indicating smaller amounts of absorbed PAm with increasing distance penetrated by the 10% PAm solutions.

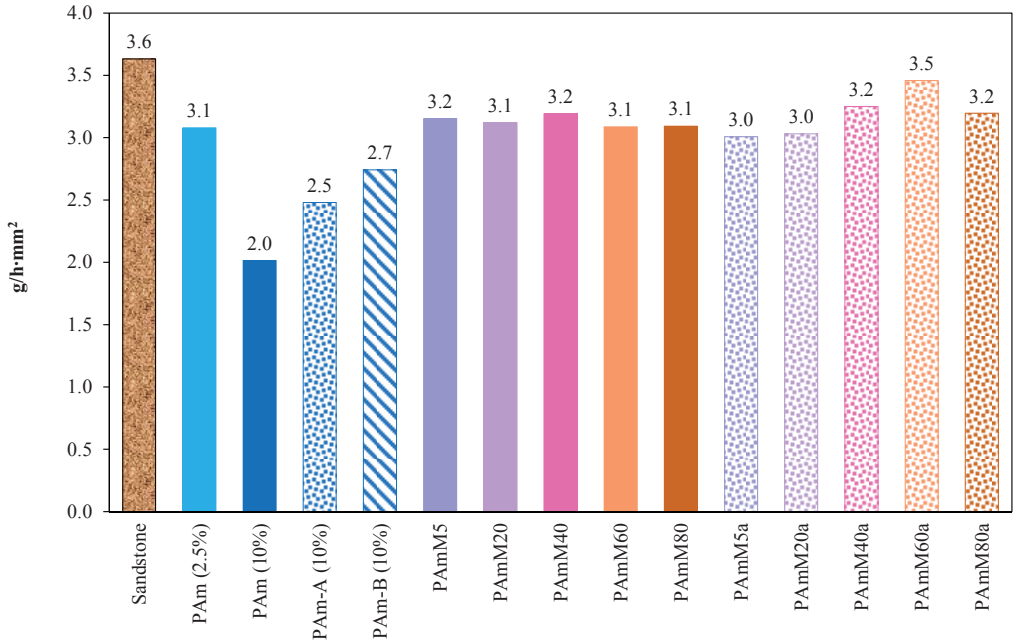

Figure 7.3.6. WVT values averaged from the sandstones consolidated with PAm and PAm-MMT composites

Figure 7.3.7 compares the values of WVT, presenting the changes in water vapour permeability of the sandstones penetrated by capillarity with PAm and PAm-MMT composites. With increasing MMT content, the WVT values tended to increase and the negligible effect of acidified MMT were revealed by the virtually identical results given by the composites formed by PAm filled with unmodified or acidified MMT. There

appeared noticeable rises in the WVT values upon the change from 20 to 40% MMT for the middle sections and from 40 to 60% MMT for the top sections and the values of WVT were generally higher for the top sections, apart from PAmM5 and PAmM80a. The observed deviations indicated reductions in the capillary penetration of PAm-MMT composites with increasing MMT concentrations and decreased WVT values of the penetrated portions of the treated sandstones allowed to presume that PAm or PAm-MMT were penetrated through the sandstones. Figure 7.3.6 exhibits only slight reductions in the WVT values compared with the untreated sandstones and the consistent changes in the permeability observed for 10% PAm, together with the reduced permeability of the sandstones penetrated by PAm and PAm-MMT composites, reflected the fair correlation between the WVT values and absorption data.

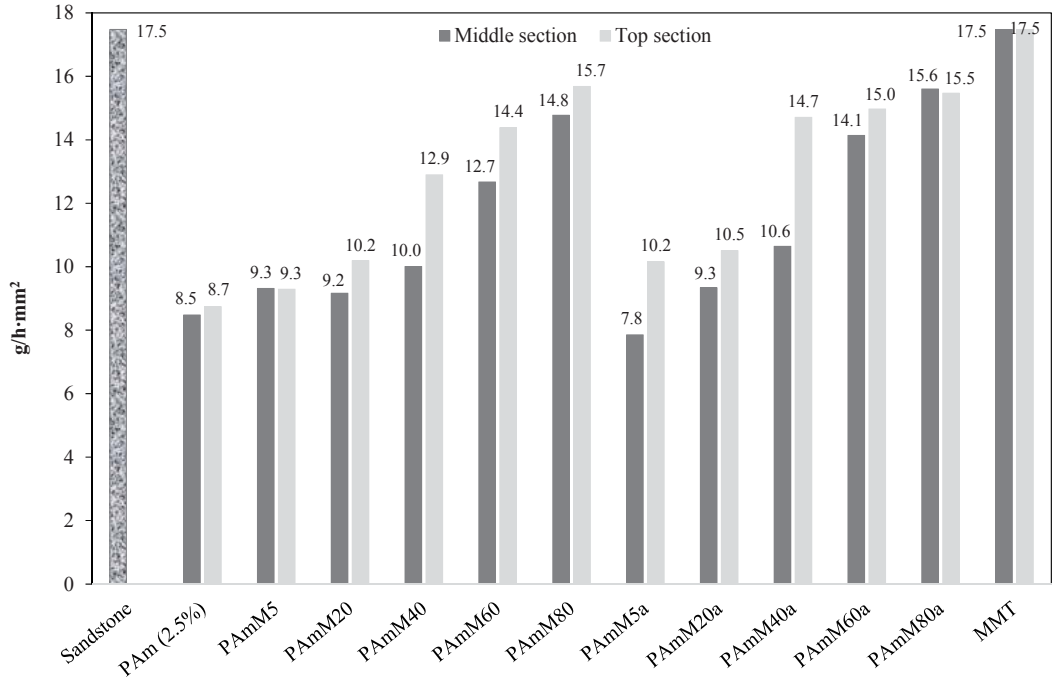

Figure 7.3.7. Mean WVT values obtained by the penetrated sections of the sandstones treated with PAm and PAm-MMT composites

7.3.4. Bending tests

The changes in mechanical properties of the consolidated sandstones were measured by bending tests and the results were used to study the efficiency of the consolidants to bind

and consolidate the sandstone surface. The bending strength results obtained for the sandstones treated by the immersion in 2.5% PAm, 2.5% PAmM5 and 2.5% PAmM5a solutions are presented in Figure 7.3.8. Compared to the untreated sandstones, the bending strengths of the consolidated sandstones were increased and the treatment with PAmM5a produced the highest increase in bending strength (34%), followed by PAmM5 (29%) and PAm (19%). In terms of mean values for their bending strength and standard deviation, the effects of acidification treatment of MMT were small but the efficiency of PAmM5a was slightly higher. The consolidation of sandstones by PAm was found to yield the lowest bending strength values. The observed values indicate that the consolidation treatments with PAmM5 and PAmM5a were more effective in increasing the mechanical strength and producing more homogeneously treated sandstones.

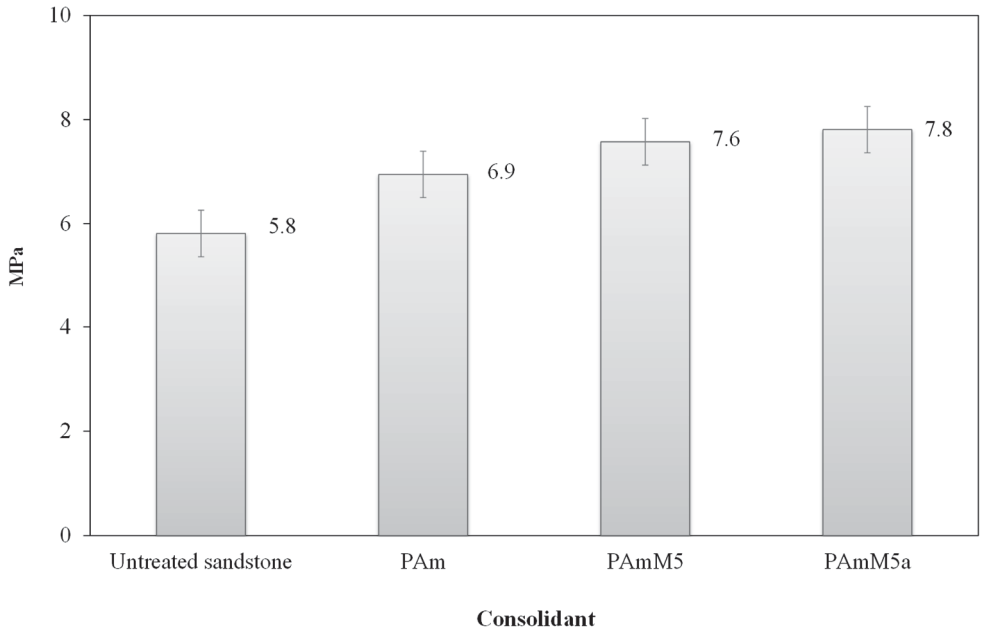

Figure 7.3.8. Mean flexural stress of the sandstones treated with 2.5% PAm, 2.5% PAmM5 and 2.5% PAmM5a

Generally, the mechanical strength of the consolidated sandstones was increased by higher concentrations of consolidant and PAm concentrations of the PAm-MMT composites. Considering the principles of sandstone consolidation, increase in the mechanical property is critical for the treated sandstone exposed to external forces caused by various weathering effects. Consequently, the increased mechanical strengths of the

treated sandstones treated with PAm and PAm-MMT at low MMT loadings decreased the impact of sandstone weathering on the treated sandstone and PAm and PAm-MMT increased the consolidation action on the treated sandstones.

7.3.5. Summary of consolidation treatment with PAm and PAm-MMT

The capillary rise observations presented slower penetration of MMT than PAm and the better penetration of the acidified MMT. Despite the negligible effects of MMT contents on the penetration ability of PAm-MMT composites, the absorption of the composites was decreased with increasing MMT contents. Compared with PAm alone, the better penetration and uptake of PAm-MMT composites containing low MMT contents was observed and the results suggested to make more effective use of PAm-MMT composites at less than 20% MMT. In agreement with capillary penetration and uptake, the reduced water vapour permeability of the consolidated sandstones was generally associated with the penetrated and absorbed consolidants that caused the delay in diffusion of water vapour through the treated sandstones. The water vapour permeabilities were unaffected by the acid-modified MMT and were reduced with increasing PAm concentrations in the presence or absence of MMT or with decreasing capillary penetration depth.

The visual and calorimetric assessment of the consolidated sandstones revealed the colour alterations followed the order PAm-MMT > unmodified MMT > PAm, demonstrating the better colour compatibility of PAm and MMT than the PAm-MMT samples, which darkened the consolidated sandstones. While the consolidated sandstones showed slight increase in redness and yellowness, the overall colour changes were mostly induced by the darkening effect. The PAm-MMT composites darkened the treated sandstones compared with PAm and unmodified MMT was more efficient to lessen the colour alterations than the acidified MMT. Likewise, the measured bending strength indicated the more compatible treatment with PAm than PAmM5 and the composites containing the unmodified MMT than the ones prepared with the acidified MMT.

Among the tested consolidants, PAm-MMT composites at high MMT contents showed lower product uptake, slower capillary rise penetration and greater water vapour permeability while increasing PAm concentrations in PAm-MMT resulted in better

consolidation performance to provide greater uptake and mechanical properties of the treated sandstone. Compared with the composites, PAm presented slightly better compatibility with smaller changes in colour and bending strength, but decreased penetration depth. The results suggested the use of PAm-MMT composites at less than 20% MMT to increase the composite uptake and the enhanced compatibility of the composite containing the unmodified MMT.

7.4. PEG and PEG-MMT composite system

7.4.1. Application of PEG and PEG-MMT

The absorption studies of PEG and PEG-MMT composite included the dispersions of PEG-MMT composites prepared using PEG25, PEG35, unmodified MMT, or acidified MMT. Figure 7.4.1 presents the capillary rise absorptions of DW and solutions containing PEG35, MMT and PEG35M. The capillary rise absorption profiles showed the rapid upward penetration of DW, MMT suspension solutions and 2.5% PEG-MMT composite dispersion solutions. Upon the completion of capillary rise, the sandstones absorbed over 70% of the total amount of most applied solutions, which were followed by the slow absorptions until they became fully saturated by the applied solutions. Based on the observed capillary rise curves of the consolidant solutions, it is likely that the diffusion of water was fast and the consolidants were slowly diffused. The solvent front in the 2.5% PEG25 and PEG35 solutions rose the full extent of the specimens within 4 hours and the penetration rates of these solutions were similar to the one of DW due to their low solution viscosities.

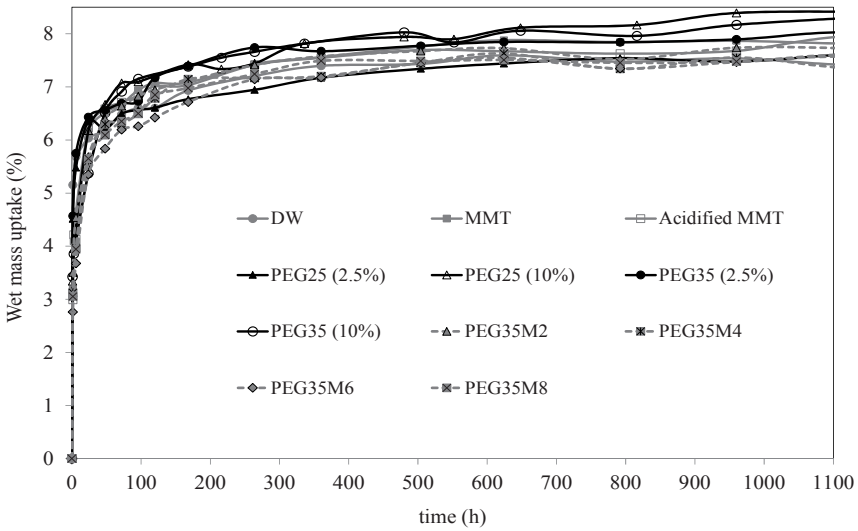

Figure 7.4.1. Capillary rise absorption curves of DW, PEG25, PEG35, MMT and PEG35M

Although the slower movement of solvent front from for the 10% PEG solutions was observed, both 2.5 and 10% PEG solutions showed the similar absorption curves and the solvent front for both 2.5 and 10% PEG solutions was brought up to the top of sandstone

specimens. The 10% PEG solutions increased the uptake of PEG25 and PEG35 by almost four and two and half times greater than the ones for 2.5% PEG25 and PEG35 respectively. It was found that higher PEG concentrations were effective to increase PEG uptake and to provide good penetration rate and extent. The 10% PEG25 solutions were penetrated faster and absorbed to a greater extent, which may indicate the smaller molecule of PEG was able to penetrate with increasing PEG concentrations.

Similar to the PEG solutions and the MMT suspensions, the completion of capillary rise for all 2.5% PEG-MMT dispersions was observed after 24 hours (Figure 7.4.1). All PEG-MMT dispersions also produced comparable results and showed similar uptake (Figure 7.4.2). The observed results are apparently independent of molecular weights of PEG and acidification of MMT used in PEG-MMT composites. It was found for all PEG-MMT composites that the uptakes of the PEG-MMT composites were small and the comparison of 2.5% PEG-MMT dispersions showed that PEGM10 samples were best absorbed. Although the uptakes of PEG-MMT composites by the sandstones were similar to or smaller than PEG, the 2.5% PEG-MMT dispersions were penetrated more slowly than the 2.5% PEG solutions, but faster than the 2.5% MMT suspensions.

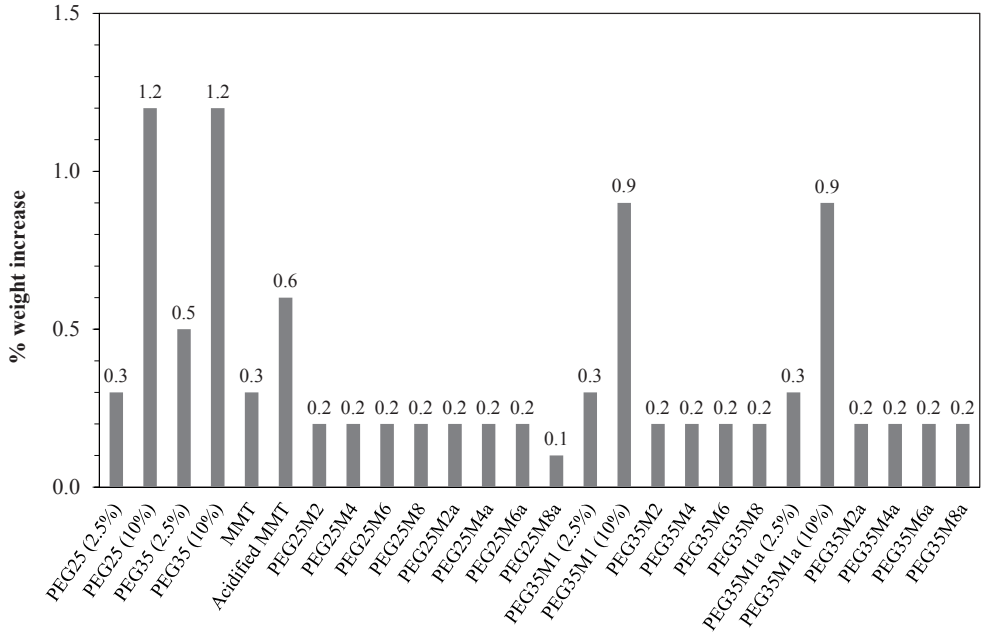

Figure 7.4.2. Uptake of PEG25, PEG35, MMT and PEG-MMT

Despite the slower capillary rise of the 2.5% MMT suspensions, the rates of capillary rise were found to be almost comparative for the PEG-MMT dispersions at all MMT concentrations. The similar rates of capillary rise penetration of PEG-MMT dispersions at all MMT contents may be a reflection of the fact that PEG chains present in the PEG-MMT composites did not prevent MMT from absorbing water agreeing with the work of Parfitt and Greenland (1970). Upon the introduction of the 10% PEGM10 dispersion, the completion of capillary rise took twice as long as the 2.5% PEGM10 dispersions, but the absorbed amounts of PEGM10 were three times greater. The capillary penetration rates were reduced to a greater extent than the 10% PEG solutions and the observed results indicated increasing MMT concentrations was ineffective in enhancing penetration and absorption of the PEG-MMT composites. At the 2.5% concentrations of PEG, MMT and PEGM10, the observed absorptions were too small and the treatments of sandstones with their higher concentrations are apparently needed to improve their uptakes by sandstones. In the case of MMT and PEG-MMT composites, higher MMT concentrations are impractical due to low uptake by the sandstones, except PEGM10. The treatment with 10% PEGM10 dispersions were found to be best in the tested PEG-MMT composites, but PEG was able to produce the faster penetrations and better absorptions.

7.4.2. Variations in appearance and colour

The visual appearance and colour of the sandstones treated with PEG and PEG-MMT composites were compared to study their effects on colour and appearance (Figure 7.4.3). The treatments with PEG25 and PEG25M composites produced perceptually similar appearance, texture and colour to the untreated sandstones and there seemed no apparent changes along their capillary penetrations. Similarly, the colour-appearance issues arising from the treatments with PEG25Ma, PEG35, PEG35M and PEG35Ma were not detected. This can be interpreted as either desirable variations in sandstone appearance after the treatments with PEG25 and PEGM composites or poor capillary penetrations. However, the comparable colour appearance of the immersed (Figure 7.4.3 (A)) and penetrated (Figure 7.4.3 (B) and (C)) sections may indicate no impact of the treatments on visual colour appearance.

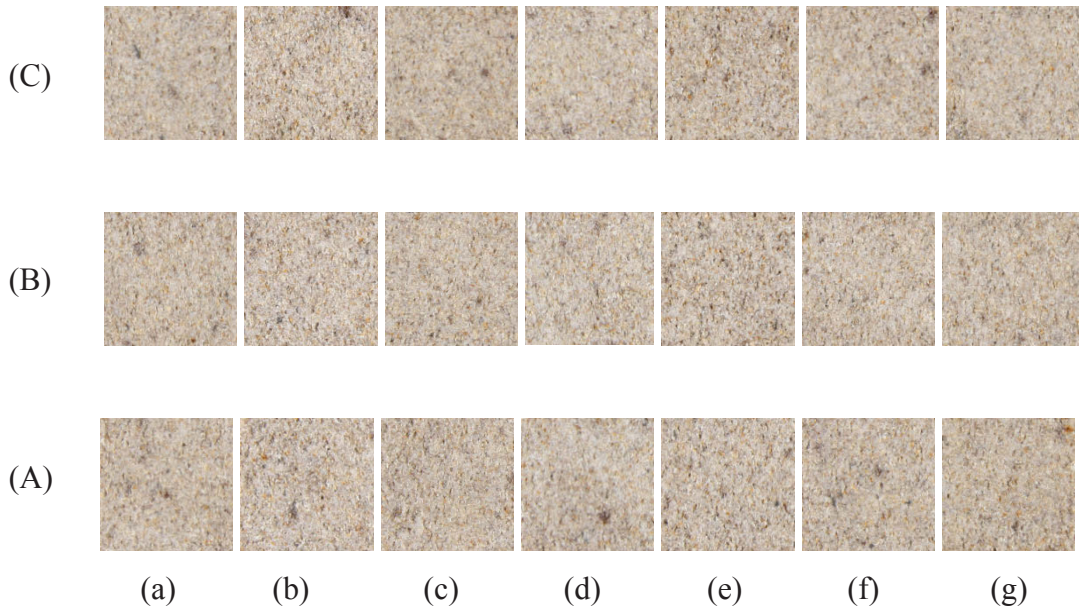

Figure 7.4.3. Photographic images of sandstones treated with PEG25, MMT and PEG25M composites taken from (A) immersed, (B) middle and (C) top sections treated with (a) DW, (b) PEG25, (c) PEG25M2, (d) PEG25M4, (e) PEG25M6, (f) PEG25M8 and (g) MMT

The chromatic determinations of the sandstones treated with PEG25, PEG35, MMT, PEG25M, and PEG25Ma, PEG35, PEG35M, PEG35Ma composites are presented in Figure 7.4.4. The color alterations of all treated sandstones exhibited the reduced brightness (L*) values, increases in the a* values, small changes in the b* values and increase in total color variation ΔE*. The treatments induced darkening and red-green colour changes and showed insignificant variations caused by yellow-blue colour alterations. The significant decreases in L*values indicated the major darkening effect on the overall colour alterations. In contrast to visual evaluations, the colour measurements showed increased redness and darkness of the sandstones treated with PEG35 and reduced colour changes of the sandstones treated with PEG25. The treatments with the composites containing PEG25 or PEG35 resulted in the similar redness and darkness of the sandstones treated with the composites indicated by the relatively similar Δa* and ΔL* values. The MMT concentrations showed negligible influence on reddening and darkening of the sandstones treated with the PEG-MMT composites and there appeared no detectable effects produced by acidified MMT. The colorimetric determinations indicated the color variations of the treated sandstones towards a darker appearance, and the total colour variations in all treated sandstones were found to be greater than 5 and

less than 10, indicating the considerable effects on the visual appearance of the treated sandstones (Rodrigues & Grossi 2007).

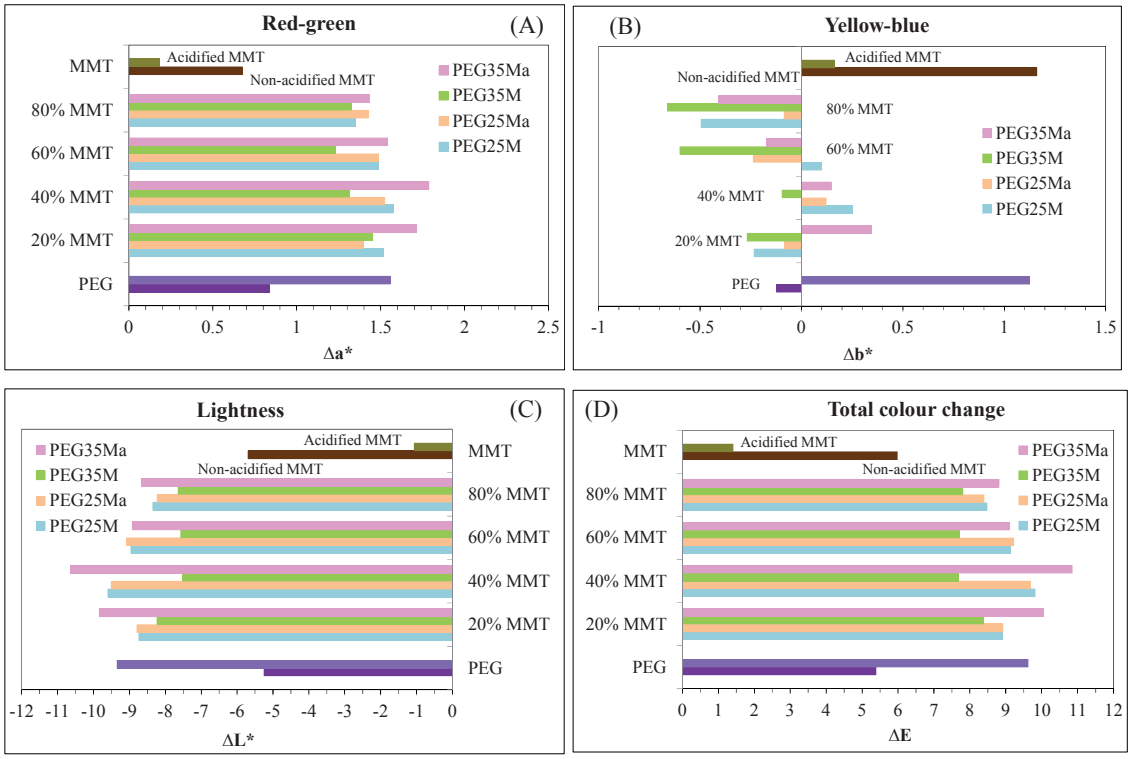

Figure 7.4.4. Differences in (A) red-green component (a*), (B) yellow-green component (b*), (C) luminosity (L*) and (D) total colour alterations (ΔE*) due to PEG25, PEG35, MMT and PEG-MMT composites

7.4.3. Water vapor permeability of consolidated sandstones

The effects of PEG, MMT and PEG-MMT composites on permeability of the treated sandstones to water vapour and penetration degree were studied, based on the changes in weight of the silica gel and the WVT values. Figure 7.4.5 presented the weight increases in desiccant due to the absorbed water vapour through some consolidated sandstones, and the changes in the WVT values of the sandstones consolidated with PEG and PEG-MMT composites were demonstrated in Figure 7.4.6. The reduced values of WVT were observed when PEG concentrations were increased from 2.5 to 10% and signified the decreased diffusion rate of water vapour through the treated sandstones that absorbed the greater amounts of PEG.

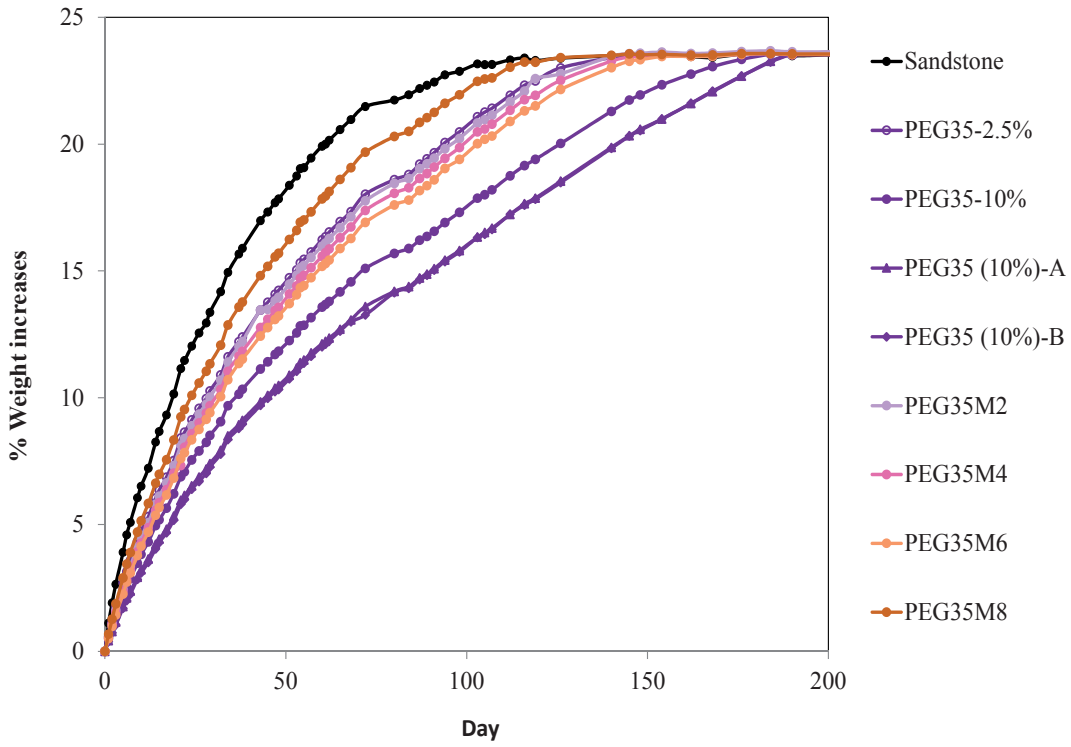

Figure 7.4.5. Increases in moisture absorption of desiccant plotted against time measured from the consolidated sandstones immersed in PEG and PEG-MMT composites and from the middle (A) and top (B) sections of the sandstones penetrated by 10% PEG35

At identical concentrations of PEG25 and PEG35, the WVT values of the treated sandstones were found to be similar at each section of the treated sandstones and the tested molecular weights of PEG had no effect on water vapour permeability of the treated sandstones indicative of the comparable penetration level of PEG25 and PEG35. The immersion of the sandstones in PEG or PEG-MMT composites resulted in the WVT values, which seemingly changed on more-or-less the same level. There appeared to be uncertain variations influenced by PEG-MMT ratios, molecular weight of PEG and acid-modified MMT. The observed results reflected similar changes in the amounts absorbed by the sandstones.

Figure 7.4.7 was included to show the WVT values corresponding to the changes in water vapour permeability of the sandstones after being penetrated by PEG and PEG-MMT composites. As with 10% PEG, the capillary penetration of 2.5% PEG resulted in similar WVT values and these results indicate good penetration ability of PEG through the sandstones and enhanced distribution of PEG across the sandstones. Upon increasing the

MMT concentrations, all PEG-MMT composites increased the WVT values for the middle parts of the treated sandstones and produced higher WVT values of the uppermost section of the treated sandstones.

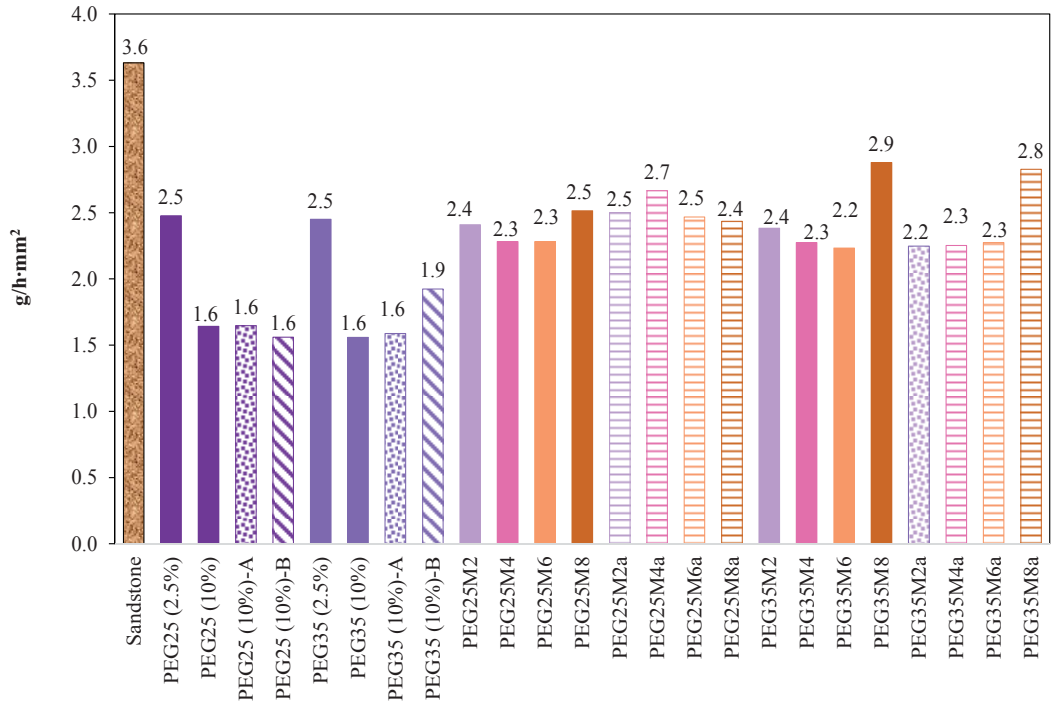

Figure 7.4.6. Average values of WVT measured from the sandstones immersed in PEG and PEG-MMT composites and from the middle (A) and top (B) sections of the sandstones treated with 10% PEG

The WVT values obtained from the uppermost parts of the sandstones treated with the composites over 20% MMT were comparable to the one of the untreated sandstones and presented similar changes, regardless of molecular weight of PEG and acid-modification of MMT. Apparently, increasing MMT concentrations led to the reduced capillary penetration of PEG-MMT composites and the composites were penetrated to the top parts of the sandstones at only 20% MMT. In contrast to PEG with no obvious changes in water vapour permeation, the observed results showed the negligible role of molecular weight of PEG and acid-modification of MMT, but the significant effect of MMT in limiting the penetrating ability of PEG-MMT composites.

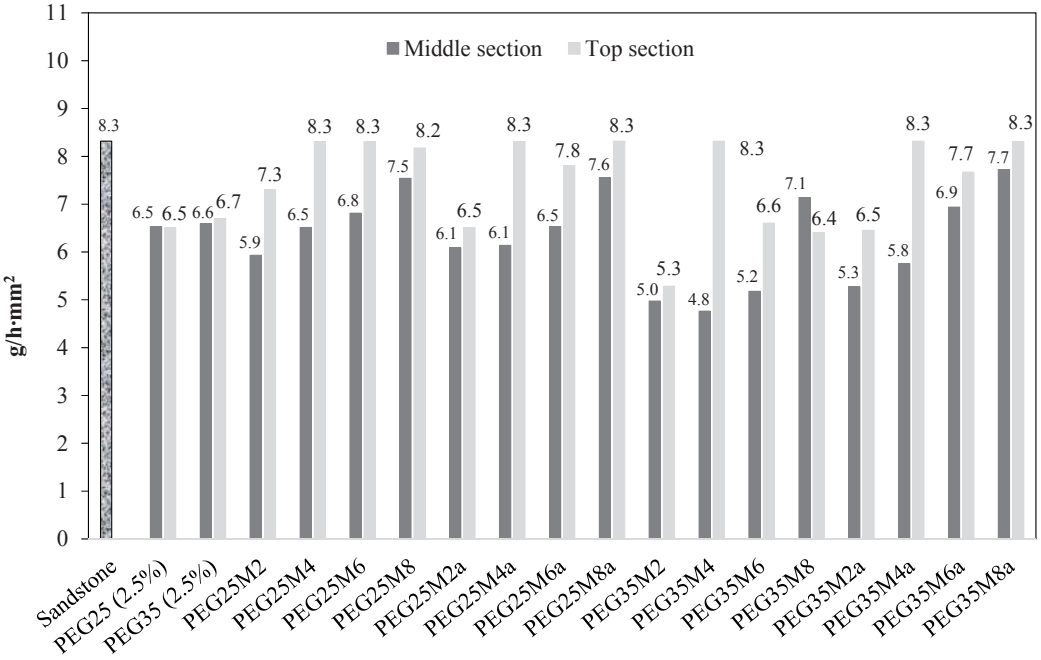

Figure 7.4.7. Average WVT values resulted from the penetrated sections of the sandstones treated with PEG and PEG-MMT composites

7.4.4. Bending tests

In order to study the effect of consolidants on the mechanical properties of the consolidated sandstones and the consolidating efficiency to bind and consolidate the sandstone surface, the bending tests were measured and compared. In Figure 7.4.8, the flexural stress of the untreated sandstones and the sandstones consolidated with 2.5% solutions of PEG25, PEG25M2, PEG25M2a, PEG35, PEG35M2, and PEG35M2a are presented. The sandstones treated with PEG25 showed 7.5% increase in bending strength. The results indicated the greater bending strengths for the sandstones treated with PEG25 than PEG35 and PEG-MMT composites at 20% MMT and the treatments with PEG25-MMT resulted in better bending strengths than the PEG35-MMT composites. The standard deviation of the measured values for the sandstone samples treated with PEG and PEG-MMT containing 20% MMT ranged from 0.1 to 0.8 but the treatment with PEG25 produced the largest standard deviation.

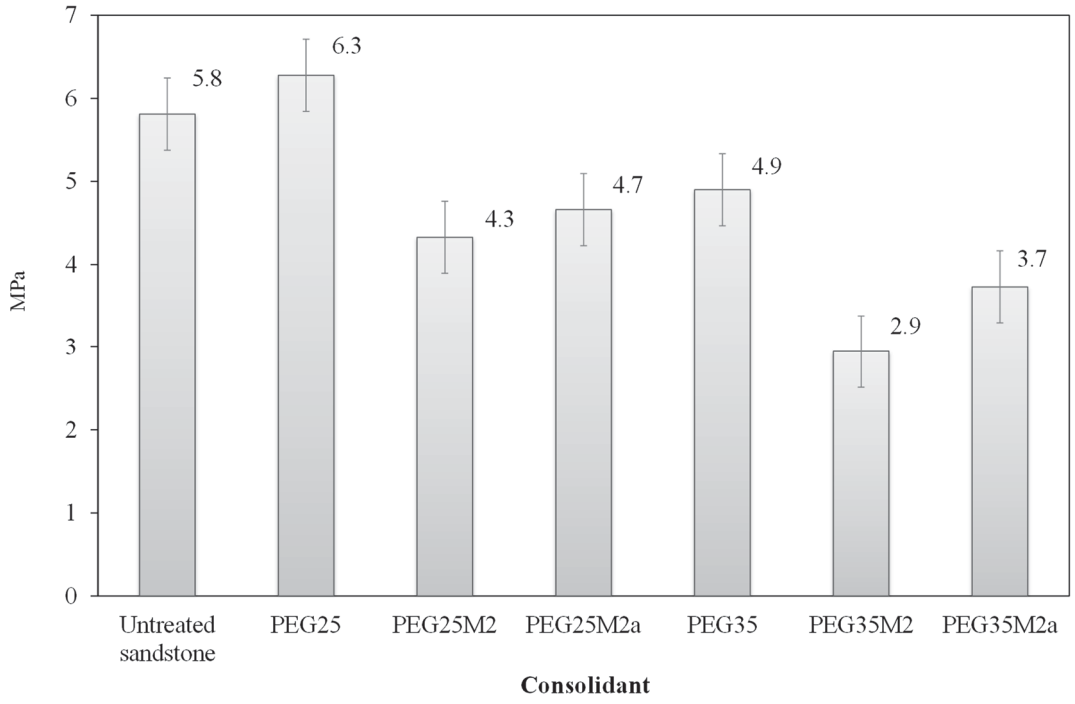

Figure 7.4.8. Averaged flexural stresses of the untreated sandstones and the sandstones consolidated with 2.5% solutions of PEG25, PEG25M2, PEG25M2a, PEG35, PEG35M2 and PEG35M2a

Except for PEG25, the bending strengths for the sandstones treated with PEG25M2, PEG25M2a, PEG35, PEG35M2 and PEG35M2a were reduced about up to 50% compared to the ones of untreated sandstone and the results obtained did not show meaningful results to evaluate their consolidation effects compared to the untreated sandstones. The reduced bending strength could be originated from water absorption, despite being dried, of the sandstones treated with PEG25M2, PEG25M2a, PEG35, PEG35M2 and PEG35M2a, thus reducing the mechanical strength of the sandstones. It has to be mentioned that the considerably different results between PEG25 and the other samples may indicate the errors for these values possibly due to the presence of defects in the material. Moreover, the decreased bending strengths for most tested sandstones suggested the use of higher concentrations of PEG35 and PEG-MMT composites to improve their mechanical properties.

7.4.5. Summary of consolidation treatment with PEG and PEG-MMT

The potential use of water based sandstone consolidants, containing PEG, MMT or PEG-MMT composites, was examined for the consolidation work of unweathered yellow block Sydney sandstone. To evaluate whether the treatments with PEG, MMT, or PEG-MMT composites were effective as sandstone consolidants the preparation of consolidated sandstones was conducted using capillary rise method. Their consolidation performance relative to the commercial consolidants and the effects of PEG molecular weights, PEG, or MMT concentrations and acid-treatment of MMT were assessed, based on colour changes, water vapour permeability, bending strength and rate and extent of penetration, and uptake of the applied consolidants.

The capillary rise experiments showed the slower penetration with increasing PEG or composites concentrations, PEG molecular weight and solution viscosities. Conversely, the effect of MMT contents on the penetration and absorption of PEG-MMT composites was small and the intercalated or absorbed PEG chains played the negligible part in limiting the water absorption of MMT. Similarly, all PEG-MMT composites and PEGs revealed similar changes and the penetration behaviours of the composites were unaffected by the acidification process of MMT and PEG molecular weight. With the similar penetration depths to PEG-MMT, PEG exhibited faster penetration and better uptake than MMT, PEG-MMT and 10% PEGM10 dispersions yielded the best uptake and good penetration in the tested PEG-MMT composites.

The changes in the water vapour permeability also showed reducing permeabilities of the treated sandstones with increasing PEG and PEG-MMT concentrations, but no significant effect of acid-modified MMT and the tested PEG molecular weights. The similar water vapour permeabilities, after the immersion and penetration of PEG, revealed the good penetrating ability of PEG, which subsequently, contributed to the attainment of good uptake of PEG. With the comparable uptake under the identical concentrations of PEG and PEG-MMT, the increased diffusion rates of water vapour on increasing the MMT concentration of PEG-MMT composites indicated the decreased penetrating capacity due to water absorption of MMT, which could prevent their penetrations.

The visual and colorimetric evaluations showed negligible effects of PEG molecular weights, acidification of MMT and PEG-MMT ratios. PEG, MMT and PEG-MMT

composites presented perceptually smaller variations than the untreated sandstone but the major contribution to the total colour change colorimetrically came from the increased darkness for all tested treatments. The treatments with PEG, MMT and PEG-MMT composites similarly underwent small changes in the mechanical properties of treated sandstones corresponding to low-risk incompatible treatments and resulted in the slight improvements in the mechanical strength of treated sandstones.

The consolidation treatment using PEG solution was found to be more effective than PEG-MMT composites, which limited their penetrations and uptakes, attributed to the MMT providing physical cross links binding the consolidants together. As with PEG, the PEG-MMT composites at low MMT contents provided improved consolidation effects. The consolidation action of PEG was greater than the PEG-MMT composite due to the good penetration depth, higher PEG uptake by the sandstones and similar visual appearance of PEG to the ones of the PEG-MMT composites. Despite the higher capillary absorption from the PEG solutions than the ones for PAA and PAm, PEG and PEG-MMT composites were found to be ineffective to improve the mechanical properties of the treated sandstones and the major weakness of PEG and PEG-MMT was low mechanical strength of the treated sandstones, especially for PEG-MMT composites at high MMT contents.

7.5. In situ polymerisation of AA

7.5.1. Application of AA solutions with or without KPS

In order to investigate the penetration and absorptions of AA, a wide range of AA concentrations from 5 to 50% were first tested to study the capillary penetration behaviours of AA in the absence of KPS. In Figure 7.5.1, weight variations of sandstones treated with AA solutions are presented. For all AA concentrations, the absorption curves were similar and the rapid absorption of the consolidant system was observed. The capillary penetrations of the 5-20% AA solution occurred at a similar rate to DW and ended after 4 hours. Although the 30-50% AA solutions were penetrated slowly via capillary rise with complete penetration based on solvent front rise to the top of the specimens after 24 hours, the viscosity of AA solutions was apparently unaffected even at 50% AA and the markedly fast penetrating ability of AA solutions was observed. After the completion of capillary rise, where the treated sandstones absorbed over 70% of the total amounts of the most AA solutions, the weights of the sandstones were slowly increased, and the sandstones treated with the AA solutions were saturated before the sandstones were saturated with DW. Despite the similar absorbed amounts of AA solution

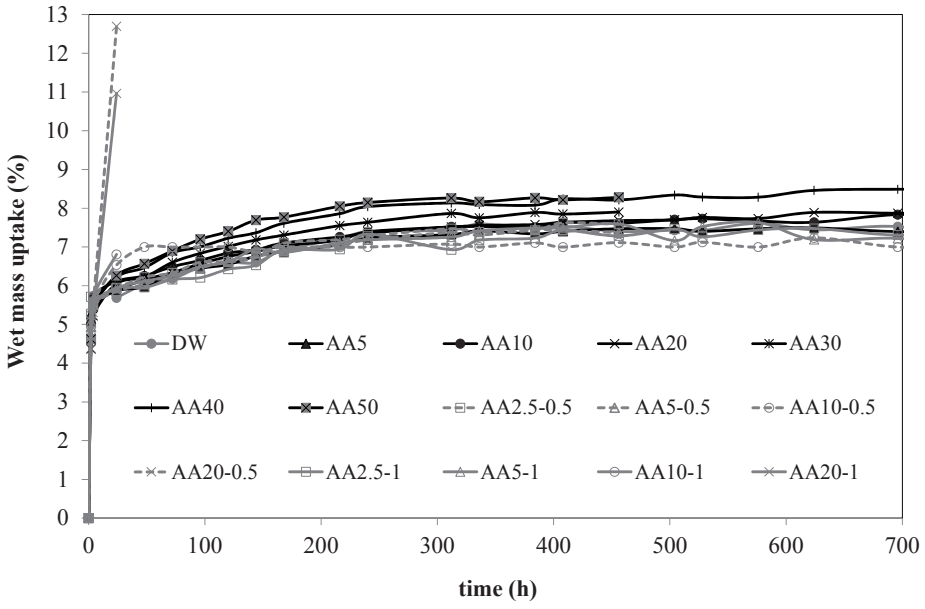

Figure 7.5.1. Capillary rise absorption tests of DW and solutions of AA with or without KPS

between 7.6 and 8.5% and high AA solution concentrations, the uptakes of AA by sandstones were found to be only 0.2-0.6% due to volatile AA on drying (Figure 7.5.2).

A second series of consolidation treatments using AA was conducted using AA solutions in presence of KPS in an effort to facilitate better absorption of AA through the use of water soluble AA monomers, which can be polymerised to form the polymer network within the porous stone system. The effects of AA and KPS concentrations on penetration, absorption and polymerisation process of AA were studied. As observed for the AA solutions without KPS, all AA solutions in the presence of 0.5 and 0.1wt% KPS rapidly penetrated the sandstone and the solvent front reached the top of the sandstone specimens after 4 hours. The results showed that the concentrations of both AA and KPS had negligible effects on the extent and rate of capillary penetrations at this stage. The obviously different changes resulted from the AA20-0.5 and AA20-1 solutions that were polymerised after 24 hours. The weight increase in dried sandstones treated by the 20% AA solutions were rapid and high but the use of AA solutions at and higher than 20% is impracticable due to the formation of hard and insoluble films formed by the polymerisation of AA.

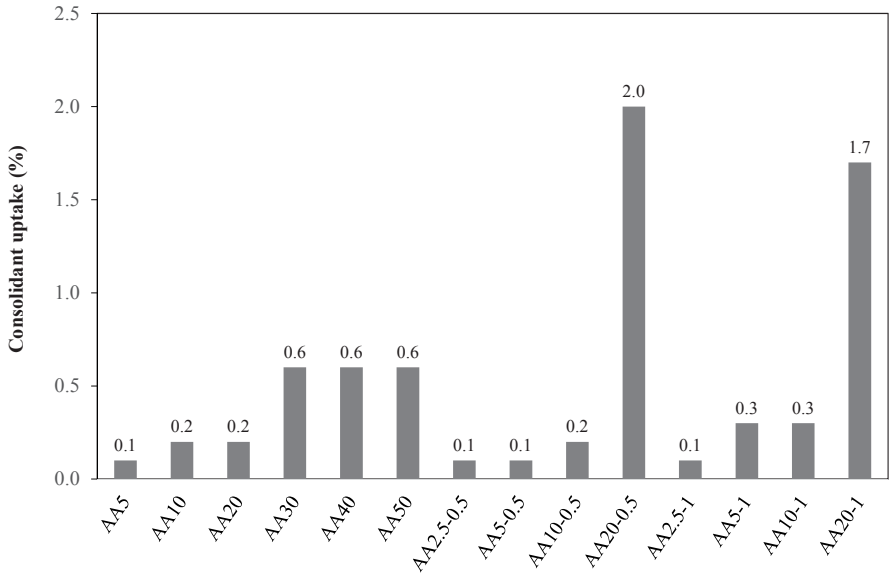

Figure 7.5.2. Uptake of AA solutions and in situ polymerisation of AA with 0.5 or 1.0 wt% KPS

With the exception of AA20-0.5 and AA20-1 solutions, the 2.5, 5 and 10% AA solutions containing 0.5 or 1.0 wt% KPS produced similar absorption curve and weight increases of the dried sandstones were comparable to the AA solutions tested without KPS (Figure 7.5.1 and 7.5.2). Of the AA2.5-0.5 and AA2.5-1.0 solutions, only 0.1% weight increases in the treated sandstones resulted. On increasing the KPS concentration from 0.5 to 1.0 wt%, the weights of sandstones after drying were also found to be increased slightly from 0.1% to 0.3 % for AA5 and 0.2% to 0.3% for AA10 respectively. While the uptakes of both AA5 and AA10 by the sandstones were small, the applied solutions became viscous after 2 days for AA10-0.5 and 1 day for AA10-1, presumably due to the polymerisation of 10% AA solutions. In contrast to AA20-0.5 and AA20-1, the treatments with AA10-0.5 and AA10-1 resulted in viscous, but water soluble solutions. Therefore, the AA5-1 and AA10-1 were better consolidating materials, though the absorbed amounts of AA5-1 and AA10-1 were smaller than the in situ polymerised 20% AA.

7.5.2. Variations in appearance and colour

The effects of AA and in situ polymerisation of AA on appearance and colour of the treated sandstones were assessed in comparison with the untreated sandstone. Figure 7.5.3 includes the selected photo images of the sandstones after the treatments with various concentrations of AA, with or without KPS. The colour change is due to the acidity of the AA reacting with the siderite $FeCO_3$ which presumably results in oxidation to iron oxide hydroxides leading to the yellow colour. The oxidation of Fe(II) is catalised by the acid. The capillary penetrations of the AA solutions without KPS produced an intense red colour on the treated sandstone surfaces and increasing AA concentrations intensified the redness of the treated sandstones. There appeared to be insignificant variations in redness of the sandstones with increasing capillary penetration length of the AA solutions; the significant colour changes in the treated sandstones above the immersed sections may indicate good penetration of AA. The treated surfaces were inhomogeneous and the formation of the red surface may be related to the reaction of AA with the iron-rich components in the sandstones.

The treatments with 2.5 and 5% AA in the presence of KPS changed the sandstone colour in a similar way to AA without KPS. The colour alterations were decreased by the

treatments with 10 and 20% AA in the presence of KPS and the colour changes were reduced when the polymerisation reaction of 10 and 20% AA in the presence of KPS. As with the sandstones treated with various AA concentrations without KPS, similar colour and appearance changes for both face-up and face-down sides of treated sandstone were observed for the treatments with 2.5 and 5% AA in the presence of KPS, indicating the negligible effect of the drying method. Conversely, the treatments with 10 and 20% AA in the presence of KPS resulted in orange coloured surfaces exposed to air due to the oxidation of the Fe(II) to Fe(III) to produce rust compounds iron oxide hydroxides, similar to AA10-1(a) in Figure 7.5.3, while the colour changes induced by AA were considerably reduced for the side placed down, as seen from AA10-1(b) in Figure 7.5.3. In contrast to drastic appearance changes in the immersed sandstones due to cracks caused by the polymerisation of AA20-0.5 and AA20-1, the treatments with AA10-0.5 and AA10-1 managed to polymerise AA, without visually identified broken and cracked sandstones.

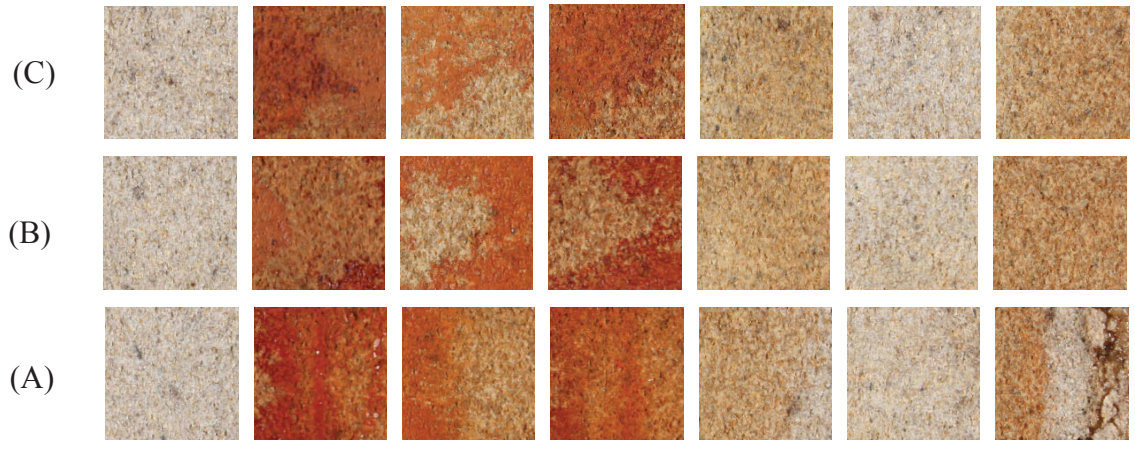

Figure 7.5.3. Images of sandstones treated with 10% AA without KPS or 2.5, 5.0, 10 and 20% AA with 1.0 wt% KPS obtained from (A) immersed, (B) middle and (C) topmost sections

Colour analysis from the sandstones treated with 10% AA without KPS also showed large colour differences where the red, yellow and darkness components significantly increased in comparison to the ones of 10% AA with 1.0 wt% KPS (Figure 7.5.4). The colorimetric determinations of the sandstones treated with AA10-1 still revealed considerable

variations in the L*, a* and b* colour coordinate values for AA10-1(a), with small changes of L*, a * and b * colour coordinate values for AA10-1(b). It is obvious the results obtained from AA10-1(b) revealed little overall colour change and AA10-1(a) showed the smaller contribution of redness than the yellowness and darkness of the surfaces.

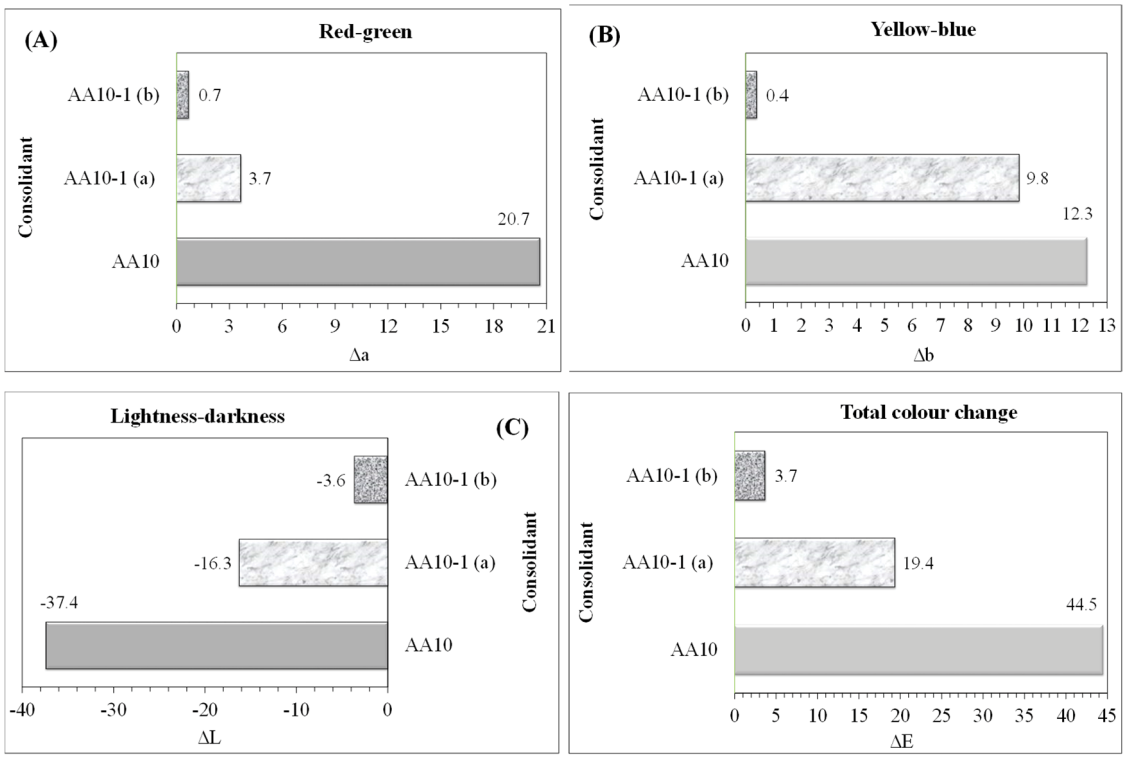

Figure 7.5.4. Differences in (A) red-green component (a*), (B) yellow-green component (b*), (C) luminosity (L*) and (D) total colour alterations caused by AA10 and AA10-1

The increased colour changes in the face-up positions of the treated sandstones showed a tendency to raise the concentrations of polymerised AA on the surface. A possible reason for the increased colour changes is the AA solutions were transported to the upper surface upon drying. The iron concentrations are transported by the evaporation causing moisture to move to the top surface. Another consideration is that the PAA film/network reduces the permeability of the oxygen required to cause oxidation of the Fe(II) to Fe(III). Although the significant colour changes were observed for the sandstone treatments with AA, it has to be mentioned that the results presented in this work were obtained for the sandstones applied to AA solutions after the extended period with the aims to understand the process of consolidation through penetration and polymerisation of AA. The colour

changes caused by the reaction of AA with the treated sandstones suggested the need to minimise acid reaction with siderite.

7.5.3. Water vapor permeability of consolidated sandstones

In order to study the effect of the treatments with AA in the presence of KPS on water vapour permeability of the treated sandstones and penetration depth, the changes in weight of the silica gel and the WVT values were compared. Shown in Figure 7.5.5 are the increased weights of desiccant caused by the absorption of water vapour passing through the sandstones immersed in the AA solutions in the presence of KPS and Figure 7.5.6 summarizes the values of WVT determined from the sandstone treatments with 2.5, 5 or 10 w/w% AA in the presence of either 0.5 or 1.0 wt% KPS. In comparison to the untreated sandstones, the treatments with all tested AA solutions decreased the values of WVT and the lower rates of water vapour diffusing through the treated sandstones were observed as a result of absorption of AA. At 0.5 wt% KPS, the WVT values showed

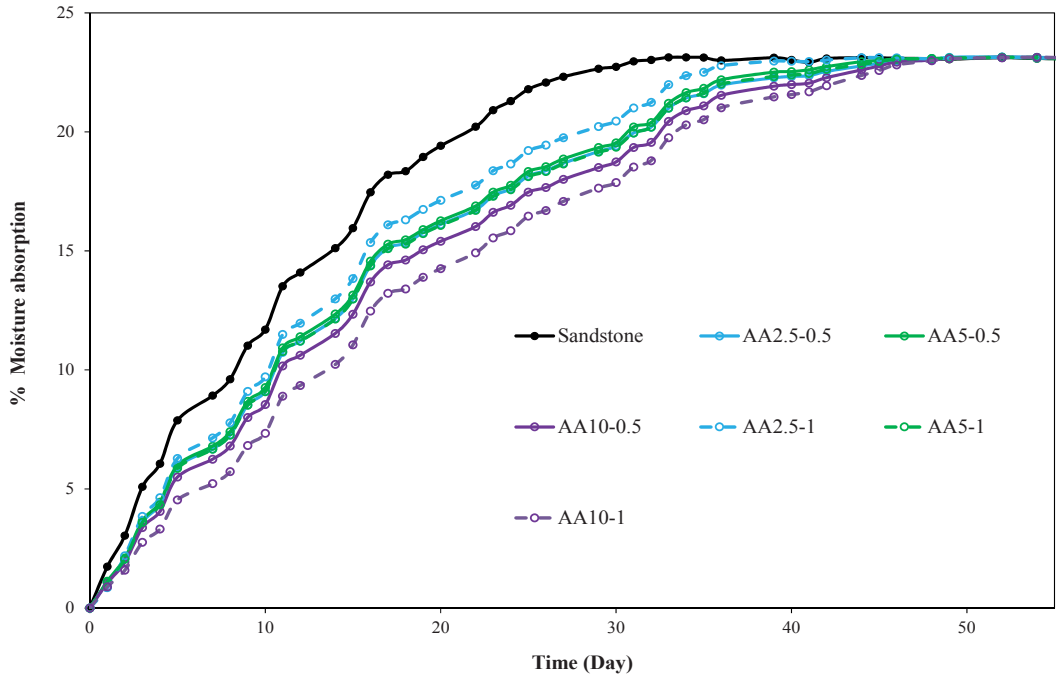

Figure 7.5.5. Changes in water vapour absorption of desiccant plotted against time measured from consolidated sandstones immersed in 2.5, 5 or 10 w/w % AA with 0.5 or 1.0 wt% KPS

decreased flow rates of water vapour from the top portions of the sandstones treated with 2.5 and 5 w/w% AA, but there appeared no significant changes in the WVT values of 10 w/w% AA. These values indicated reduced water vapour permeabilities of the penetrated sections of the sandstones treated with 2.5 and 5 w/w % AA and the unchanged permeabilities of the sandstones treated using 10 w/w% AA to water vapour.

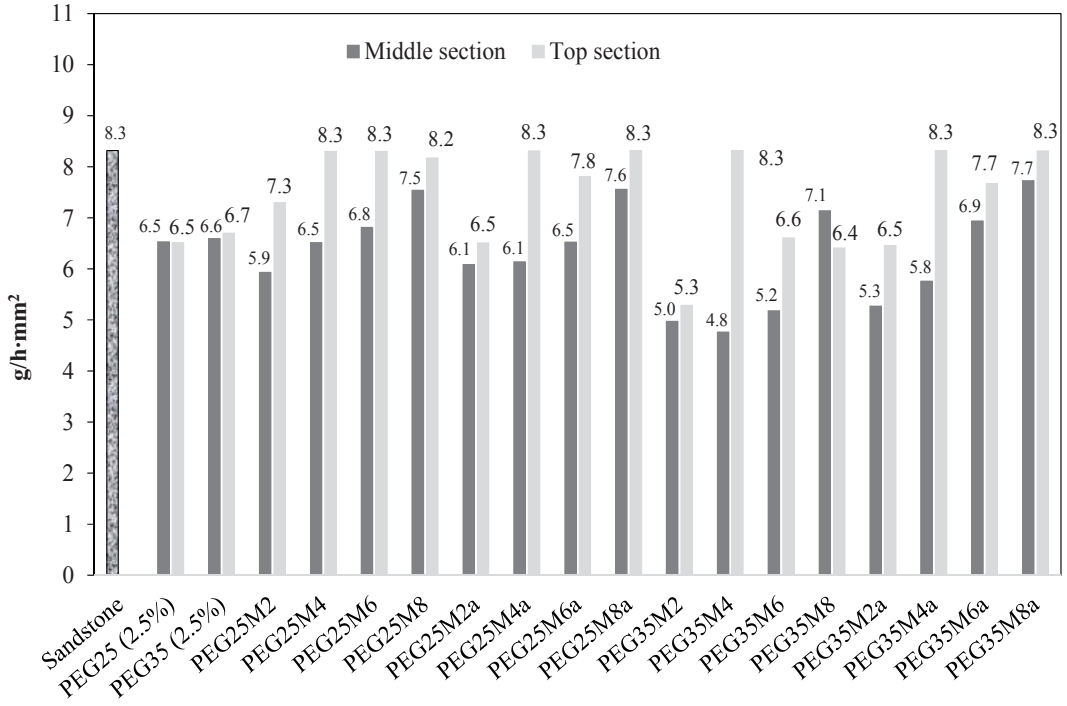

Figure 7.5.6. WVT values averaged from the sandstones consolidated with the solutions containing 2.5, 5 or 10 w/w% AA in the presence of 0.5 or 1.0 wt% KPS

On increasing KPS concentrations from 0.5 to 1.0 wt %, the WVT values were slightly reduced and tended to decrease with AA concentrations. With increasing capillary penetration, the sandstones treated with 2.5 and 5 w/w% AA reflected slightly lower WVT values, whereas the 10% AA solutions resulted in increased WVT values at 1.0 wt % KPS. The decreases in water vapour permeability with increasing AA and KPS concentrations can be described in part on the basis of increased polymerisation reaction of AA, which could reduce the pathway for diffusion of water vapour. In agreement with the absorbed amounts of AA, the observed changes were rather similar under the identical AA concentration and the AA concentrations showed only little overall changes in the values of WVT, even for the treatments with 10% concentrations, which displayed the

polymerisation of AA.

7.5.4. Bending tests

The efficiency of the consolidants to bind and consolidate the sandstone surface was studied by the changes in mechanical properties of the consolidated sandstones. Figure 7.5.7 shows the changes in flexural stress caused by the sandstones consolidated with 10% AA in the presence of 0.5 or 1.0 wt% KPS. In order to measure the changes in the mechanical properties of the treated sandstone specimens, representative samples were investigated in triplicate. Based on all of the discussed changes in the treated sandstones with varying AA and KPS concentrations, the in situ polymerisation of 20% AA resulted in cracked sandstone specimens while the AA concentrations less than 10% showed obvious colour variations. Therefore, the most representative sandstone sample to measure the consolidation effect was found from the treatments with the in situ polymerisation of 10% AA The bending strengths were improved after the consolidation treatment and increased with AA10-0.5 and AA10-1 by up to 26 and 93% respectively.

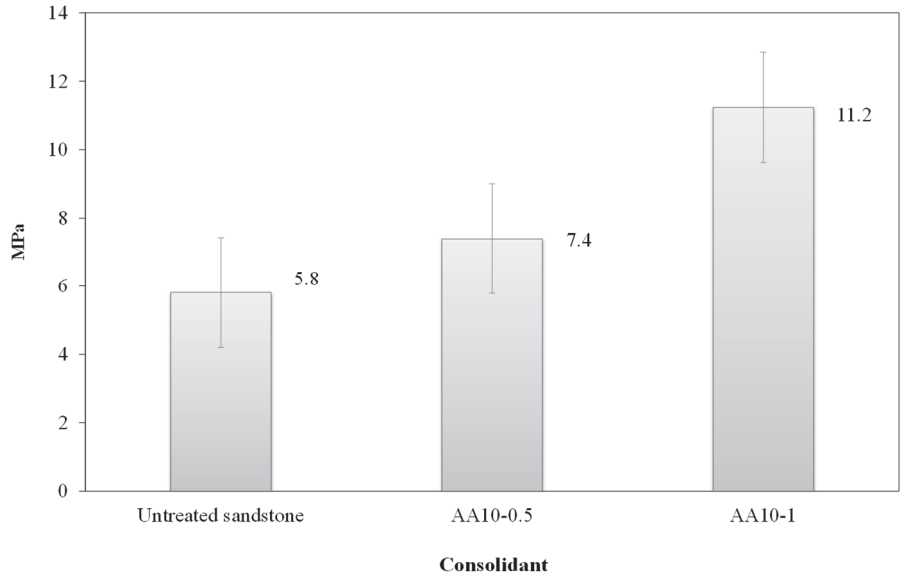

Figure 7.5.7. Average values of flexural stress of the sandstones treated with 10% AA in the presence of 0.5 or 1.0 wt% KPS

Despite their uptakes by the sandstones similar to the treatments without KPS, significant

increases in bending strength may indicate in situ polymerisation of AA within the sandstones. There was as significant time gap between consolidation, drying and strength testing. When the concentration of the KPS was increased, the polymerisation of AA occurred to a greater extent, thus the bending strength of the sandstones treated with AA10-1 was increased correspondingly. Generally, the mechanical strength of the treated sandstones increased with increasing concentrations of AA and KPS and the extent to which the mechanical strength of the treated sandstones increases can be directly related to these concentrations. The increases in bend strength of the tested sandstones can also be interpreted as evidence that the consolidation action of in situ polymerisation at 10% AA was enhanced to resist mechanical stress from external forces induced by sandstone weathering processes.

7.5.5. Summary of consolidation treatment with in situ polymerisation of AA

The consolidation treatments were performed on unweathered yellow block Sydney sandstone using AA applied, with or without KPS, by means of capillary rise technique to assess its potential use and suitability as water based stone consolidant prepared through the in situ polymerisation of AA in the treated sandstones. The evaluation of the consolidation effect of in situ polymerised AA was made in terms of colour modifications, water vapour permeability, bending strength, rate and depth of penetration and uptake of the applied consolidants. The influence of AA and KPS concentrations on polymerisation reaction and consolidation action of AA was studied in order to obtain the optimal concentrations of AA and KPS used for the consolidation work in Sydney sandstone.

It was found from the capillary rise penetration of AA solutions that the concentrations of AA had small effect on their abilities to penetrate through the sandstones and to produce low viscous states, even at 50% AA. The penetration rates of the AA solutions were found to be virtually unaffected, but reduced to similar rates observed for 2.5% PAA solution over 20% AA, which demonstrated faster transport of monomeric AA compared with the larger sized polymeric form. Despite the fast penetrations of AA solutions and polymerisation of AA over 5% AA, increasing AA and KPS concentrations produced small increases in the absorbed quantity of AA up to 10% AA concentrations. Above 10% AA, larger weight increases were observed indicating significantly increased penetration.

On increasing the concentrations of KPS and AA, the water vapour permeabilities of the treated sandstones tended to be slightly reduced with decreasing capillary rise distance. The observed changes in water vapour permeabilities corresponded to uptake measurements and were found to be rather small at the tested concentrations of AA and KPS. The slight decreases in the permeabilities of the treated sandstones to water vapour with increasing AA and KPS concentrations revealed the small effect of AA concentrations on the incompatibility of the treatments up to 10% AA in the presence of KPS. The observations can be related to even penetration of the consolidants through the specimens.

The main problem regarding in situ polymerisation of AA is the red colour of the treated sandstones, especially when AA was unreacted at low AA concentrations. Over 5% AA concentrations in the presence of KPS, the polymerisation reaction of AA was associated with the decreased colour alterations as demonstrated by the orange appearance and the reduced reddening, yellowing, and darkening of the treated sandstones and the in situ polymerisation at 10% AA resulted in the formation of the crack-free sandstones, unlike 20% AA, which caused the undesirable cracks. The mechanical strengths of the treated sandstones increased with AA and KPS concentrations and the in situ polymerisation of 10% AA resulted in considerable increments in mechanical strength and consolidation actions.

Increasing the concentrations of AA and KPS presented the slightly increased uptake of AA by the sandstones and polymerisation reaction of AA, which in turn, resulted in decreased water vapour permeability and colour alterations and increased bending strength of the treated sandstones. While the changes in the uptake and water vapour permeability of the treated sandstones were comparable under 20% AA, the in situ polymerisation at 10% AA reduced the colour alterations and increased the bending strength without crack formation, suggesting the best concentration of 10% AA for the consolidation of Sydney sandstones. The colour alteration caused by the acid makes this system unusable as a consolidant, however, the high degree of penetration, good permeability and mechanical strength demonstrates the potential of in situ polymerisation as a means of sandstone consolidation.

7.6. In situ polymerisation of Am

7.6.1. Application of Am solutions with or without KPS

The capillary rise absorption studies of Am solutions using various Am and KPS concentrations were examined as potential consolidant systems. The first experimental runs were conducted using 5-50% Am solutions in the absence of KPS to study the effects of Am concentrations on their capillary rise absorptions and penetration behaviours into the sandstones. In the second experimental series, sandstones were treated with the various concentrations of Am and KPS to study their capillary rise absorptions, penetrations and polymerisation of Am. A plot of the absorbed amounts of DW and the solutions containing Am are presented in Figure 7.6.1.

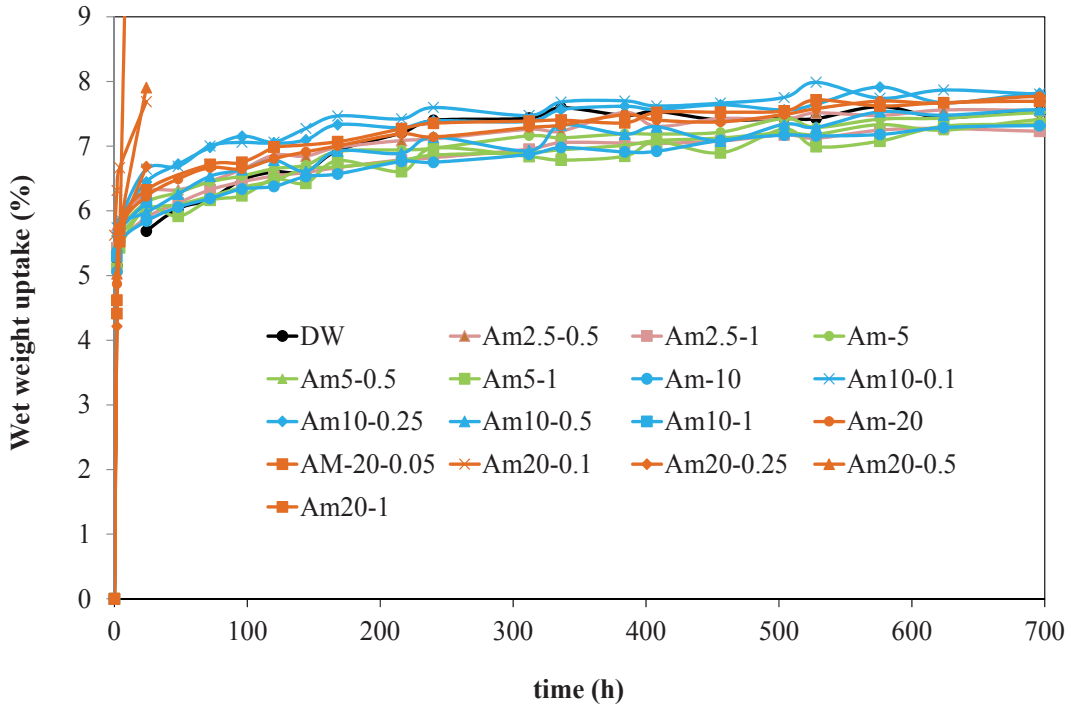

Figure 7.6.1. Capillary rise absorption curves vs. time for sandstone samples treated by DW and Am solutions

The absorption curves and the absorbed amounts of the most tested Am solutions were similar and the wet weights of the treated sandstones were increased by 7.4-8.3 %, which appeared independent of the Am and KPS concentrations. For the low-viscous solutions of 5-20% Am in absence of KPS and the Am solutions up to 10% Am with KPS, the capillary rise was found to be rapid and completed after 4 hours and the penetrating

behaviours were unaffected by the presence of 0.5 or 1.0 wt % KPS. The penetrations of the Am solutions above 20% Am without KPS were slower and their capillary rises were completed after 24 hours. Similarly, the Am solutions greater than 10% Am in the presence of KPS were penetrated to complete their capillary rises after 24 hours. Except for some solutions of high Am concentrations, which were rapidly polymerised, the observation of capillary penetrations of the Am solutions with various Am and KPS concentrations showed that the penetration rates of the Am solutions depended on the Am concentrations.

As shown in Figure 7.6.2, the uptake of Am by the treated sandstones increased from 0.2% for Am5 to 1.8% for Am50 and the final weight increases in the dried sandstones after the treatments with the Am solutions without KPS were found to increase with increasing Am concentrations. With 2.5 and 5% Am solutions in the presence of KPS, no obvious changes in solution viscosities and weight increase of sandstones were detected.

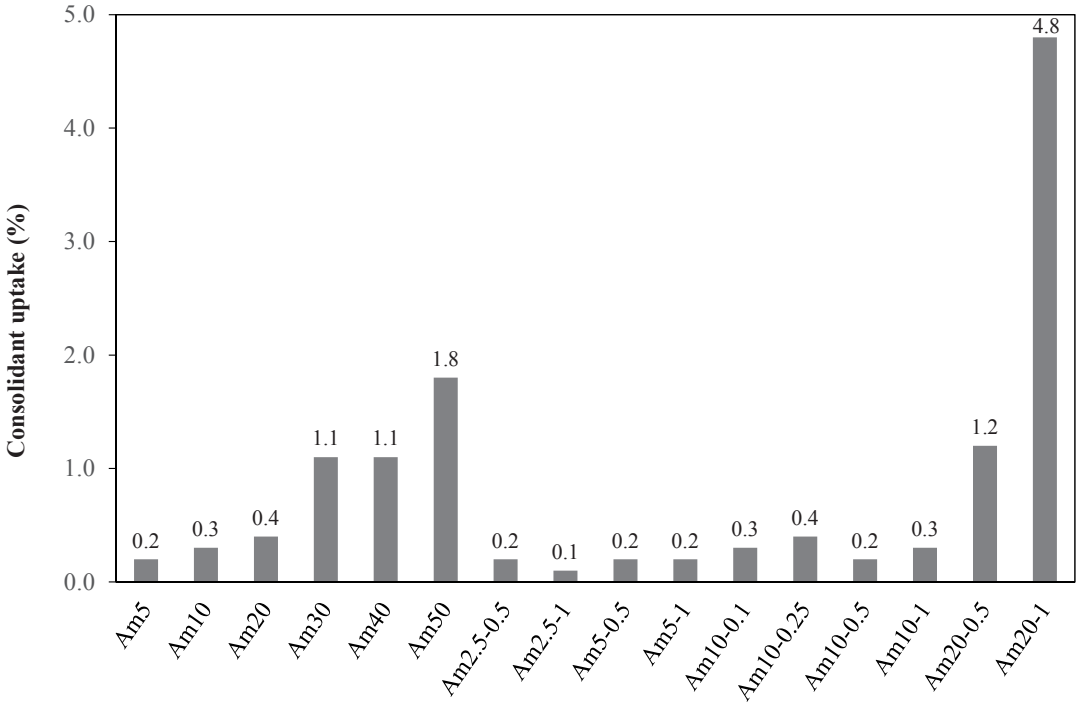

Figure 7.6.2. Uptake of Am with or without KPS

The 10% Am solutions in the presence of 1% KPS became viscous and penetrated much slower but the dry weights of the sandstones treated with 10% Am using varying KPS

concentrations were found to be similar to the ones for 2.5 and 5% Am solutions with KPS. The applications of 20% Am with KPS resulted in the rapid polymerisation of Am after 24 hours and the formation of rigid water insoluble materials was obtained. In order to study the effects of KPS on the in situ polymerisation of Am, the higher Am concentrations in the range of 30 to 50% Am were also investigated using low KPS concentrations at 0.05-0.5 wt% KPS. The sandstone treatments with these Am solutions showed the same results as the 20% Am solutions, which were polymerised after 24 hours. The observed results indicated the negligible effect of KPS concentrations. The Am concentration, however, was found to be important in determining the in situ polymerisation process of Am.

In marked contrast, the absorbed amounts in the dried sandstones treated with the Am solutions containing less than 20% Am were much lower than those with 20% Am in the presence of KPS. For the concentrations less than 10% Am, premature solution polymerisation of the Am coupled with the low uptake of the consolidant solution make the consolidation treatment unsatisfactory. Similarly, the consolidation treatments with 20% Am were seemingly unsuitable due to the hard materials formed by the polymerisation reaction of 20% Am. Although the absorbed amounts of 10% Am in the presence of KPS by sandstones were mostly similar to the 2.5 and 5% Am solution, the water soluble solutions and more flexible dried films obtained for the 10% Am with KPS reflected its potential use for in situ polymerisation in sandstone treatment.

7.6.2. Variations in appearance and colour

The sandstones treated with Am, with or without KPS, were first assessed by the perceptual changes related to the altering colour and appearance and the selected images of the treated sandstones are shown in Figure 7.6.3. Irrespective of Am concentrations, the treated sandstones showed a homogeneous surface, suggesting a uniform distribution of penetrated Am. The perceptual change in colour of the consolidated sandstones was trivial. The appearance of the treated sandstones, however, was severely affected by the crack formations, which increased with increasing concentrations of Am and KPS. Using greater than 10% Am, the treated sandstones were severely cracked due to the stresses caused by the polymerisation of Am. At 10% Am, the treated sandstones using 1.0 wt%

KPS showed some cracks, but no crack formation was observed in the presence of 0.5 wt% KPS. The results indicate that in situ polymerisation of Am below 20% concentrations are feasible for the sandstone consolidation.

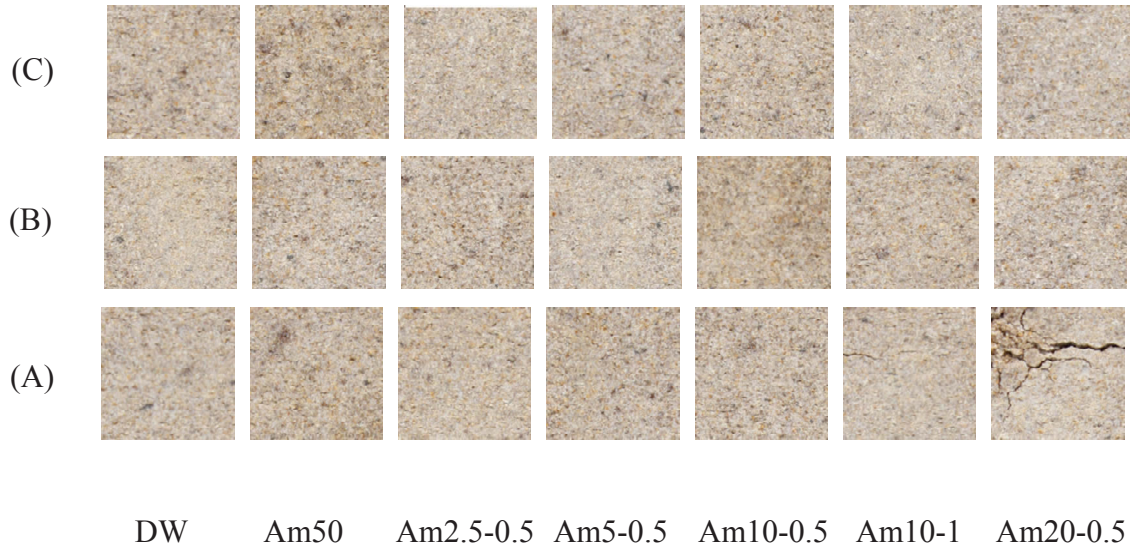

Figure 7.6.3. Images obtained from (A) immersed, (B) middle and (C) top sections of sandstones treated with Am in the presence or absence of KPS

The colour changes of the treated sandstones were measured colorimetrically and were monitored through redness/greenness, yellowness/blueness, lightness/darkening and total colour difference changes as shown in Figure 7.6.4. On the sandstones treated by Am, with or without KPS, increases in Δa* and reductions in Δb* and ΔL* were produced due to a small degree of reddening, blueing and darkening effects of the treatments. As far as blueing of the treated sandstones, the blueness was increased for the samples treated with Am2.5-1, Am5-1 and Am10-1 and appeared to be associated with increasing KPS concentrations, but the change in color was small overall. All the treated sandstones had similar Δa* and ΔL* after the treatments with Am, with or without KPS. Only minor influences of Am and KPS concentrations on the reddening and darkening were observed. While the changes in redness and blueness contributed little to overall color differences, the variations in ΔL* were considerably larger and the colour changes mostly caused by the darkening of the treated sandstones. According to the indicators reported for the incompatibility levels of the consolidants, the total colour changes were found to be over 5 and less than 7.5, which may be regarded as high risk of incompatible treatments (Rodrigues & Grossi 2007). However, the changes in the appearance of the treated

sandstones are perceptually not pronounced and there is little change in the colour relative to the virgin sandstone.

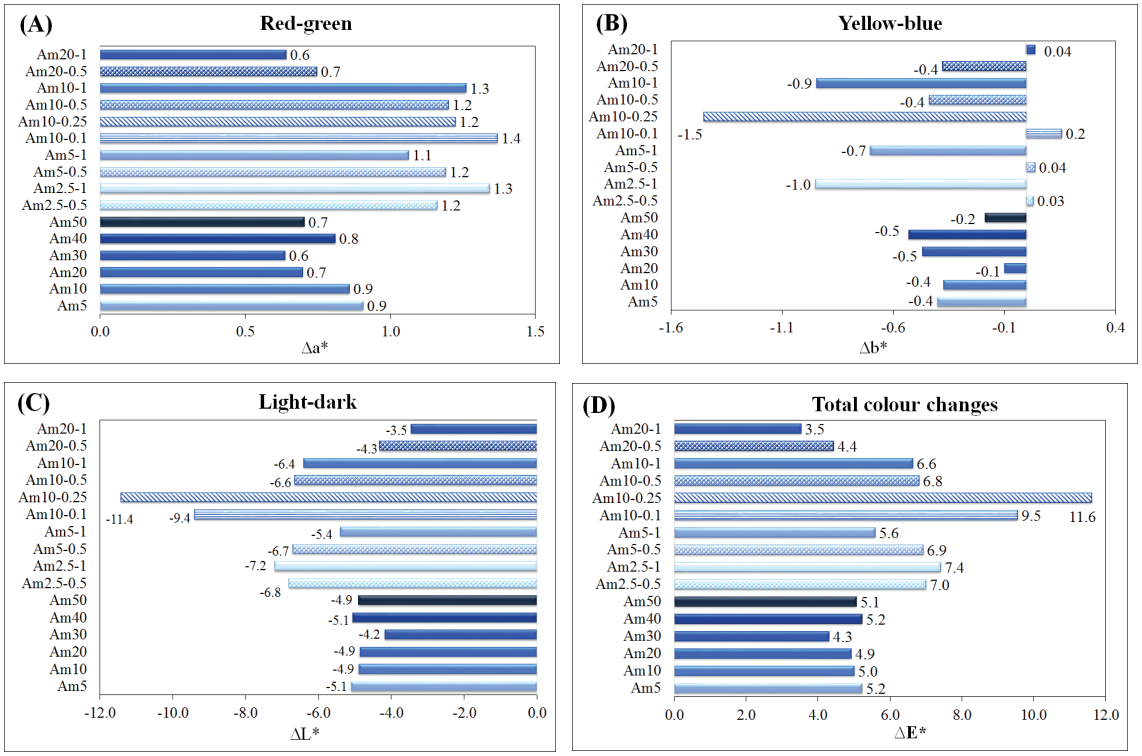

Figure 7.6.4. Differences in (A) red-green component (a*), (B) yellow-green component (b*), (C) luminosity (L*) and (D) total colour alterations caused by Am with or without KPS

7.6.3. Water vapor permeability of consolidated sandstones

Water vapour permeability of the treated sandstones and penetration depth caused by the treatments with Am in the presence of KPS were compared by the changes in weight of the silica gel and the WVT values. Figure 7.6.5 shows the weight increases due to water-vapour absorption of silica gel through the sandstone treated by immersion in 2.5, 5 or 10 w/w % Am solution containing 0.5 or 1 wt% KPS. The measured WVT values after the immersion or penetration of 2.5, 5 or 10 w/w% Am in the presence of either 0.5 or 1.0 wt% KPS were shown in Figure 7.6.6. After all the tested Am and KPS concentrations,

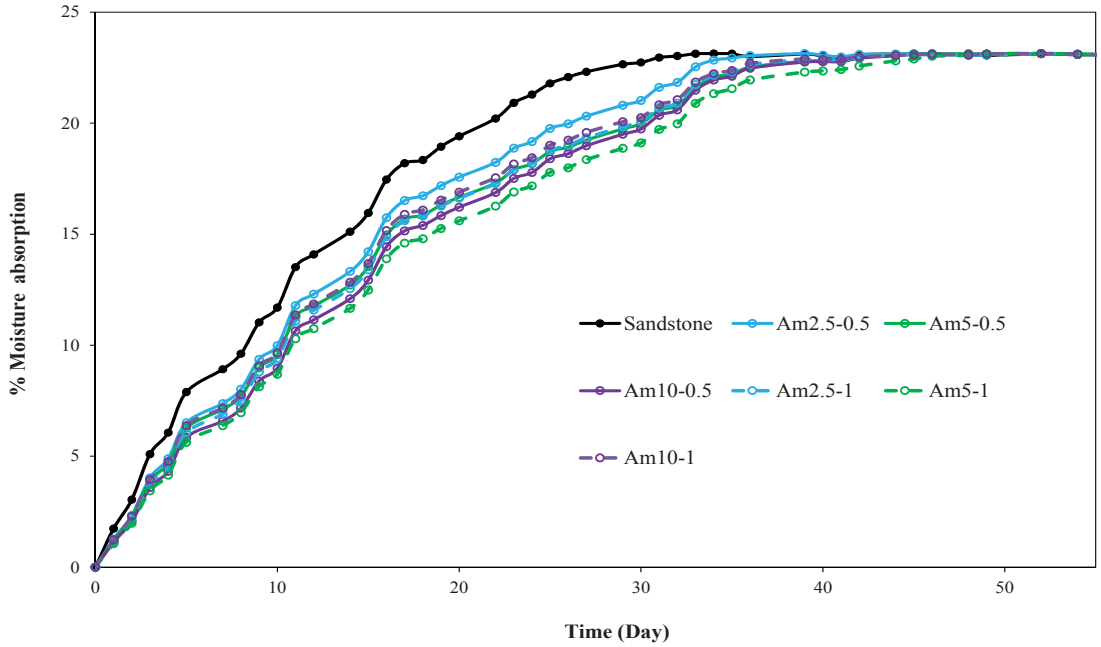

Figure 7.6.5. Plot of water vapour absorptioon of desiccant versus time found from consolidated sandstones immersed in 2.5, 5 or 10 w/w % Am with 0.5 or 1.0 wt% KPS

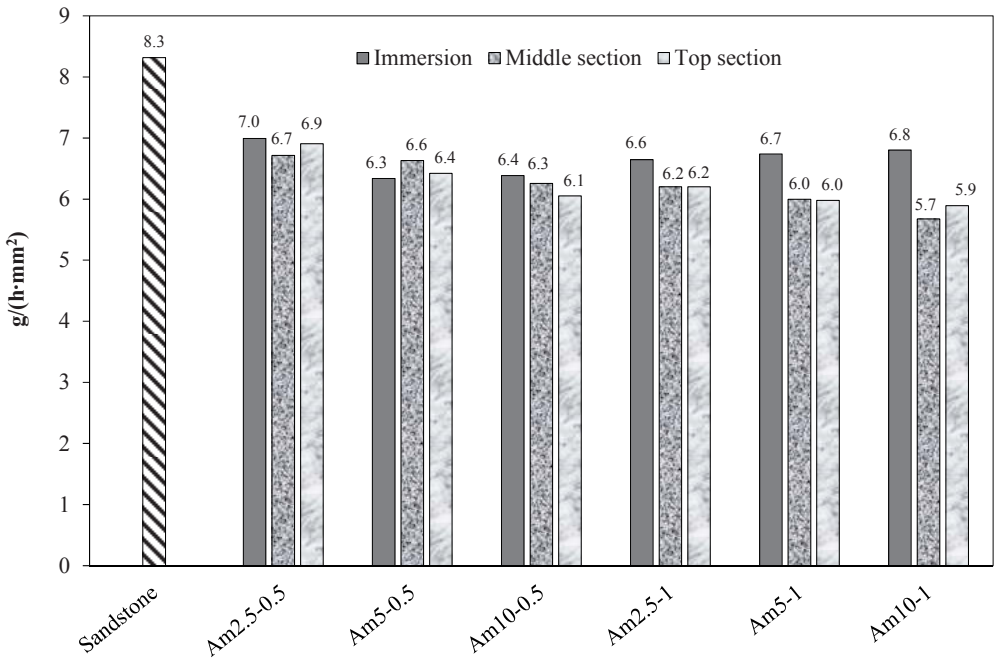

Figure 7.6.6. Mean WVT values of the sandstones consolidated with the solutions containing 2.5, 5 or 10 w/w% Am in the presence of 0.5 or 1.0 wt% KPS

the treated sandstones produced lower values of WVT due to the reduced water vapour

transmission rates and a reduction in water vapour permeability by 15.9 to 31.8 %, indicating the absorption of Am by the sandstones from the applied solutions. In the presence of 0.5 wt % KPS, similar values of WVT were observed for all parts of the treated sandstones at 2.5 and 5 w/w% Am, while treatment with 10% Am slightly reduced the WVT values with increasing the height of capillary rise. When 1.0 wt % KPS was used, the WVT values tended to be reduced compared with the ones of the sandstones treated using 0.5% KPS and the penetrated sections of the treated sandstones showed reduced WVT values.

Close inspection of the WVT values in Figure 7.6.6 revealed the decreased rates of water vapour diffusion with increasing Am and KPS concentrations for the penetrated sections of the treated sandstones. In addition to the increased amounts of absorbed Am, the observed changes could partially originate from the higher degree of Am polymerisation that can cause the delay in the permeation of water vapour though the sandstones. Although the treatment of the sandstones reduced the permeabilities to water vapour, the effect of Am concentrations below 20% Am were found to be relatively small. Even at the treatments with 10% Am, which showed the polymerisation of Am in the presence of KPS, the water vapour permeability of the treated sandstones were not significantly reduced and the good permeability characteristics observed for the in situ polymerisation at 10% Am showed additional experimental evidence for 10 % Am being the optimal concentration for the sandstone treatment.

7.6.4. Bending tests

The effect of Am in the presence of KPS on the mechanical properties of the consolidated sandstones on the consolidating effectiveness to bind and consolidate the sandstone surface was studied by the bending tests. The bending tests of the sandstones consolidated with 10% Am in the presence of 0.5 or 1.0 wt% KPS were conducted and the average flexural stress values were compared with the untreated sandstones in Figure 7.6.7. Based on the results discussed above, the in situ polymerisation at 10% Am produced apparently the best performance among the tested concentrations and the effect of the treatments with 10% Am on the mechanical properties of the treated sandstones was tested as representative consolidant. The bending strength of the sandstones consolidated by

Am10-0.5 reduced by 49% while the use of Am10-1 increased the bending strength of the consolidated sandstones by 42%. Although the concentrations of Am were identical, the bend strength of the sandstones consolidated with Am10-0.5 was as low as one-third of the strength after the treatments with Am10-1. The obvious alterations may be caused by the different extents of Am polymerisation as the polymerisation rate of Am was expected to be reduced for the 0.5% KPS.

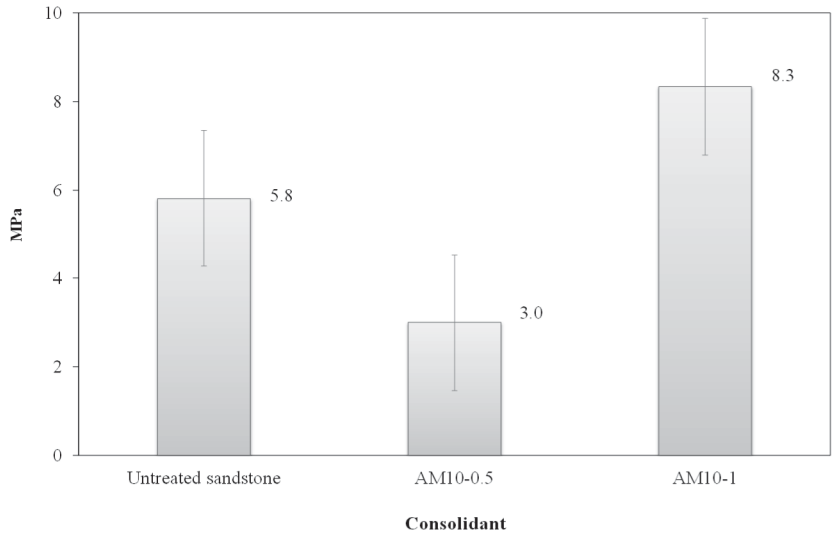

Figure 7.6.7. Flexural stress values averaged for the untreated and treated sandstones with 10% Am in the presence of 0.5 or 1.0 wt% KPS

Based on the significant reduction in the bending strength of the sandstones treated with 0.5% KPS, it is probable that the polymerisation of Am was incomplete under the tested condition and the moisture absorption of the treated sandstones possibly accounts for the decreased sandstone strength. From the physical point of view, the higher tensile strength after the in situ polymerisation at 10% Am also increased the ability of the treated sandstones to withstand the shear or tensile forces and the treatments provided the better consolidation action against the weathering and degradation processes.

7.6.5. Summary of consolidation treatment with in situ polymerisation of Am

In order to assess suitability for potential use as water based stone consolidant, the consolidation treatments were tested on unweathered Sydney's yellow block sandstone,

which were consolidated using various Am and KPS concentrations applied through capillary rise technique. The consolidation efficiency of in situ polymerised Am was determined by water vapour permeability, colour modifications, bending strength and rate, and depth of penetration and uptake of the applied consolidants. In search for the optimum concentrations of Am and KPS required to consolidate Sydney sandstone, the effects of Am and KPS concentrations on in situ polymerisation reaction compared and evaluated.

The changes in the capillary penetration of Am solutions, with or without KPS, showed little effect of their concentrations on the penetration depth and viscosity of the tested solutions. The penetration of the Am solutions into the sandstones was faster than the polymer solutions and the solutions containing less than 20% Am had practically no influence upon their penetration rates. The solutions at higher Am were found to penetrate the sandstones with slower penetration rate comparable to the ones of 2.5% PAm. Below 20% Am concentrations in the presence of KPS, increasing Am concentrations only produced slight weight increases and small uptakes of consolidant by the treated sandstones. Even though the uptakes were considerably increased at 20% Am concentrations, the in situ polymerised 10% Am resulted in more flexible and water soluble materials suitable as consolidant.

The visual comparison of the consolidated sandstones demonstrated insignificant colour changes at all Am and KPS concentrations. Although the concentrations of Am and KPS had negligible effect on the colour, crack formation by the in situ polymerisation limits the potential use of the Am solution at concentrations above 10% Am concentrations of KPS. The in situ polymerisation of Am reduced the water vapour permeability but not significantly. As the concentrations of Am and KPS and penetration depth of penetrated and polymerised Am increased, the water vapour permeabilities of the treated sandstones were decreased. Although the in situ polymerisation under 20% Am had practically small influence upon the changes, colour variations and water vapour permeabilities, the mechanical strengths of the treated sandstones were increased with higher KPS concentrations.

The use of high concentration Am consolidation solutions at > 10% Am and KPS resulted in crack formation. This effect limits the applicable concentrations of Am in consolidants

to circa 10% but further testings is required to confirm this limit. Despite small uptake for the in situ polymerisation of 10% Am, it produced substantial increase in the tensile strength. Increased tensile strength indicates that the consolidant is binding the sandstone particles together aiding the consolidation process. Without developing colour alterations and cracks, the in situ polymerisation of 10% Am with good level of water vapour permeability and increased bend strength demonstrated the best effectiveness.

7.7. Commercial consolidants

7.7.1. Application of commercial consolidants

The capillary rise experiments were performed on the unweathered sandstones using commercially available consolidants and Figure 7.7.1 compares their absorptions. As for MMT, monomers, polymers and composites solutions, the absorption profiles of B67, B72, Lascaux and Silres initially showed the rapid absorption, which was followed by slow wet weight increase until the saturated state was achieved. With treatments of the applied monomer liquid Silres and Lascaux solutions, the solvent front had reached the top of the sandstone specimen within 24 hours and the weights of wet sandstone samples were increased by 8.1% at the saturated state after 41 days. For the Lascaux and Silres solutions, the rate and extent of their penetrations were comparable and presented the comparable rate and extent of solution penetration and similar behaviours concerning their penetration and absorptions were observed.

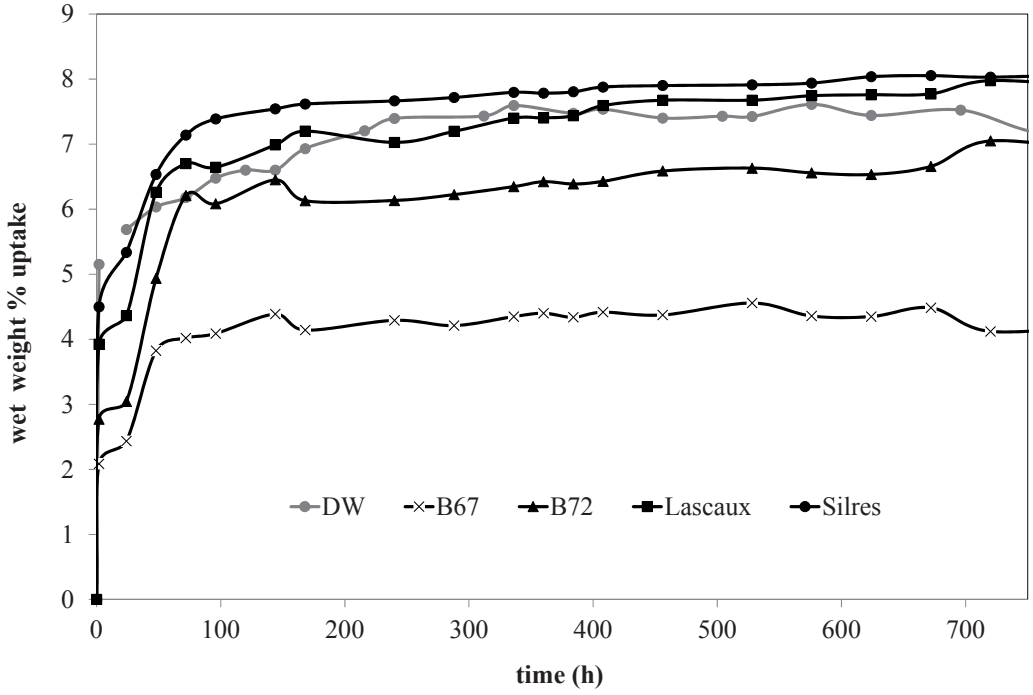

Figure 7.7.1. Absorption curves of DW, B67, B72, Lascaux and Silres solutions versus time

In contrast, the capillary rise absorption profiles showed the slower upward penetration of B67 and B72 solutions and the clear differences in the penetration degree and rates of the tested hydrophobic solutions. The B67 and B72 solutions much more slowly penetrated up to ~10 mm and 35 mm and the weights of wet sandstone samples increased by 4.6% after 29 days for B67 and by 7.1% after 40 days for B72. The treated sandstones were saturated by the B67 solution before the capillary saturations of the sandstones consolidated by the B72 solution but the penetration and absorption of the B72 solution were greater than the ones of the B67 solution. As expected from the B67 and B72 solutions which were apparently very viscous, the highly viscous solutions of B67 and B72 were more difficult to penetrate the sandstones and the penetration of B67 and B72 can be restricted due to large polymer molecules. Conversely, the non-viscous Lascaux solution and liquid monomer Silres showed good penetration rate and levels. The better penetrating capacity was observed for the non-viscous Lascaux solution and liquid monomer of Silres. Despite the high concentration of Silres, the monomer liquid Silres showed marked ability to penetrate in agreement with the previous reports showing good penetration depth and absorption of silane-based consolidants (Mosquera, de los Santos & Rivas 1986, Salazar-Hernández et al. 2010).

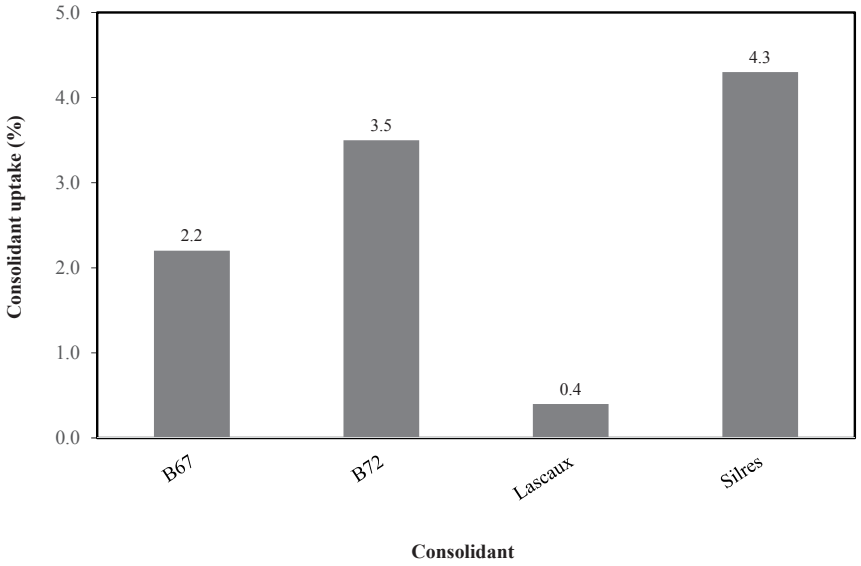

Figure 7.7.2. Comparison of uptake of B67, B72, Silres and Lascaux

From Figure 7.7.2, it is obvious that the uptakes of the commercial products were found to be high with the exception of Lascaux. The increase in the weights of dried sandstone samples were found to be greatest when consolidated with Silres. Silres and Lascaux showed good penetration depth and levels, but it is most likely that the higher amounts of Silres were absorbed from the liquid monomer of Silres which was almost five times more concentrated than the Lascaux solution. Although the penetration of the B67 solution was limited and the wet weight of the sandstone samples were smaller for the consolidation with the B67 and B72 solution, the amounts of B67 and B72 absorbed by the dried sandstones were found to be much higher than when testing Lascaux and the tested hydrophobic products showed better abilities to be absorbed by the sandstones than Lascaux. Despite the fact that the concentrations of the applied solutions containing B67, B72 and Lascaux were equivalent, the lowest uptake of Lascaux by the sandstones indicated that the absorption capacity of sandstone was reduced by water-based Lascaux.

7.7.2. Variations in appearance and colour

Figure 7.7.3 includes the images taken from the consolidated sandstones with B67, B72, Lascaux and Silres, which were visually compared. The visual observations of the sandstones, consolidated with B67, B72 and Silres, clearly showed the increased darkness in appearance and the sandstone samples became darker than the untreated sandstone surfaces after the treatments with all commercial consolidants. Particularly they were intensified for the hydrophobic B67 and B72 and significantly darker than Silres and Lascaux. The visual comparisons of the sandstones consolidated with B67 and B72 showed the wet and dark-coloured sandstones up to about 10 mm above the immersed sections while the similar darken and brownish appearance of the sandstones consolidated with B72 was only observed from the middle and top sections beyond this level, where visible changes attributed to the penetration of B67 were not detected. Although the consolidation treatments with Lascaux and Silres also darkened the sandstone appearance, the sandstones consolidated with Silres appear darker when compared with the resulting appearance of the sandstones treated with Lascaux. In contrast, the visual effect of Lascaux was considerably reduced and the consolidated sandstones resulted in the more visually similar appearance to the untreated sandstones.

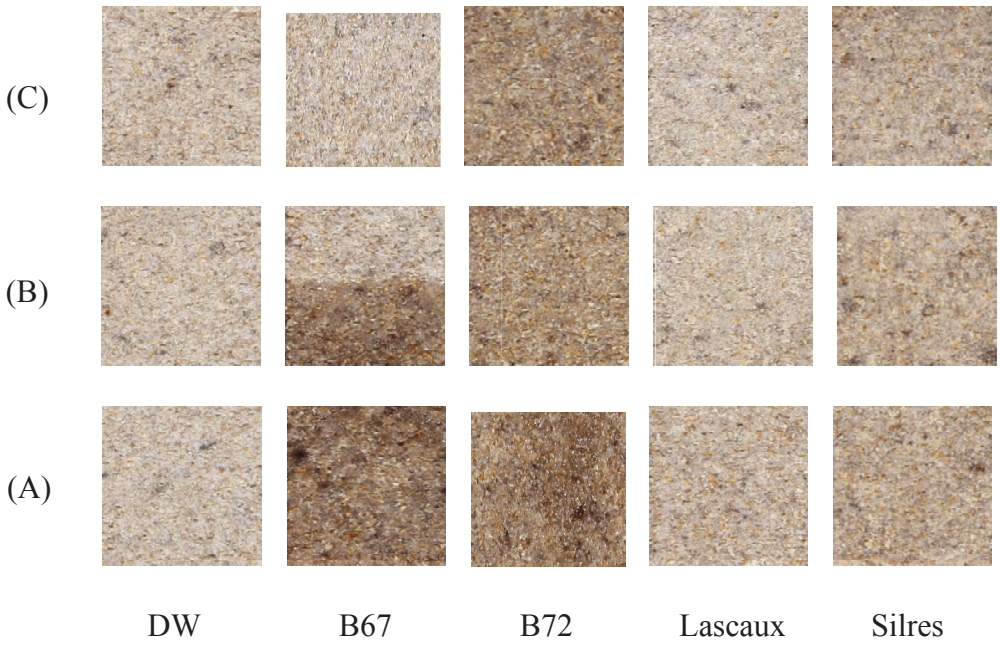

Figure 7.7.3. Comparison of the visual effects of B67, B72, Lascaux and Silres based on photographic images of consolidated sandstones obtained from (A) immersed, (B) middle and (C) top sections of the consolidated sandstone

Figure 7.7.4. compares the L *, a * and b * colour coordinate values of Silres, Lascaux, B72, and B67 and the reddening, yellowing and darkening of colours produced by all these consolidants were recognized by the increased a * and b * colour coordinate values and the decreased L* values. In comparison to Silres and Lascaux, the consolidation with B67 and B72 showed greater positive values of Δa*, Δb*, and ΔE and more negative values of ΔL* indicated extensive darkening, yellowing and reddening of the treated sandstones. Although the colour variations in the sandstones treated by B67 and B72 were visually comparable, the colorimetric analysis identified slightly increased reddening, yellowing and darkening effects of B72. Silres yielded greater reddening, yellowing and darkening effects than Lascaux, both of which were significantly lower than B67 and B72.

Agreeing with the visual appearance modifications, the colorimetric measurements detected that the total colour changes of the treated sandstones were found to decrease in the following order: B72 > B67 > Silres > Lascaux. All the consolidated sandstones had a ΔE greater than 10 and the observed total colour changes also indicated significant

colour changes and high incompatible risk of these consolidation treatments (Rodrigues & Grossi 2007).

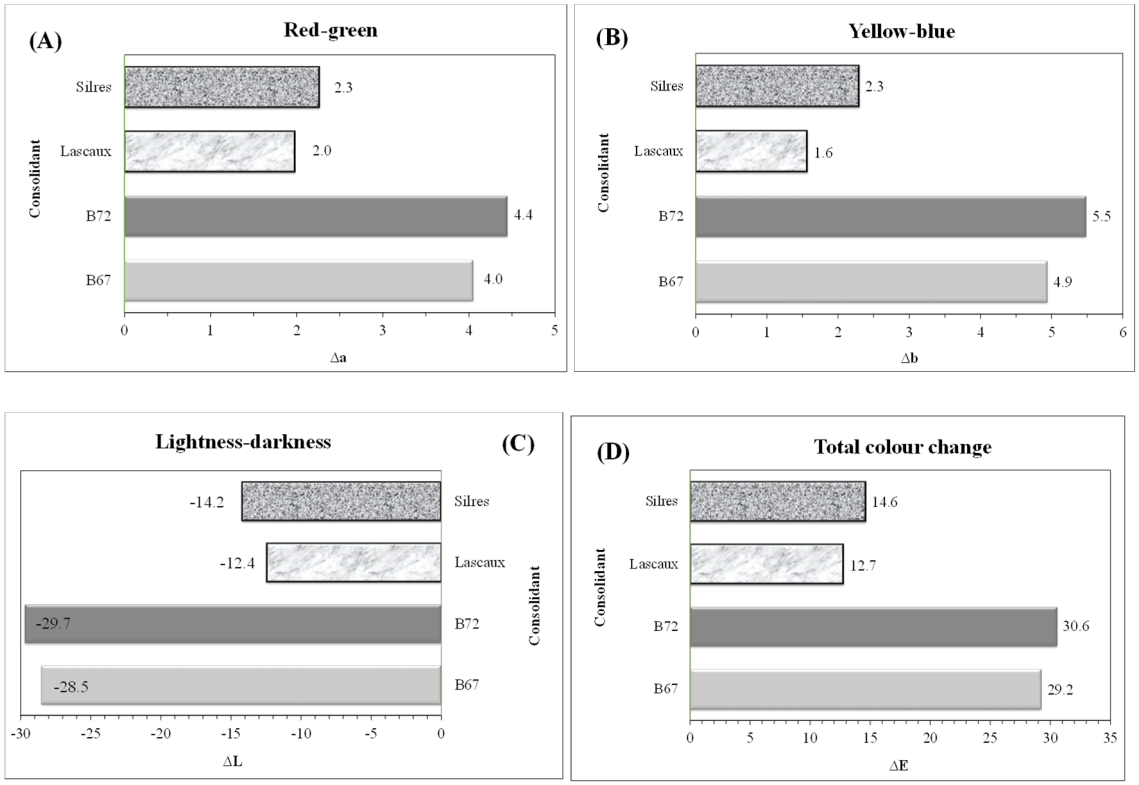

Figure 7.7.4. Comparison of (A) red-green component (a*), (B) yellow-green component (b*), (C) luminosity (L*) and (D) total colour caused by B67, B72, Lascaux and Silres from the images taken from the immersed sections of the treated sandstones

7.7.3. Water vapor permeability of consolidated sandstones

Water vapour permeability of the consolidated sandstone and their penetration depth were evaluated by the changes in weight of the silica gel and WVT values. Figure 7.7.5 shows the weight gains due to absorbed water vapour by silica gel which permeates through the sandstone samples consolidated by B67, B72, Silres and Lascaux and Figure 7.7.6 compares the averaged WVT values measured from the immersed, middle and top sections of the consolidated sandstones except for the middle section of the sandstones treated with B67. As can be seen from these Figures, the absorption curves and the WVT values measured from the all parts of the sandstone samples consolidated with all

commercial products showed decreased WVT values and diffusion rates of water vapour through the consolidated sandstones as compared with the untreated sandstone, suggesting that the water vapour permeabilities of the treated sandstones were reduced by the absorption and penetration of the consolidants. Besides the high WVT values for the topmost part of the sandstones treated with B67, both B67 and B72 produced the least permeable sandstones and the absorbed hydrophobic products significantly reduced the flow rate of water vapour through the treated sandstones.

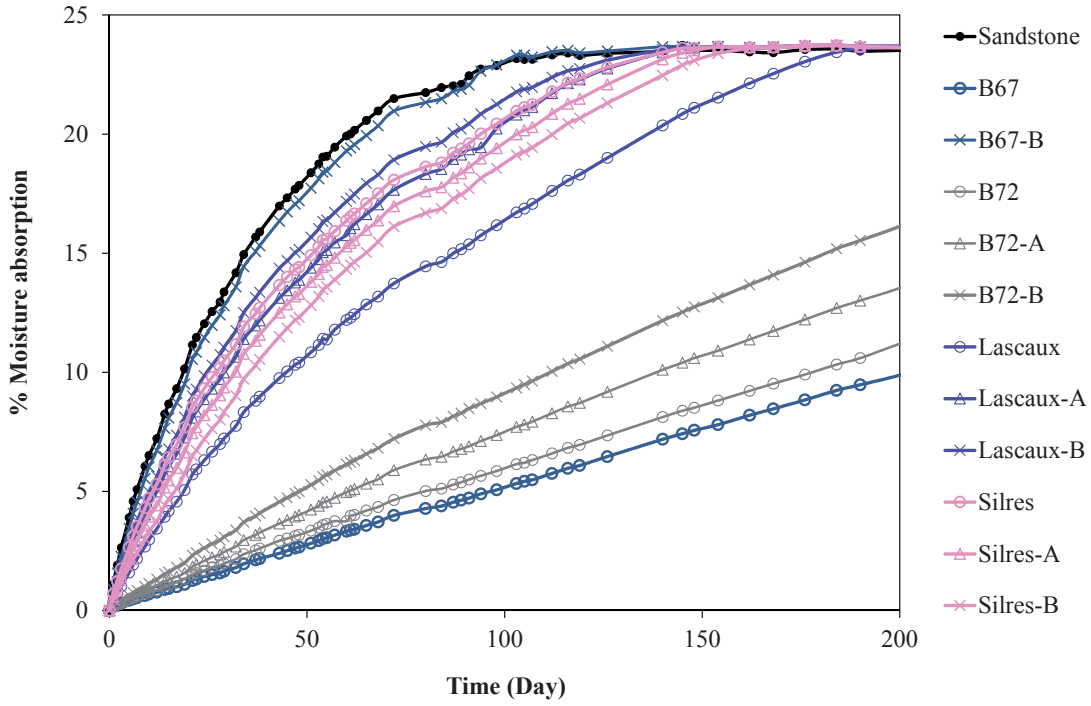

Figure 7.7.5. Moisture absorption by desiccant plotted against time detected from the untreated sandstone and the immersed, middle (A) and top (B) sections of sandstones consolidated with B67, B72, Silres and Lascaux

From the moisture absorption curves and the WVT values, considerable changes in water vapour permeabilities across the treated sandstones were detected. Lower WVT was observed for B67 as there was a tide mark in the B67 sample. The B67 sample has a WVT which is similar to sandstone suggesting that B67 did not penetrate to the top of the sample. B72 showed similar permeability for the immersed samples B67. B72, however,

penetrated through the whole sample. Increased permeability at middle and top suggests smaller amount of consolidants penetrating the sandstone with increasing height.

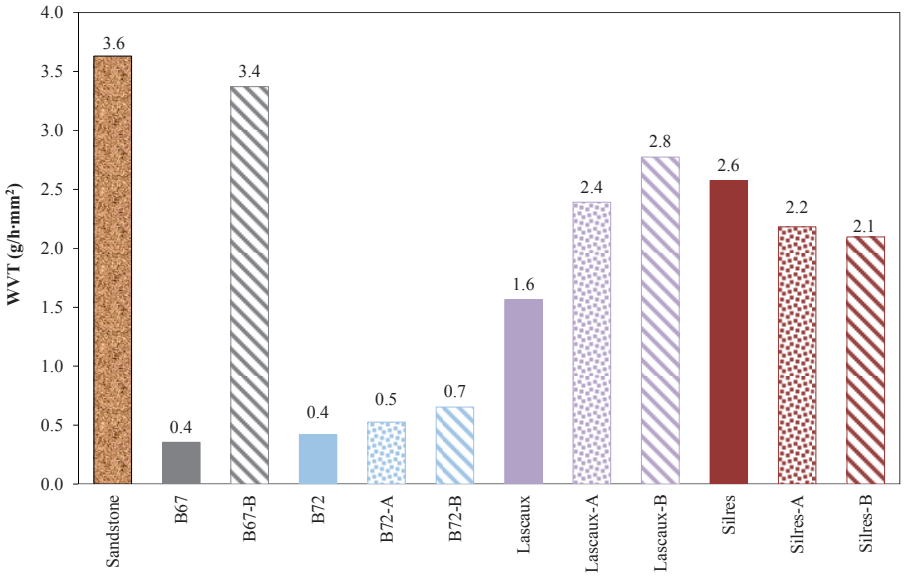

Figure 7.7.6. WVT values averaged from the immersed, middle (A) and top (B) sections of the sandstones treated with B67, B72, Lascaux and Silres

The greater WVT values of the sandstones consolidated with Lascaux were observed with increasing capillary rise length and the water vapour permeability was increased with increasing capillary rise penetration of Lascaux. The increased water vapour permeabilities of the sandstones treated with Lascaux on increasing capillary rise length were associated with the reduced amounts of Lascaux by capillary rise absorptions. In the case of Silres, a change in the opposite direction occurred. The WVT values were reduced with increasing capillary rise and the permeabilities of the penetrated section of the consolidated sandstones to water vapour were smaller than the ones observed for the immersed section. The penetrated parts exposed to moisture in air could undergo hydrolysis reaction with Silres and resulted in decreased permeability with increasing capillary rise distance.

By comparing the moisture absorption curves and the WVT values of Silres and Lascaux, it became obvious that water vapour diffusion through the sandstone treated with Silres was faster and the WVT values for Silres were greater than the ones for the immersed

section of Lascaux but comparable to the penetrated section of Lascaux. Despite the lower capillary absorption, Lascaux showed the slower or similar diffusion of water vapour and was incapable of producing better water vapour permeability than Silres. Provided the greater uptakes of Silres by the sandstones, Silres was more efficient to achieve the permeable samples compared with the immersed B67 sample and B72 which considerably restricted the permeabilities of the treated sandstones to water vapour. The high uptakes of Silres by the sandstones and the ability of Silres to prepare the consolidated sandstones that remained permeable to water vapour indicate the best result from the permeability test of the consolidated sandstones was produced by Silres.

7.7.4. Summary of consolidation treatment with commercial consolidants

The consolidation treatment of Sydney's yellow block sandstone was performed with four commercially available hydrophobic isobutyl methacrylate polymers, water soluble acrylic adhesive and ethyl silicate. In order to study the consolidation effects of different chemical nature on Sydney sandstone, the commercially synthesised stone consolidants were selected from the hydrophobic and hydrophilic polymers and silane-based material and their consolidation actions were compared. The evaluation of their consolidation performance on Sydney sandstone was made in terms of colour modifications, water vapour permeability, rate and depth of penetration and uptake of the applied consolidants.

The capillary rise penetration of the Lascaux and Silres solutions resulted in the almost identical rates and extents of their penetrations. Conversely, the penetration rate of the B67 and B72 solutions were considerably reduced and it is also notable that B67 has a much reduced capillary rise. It appears to indicate that the penetration rate of solvent is high for Lascaux and Silres and low for B67 and B72. The dry uptake of consolidant is greater for Silres and lower for Lascaux. Despite the better penetration of the Lascaux solutions, the absorbed amount of Lascaux was significantly restricted and the observed uptake of Lascaux was much smaller than B67 and B72. Silres resulted in the highest uptake after B72 and B67. With the fast and deep penetration of the Silres solution, the

treatment with Silres produced the best result, whereas the results showed the low penetration of B67 and uptake of Lascaux.

The water vapour permeabilities of the sandstones were reduced after the consolidation treatments. The permeabilities of the sandstones consolidated with Lascaux to water vapour did not differ considerably from the ones observed for Silres. In marked contrast, the hydrophobic consolidants resulted in low permeabilities of the consolidated sandstones to water vapour and produced the impermeable polymer films in the treated sandstones. Except for Silres, the water vapour permeabilities of the consolidated sandstones were increased with increasing capillary rise length and reducing absorbed amount of B67, B72 and Lascaux. Silres produced the decreased peameabilities for the penetrated sections of the treated sandstones that likely occurred by the hydrolysis reaction of Silres with moisture in air. Water vapour permeabilities give an indication of the permeability of the consolidant particularly for the immersed section showing high degree of permeability for Silres with a lower, but still high permeability for Lascaux. The permeability for the middle and to sections give an indication of the relative penetration of the consolidant which shows good penetration for B72, Silres and Lascaux. B67 has limited penetration. The water vapour permeability tests demonstrated the best ability of Silres to preserve the water vapour permeability of the consolidated sandstones with the highest uptake of Silres.

The consolidation with the commercial products presented obvious colour changes, but there was no considerable differences in appearance and colour measured by the visual and colorimeric analysis from the immersed, middle and top sections of the treated sandstones. The consolidants produced a darker appearance of the treated sandstones and the colorimetric evidence for the redder, yellower and darker sandstones, whereas the major contribution to the total colour change came from the increased darkness for all tested treatments. The colorimetric evaluations showed decreased total colour changes in the following order: B72 > B67 > Silres > Lascaux. Although the observed total colour changes were found to be greater than 10, indicating the significant changes in colour and appearance and high incompatible risk with respect to the appearance of treated

sandstones, Lascaux visually showed only a small colour change. Silres showed more colour changes but less than the B67 and B72.

Among the tested commercial consolidants, Silres outperformed in terms of uptake, penetration depth and water vapour permeability. Lascaux, however, showed much lower degree of colour change. The consolidation treatment with B67 and B72 was found to be incompatible with the tested sandstone as reflected by low permeability towards water vapour, low penetration depth and significant difference in colour change, apart from the higher absorptions. In comparison with B67 and B72, the treatment with Lascaux resulted in more compatible and better consolidation actions as to water vapour permeability, penetration depth and colour variations, but low uptake of Lascaux by the treated sandstone was observed.

7.8. Comparison of consolidation performance

7.8.1. Application of consolidants

In the current consolidation work, two approaches were employed to treat unweathered sandstone. Water based polymer consolidant systems were applied as polymer solutions or as monomer for in situ polymerisation. In the application of the preformed water-based consolidating systems, MMT, hydrophilic polymer and their composites were tested to evaluate the effects of their concentrations on their penetrations into and absorptions by sandstones. A key aspect of in situ polymerisation of AA and Am is to investigate the effects of changing concentrations of monomers and initiators on the in situ polymerisation process in an effort to improve the uptake of in situ polymerised AA and Am by sandstones. The rate and extent of penetration from the applied consolidating materials were visually evaluated by the capillary rise experiments and the absorbed amounts of applied consolidants were compared.

Comparisons in terms of capillary rise penetrations of the consolidating solutions showed clear differences in the penetration rates of the polymer and monomer solutions. Particularly, the absorption behaviours of sandstones were less affected by the low viscous solutions of all monomer concentrations. Despite the higher AA and Am concentrations, penetration rates of 2.5-20% monomer solutions were similar to DW and higher than the 2.5% PAA and PEG solutions. Even at 30-50% AA or Am concentrations, the AA and Am solutions penetrated at similar rates to 2.5% MMT, PAA-MMT, PAm, PAm-MMT and PEG-MMT solutions, 10% PEG solutions and 20% Lascaux solutions and they penetrated almost six times slower than DW. As observed for the monomer liquid Silres, the capillary rise experiments showed fast penetration of the AA and Am solutions through the pore network in the sandstone and demonstrated the obvious advantage of using the monomer solutions. In contrast, the penetration rates of polymer solutions were reduced, especially for 10% PAA and PAm solutions and 20% B72 and B67 solutions. Their penetrations were limited to 10~20 mm, and their penetration rates were significantly reduced by the high viscous solutions. Although the rates and extents of capillary rise penetration for the PAA and PAm solutions were reduced with increasing polymer concentrations, the penetration capacities of PEG were found to be superior to

PAm and PAA. Additionally, it was observed from PAA and PEG that the lower molecular weights of polymers resulted in higher capillary rise rates and the extent of capillary penetration was reduced for PAA250 solutions.

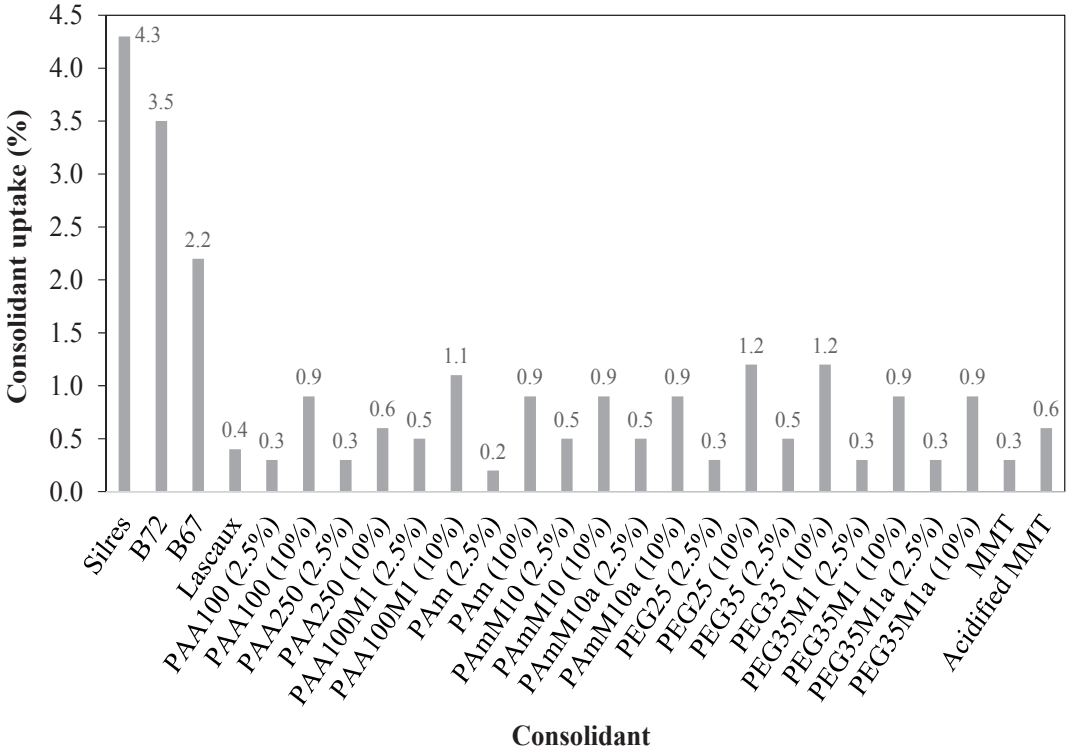

Figure 7.8.1. Dry weight increases in sandstones treated with PAA, PAm, PEG, MMT, composites, B67, B72, Lascaux and Silres

Considering the slower penetration rate of MMT suspension than polymer solutions at the same concentrations, the negative effect of MMT on the penetration rate was larger than polymers and the penetration ability of MMT was limited by water absorption of MMT in DW. For the PAA-MMT and PAm-MMT dispersions, the rates of penetration measured using the capillary rise method were slightly increased with decreasing MMT content and it seemed the water absorption of MMT was slightly inhibited due to the presence of PAA and PAm. In the case of PEGM dispersions, the rates of capillary rise of PEGM dispersions were similar at all MMT concentrations and the inhibitory effect of PEG was not clearly observed. For all polymer-MMT dispersions, the applied dispersions became viscous and it is likely the composite systems with high MMT loading are

inappropriate for the stone consolidation work. The reduced penetration observed for the composite systems at high MMT loading suggests the necessity of the polymer present in excess to form the network which acts as the consolidant. Overall, it was found that all applied consolidating materials penetrated to greater than 10 mm, although the presence of polymer and MMT decreased their capillary rise penetration rates.

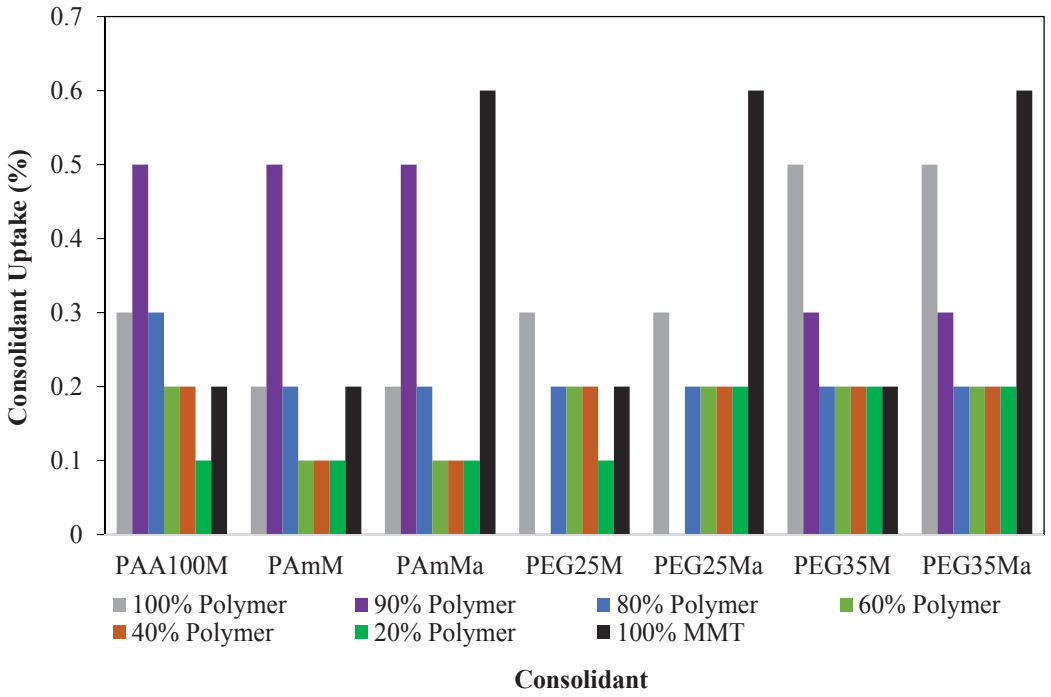

Figure 7.8.2. Capillary uptake of polymer-MMT composites by the sandstones

Despite the different capillary penetration rates observed for the polymer, MMT and their composite solutions, the uptakes of these consolidating materials on the sandstones after drying were relatively similar and the effect of different polymers on their absorbed amounts were found to be small as seen in Figure 7.8.1. At 10% polymer concentrations, the polymer uptakes ranged from 0.6% and 1.2% and the polymer uptakes by the sandstones were decreased in the order PEG > PAm, PAA100 > PAA250 and all polymer uptakes were increased with increasing polymer concentrations. The uptakes of PAA100M1 and PAmM10 were slightly larger than 10% PAA100 and similar to 10% PAm, whereas PEG uptakes by the sandstones were larger than the PEGM10. The uptakes of 10% PAA100M, 10% PAmM10 and 10% PEGM10 were found to be between

0.9 and 1.1% and the observed results were similar for all composites. Likewise, no effect of different polymers on the composite uptakes into the sandstones was observed for the 2.5% composites, but the weights of the treated sandstones were smaller (Figure 7.8.2).

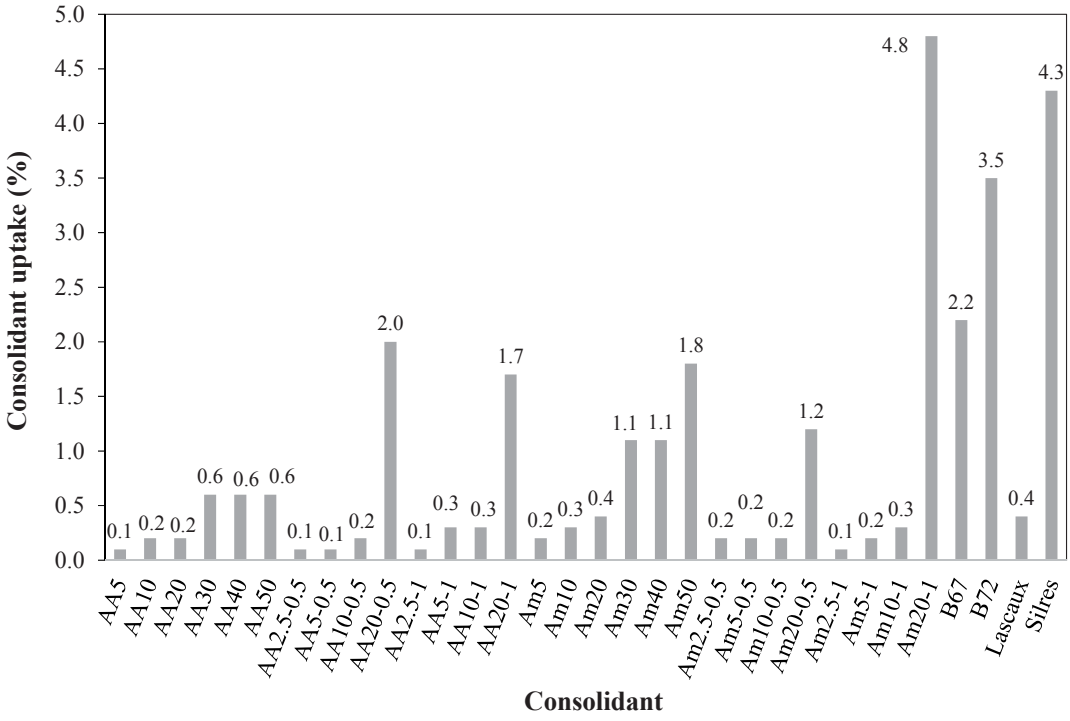

Figure 7.8.3. Dry weight increases in sandstones consolidated with B72, B67, Lascaux, Silres and AA and Am solutions with or without KPS

When the commercially available consolidants were compared, the consolidant uptakes were decreased in the order Silres > B72 > B67 > Lascaux. The uptakes of Lascaux were significantly smaller as seen for the tested series of polymers, MMT and composites, whereas the weight increases of the treated sandstones absorbed from the 10% polymers, 10% polymer-MMT10 and acidified MMT were found to be higher than Lascaux. These results revealed the water based consolidation systems were less effective in increasing the consolidant uptake from water compared with the hydrophobic B72 and B67 polymers from acetone and the uptakes of PAA, PAm and all polymer-MMT composites were limited by the increased viscosity of PAA and PAm and the swelling behaviour of MMT. PEG-MMT systems showed reduced consolidant uptake relative to PAA and PAm for MMT content with the higher MW polymer absorbing to a greater extent. For all of the

polymer-MMT consolidant systems, 90% polymer and 10% MMT appeared to be the optimised blend for consolidant uptake.

The consolidation treatment efficiency in terms of improving the consolidant uptake to sandstone caused by in situ polymerised water soluble AA and Am was evaluated. At 2.5-10% AA and Am in the presence of KPS, the weight increases of the treated sandstones were comparable at the same monomer and KPS concentrations (Figure 7.8.3). Several changes were observed when comparing the uptakes of AA with those of Am. In the absence of KPS, the Am uptakes on the sandstones were greater than the ones of AA and the results demonstrated better uptakes of Am than AA. Similarly, the weights of sandstones treated by 20% monomer solutions in the presence of KPS were larger, especially for the Am20-1 and the observed weight increases of sandstone after the in situ polymerisation of high Am concentration reacted with KPS were greater than Silres. At monomer concentrations lower than 20%, the uptakes of AA and Am were much smaller than Silres, B72 and B67. The weight increases of sandstones treated by 5-10% monomers in the presence of KPS were lower than Lascaux, 10% polymers and 10% composites. The observations revealed the in situ polymerisation of both AA and Am using less than 20% did not effectively improve the uptake of polymerised AA or Am.

7.8.2. Variations in appearance and colour

The consolidation efficiencies related to preservation of the original color and appearance of sandstones were visually and instrumentally assessed and the influences of MMT, polymers, polymer-MMT composites, in situ polymerised AA and Am, B72, B67, Lascaux and Silres were compared (Figure 7.8.4). The differences in the visual aspects of the sandstones treated with PAA and PAA-MMT composites were found by the darker and orange coloured surfaces, accounting for the oxidization reaction of iron-containing materials present in the sandstones. The treated sandstones showed the irregular distribution of the oxidized iron components and the treated surfaces became darker and

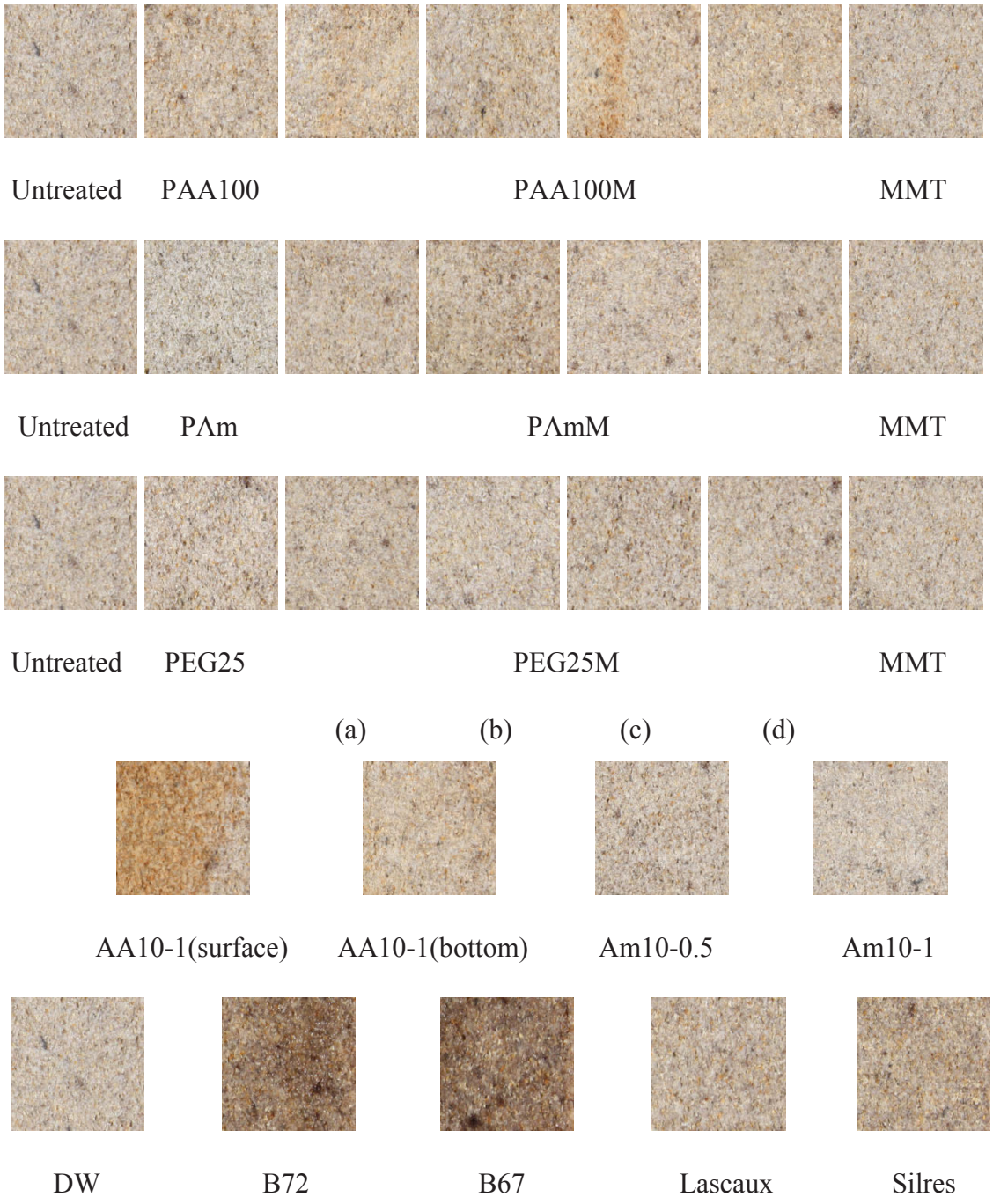

Figure 7.8.4. Images from immersed sections of sandstones treated with B72, B67, Lascaux, Silres, PAA100, PAm, PEG25 and polymer-MMT composites at (a) 20% MMT, (b) 40% MMT, (c) 60% MMT and (d) 80% MMT

more orange with increasing PAA concentrations. The sandstone appearance resulting from the treatments with PAm and PEG seemed to be more uniform and closer to the untreated sandstones and the sandstone surfaces treated with the composites comprising

of PAm or PEG with MMT as filler did not appear to be different, presenting the lower visual effects of PAm and PEG, as their colour and appearance remained unaltered at all MMT concentrations. The sandstones treated with PAm appear lighter in colour than the ones treated with the PAm-MMT composites, whereas PEG and PEG-MMT composites produced the similar changes in colour and appearance of the treated sandstones.

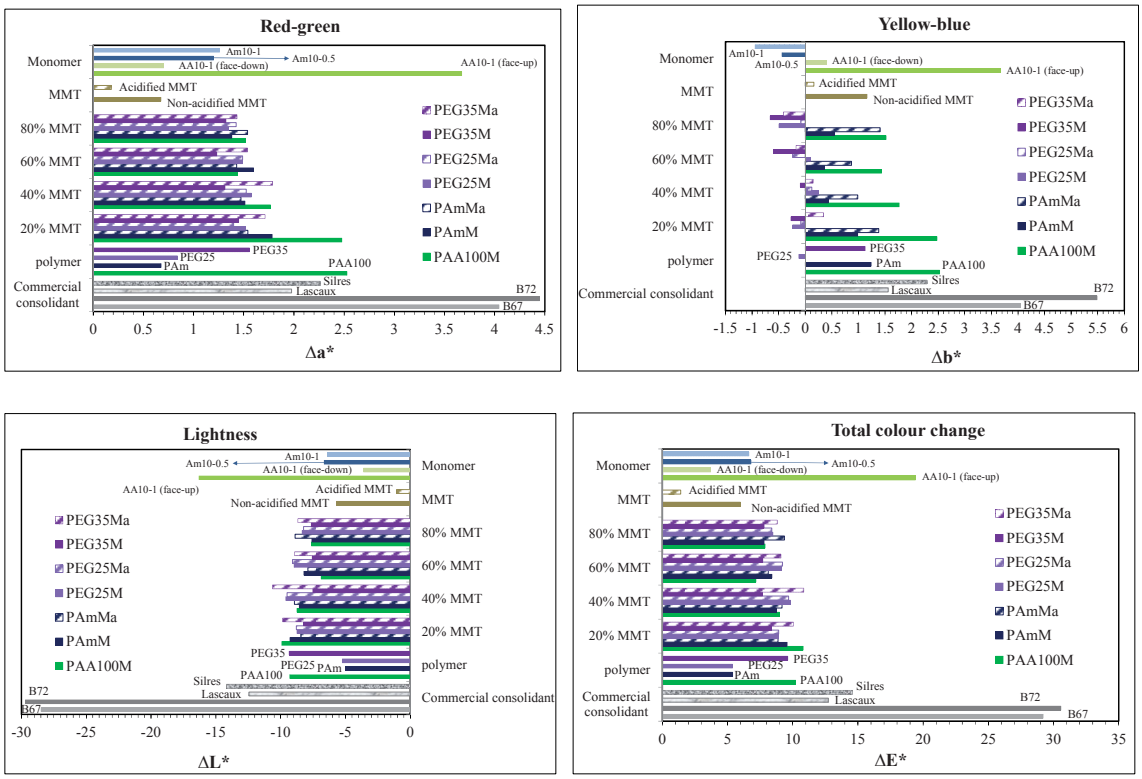

Figure 7.8.5. Variations in (A) red-green component (a*), (B) yellow-green component (b*), (C) luminosity (L*) and total colour alterations changed by MMT, PAA100, PAA250, PAm, PEG25, PEG35, B72, B67, Lascaux and Silres

In response to AA or in situ polymerised AA, the changes in oxidation state of the iron-bearing materials occurred and the treated sandstones resulted in the inhomogeneous treated surfaces similar to the treatments with PAA. The colour variations in the treated sandstones were greater than the ones observed for PAA and the treatments with AA, which resulted in the increased color modifications of the treated surfaces as seen from the images for AA10-1(surface). The tested Am assessed pertaining to appearance, color

and uniformity of the treated sandstones showed the similar visual effects to PAm, except for the visual observation of the cracks produced at Am concentrations greater than 10%.

The treated sandstones appeared relatively uniform, except for B67, which showed visible color changes up to 10mm positioned above the immersed sections. The sandstones treated with B72 and B67 showed the wet and darker appearance of sandstone surface and significant colour alterations were seen. The colour variations of the treatments with Lascaux and Silres were decreased, but the sandstones treated with Silres looked darker than the Lascaux. Based on the visually assessed sandstones, apparent changes of color to a red or orange color were observed for the sandstones treated with AA or PAm, but the changes in the colour and appearance of the treated sandstones were smaller after the treatments with MMT, PAm, PEG, PAm-MMT and PEG-MMT composites and in situ polymerised Am in comparison to B72, B67, Lascaux and Silres that produced darker surface appearance of the consolidated sandstones.

Figure 7.8.5 shows decreases in values for L* parameter and increased values for chromatic changes for all the samples. All treatments resulted in a decrease of stone surface brightness and an increase in redness. The treatment with PAA100 and PAA100M2 essentially affected a* and b* chromatic change due to increased yellowness and redness. The variations of the redness and darkness Δa^* and ΔL^* produced by PAm and PEG25 are similar and they underwent lower colour alterations than PAA and PEG35. PEG25 and PEG-MMT composites resulted in b* values toward the blueness, whereas yellowing effects of PAm and PAm-MMT composites were slightly increased. The comparable values of a* and L* were observed for all the polymer-MMT composites and the tested polymers and acid-treatment of MMT showed insignificant effects on the overall colour changes as reflected by their similar ΔE values. The change in the appearance of the exposed sandstone surface treated with KPS in situ polymerised AA, as shown in Figure 7.8.5, increased variation of the darkness, redness and yellowness and resulted in the largest colour changes of all tested consolidating materials in this study due to the high acidity reacting with the siderite releasing iron to the surface resulting in a rust colour. Conversely, the one side of the applied sandstone sample was laid down and dried and this bottom sides of the treated sandstones revealed smaller colour

alterations than polymers and composite samples as seen from the image of AA10-1(bottom) in Figure 7.8.4. Contrary to AA, both sides of the sandstone applied via capillary rise method indicated similar darkening, reddening and blueing effects and slight increases in total colour changes of Am more than PAm. Consistent with the visual observations, B67 and B72 produced drastic reductions in their L* values, the highest a*, b*, and ΔE values and exhibited the greatest darkening, yellowing and reddening effects to result in the highest total colour valuations. Silres and Lascaux induced darkening, yellowing and reddening of the treated sandstones and the darkening effect of Silres was greater. The sandstones treated with Silres reflected the darkest surface and the highest total colour valuations after B67 and B72.

With the exception of the difference in chromatic parameters towards the red and yellow associated with the treatments with PAA and AA, the main contribution to the total colour variations in ΔE was originated from the increases in darkness of the treated sandstones and the effects of a* and b* values were found to be small for most treated sandstones. Data obtained from the colorimetric measurements of the consolidated sandstones did not exhibit significant changes along with the capillary rise penetrations of the consolidants, but B67 only showed noticeable colour changes above the penetrated sections. The total colour alterations were found to decrease in the following order: B72 > B67 > AA10-1 > Silres > Lascaux > PAA > polymer-MMT composites, PEG35 > Am10 > MMT > PAm, PEG25 > acidified MMT. The measured ΔE values of most tested polymers and composites were in the range ΔE = 5 to 10 whereas B72, B67, AA10-1, Silres and Lascaux were found to be greater than 10. The combined results from the colorimetric detection and visual appearance indicated smaller alterations in colour and appearance of the consolidation treatments with polymers, polymer-MMT composites and Am in comparison to B72, B67, Silres and Lascaux.

7.8.3. Water vapor permeability of consolidated sandstones

The water vapour permeabilities of the sandstones consolidated with different consolidants and their penetrations were compared by the WVT values. Several changes

were observed when comparing the WVT values of the sandstones after the immersion of sandstone specimens in PAA, PAm, PEG, PAA-MMT, PAm-MMT, PEG-MMT composites, B67, B72, Lascaux and Silres solutions in Figure 7.8.6. Decreases in the WVT values of the sandstones treated with PEG and PEG-MMT composites were observed and PEG consolidants showed reduced permeability. While increasing polymer concentrations from 2.5 to 10% reduced the WVT values considerably, the sandstone treatments with PAA and PAm resulted in almost twice the reduction in the WVT values of the sandstone treated with PEG and the extents of decreases in the water vapour permeability of the sandstones treated with the higher concentrations of PAA and PAm were found to be greater than the ones of PEG.

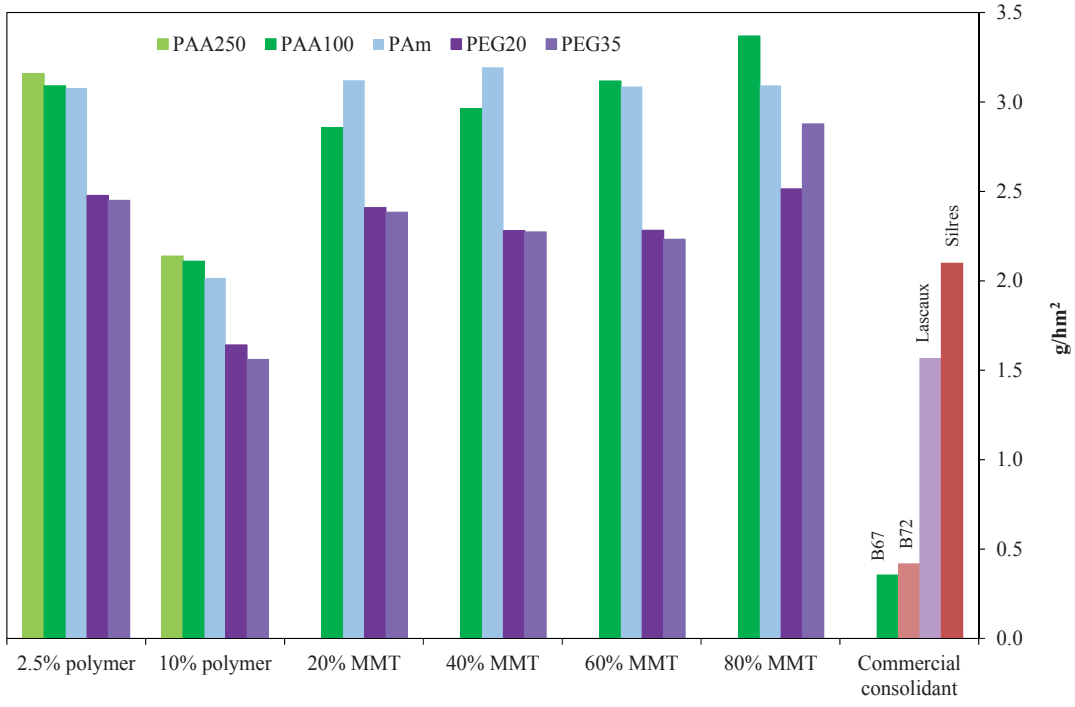

Figure 7.8.6. Comparison of WVT values measured after the immersion of 2.5 or 10% PAA, PAm and PEG and 2.5% composites comprising PAA, PAm or PEG with various MMT concentrations and commercial consolidants

As the MMT concentrations were increased, the sandstones immersed in PAA-MMT composites showed increased WVT values, whereas similar WVT values were observed for the treatments with PAm-MMT and PEG-MMT composites. After the immersion of

the sandstones in the polymer-MMT composites dispersions, the PAA-MMT composites increased the water vapour permeability of the treated sandstones with increasing MMT concentrations, but the effect of MMT concentrations on the water vapour permeability of the treated sandstones was found to be less important for the PAm-MMT and PEG-MMT composites. The PAm-MMT and PEG-MMT composites dispersions, regardless of acidification process of MMT, showed increased WVT values of the treated sandstones with increasing MMT concentrations, but the PEG-MMT composites over 20% MMT showed similar WVT values to the untreated sandstones from the topmost parts of the treated sandstones. The results indicated that by increasing the MMT concentration, the water vapour permeability of the treated sandstones was reduced by the PAA-MMT composite and the penetration of the PAm-MMT and PEG-MMT composites and the penetration was likely to be more limited by PEG-MMT composites.

In contrast to the composites that increased permeability of the treated sandstones with their penetration depths, the treatments with polymers produced similar WVT values measured from the penetrated portions of sandstones and the diffusion of all polymers were apparently allowed across the penetrated parts. Compared with the values obtained from the polymer penetrations, the immersed parts of the sandstones revealed smaller WVT values for treatments with PAA and PAm and similar WVT values for PEG. Apparently, the higher water vapour permeability resulted from the reduced penetration of PAA and PAm and similar water vapour permeability of the immersed and penetrated sandstones was attributed to the better penetrating ability of PEG through the sandstones. Unlike the tested water soluble polymers, the WVT values of the sandstones treated with the composites, B67, B72, and Lascaux were reduced with capillary penetration length and better penetration was observed by PAA, PAm and PEG.

Provided polymers penetrated evenly through the sandstones, the inhibitive effect of MMT caused by the water absorption of MMT was likely to be responsible for the increased water vapour permeability of the sandstones penetrated by the composites. It was suggested from the reduced penetration of the composites revealed by lower water vapour diffusion rates observed for composite penetration that the lower penetration of the composites through the sandstones decreased the uptake of the composites. The water

vapour permeability of the treated sandstone was found to decrease in the following order: MMT > composites > PAA, PAm > PEG > Lascaux > B67, B72, which mostly correlated with the amount of consolidant adsorbed by the sandstones and the penetration depth. The different results given by Silres was striking and the reduced permeability of the treated sandstones with increasing penetration depth reflected the best penetrating and consolidating ability of Silres, while the virtually impermeable sandstone surface to water vapour produced by the hydrophobic products likely resulted from their low penetrations though the sandstones. The higher penetration and absorption of PAA, PAm and PEG demonstrated better effectiveness of PAA, PAm and PEG than Lascaux.

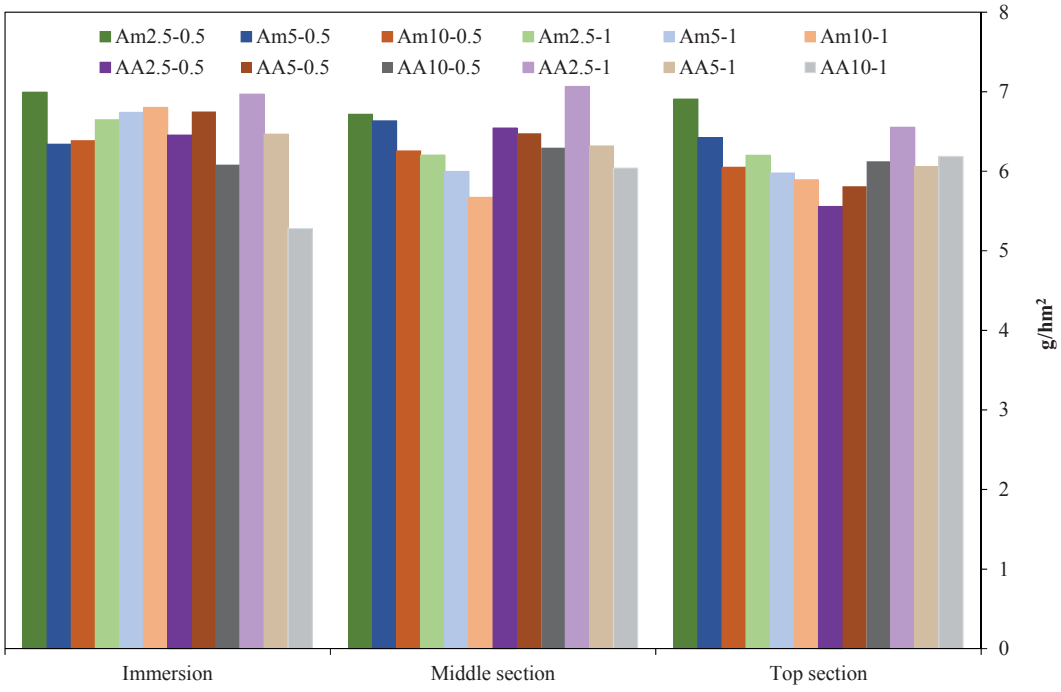

Figure 7.8.7. WVT values measured from the immersed, middle and topmost parts of the sandstones treated with 2.5, 5 and 10% AA or Am in the presence of 0.5 or 1.0 wt% KPS

Figure 7.8.7 shows the WVT values for the sandstones treated in the concentration range 2.5-10% of AA and Am with 0.5 or 1 % KPS. With increasing concentrations of AA and Am under the same KPS concentration, the values of WVT generally decreased after the treatments and the water vapour permeability of the treated sandstones were reduced. It showed for each identical concentration of monomer, increasing KPS concentration

resulted in smaller values of WVT from the penetrated parts of the treated sandstones, whereas higher KPS concentration did not show noticeable decreases in the WVT values of the sandstones treated with AA, except 10% AA, which produced the decreased WVT values of the immersed sandstones. As the concentrations of Am or KPS increased, the reductions in WVT values were seen from the penetrated parts of the treated sandstones and there was no clear difference in the WVT values between the middle and upper parts of the treated sandstones. Upon increasing AA and KPS concentration, the WVT values tended to decrease with increasing penetration depth of 2.5 or 5 % AA, but with decreasing penetration depth of 10% Am.

The observed changes in the WVT values showed decreases in the permeability of the treated sandstones to water vapour with increasing concentrations of monomer and KPS and were considered to be associated with increases in absorption and polymerisation degree of Am or AA. The decreased water vapour permeability observed for the penetrated sections of the sandstones treated with 1 wt % KPS with all Am or 2.5 and 5% AA could be caused by higher amounts of penetrated and polymerised Am or AA with time delay in the diffusion of water vapour through the treated sandstones. The tendencies of 10% AA to decrease the water vapour permeability of the immersed sandstones may be related to faster polymerisation of AA, resulting in the increased amount of absorbed and polymerised AA in the immersed sections and in the decreased penetration of AA. Even though the permeabilities of the treated sandstones to water vapour were reduced as with the increased uptake of the monomers, the WVT values produced by AA and Am showed relatively similar variations and the overall impacts of monomer type and the different concentrations of monomers and KPS on the changes in water vapour permeability of the treated sandstones were found to be small. In the range of tested concentrations, similar permeable sandstones to water vapour indicated unaltered risk of incompatible sandstone treatments, which in turn, revealed effective treatments at 10% AA or Am, without being significantly affected by the polymerised monomers in the treated sandstones.

7.8.4. Bending tests

This bending test of the consolidated sandstones was performed to evaluate the effects of selected consolidants on their mechanical characteristics in terms of their flexural stress and to compare their capabilities to consolidate the sandstone. As seen in Figure 7.8.8, the wide range of the flexural stress values obtained for the consolidated sandstones ranged from 382 to 1469 MPa. The measured standard deviation range from 0.1 to 1.1. The treatments with 10% monomer using 1.0 wt% KPS had greater bending strengths than any of the tested consolidants, but AA10-1 had significantly higher influence on the bending strength. The bending strengths were reduced for both Am and AA by 0.5 wt% KPS compared with 1.0 wt% KPS and the reduced strength of the sandstones consolidated with Am10-0.5 may be caused by the slower polymerisation reaction of Am. For the tested polymers, PAA100 showed the highest effect, followed by PAA250, PAm and PEG25, respectively. The results indicated PEG and PEG-MMT produced lower influences by attributing lesser and reduced bending strengths than PAA, PAm and their composites. Except for PAmM5, the composites reduced the bending strength of treated sandstones more than the polymers, but no effect, regarding acidification of MMT was observed.

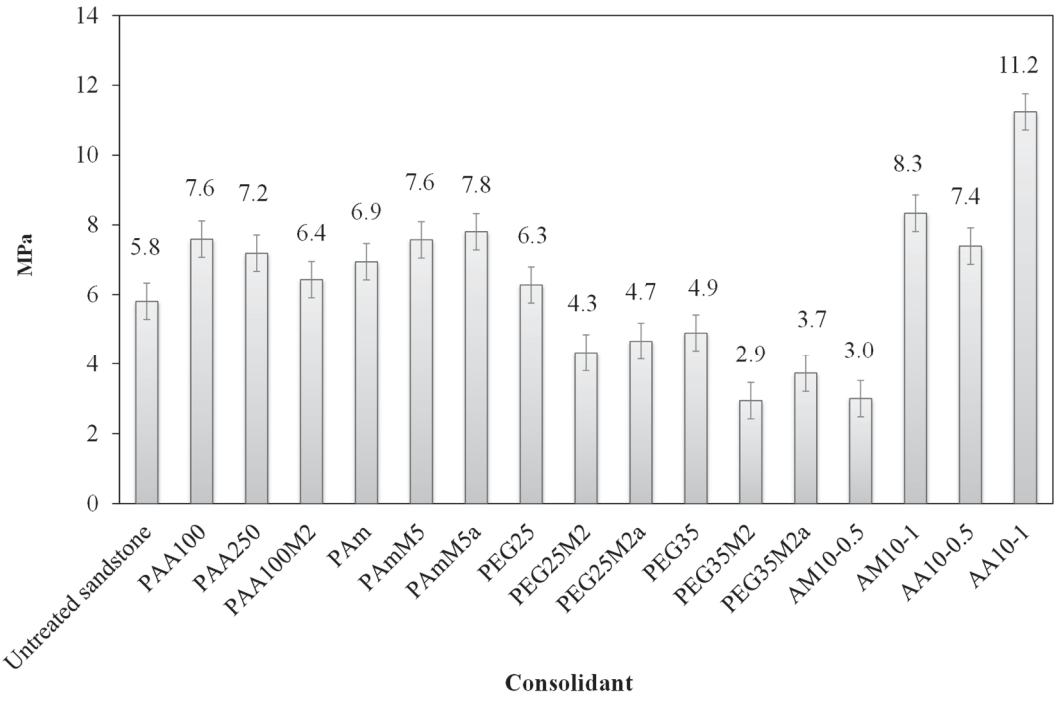

Figure 7.8.8. Overview bending strength results on Sydney sandstone

Based on the data determined for the bending strength of the consolidated sandstones, the potential durability of the consolidated sandstone can be evaluated and the results can be expressed in terms of binding and consolidating ability of the applied consolidating materials. Among the tested sandstones, the effect of PAA, PAm and their composites on the bending strength of the treated sandstones were found to be relatively similar but PAA was slightly greater than PAm and PAA100M2. Reinforcements were observed for the treatments with PAA and PEG in comparing with the sandstones consolidated with their composites. In contrast, the PAmM5 and PAmM5a were more effective to increase the consolidation action than PAm alone. The in situ polymerisation of AA and Am proved to produce the higher bending strengths with increasing KPS than the ones of PAA, PAm, PEG or their composite systems and the results indicate the better ability of in situ polymerised AA or Am to improve the binding and consolidating action.

7.8.5. Incompatibility of consolidation treatment

For consolidation treatment, the compatibility between consolidant and stone is an important consideration and the incompatible action of consolidant should be minimised (Rodrigues & Grossi 2007, Stück et al. 2008). The guidelines were given by Rodrigues & Grossi (2007) for treatment incompatibility in terms of bending strength, total colour difference and penetration depth. The reported indicators suggest the high risk of incompatible treatment when total colour difference is higher than 5 (Rodrigues & Grossi 2007). With the exception of acidified MMT, the polymers, MMT and composites resulted in the ΔE values greater than 5 and this indicator suggests high incompatibility risks for both consolidation treatments tested in this work and the commercial consolidants (Rodrigues & Grossi 2007). The total colour change was between 5 and 10 for the polymer, polymer-MMT composite and in situ polymerised AA and Am, whereas the total colour difference for the commercial consolidants showed greater than 10. Although the colorimetric analysis reveals high incompatibility risks and, therefore, considerable colour alteration of most treated sandstones, the higher degrees of incompatibility were observed for B67, B72, Silres and Lascaux in agreement with the visual inspection of the consolidated sandstones.

Considering incompatibility criteria, regarding penetration depth of consolidants, the risks of increasing harmful effects are high for consolidant penetration less than 5 mm, medium for 5-20 mm and low for higher than 20mm, according to the proposed indicators for consolidation treatment (Rodrigues & Grossi 2007). Comparison of the capillary rise penetration and water vapour permeability for the sandstones consolidated with polymers, polymer-MMT composite and in situ polymerised systems indicates the increased penetration of consolidants with increasing MMT content and the in situ polymerised AA or Am, compared with PAA or PAm. It follows that the incompatibility risk of consolidation treatment could be reduced by the higher concentrations of polymer in the composites and the in situ polymerisation of AA or Am. Although a higher risk of developing surface coating to impede diffusion of water vapour could be caused by the low penetration of MMT or the composites with high MMT contents, according to the proposed scale, the observed water vapour permeability remained unaffected by these treatments and the potential risk associated with the surface absorption of MMT and the composite systems was likely to be small. The low penetration determined by low water vapour permeability for B67 and B72 indicates increased incompatibility risk due to the superficial layer producing a barrier to diffusion of water vapour. The observed penetrations of Silres and Lascaux indicate reduced and similar incompatibility risk, compared with the ones of the polymers.

It has been proposed that an incompatibility in the mechanical properties of consolidated surface layers with the bulk sandstone could accelerate degradation. This may result from differing thermal expansions and strengths of the surface and bulk layers, producing a stress gradient in the sandstone, which may lead to fracture. Based on this potential risk for failure, Rodrigues and Grossi (2007) proposed a scale of high, moderate and low based on the relative strengths (25%, 10-25%, 0-10%). It suggests the high, medium and low incompatibility risks for the consolidation treatments with PAA100, PAA250 and PAA100M2, respectively (Rodrigues & Grossi 2007). The differences in bending strength between the untreated and sandstones consolidated with PAm, PAmM5 and PAmM5a were found to be greater than 10% and the results presented increased bending strength after the consolidation treatments with PAm, PAmM5 and PAmM5a at medium risk (Rodrigues & Grossi 2007). The sandstones treated with PEG25 showed 7.5% increase in bending strength and represented low incompatibility risk of this consolidation

treatment. The determined increases in mechanical strength indicated medium and high risks for the consolidation treatment with AA10-0.5 and AA10-1. The increased bend strength observed for Am10-1 indicated high risk of incompatible consolidation treatment.

The bending strengths observed for PAA, PAm and PAmM5 increased by more than 25%, indicating the levels of their incompatibility risks are greater than medium. Because the mechanical strengths of PAA-MMT or PAm-MMT composites appeared to be reduced with increasing MMT content, based on physical inspections of the treated sandstones, PAA-MMT or PAm-MMT composites with high MMT loading may be more favourable in view of better compatibility of MMT. Similarly, the large increases in bending strengths, resulting from the 10% monomer with 1.0 wt% KPS, may present incompatible treatments and the lower concentrations of monomers or KPS could be used to produce more compatible results. For the consolidation treatment of sandstone, however, consolidants are used as a means of imparting the structural strength of stones and adequate mechanical strength of the treated sandstones is essential to bind and to preserve the stone structure under combined actions of weathering processes. The bending test performed on the consolidated sandstones measured the changes in tensile forces of the treated sandstone. Therefore, the increased tensile forces of most consolidated sandstones indicate the greater consolidation action to reduce crack propagation and the in situ polymerisation method presented the better consolidation result to make the treated sandstones mechanically more durable. Based on the scale, the tested consolidants are in the low-high risk category; however, the development of a consolidant system will require durability trials in addition to the experiments carried out in this study.

7.9. Conclusions on consolidation of Sydney sandstone

This chapter intended to evaluate the consolidation performance of water soluble polymers, MMT and polymer-MMT composites in Sydney sandstones consolidated with aqueous polymers or monomers for in situ polymerisation. The consolidation effects of water based consolidation systems on Sydney sandstone was compared with the stone consolidating materials which are commonly used in consolidation work and their effectiveness were evaluated based on penetration and uptake of consolidants as well as

changes in colour, appearance, water vapour permeability and mechanical strength. In effort to establish the optimal conditions for the tested water based consolidating materials, the effects of their concentration and preparation conditions on the consolidation performance were studied.

The capillary rise experiments performed on Sydney sandstone revealed the similar extent of penetration of most tested consolidating solutions. The penetration rate and extent of consolidating solutions to sandstones were affected by not only solution viscosity but also the molecular size. The obvious benefit of using in situ polymerisation method was their fast penetration. The penetration rates were reduced with increasing solution viscosity caused by water absorbing MMT and higher concentration of polymer and composites. The observations presented better penetrating ability of PEG than the other tested polymers but the limiting effect of MMT on the rate and depth of penetrations was greater than the polymers. The penetration depth of all the tested consolidants exceeded 10 mm and all tested polymers, MMT, composites and monomers showed satisfactory penetration for Sydney sandstone.

The major concern of using the tested polymer, MMT, their composites and in situ polymerisation of Am and AA was their low uptake by the sandstones. The problem regarding the absorptions of such aqueous consolidants made of water soluble polymers or MMT was the increment in solution viscosity especially for MMT that absorbed water, restricted their penetrations and concentrations and resulted in the reduced absorption of the composite using low concentration of polymer-MMT composite. In addition to the better penetration ability, the in situ polymerisation of AA and Am provided the higher weight gains comparable to Silres and the hydrophobic consolidants but the limiting factor to this method has been the detrimental effects of rigid polymerised materials over 10% monomers.

Consistent with capillary rise absorption studies, the water vapour permeabilities of the treated sandstones were generally reduced with the absorbed amounts of consolidants, the presence of MMT and increasing concentrations of polymers, monomers and initiator and

the similar results were observed for the composites and the in situ polymerisation under 20% AA or Am. The hydrophobic consolidants produced the lowest water vapor permeabilities but Silres was most effective to preserve the water vapor permeability. All tested water soluble polymers showed better ability to maintain more permeable sandstones than Lascaux but PEG reduced water vapor permeability due to its higher absorption and better penetration compared with PAA and PAm. Due to the greater restriction of MMT on the penetration depth, the water vapour permeabilities of the composites were higher than polymers. With unaltered compatibility deprived of significant effect of the in situ polymerised monomers, using 10% monomers was most effective.

As far as the visual and colorimetric comparisons of the treated sandstones are concerned, the effects of PAm, PAm-MMT, PEG, PEG-MMT and in situ polymerisation of Am on the changes in color and appearance of treated sandstones were smaller than those of the commercial consolidants and they produced more uniformly coloured surfaces. Conversely, AA, PAA and PAA-MMT in response to the oxidization reaction of iron-containing materials existing in the sandstones imparted darker and orange coloured sandstones and their irregular distributions exhibited the inhomogeneous appearance. While the in situ polymerisation of Am produced the small chromatic aspects of the treated sandstones, the undesirable cracks formed by the in situ polymerisation reactions over 10% monomers together with the color reduction observed for the in situ polymerisation of AA suggested the in situ polymerisation of 10% AA or Am to satisfy the need for the preservation of Sydney sandstone appearance.

Despite the smaller or comparable uptakes compared with those of the polymers and composites, the in situ polymerisation of 10% AA or Am displayed the greater effects on the mechanical characteristics and the increase in bending strength with increasing KPS concentrations likely due to the higher degree of polymerisation of the monomer at ambient temperature. The order of the increase in bending strength after the treatments with the polymers was PAA100 > PAA250 > PAm > PEG25 > PEG35 and the composites reduced the bend strengths irrespective of the acid-modification of MMT. The results suggested the higher concentrations of PEG or PEG-MMT composites to improve the

mechanical strength of the treated sandstones. The in situ polymerisation method is considered to be more favourable than polymers or composites to improve the consolidation action on the treated sandstones. As far as the incompatibility level of the treated sandstones is concerned, the composites or the in situ polymerised Am or AA using the lower KPS concentrations may be more effective than PAA, PAm or high monomer/initiator concentrations.

Considered from compatibility criteria, the hydrophobic B67 and B72 consolidants were least compatible treatments due to significant colour changes and low penetrations and water vapour permeabilities. While the tested consolidants are incompatible based on the evaluation of the total colour changes, Silres and Lascaux showed the higher levels of visual and calorimetric compatibility. Regarding the incompatibilities associated with the consolidation penetrations, Silres was found to be the most compatible and Lascaux produced similar incompatibility degree to the tested water soluble polymers. Although increasing polymer concentrations can enhance consolidation action and penetration, the higher MMT contents may be used to improve the chemical compatibility. The increased penetration and mechanical strength of the in situ polymerisation was the considerable advantage relative to the polymers but using minimum KPS concentrations could be more effective, considering the increased risk of incompatible effect, as revealed by the substantial increases in bending strength and crack formation with increasing KPS concentrations.

From the practical viewpoint of the consolidation treatment of Sydney sandstone, Silres and the water based materials were more suitable than the hydrophobic consolidants based on the color modifications and low water vapour permeability of the treated sandstones. While offering deep penetration depth, high absorption and good water vapor permeability, Silres can limit the successful consolidation treatments of Sydney sandstones mainly due to the darken color appearance. Compared with Lascaux, the consolidation performances of pre-formed polymers were found to be better whereas the composites and the in situ polymerisation under 20% monomers were comparable. Despite their small absorptions, the water based systems can offer a means of providing mild surface treatments that are compatible with Sydney sandstone without significantly modifying the sandstone properties.

CHAPTER 8. CONCLUSIONS

8.1. Introduction

The weathering of Sydney sandstone in Sydney's heritage buildings is of concern as it has the potential to result in loss of buildings of significant cultural value. In response to the weathering of the heritage buildings in Sydney, this research attempted to develop consolidating systems to prevent or to slow down further deterioration of the sandstone. The most classes of commercially available consolidating materials present some disadvantages because they do not satisfy the fundamental requirement of physico-chemical compatibility with Sydney sandstone and consequently the development of more effective and compatible consolidation treatment for Sydney sandstone buildings is a goal of this thesis. A good consolidant for Sydney sandstone building should meet considerations concerning the important role of water flow in the sandstone building system and the structural deterioration of natural clay mineral binder in the weathered Sydney sandstone reported as the major cause of Sydney sandstone weathering.

This research, dealing with the development of water based consolidating materials, was performed to assess their suitability for use in stone consolidation work on Sydney sandstone. The experimental work, as discussed in the previous chapters, involved preparing, characterising and evaluating sandstone consolidating systems based on water soluble or dispersible materials and was tasked with achieving the identification of optimal preparation conditions and establishment of the rationale behind their consolidation performances in pursuit of the research objectives. This project assessed the degree to which the water based materials are suitable as sandstone consolidants and this research objective was achieved to the extent that the laboratory tests have demonstrated the effective use of the aqueous consolidants for the surface treatment of unweathered Sydney sandstones, which may provide the structural and mechanical performance of the treated sandstones subjected to progressive weathering.

The aim of the development of consolidation treatment for Sydney sandstone was to use water dispersible MMT, as well as water soluble polymers, monomers and initiators. Among the water based systems prepared using preformed polymers or polymer precursors in the presence or absence of MMT, the consolidation treatments were conducted using PAA, PAm or PEG, with or without their intercalation process into MMT gallery, or in situ polymerisation of AA or Am without MMT. Due to the hydrophilic interaction and miscibility with MMT, the water soluble polymer was an effective intercalating agent for providing the uniform and easy dispersion of MMT particles. The development of consolidating treatments using water based consolidation systems was considered to be satisfactory to some degree in the sense of achieving the reasonably simplified and fast consolidation treatments of Sydney sandstone.

8.2. Hydrophilic polymer-MMT composites

In order to realise the full potential of the tested water soluble polymers, monomers or initiator, or water dispersive MMT and their composites, this study has determined the effects of various experimental parameters, such as preparation conditions, their concentrations, nature and molecular weight of polymers and acid-modification of MMT. In the range of parameters employed, the contributions of temperature, time, molecular weights and acidification of MMT were negligible in modifying the structural, morphological and interactional aspects of the composites and their effects upon the intercalation behaviours of polymers, interlayer separation of MMT or consolidation actions were insignificant. The pre-treatment of MMT through the disagglomeration process and homogenization of MMT aided by ultrasonication was the most important preparation step governing the absorption behaviour of polymers.

Undoubtedly, the ratio of polymer and MMT was a key factor in determining the characteristics and consolidation efficiency of the composites and all composites generally followed similar changes in the intercalation behaviour, MMT dispersion, structural variations, intermolecular interactions between polymer and MMT, thermal stability and consolidation effectiveness. The interlayer absorption of polymers is likely

to reduce swelling capacity of the MMT while the crosslinking effect of MMT is likely to aid surface consolidation. On the other hand, the intercalation process of all polymers produced the intercalated structure of MMT at all ratios of MMT to all polymers, with the possible partial exfoliation at low MMT contents and the overall effect of polymer-MMT ratios on the interlayer penetrations of the polymers were largely limited.

The changes in the morphology and interlayer space of MMT, bonding environment and thermal stability of polymer with MMT identified critical concentration of 50-60% MMT for saturation of the MMT galleries, above which little or no further intercalation occurs, where the composite structures considerably changed and the upper limit on the interlayer expansion of MMT occurred. At high MMT concentrations there is too little polymer. At low MMT concentrations there is an excess of polymer thus galleries are filled. With increasing polymer concentrations, there were gradual increases in adsorbed polymer chains, separation of MMT particles, uniformity and transparency of the produced films, going from states of varying degrees of MMT agglomeration to states of micro-particles dispersed in the polymer based system due to this structural transition. In contrast, the large MMT agglomerates mostly existed in the non-intercalated form, where the swelling phenomena was caused by the absorbed interlayer water and the reduced penetration through the sandstones render the microstructure unsuitable for sandstone consolidation.

In addition to the ratios of polymer:MMT in the composites, the nature of polymers had direct effect on the characteristics of the composites and consolidation efficiency of the polymers and their composites. The results obtained by all three polymers and their composites loaded with MMT have shown a similar trend, but the extents to which the observed changes occurred were dependent on the nature of polymers. Compared with PAA and PEG, the changes in the lattice expansion of MMT and thermal stability of pre- and in situ formed PAm were more gradual and continuous upon increasing PAm concentrations and the intercalation degree of PAm was greater than those of PAA and PEG, causing the formation of the smaller stacked MMT layers in the PAm-MMT composites. The extent of interlayer expansion of MMT was greater after the in situ polymerisation of Am and was increased for short mixing times. Even though the extents

and behaviours of PAA and PEG intercalation were rather similar, the stacked MMT lamellae in the PAA matrix were more random in orientation.

Because of the hydrophilic nature of the polymers, the similar dispersion patterns of MMT resulted from the hydrophilic interaction and the polymers were linked with MMT through the physical interaction involved in changes in hydrogen bonds of carboxyl or amide group and ion-dipole forces without the formation of strong covalent bonds. In the MMT rich side, corresponding to the extensive polymer intercalation, the polymer incorporation into MMT was associated with breaking self-associated hydrogen bonds of PAA or PAm, or distorting conformation and reducing crystallinity of intercalated PEO chains. Beyond the upper limit, PAm interacted with the hydrated interlayer sodium cation or hydroxyl group of MMT and established a stronger hydrogen bond than in situ polymerised PAm in the presence of MMT. The most of intercalated PAA was found to be in undissociated form and the better interaction between PAA and MMT is demonstrated by the increased thermal stability of PAA in the composites than PAm and PEG. Unlike PAA or PAm, the absorbed PEG interacted with the internal MMT surface and considerably improved thermal stability.

8.3. Consolidation treatment of Sydney sandstone

Despite the possible use of the composites up to 60% MMT for the consolidation treatment of Sydney sandstones, according to the structural characterisation, the uptake and penetration of the composites by the sandstones were reduced with increasing the MMT concentrations and the absorption of the composites were significantly reduced over 10% MMT. As the ability of intercalated and adsorbed polymers to prevent the swelling of MMT due to water absorption was limited, increasing polymer concentration was more effective in improving uptake and penetration and the intercalated or adsorbed PEG was a less effective inhibitor than PAA and PAm. Since the inhibitory effect of MMT on the penetration or absorption of the composites into the sandstone was greater than polymer and the overall influence of MMT on appearance and water vapour permeability of the sandstones treated with the composites was negligible, it was more practical to

apply low MMT contents, less than 20% MMT. The reduced penetration of MMT composites does however have an advantage that the surface of porous degraded stones may be better consolidated by these composites and further testings is required to demonstrate their efficacy. Higher MMT contents could be effectively applied to improve the compatibility levels associated with not only chemical aspect, but also the reduced impacts of colour changes caused by PAA and excessive strength produced by PAA and PAm.

The higher polymer concentrations were effective in increasing polymer uptakes, but increased concentration adversely affected penetration, colour and water vapour permeability, suggesting the importance of designing optimised concentrations that maximise consolidation effectiveness and minimise these negative influences. Although PEG provided good colour match with the sandstone and higher levels of penetration and uptake than PAA and PAm, using higher PEG concentrations to enhance the mechanical strength of the treated sandstone can also reduce the water vapour permeability and colour compatibility. Even with the reduced penetration and uptake of PAA and PAm, the better consolidation performance of PAm was revealed by penetration in the Sydney sandstone and the reduced colour variations, unlike PAA, which caused the orange coloured appearance due to acid catalysed oxidization of the Fe(II) in siderite.

Comparisons made between commercial consolidants and water based consolidants provided a way of determining the consolidation performance under the identical consolidation condition. The higher uptakes in the treated sandstone from the hydrophobic polymeric consolidants than the aqueous consolidation systems were achieved, but their low penetrations, significant colour change and poor permeability made them unsuitable and incompatible as consolidants in Sydney sandstone. The consolidating capacity of Silres was well above those of the hydrophobic and aqueous consolidants as determined by higher uptake, good penetration and water vapour permeability, but the satisfactory use of Silres as sandstone consolidant was restricted by the darker appearance caused by the treatment. In contrast, the results did not show considerable differences in its consolidating capacity between Lascaux and the aqueous consolidants, based on PAA, PAm, PEG and their composites.

This work also considered the suitability of in situ polymerisation of water soluble monomers and initiators, so that the unreacted and smaller monomers were applied onto and polymerised within the sandstone in an attempt to increase uptake and penetration. The consolidation effectiveness, performed with persulfate as initiator, revealed the upper limit of 10% AA or Am for this method. In contrast to the polymers and composites, the in situ polymerisation method showed fast and good penetrating capability, but the crack formation developed at 20% AA and at 10% Am + 1% KPS solution. Despite the general increase in the uptake and water vapour permeability with increasing the concentration of monomer and KPS, the impact of monomer and KPS concentrations on overall performance was considered to be small under 20% monomers. The optimum concentrations were found to be 10% for the treatment with both AA and Am resulting in improved consolidating properties while reducing incompatibility such as those colour change. Even with the small uptakes by the sandstones, the in situ polymerisation at 10% monomers produced higher mechanical strength than the polymers and composite. The better consolidation action though the in situ polymerisation of Am indicated some practical implications in the treatments of Sydney sandstones, but the situ polymerisation of AA indicated some limitations arising from the greater colour changes and decreased penetration due to its slightly higher polymerisation rate.

8.4. Concluding remarks

In terms of overall impact on the consolidation performance of the aqueous consolidants, the effects of different polymers were likely to be low and the consolidation effectiveness of all composites was considered to be similar. Compared with Lascaux, the consolidation effects of the polymers and composites were comparable or improved properties of the polymer, polymer-MMT composite and in situ polymerised consolidants were yielded with respect to the commercial Lascaux consolidant based on the laboratory tests carried out. The consolidation treatments with the tested polymers, composites and the in situ polymerisation method showed satisfactory results in comparison to Lascaux and the consolidating efficiencies of the developed water based consolidating materials has been satisfied to the extent that the consolidation performance demonstrated mild action, without letting the treated sandstones change their characteristics significantly and the

alterations mainly found from the treated surfaces could possibly be reversed to some degree.

In summary, the experiments performed using ultrasonication technique to disperse MMT in the matrixes of PAA, PAm and PEG demonstrated the fast, straightforward and efficient preparation of the polymer-MMT composite dispersions for the consolidation treatments of Sydney sandstone. In summary, it can be concluded that encouraging results were obtained from the water soluble polymer alone or in combination with low contents of MMT and the in situ polymerisation of 10% AA or Am as aqueous consolidants offer a potential means to develop more effective and compatible consolidation treatment of weathered Sydney yellow block sandstone.

REFERENCES

Abdelhak, M., Abdelkarim, H. & Barbara, I. 2012, 'Effect of plant fiber-polyacrylamide blend on retention and evaporation water at arid and semi-arid soils of Algeria', *Journal of Chemistry and Chemical Engineering*, vol. 6, no. 1, pp. 7-17.

Abraham, T., Ratna, D., Siengchin, S. & Karger-Kocsis, J. 2009, 'Structure and properties of poly (ethylene oxide)-organo clay nanocomposite prepared via melt mixing', *Polymer Engineering & Science*, vol. 49, no. 2, pp. 379-90.

Adams, J.M. & McCabe, R.W. 2013, 'Clay minerals as catalysts' in Bergaya, F. Legaly (eds), *Handbook of clay science*, 2nd edn, Elsevier, Amsterdam, pp. 541-581.

Ahmadi, S., Huang, Y. & Li, W. 2004, 'Synthetic routes, properties and future applications of polymer-layered silicate nanocomposites', *Journal of materials science*, vol. 39, no. 6, pp. 1919-25.

Akelah, A. 1995, 'Nanocomposites of Grafted Polymers onto Layered Silicate', in P. Prasad, J. Mark & T. Fai (eds), *Polymers and Other Advanced Materials*, Springer US, pp. 625-44.

Akimkhan, A. 2013, 'Adsorption of polyacrylic acid and polyacrylamide on montmorillonite', *Russian Journal of Physical Chemistry A*, vol. 87, no. 11, pp. 1875-80.

Al Gahtani F. 2017, 'Petrology, Diagenesis and Reservoir Quality in the Hawkesbury Sandstone, Southern Sydney Basin, Australia', *Journal of Geology & Geophysics*, vol. 6, no. 3, p. 283.

Alateyah, A.I., Dhakal, H.N. & Zhang, Z.Y. 2013, 'Processing, Properties, and Applications of Polymer Nanocomposites Based on Layer Silicates: A Review', *Advances in Polymer Technology*, vol. 32, no. 4, pp. n/a-n/a.

Albdiry, M., Yousif, B., Ku, H. & Lau, K. 2013, 'A critical review on the manufacturing processes in relation to the properties of nanoclay/polymer composites', *Journal of Composite Materials*, vol. 47, no. 9, pp. 1093-115.

Alessandrini, G., Aglietto, M., Castelvetro, V., Ciardelli, F., Peruzzi, R. & Toniolo, L. 2000, 'Comparative evaluation of fluorinated and unfluorinated acrylic copolymers as

water-repellent coating materials for stone', *Journal of Applied Polymer Science*, vol. 76, no. 6, pp. 962-77.

Alexander, L.E. 1969, 'X ray diffraction methods in polymer science', Wiley Interscience, New York.

Alexander, M.R., Payan, S. & Duc, T.M. 1998, 'Interfacial interactions of plasma-polymerized acrylic acid and an oxidized aluminium surface investigated using XPS, FTIR and poly (acrylic acid) as a model compound', *Surface and interface analysis*, vol. 26, no. 13, pp. 961-73.

Alexandre, M. & Dubois, P. 2000, 'Polymer-layered silicate nanocomposites: preparation, properties and uses of a new class of materials', *Materials Science and Engineering: R: Reports*, vol. 28, no. 1–2, pp. 1-63.

Anandhan, S. & Bandyopadhyay, S. 2011, *Polymer nanocomposites: from synthesis to applications*, INTECH Open Access Publisher, Rijeka

Anderson, R., Ratcliffe, I., Greenwell, H., Williams, P., Cliffe, S. & Coveney, P. 2010, 'Clay swelling—a challenge in the oilfield', *Earth-Science Reviews*, vol. 98, no. 3, pp. 201-16.

Aranda, P., Mosqueda, Y., Pérez-Cappe, E. & Ruiz-Hitzky, E. 2003, 'Electrical characterization of poly(ethylene oxide)–clay nanocomposites prepared by microwave irradiation', *Journal of Polymer Science Part B: Polymer Physics*, vol. 41, no. 24, pp. 3249-63.

Aranda, P. & Ruiz-Hitzky, E. 1992, 'Poly (ethylene oxide)-silicate intercalation materials', *Chemistry of Materials*, vol. 4, no. 6, pp. 1395-403.

Aranda, P. & Ruiz-Hitzky, E. 1994, 'New polyelectrolyte materials based on smectite polyoxyethylene intercalation compounds', *Acta Polymerica*, vol. 45, no. 2, pp. 59-67.

Aranda, P. & Ruiz-Hitzky, E. 1999, 'Poly(ethylene oxide)/NH4+-smectite nanocomposites', *Appl. Clay Sci.*, vol. 15, no. 1-2, pp. 119-35.

Arnold, H. & Chung, D.D.L. 1993, 'Review of X-ray diffraction', in D.D.L. Chung, P.W. DeHaven, H. Arnold, D. Ghosh (ed.), X-ray diffraction at elevated temperatures, VCH Publishers Inc., New York, pp.1-74.

ASTM Standard international 2010, Standard Test Methods for Flexural Properties of Unreinforced and Reinforced Plastics and Electrical Insulating Materials, D790–10, *ASTM international*, West Conshohocken, PA 19428-2959, United States.

ASTM Standard international 2011a, Standard Practice for Calculation of Color Tolerances and Color Differences from Instrumentally Measured Color Coordinates, D2244 – 09b, *ASTM international*, West Conshohocken, PA 19428-2959, United States.

ASTM Standard international 2011b, 'Standard Test Methods for Water Vapor Transmission of Materials', E96/E96M–10, *ASTM international*, West Conshohocken, PA 19428-2959, United States.

ASTM Standard international 2012, 'Standard Practice for Maintaining Constant Relative Humidity by Means of Aqueous Solutions', E104–02, *ASTM international*, West Conshohocken, PA 19428-2959, United States.

Australian Bureau of Statistics 2016, *3101.0 - Australian Demographic Statistics, Dec 2015,* Canberra, viewed 18 August 2016, < http://www.abs.gov.au/ausstats/abs@.nsf/mf/3101.0>.

Australian Government Bureau of Meteorology 2016a, *Monthly highest temperature*, Canberra, viewed 18 August 2016,< http://www.bom.gov.au/jsp/ncc/cdio/weatherData/av?p_nccObsCode=40&p_display_type=dataFile&p_startYear=&p_c=&p_stn_num=066062 >.

Australian Government Bureau of Meteorology 2016b, *Monthly rainfall*, Canberra, viewed 18 August 2016, <http://www.bom.gov.au/jsp/ncc/cdio/weatherData/av?p_nccObsCode=139&p_display_type=dataFile&p_startYear=&p_c=&p_stn_num=066062>.

Australian Government Department of the Environment n.d., *Australia's World Heritage List*, Canberra, viewed 27 May 2016, <https://www.environment.gov.au/heritage/places/world-heritage-list>.

Australian Government Department of the Environment and Energy n.d., *Climate change impacts in Australia*, Canberra, viewed 18 August 2016, <https://www.environment.gov.au/climate-change/climate-science/impacts>.

Australian Government Productivity Commission 2006, *Conservation of Australia's Historic Heritage Places: Productivity Commission Inquiry Report*, April 2006, No. 37, Canberra, viewed 24 May 2016, <http://www.pc.gov.au/__data/assets/pdf_file/0011/92369/ heritage.pdf>.

Australian Radiation Protection and Nuclear Safety Agency 2016, *Australian UV Index Models*, Canberra, viewed 18 August 2016, <http://www.arpansa.gov.au/uvindex/models/syduvmodel.htm>.

Avena, M. J., Pauli, C. P. D., 1998, 'Proton Adsorption and Electrokinetics of an Argentinean Montmorillonite', *Journal of colloid and interface science*, vol.202, no.1, pp. 195–204.

Bae, S. & Inyang, H.I. 2006, 'Confirmation of aqueous polymer sorption on contaminant barrier clay using TGA', *Journal of materials in civil engineering*, vol. 18, no. 2, pp. 307-10.

Baglioni, P., Giorgi, R. & Dei, L. 2009, 'Soft condensed matter for the conservation of cultural heritage', *Comptes Rendus Chimie*, vol. 12, no. 1-2, pp. 61-9.

Balek, V., Málek, Z., Yariv, S. & Matuschek, G. 1999, 'Characterization of Montmorillonite Saturated with Various Cations', *Journal of Thermal Analysis and Calorimetry*, vol. 56, no. 1, pp. 67-76.

Baltá-Calleja, F.J. & Vonk, C.G. 1989, *X-ray scattering of synthetic polymers*, vol. 8, Elsevier, New York.

Bell, F.G. 1993, 'Durability of carbonate rock as building stone with comments on its preservation', *Environmental Geology*, vol. 21, no. 4, pp. 187-200.

Bellamy, L.J. 1980, The infrared spectra of complex molecules, 2nd edn, Chapman and Hall, New York.

Belova, V., Andreeva, D.V., Möhwald, H. & Shchukin, D.G. 2009, 'Ultrasonic Intercalation of Gold Nanoparticles into Clay Matrix in the Presence of Surface-Active

Materials. Part I: Neutral Polyethylene Glycol', *The Journal of Physical Chemistry C*, vol. 113, no. 14, pp. 5381-9.

Benavente, D., Martínez-Martínez, J., Cueto, N. & García-del-Cura, M.A. 2007, 'Salt weathering in dual-porosity building dolostones', *Engineering Geology*, vol. 94, no. 3–4, pp. 215-26.

Bergaya, F., Legaly, G. 2013, 'General introduction: clays, clay minerals, and clay science' in Bergaya, F. Legaly (eds), *Handbook of clay science*, 2nd edn, Elsevier, Amsterdam, pp. 1-19.

Bernabeu, A., Expósito, E., Montiel, V., Ordóñez, S. & Aldaz, A. 2001, 'A new electrochemical method for consolidation of porous rocks', *Electrochemistry Communications*, vol. 3, no. 3, pp. 122-7.

Berry, J. 1994, 'The encapsulation of salt by consolidants used in stone conservation', *Institute of archaeology*, vol. 5, pp. 29-37.

Berry, R.W., Bergaya, F & Lagaly, G 2006, 'Teaching clay science: a great perspective' in Bergaya, F. Legaly (eds), *Handbook of clay science*, 1st edn, Elsevier, Amsterdam, pp. 1183-1194.

Besra, L., Sengupta, D., Roy, S. & Ay, P. 2004, 'Influence of polymer adsorption and conformation on flocculation and dewatering of kaolin suspension', *Separation and Purification technology*, vol. 37, no. 3, pp. 231-46.

Besson, G. & Drits, V. 1997, 'Refined relationships between chemical composition of dioctahedral fine-grained mica minerals and their infrared spectra within the OH stretching region. Part I: Identification of the OH stretching bands', *Clays and Clay Minerals*, vol. 45, no. 2, pp. 158-69.

Bhat, V., Shivakumar, H.R., Rai, K.S. & Sanjeev, G. 2014, 'Effect of electron beam irradiation on physico-chemical properties of polyacrylamide films', *Radiat. Eff. Defects Solids*, vol. 169, no. 2, pp. 137-43.

Biasci, L., Aglietto, M. & Ruggeri, G. 1995, 'Functionalization of montmorillonite by acrylamide polymers containing side-chain ammonium cations', *Polymers for Advanced Technologies*, vol. 6, no. 10, pp. 662-70.

Billingham, J., Breen, C. & Yarwood, J. 1997, 'Adsorption of polyamine, polyacrylic acid and polyethylene glycol on montmorillonite: an in situ study using ATR-FTIR', *Vibrational Spectroscopy*, vol. 14, no. 1, pp. 19-34.

Bishop, M.D., Kim, S., Palomino, A.M. & Lee, J.-S. 2014, 'Deformation of "tunable" clay–polymer composites', *Applied Clay Science*, vol. 101, pp. 265-71.

Biswal, D.R. & Singh, R.P. 2004, 'Characterisation of carboxymethyl cellulose and polyacrylamide graft copolymer', *Carbohydrate Polymers*, vol. 57, no. 4, pp. 379-87.

Biswas, M. & Ray, S.S. 2001, 'Recent progress in synthesis and evaluation of polymer-montmorillonite nanocomposites', *New polymerization techniques and synthetic methodologies*, Springer, pp. 167-221.

Blake, C.D. 1967, *Fundamentals of modern agriculture*, Sydney University Press, Sydney.

Bleam, W.F., 1990, 'The nature of cation-substitution sites in phyllosilicates', *Clays and Clay Minerals*, vol.38, no.5, pp.527-536.

Bohor, B. & Hughes, R.E. 1971, 'Scanning electron microscopy of clays and clay minerals', *Clays and Clay Minerals*, vol. 19, no. 1.

Bolto, B. & Gregory, J. 2007, 'Organic polyelectrolytes in water treatment', *Water Research*, vol. 41, no. 11, pp. 2301-24.

Borgia, G.C., Camaiti, M., Cerri, F., Fantazzini, P., & Piacenti, F. 2003, 'Hydrophobic Treatments for Stone Conservation: Influence of the Application Method on Penetration, Distribution and Efficiency', *Studies in Conservation*, vol.48, no.4, pp. 217-226.

Bortel, E., Hodorowicz, S. & Lamot, R. 1979, 'Relation between crystallinity degree and stability in solid state of high molecular weight poly (ethylene oxide) s', *Die Makromolekulare Chemie*, vol. 180, no. 10, pp. 2491-8.

Bossert, J., Ožbolt, J. & Grassegger, G. 2004, 'Finite-element modelling of the conservation effects of an artificial resin on deteriorated heterogeneous sandstone in building restoration', *Environmental Geology*, vol. 46, no. 3, pp. 323-32.

Bottero, J., Bruant, M., Cases, J., Canet, D. & Fiessinger, F. 1988, 'Adsorption of nonionic polyacrylamide on sodium montmorillonite: Relation between adsorption, ξ potential, turbidity, enthalpy of adsorption data and 13C-NMR in aqueous solution', *Journal of colloid and interface science*, vol. 124, no. 2, pp. 515-27.

Boulet, P., Bowden, A.A., Coveney, P.V. & Whiting, A. 2003, 'Combined experimental and theoretical investigations of clay-polymer nanocomposites: intercalation of single bifunctional organic compounds in Na+-montmorillonite and Na+-hectorite clays for the design of new materials', *J. Mater. Chem.*, vol. 13, no. 10, pp. 2540-50.

Bowen, D.K. & Tanner, B.K. 1998, *High resolution X-ray diffractometry and topography*, Taylor & Francis, London; Bristol, PA.

Boyer, D.W. 1987, 'A Field and Laboratory Testing Program: Determining the Suitability of Deteriorated Masonries for Chemical Consolidation', *APT Bulletin*, vol. 19, no. 4, pp. 45-52.

Brigatti, M. F., Galan, E., Theng, B.K.G. 2013, 'Structure and mineralogy of clay mineralogy of clay minerals' in Bergaya, F. Legaly (eds), *Handbook of clay science*, 2nd edn, Elsevier, Amsterdam, pp. 21-51.

Broadbent, J. 2002, 'Attitudes', in G. Deirmendjian (ed.), Sydney sandstone, Craftsman House, Sydney, pp. 95-97.

Brus, J.í. & Kotlík, P. 1996a, 'Cracking of Organosilicone Stone Consolidants in Gel Form', *Studies in Conservation*, vol. 41, no. 1, pp. 55-9.

Brus, J. & Kotlík, P. 1996b, 'Consolidation of Stone by Mixtures of Alkoxysilane and Acrylic Polymer', *Studies in Conservation*, vol. 41, no. 2, pp. 109-19.

Bugani, S., Camaiti, M., Morselli, L., Van de Casteele, E. & Janssens, K. 2007, 'Investigation on porosity changes of Lecce stone due to conservation treatments by means of x-ray nano- and improved micro-computed tomography: preliminary results', *X-Ray Spectrometry*, vol. 36, no. 5, pp. 316-20.

Bugani, S., Camaiti, M., Morselli, L., Van de Casteele, E. & Janssens, K. 2008, 'Investigating morphological changes in treated vs. untreated stone building materials by x-ray micro-CT', *Analytical and Bioanalytical Chemistry*, vol. 391, no. 4, pp. 1343-50.

Bujdák, J., Hackett, E. & Giannelis, E.P. 2000, 'Effect of Layer Charge on the Intercalation of Poly(ethylene oxide) in Layered Silicates: Implications on Nanocomposite Polymer Electrolytes', *Chemistry of Materials*, vol. 12, no. 8, pp. 2168-74.

Bumbaru, D. 2002, Heritage at risk: ICOMOS world report 2001/2002 on monuments and sites in danger, Saur.

Burchill, S., Hall, P., Harrison, R., Hayes, M., Langford, J., Livingston, W., Smedley, R., Ross, D. & Tuck, J. 1983, 'Smectite-polymer interactions in aqueous systems', *Clay Miner*, vol. 18, no. 4, pp. 373-97.

Burrows, H.D., Ellis, H.A. & Utah, S.I. 1981, 'Adsorbed metal ions as stabilizers for the thermal degradation of polyacrylamide', *Polymer*, vol. 22, no. 12, pp. 1740-4.

Çatalgil-Giz, H., Giz, A., Alb, A.M. & Reed, W.F. 2004, 'Absolute online monitoring of acrylic acid polymerization and the effect of salt and pH on reaction kinetics', *Journal of applied polymer science*, vol. 91, no. 2, pp. 1352-9.

Cardell, C., Delalieux, F., Roumpopoulos, K., Moropoulou, A., Auger, F. & Van Grieken, R. 2003, 'Salt-induced decay in calcareous stone monuments and buildings in a marine environment in SW France', *Construction and Building Materials*, vol. 17, no. 3, pp. 165-79.

Cardiano, P., Ponterio, R.C., Sergi, S., Lo Schiavo, S. & Piraino, P. 2005, 'Epoxy-silica polymers as stone conservation materials', *Polymer*, vol. 46, no. 6, pp. 1857-64.

Cariati, F., Rampazzi, L., Toniolo, L. & Pozzi, A. 2000, 'Calcium Oxalate Films on Stone Surfaces: Experimental Assessment of the Chemical Formation', *Studies in Conservation*, vol. 45, no. 3, pp. 180-8.

Carrado, K.A. 2000, 'Synthetic organo- and polymer-clays: preparation, characterization, and materials applications', *Applied Clay Science*, vol. 17, no. 1-2, pp. 1-23.

Carretero-Gonzalez, J., Valentin, J.L., Arroyo, M., Saalwaechter, K. & Lopez-Manchado, M.A. 2008, 'Natural rubber/clay nanocomposites: Influence of poly(ethylene glycol) on the silicate dispersion and local chain order of rubber network', *Eur. Polym. J.*, vol. 44, no. 11, pp. 3493-500.

Carretti, E., Dei, L. & Baglioni, P. 2003, 'Solubilization of Acrylic and Vinyl Polymers in Nanocontainer Solutions. Application of Microemulsions and Micelles to Cultural Heritage Conservation', *Langmuir*, vol. 19, no. 19, pp. 7867-72.

Carretti, E. & Dei, L. 2004, 'Physicochemical characterization of acrylic polymeric resins coating porous materials of artistic interest', *Progress in Organic Coatings*, vol. 49, no. 3, pp. 282-9.

Carta, L., Calcaterra, D., Cappelletti, P., Langella, A. & de'Gennaro, M. 2005, 'The stone materials in the historical architecture of the ancient center of Sassari: distribution and state of conservation', *Journal of Cultural Heritage*, vol. 6, no. 3, pp. 277-86.

Carver, S.R. 1940, Official Year Book of the Commonwealth of Australia No. 33 - 1940, Commonwealth Bureau of Census and Statistics, Canberra.

Casadio, F. & Toniolo, L. 2004, 'Polymer Treatments for Stone Conservation: Methods for Evaluating Penetration Depth', *Journal of the American Institute for Conservation*, vol. 43, no. 1, pp. 3-21.

Caulfield, M.J., Hao, X., Qiao, G.G. & Solomon, D.H. 2003, 'Degradation on polyacrylamides. Part I. Linear polyacrylamide', *Polymer*, vol. 44, no. 5, pp. 1331-7.

Celik, M.S., 2004, 'Electrokinetic behaviour of clay surfaces' in F. Whypych & K.G. Satyanarayana (eds), *Clay surfaces: Fundamentals and applications*, 1st edn, Elsevier, London, pp. 57-89.

Chaiko, D.J. 2003, 'New Poly(ethylene oxide)-Clay Composites', *Chem. Mater.*, vol. 15, no. 5, pp. 1105-10.

Chang, F.-R.C., Skipper, N. & Sposito, G. 1995, 'Computer simulation of interlayer molecular structure in sodium montmorillonite hydrates', *Langmuir*, vol. 11, no. 7, pp. 2734-41.

Chang, F.-R.C., Skipper, N. & Sposito, G. 1998, 'Monte Carlo and molecular dynamics simulations of electrical double-layer structure in potassium-montmorillonite hydrates', *Langmuir*, vol. 14, no. 5, pp. 1201-7.

Charola, A.E., Tucci, A. & Koestler, R.J. 1986, 'On the Reversibility of Treatments with Acrylic/Silicone Resin Mixtures', *Journal of the American Institute for Conservation*, vol. 25, no. 2, pp. 83-92.

Chauhan, A. & Chauhan, P. 2014, 'Powder XRD technique and its applications in science and technology', *Journal of Analytical & Bioanalytical Techniques*, vol. 2014.

Chen, B. & Evans, J.R.G. 2005a, 'X-ray diffraction studies and phase volume determinations in poly(ethylene glycol)-montmorillonite nanocomposites', *Polym. Int.*, vol. 54, no. 5, pp. 807-13.

Chen, B. & Evans, J. 2005b, 'On the thermodynamic driving force for polymer intercalation in smectite clays', *Philosophical magazine*, vol. 85, no. 14, pp. 1519-38.

Chen, B., Evans, J.R., Greenwell, H.C., Boulet, P., Coveney, P.V., Bowden, A.A. & Whiting, A. 2008, 'A critical appraisal of polymer-clay nanocomposites', *Chemical Society Reviews*, vol.37, no.3, pp.568-594.

Cheraghian, G., Nezhad, S.S.K., Kamari, M., Hemmati, M., Masihi, M., Bazgir, S., 2014, 'Adsorption polymer on reservoir rock and role of the nanoparticles, clay and SiO2', *Int Nano Lett*, vol. 4, no. 9, pp. 38-41.

Cheremisinoff, N.P. 1996, *Polymer characterization*, Noyes Publications, Westwood, N.J.

Chiantore, O., Lazzari, M., Aglietto, M., Castelvetro, V. & Ciardelli, F. 2000, 'Photochemical stability of partially fluorinated acrylic protective coatings I. Poly(2,2,2-trifluoroethyl methacrylate) and poly(1H,1H,2H,2H-perfluorodecyl methacrylate-co-2-ethylhexyl methacrylate)s', *Polymer Degradation and Stability*, vol. 67, no. 3, pp. 461-7.

Chiavarini, M., Gaggini, F., Guidetti, V. and Massa, V 1993, 'Stone protection: from perfluoropolyethers to polyfluorourethanes. Proc. Int. Symp. UNESCO/RILEM, Paris', pp. 725-32.

Chin, I.-J., Thurn-Albrecht, T., Kim, H.-C., Russell, T.P. & Wang, J. 2001, 'On exfoliation of montmorillonite in epoxy', *Polymer*, vol. 42, no. 13, pp. 5947-52.

Chrissopoulou, K., Andrikopoulos, K.S., Fotiadou, S., Bollas, S., Karageorgaki, C., Christofilos, D., Voyiatzis, G.A. & Anastasiadis, S.H. 2011, 'Crystallinity and Chain

Conformation in PEO/Layered Silicate Nanocomposites', *Macromolecules (Washington, DC, U. S.)*, vol. 44, no. 24, pp. 9710-22.

Chrissopoulou, K., Fotiadou, S., Frick, B. & Anastasiadis, S.H. 2013, 'Structure and Dynamics in Hydrophilic Polymer/Layered Silicate Nanocomposites', *Macromol. Symp.*, vol. 331-332, no. 1, New Polymeric Materials and Applications, pp. 50-7.

Choi, H.J., Kim, S.G., Hyun, Y.H. & Jhon, M.S. 2001, 'Preparation and rheological characteristics of solvent-cast poly (ethylene oxide)/montmorillonite nanocomposites', *Macromolecular rapid communications*, vol. 22, no. 5, pp. 320-5.

Choudhary, S. & Sengwa, R. 2011, 'Ionic conduction and relaxation processes in melt compounded poly(ethylene oxide)-lithium perchlorate trihydrate-montmorillonite nanocomposite electrolyte', *Indian Journal of Engineering & Materials Sciences*, vol. 18, no. 2, pp. 147-56.

Choudhary, S. & Sengwa, R.J. 2014, 'Intercalated clay structures and amorphous behavior of solution cast and melt pressed poly (ethylene oxide)–clay nanocomposites', *Journal of Applied Polymer Science*, vol. 131, no. 4.

Choy, J.H. & Park, M., 2004, 'Cationic and anionic clays for biological applications' in F. Whypych & K.G. Satyanarayana (eds), *Clay surfaces: Fundamentals and applications*, 1st edn, Elsevier, London, pp. 403-424.

Chung, D.D.L. 1993, 'In situ process analysis at elevated temperature', in D.D.L. Chung, P.W. DeHaven, H. Arnold, D. Ghosh (ed.), X-ray diffraction at elevated temperatures, VCH Publishers Inc., New York, pp.189-208.

Churchman, G.J. 2002, 'Formation of complexes between bentonite and different cationic polyelectrolytes and their use as sorbents for non-ionic and anionic pollutants', *Applied Clay Science*, vol. 21, no. 3, pp. 177-89.

Churchman, G.J., Gates, W.P., Theng, B.K.G., Yuan, G. 2006, 'Clays and clay minerals for pollution control' in Bergaya, F. Legaly (eds), *Handbook of clay science*, 1st edn, Elsevier, Amsterdam, pp. 625-676.

Clegg, F., Breen, C. & Khairuddin 2014, 'Synergistic and Competitive Aspects of the Adsorption of Poly(ethylene glycol) and Poly(vinyl alcohol) onto Na-Bentonite', *J. Phys. Chem. B*, vol. 118, no. 46, pp. 13268-78.

Cnudde, V., Cnudde, J.P., Dupuis, C. & Jacobs, P.J.S. 2004, 'X-ray micro-CT used for the localization of water repellents and consolidants inside natural building stones', *Materials Characterization*, vol. 53, no. 2-4, pp. 259-71.

Cnudde, V., Dierick, M., Masschaele, B. & Jacobs, P.J. 2006, 'A high-resolution view at water repellents and consolidants: critical review and recent developments', in S.K. Kourkoulis (ed.), *Fracture and Failure of Natural Building Stones: Applications in the Restoration of Ancient Monuments*, Springer Netherlands, Dordrecht, pp. 519-40.

Cocca, M., D'Arienzo, L., D'Orazio, L., Gentile, G. & Martuscelli, E. 2004, 'Polyacrylates for conservation: chemico-physical properties and durability of different commercial products', *Polymer Testing*, vol. 23, no. 3, pp. 333-42.

Cocca, M., D'Arienzo, L., D'Orazio, L., Gentile, G. & Martuscelli, E. 2005, 'Synthesis of poly (urethane urea) by in situ polymerization inside stone', *Journal of Polymer Science Part B: Polymer Physics*, vol. 43, no. 5, pp. 542-52.

Connell, J. 2000, *Sydney:the emergence of a world city,* Oxford University Press, Melbourne.

Cooke, R.U. 1989, 'Geomorphological Contributions to Acid Rain Research: Studies of Stone Weathering', *The Geographical Journal*, vol. 155, no. 3, pp. 361-6.

Costa, L., Gad, A.M., Camino, G., Cameron, G.G. & Qureshi, M.Y. 1992, 'Thermal and thermooxidative degradation of poly (ethylene oxide)-metal salt complexes', *Macromolecules*, vol. 25, no. 20, pp. 5512-8.

Cox, P. 2002, 'Architecture', in G. Deirmendjian (ed.), Sydney sandstone, Craftsman House, Sydney, pp. 53-55.

Cramer, D. 2002, 'Shaping the stone', in G. Deirmendjian (ed.), Sydney sandstone, Craftsman House, Sydney, pp.115-119.

Crompton, T.R. 2008, *Characterisation of polymers*, Smithers Rapra, Shawbury.

Crompton, T.R. 2010, *Thermal methods of polymer analysis*, Smithers Rapra Technology, Shawbury.

Crompton, T.R. 2013, *Thermal Methods of Polymer Analysis*, ISmithers Rapra Publishing, Shrewsbury.

Cui, Y. & van Duijneveldt, J.S. 2010, 'Adsorption of Polyetheramines on Montmorillonite at High pH', *Langmuir*, vol. 26, no. 22, pp. 17210-7.

Cullity, B.D. 1978, *Elements of x-ray diffraction*, 2nd edn, Addison-Wesley Pub. Co., Reading, Massachusetts.

Cullity, B.D. & Stock, S.R. 2001, *Elements of X-ray Diffraction*, 3rd edn, Prentice-Hall, Englewood Cliffs.

D'Arienzo, L., Scarfato, P. & Incarnato, L. 2008, 'New polymeric nanocomposites for improving the protective and consolidating efficiency of tuff stone', *Journal of Cultural Heritage*, vol. 9, no. 3, pp. 253-60.

Dangge, G., Jianzhong, M., Bin, L. & Yun, L. 2009, 'Study on PDM-AM-GL/MMT nanocomposites and their application', *Materials and Manufacturing Processes*, vol. 24, no. 12, pp. 1306-11.

Daniliuc, L., De Kesel, C. & David, C. 1992, 'Intermolecular interactions in blends of poly (vinyl alcohol) with poly (acrylic acid)—1. FTIR and DSC studies', *European polymer journal*, vol. 28, no. 11, pp. 1365-71.

De, P.P. 2010, 'Instrumental Techniques used for Thermal Analysis of Rubbers and Rubbery Materials', in N.R. Choudhury, P.P. De & N.K. Dutta (eds), *Thermal Analysis of Rubbers and Rubbery Materials*, Elsevier, Shawbury, pp. 11-64.

De Buergo, M.A., Fort, R. & Gomez-Heras, M. 2004, 'Contributions of scanning electron microscopy to the assessment of the effectiveness of stone conservation treatments', *Scanning*, vol. 26, no. 1, pp. 41-7.

D'Esposito, L. & Koenig, J.L. 1978, 'Applications of fourier transform infrared to synthetic polymers and biological macromolecules', in J.R. Ferraro & L. J. Basile (ed.), *Fourier transform infrared spectroscopy*, Academic Press, New York, pp. 61-97

Dei, L. & Salvadori, B. 2007, 'Nanotechnology in cultural heritage conservation: nanometric slaked lime saves architectonic and artistic surfaces from decay', *Journal of Cultural Heritage*, vol. 7, no. 2, pp. 110-5.

Deirmendjian, G. 2002, '*Sydney sandstone*', Craftsman House, Sydney.

Deka, M. & Kumar, A. 2013, 'Dielectric and conductivity studies of 90 MeV O7+ ion irradiated poly(ethylene oxide)/montmorillonite based ion conductor', *J. Solid State Electrochem.*, vol. 17, no. 4, pp. 977-86.

Delgado Rodrigues, J. 2001, 'Swelling behaviour of stones and its interest in conservation. An appraisal', *Materiales de construccion*, vol. 51, no. 263-264, pp. 183-95.

Deng, Y., Dixon, J.B., White, G.N., Loeppert, R.H. & Juo, A.S.R. 2006, 'Bonding between polyacrylamide and smectite', *Colloids and Surfaces A: Physicochemical and Engineering Aspects*, vol. 281, no. 1–3, pp. 82-91.

Department of Environment and Climate Change NSW 2008a, 'Building in a saline environment', Sydney, viewed 20May 2016, < http://www.environment.nsw.gov.au/ resources/ salinity/booklet6buildininasalineenvironment.pdf>.

Department of Environment and Climate Change NSW 2008b, *Summary of climate change impacts: Sydney Region: NSW Climate Change Action Plan*, Sydney

Department of the Environment and Heritage 2004, *Preserving our Past, Building our Future*, Department of the Environment and Heritage, Canberra, viewed 17 May 2016, < http://www.environment.gov.au/system/files/resources/3845f27a-ad2c-4d40-8827-18c643c7adcd/files/adaptive-reuse.pdf >.

Derho, J., Soulestin, J. & Krawczak, P. 2014, 'Structural evolution of poly (lactic acid)/poly (ethylene oxide)/unmodified clay upon ambient ageing', *Journal of Applied Polymer Science*, vol. 131, no. 13.

Diaz-Perez, A., Cortés-Monroy, I. & Roegiers, J. 2007, 'The role of water/clay interaction in the shale characterization', *Journal of Petroleum Science and Engineering*, vol. 58, no. 1, pp. 83-98.

Doehne, E. & Price, C.A. 2011, *Stone Conservation: An Overview of Current Research*, Getty Publications.

Dollimore, D. & Heal, G. 1967, 'The degradation of selected polymers to carbons in an inert atmosphere', *Carbon*, vol. 5, no. 1, pp. 65-72.

Domaslowski, W. 1969, 'Consolidation of stone objects with epoxy resins', *Monumentum*, vol. 4, pp. 51-64.

Domingo, C., Alvarez de Buergo, M., Sánchez-Cortés, S., Fort, R., García-Ramos, J.V. & Gomez-Heras, M. 2008, 'Possibilities of monitoring the polymerization process of silicon-based water repellents and consolidants in stones through infrared and Raman spectroscopy', *Progress in Organic Coatings*, vol. 63, no. 1, pp. 5-12.

Dong, J., Ozaki, Y. & Nakashima, K. 1997a, 'FTIR studies of conformational energies of poly (acrylic acid) in cast films', *Journal of Polymer Science Part B: Polymer Physics*, vol. 35, no. 3, pp. 507-15.

Dong, J., Ozaki, Y. & Nakashima, K. 1997b, 'Infrared, Raman, and near-infrared spectroscopic evidence for the coexistence of various hydrogen-bond forms in poly (acrylic acid)', *Macromolecules*, vol. 30, no. 4, pp. 1111-7.

Douillard, J.M. & Salles, F., 2004, 'Phenomenology of water adsorption at clay surfaces' in F. Whypych & K.G. Satyanarayana (eds), *Clay surfaces: Fundamentals and applications*, 1st edn, Elsevier, London, pp. 118-152.

Dragovich, D. & Egan, M. 2011, 'Salt weathering and experimental desalination treatment of building sandstone, Sydney (Australia)', *Environmental Earth Sciences*, vol. 62, no. 2, pp. 277-88.

Dreesen, R. & Dusar, M. 2004, 'Historical building stones in the province of Limburg (NE Belgium): role of petrography in provenance and durability assessment', *Materials Characterization*, vol. 53, no. 2-4, pp. 273-87.

Duarte, A.S.R., Amorim da Costa, A.M. & Amado, A.M. 2005, 'On the conformation of neat acrylamide dimers-a study by ab initio calculations and vibrational spectroscopy', *J. Mol. Struct.: THEOCHEM*, vol. 723, no. 1-3, pp. 63-8.

Dubinsky, S., Grader, G.S., Shter, G.E. & Silverstein, M.S. 2004, 'Thermal degradation of poly(acrylic acid) containing copper nitrate', *Polymer Degradation and Stability*, vol. 86, no. 1, pp. 171-8.

Dunn, J.R. and Hudec, P.P. 1966, 'Water, Clay and Rock Soundness', *The Ohio Journal of Science*. Vol. 66, no. 2, pp. 153-168.

Durand-Piana, G., Lafuma, F. & Audebert, R. 1987, 'Flocculation and adsorption properties of cationic polyelectrolytes toward Na-montmorillonite dilute suspensions', *Journal of colloid and interface science*, vol. 119, no. 2, pp. 474-80.

Durán-Suárez, J., García-Beltrán, A. & Rodríguez-Gordillo, J. 1995, 'Colorimetric cataloguing of stone materials (biocalcarenite) and evaluation of the chromatic effects of different restoring agents', *Science of The Total Environment*, vol. 167, no. 1-3, pp. 171-80.

E. Silva, M.E.S.R., Dutra, E.R., Mano, V. & Machado, J.C. 2000, 'Preparation and thermal study of polymers derived from acrylamide', *Polym. Degrad. Stab.*, vol. 67, no. 3, pp. 491-5.

EL-GOHARY, M. 2011, 'Chemical deterioration of Egyptian limestone affected by saline water', *International Journal of Conservation Science*, vol. 2, no. 1, pp. 17-28.

Echlin, P. 2009, *Handbook of sample preparation for scanning electron microscopy and x-ray microanalysis*, Springer, London.

Eisenberg, A., Yokoyama, T. & Sambalido, E. 1969, 'Dehydration kinetics and glass transition of poly (acrylic acid)', *Journal of Polymer Science Part A-1: Polymer Chemistry*, vol. 7, no. 7, pp. 1717-28.

Elmahdy, M., Chrissopoulou, K., Afratis, A., Floudas, G. & Anastasiadis, S. 2006, 'Effect of confinement on polymer segmental motion and ion mobility in PEO/layered silicate nanocomposites', *Macromolecules*, vol. 39, no. 16, pp. 5170-3.

El-Zahhar, A.A., Abdel-Aziz, H.M. & Siyam, T. 2007, 'Gamma Radiation-Induced Preparation of Polymeric Composite Sorbents and Their Structure Assignments', *Journal of Macromolecular Science, Part A*, vol. 44, no. 2, pp. 215-22.

Erceg, M., Jozić, D., Banovac, I., Perinović, S. & Bernstorff, S. 2014, 'Preparation and characterization of melt intercalated poly(ethylene oxide)/lithium montmorillonite nanocomposites', *Thermochimica Acta*, vol. 579, pp. 86-92.

Essington, M.E. 2003, *Soil and water chemistry: an integrative approach,* CRC Press, Boca Raton.

Excoffon, P. & Marechal, Y. 1972, 'Infrared spectra of H-bonded systems: saturated carboxylic acid dimers', *Spectrochimica Acta Part A: Molecular Spectroscopy*, vol. 28, no. 2, pp. 269-83.

Fan, L., Nan, C.-W. & Li, M. 2003, 'Thermal, electrical and mechanical properties of $(PEO)_{16}$ $LiClO_4$ electrolytes with modified montmorillonites', *Chemical physics letters*, vol. 369, no. 5, pp. 698-702.

Fares, M., Hacaloglu, J. & Suzer, S. 1994, 'Characterization of degradation products of polyethylene oxide by pyrolysis mass spectrometry', *European polymer journal*, vol. 30, no. 7, pp. 845-50.

Farmer, V.C. & Russell, J.D. 1964, 'The infra-red spectra of layer silicates', *Spectrochimica Acta*, vol. 20, no. 7, pp. 1149-73.

Fassina, V. 1995, 'New findings on past treatments carried out on stone and marble monuments' surfaces', *Science of The Total Environment*, vol. 167, no. 1-3, pp. 185-203.

Favaro, M., Mendichi, R., Ossola, F., Russo, U., Simon, S., Tomasin, P. & Vigato, P.A. 2006, 'Evaluation of polymers for conservation treatments of outdoor exposed stone monuments. Part I: Photo-oxidative weathering', *Polymer Degradation and Stability*, vol. 91, no. 12, pp. 3083-96.

Favaro, M., Mendichi, R., Ossola, F., Simon, S., Tomasin, P. & Vigato, P.A. 2007, 'Evaluation of polymers for conservation treatments of outdoor exposed stone monuments. Part II: Photo-oxidative and salt-induced weathering of acrylic-silicone mixtures', *Polymer Degradation and Stability*, vol. 92, no. 3, pp. 335-51.

Ferfera-Harrar, H., Aiouaz, N., Dairi, N. & Hadj-Hamou, A.S. 2014, 'Preparation of chitosan-g-poly(acrylamide)/montmorillonite superabsorbent polymer composites: Studies on swelling, thermal, and antibacterial properties', *Journal of Applied Polymer Science*, vol. 131, no. 1, pp. n/a-n/a.

Fernandes, P. 2006, 'Applied microbiology and biotechnology in the conservation of stone cultural heritage materials', *Applied Microbiology and Biotechnology*, vol. 73, no. 2, pp. 291-6.

Ferreira Pinto, A.P. & Delgado Rodrigues, J. 2008, 'Stone consolidation: The role of treatment procedures', *Journal of Cultural Heritage*, vol.9, no.1, pp. 38-53.

Fidler, J. 1995, 'Lime Treatments: Lime Watering and Shelter Coating of Friable Historic Masonry', *APT Bulletin*, vol. 26, no. 4, pp. 50-6.

Filippi, S., Mameli, E., Marazzato, C., Magagnini, P. 2007, 'Comparison of solution-blending and melt-intercalation for the preparation of poly (ethylene-co-acrylic acid)/organoclay nanocomposites', *European polymer journal*, vol.43, no.5, pp. 1645-1659.

Finocchio, E., Cristiani, C., Dotelli, G., Stampino, P.G. & Zampori, L. 2014, 'Thermal evolution of PEG-based and BRIJ-based hybrid organo-inorganic materials. FT-IR studies', *Vibrational Spectroscopy*, vol. 71, pp. 47-56.

Fitzgerald, S. 2002, 'Hewing the stone', in G. Deirmendjian (ed.), Sydney sandstone, Craftsman House, Sydney, pp. 53-55.

Fitzner, B. & Heinrichs, K. 2001, 'Damage diagnosis at stone monuments-weathering forms, damage categories and damage indices', *ACTA-UNIVERSITATIS CAROLINAE GEOLOGICA*, no. 1, pp. 12-3.

Flannery, T. 2002, 'The stone', in G. Deirmendjian (ed.), Sydney sandstone, Craftsman House, Sydney, pp. 31-35.

Franklin, B. 2000, 'The role of petrography in the selection of sandstone for repair', *Seminar on Material evidence. Conserving historic building fabric*.

Frost, R.L., Kristof, J. 2004, 'Raman and infrared spectroscopic studies of kaolinite surfaces modified by intercalation' in F. Whypych & K.G. Satyanarayana (eds), *Clay surfaces: Fundamentals and applications*, 1st edn, Elsevier, London, pp.184-215.

Frost, R.L., Kristof, J., Paroz, G.N. & Kloprogge, J. 1998, 'Role of water in the intercalation of kaolinite with hydrazine', *Journal of Colloid and Interface Science*, vol. 208, no. 1, pp. 216-25.

Galán, E 2013, ‘Genesis of clay minerals’ in Bergaya, F. Legaly (eds), *Handbook of clay science*, 2nd edn, Elsevier, Amsterdam, pp. 89-113.

Galwey, A.K. & Craig, D.Q.M. 2007, 'Thermogravimetric Analysis: Basic Principles', in D.Q.M. Craig & M. Reading (eds), *Thermal analysis of pharmaceuticals*, CRC Press, London, pp. 139-191.

Gao, F. 2004, 'Clay/polymer composites: the story', *Materials today*, vol. 7, no. 11, pp. 50-5.

Gao, D. & Heimann, R.B. 1993, 'Structure and mechanical properties of superabsorbent polyacrylamide-montmorillonite composite hydrogels', *Polym. Gels Networks*, vol. 1, no. 4, pp. 225-46.

García-Talegon, J., Vicente, M.A., Vicente-Tavera, S. & Molina-Ballesteros, E. 1998, 'Assessment of chromatic changes due to artificial ageing and/or conservation treatments of sandstones', *Color Research & Application*, vol. 23, no. 1, pp. 46-51.

Ghedini, N., Gobbi, G., Sabbioni, C. & Zappia, G. 2000, 'Determination of elemental and organic carbon on damaged stone monuments', *Atmospheric Environment*, vol. 34, no. 25, pp. 4383-91.

Giannelis, E.P. 1996, 'Polymer layered silicate nanocomposites', *Advanced materials*, vol. 8, no. 1, pp. 29-35.

Giavarini, C., Santarelli, M.L., Natalini, R. & Freddi, F. 2007, 'A non-linear model of sulphation of porous stones: Numerical simulations and preliminary laboratory assessments', *Journal of Cultural Heritage*, vol. 9, no. 1, pp. 14-22.

Gibbs, R.J. 1965, ‘Rrror due to segregation in quantitative clay mineral x-ray diffraction mounting techniques’, *The American Mineralogist*, vol.50, no.4, pp. 741-751.

Giese, R.F. & Van Oss, C.J. 2001, *Colloid and surface properties of clays and related materials,* Marcel Dekker, Inc., New York.

Gillott, J.E. 1968, *Clay in engineering geology*, Elsevier Science Pub. Co., USA.

Ginell, W.S. & Coffman, R. 1998, 'Epoxy Resin-Consolidated Stone: Appearance Change on Aging', *Studies in Conservation*, vol. 43, no. 4, pp. 242-8.

Giorgi, R., Baglioni, M., Berti, D. & Baglioni, P. 1986, 'New Methodologies for the Conservation of Cultural Heritage: Micellar Solutions, Microemulsions, and Hydroxide Nanoparticles', *Accounts of Chemical Research*, vol. 43, no. 6, pp. 695-704.

Giovanni Brunetti, B., Sgamellotti, A. & Clark, A.J. 1986, 'Advanced Techniques in Art Conservation', *Accounts of Chemical Research*, vol. 43, no. 6, pp. 693-4.

Glikman, J.-F., Arnaud, R., Lemaire, J. & Seinera, H. 1986, 'Photolysis and photo-oxidation of ethylene-ethyl acrylate copolymers', *Polymer Degradation and Stability*, vol. 16, no. 4, pp. 325-35.

Goudie, A. & Viles, H.A. 1997, *Salt weathering hazard*, Wiley, Chichester

Grassie, N. & Mendoza, G.A.P. 1984, 'Thermal degradation of polyether-urethanes: Part 1—Thermal degradation of poly (ethylene glycols) used in the preparation of polyurethanes', *Polymer degradation and stability*, vol. 9, no. 3, pp. 155-65.

Grassi, S., Favaro, M., Tomasin, P. & Dei, L. 2009, 'Nanocontainer aqueous systems for removing polymeric materials from marble surfaces: A new and promising tool in cultural heritage conservation', *Journal of Cultural Heritage*, vol. 10, no. 3, pp. 347-55.

Greenland, D. 1963, 'Adsorption of polyvinyl alcohols by montmorillonite', *Journal of Colloid Science*, vol. 18, no. 7, pp. 647-64.

Gridi-Bennadji, F., Lecomte-Nana, G., Bonnet, J.-P. & Rossignol, S. 2012, 'Rheological properties of montmorillonitic clay suspensions: Effect of firing and interlayer cations', *Journal of the European Ceramic Society*, vol. 32, no. 11, pp. 2809-17.

Griffin, P.S., Indictor, N. & Koestler, R.J. 1991, 'The biodeterioration of stone: a review of deterioration mechanisms, conservation case histories, and treatment', *International Biodeterioration*, vol. 28, no. 1-4, pp. 187-207.

Griffiths, P.R. & De Haseth, J.A. 2007, *Fourier transform infrared spectrometry*, vol. 171, John Wiley & Sons.

Grim, R.E. 1968, 'Clay mineralogy', McGraw-Hill, Boca Raton.

Girma, K., Lorenz, V., Blaurock, S. & Edelmann, F.T. 2006, 'Coordination chemistry of acrylamide 3: Synthesis, crystal structure and IR spectroscopic properties of dichloro-

tetrakis (O–acrylamide) copper (II),[Cu (O–OC (NH 2) CH CH 2) 4 Cl 2]', *Inorganica chimica acta*, vol. 359, no. 1, pp. 364-8.

Griswold, J. & Uricheck, S. 1998, 'Loss Compensation Methods for Stone', *Journal of the American Institute for Conservation*, vol. 37, no. 1, pp. 89-110.

Güngör, N. & Karaoğlan, S. 2001, 'Interactions of polyacrylamide polymer with bentonite in aqueous systems', *Materials Letters*, vol. 48, no. 3, pp. 168-75.

Günzler, H. & Gremlich, H.-U. 2002, *IR spectroscopy: an introduction*, Wiley-VCH, Cambridge.

Gúven, N., 1992, 'Molecular aspects of clay-water interactions' in N. Gúven & R.M. Pollastro (eds), *Clay-water interface and its rheological implications*, 2nd edn, The Clay Minerals Society, Colorado, pp. 2-79.

Guerrero, S.J., Boldarino, P. & Zurimendi, J.A. 1985, 'Characterization of polyacrylamides used in enhanced oil recovery', *Journal of Applied Polymer Science*, vol. 30, no. 3, pp. 955-67.

Guggenheim, S. & Van Groos, A.K. 2001, 'Baseline studies of the clay minerals society source clays: thermal analysis', *Clays and Clay Minerals*, vol. 49, no. 5, pp. 433-43.

Gunn, S. 2012, Stone house construction, 1st edn, CSIRO Publishing, Collingwood.

Gupta, S.P. 2011, 'Conservation of Stone Structure by Impregnation with Tetraethoxysilane', *International Journal of Chemical and Analytical Science*, vol. 2, no. 8, pp. 115-9.

Gupta, R.K., Kennel, E. & Kim, K. 2010, 'Polymer nanocomposites handbook', CRC Press, Boca Raton.

Gurkaynak, A., Tubert, F., Yang, J., Matyas, J., Spencer, J. & Gryte, C.C. 1996, 'High-temperature degradation of polyacrylic acid in aqueous solution', *Journal of Polymer Science Part A: Polymer Chemistry*, vol. 34, no. 3, pp. 349-55.

Hackett, E., Manias, E. & Giannelis, E.P. 1995, 'Computer Simulation Studies of PEO/Layer Silicate Nanocomposites', *Chemistry of Materials*, vol. 12, no. 8, pp. 2161-7.

Hall, C.M., McArthur, S. & Foundation, N.Z.N.H. 1993, *Heritage management in New Zealand and Australia: visitor management, interpretation and marketing*, Oxford University Press.

Hall, P.L. 1987, Clay: their significance, properties, origins and uses', in M.J. Wilson (ed.), *A handbook of determinative methods in clay mineralogy*, Blackie & Son Limited, Glasgow, pp. 1-22.

Han, D., Wang, T., Lin, Z., Hu, Y., Zhao, F., Yi, J. & Li, S. 2010, 'Promoting effects of polyacrylamide on ignition and combustion of Al/H2O based fuels: Experimental studies of polyacrylamide aqueous solution flash pyrolysis', *J. Anal. Appl. Pyrolysis*, vol. 87, no. 1, pp. 56-64.

Hameed, F., Schillinger, B., Rohatsch, A., Zawisky, M. & Rauch, H. 2009, 'Investigations of stone consolidants by neutron imaging', *Nuclear Instruments and Methods in Physics Research Section A: Accelerators, Spectrometers, Detectors and Associated Equipment*, vol. 605, no. 1-2, pp. 150-3.

Hansen, E., Doehne, E., Fidler, J., Larson, J., Martin, B., Matteini, M., Rodriguez-Navarro, C., Pardo, E.S., Price, C. & de Tagle, A. 2003, 'A review of selected inorganic consolidants and protective treatments for porous calcareous materials', *Studies in Conservation*, vol. 48, no. sup1, pp. 13-25.

Harper, C.A. & Petrie, E.M. 2003, *Plastics Materials and Processes: A Concise Encyclopedia*, Wiley, Berlin.

He, B.B. 2009, *Two-dimensional X-ray diffraction,* Wiley, Hoboken, NJ.

Hedley, C., Yuan, G. & Theng, B. 2007, 'Thermal analysis of montmorillonites modified with quaternary phosphonium and ammonium surfactants', *Applied Clay Science*, vol. 35, no. 3, pp. 180-8.

Heiman, J.L. 1981a, *The preservation of Sydney sandstone by chemical impregnation,* Experimental Building Station, Sydney

Heiman, J.L. 1981b, *Durability tests on sandstone treated with silanes,* Experimental Building Station, Sydney.

Helvacıoğlu, E., Aydın, V., Nugay, T., Nugay, N., Uluocak, B.G. & Şen, S. 2011, 'High strength poly (acrylamide)-clay hydrogels', *Journal of Polymer Research*, vol. 18, no. 6, pp. 2341-50.

Hempel, K. 1976, 'An Improved Method for the Vacuum Impregnation of Stone', *Studies in Conservation*, vol. 21, no. 1, pp. 40-3.

Hensen, E., Tambach, T., Bliek, A. & Smit, B. 2001, 'Adsorption isotherms of water in Li–, Na–, and K–montmorillonite by molecular simulation', *The Journal of Chemical Physics*, vol. 115, no. 7, pp. 3322-9.

Hikosaka, M.Y., Pulcinelli, S.H., Santilli, C.V., Dahmouche, K. & Craievich, A.F. 2006, 'Montmorillonite (MMT) effect on the structure of poly(oxyethylene) (PEO)-MMT nanocomposites and silica-PEO-MMT hybrid materials', *J. Non-Cryst. Solids*, vol. 352, no. 32-35, pp. 3705-10.

Horie, C.V. 2010, *Materials for Conservation: Organic Consolidants, Adhesives and Coatings*, Taylor & Francis Group, Amsterdam.

Hu, H., Saniger, J., Garcia-Alejandre, J. & Castaño, V. 1991, 'Fourier transform infrared spectroscopy studies of the reaction between polyacrylic acid and metal oxides', *Materials Letters*, vol. 12, no. 4, pp. 281-5.

Huang, P. & Ye, L. 2014a, 'In situ polymerization of cationic polyacrylamide/montmorillonite composites and its flocculation characteristics', *Journal of Thermoplastic Composite Materials*, p. 0892705713518787.

Huang, P. & Ye, L. 2014b, 'Enhanced dewatering of waste sludge with polyacrylamide/montmorillonite composite and its conditioning mechanism', *Journal of Macromolecular Science, Part B*, vol. 53, no. 9, pp. 1465-76.

Hugues, T., Steiger, L. & Weber, J. 2005, *Dressed stone: types of stone, details, examples*, 1st edn, Edition Detail, Munich.

Hunt, H.G. 2014, Release of the draft Australian Heritage Strategy, media release, 15 April 2014, BHP Limited, Melbourne, viewed 11 May 2015, <http://www.environment.gov.au/minister/hunt/2014/ mr20140415.html >.

Hunt, R.W.G. & Pointer, M.R. 2011, *Measuring Colour*, Wiley, Hoboken.

Iñigo, A.C., Vicente-Tavera, S. & Rives, V. 2004, 'MANOVA-biplot statistical analysis of the effect of artificial ageing (freezing/thawing) on the colour of treated granite stones', *Color Research & Application*, vol. 29, no. 2, pp. 115-20.

Iñigo, A.C., Vicente-Tavera, S., Rives, V. & Vicente, M.A. 1997, 'Color changes in the surface of granitic materials by consolidated and/or water repellent treatments', *Color Research & Application*, vol. 22, no. 2, pp. 133-41.

IJdo, W.L., Kemnetz, S. & Benderly, D. 2006, 'An infrared method to assess organoclay delamination and orientation in organoclay polymer nanocomposites', *Polymer Engineering & Science*, vol. 46, no. 8, pp. 1031-9.

Inyang, H.I. & Bae, S. 2005, 'Polyacrylamide sorption opportunity on interlayer and external pore surfaces of contaminant barrier clays', *Chemosphere*, vol. 58, no. 1, pp. 19-31.

Inyang, H.I., Bae, S., Mbamalu, G. & Park, S.-W. 2007, 'Aqueous polymer effects on volumetric swelling of Na-montmorillonite', *Journal of materials in civil engineering*, vol. 19, no. 1, pp. 84-90.

Ip, K.H., Stuart, B.H. & Ray, A.S. 2003, 'Characterisation of weathering of Sydney sandstones in heritage buildings', *Journal of Cultural Heritage*, vol. 4, no. 3, pp. 211-20.

Ip, K.H., Ray, A.S., Stuart, B.H. & Thomas, P.S. 2004, 'Degradation of historic sandstone buildings of Sydney', *Proceedings of the 7th Australasian Masonry Conference*, ed. M. Masia, Newcastle, Australia: University of Newcastle, pp. 420-7.

Ip, K.H., Ray, A.S., Stuart, B.H. & Thomas, P S. 2005a, 'Investigation of the degradation of sandstones in Sydney's heritage buildings', in L. Modena, Roca (ed.), *Structural analysis of historical constructions,* Taylor & Francis Group, London, pp. 239-44.

Ip, K.H., Ray, A.S., Stuart, B.H. & Thomas, P.S. 2005b, 'Thermal analysis of heritage stones', *Journal of Thermal Analysis and Calorimetry*, vol. 80, no. 3, pp. 559-63.

Ip, K.H. 2007, 'Investigation into clay-based consolidants for conservation of 'yellow block sandstones' in Sydney's heritage buildings', University of Technology Sydney.

Ip, K.H., Stuart, B.H., Ray, A.S. & Thomas, P.S. 2008a, 'A spectroscopic investigation of the weathering of a heritage Sydney sandstone', *Spectrochimica Acta Part A: Molecular and Biomolecular Spectroscopy*, vol. 71, no. 3, pp. 1032-5.

Ip, K.H., Stuart, B.H., Thomas, P.S. & Ray, A.S. 2008b, 'Thermal characterization of the clay binder of heritage Sydney sandstones', *Journal of Thermal Analysis and Calorimetry*, vol. 92, no. 1, pp. 97-100.

Ip, K.H., Stuart, B.H., Ray, A.S. & Thomas, P.S. 2011a, 'ESEM-EDS Investigation of the Weathering of a Heritage Sydney Sandstone', *Microscopy and Microanalysis*, vol. 17, no. 02, pp. 292-5.

Ip, K.H., Stuart, B.H., Thomas, P.S. & Ray, A.S. 2011b, 'Characterisation of poly(vinyl alcohol)–montmorillonite composites with higher clay contents', *Polymer Testing*, vol. 30, no. 7, pp. 732-6.

Işik-Yürüksoy, B., Kiş, M. & Güven, O. 1998, 'The preservation of Çankiri limestone in sulfur dioxide atmosphere by in situ polymerization of ethyl methacrylate', *Journal of Applied Polymer Science*, vol. 69, no. 9, pp. 1761-4.

Jaggi, N. & Vij, D.R. 2006, 'Fourier transform infrared spectroscopy', in D.R. Vij (ed.), Handbook of applied solid state spectroscopy, Springer, New York, pp. 411-450.

Jeong, H.M., Kim, D.H., Yoon, K.S., Jung, J.S., Kim, Y.S., Kim, T.K., Cho, Y.L. & Hwang, J.M. 2007, 'Sodium montmorillonite intercalated with poly(ethylene glycol): a modifier of reactive hot-melt polyurethane adhesive', *J. Adhes. Sci. Technol.*, vol. 21, no. 9, pp. 841-53.

Jimenez-Lopez, C., Rodriguez-Navarro, C., Piñar, G., Carrillo-Rosúa, F.J., Rodriguez-Gallego, M. & Gonzalez-Muñoz, M.T. 2007a, 'Consolidation of degraded ornamental porous limestone stone by calcium carbonate precipitation induced by the microbiota inhabiting the stone', *Chemosphere*, vol. 68, no. 10, pp. 1929-36.

Jimenez-Lopez, C., Jroundi, F., Rodríguez-Gallego, M., Arias, J. & Gonzalez-Muñoz, M. 2007b, 'Biomineralization induced by Myxobacteria', *Communicating current research and educational topics and trends in applied microbiology*, vol. 1, pp. 143-54.

Jimenez-Lopez, C., Jroundi, F., Pascolini, C., Rodriguez-Navarro, C., Pinar-Larrubia, G., Rodriguez-Gallego, M. & González-Muñoz, M.T. 2008, 'Consolidation of quarry calcarenite by calcium carbonate precipitation induced by bacteria activated among the microbiota inhabiting the stone', *International Biodeterioration & Biodegradation*, vol. 62, no. 4, pp. 352-63.

Jo, W., Cruz, C. & Paul, D. 1989, 'FTIR investigation of interactions in blends of PMMA with a styrene/acrylic acid copolymer and their analogs', *Journal of Polymer Science Part B: Polymer Physics*, vol. 27, no. 5, pp. 1057-76.

Johnston, C., Sposito, G. & Erickson, C. 1992, 'Vibrational probe studies of water interactions with montmorillonite', *Clays and Clay Minerals*, vol. 40, no. 6, pp. 722-30.

Jokilehto, J. 1999, *A history of architectural conservation*, Butterworth-Heinemann.

Jonathan, N. 1961, 'The infrared and Raman spectra and structure of acrylamide', *Journal of Molecular Spectroscopy*, vol. 6, pp. 205-14.

Jones, F., Farrow, J. & Van Bronswijk, W. 1998, 'An infrared study of a polyacrylate flocculant adsorbed on hematite', *Langmuir*, vol. 14, no. 22, pp. 6512-7.

Jordan, J., Jacob, K.I., Tannenbaum, R., Sharaf, M.A. & Jasiuk, I. 2005, 'Experimental trends in polymer nanocomposites—a review', *Materials science and engineering: A*, vol. 393, no. 1, pp. 1-11.

Jroundi, F., Fernández-Vivas, A., Rodriguez-Navarro, C., Bedmar, E. & González-Muñoz, M. 2010, 'Bioconservation of Deteriorated Monumental Calcarenite Stone and Identification of Bacteria with Carbonatogenic Activity', *Microbial Ecology*, vol. 60, no. 1, pp. 39-54.

Kabanov, V., Dubnitskaya, V. & Khar'kov, S. 1975, 'Thermal properties of polyacrylic acid', *Polymer Science USSR*, vol. 17, no. 7, pp. 1848-55.

Kalaleh, H.-A., Tally, M. & Atassi, Y. 2013, 'Preparation of a clay based superabsorbent polymer composite of copolymer poly (acrylate-co-acrylamide) with bentonite via microwave radiation', *arXiv preprint arXiv:1311.6445*.

Kamal, M.R. & Ionescu-Vasii, L.L. 2010, 'Thermal Characterisation of Polymer Nanocomposites', in N.R. Choudhury, P.P. De & N.K. Dutta (eds), *Thermal Analysis of Rubbers and Rubbery Materials*, Elsevier, Shawbury, pp. 277-319.

Kanellopoulou, D.G. & Koutsoukos, P.G. 2003, 'The Calcitic Marble/Water Interface: Kinetics of Dissolution and Inhibition with Potential Implications in Stone Conservation', *Langmuir*, vol. 19, no. 14, pp. 5691-9.

Karatasios, I., Theoulakis, P., Kalagri, A., Sapalidis, A. & Kilikoglou, V. 2009, 'Evaluation of consolidation treatments of marly limestones used in archaeological monuments', *Construction and Building Materials*, vol. 23, no. 8, pp. 2803-12.

Karpovich-Tate, N. & Rebrikova, N.L. 1991, 'Microbial communities on damaged frescoes and building materials in the Cathedral of the Nativity of the Virgin in the Pafnutii-Borovskii monastery, Russia', *International Biodeterioration*, vol. 27, no. 3, pp. 281-96.

Kasai, N. & Kakudo, M. 2005, *X-ray diffraction by macromolecules*, vol. 80, Kodansha, Tokyo.

Khursheed, A. 2011, *Scanning electron microscope optics and spectrometers,* World Scientific Pub. Co., Singapore.

Kickelbick, G. 2007, *Hybrid materials: synthesis, characterization, and applications*, John Wiley & Sons.

Kiliaris, P. & Papaspyrides, C. 2010, 'Polymer/layered silicate (clay) nanocomposites: an overview of flame retardancy', *Progress in Polymer Science*, vol. 35, no. 7, pp. 902-58.

Kim, S. & Park, S.-J. 2007, 'Preparation and ion-conducting behaviors of poly (ethylene oxide)-composite electrolytes containing lithium montmorillonite', *Solid State Ionics*, vol. 178, no. 13, pp. 973-9.

Kim, E. K., Won, J., Do, J., Kim, S.D., Kang, Y.S., 2009, 'Effects of silica nanoparticle and GPTMS addition on TEOS-based stone consolidants', *Journal of Cultural Heritage,* vol. 10, no. 2, pp. 214-221.

Kim, S. & Palomino, A.M. 2011, 'Factors influencing the synthesis of tunable clay–polymer nanocomposites using bentonite and polyacrylamide', *Applied Clay Science*, vol. 51, no. 4, pp. 491-8.

Koç, Z., Çelik, M., Önal, M., Sarıkaya, Y., Öner, Y. & Açık, L. 2014, 'Study on the synthesis and properties of polyacrylamide/Na-montmorillonite nanocomposites', *Journal of Composite Materials*, vol. 48, no. 4, pp. 439-46.

Kok, M.V. 2002, 'Thermogravimetry of selected bentonites', *Energy Sources*, vol. 24, no. 10, pp. 907-14.

Komadel, P., Schmidt, D., Madejová, J. & Cĭčel, B. 1990, 'Alteration of smectites by treatments with hydrochloric acid and sodium carbonate solutions', *Applied Clay Science*, vol. 5, no. 2, pp. 113-22.

Komadel, P. 2003, 'Chemically modified smectites', *Clay Minerals*, vol. 38, no. 1, pp. 127-38.

Komadel, P. & Madejová, J. 2013, 'Acid activation of clay minerals' in Bergaya, F. Legaly (eds), *Handbook of clay science*, 2nd edn, Elsevier, Amsterdam, pp. 385-409.

Komarneni, S. 1992, 'Nanocomposites', *Journal of Materials Chemistry*, vol. 2, no. 12, pp. 1219-30.

Kornmann, X. 1999, 'Synthesis and Characterization of Thermoset–clay Nanocomposites', PhD Thesis, Luleå University of Technology, Luleå.

Kotlík, P., Justa, P. & Zelinger, J. 1983, 'The Application of Epoxy Resins for the Consolidation of Porous Stone', *Studies in Conservation*, vol. 28, no. 2, pp. 75-9.

Kovacs, T. 1969, *Principles of x-ray metallurgy*, 1st edn, Iliffe, London.

Kramar, S., Urosevic, M., Pristacz, H. & Mirtič, B. 2010, 'Assessment of limestone deterioration due to salt formation by micro-Raman spectroscopy: application to architectural heritage', *Journal of Raman Spectroscopy*, vol. 41, no. 11, pp. 1441-8.

Krishnan, M., Saharay, M. & Kirkpatrick, R.J. 2013, 'Molecular Dynamics Modeling of CO_2 and Poly(ethylene glycol) in Montmorillonite: The Structure of Clay-Polymer

Composites and the Incorporation of CO_2', *J. Phys. Chem. C*, vol. 117, no. 40, pp. 20592-609.

Krzaczkowska, J., Strankowski, M., Jurga, S., Jurga, K. & Pietraszko, A. 2010, 'NMR dispersion studies of poly(ethylene oxide)/sodium montmorillonite nanocomposites', *J. Non-Cryst. Solids*, vol. 356, no. 20-22, pp. 945-51.

Kulicke, W.M. & Siesler, H.W. 1982, 'IR studies of the deuteration of polyacrylamide', *Journal of Polymer Science: Polymer Physics Edition*, vol. 20, no. 3, pp. 553-6.

Kulicke, W.M., Kniewske, R. & Klein, J. 1982, 'Preparation, characterization, solution properties and rheological behaviour of polyacrylamide', *Progress in Polymer Science*, vol. 8, no. 4, pp. 373-468.

Kurochkina, G. & Pinskii, D. 2012, 'Development of a mineralogical matrix at the adsorption of polyelectrolytes on soil minerals and soils', *Eurasian Soil Science*, vol. 45, no. 11, pp. 1057-67.

Kwiatkowski, J. & Whittaker, A.K. 2001, 'Molecular motion in nanocomposites of poly (ethylene oxide) and montmorillonite', *Journal of Polymer Science Part B: Polymer Physics*, vol. 39, no. 14, pp. 1678-85.

Lagaly, G. & Dékány. 2013, 'Colloid clay science' in Bergaya, F. Legaly (eds), *Handbook of clay science*, 2nd edn, Elsevier, Amsterdam, pp. 243-346.

Lagaly, G., Ogawa, M., Dékány, I. 2013, 'Clay mineral-organic interactions' in Bergaya, F. Legaly (eds), *Handbook of clay science*, 2nd edn, Elsevier, Amsterdam, pp. 435-506.

Lagashetty, A. & Venkataraman, A. 2005, 'Polymer nanocomposites', *Resonance*, vol. 10, no. 7, pp. 49-57.

LeBaron, P.C., Wang, Z. & Pinnavaia, T.J. 1999, 'Polymer-layered silicate nanocomposites: an overview', *Applied clay science*, vol. 15, no. 1, pp. 11-29.

Lebovka, N.I., Lysenkov, E.A., Goncharuk, A.I., Gomza, Y.P., Klepko, V.V. & Boiko, Y.P. 2011, 'Phase behaviour, microstructure, and percolation of poly(ethylene glycol) filled by multiwalled carbon nanotubes and organophilic montmorillonite', *J. Compos. Mater.*, vol. 45, no. 24, pp. 2555-66.

Lee, J.Y., Tanaka, H., Takezoe, H., Fukuda, A., Kuze, E. & Iwanaga, H. 1984, 'Novel method of preparing Ag–Hg alloy on polyacrylamide films and their structure', *Journal of Applied Polymer Science*, vol. 29, no. 3, pp. 795-802.

Lemmon, J.P. & Lerner, M.M. 1994, 'Preparation and Characterization of Nanocomposites of Polyethers and Molybdenum Disulfide', *Chemistry of Materials*, vol. 6, no. 2, pp. 207-10.

Lepine, L. & Gilbert, R. 2002, 'Thermal degradation of polyacrylic acid in dilute aqueous solution', *Polymer degradation and stability*, vol. 75, no. 2, pp. 337-45.

Leung, W.M., Axelson, D.E. & Van Dyke, J.D. 1987, 'Thermal degradation of polyacrylamide and poly(acrylamide-co-acrylate)', *J. Polym. Sci., Part A: Polym. Chem.*, vol. 25, no. 7, pp. 1825-46.

Lewin, S.Z. & Baer, N.S. 1974, 'Rationale of the Barium Hydroxide-Urea Treatment of Decayed Stone', *Studies in Conservation*, vol. 19, no. 1, pp. 24-35.

Li, H. & Gao, D. 2011, 'Characterisation of poly (acrylamide)/montmorillonite nanocomposite synthesised by polymerisation induced by UV radiation', *Pigment & Resin Technology*, vol. 40, no. 2, pp. 79-83.

Liao, B., Song, M., Liang, H. & Pang, Y. 2001, 'Polymer-layered silicate nanocomposites. 1. A study of poly(ethylene oxide)/Na+-montmorillonite nanocomposites as polyelectrolytes and polyethylene-block-poly(ethylene glycol) copolymer/Na+-montmorillonite nanocomposites as fillers for reinforcement of polyethylene', *Polymer*, vol. 42, no. 25, pp. 10007-11.

Licchelli, M., Marzolla, S.J., Poggi, A. & Zanchi, C. 2011, 'Crosslinked fluorinated polyurethanes for the protection of stone surfaces from graffiti', *Journal of Cultural Heritage*, vol. 12, no. 1, pp. 34-43.

Lipson, H. & Steeple, H. 1970, *Interpretation of x ray powder diffraction patterns*, 1st edn, Macmillan, London.

Lisci, M., Monte, M. & Pacini, E. 2003, 'Lichens and higher plants on stone: a review', *International Biodeterioration & Biodegradation*, vol. 51, no. 1, pp. 1-17.

Litomyšl 2010, *Recent progress in the consolidation of calcareous materials*, Czech Republic.

Liu, P. 2007, 'Polymer modified clay minerals: A review', *Applied Clay Science*, vol. 38, no. 1–2, pp. 64-76.

Liu, Q. & Zhang, B.-J. 2007, 'Syntheses of a novel nanomaterial for conservation of historic stones inspired by nature', *Materials Letters*, vol. 61, no. 28, pp. 4976-9.

Liu, Q., Zhang, B., Shen, Z. & Lu, H. 2006, 'A crude protective film on historic stones and its artificial preparation through biomimetic synthesis', *Applied Surface Science*, vol. 253, no. 5, pp. 2625-32.

Liufu, S., Xiao, H. & Li, Y. 2005, 'Adsorption of poly (acrylic acid) onto the surface of titanium dioxide and the colloidal stability of aqueous suspension', *Journal of colloid and interface science*, vol. 281, no. 1, pp. 155-63.

Lombardo, P.C., Poli, A.L., Neumann, M.G., Machado, D.S. & Schmitt, C.C. 2013, 'Photodegradation of poly (ethyleneoxide)/montmorillonite composite films', *Journal of Applied Polymer Science*, vol. 127, no. 5, pp. 3687-92.

Long, B., Wang, C.-A., Lin, W., Huang, Y. & Sun, J. 2007, 'Polyacrylamide-clay nacre-like nanocomposites prepared by electrophoretic deposition', *Composites Science and Technology*, vol. 67, no. 13, pp. 2770-4.

Loo, L.S. & Gleason, K.K. 2003, 'Fourier transform infrared investigation of the deformation behavior of montmorillonite in nylon-6/nanoclay nanocomposite', *Macromolecules*, vol. 36, no. 8, pp. 2587-90.

Lopez-Arce, P., Doehne, E., Martin, W. & Pinchin, S. 2008, 'Magnesium sulfate salts and historic building materials: experimental simulation of limestone flaking by relative humidity cycling and crystallization of salts', *Materiales de Construcción*, vol. 58, no. 289-290, pp. 125-42.

Lopez-Arce, P., Garcia-Guinea, J., Benavente, D., Tormo, L. & Doehne, E. 2009a, 'Deterioration of dolostone by magnesium sulphate salt: An example of incompatible building materials at Bonaval Monastery, Spain', *Construction and Building Materials*, vol. 23, no. 2, pp. 846-55.

López-Arce, P., Doehne, E., Greenshields, J., Benavente, D. & Young, D. 2009b, 'Treatment of rising damp and salt decay: the historic masonry buildings of Adelaide, South Australia', *Materials and structures*, vol. 42, no. 6, pp. 827-48.

López-Arce, P., Gomez-Villalba, L.S., Pinho, L., Fernández-Valle, M.E., de Buergo, M.Á. & Fort, R. 2010, 'Influence of porosity and relative humidity on consolidation of dolostone with calcium hydroxide nanoparticles: Effectiveness assessment with non-destructive techniques', *Materials Characterization*, vol. 61, no. 2, pp. 168-84.

López-Arce, P., Fort, R., Gómez-Heras, M., Pérez-Monserrat, E. & Varas-Muriel, M. 2011, 'Preservation strategies for avoidance of salt crystallisation in El Paular Monastery cloister, Madrid, Spain', *Environmental Earth Sciences*, vol. 63, no. 7-8, pp. 1487-509.

López-Arce, P., Zornoza-Indart, A., Gomez-Villalba, L. & Fort, R. 2012, 'Short-and Longer-Term Consolidation Effects of Portlandite (CaOH) 2 Nanoparticles in Carbonate Stones', *Journal of Materials in Civil Engineering*, vol. 25, no. 11, pp. 1655-65.

López-Galindo, A. & Viseras, C. 2004, 'Pharmaceutical and cosmetic applications on clays' in F. Whypych & K.G. Satyanarayana (eds), *Clay surfaces: Fundamentals and applications*, 1st edn, Elsevier, London, pp.267-289.

Lopes, A.C., Martins, P. & Lanceros-Mendez, S. 2014, 'Aluminosilicate and aluminosilicate based polymer composites: Present status, applications and future trends', Progress in Surface Science, vol. 89, no. 3–4, pp. 239-277.

Loughnan, F.C. 1969, *Chemial weathering of the silicate minerals*, American Elsevier Publishing Co. New York.

Lu, J. & Wu, L. 2002, 'Spectrophotometric determination of substrate-borne polyacrylamide', *Journal of agricultural and food chemistry*, vol. 50, no. 18, pp. 5038-41.

Lu, T., Shan, G. & Shang, S. 2010, 'Intermolecular interaction in aqueous solution of binary blends of poly(acrylamide) and poly(ethylene glycol)', *J. Appl. Polym. Sci.*, vol. 118, no. 5, pp. 2572-81.

Luo, J.-J. & Daniel, I.M. 2003, 'Characterization and modeling of mechanical behavior of polymer/clay nanocomposites', *Composites science and technology*, vol. 63, no. 11, pp. 1607-16.

Ma, Y.-H., Wu, S.-Y., Wu, T., Chang, Y.-J., Hua, M.-Y. & Chen, J.-P. 2009, 'Magnetically targeted thrombolysis with recombinant tissue plasminogen activator bound to polyacrylic acid-coated nanoparticles', *Biomaterials*, vol. 30, no. 19, pp. 3343-51.

MacMahon, B. 2001, *The architecture of East Australia:an architectural history in 432 individual presentations,* Edition Axel Menges, Stuttgart.

Madejová, J. 2003, 'FTIR techniques in clay mineral studies', *Vibrational Spectroscopy*, vol. 31, no. 1, pp. 1-10.

Madejova, J. & Komadel, P. 2001, 'Baseline studies of the clay minerals society source clays: infrared methods', *Clays and clay minerals*, vol. 49, no. 5, pp. 410-32.

Madejová, J., Bujdák, J., Janek, M. & Komadel, P. 1998, 'Comparative FT-IR study of structural modifications during acid treatment of dioctahedral smectites and hectorite', *Spectrochimica Acta Part A: Molecular and Biomolecular Spectroscopy*, vol. 54, no. 10, pp. 1397-406.

Madejová, J., Janek, M., Komadel, P., Herbert, H.-J. & Moog, H. 2002, 'FTIR analyses of water in MX-80 bentonite compacted from high salinary salt solution systems', *Applied Clay Science*, vol. 20, no. 6, pp. 255-71.

Mahdavinia, G.R. & Asgari, A. 2013, 'Synthesis of kappa-carrageenan-g-poly (acrylamide)/sepiolite nanocomposite hydrogels and adsorption of cationic dye', *Polymer bulletin*, vol. 70, no. 8, pp. 2451-70.

Malathi, M. & Tamilarasan, K. 2014, 'Synthesis and characterization of polyethylene oxide based nano composite electrolyte', *Sadhana*, vol. 39, no. 4, pp. 999-1007.

Manias, E., Polizos, G., Nakajima, H. & Heidecker, M.J. 2007, 'Fundamentals of Polymer Nanocomposite Technology', in A.B.M.a.C.A. Wilkie (ed.), *Flame Retardant Polymer Nanocomposites*, John Wiley & Sons, Inc., pp. 31-66.

Mata, M., Peacor, D. & Gallart-Martí, M. 2002, 'Transmission electron microscopy (TEM) applied to ancient pottery', *Archaeometry*, vol. 44, no. 2, pp. 155-76.

Matero, F.G. & Tagle, A.A. 1995, 'Cleaning, Iron Stain Removal, and Surface Repair of Architectural Marble and Crystalline Limestone: The Metropolitan Club', *Journal of the American Institute for Conservation*, vol. 34, no. 1, pp. 49-68.

Maurer, J.J., Eustace, D.J. & Ratcliffe, C.T. 1987, 'Thermal characterization of poly(acrylic acid)', *Macromolecules*, vol. 20, no. 1, pp. 196-202.

Max, J.-J. & Chapados, C. 2004, 'Infrared Spectroscopy of Aqueous Carboxylic Acids: Comparison between Different Acids and Their Salts', *The Journal of Physical Chemistry A*, vol. 108, no. 16, pp. 3324-37.

McAfee, P. 2001, Stone buildings: conservation, repair, building, O'Brien Press, Dublin.

McAfee, P. 2011, Irish stone walls, 1st edn, O'Brien Press, New York.

McCluskey, P.H., Snyder, R.L. & Condrate Sr, R. 1989, 'Infrared spectral studies of various metal polyacrylates', *Journal of Solid State Chemistry*, vol. 83, no. 2, pp. 332-9.

McFarlane, A., Bremmell, K. & Addai-Mensah, J. 2005, 'Microstructure, rheology and dewatering behaviour of smectite dispersions during orthokinetic flocculation', *Minerals Engineering*, vol. 18, no. 12, pp. 1173-82.

McGaugh, M.C. & Kottle, S. 1967, 'The thermal degradation of poly(acrylic acid)', *Journal of Polymer Science Part B: Polymer Letters*, vol. 5, no. 9, pp. 817-20.

McGaugh, M. C. & Kottle, S. 1968, 'The thermal degradation of acrylic acid–ethylene polymers', *Journal of Polymer Science Part A-1: Polymer Chemistry*, vol. 6, no. 5, pp. 1243-8.

McGuire, M.J., Addai-Mensah, J. & Bremmell, K.E. 2006, 'Spectroscopic investigation of the adsorption mechanisms of polyacrylamide polymers onto iron oxide particles', *J. Colloid Interface Sci.*, vol. 299, no. 2, pp. 547-55.

Mckinley, J.M., Worden, R.H. & Ruffell, A.H. 2003, 'Smectite in sandstones: a review of the controls on occurrence and behaviour during diagenesis' in Worden, R.H.,

Morad. S (eds), *Clay mineral cements in sandstones*, Blackwell Publishing company, Malden, pp. 110-111.

McNeill, I. & Zulfiqar, M. 1978, 'Thermal degradation of ammonium polymethacrylate and polymethacrylamide', *Journal of Polymer Science: Polymer Chemistry Edition*, vol. 16, no. 10, pp. 2465-74.

McNeill, I.C. & Sadeghi, S.M.T. 1990, 'Thermal Stability and Degradation Mechanisms of Poly(Acrylic Acid) and its Salts: Part 1 Poly(Acrylic Acid)', *Polymer Degradation and Stability*, vol. 29, pp. 233-46.

Mazzola, M., Frediani, P., Bracci, S. & Salvini, A. 2003, 'New strategies for the synthesis of partially fluorinated acrylic polymers as possible materials for the protection of stone monuments', *European Polymer Journal*, vol. 39, no. 10, pp. 1995-2003.

McNally, G.H. & Franklin, B.J. 2000, *Sandstone City, Monograph No. 5: Sydney's Dimension Stone and Other Sandstone Geomaterials: Proceedings of a symposim held on 7th July 2000, during the 15th Australian Geological Convention at the University of Technology Sydney*, Geological Society of Australia Incorporated.

McNally, G. & Whitehouse, J. 2004, 'Sydney sandstone geomaterials-broken, crushed and friale rock products', *Australian Geomechanics: Journal and News of the Australian Geomechanics Society*, vol. 39, no. 4, pp. 47-54.

McSkimming, E.R. 2012, 'Deterioration & Weathering Effects on the Engineering Properties of Sydney (Yellow Block) Sandstone when used as a Building Material', *The UNSW Canberra at ADFA Journal of Undergraduate Engineering Research*, vol. 4, no. 1. pp. 1-24.

Melo, M.J., Bracci, S., Camaiti, M., Chiantore, O. & Piacenti, F. 1999, 'Photodegradation of acrylic resins used in the conservation of stone', *Polymer Degradation and Stability*, vol. 66, no. 1, pp. 23-30.

Menczel, J.D., Prime, R.B. & Gallagher, P.K. 2009, 'Introduction', in J.D. Menczel & R.B. Prime (eds), *Thermal analysis of polymers: fundamentals and applications*, John Wiley & Sons, New Jersey, pp. 1-6.

Miliani, C., Velo-Simpson, M.L. & Scherer, G.W. 2007, 'Particle-modified consolidants: A study on the effect of particles on sol-gel properties and consolidation effectiveness', *Journal of Cultural Heritage*, vol. 8, no. 1, pp. 1-6.

Millot, G., 1970, *Geology of clays*, trans. W. R. Farrand, H. Paquet, Chapman & Hall, London.

Minichelli, D. 1982, 'THE QUANTITATIVE PHASE ANALYSIS OF CLAY MINERALS BY X-RAY DIFFRACTION. MODERN ASPECTS OF INDUSTRIAL ROUTINE CONTROL', *Clay Minerals*, vol. 17, no. 4, pp. 401-8.

Miranda-Trevino, J.C. & Coles, C.A. 2003, 'Kaolinite properties, structure and influence of metal retention on pH', *Applied Clay Science*, vol. 23, no. 1-4, pp. 133-9.

Mittal, V. 2010, 'Polymer nanocomposites: synthesis, microstructure, and properties', *Optimization of polymer nanocomposite properties. Wiley-VCH Verlag GmbH & Co. KGaA, Weinheim*, pp. 1-19.

Mittal, V. 2012, *Characterization Techniques for Polymer Nanocomposites*, Wiley-VCH, Weinheim.

Moharram, M.A. & El-Gendy, H.M. 2002, 'Infrared spectroscopy and electrical properties of ternary poly(acrylic acid)-metal-poly(acrylamide) complexes', *J. Appl. Polym. Sci.*, vol. 85, no. 13, pp. 2699-705.

Moharram, M. & Khafagi, M. 2007, 'Application of FTIR spectroscopy for structural characterization of ternary poly (acrylic acid)–metal–poly (vinyl pyrrolidone) complexes', *Journal of applied polymer science*, vol. 105, no. 4, pp. 1888-93.

Moharram, M.A., Rabie, S. & El-Gendy, H. 2002, 'Infrared spectra of γ-irradiated poly (acrylic acid)–polyacrylamide complex', *Journal of applied polymer science*, vol. 85, no. 8, pp. 1619-23.

Mola, F.Z. 2011, Natural stone houses, 1st edn, Frechmann Kolón GmbH, Barcelona.

Moncrieff, A. 1976, 'The Treatment of Deteriorating Stone with Silicone Resins: Interim Report', *Studies in Conservation*, vol. 21, no. 4, pp. 179-91.

Moncrieff, A. & Hempel, K.F.B. 1977, 'Conservation of Sculptural Stonework: Virgin & Child on S. Maria dei Miracoli and the Loggetta of the Campanile, Venice', *Studies in Conservation*, vol. 22, no. 1, pp. 1-11.

Moore, D.M. & Reynolds, R.C., 1997, *X-ray diffraction and the identification and analysis of clay minerals*, 2nd edn, Oxford university press, New York

Moreno, F., Vilela, S.A.G., Antunes, Â.S.G. & Alves, C.A.S. 2006, 'Capillary-rising salt pollution and granitic stone erosive decay in the parish church of Torre de Moncorvo (NE Portugal)-implications for conservation strategy', *Journal of Cultural Heritage*, vol. 7, no. 1, pp. 56-66.

Morent, R., De Geyter, N., Van Vlierberghe, S., Vanderleyden, E., Dubruel, P., Leys, C. & Schacht, E. 2009, 'Deposition of Polyacrylic Acid Films by Means of an Atmospheric Pressure Dielectric Barrier Discharge', *Plasma Chemistry and Plasma Processing*, vol. 29, no. 2, pp. 103-17.

Morgan, A.B. & Gilman, J.W. 2003, 'Characterization of polymer-layered silicate (clay) nanocomposites by transmission electron microscopy and X-ray diffraction: A comparative study', *Journal of Applied Polymer Science*, vol. 87, no. 8, pp. 1329-38.

Moronta. A., 2004, 'Catalytic and adsorption properties of modified clay surfaces' in F. Whypych & K.G. Satyanarayana (eds), *Clay surfaces: Fundamentals and applications*, 1st edn, Elsevier, London, pp. 321-344.

Moropoulou, A., Haralampopoulos, G., Tsiourva, T., Auger, F. & Birginie, J. 2003a, 'Artificial weathering and non-destructive tests for the performance evaluation of consolidation materials applied on porous stones', *Materials and Structures*, vol. 36, no. 4, pp. 210-7.

Moropoulou, A., Kouloumbi, N., Haralampopoulos, G., Konstanti, A. & Michailidis, P. 2003b, 'Criteria and methodology for the evaluation of conservation interventions on treated porous stone susceptible to salt decay', *Progress in Organic Coatings*, vol. 48, no. 2-4, pp. 259-70.

Mosquera, M.J., Benítez, D. & Perry, S.H. 2002, 'Pore structure in mortars applied on restoration: Effect on properties relevant to decay of granite buildings', *Cement and Concrete Research*, vol. 32, no. 12, pp. 1883-8.

Mosquera, M.J., de los Santos, D.M. & Rivas, T. 1986, 'Surfactant-Synthesized Ormosils with Application to Stone Restoration', *Langmuir*, vol. 26, no. 9, pp. 6737-45.

Mosquera, M.J., de los Santos, D.M., Montes, A. & Valdez-Castro, L. 2005, 'New Nanomaterials for Consolidating Stone', *Langmuir*, vol. 24, no. 6, pp. 2772-8.

Mosquera, M.J., Pozo, J. & Esquivias, L. 2003, 'Stress During Drying of Two Stone Consolidants Applied in Monumental Conservation', *Journal of Sol-Gel Science and Technology*, vol. 26, no. 1, pp. 1227-31.

Mosquera, M.J., Pozo, J., Esquivias, L., Rivas, T. & Silva, B. 2002, 'Application of mercury porosimetry to the study of xerogels used as stone consolidants', *Journal of Non-Crystalline Solids*, vol. 311, no. 2, pp. 185-94.

Mpofu, P., Addai-Mensah, J. & Ralston, J. 2004, 'Flocculation and dewatering behaviour of smectite dispersions: effect of polymer structure type', Minerals Engineering, vol. 17, no. 3, pp. 411-23.

Mpofu, P., Addai-Mensah, J. & Ralston, J. 2005, 'Interfacial chemistry, particle interactions and improved dewatering behaviour of smectite clay dispersions', International Journal of Mineral Processing, vol. 75, no. 3–4, pp. 155-71.

Mukherjee, S. 2013, *The Science of Clays*, Springer, Heidelberg, Germany.

Munnikendam, R.A. 1967, 'Preliminary Notes on the Consolidation of Porous Building Materials by Impregnation with Monomers', *Studies in Conservation*, vol. 12, no. 4, pp. 158-62.

Munnikendam, R.A. 1973, 'A New System for the Consolidation of Fragile Stone', *Studies in Conservation*, vol. 18, no. 2, pp. 95-7.

Nadler, A., Malik, M. & Letey, J. 1992, 'Desorption of polyacrylamide and polysaccharide polymers from soil materials', *Soil technology*, vol. 5, no. 1, pp. 91-5.

Naskar, A.K. & De, P.P. 2010, 'Applications of DSC and TGA for the Characterisation of Rubbers and Rubbery Materials', in R. Brown (ed.), *Thermal Analysis of Rubbers and Rubbery Materials*, Elsevier, Shawbury, pp. 65-148.

Natkański, P., Kuśtrowski, P., Białas, A., Piwowarska, Z. & Michalik, M. 2012, 'Controlled swelling and adsorption properties of polyacrylate/montmorillonite composites', *Materials Chemistry and Physics*, vol. 136, no. 2, pp. 1109-15.

Natkański, P., Kuśtrowski, P., Białas, A., Piwowarska, Z. & Michalik, M. 2013, 'Thermal stability of montmorillonite polyacrylamide and polyacrylate nanocomposites and adsorption of Fe (III) ions', *Applied Clay Science*, vol. 75, pp. 153-7.

National Research Council (U.S.). Committee on Conservation of Historic Stone Buildings and Monuments. 1982, *Conservation of historic stone buildings and monuments: report of the Committee on Conservation of Historic Stone Buildings and Monuments, National Materials Advisory Board, Commission on Engineering and Technical Systems, National Research Council*, National Academy Press, Washington D.C.

Nemecz, E. 1981, *Clay minerals*, Akadémiai Kiadó, Budapest.

Nguyen, Q.T. & Baird, D.G. 2006, 'Preparation of polymer–clay nanocomposites and their properties', *Advances in Polymer Technology*, vol. 25, no. 4, pp. 270-85.

NSW Government: Office of Environment and Heritage 2012, *Built heritage*, Sydney, viewed 10 June 2015, <http://www.environment.nsw.gov.au/Heritage/aboutheritage/builtheritage.htm>.

NSW Government: Office of Environment and Heritage 2016, *Air quality index values - updated hourly*, Sydney, viewed 18 August 2016, <http://www.environment.nsw.gov.au/aqms/aqitable.htm>.

NSW Government: NSW Public Works 2009, Centenary Stonework Program 2008/2009 Program Achievements, Pamphlet, NSW Public Works, Sydney.

NSW Government: Public Works Advisory n.d., Minister's Stonework Probram, viewed 26 June 2016, <http://www.publicworks.nsw.gov.au/architecture-heritage/ministers-stonework>.

Nyquist, R., Platt, A. & Priddy, D. 1982, 'Infrared studies of styrene-acrylic acid and styrene-acrylamide copolymers at variable temperature', *Applied Spectroscopy*, vol. 36, no. 4, pp. 417-20.

Önal, M. & Sarıkaya, Y. 2007, 'Thermal behavior of a bentonite', *Journal of Thermal Analysis and Calorimetry*, vol. 90, no. 1, pp. 167-72.

O'Connor, J.R., Abhi; Franklin, Brenda; Stuart, Barbara 2001, 'Changes in the physical and chemical properties of weathered maroubra sandstone in Sydney', *AICCM bulletin*, vol. 26, pp. 20-5.

Ogawa, M., Kuroda, K. & Kato, C. 1989, 'Preparation of montmorillonite-polyacrylamide intercalation compounds and the water absorbing property', *Clay Science*, vol. 7, no. 4, pp. 243-51.

Okada, A. & Usuki, A. 2006, 'Twenty Years of Polymer-Clay Nanocomposites', *Macromolecular Materials and Engineering*, vol. 291, no. 12, pp. 1449-76.

Olad, A. 2011, 'Polymer/clay nanocomposites', in B. Reddy (ed.), *Advances in diverse industrial applications of nanocomposites*, pp. 113-38.

Oliver, A.B. 2002, 'The Variable Performance of Ethyl Silicate: Consolidated Stone at Three National Parks', *APT Bulletin*, vol. 33, no. 2/3, pp. 39-44.

Olodovskii, P. & Murashko, M. 1976, 'Influence of water-soluble polymers and electrolytes on the permeability of weak-filtering dispersed systems', *Journal of engineering physics*, vol. 30, no. 2, pp. 222-7.

Onder, E., Sarier, N., Ukuser, G., Ozturk, M. & Arat, R. 2013, 'Ultrasound assisted solvent free intercalation of montmorillonite with PEG1000: a new type of organoclay with improved thermal properties', *Thermochimica Acta*, vol. 566, pp. 24-35.

Orwell & Peter Phillips 2008, *Who's responsible for this?*, extracts from a keynote address to the CSAAR Conference, viewed 01 May 2016, < http://www.opp.net.au/240/articles/whos-responsible-for-this/ >.

Osete-Cortina, L. & Doménech-Carbó, M.T. 2006, 'Characterization of acrylic resins used for restoration of artworks by pyrolysis-silylation-gas chromatography/mass spectrometry with hexamethyldisilazane', *Journal of Chromatography A*, vol. 1127, no. 1-2, pp. 228-36.

Pan, W. & Chen, Y. 2011, 'Preparation of Ag–polyacrylamide nanocomposites by ultraviolet irradiation technique', *Applied Mechanics and Materials*, vol. 44, Trans Tech Publ, pp. 2199-202.

Papke, B., Ratner, M.A. & Shriver, D. 1981, 'Vibrational spectroscopy and structure of polymer electrolytes, poly (ethylene oxide) complexes of alkali metal salts', *Journal of Physics and Chemistry of Solids*, vol. 42, no. 6, pp. 493-500.

Parfitt, R. & Greenland, D. 1970a, 'Adsorption of water by montmorillonite-poly (ethylene glycol) adsorption products', *Clay Mineralogy*, vol. 8, pp. 317-24.

Parfitt, R. & Greenland, D. 1970b, 'The adsorption of poly (ethylene glycols) on clay minerals', *Clay Minerals*, vol. 8, no. 3, pp. 305-15.

Park, H.D. & Shin, G.H. 2009, 'Geotechnical and geological properties of Mokattam limestones: Implications for conservation strategies for ancient Egyptian stone monuments', *Engineering Geology*, vol. 104, no. 3-4, pp. 190-9.

Paul, D. & Robeson, L. 2008, 'Polymer nanotechnology: nanocomposites', *Polymer*, vol. 49, no. 15, pp. 3187-204.

Pavlidou, S. & Papaspyrides, C.D. 2008, 'A review on polymer–layered silicate nanocomposites', *Progress in Polymer Science*, vol. 33, no. 12, pp. 1119-98.

Pecharsky, V.K. & Zavalij, P.Y. 2009, *Fundamentals of powder diffraction and structural characterization of materials,* 2nd edn, Springer, New York.

Pefferkorn, E. 1999, 'Polyacrylamide at Solid/Liquid Interfaces', *Journal of Colloid and Interface Science*, vol. 216, no. 2, pp. 197-220.

Pells, P. 1977, 'Measurement of engineering properties of Hawkesbury Sandstone', *Australian Geomechanics Journal*, vol. 7, no. 1, pp. 10-20.

Petit, S. 2006, 'Fourier transform infrared spectroscopy' in Bergaya, F. Legaly (eds), *Handbook of clay science*, 1st edn, Elsevier, Amsterdam, pp. 213–231.

Petrie, E.M. 2006, *Epoxy adhesive formulations*, McGraw-Hill, London.

Pettijohn, F.J., Potter, P.E. & Siever, R. 2005, Sand and sandstone, 2nd edn, Springer-Verlag, New York.

Pham, H. & Nguyen, Q.P. 2014, 'Effect of silica nanoparticles on clay swelling and aqueous stability of nanoparticle dispersions', *Journal of Nanoparticle Research*, vol. 16, no. 1, pp. 1-11.

Piacenti, F. 1994, 'Chemistry for the conservation of the cultural heritage', *Science of The Total Environment*, vol. 143, no. 1, pp. 113-20.

Pieper, R. 1995, 'Symposium on Preservation Treatments for Historic Masonry: An Introduction', *APT Bulletin*, vol. 26, no. 4, pp. 6-8.

Piñar, G., Jimenez-Lopez, C., Sterflinger, K., Ettenauer, J., Jroundi, F., Fernandez-Vivas, A. & Gonzalez-Muñoz, M. 2010, 'Bacterial Community Dynamics During the Application of a & a Myxococcus xanthus-Inoculated Culture Medium Used for Consolidation of Ornamental Limestone', *Microbial Ecology*, vol. 60, no. 1, pp. 15-28.

Pinna, D., Salvadori, B. & Porcinai, S. 2011, 'Evaluation of the application conditions of artificial protection treatments on salt-laden limestones and marble', *Construction and Building Materials*, vol. 25, no. 5, pp. 2723-32.

Pinnavaia, T.J. 1983, 'Intercalated clay catalysts', *Science*, vol. 220, no. 4595, pp. 365-71.

Pinto, A.P.F. & Rodrigues, J.D. 2008, 'Stone consolidation: The role of treatment procedures', *Journal of Cultural Heritage*, vol. 9, no. 1, pp. 38-53.

Pomogailo, A. 2005, 'Hybrid Intercalative Nanocomposites', *Inorganic Materials*, vol. 41, no. 0, pp. S47-S74.

Pope, G.A., Meierding, T.C. & Paradise, T.R. 2002, 'Geomorphology's role in the study of weathering of cultural stone', *Geomorphology*, vol. 47, no. 2-4, pp. 211-25.

Prime, R.B., Bair, H.E., Vyazovkin, S., Gallagher, P.K. & Riga, A. 2009, "Thermogravimetric Analysis (TGA)', in J.D. Menczel & R.B. Prime (eds), *Thermal analysis of polymers: fundamentals and applications*, John Wiley & Sons, New Jersey, pp. 241-317.

Proietti, N., Capitani, D., Cozzolino, S., Valentini, M., Pedemonte, E., Princi, E., Vicini, S. & Segre, A.L. 2006, 'In Situ and Frontal Polymerization for the Consolidation of Porous Stones: A Unilateral NMR and Magnetic Resonance Imaging Study', *The Journal of Physical Chemistry B*, vol. 110, no. 47, pp. 23719-28.

Pusino, A., Gennari, M., Premoli, A. & Gessa, C. 1990, 'Formation of polyethylene glycol on montmorillonite by sterilization with ethylene oxide', *Clays and Clay Minerals*, vol. 38, no. 2, pp. 213-5.

Rady, M. 2009, 'Study of phase changing characteristics of granular composites using differential scanning calorimetry', *Energy Conversion and Management*, vol. 50, no. 5, pp. 1210-7.

Rakhshani, M., Kamrannejad, M.M., Babaluo, A.A., Rezaei, M. & Aghjeh, M.R. 2012, 'Thermal degradation behavior and kinetic studies of polyacrylamide gel in TiO2 nanoparticles synthesis', *Iran. Polym. J.*, vol. 21, no. 12, pp. 821-8.

Ramachandran, V.S., Paroli, R.M., Beaudoin, J.J. & Delgado, A.H. 2002, *Handbook of thermal analysis of construction materials*, William Andrew, New York.

Ratanarat, K., Nithitanakul, M., Martin, D. & Magaraphan, R. 2003, 'Polymer-layer silicate nanocomposites: linear PEO and highly branched dendrimer for organic wastewater treatment', *Reviews on Advanced Materials Science*, vol. 5, no. 3, pp. 187-92.

Ratna, D. & Abraham, T. 2011, 'Rheological properties and crystal morphology of poly (ethylene oxide)/clay nanocomposites', *Polymer Composites*, vol. 32, no. 8, pp. 1210-7.

Rao, S.M., Brinker, C.J. & Ross, T.J. 1996, 'Environmental microscopy in stone conservation', *Scanning*, vol. 18, no. 7, pp. 508-14.

Ray, H.N. 1982, 'Weathering of Sydney sandstone in buildings and outcrop', Master thesis, New South Wales Institute of Technology, Sydney.

Reddy, K.S., Prabhakar, M.N., Babu, P.K., Venkatesulu, G., Rao, U.S.K., Rao, K.C. & Subha, M.C.S. 2012, 'Miscibility studies of hydroxypropyl cellulose/poly(ethylene glycol) in dilute solutions and solid state', *Int. J. Carbohydr. Chem.*, pp. 906389, 9 pp.

Reeves, G. M., Sims, I. & Cripps, J.C. 2006, *Clay materials used in construction*, Engineering Geology Special Publication, London, pp. 1-75.

Reichelt, R. 2007, 'Scanning electron microscopy ', in P. W. Hawkes & J. C.H. Spence (ed.), *Science of microscopy*, Springer, New York, pp. 133-272.

Reinholdt, M.X., Kirkpatrick, R.J. & Pinnavaia, T.J. 2005, 'Montmorillonite-Poly(ethylene oxide) Nanocomposites: Interlayer Alkali Metal Behavior', *J. Phys. Chem. B*, vol. 109, no. 34, pp. 16296-303.

Reynolds, R.C. Jr. 1989, 'Principles of powder diffraction', in D.L. Bish & J.E. Post (ed.), T Modern powder diffraction, Mineralogical Society of America, Washington, D.C., pp. 1-17.

Robert, J.-L. & Kodama, H. 1988, 'Generalization of the correlations between hydroxyl-stretching wavenumbers and composition of micas in the system K2O-MgO-Al2O3-SiO2-H2O: a single model for trioctahedral and dioctahedral micas', *American Journal of Science. A*, vol. 288, pp. 196-212.

Rodrigues, J.D. 2001, 'Consolidation of decayed stones. A delicate problem with few practical solutions', *Historical Constructions*, pp. 3-14.

Rodrigues, J.D. & Grossi, A. 2007, 'Indicators and ratings for the compatibility assessment of conservation actions', *Journal of Cultural Heritage*, vol. 8, no. 1, pp. 32-43.

Rodrigues, J.D., Pinto, A.F. & da Costa, D.R. 2002, 'Tracing of decay profiles and evaluation of stone treatments by means of microdrilling techniques', *Journal of Cultural Heritage*, vol. 3, no. 2, pp. 117-25.

Rodriguez-Navarro, C. & Doehne, E. 1999, 'Salt weathering: influence of evaporation rate, supersaturation and crystallization pattern', *Earth Surface Processes and Landforms*, vol. 24, no. 3, pp. 191-209.

Rodriguez-Navarro, C., Rodriguez-Gallego, M., Ben Chekroun, K. & Gonzalez-Munoz, M.T. 2003, 'Conservation of Ornamental Stone by Myxococcus xanthus-Induced Carbonate Biomineralization', *Appl. Environ. Microbiol.*, vol. 69, no. 4, pp. 2182-93.

Ross, B. & Guggenheim, S. 2002, ‘Interlayer reactions in expandable clays: exchange, salvation, and intercalation experiments’ in Rule, A.C., Guggenheim, S. (eds), *teaching clay science*, The Clay Mineral Society, Aurora, pp. 162-164.

Rossi, S., Luckham, P.F. & Tadros, T.F. 2003, 'Influence of non-ionic polymers on the rheological behavior of Na+-montmorillonite clay suspensions. Part II. Homopolymer ethyleneoxide and polypropylene oxide-polyethylene oxide ABA copolymers', *Colloids Surf., A*, vol. 215, no. 1-3, pp. 1-10.

Rozenbaum, O., Barbanson, L., Muller, F. & Bruand, A. 2008, 'Significance of a combined approach for replacement stones in the heritage buildings’ conservation frame', *Comptes Rendus Geoscience*, vol. 340, no. 6, pp. 345-55.

Ruiz-Agudo, E., Rodriguez-Navarro, C. & Sebastián-Pardo, E. 2006, 'Sodium Sulfate Crystallization in the Presence of Phosphonates: Implications in Ornamental Stone Conservation', *Crystal Growth & Design*, vol. 6, no. 7, pp. 1575-83.

Ruiz-Hitzky, E. 1993, 'Conducting polymers intercalated in layered solids', *Advanced Materials*, vol. 5, no. 5, pp. 334-40.

Ruiz-Hitzky, E. 2003, 'Functionalizing Inorganic Solids: Towards Organic–Inorganic Nanostructured Materials for Intelligent and Bioinspired Systems', *The Chemical Record*, vol. 3, no. 2, pp. 88-100.

Ruiz-Hitzky, E. & Aranda, P. 1990, 'Polymer-salt intercalation complexes in layer silicates', *Advanced Materials*, vol. 2, no. 11, pp. 545-7.

Ruiz-Hitzky, E. & Van Meerbeek, A. 2006, 'Clay Mineral–and Organoclay–Polymer Nanocomposite', *Developments in Clay Science*, vol. 1, pp. 583-621.

Russell, J.D. 1987, ‘Infrared methods', in M.J. Wilson (ed.), *A handbook of determinative methods in clay mineralogy*, Blackie & Son Limited, Glasgow, pp. 133-173.

Sabbioni, C. 2003, ‘In The Effects of Air Pollution on the Built Environment’, P. Brimblecombe (ed.), *Mechanisms of air pollution damage to stone*, Imperial College Press, London, pp. 63-106.

Sadat-Shojai, M. & Ershad-Langroudi, A. 2009, 'Polymeric coatings for protection of historic monuments: Opportunities and challenges', *Journal of Applied Polymer Science*, vol. 112, no. 4, pp. 2535-51.

Salazar-Hernández, C., Alquiza, M.J.P., Salgado, P. & Cervantes, J. 2010, 'TEOS–colloidal silica–PDMS-OH hybrid formulation used for stone consolidation', *Applied Organometallic Chemistry*, vol. 24, no. 6, pp. 481-8.

Salazar-Hernández, C., Zárraga, R., Alonso, S., Sugita, S., Calixto, S. & Cervantes, J. 2009, 'Effect of solvent type on polycondensation of TEOS catalyzed by DBTL as used for stone consolidation', *Journal of Sol-Gel Science and Technology*, vol. 49, no. 3, pp. 301-10.

Saleh, S.A., Helmi, F.M., Kamal, M.M. & El-Banna, A.-F.E. 1992, 'Study and Consolidation of Sandstone: Temple of Karnak, Luxor, Egypt', *Studies in Conservation*, vol. 37, no. 2, pp. 93-104.

Salimbeni, R., Pini, R., Siano, S. & Calcagno, G. 2000, 'Assessment of the state of conservation of stone artworks after laser cleaning: comparison with conventional cleaning results on a two-decade follow up', *Journal of Cultural Heritage*, vol. 1, no. 4, pp. 385-91.

Saravanan, R. & Rani, M.P. 2012, 'Charge Density Analysis from X-Ray Diffraction', *Metal and Alloy Bonding-An Experimental Analysis*, Springer, pp. 31-64.

Sarier, N. & Onder, E. 2010, 'Organic modification of montmorillonite with low molecular weight polyethylene glycols and its use in polyurethane nanocomposite foams', *Thermochimica Acta*, vol. 510, no. 1, pp. 113-21.

Saujanya, C. & Radhakrishnan, S. 1997, 'Crystallization behavior of polyethylene oxide/para-nitroaniline microdispersed composites', *Journal of applied polymer science*, vol. 65, no. 6, pp. 1127-37.

Sawyer, L.C., Grubb, D.T., Meyers, G.F. 2008, *Polymer microscopy*, vol. 3, Springer, New York.

Schaffer, R.J. 2016, *The weathering of natural building stones*, Routledge, London.

Schild, H. 1996, 'Thermal decomposition of PNIPAAM: TGA–FTIR analysis', *Journal of Polymer Science Part A: Polymer Chemistry*, vol. 34, no. 11, pp. 2259-62.

Schmuckler, G. & Limoni, B. 1977, 'Interaction of platinum chloride with a polyacrylamide gel and its monomeric analogues', *Journal of Inorganic and Nuclear Chemistry*, vol. 39, no. 1, pp. 137-41.

Schoonheydt, R.T. & Johnston, C.T. 2013, 'Surface and interface chemistry of clay minerals' in Bergaya, F. Legaly (eds), *Handbook of clay science*, 2nd edn, Elsevier, Amsterdam, pp. 139-172.

Sengwa, R.J. & Choudhary, S. 2014, 'Structural characterization of hydrophilic polymer blends/montmorillonite clay nanocomposites', *J. Appl. Polym. Sci.*, vol. 131, no. 16, pp. 40617/1-/11.

Sengwa, R., Choudhary, S. & Sankhla, S. 2009, 'Dielectric spectroscopy of hydrophilic polymers–montmorillonite clay nanocomposite aqueous colloidal suspension', *Colloids and Surfaces A: Physicochemical and Engineering Aspects*, vol. 336, no. 1, pp. 79-87.

Sengwa, R., Choudhary, S. & Dhatarwal, P. 2015, 'Influences of ultrasonic-and microwave-irradiated preparation methods on the structural and dielectric properties of (PEO–PMMA)–LiCF3SO3–x wt% MMT nanocomposite electrolytes', *Ionics*, vol. 21, no. 1, pp. 95-109.

Selwitz, C. 1995, 'The Use of Epoxy Resins for the Stabilization of Deteriorated Masonry', *APT Bulletin*, vol. 26, no. 4, pp. 27-34.

Setoguchi, Y., Monobe, H., Wan, W., Terasawa, N., Kiyohara, K., Nakamura, N. & Shimizu, Y. 2004, 'Infrared Spectral Studies of Triphenylene Mesogens Possessing Terminal Functional Groups in the Peripheral Chains for Hydrogen-Bond Interaction', *Molecular Crystals and Liquid Crystals*, vol. 412, no. 1, pp. 9-18.

Shami, Z., Sharifi-Sanjani, N., Khanyghma, B., Farjpour, S. & Fotouhi, A. 2014, 'Ordered exfoliated silicate platelets architecture: hydrogen bonded poly(acrylic acid)-poly(ethylene oxide)/Na-montmorillonite complex nanofibrous membranes prepared by electrospinning technique', *RSC Advances*, vol. 4, no. 77, pp. 40892-7.

Sharma, R., Bisen, D., Shukla, U. & Sharma, B. 2012, 'X-ray diffraction: a powerful method of characterizing nanomaterials', *Recent Research in Science and Technology*, vol. 4, no. 8, pp. 77-9.

Shen, Y.-H. 2002, 'Estimation of surface area of montmorillonite by ethylene oxide chain adsorption', *Chemosphere*, vol. 48, no. 10, pp. 1075-9.

Shen, Z., Simon, G.P. & Cheng, Y.-B. 2002, 'Comparison of solution intercalation and melt intercalation of polymer–clay nanocomposites', *Polymer*, vol. 43, no. 15, pp. 4251-60.

Shen, Z., Simon, G.P. & Cheng, Y.-B. 2003, 'Saturation ratio of poly(ethylene oxide) to silicate in melt intercalated nanocomposites', *Eur. Polym. J.*, vol. 39, no. 9, pp. 1917-24.

Shi, L. 2000, 'An approach to the flame retardation and smoke suppression of ethylene–vinyl acetate copolymer by plasma grafting of acrylamide', *Reactive and Functional Polymers*, vol. 45, no. 2, pp. 85-93.

Shimizu, K. & Mitani, T. 2010, New horizons of applied scanning electron microscopy, vol. 45, Springer-Verlag, Heidelberg.

Siegesmund, S. & Snethlage, R. 2010, *Stone in Architecture: Properties, Durability*, Springer Verlag, Berlin.

Siegesmund, S., Weiss, T. & Vollbrecht, A. 2002, 'Natural stone, weathering phenomena, conservation strategies and case studies: introduction', *Geological Society, London, Special Publications*, vol. 205, no. 1, pp. 1-7.

Siesler, H.W. & Holland-Moritz, K. 1980, *Infrared and Raman spectroscopy of polymers*, vol. 4, M. Dekker.

Sinha Ray, S. & Okamoto, M. 2003, 'Polymer/layered silicate nanocomposites: a review from preparation to processing', *Progress in Polymer Science*, vol. 28, no. 11, pp. 1539-1641.

Skipper, N., Sposito, G. & Chang, F.-R.C. 1995, 'Monte Carlo simulation of interlayer molecular structure in swelling clay minerals. 2. Monolayer hydrates', *Clays and Clay minerals*, vol. 43, no. 3, pp. 294-303.

Skoulikidis, T., Vassiliou, P. & Tsakona, K. 2005, 'Surface Consolidation of Pentelic Marble: Criteria for the selection of methods and materials-The Acropolis case (6 pp)', *Environmental Science and Pollution Research*, vol. 12, no. 1, pp. 28-33.

Slonimskaya, M., Besson, G., Dainyak, L., Tchoubar, C. & Drits, V. 1986, 'Interpretation of the IR spectra of celadonites and glauconites in the region of OH-stretching frequencies', *CLAY MINER. Clay Miner.*, vol. 21, no. 3, p. 377.

Smith, B.C. 2011, *Fundamentals of Fourier transform infrared spectroscopy*, CRC press, Boca Raton.

Smith, B.J., Baptista-Neto, J.A., Silva, M.A.M., McAlister, J.J., Warke, P.A. & Curran, J.M. 2004, 'The decay of coastal forts in southeast Brazil and its implications for the conservation of colonial built heritage', *Environmental Geology*, vol. 46, no. 3, pp. 493-503.

Sofianopoulos, A.J. 1951, 'Conservation of ancient marble monuments', *Journal of Chemical Education*, vol. 28, no. 2, pp. 79-81.

Son, S., Won, J., Kim, J.-J., Jang, Y.D., Kang, Y.S. & Kim, S.D. 2009, 'Organic−Inorganic Hybrid Compounds Containing Polyhedral Oligomeric Silsesquioxane for Conservation of Stone Heritage', *ACS Applied Materials & Interfaces*, vol. 1, no. 2, pp. 393-401.

Song, Y., Petty, M., Yarwood, J., Feast, W., Tsibouklis, J. & Mukherjee, S. 1992, 'Fourier transform infrared studies of molecular ordering and interactions in Langmuir-Blodgett films containing nitrostilbene and stearic acid', *Langmuir*, vol. 8, no. 1, pp. 257-61.

Song, T., Goh, S. & Lee, S. 2002, 'Interpolymer complexes through hydrophobic interactions: C60-end-capped linear or four-arm poly (ethylene oxide)/poly (acrylic acid) complexes', *Macromolecules*, vol. 35, no. 10, pp. 4133-7.

Sowwan, M., Faroun, M., Musa, I., Ibrahim, I., Makharza, S., Sultan, W. & Dweik, H. 2008, 'Study on the morphology of polyacrylamide–silica fumed nanocomposite thin films', *Int J Phys Sci*, vol. 3, no. 6, pp. 144-7.

Steudel, A., Batenburg, L., Fischer, H., Weidler, P. & Emmerich, K. 2009, 'Alteration of swelling clay minerals by acid activation', *Applied Clay Science*, vol. 44, no. 1, pp. 105-15.

Strawhecker, K.E. & Manias, E. 2000, 'Structure and Properties of Poly(vinyl alcohol)/Na+ Montmorillonite Nanocomposites', *Chemistry of Materials*, vol. 12, no. 10, pp. 2943-9.

Strawhecker, K.E. & Manias, E. 2003, 'Crystallization Behavior of Poly(ethylene oxide) in the Presence of Na+ Montmorillonite Fillers', *Chem. Mater.*, vol. 15, no. 4, pp. 844-9.

Striegel, M.F., Bede Guin, E., Hallett, K., Sandoval, D., Swingle, R., Knox, K., Best, F. & Fornea, S. 2003, 'Air pollution, coatings, and cultural resources', *Progress in Organic Coatings*, vol. 48, no. 2-4, pp. 281-8.

Stuart, B. & Ando, D.J. 1997, *Biological applications of infrared spectroscopy*, John Wiley, New York.

Stuart, B.H. 2007, 'Conservation Materials', *Analytical Techniques in Materials Conservation*, John Wiley & Sons, Ltd, Chichester, pp. 1-42.

Stuart, G. 1993, Secrets in stone: discover the history of Sydney, 1st edn, Brandname Properties Ltd, Sydney.

Stuart, M., Scheutjens, J.M.H. & Fleer, G. 1980, 'Polydispersity effects and the interpretation of polymer adsorption isotherms', *Journal of Polymer Science: Polymer Physics Edition*, vol. 18, no. 3, pp. 559-73.

Stück, H., Forgó, L., Rüdrich, J., Siegesmund, S. & Török, A. 2008, 'The behaviour of consolidated volcanic tuffs: weathering mechanisms under simulated laboratory conditions', *Environmental geology*, vol. 56, no. 3-4, pp. 699-713.

Su, C.-C. & Shen, Y.-H. 2008, 'Effects of poly (ethylene oxide) adsorption on the dispersion of smectites', *Colloids and Surfaces A: Physicochemical and Engineering Aspects*, vol. 312, no. 1, pp. 1-6.

Sudo, T., Shimoda, S., Yotsumoto, H. & Aita, S. 1981, *Electron micrographs of clay minerals*, Elsevier Scientific Pub. Co., New York.

Sugahara, Y., Satokawa, S., Kuroda, K. & Kato, C. 1990, 'Preparation of a kaolinite-polyacrylamide intercalation compound', *Clays Clay Miner.*, vol. 38, no. 2, pp. 137-43.

Sun, L., Kepley, L.J. & Crooks, R.M. 1992, 'Molecular interactions between organized, surface-confined monolayers and vapor-phase probe molecules: Hydrogen-bonding interactions', *Langmuir*, vol. 8, no. 9, pp. 2101-3.

Sun, J., Wu, T., Liu, F., Wang, Z., Zhang, X. & Shen, J. 2000, 'Covalently attached multilayer assemblies by sequential adsorption of polycationic diazo-resins and polyanionic poly (acrylic acid)', *Langmuir*, vol. 16, no. 10, pp. 4620-4.

Sun, L., Ertel, E.A., Zhu, L., Hsiao, B.S., Avila-Orta, C.A. & Sics, I. 2005, 'Reversible de-intercalation and intercalation induced by polymer crystallization and melting in a poly (ethylene oxide)/organoclay nanocomposite', *Langmuir*, vol. 21, no. 13, pp. 5672-6.

Suter, J.L. & Coveney, P.V. 2009, 'Computer simulation study of the materials properties of intercalated and exfoliated poly(ethylene)glycol clay nanocomposites', *Soft Matter*, vol. 5, no. 11, pp. 2239-51.

Swann, J. 2008, 'The role The Sydney Yellowblock Revival – Is its Revival a Blessing or a Curse?', *discovering Stone*, vol. 13.

Swann, J. 2011, 'Modes of decay', *Discovering stone*, issue 20, pp. 24-29, viewed 20 May 2016, <www.infotile.com/pdfFile/advicetopic/7122011113752.pdf>.

Swanson, J., Ward, C.R. & Franklin, B.J. 2002, 'Mineralogy of Sydney Building Sandstones in Relation to Geotechnical Properties-1: Relation of Quantitative X-ray Diffraction Data to Other Chemical and Petrographic Indicators', *Australian Geomechanics: Journal and News of the Australian Geomechanics Society*, vol. 37, no. 4, pp. 53-69.

Szekely, G., Nebuloni, M. & Zerilli, L. 1992, 'Thermal analysis-mass spectrometry coupling and its applications', *Thermochimica acta*, vol. 196, no. 2, pp. 511-32.

Tabasso, M.L. 1995, 'Acrylic Polymers for the Conservation of Stone: Advantages and Drawbacks', *APT Bulletin*, vol. 26, no. 4, pp. 17-21.

Tarasov, V.I. 2001, 'New Colloid Silicate Solutions for Restoration and Conservation of Stone Facades', *Russian Journal of Applied Chemistry*, vol. 74, no. 12, pp. 1985-9.

Thanh, T.D., Mao, N.D., Ngan, N.T.K., Nhan, H.T.C., Huy, H.T. & Grillet, A.-C. 2012, 'Study structure and properties of nanocomposite material based on unsaturated polyester with clay modified by poly (ethylene oxide)', *Journal of Nanomaterials*, vol. 2012, p. 21.

The Australian National University 2009, *Implications of Climate Change for Australia's World Heritage Properties: A Preliminary Assessment*, Department of climate change and the Department of the environment, water, heritage and the arts, Canberra.

Theng, B. 1982, 'Clay–polymer interactions: summary and perspectives', *Clays and Clay Minerals*, Citeseer.

Thomas, F., Michot, L.J., Vantelon, D., Montarge`s, E., Pre´lot, B., Cruchaudet, M. & Delon, J.F., 1999, 'Layer charge and electrophoretic mobility of smectites', *Colloids and Surfaces A: Physicochemical and Engineering Aspects,* vol.159, no. 2-3, pp. 351–358.

Thomson, G. & White, R. 1974, 'The pH of Rain and the Destruction of Alkaline Stone', *Studies in Conservation*, vol. 19, no. 3, pp. 190-1.

Thuc, C.-N.H., Grillet, A.-C., Reinert, L., Ohashi, F., Thuc, H.H. & Duclaux, L. 2010, 'Separation and purification of montmorillonite and polyethylene oxide modified montmorillonite from Vietnamese bentonites', *Appl. Clay Sci.*, vol. 49, no. 3, pp. 229-38.

Tiano, P. 1995, 'Stone Reinforcement by Calcite Crystal Precipitation Induced by Organic Matrix Macromolecules', *Studies in Conservation*, vol. 40, no. 3, pp. 171-6.

Tiano, P. 2002, 'Biodegradation of cultural heritage: decay mechanisms and control methods', *Seminar article, New University of Lisbon, Department of Conservation and Restoration*, pp. 7-12.

Tiano, P., Biagiotti, L. & Mastromei, G. 1999, 'Bacterial bio-mediated calcite precipitation for monumental stones conservation: methods of evaluation', *Journal of Microbiological Methods*, vol. 36, no. 1-2, pp. 139-45.

Tiano, P., Cantisani, E., Sutherland, I. & Paget, J.M. 2006, 'Biomediated reinforcement of weathered calcareous stones', *Journal of Cultural Heritage*, vol. 7, no. 1, pp. 49-55.

Tkac, I., Kodamel, P. & Müller, D. 1994, 'Acid-treated montmorillonites. A study by 29Si and 27Al MAS NMR', *Clay Minerals*, vol. 29, no. 1, pp. 11-9.

Török, Á. 2010, 'In Situ Methods of Testing Stone Monuments and the Application of Nondestructive Physical Properties Testing in Masonry Diagnosis', in M.B. Dan, R. Přikryl & Á. Török (eds), *Materials, Technologies and Practice in Historic Heritage Structures*, Springer Netherlands, pp. 177-93.

Török, Á. & Přikryl, R. 2010, 'Current methods and future trends in testing, durability analyses and provenance studies of natural stones used in historical monuments', *Engineering Geology*, vol. 115, no. 3, pp. 139-42.

Tolle, T.B. & Anderson, D.P. 2002, 'Morphology development in layered silicate thermoset nanocomposites', *Composites Science and Technology*, vol. 62, no. 7, pp. 1033-41.

Tomaselli, L., Lamenti, G., Bosco, M. & Tiano, P. 2000, 'Biodiversity of photosynthetic micro-organisms dwelling on stone monuments', *International Biodeterioration & Biodegradation*, vol. 46, no. 3, pp. 251-8.

Toniolo, L., Paradisi, A., Goidanich, S. & Pennati, G. 2011, 'Mechanical behaviour of lime based mortars after surface consolidation', *Construction and Building Materials*, vol. 25, no. 4, pp. 1553-9.

Toth, I., Szepvolgyi, J., Jakab, E., Szabo, P. & Szekely, T. 1990, 'Thermal decomposition of a bentonite-polyacrylamide complex', *Thermochim. Acta*, vol. 170, pp. 155-66.

Tran, N.H., Dennis, G.R., Milev, A.S., Kannangara, G.S.K., Wilson, M.A. & Lamb, R.N. 2005, 'Interactions of sodium montmorillonite with poly(acrylic acid)', *Journal of Colloid and Interface Science*, vol. 290, no. 2, pp. 392-6.

Tran, N.H., Wilson, M.A., Milev, A.S., Dennis, G.R., Kannangara, G.S.K. & Lamb, R.N. 2006, 'Dispersion of silicate nano-plates within poly(acrylic acid) and their interfacial interactions', *Science and Technology of Advanced Materials*, vol. 7, no. 8, pp. 786-91.

Tsakalof, A., Manoudis, P., Karapanagiotis, I., Chryssoulakis, I. & Panayiotou, C. 2007, 'Assessment of synthetic polymeric coatings for the protection and preservation of stone monuments', *Journal of Cultural Heritage*, vol. 8, no. 1, pp. 69-72.

Tuminello, W.H., Bracci, S. & Piacenti, F. 2002, 'New Developments in Fluorinated Materials for Stone Preservation', *APT Bulletin*, vol. 33, no. 4, pp. 19-22.

Turkington, A.V. & Paradise, T.R. 2005, 'Sandstone weathering: a century of research and innovation', *Geomorphology*, vol. 67, no. 1-2, pp. 229-53.

Tutas, M., Saglam, M., Yuksel, M. & Guler, C. 1987, 'Investigation of the thermal decomposition kinetics of polyacrylamide using a dynamic TG technique', *Thermochim. Acta*, vol. 111, pp. 121-6.

Twardowski, T.E. 2007, *Introduction to nanocomposite materials: properties, processing, characterization*, DEStech publications, Inc.

Tzavalas, S. & Gregoriou, V.G. 2009, 'Infrared spectroscopy as a tool to monitor the extent of intercalation and exfoliation in polymer clay nanocomposites', *Vibrational Spectroscopy*, vol. 51, no. 1, pp. 39-43.

Ulusoy, U., Şimşek, S. & Ceyhan, Ö. 2003, 'Investigations for Modification of Polyacrylamide-Bentonite by Phytic Acid and its Usability in Fe3+, Zn2+ and UO2 2+ Adsorption', *Adsorption*, vol. 9, no. 2, pp. 165-75.

Utracki, L., Sepehr, M. & Boccaleri, E. 2007, 'Synthetic, layered nano-particles for polymeric nanocomposites (PNC's)', *Polymers for advanced technologies*, vol. 18, no. 1, pp. 1-37.

Vacchiano, C.D., Incarnato, L., Scarfato, P. & Acierno, D. 2008, 'Conservation of tuff-stone with polymeric resins', *Construction and Building Materials*, vol. 22, no. 5, pp. 855-65.

Vaia, R.A. & Giannelis, E.P. 1997, 'Polymer Melt Intercalation in Organically-Modified Layered Silicates: Model Predictions and Experiment', *Macromolecules*, vol. 30, no. 25, pp. 8000-9.

Vaia, R.A. & Liu, W. 2002, 'X-ray powder diffraction of polymer/layered silicate nanocomposites: Model and practice', *Journal of Polymer Science Part B: Polymer Physics*, vol. 40, no. 15, pp. 1590-600.

Vaia, R.A., Sauer, B.B., Tse, O.K. & Giannelis, E.P. 1997, 'Relaxations of confined chains in polymer nanocomposites: glass transition properties of poly (ethylene oxide)

intercalated in montmorillonite', *J. Polym. Sci., Part B: Polym. Phys.*, vol. 35, no. 1, pp. 59-67.

Van Dyke, J.D. & Kasperski, K.L. 1993, 'Thermogravimetric study of polyacrylamide with evolved gas analysis', *Journal of Polymer Science Part A: Polymer Chemistry*, vol. 31, no. 7, pp. 1807-23.

Vasiliev, V.V. & Morozov, E. 2001, *Mechanics and analysis of composite materials*, Elsevier.

Velde, B. 1977, *Clays and clay minerals in natural and synthetic systems*, Elsevier Scientific Pub. Co, Amsterdam.

Velde, B. 1983, 'Infrared OH-stretch bands in potassic micas, talcs and saponites; influence of electronic configuration and site of charge compensation', *American Mineralogist*, vol. 68, pp. 1169-73.

Velde, B. 1992, Introduction to clay minerals: chemistry, origins, uses and environmental significance, Chapman & Hall, London.

Velde, B. 1995, 'Composition and mineralogy of clay minerals' in B. Velde (ed), *Origin and mineralogy of clays*, 1st edn, Springer, Germany, pp. 8-41.

Velde, B. & Meunier, A. 2008, *The origin of clay minerals in soils and weathered rocks*, Springer, Berlin.

Vicini, S., Margutti, S., Moggi, G. & Pedemonte, E. 2001, 'In situ copolymerisation of ethylmethacrylate and methylacrylate for the restoration of stone artefacts', *Journal of Cultural Heritage*, vol. 2, no. 2, pp. 143-7.

Vicini, S., Mariani, A., Princi, E., Bidali, S., Pincin, S., Fiori, S., Pedemonte, E. & Brunetti, A. 2005, 'Frontal polymerization of acrylic monomers for the consolidation of stone', *Polymers for Advanced Technologies*, vol. 16, no. 4, pp. 293-8.

Vicini, S., Margutti, S., Princi, E., Moggi, G. & Pedemonte, E. 2002, 'In situ copolymerization for the consolidation of stone artefacts', *Macromolecular Chemistry and Physics*, vol. 203, no. 10-11, pp. 1413-9.

Vicini, S., Princi, E., Pedemonte, E., Lazzari, M. & Chiantore, O. 2004, 'In situ polymerization of unfluorinated and fluorinated acrylic copolymers for the conservation of stone', *Journal of Applied Polymer Science*, vol. 91, no. 5, pp. 3202-13.

Vicini, S., Princi, E., Pedemonte, E. & Moggi, G. 2006, 'Surface Treatment', in S.K. Kourkoulis (ed.), *Fracture and Failure of Natural Building Stones*, Springer Netherlands, pp. 565-75.

Viani, A., Gualtieri, A.F. & Artioli, G. 2002, '*The nature of disorder in montmorillonite by simulation of X-ray powder patterns*', American Mineralogist, vol.87, no.5, pp. 966-975.

Vilcu, R., Bujor, I.I., Olteanu, M. & Demetrescu, I. 1987, 'Thermal stability of copolymer acrylamide-maleic anhydride', *J. Appl. Polym. Sci.*, vol. 33, no. 7, pp. 2431-7.

Vilcu, R., Irinei, F., Ionescu-Bujor, J., Olteanu, M. & Demetrescu, I. 1985, 'Kinetic parameters obtained from TG and DTG curves of acrylamide-maleic anhydride copolymers', *Journal of thermal analysis*, vol. 30, no. 2, pp. 495-502.

Viles, H.A. 2005, 'Can stone decay be chaotic?' in A.V. Turkington (eds), *Stone Decay in the Architectural Environment*, 1st edn, Geological Society of America Special Papers, London, vol. 390, pp. 11-16.

Volpert, E., Selb, J., Candau, F., Green, N., Argillier, J. & Audibert, A. 1998, 'Adsorption of hydrophobically associating polyacrylamides on clay', *Langmuir*, vol. 14, no. 7, pp. 1870-9.

Volzone, C., 2004, 'Removal of metals by natural and modified clays' in F. Whypych & K.G. Satyanarayana (eds), *Clay surfaces: Fundamentals and applications*, 1st edn, Elsevier, London, pp. 290-320.

Voorn, D., Ming, W. & Van Herk, A. 2006, 'Polymer-clay nanocomposite latex particles by inverse pickering emulsion polymerization stabilized with hydrophobic montmorillonite platelets', *Macromolecules*, vol. 39, no. 6, pp. 2137-43.

Wang, J., Hu, Y., Li, B., Gui, Z. & Chen, Z. 2004, 'Preparation of polyacrylamide and gamma-zirconium phosphate nanocomposites by intercalative polymerization', *Ultrasonics sonochemistry*, vol. 11, no. 5, pp. 301-6.

Wang, L., Wang, Z., Zhang, X., Shen, J., Chi, L. & Fuchs, H. 1997, 'A new approach for the fabrication of an alternating multilayer film of poly (4-vinylpyridine) and poly (acry1ic acid) based on hydrogen bonding', *Macromol. Rapid Commun*, vol. 18, pp. 509-14.

Wang, Y., Zeng, L., Ren, X., Song, H. & Wang, A. 2010, 'Removal of Methyl Violet from aqueous solutions using poly (acrylic acid-co-acrylamide)/attapulgite composite', *Journal of Environmental Sciences*, vol. 22, no. 1, pp. 7-14.

Ward-Harvey, K. 2009, *Fundamental Building Materials*, 4th edn, Universal-Publishers, Boca Raton.

Warke, P.A., Curran, J.M., Turkington, A.V. & Smith, B.J. 2003, 'Condition assessment for building stone conservation: a staging system approach', *Building and Environment*, vol. 38, no. 9-10, pp. 1113-23.

Warke, P.A., McKinley, J. & Smith, B.J. 2006, 'Weathering', in S.K. Kourkoulis (ed.), *Fracture and Failure of Natural Building Stones*, Springer Netherlands, pp. 313-27.

Warscheid, T. & Braams, J. 2000, 'Biodeterioration of stone: a review', *International Biodeterioration & Biodegradation*, vol. 46, no. 4, pp. 343-68.

Waseda, Y., Matsubara, E. & Shinoda, K. 2011, X-Ray diffraction crystallography: introduction, examples and solved problems, Springer.

Weaver, C.E. & Pollard, L.D. 1973, *The chemistry of clay minerals,* vol. 15, Elsevier Scientific, Amsterdam.

Weber, H. 1985, 'Conservation and Restoration of Natural Stone in Europe', *Bulletin of the Association for Preservation Technology*, vol. 17, no. 2, pp. 15-23.

Webster, A. & May, E. 2006, 'Bioremediation of weathered-building stone surfaces', *Trends in Biotechnology*, vol. 24, no. 6, pp. 255-60.

Weiss, N.R. 1995, 'Chemical Treatments for Masonry: An American History', *APT Bulletin*, vol. 26, no. 4, pp. 9-16.

Werner, A. 1981, 'Synthetic materials in art conservation', *Journal of Chemical Education*, vol. 58, no. 4, pp. 321-4.

Wheeler, G. 2005, *Alkoxysilanes and the consolidation of stone*, Getty Publications, California.

Wheeler, G.S., Schein, A., Shearer, G., Su, S.H., Scott Blackwell, C. 1992, 'Preserving our heritage in stone', *Anal Chem*, vol. 64, no. 5, pp. 347–56.

Will, G. 2006, *Powder diffraction: the Rietveld method and the two-stage method to determine and refine crystal structures from powder diffraction data*, vol. 1, Springer, Berlin.

Wills, P. & Eves, C. 2005, *Heritage Australia: a review of Australian material regarding the economic and social benefits of heritage property*, New South Wales Heritage Office.

Wilson, G.M. 1985, 'Oölitic Limestone Conservation: A Case Study in Conservation and Maintenance, Governor's Mansion, Salt Lake City, Utah', *Bulletin of the Association for Preservation Technology*, vol. 17, no. 2, pp. 25-33.

Winkler, E. 1987, 'Weathering and weathering rates of natural stone', *Environmental Geology*, vol. 9, no. 2, pp. 85-92.

Winkler, E.M. 1973, *Stone: properties, durability in man's environment*, Springer-verlag, New York.

Witkowski, A. 1967, 'Infrared Spectra of the Hydrogen-Bonded Carboxylic Acids', *The Journal of Chemical Physics*, vol. 47, no. 9, pp. 3645-8.

Witte, E.D., Huget, P. & Broeck, P.V.D. 1977, 'A Comparative Study of Three Consolidation Methods on Limestone', *Studies in Conservation*, vol. 22, no. 4, pp. 190-6.

Witucki, G.L. 1993, 'A silane primer: chemistry and applications of alkoxy silanes', *Journal of coatings technology*, vol. 65, pp. 57-60.

Wolff, A. 2004, 'Restoration and maintenance: A case study of cologne cathedral' in C. Mäckler (eds), *Material stone*, Birkhäuser, Berlin, pp. 110-111.

Worden, R.H., Morad, S. 2003, 'Clay minerals in sandstones: controls on formation, distribution and evolution' in Worden, R.H., Morad. S (eds), *Clay mineral cements in sandstones*, 1st edn, Blackwell Publishing company, Malden, pp. 3-10.

Worrall, W.E. 1968, *Clays: their nature, origin and general properties*, Maclaren & Sons Ltd, London.

Wright, J.S. 2002, 'Geomorphology and stone conservation: sandstone decay in Stoke-on-Trent', *Structural Survey*, vol. 20, no. 2, pp. 50-61.

Wu, J. & Lerner, M.M. 1993, 'Structural, thermal, and electrical characterization of layered nanocomposites derived from sodium-montmorillonite and polyethers', *Chemistry of Materials*, vol. 5, no. 6, pp. 835-8.

Wu, J., Lin, J., Li, G. & Wei, C. 2001, 'Influence of the COOH and COONa groups and crosslink density of poly (acrylic acid)/montmorillonite superabsorbent composite on water absorbency', *Polymer International*, vol. 50, no. 9, pp. 1050-3.

Wendlandt, W.W. & Gallagher, P.K. 1981, 'CHAPTER 1 - Instrumentation A2 - TURI, EDITH A', *Thermal Characterization of Polymeric Materials*, Academic Press, pp. 1-90.

Wypych, F., 2004, 'Chemical modification of clay surfaces' in F. Whypych & K.G. Satyanarayana (eds), *Clay surfaces: Fundamentals and applications*, 1st edn, Elsevier, London, pp. 2-56.

Xie, W. & Pan, W.-P. 2001, 'Thermal characterization of materials using evolved gas analysis', *Journal of Thermal Analysis and Calorimetry*, vol. 65, no. 3, pp. 669-85.

Yahiaoui, A., Hachemaoui, A. & Belbachir, M. 2009, 'Cationic polymerization of ethylene oxide with Maghnite-H as a clay catalyst in the presence of ethylene glycol', *J. Appl. Polym. Sci.*, vol. 113, no. 1, pp. 535-40.

Yan, X. & Zhang, X. 2014, 'Interactive effects of clay and polyacrylamide properties on flocculation of pure and subsoil clays', *Soil Research.*, vol. 52, no. 7, pp. 727–737.

Yang, L., Heatley, F., Blease, T.G. & Thompson, R.I. 1996, 'A study of the mechanism of the oxidative thermal degradation of poly (ethylene oxide) and poly (propylene oxide) using 1 H-and 13 C-NMR', *European polymer journal*, vol. 32, no. 5, pp. 535-47.

Yang, M.-H. 1998, 'The two-stages thermal degradation of polyacrylamide', *Polymer testing*, vol. 17, no. 3, pp. 191-8.

Yang, M.-H. 1999, 'The thermal degradation of polyacrylamide with adsorbed metal ions as stabilizers', *Polym. Test.*, vol. 19, no. 1, pp. 85-91.

Yang, M.-H. 2002, 'On the thermal degradation of poly(styrene sulfone)s. V. Thermogravimetric kinetic simulation of polyacrylamide pyrolysis', *J. Appl. Polym. Sci.*, vol. 86, no. 7, pp. 1540-8.

Yano, K., Usuki, A., Okada, A., Kurauchi, T. & Kamigaito, O. 1993, 'Synthesis and properties of polyimide–clay hybrid', *Journal of Polymer Science Part A: Polymer Chemistry*, vol. 31, no. 10, pp. 2493-8.

Yeh, J.-M., Liou, S.-J. & Chang, Y.-W. 2004, 'Polyacrylamide-clay nanocomposite materials prepared by photopolymerization with acrylamide as an intercalating agent', *J. Appl. Polym. Sci.*, vol. 91, no. 6, pp. 3489-96.

Young, G. 1988, *Conservation, history and development,* New South Wales Government Information Service, Sydney.

Zárraga, R., Alvarez-Gasca, D.E. & Cervantes, J. 2002, 'Solvent effect on TEOS film formation in the sandstone consolidation process', *Silicon Chemistry*, vol. 1, no. 5, pp. 397-402.

Zárraga, R., Cervantes, J., Salazar-Hernandez, C. & Wheeler, G. 2010, 'Effect of the addition of hydroxyl-terminated polydimethylsiloxane to TEOS-based stone consolidants', *Journal of Cultural Heritage*, vol. 11, no. 2, pp. 138-44.

Zadaka, D., Radian, A. & Mishael, Y.G. 2010, 'Applying zeta potential measurements to characterize the adsorption on montmorillonite of organic cations as monomers, micelles, or polymers', *Journal of Colloid and Interface Science*, vol. 352, no. 1, pp. 171-7.

Zampori, L., Stampino, P.G., Cristiani, C., Cazzola, P. & Dotelli, G. 2010, 'Intercalation of poly (ethylene-oxides) in montmorillonite: tailor-made nanocontainers for drug delivery systems', *Applied Clay Science*, vol. 50, no. 2, pp. 266-70.

Zanardini, E., Abbruscato, P., Ghedini, N., Realini, M. & Sorlini, C. 2000, 'Influence of atmospheric pollutants on the biodeterioration of stone', *International Biodeterioration & Biodegradation*, vol. 45, no. 1-2, pp. 35-42.

Zanetti, M., Lomakin, S. & Camino, G. 2000, 'Polymer layered silicate nanocomposites', *Macromolecular Materials and Engineering*, vol. 279, no. 1, pp. 1-9.

Zendri, E., Biscontin, G., Nardini, I. & Riato, S. 2007, 'Characterization and reactivity of silicatic consolidants', *Construction and Building Materials*, vol. 21, no. 5, pp. 1098-106.

Zhao, X., Wang, B. & Li, J. 2008, 'Synthesis and electrorheological activity of a modified kaolinite/carboxymethyl starch hybrid nanocomposite', *Journal of Applied Polymer Science*, vol. 108, no. 5, pp. 2833-9.

Zhou, W., Apkarian, R.P., Wang, Z.L., Joy, D. 2007, 'Fundamentals of Scanning Electron Microscopy', in W. Zhou, Z.L. Wang (ed.), Scanning microscopy for nanotechnology, Springer, New York, pp.1-40.

Zhou, X., Goh, S.H., Lee, S.Y. & Tan, K.L. 1998, 'XPS and FTi.r. studies of interactions in poly(carboxylic acid)/poly(vinylpyridine) complexes', *Polymer*, vol. 39, no. 16, pp. 3631-40.

Zhu, J. & Wilkie, C.A. 2007, *Intercalation compounds and clay nanocomposites*, Wiley-VCH, Weinheim.

Zhu, S., Chen, J. & Li, H. 2009, 'Influence of poly(ethylene glycol)/montmorillonite hybrids on the rheological behaviors and mechanical properties of polypropylene', Polym. Bull. (Heidelberg, Ger.), vol. 63, no. 2, pp. 245-57.

Zhu, S., Chen, J., Li, H. & Cao, Y. 2013a, 'Structure and conformation of poly(ethylene glycol) in confined space of montmorillonite', *Appl. Surf. Sci.*, vol. 264, pp. 500-6.

Zhu, S., Peng, H., Chen, J., Li, H., Cao, Y., Yang, Y. & Feng, Z. 2013b, 'Intercalation behavior of poly(ethylene glycol) in organically modified montmorillonite', *Appl. Surf. Sci.*, vol. 276, pp. 502-11.

Zornoza-Indart, A. & Lopez-Arce, P. 2016a, 'Silica nanoparticles (SiO_2): Influence of relative humidity in stone consolidation', *Journal of Cultural Heritage*, vol. 18, pp. 258-70.

Zornoza-Indart, A., Lopez-Arce, P., Leal, N., Simão, J. & Zoghlami, K. 2016b, 'Consolidation of a Tunisian bioclastic calcarenite: From conventional ethyl silicate

products to nanostructured and nanoparticle based consolidants', *Construction and Building Materials*, vol. 116, pp. 188-202.